UNIVERSITA' DEGLI STUDI DI TORINO
Dipartimento di Chimica
Ciclo XXXV

PhD thesis in: "Technology driven sciences: technologies for cultural heritage (TECH4CULTURE)"

AN ARCHAEOMETRIC STUDY OF GLASS PRODUCTION AND SUPPLY IN IRON AGE ETRURIA AND LATIUM

Name of the candidate:

Oleh Yatsuk

Supervisors:

Prof. Monica Gulmini

Prof. Cristiano Iaia

Academic years: 2019-2023
SSD: CHIM01

Torino, 2023

To my friend Ivan and my godfather Victor,

may this work serve their good memory

Table of Contents

ACKNOWLEDGEMENTS

The world appeared to be a different place in 2019 when the work started. Somehow, despite all the disruptive circumstances of recent years, this work continued being both soothing and calming (by providing direction in life and distracting from the world) as well as the source of madness. Looking back at the work done, it is apparent that it continued and arrived until this stage only because people believed what I was doing was good and worthy.

People started to believe and support the idea of glass analysis from the Iron Age Central Italy contexts at the interview during the Tech4Culture PhD program selection process. It must have been compelling enough to benefit from funding attached to the candidate's position. I appreciate the program's openness to prospective students' proposals, allowing me to start something that felt like my idea. This feeling of pursuing something of your own gave much encouragement as well as anxiety and opened the way to the experience unattainable otherwise.

I have been lucky to work under the supervision of people who shared my enthusiasm for the project and put a lot of their energy and time for this thesis to see the light of day. Prof. Monica Gulmini always had ideas of how to organise the work, design the study and present the data. She was solving the problems on our way most efficiently, making this study feasible. And there were many obstacles on the way, indeed. At times, she had more faith in our research than me, and only thanks to her endless encouragement this thesis has been finally written. Without her role, this story would look much more like a story of failure.

I am grateful to a supervisor from the archaeological side – Prof. Cristiano Iaia. He put up with my limited knowledge of archaeological contexts and the Italian language – a prerequisite for working with archaeological scholarship. I feel that my knowledge has grown substantially with his suggestions and guidance. His role was crucial to finding our way to systematise the materials we were studying.

This study would only be possible if we could access the collections of archaeological glass beads. I remember with great warmth the reply of Dr Vittoria Lecce saying I was welcome to study their glasses even before I officially started the project. The whole administration of the Museo Nazionale Etrusco di Villa Giulia also deserves thanks for authorising us to work with the collection and accommodating our needs during the time of pandemic when most of the museums remained closed to external researchers.

The same goes for the administration of the Museo delle Civiltà (particularly its division known as Museo Preistorico Etnografico "L. Pigorini"). Despite the reorganisation, changes in the administration and strict schedule, we managed to accomplish a lot together with Dr Alessandra Serges and Serena Francone, who helped a lot with orientation, managing the objects and general organisation of work.

Both administrations trusted us enough to release substantial sets of objects to be studied in the laboratories. This was crucial for achieving the desired depth of insight into the objects' composition and structure, and I am grateful that it was possible.

The archaeological side of the study was much reinforced by the support of Dr Leonie Koch, who was studying glass beads from the Iron Age contexts in Italy for a long time and provided the necessary expertise on specific sets of beads within this study. She also agreed to provide her opinion on the thesis, which was difficult because it was a challenging reading.

The reader will see that we used a reasonably wide range of analytical methods to collect the data we were interested in. Behind each piece of equipment there were people that were keen to do glass analyses and who taught me a lot about data collection and processing. They all contributed their time to supervise me or to do the analyses themselves. Sometimes it happened in unfavourable circumstances, showing they cared about the project.

I am grateful for suggestions on the colour measurements to Dr Paola Iacomussi, who did not take part in the assessment and presentation of the colour information though. I am grateful to Corning Museum of Glass for providing the reference materials that were more than useful on multiple occasions during the study. XRF measurements in the Villa Giulia museum were done by Dr Astrik Gorghinian and Dr Marco Ferretti, who also extended my knowledge of the technique and data treatment, making the outcome of the study much better. Dr Giacomo Fiocco and Prof. Marco Malagodi are commended for coming all the way from Cremona for the XRF session in Rome and helping with the acquisition of hundreds of spectra in a very short time. FORS measurements were possible thanks to the support of Prof. Alessandro Re and Prof. Alessandro Lo Giudice, who trained me and lent the FORS setup. On this occasion, special mention goes to Dr Leandro Sottili for helping with its transportation.

In the laboratory setting, the first instrument we used was SEM-EDS. Dr Patrizia Davit and Dr Roberto Cossio have helped a lot with establishing the protocol of analysis and calibration of the instrument. Prof. Roberto Giustetto and Giulia Berruto supported us with the XRD measurements that were invaluable in the characterisation of the inclusions inside the glass. I am highly grateful for the hospitality I received at the University of Bari Aldo Moro. Raman and LA-ICP-MS measurements were possible thanks to the support of Prof Annarosa Mangone and Dr Lorena Carla Giannossa. They taught me a lot about the methods and addressed any obstacles we encountered during the analytical campaign. Further help was received from Dr Tiziana Forleo, Dr Vincent Gardette and Prof Pedro Barrulas. I also thank Sabrina Molinaro, who helped a lot during the data acquisition.

The acknowledgements would only be complete with mentioning how much support I received from my family and friends. My parents and grandparents, siblings and cousins were forgiving and are still forgiving of my long absences and are very enthusiastic about my work, even though they hardly can remember what I do exactly. My friends that are based in Turin and those with whom I was primarily interacting online through all these years probably do not know how much they have helped me to stay on track and how much I appreciate their friendship and every moment together because I do not show it enough. Now it is on the record.

This work would not be accomplished without those who defend their homes in Ukraine (my country of origin). Their bravery and resilience allowed me to proceed with my minuscule and seemingly irrelevant (in these circumstances) research being confident that my world will not collapse, no matter the perils. For this, I am eternally grateful.

Finally, I am grateful to the reviewers – Prof Alberta Silvestri and Prof Thilo Rehren, for their willingness to read the thesis and suggestions that were the product of their reflections on the content. I hope that most of them are addressed in the text.

ABSTRACT

The primary focus of this work is the chemical composition of vitreous beads dated to the first half of the first millennium BCE. The majority of them were unearthed in the present-day Lazio region of Italy. By cross-checking their contexts with the composition, it was possible to make inferences about the glass-making technology of the time, which led to a better understanding of the development of the glass industry as a whole. The period discussed in the thesis is seldom considered by glass researchers, which makes the newly obtained data more valuable.

The study was organised in three stages: during the first one, the collections of glass objects were studied, and representative objects were selected for documentation of appearance and state of preservation; selected samples were studied during stage two with non-invasive analytical techniques using portable equipment without taking them outside the museums; even smaller but still representative number of samples was then subjected to the laboratory study during the stage three.

Among the significant outcomes of the study, we can mention tracking the transition of the use of fluxing materials, glass stabilisers and colourants. It became evident that glass was primarily supplied from several specialised workshops in the Eastern Mediterranean, though evidence of local glass-making was also discovered. Based on the data, the Iron Age appears to be a very important period in the history of glass-making, featuring multiple accounts of innovation.

List of figures

List of tables

List of abbreviations

BCE – Before the Common Era;
CCD – Charge-Coupled Device (detector);
CMOG – Corning Museum of Glass;
CRM – Certified Reference Material;
DNG – Digital Negative Specification;
EA – Early Archaic;
EDOF – Extended Depth Of Field;
EIA – Early Iron Age;
EO – Early Orientalising;
EPMA – Electron Probe Micro Analysis;
FBA – Final Bronze Age;
FORS – Fibre Optic Reflectance Spectroscopy;
FP – Fundamental Parameters;
FWHM – Full Width at Half Maximum;
HCA – Hierarchical Cluster Analysis;
HIMT – High Iron Manganese Titanium glass;
HMG – High Magnesium Glass;
IA – Iron Age;
LA – Late Archaic;
LA-ICP-MS – Laser Ablation – Inductively Coupled Plasma – Mass Spectrometry;
LBA – Late Bronze Age;
LED – Light Emitting Diode;
LMG – Low Magnesium Glass;
LMHK – Low Magnesium High potassium (K);
LMMK – Low Magnesium Medium potassium (K);
LO – Late Orientalising;
LOQ – Limit of Quantification;
MO – Middle Orientalising;
MRO – Medium-Range Order;
NIST – National Institute of Standards and Technology;
OM – Optical Microscopy;
PC – Principal Component;
PCA – Principal Component Analysis;
PIXE – Particle Induced X-Ray Emission;
p-XRF – portable X-Ray Fluorescence spectrometry;
QC – Quality Control;
REE – Rare-Earth Elements;
RGB – Red Green Blue;
RoI – Regions of Interest;
RSD – Relative Standard Deviation;

SDD – Silicon Drift Detector;

SGT – Society of Glass Technology;

SIMS – Secondary Ion Mass Spectrometry;

SNV – Standard Normal Variate;

SRO – Short-Range Order;

TIMS – Thermal Ionisation Mass Spectrometry;

UCC – Upper Continental Crust;

USB – Universal Serial Bus;

UV-Vis-NIR – UltraViolet-Visible-Near-InfraRed;

(VP)-SEM-EDS – (Variable Pressure) – Scanning Electron Microscopy coupled with Energy Dispersive Spectrometry;

WDS – Wavelength Dispersive Spectrometer;

XANES – X-Ray Absorption Near Edge Structure;

XRD – X-Ray Diffraction;

PREFACE.

Glass has been produced and used by people in different parts of the world for almost five thousand years (Tait 1991; Shortland and Degryse 2021), though the more systematic (and better studied) occurrences are dated to the second millennium BCE (Brill 1963; Rehren 2021). At the beginning of its production, glass was regarded with extraordinary value, even as if it had magical properties (Barag 2009; Hodgkinson 2019; Schenkel 2019), and glass objects were highly appreciated for their gloss and richness of colours.

In addition to beauty, nowadays, we are continuing to explore the glass structure to obtain unique technological properties, and glass is one of the most promising directions material science is progressing in (Pellitier and Quiao 2019).

We have yet to determine precisely how the first glass came into being and who made it first (Shortland and Degryse 2021). Archaeology and history on their own sometimes provide only limited information about the technology and production places of most of the ancient glass objects that are found in thousands each year worldwide.

On the other hand, archaeometry can support the archaeological research on many aspects of the development of the glass industry. This task can be approached successfully only if the results of the archaeometric investigations are set correctly in the archaeological context of the finds. Such an interdisciplinary search for new evidence is the main idea behind the present PhD research project, focusing on glass from the Iron Age Mediterranean and neighbouring regions. The period, in the context of this study, corresponds to the first half of the first millennium BCE.

In archaeometric studies of the Iron Age glasses, the interest has increased in the last twenty years. However, such scholarship is less extensive than the one for Bronze Age or Hellenistic-Roman glass (Arletti et al. 2010; Schmidt 2019; Reade 2021). In the Iron Age Mediterranean, Etruscan contexts are among the most attractive ones to study. Etruscans had advanced technology and a vast exchange network for the time, and they had both commercial connections and knowledge of high-temperature processes (such as metallurgy and pottery making) to make their own glass. Several hints support this hypothesis: glass working was attested in Northern Italy in the Final Bronze Age (Henderson 1988; Towle et al. 2001); therefore, it is reasonable to assume primary glass production could have been continued in the Iron Age. Even if it did not happen, the Mediterranean trade network established by Phoenicians and Greeks provided a steady flow of materials, skills and craftspeople from the East, which in the Italian peninsula were probably making their own glass vessels and other objects (Harden 1968; Sternini 2017; Koch 2020) by working imported glass.

The archaeological question is if they were actually making glass out of raw materials or if only secondary glass production and glass shaping occurred. Even though researchers have focussed on Etruscan antiquities since the 18th century, glass beads were seldom the main interest of archaeologists.

Putting the geographical aspect aside, Iron Age was a time of significant developments in the glass industry, as new techniques of glass shaping and a new flux for primary glass production were introduced. These changes shall also find their reflection in Etruscan contexts, even if the primary production sites were thousands of kilometres away. This period is interesting because chemical analysis of glass finds highlighted different main compositional groups that show further minor

divisions (Lončarić and Costa 2023). This evidence led to the conclusion that the glass industry at that time was not centralised as it happened to be, for example, in Roman times (Henderson 2013; Rehren and Freestone 2015).

The Etruscans - set geographically in the middle of the Mediterranean – are an essential element of a puzzle that is definitely worth examining from the particular perspective of the glass trade. With this premise, it is evident that an interdisciplinary study of technology and provenance of glass unearthed from Etruscan contexts has great potential.

In this PhD research project, the focus is on the glass finds (mostly beads) found in 10th – 5th centuries BCE Southern Etruria (namely from Bisenzio, Capena, Cerveteri, Falerii, Narce, Tarquinia, Veio, Vulci) and Latium (Marino, Osteria dell'Osa, Sermoneta, Tivoli). These sites are all located in the modern Lazio region of Italy. However, the list of archaeological sites considered in this work would not be exhaustive without Terni (located in Umbria) and Verucchio (Emilia Romagna). Most of the objects were recovered from the funerary contexts. All the studied objects are presently kept in the valuable collections of the *Museo delle Civiltà* and the *Museo Nazionale Etrusco di Villa Giulia*, both in Rome (Italy).

Several hundreds of archaeological objects were analysed under high magnification to observe the morphology and then using spectroscopic methods to gather compositional information.

The diversity of glass beads in terms of appearance is astonishing; that is why there was the need to establish a cost-efficient methodology that would allow analysing a large number of samples, providing essential information on how each particular piece was made and how it is related to others. This information was then refined with the application of more accurate - but costly and invasive - methods of analyses, which were performed on a smaller number of representative samples. In this way, it was intended to keep the representativity of the extensive collections and provide a depth of insight into each compositional group previously defined through the extensive preliminary analytical campaign.

This approach allowed the production of many new morphological and compositional data. They were then interpreted to contribute new knowledge on the technology used at the time for glass-making, with particular attention on raw materials. Attention was set on data that brought some clues to respond to the question of the existence of local (primary or secondary) glass production in the lands under the Etruscan influence. The published corpus of data was scrutinised in search of compositional matches with the new data produced in this research, as those matches would be of extreme value to suggest specific provenance of the primary glass, contributing new inferences to the questions of trade and exchange in the whole Mediterranean.

The above-outlined work was organised into the following three stages.

- Stage 1: the beads and the other glass objects were observed focussing on their preservation state and registering typologically relevant features. An extensive photographic campaign, with both a digital camera and a digital microscope, allowed the documentation of the objects as a whole and of informative details on their surface.
- Stage 2: was limited to strictly non-invasive approaches performed inside the museums' premises using FORS and p-XRF. Collected data were used for the compositional subdivision of the objects. They set the basis for the selection of the smaller number of samples to be included in the final stage.

- Stage 3: was conducted in the laboratory with SEM-EDS, LA-ICP-MS, μ-Raman spectroscopy and μ-XRD to gather accurate and exhaustive compositional data.

The overall research is presented here in two parts.

Part one consists of four chapters and gives an overview of the study's theoretical framework and the archaeometric investigation methods. It contains all the essential knowledge that was needed to approach the archaeometric results and their discussion given in part two.

Glass as a material and ancient glass technologies are discussed in Chapter 1 to set the frame for the archaeometric research; Chapter 1 also reports the review of the archaeometric literature on ancient glasses, focusing on the Iron Age Mediterranean and, specifically, the Italian peninsula.

Chapter 2 outlines the archaeological and historical records that built the chronological and geographical framework of the study and includes some information on the economic, technological and trade development of the society relevant for discussing the analytical data within the archaeological frame.

Chapter 3 presents the samples and the criteria employed to build a typology based on suitable features, including shape, size, colour, translucency, and decoration.

Methods of analysis and methodological limitations that were recognised and addressed during the study are considered in Chapter 4, in which the quality and overall reproducibility of the results is also assessed.

Part two consists of seven chapters, six of which present the results obtained for one specific set of objects. In each chapter, the discussion section aims at reconstructing glass-making technology and provenance based on the evidential reasoning and comparison of the results with those available in the literature.

The last chapter (Chapter 11) considers the overall archaeometric outcome of this research and highlights its contribution to the knowledge on glass production and circulation within the studied area.

PART I

CONTEXTS, MATERIALS, METHODS.

This part of the thesis provides the framework of knowledge that will be used in the second part, where new data are presented. From the narrative point of view, here is the place for outlining the concepts that will support the description of the materials and the interpretation of compositional data or in the data interpretation. The information presented in this part comes from four directions, each organised into a chapter of its own (see Preface).

CHAPTER 1. SHORT HISTORY OF GLASS PRODUCTION AND CIRCULATION IN THE MEDITERRANEAN IN THE FIRST HALF OF THE FIRST MILLENNIUM BCE.

1.1. Glass as a material.

Glass, by no doubt, is a fascinating material. Applications of glassy materials are today wider than ever, and we are continuing to discover new ones. The versatility of glass as a material is largely due to its atomic arrangement, which is different from the one of the crystalline solids, and almost all the definitions of the vitreous state are based on this key difference. In some instances, definitions even grant glasses a separate state of matter, such as the quite popular, although debated (Rao 2002; Condradt 2019), definition of Paul (1989): "glass is a state of matter which maintains the energy, volume and atomic arrangement of a liquid, but for which the changes in energy and volume with temperature and pressure are similar in magnitude to those of a crystalline solid".

One of the latest, most general definitions of glass has been given by Condradt: "Glasses are dense (nonfractal) isotropic and homogeneous non-crystalline solids characterised by the absence of any internal phase boundaries", although the author himself gives several examples in which his definition fails in fitting to all glassy materials (Condradt 2019). As for the subject of the present work, it is evident that glass definition by Condradt is quite unsuitable for ancient glasses that normally contain various inclusions of crystalline phases (Shortland 2002; Duckworth et al. 2012; Maltoni and Silvestri 2018).

The issue of isotropy in glasses needs to be discussed further regarding both modern (Murai et al. 2013), some ancient glasses, such as the late Roman dichroic glass (Barber and Freestone 1990) and opaque glass, keeping in mind that the inhomogeneity of ancient glass may give the scientists valuable information on technology and provenance.

Another definition, which better suits ancient glasses, is the one from the Art and Architecture Thesaurus developed by the Getty Trust. It defines glass as: "An amorphous, inorganic substance made by fusing silica (silicon dioxide) with a basic oxide; generally transparent but often translucent or opaque. Its characteristic properties are its hardness and rigidity at ordinary temperatures, its capacity for plastic working at elevated temperatures, and its resistance to weathering… Used for both utilitarian and decorative purposes, it can be formed into various shapes, coloured or decorated…" (Getty Trust Art and Architecture Thesaurus). This definition mostly touches the appearance of common glass and some important features such as its good workability at high temperature. However, it has at least two main flaws. First, the use of the term "substance" is not proper from a chemical point of view and second, it leaves out all natural vitreous materials, among which obsidian and the so called "desert glass" formed upon high energy impact (Fudall 1981; Riemer 2007), which have their place among the materials relevant for cultural heritage studies.

Moreover, silica is not the only substance capable of glass network forming (see Angelini et al. 2019, and references within). Finally, durability or resistance to weathering does not reflect the behaviour of the so called "wood-ash glasses", which were popular in medieval Europe, and were very susceptible to weathering (Pollard and Heron 2015; Heinmann 2018).

All these definitions highlight one, most crucial feature of glass: its amorphous nature. In this work we will focus on artificial, silica-based glasses, so all the three definitions reported above have merit.

Silica, as a main component of glass, forms a network of silicon atoms linked by oxygens without any detectable order (Figure 1.1). Zachariansen (1932) proposed the so-called "random network" theory describing glass as infinitely complex unit cell lacking any long-range order, arranged according to several rules. Among these rules, one is that the cation coordination number is small (3 or 4). As for silicon, this number is four and the central cation is arranged in the tetrahedral coordination. According to Zachariasen's rules, the polyhedra must be joined one to another by the corners, without sharing edges or faces. These rules are sometimes termed a short-range order (SRO) for the coordination of polyhedra and medium range order (MRO) for the bonds between them (Condradt 2019). The glass network of atoms represented in Figure 1.1 complies with these rules.

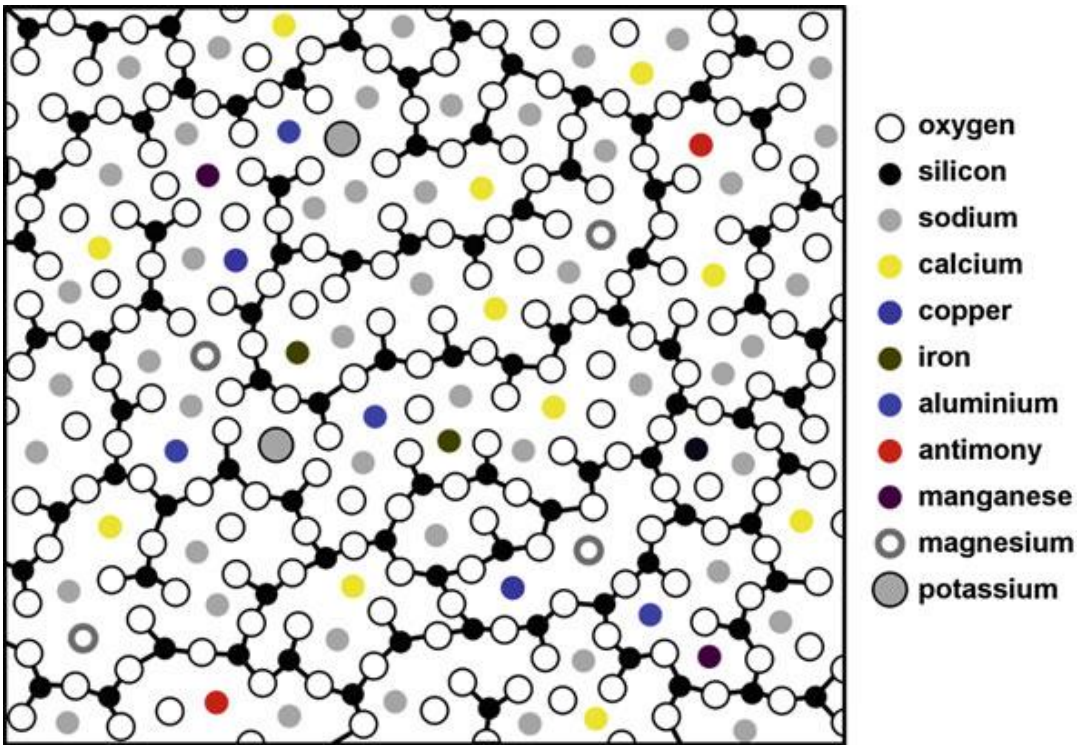

Figure 1.1. scheme of typical roman glass structure (image from Rasmussen 2012).

The main sources of silica for ancient glasses were quartz-rich sands and quartz pebbles (Henderson 1985). Quartz is a mineral that (ideally) consists of pure silica, and it is one of the most common minerals of the Earth's crust (Clarke and Washington 1924). Turning quartz into glass requires a lot of energy, as at normal pressure it melts at 1710 C° and it adopts the glassy structure on cooling of the molten material (Sosman 1927); the melting point of quartz is well above the temperatures that ancient kilns could reach (Levey 1955; Goffer 2006), that is why ancient glass makers exploited additional components, called fluxing agents or fluxes, to produce a eutectic

mixture (Verheijen and Hubert 2019). This mixture, called the glass batch, is obtained by finely grinding the pre-treated raw materials ready for fusion.

Throughout history, the fluxing function was performed by alkali carbonates. The alkali (Na and K ions) do not play a role in the formation of the glass structure; on the contrary, they break the covalent bonds between the silicon tetrahedra and occupy the octahedrally coordinated sites in the glass network (Figure 1.1). Therefore, these ions are called network modifiers (Zachariasen, 1932). Along with the heating of the glass batch, both chemical and physical transformations occur, namely dehydration, solid state reactions, formation of the primary melt and dissolution. For the silica-soda glass, the chain of reactions leads to the formation of a solid mixture of SiO_2 and Na_2O. A eutectic point as low as 800 C° is expected for the proper mixture between SiO_2 and Na_2O, although higher temperature is needed to melt real glass batches, which also contained a set of other components that are contributed by the set of natural raw materials. Nevertheless, those temperatures could be obtained in ancient furnaces, so that glass could be actually produced in the past with suitable (and available) natural raw materials.

Energies of the chemical bonds that are present in the glassy structure are not the same, they are within a wide interval, which is determined by the composition of the glass; therefore, glass does not show a specific melting point, but it softens through a range of temperatures, called the glass transition range. The heating diminishes/rises its viscosity on heating or cooling, respectively (Pollard and Heron 2015). The process of glass formation is presented in Figure 1.2.

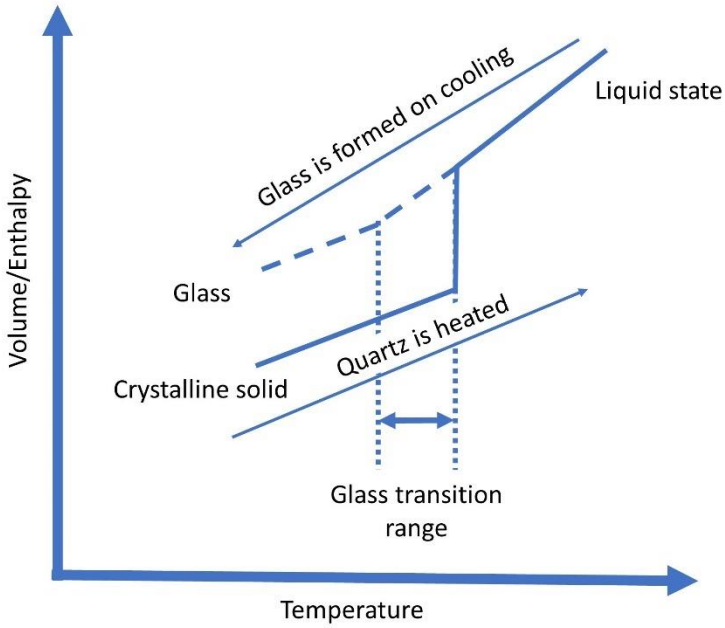

Figure 1.2. Graph of transformation of the crystalline solid (quartz) to the glass through melting (after Paul 1989).

Figure 1.2. shows that if the crystalline solid is formed from a melt, then the energy of the material suddenly decreases at the solidification point, reaching a lower value. On the other hand, this drop of energy is not observed in glass, and the final solid has higher enthalpy and volume in respect to the crystalline form. This transformation is represented by the dotted line in Figure 1.2. The transformation must be fast enough to prevent crystal growth (Rao 2002). At the glass transition temperature (the lower limit of glass transition temperature range) the system becomes rigid, with a viscosity above 10^{13} Poise (10^{12} Pa*s). The resulting solid shall then be annealed to release the internal stress (Debenedetti and Stillinger 2001; Pollard and Heron 2015).

Among the components of soda-lime-silica glasses, alkali-earth elements, and calcium in particular, play the pivotal role of making the network more resistant to water. Without the stabilising effect of calcium, which have higher bonding energy, the alkalis tend to be leached from the network, making the whole system unstable in the presence of water (Henderson 1985; Abd-Alla 2007; Henderson 2013; Angelini et al. 2019).

This set of functional components of glass – network formers, modifiers, and stabilisers – shall be in a strict quantitative proportion to yield a good-quality, durable glass. With an excess of network former, the melting temperature of the batch would be too high, and residues of crystalline material would remain in the final glass. An excess of stabiliser might make the fusion too hard to achieve, and final glass would be prone to devitrification, with portions of glass turning to a crystalline state (Vogel et al. 1989; Abd-Alla 2007; Pollard and Heron 2015). It is likely that the batch did not turned into glass in its entirety in the ancient furnaces. It is reasonable to assume that different phases and compositions of the product could be formed in different part of the heating system, but only “good” portions were collected for the subsequent glass-working, with the remaining portions included again in the production process, or discarded (Rehren 2000).

Other important components in glass are the so-called intermediates, that might substitute the main network ions in the glassy network, although they cannot perform their functions on their own (Zachariasen, 1932). One significant example is aluminium, which also stabilises the glass and improves its mechanical properties if added in moderate quantities (Vogel et al 1989; Le Losq et al 2019). Iron and lead are also known to influence stability and viscosity of glass.

All other significant components that were added to glass batch since the invention of glass until Hellenistic times (i.e., the entire time span covered in this study) contribute only to the final appearance of the glasses. Nevertheless, this is quite an important function in ancient glass-making, as glass was produced mainly for decorative and aesthetic purposes.

Elements and compounds that contribute colour are called colorants, and those that interfere with transparency giving opacity are called opacifiers (Pollard and Heron 2015; Rehren and Freestone 2015). Some agents, such as lead antimonate, make the glass both opaque and coloured (Lahlil et al. 2010).

In most of the cases, colorants are cations of transition metals, such as Fe, Cu, Co, Mn, the state of oxidation of which can be adjusted to obtain desired colour in the glass. The light absorption, and hence the colour, depends in fact on both the oxidation state and the place that such ions occupy in the glass network, which affects the number of oxygens that can be arranged in their coordination sphere.

For example, Co^{2+} can substitute silicon or sodium ions, having either tetrahedral or octahedral coordination with oxygen. This will change the colour of glass from deep blue to pink. On the other

hand, iron can be found in octahedral coordination both as Fe^{2+} and as Fe^{3+}, giving blue or yellow, respectively; The co-existence of Fe^{2+} and Fe^{3+} produces all the hues between yellow and blue, depending on their relative amount, which can be modified by varying the redox condition of the furnace or with proper raw materials added to the glass. Colorants and opacifiers used in glass making before 500 BCE are summarized in Table 1.1.

Colourants and opacifiers can be used together to achieve more shades within a specific hue, or to produce a different one, such as when a yellow opacifier is dispersed in a blue transparent glass to obtain a green, opaque glass.

Table 1.1. Main chromophores used in the Iron Age glass-making, colours they produce and the furnace conditions needed to achieve that colour (after Weyl 1999).

Colour	**Chromophore/opacifier**	**Furnace environment**
Yellow	Fe^{3+}	Oxidising
Yellow (opaque)	$Pb_2Sb_2O_7$	-
White (opaque)	$Ca_2Sb_2O_7/CaSb_2O_6$	-
Blue	Fe^{2+}	Reducing
Blue	Cu^{2+}	Oxidising
Blue	Co^{2+}	Reducing
Purple	Mn^{3+}	Reducing
Red (opaque)	Cu^{0}	Reducing
Black appearing	Fe^{2+}/Fe^{3+}-S^{2-}	Reducing

Glass chemistry is far more complex than presented in this section. Nevertheless, this short representation of the chemical relation between glass batch components aims to give a general framework for compositional studies on ancient glass and it is necessarily limited to some simple features. In addition to this general frame, ancient glass technology and selection of raw materials shall be considered for the interpretation of the compositional results.

1.2. Raw materials for ancient glass making and technologies for glass shaping.

It is hard to say precisely where and when first vitreous materials were produced. Many researchers agree that it was in the 3rd millennium BCE either in Egypt or Mesopotamia (Moorey 1999). Pliny the Elder has his own record on how the first glass was discovered. He even names the exact place in Phoenicia – the Belus river mouth – modern name Na'aman stream in Israel (Scott and Degryse 2014). He tells the story of merchants, who came on that shore and supported their cauldrons with "nitre" chunks. When they started the fire, they noticed flows of liquid that was, in

fact, first glass (Pliny 36:65). His words have very small credibility, first of all because it is very hard to reach sufficient temperatures to fuse silica with "nitre" (probably natron) with the open fire, and then because natron was probably not the first fluxing agent used in in glass-making (Shortland and Tite (2000) and references therein).

The work presented here deals with more recent glasses, therefore the discussion can move to the technological aspects of the glass-making industry that developed by the end of the second millennium BCE, focussing on raw materials and their role in supporting us in "telling the story" of glass productions by detecting their "fingerprints" in the composition of the final glass.

The main component in the glass batch was silica, as no other network former was used in that period. Silica was introduced in the batch in the form of quartz sand, pebbles or pure vein chunks. Sand was probably the most used material, as it is suggested by the impurities found in glass composition (Henderson 1985; Aerts et al. 2003; Silvestri et al. 2008). The most common and at the same time important impurities in quartz sands are feldspars and iron bearing minerals. Both may have positive effect on the glass network, but they were most likely unintentional additions, although iron compounds could be intentionally added for colouring. It is well supported theory that a stabilising component – Ca, was also added unintentionally with fragments of shells (predominantly composed of calcium carbonate) that are abundant in beach sands (Brill 1999; Scott and Degryse 2014), although they also could be crushed and added separately. Another source of calcium carbonate could be limestone (Henderson et al. 2005) which can also be a component of sand from carbonate rocks. The most frequent impurity that can be present in limestone is magnesium carbonate from dolomitic limestones, that can also enter the glass batch with flux and/or sand.

If only major glass components are considered, the most relevant characteristic of ancient glasses produced before 500 BCE is the kind of fluxing agent. The fluxes available and known to the ancient craftsmen were either of plant or of mineral origin. Plant ash was probably the first flux used to make glass (Rehren and Freestone 2015), whereas mineral sources of alkali were used in the production of faience and Egyptian blue (Shortland et al. 2006).

For preparing the plant ash, halophytic (salt tolerant) plants were used. Such plants, that can be found across the Mediterranean, are those of the *Chenopodiaceae* family, such as *Salsola kali, S. turcmanica, S. rigida, S. soda, Anabasis articulata, Salicornia, Suaeda*.

Ashes obtained from these species are rich in sodium and potassium carbonates, with different ratios of the two, which enable the distinction between soda-rich and mixed alkali plant ashes. The former ones were used in production of the so-called High Magnesium Glass or HMG. The latter ones can have potassium content higher than that of sodium, and would produce Low Magnesium High potassium glasses (LMHK), though the nature of the flux in these glasses is still the subject of debate (Henderson 2013; Paynter and Jackson 2022). Unfortunately, the composition of the ash is variable even if plants of a same species are used; therefore, the glass composition does not strictly mirror the composition of the ash at the species level (Tite at al. 2006). Moreover, not all the components of plant ashes are incorporated in the glass network (Shugar and Rehren 2002).

Mineral sources of alkali were of evaporitic origin. The best-known open deposits that were exploited in the past are those of Wadi al-Natrun in Egypt. The crust of the evaporites, called natron, contains predominantly hydrated sodium carbonates, sulphates and sodium chloride. Mineralogical composition of those deposits is predominantly trona and natron, and to the lesser extent burkeite, thenardite, mirabilite and halite (Shortland et al. 2006; Angelini et al. 2019). Natron started to be

used as a flux for glass making probably in the beginning of 1st millennium BCE and, by the middle of that millennium, became the most popular flux in the Mediterranean glass production (Shortland et al. 2006; Dardeniz 2015). It is apparent that it was traded internationally (Saguì 2008; Reade et al. 2009). Glasses produced with mineral source of alkali is classified as Low Magnesium Glass group (LMG).

Most of the compositional varieties in Bronze and Iron Age glasses are distinguished through the kind of flux and through some minor sand impurities that leave their fingerprint in the final glass. (Gratuze and Janssens 2004; Brems and Degryse 2014; Rehren and Freestone 2015).

On the other hand, the most evident feature of a glass object is the colour. Most of the glasses of the Bronze and Iron Age were semi-translucent or opaque, and colours of such glasses were achieved with the addition of minor quantities of mineral-origin materials into the batch. These materials are listed in Table 1.1, and their origin may be traced through the composition of the glass.

Calcium antimonate (in the form of $CaSb_2O_6$ or $Ca_2Sb_2O_7$) gives the opaque-white appearance to the glass if a proper number of crystals is suspended in the glass matrix. It was probably produced by heating stibnite (antimony (III) oxide) and calcium carbonate, and then added as a powder to the molten glass (Lahlil 2010).

Lead antimonate ($Pb_2Sb_2O_7$) is widely known for its bright yellow colour and used to give the opaque effect to early glass. The compound was probably produced by sintering galena (or other lead-containing mineral or metallurgical product) and stibnite (lead and antimony sulphides, respectively). the early Egyptian technology was somewhat different form the later Roman one (Molina et al. 2014).

Bone ash was also suggested as a possible opacifier in some Iron Age glasses, but its occurrences need further study (Towle and Henderson 2004). Finally, it is important to note that visual opacification of glass could be reached also by a fine the dispersion of bubbles, or minute quartz grains in the glass.

Co^{2+} is a very strong chromophore. Some hundreds of ppm in glass is enough to turn it deep blue. Egyptian glassmakers probably used cobalt-bearing alums to obtain various colouring materials. It is difficult to say what kind of intermediate steps were employed for the raw material on its way to the glass batch, but the use of natron for a precipitation reaction with the alum was suggested (Rehren 2001; Shortland et al. 2006). Besides Egyptian alum, other sources of cobalt ores were also known since the Bronze Age (Towle et al. 2001; Costa et al. 2021).

Some amount of iron was entering the glass batch with the sand, and the natural greenish tinge of glass is due to the iron presence, which influences colour of almost any glass. Additional amount (probably in the form of oxide) could be added to give a more intense colour, up to a level that turns the glass “black” as all the visible portion of the electromagnetic spectrum is adsorbed. Moreover, intense green can develop as a mixture of the yellow hue given by Fe^{3+} and the blue one given Fe^{2+} ions. A careful control of the redox conditions in the furnace was needed to obtain a specific colour (Ceglia et al. 2014; 2015; Conte et al. 2018). Some sands naturally contain Fe in high quantities could be used to produce glass in ancient times (like HIMT glass (Bugoi et al. 2021) or other heavily coloured glasses (Cagno et al. 2014; Conte et al. 2016)) or by the addition of high-Fe metallurgical products (Panighello et al. 2012; Giachet et al. 2019).

Another element that was used to produce black-appearing glass was manganese (Polikreti et al. 2011), although its use for black glass was not very common in Iron Age and the element was

more popular as a purple colourant in the form of dissolved Mn^{3+} (Sayre 1964; Reade et al. 2009; Möncke et al. 2014).

Cu^{2+} was responsible for many shades (almost always together with iron) of blue and green glass, and was one of the most important colouring agents in ancient glass-making. Same as for iron, the coordination number of the ion determines the colour of the glass and was regulated through the redox conditions of the furnace (Möncke et al. 2014; Rehren and Freestone 2015). In some specific cases, bronze scrapings were suggested as the raw material for copper, testified by the presence of tin in the glass (Costa et al. 2019). Elemental copper microcrystals were used for turning glass opaque red (Bandiera et al. 2020, and references therein).

Glass making may entail the use of a preliminary treatment of the silica with the flux, to obtain a poorly melt sodium silicate frit, which might be coloured if colourants are also added. The frit was used both for colouring and for facilitated the melting process (Wang et al. 2022). Finally, after the glass melt is prepared, it could be shaped into an object. For the times discussed here, glass was employed for jewellery and small luxury vessels. Bronze and Iron Age artisans were able to prepare polychrome objects from differently coloured glasses (Rehren and Pusch 2005; Venclová et al. 2011; Blomme et al. 2017).

Beads could be produced in small batches using moulds, or winding glass around a metal or ceramic rod. The apertures could be those left by the rod after the bead is formed or could be pierced with special tools while the glass was still hot. Decorative elements could be also tooled or shaped on the surface, making plicate ornaments or other reliefs made with attaching more glass, pressing or pinching etc.

The polychrome decorations on beads or other objects included droplets of glass on the surface of the “base”, lines, waves, spirals, rings of the very thin threads of glass on the surface. A very popular decoration for beads was in the form of eyes. Each eye was obtained by dropping of small portions of glass on the base surface in a sequence to form a stratified polychrome eye (Eisen 1916; Beck 1928; Harden 1968; Spague and Bowers 1985; Hughes-Brock 1999; Bellintani 2011; Koch 2011; Karklins 2012).

Vessel makers developed several techniques of forming. Glass blowing was not known at that time, that is why all the vessels needed some kind of support and glass was shaped around or within it. One of the most popular techniques was core forming. In that case the core (probably made of clay and dung) was attached to a rod that would allow to either dip it into the melt (Jones 1995) or, more likely, wound soft glass stripes around this core, so that each stripe can attach to the others, forming the vessel. Open vessels, such as bowls, could be made on a mould that performed the same function of the core when the glass was poured on it (Moorrey 1999).

It can be seen now that glass industry, though being relatively young by the Iron age, was already quite developed, and that rudimentary technical knowledge on raw materials and glass working allowed glass artisans to make objects that were highly appreciated by ancient people.

1.3. Glass production and trade organisation.

In this section, the ancient glass industry will be described focussing on the time period from the beginning to the middle of the first millennium BCE. The overview will be necessarily synthetic and will touch briefly other time periods.

The interest to archaeometric studies on glass of this period has increased considerably in the last 20 years, but archaeological studies of such glasses have a long-lasting history (for a more comprehensive presentation see Eisen 1916; Harden 1968; Haevernick et al. 1987; Brill 1999; Koch 2011; Henderson 2013; Freestone et al. 2009; Rehren and Freestone 2015).

The Late Bronze Age (second half of 2nd millennium BCE) is known for the spreading of glass technology and for the vast trade of raw glass documented, as an example, by the Uluburun shipwreck (Jackson and Nicholson 2010) or by the abundancy of finds – such as beads - that were registered in many places (Taniichi 1992). The site of Frattesina (Veneto, Italy) features evidence of the earliest glass production in the continental Europe (Towle et al. 2001). Regarding Mycenaean glass, it is considered to be imported from Egypt (Henderson 2013; Lankton et al 2022), but has been probably worked there (Nikita and Henderson 2006).

Similarly to the glass of the Bronze Age, most of the Mediterranean and European glass of the beginning of Iron Age was probably produced in Mesopotamia, Egypt and the Levant (Henderson 2013). In Greece, glass technology reappeared in the beginning of Archaic period (Oikonomou and Triantafyllidis 2018). In the first half of the 1st millennium BCE, glass was a valued product that was used in jewellery, together with precious metal, amber, semiprecious and precious stones, and it was common among offerings in Athenian temples (Stern 1999; 2007).

The production of glass objects was carried out in two phases. The first was glass melting from raw materials, also called primary glass-making, which included colouring and opacification, if needed. Then there was the production of finished objects (beads or vessels) starting from raw glass, also called secondary glass-working.

These phases required different skills and equipment (such as furnaces and tools) and were separated in time and space in many cases. Figure 1.3 represents this division for Roman times and highlight possible use of same raw materials for objects that were actually produced in different places.

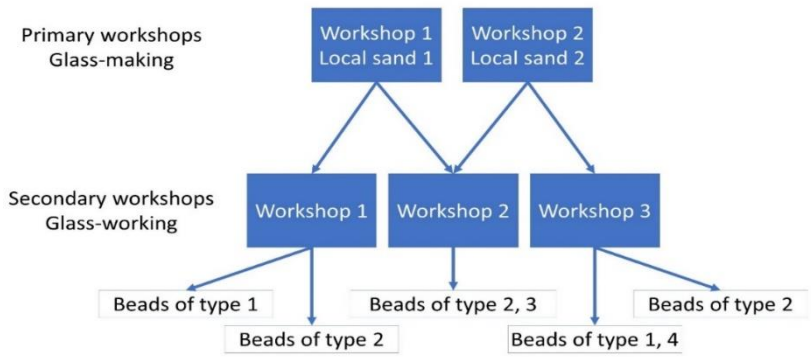

Figure 1.3. Model of Roman glass industry (after Rehren and Freestone 2015).

Each secondary workshop could specialise in production of specific objects (in Figure 1.3 they are different types of beads). This system was well established in Roman times, but its basic elements were existing from the Bronze Age (Scott and Degryse 2014). As an example, no evidence has been found yet of primary glass-making in Classical Greece, but archaeological remains documented few

secondary workshops (Stern 1999; O'Hea 2005). On the other hand, the rather exceptional site of Yahorlyk (on the north shore of the Black Sea) revealed evidence of both local glass production and imported glass-working (Kolesnychenko and Yatsuk 2021). This evidence may complicate the theoretical model for glass production and trading, but it does not change its essence.

Regarding textual evidence, glass is mentioned in many written sources, although these texts usually completely lack in the technological aspects. Probably the most famous examples for Mediterranean glass are Mesopotamian cuneiform tablets from the 7th century BCE (Oppenheim 1973) and Natural History by Pliny the Elder from the 1st century CE (Pliny, 36). These texts, especially the first one, give a very dim idea about how the glass in Iron Age was produced. Regarding the Pliny's testimony, he was writing about the industry contemporary for him that, by the end of the millennium, was significantly more advanced that the one in Bronze and Iron Age.

The most reliable sources of technological information presently available are the archaeometric studies and outcomes from experimental archaeology. The former ones revealed a slow transition from plant ash towards the use of mineral sources of alkali as a fluxing agent that occurred in the beginning of the first half of the first millennium BCE. Natron from Wadi al-Natrun started to be used in Egypt from the 10th century BCE and became the most popular flux in the Near East by the 8th century BCE (Henderson 2013). For the areas east of the Euphrates, a change in the flux was not apparent, as the composition of archaeological glass informs us that plant ash remained the most popular flux in Mesopotamia and central Asia in that period (Shortland et al. 2006).

In the first half of the 1st millennium BCE, glass was used for various purposes, mainly as a decoration, in the form of beads and pendants or plaques for inlays in wood (furniture), ivory and metals (swords) (Reade et al. 2009b). Beside this, it was used to produce small vessels for luxury products such a perfumes and balms (Panighello et al 2012). Levant was one of the most important areas for glass production (Harden 1968; Panighello et al 2012; Blomme et al. 2016). Compositionally similar glasses associated with Levantine production in the Mediterranean were found as far as France (Reade et al. 2009b). Some signs of glass production were found in modern Turkey (before the 7th century BCE) at Kaman-Kalehoyuk site. Glasses analysed from there are, actually, comparable with some Italian finds (Henderson 2018). Among Greek sites, glass working was attested at Rhodes, and the island is quite often suggested as the place of production of the so-called Mediterranean group 1 vessels glass, which was a popular choice for contain valuable liquids across the whole Mediterranean (Panighello et al. 2012; Oikonomou and Triantafyllidis 2018).

By the end of 5th century BCE glass, and beads in particular, gradually became quite ubiquitous in Mediterranean and beyond. Both glass objects and raw glass were transported along important trade routes, and various shapes and combinations of colours appeared in the Iberian peninsula (González-Ruibal 2004; Rubert and Alonso 2011; Costa et al. 2021), in North Africa (Harden and Tatton-Brown 1981; Docter and Sonneveld 2009; Eremin et al. 2012), in the Celtic realm (Cosyns et al. 2003; Purowski et al. 2012), in the Balkans (Palavestra 1997) and in the European steppe (Kolesnychenko and Yatsuk 2021), usually attributed to Near Eastern primary glass-production.

It is therefore evident that glass production and trade in the first half of the 1st millennium BCE was a complex system, that involved different stages and people for production, working, distribution and, perhaps, recycling. Through trade, a major part of which was carried by Phoenician and Greek traders, glass reached many remote places of Mediterranean and other adjacent regions

of Europe, Asia and Africa, from modern Georgia (Shortland and Schroeder 2009) to Portugal (Costa et al. 2021).

1.4. Archaeometry of ancient glass: approaches and instruments.

Ancient glass has been studied by archaeologists and art historians for a long time, but scientific analyses with chemical and physical methods have developed later, in 20^{ies} - 30^{ies} of the 20th century. First works on the analyses of historic glasses were published in the Journal of the Society of Glass Technology after its establishment in 1917 (Henderson 2013).

It would be incorrect though, to assume that glass history researchers were not aware of technology of glass making before those times, as several documentary sources were available. The already mentioned Pliny, for example. But also, Theophilus, as his treatise *"De diversis artibus"* from the 12th century describes medieval glass technology (Freestone 1992), and Antonio Neri who wrote *"L'arte vetraria"* in the 17th century describing early modern glass industry (Cable 2001).

In the middle of 20th century, the journals "Journal of Glass Studies" of the Corning museum and "Archaeometry" start to be issued, soon becoming the publishing platforms for new archaeometric studies in the field of ancient glass technology. Modern knowledge on ancient glass technology is mainly based on the works of Turner (1954; 1956; 1959 etc), Sayre (Sayre and Smith 1961; Sayre 1964), Brill (Brill and Moll 1961; Brill 1963; Brill and Cahill 1988) and others, who built the framework of archaeological glass studies with newly available scientific methods. Their ideas and views are still reiterated in countless publications.

Chemical information about ancient glass is the bedrock upon which nearly all archaeometric studies are built. In case of glass, compositional analyses are pivotal to reach comprehensive conclusions on raw materials as outlined in section 1.2.

Depending on the kind and relative amounts of the main components of the glass and their impurities, some major compositional groups were established (Sayre and Smith 1961; Rehren 2000; Brems and Degryse 2014; Angelini et al. 2019).

The final idea about the glass batch "formula" is linked to the notion of homogeneity of the resulting glass, and of the probable intermediary steps that might have been undertaken by ancient craftspeople before and during the thermal process, which are much harder to trace through the glass final composition (Rehren 2000).

Interpretation of each component of the batch is hardly straightforward as well. In the section 1.1 it was clarified that glass is a complex mixture: it derives from the molten raw materials that do not re-arrange into a crystalline structure on cooling.

On one hand, we can assume that raw materials largely determine the elemental chemical composition of the glass, and different compositions in the final glass may arise from specific choices of raw materials. For example, calcium might enter the batch with shells, but also as a component of plant ash, or as a part of the plagioclase impurity in the quartz sand (Henderson 1985; Brems and Degryse 2014). On the other hand, potassium level can rise because of the fumes of the combustive materials in the furnace and other metals can be incorporated into the glass from the crucibles during the glass preparation (Balvanović and Šmit 2020). These processes can impede the reconstruction of the batch formula.

Composition of glass can be determined by multiple methods. As for many other materials, chemical information is usually obtained by applying spectroscopic techniques. Their mechanism of interaction with matter relies on the phenomenon that atoms of different elements (individually or as a compound) have a unique "response" to a different "stimulus", the latter being beams of atomic and subatomic particles, or electromagnetic energy.

Chemical composition of ancient glasses can be obtained, at least for some elements, with relatively simple and fast methods. If sampling for invasive analyses or even transportation of the object to the laboratory is not allowed, portable, non-invasive analytical instrumentation can be employed.

XRF is a versatile and very popular technique for investigating archaeological glass composition (Liritzis and Zacharias 2011; Frahm and Doonan 2013). The use of portable instruments, equipped with an X-ray tube and a solid-state detector, can be a good option as it is not detrimental for the integrity of the objects. p-XRF analyses can be done directly in the premises where the objects are kept, eliminating the process of sampling and all the risks and constraints that it entails (Yatsuk et al. 2022). XRF has limitations though, especially if implemented with portable devices. The accurate quantification of light elements is of extreme relevance for glass studies, and Na and Mg cannot be accurately determined using portable equipment, although the use of small vacuum chambers was suggested to overcome this limitation (Liu et al. 2012; Abe et al. 2018). Quantitative data can be obtained with previous calibration of the instruments if the planarity of the sample is acceptable. For those objects that can be analysed in the laboratory, a synchrotron source of X radiation might be used to enhance the accuracy of the determination, to improve the spatial resolution of the analyses and to broaden the number of elements that can be determined due to lower LODs (Janssens et al. 1996; Figueiredo 2012).

SEM is a powerful approach for magnified imaging and in the Variable Pressure (VP) mode it is suitable to scrutinise nearly any kind of archaeological material. When coupled to and energy- or to a wavelength-dispersive spectrometer, it offers broad opportunities for elemental analyses of ancient glass, from elemental mapping to spot or area analyses. Unfortunately, for quantitative data, it is necessary to expose a flat, polished and conductive surface, therefore there is the need to prepare a sample for the analysis. Semi-quantitative data can be obtained in the variable pressure mode on unprepared samples, although the quantification of light elements can be somewhat challenging (Silvestri and Marcante 2011; Babalola et al. 2018). Recently, transportable SEM-EDS equipment for *in-situ* analyses have been introduced in the market (Frahm 2014).

Electron Probe Micro Analysis (EPMA) is basically comparable to SEM-EDS systems, although this name refers to an equipment that has lower detection limits and better accuracy of measurement as it is normally equipped with a WDS detector. It is routinely used for quantitative analyses of major, minor and some trace elements (Towle and Henderson 2004; Gallo et al. 2014).

Another technique for elemental compositional analysis is SIMS, which allows the detection of a wide range of elements, including light ones, down to ppb level of concentration (Rutten et al. 2006; Janssens 2013). This technique is presently not so widespread in the field of ancient glass analysis.

Quantitative elemental analyses on ancient glasses meets numerous obstacles. Analytical procedures are normally invasive, i.e. a sample has to be detached from the archaeological object, due to the nature of the material under analyses; there is, in fact, the need for clean surfaces of

unaltered glass to be exposed to the analytical beam, and vacuum conditions are associated with most of the analytical techniques if a non-destructive approach (i.e. the sample is preserved) is pursued.

On the other hand, if destructive approaches are allowed, methods that enable a complete elemental quantification of the glass matrix in terms of major, minor and trace components are Inductively Coupled Plasma Optical Emission or Mass Spectrometry (Mirti et al. 2008, 2009; Schenk and Almiral 2012). Recently, this latter technique has been especially appreciated when coupled to Laser Ablation systems for micro-sampling, thus significantly reducing the traces of the analyses on the archaeological object, which is an important aspect in cultural heritage analyses.

Reaching high levels of accuracy is challenging using this method. Firstly, the ablation process is matrix-dependent, and settings shall be adapted to the material, although isobaric interference cannot be avoided for some elements. Then, because of the heterogeneity of the matrix, multiple spots/areas shall be considered, and data reduction is necessary. Moreover, adequate reference materials to be employed as multiple standards are recommended. There is a tendency for some elements to yield data of poorer quality when determined using this method. Despite these issues, in most of the cases the analyst can achieve high precision and accuracy down to trace elements levels (Dussubieux et al. 2009; Bertini et al. 2013; Tzankova and Mihaylov 2019).

For a complete characterisation of the glass, several complementary approaches can be combined to obtain more robust data and/or to make a deeper insight into the glass chemistry. The set of SEM-EDS, micro-XRF and LA-ICP-MS applied by Oikonomou and Triantafyllidis (2018) for the study of archaic glasses from Rhodes is a representative example. Sometimes, additional method is required to enhance the result of the major one, such as in the case of the use of concentrations obtained with SEM-EDS or other techniques to provide the internal standard values for LA-ICP-MS data quantification (Liu et al. 2008).

Another problem on the way to accurate analysis of glass is weathering. Alkalis tend to leach out off the glass surface, which becomes depleted in these elements (Gulmini et al. 2009; Pollard and Heron 2015). This makes it almost impossible to investigate the original elemental composition with surface-sensitive techniques such as SEM-EDS, EPMA, PIXE and SIMS. Many authors resort to cross sectioning of the samples (Quartieri and Arletti 2013; Maltoni et al. 2015), abrasion with a drill (Maltoni et al. 2015), ion sputtering for SIMS (Rutten et al. 2006) or, in case of LA-ICP-MS, pre-ablation of the surface layer to remove altered surface on the analytical spot (Smirniou et al. 2018).

Glass structure can be studied at different levels. Macro-level analysis is achieved with the naked eye or by simple optical systems, broadly used by archaeologists for getting an insight into techniques of the final forming of the object, to highlight the presence of larger inclusions or the interactions between multiple layers of the glass (such as for polychrome objects and/or complex-shaped ones). Extensive practical knowledge and experiments are needed for building some conclusions with this approach (Stern 1995; Moorey 1999).

There are then a few methods that can provide information about micro-structure of the matrix. Raman spectroscopy becomes increasingly popular among the methods chosen for chemical characterisation of ancient glasses. This non-invasive method can shed light onto the flux used, characterise crystal inclusions and suggest manufacturing temperature, although with rather poor precision (Colomban 2008; Won-in et al. 2011; Costa et al. 2019). Another technique that yields information about crystal phases within the glass matrix is XRD. Since glass by its nature is

amorphous, XRD gives qualitative results only for inclusions that were used as opacifiers. A non-invasive approach with micro-XRD is preferrable for archaeological glass (Drünert et al. 2018; Matin et al. 2019).

As already mentioned in section 1.1, glass is mainly coloured by transition metals that are coordinated with oxygen in a specific arrangement. This feature of the glass structure can be investigated by several methods. One of the fastest and simplest is FORS. Portable equipment, suitable for non-invasive *in situ* analysis provides information about diffusion in the UV, visible and near IR part of electromagnetic spectrum. By the pattern of the diffused light, it is possible to distinguish between, for example, Co^{2+} and Cu^{2+} coloured glasses, or suggest the combination of colouring agents (i.e. chemical species) that give the final colour to glass (Bacci and Picollo 1996; Bacci et al. 2007; Picollo et al. 2018; Aceto et al. 2020). Similarly, but with less straightforward approach, XANES or EPR Spectroscopy can be used to determine the oxidation state of transition metals and their position in the glass structure, particularly iron (Mirti et al. 1993; Ceglia et al. 2014, 2015).

To support the inferences that can be made on raw materials and technology of ancient glass through physical and chemical analyses there is the need of mock-ups prepared by replicating experiments (Shugar and Rehren 2002; Jackson et al. 2005; Lahlil et al. 2011). Experimental glasses are usually compared by different parameters, most important of which are composition and structure. Comparison sometimes includes such parameters as density, refractive index, and energy changes with temperature observed with calorimetry analysis (Qin et al. 2016).

Composition of glass can also be the key information for provenance studies, that, for archaeological glass, are completed with different degrees of success. Suggestions for specific artefact provenance are usually done by comparing the compositional features of one artefact with the ones of another specimen for which the provenance is known (from a glass-working site, for example). It is also possible to link the artefact to a specific provenance by recognising the signs of use of the specific raw materials that were selected from specific places. In case of glass provenance, the analyses are mostly focused to disclose the provenance of the silica component (Brems and Degryse 2014; Pollard and Heron 2015). A broad idea on provenance can be obtained by attributing glass to a certain compositional group, such as LMHK, HIMT, LMG, etc. (Angelini et al. 2019; Koleini et al. 2019). In order to narrow the information down to a specific production site, most of the studies resort nowadays to trace elements analyses and isotopic ratio analyses. There are, however, other markers of provenance among minor constituents, that has been used for decades, and continue to be used, to distinguish between groups of samples of different provenance. One of the most popular ways is to check correlation and grouping of titanium and zirconium concentrations. These elements entered the glass batch exclusively with the impurities of the silica component. Their absolute and relative amount depends on the parental rock and sediment deposition mechanisms, which is then mirrored by sands and by glasses that were produced from those sands. This feature of the glasses helps to distinguish between glasses of different provenance even if they belong to the same compositional group, i.e. their batch was prepared with the same formula (Aerts et al. 2003; Polikreti et al. 2011; Brems and Degryse 2014).

Trace elements analyses are more reliable proxies for glass provenance. In this work the term “trace element” is used for constituents that are present in concentrations below 100 ppm (Morrison 1979). Various configurations of ICP and SIMS equipment are used to determine concentrations well

below this figure. Same as with Ti and Zr, what matters is both amount and proportions. Usually, binary plots of element 1 vs element 2 concentrations are built to highlight correlations or groupings (Freestone et al. 2002; Šmit et al. 2005 Conte et al. 2016; Oikonomou et al. 2023). In some cases, a sum, or a ratio of two elements, can be used against other two elements. As an example, this was done to discriminate Mesopotamian glass from Egyptian one using 1000 Zr/Ti value plotted against Cr/La. Such discrimination method is widely used (Shortland et al. 2007; Polikreti et al. 2011; Oikonomou et al. 2020; Lankton et al. 2022).

Multivariate analysis of compositional data helps to highlight trends and groups of samples on compositional bases (Genga et al. 2008; Baxter 2015). PCA is probably the most popular multivariate approach, as it supports provenance attribution and helps in visualising groups of glass produced with the same type of raw materials if major elements are considered (Schibille et al. 2011, 2017; Phelps et al. 2015). Cluster analysis (among which the hierarchical approach is the most popular) is also a valuable tool to track relations within the data set (Aerts et al. 1999). This method can be applied even on strictly qualitative data such as Raman ones (Colomban and Tournié 2007).

Another tool to graphically represent compositional data are the linear plots of REE. REE are usually included in the element list for glass analyses and these plots represent the REE pattern for each sample. The REE values shall be normalised against some standard value, the most common of which are chondrites and the upper continental crust. REE patterns support conclusions on provenance, as samples having different patterns are presumed to have different origin because the change in the REE content of silica reflects the change of geographical setting. In this kind of studies, it is important to pay some attention to the anomalies of Eu and Ce. These elements, unlike other REE, may change their oxidation state depending on the redox conditions of the environment in which their compounds are formed (namely, magma or sea water). Therefore, the ratio between Eu, Ce and their respective neighbouring elements can give the clues about the source of raw materials used for glass production (sand or shell). The total ratio between the light REE and heavy REE is also used for discrimination (Trail et al. 2012; Shields and Stille 1998, 2001; Degryse and Shortland 2009; Ganio et al. 2012).

Stable and radiogenic isotopic ratio determination is one of the most reliable methods of provenance attribution of archaeological glasses. Until recent times, isotopic studies were destructive and required some portion of the material to be sacrificed (Brill 1999; Freestone et al. 2003; Degryse and Schneider 2008; Degryse et al. 2010; Ganio et al. 2012; Brems et al. 2013; Gallo et al. 2015; Blomme et al. 2017; Henderson et al. 2020), but nowadays laser ablation systems coupled to a multi collector ICP equipment reduce sampling to micro-portions. TIMS and SIMS are also used (Janssens 2013; Chang et al. 2015; Knaf et al. 2017).

Isotopes determination is focused mainly on Sr and Nd, although Pb and O can be used as well (Brill 1999). Sr mostly reflects the lime component of glass, as it is known for substituting Ca atoms (Degryse and Schneider 2008; Janssens 2013). It can derive from the stabiliser (shells, limestone), from the network former (feldspars, heavy fraction minerals) or from the plant ash flux, making the interpretation of the results somewhat difficult and debatable (Brems and Degryse 2014; Pollard and Heron 2015).

On the other hand, Nd is associated almost exclusively with the network former (Degryse and Schneider 2008). Usually, combined Sr and Nd isotopic data are the proxies that allow to suggest

Egyptian, Mesopotamian, or mixed provenance for Eastern Mediterranean glass, including Iron Age glass (Janssens 2013; Blomme et al. 2017).

1.5. Previous archaeometric studies of glass from the Iron Age contexts in Italy.

This section gathers in a chronological order the archaeometric literature for glasses found in archaeological contexts that are chronologically and geographically close to those included in the present study. Iron Age glass is even now considered an understudied material in archaeometry (Arletti et al. 2011; Oikonomou and Triantafyllidis 2018; Koch 2021), but the finds from Italy have attracted the attention of the scientists for quite a long time, resulting in several publications. The way these authors built their methodologies may be different from the other studies, which brings us to the problem of compatibility of the data, but it is indeed possible to put the knowledge obtained by analysing glass from Central Italy into a common framework.

The first attempt of chemical study of "Etruscan glass" was carried out by Brill (1999) within his extensive work in Corning Museum. Four objects were analysed: a bracelet of dark green opaque glass, a blue oinochoe with "prunes" (probably one of the *Stachelflaschen*), a colourless bowl from the Bernardini tomb (Palestrina) and a dark blue bowl from the San Giovenale tomb (Viterbo). While the bowl from the Bernardini tomb appeared to be HMG glass, the rest of the artefacts were probably made with natron. The bracelet probably owes its colour to iron and opacity to lead. The oinochoe was coloured by copper, unlike the bowl from the San Giovenale tomb, that was coloured by cobalt. The minor and trace elements values are not very precise according to modern standards, and the analytical method used for the determination is unclear (atomic absorption or inductively coupled plasma mass or optical emission spectroscopy were used for different samples on the span of more than 30 years). In any case, it was possible to assign the objects to a specific compositional group.

Next is the comparative study of LBA glass from Frattesina (mentioned in section 1.3) and the Iron Age glass from the same area (namely, the Po valley). Electron microprobe analysis was used to identify the content of 22 elements in the samples. The necropolises of Adria (Canal Bianco, Ca' Garzoni, and Ca' Cima) are mostly dated to classic and later periods (Robino 2016) that are not in the scope of this research, but some 12 samples from archaic and late orientalising periods were represented, including two oinochoes with spikes from collections in England (Towle et al. 2001).

The above-mentioned oinochoes do not have evident similarity with the Late Bronze Age glasses from Frattesina. They were probably made with natron or soda rich-plant ash glass. Both are blue and contain some copper, which would explain the colour, but the darker one has additional cobalt in the matrix. It is noted that glasses from late orientalising and archaic periods have more calcium that the Bronze Age and the later Classical and Hellenistic ones, and they belong to LMG group (Towle et al. 2001). The authors did not find the evidence of continuity between Frattesina and Adria glasses, and they did not rise the question of provenance, therefore more data on trace elements or isotopic ratios are needed to discuss this matter.

One of the most important works relevant for the present research was carried out by Towle and Henderson (2004). Notwithstanding the paper is entitled "The glass bead game" it includes objects other than beads: 18 objects from UK museums, among which Stachelflaschen and Glasbügelfibeln (both types of objects are mentioned in Chapter 2), were analysed using EPMA. The

results were confirmed for 3 samples by SEM-EDS analyses. Both plant ash and natron glasses were identified, with the prevailing occurrence of the latter ones. The data obtained from blue ring beads featured undetectable concentration of sodium, and extremely high potassium concentrations (up to 17.7%), together with elevated phosphorus and calcium contents, which differentiated them from the glasses from Frattesina (Towle and Henderson 2004). The authors included in their paper the oinochoe (*Stachelflaschen)* from the already discussed study of Frattesina and Adria glasses (Towle et al. 2001) and they concluded that, given the evident compositional difference, it would be possible that some of the beads were made locally (Towle and Henderson 2004).

Another study performed with a different analytical approach was published by Arletti and colleagues in 2008. They focused on materials dated from 7th to 4th century BCE. A non-invasive procedure was comprised with synchrotron micro-XRF, XANES, and XRD. 5 objects were studied: 3 vessels and 2 beads. The vessels represented typical Mediterranean group 1 shapes (Harden 1968). Due to the nature of the research question (i.e. an insight into colour and opacification), no quantitative data on the glass matrix were produced. Instead, attention was paid to the detection of the different oxidation states of some chromophores (mainly iron ions). Moreover, crystalline phases were determined by micro-XRD, to disclose the nature of the opacifying agents and calcium antimonate was detected as the main opacifier (Arletti et al. 2008). Authors suggested different manufacturing sites for the objects, but this conclusion needs the support of more data.

The analyses conducted by Cecere and colleagues on variously coloured glass finds from various sites of southern Etruria and a necklace from the Castellani collection are related to objects that are similar to those considered in this study. In addition, “some sands” were analysed together with vitreous samples with SEM-EDS (variable pressure mode), which did not allow precise and accurate quantification (Cecere et al. 2008). As a consequence, no robust conclusion was possible based on the compositional data. Authors addressed the important, and yet unresolved, question of terminology: the confusion that the term “glass paste” brings when different kinds of vitreous materials are discussed.

In another study of Arletti et al. (2010), 69 samples of differently coloured glass from 16 vessels and the same number of beads and spindle whorls from 6th-4th centuries BCE were analysed by EMPA. All the objects included in that study were excavated from the Bologna (Certosa and Giardini Margarita) and from the slightly recent Spina (Vale Trebba and Valle Pega) necropolises. The analyses were carried out on samples extracted from the archaeological objects and the concentration of 18 elements was determined with WDS. Results revealed that the group of samples was quite homogeneous from a compositional point of view, and the objects were all made with the same soda-lime glass, regardless their shape and function. Authors suggest a same production site for almost all the samples (Arletti et al. 2010).

Polla et al. (2010) investigated Villanovan period glasses from Bologna. 34 beads were selected to constitute a typologically representative set of samples. Different colours of glass were analysed: blue, amber, yellow, red, black and white. Compositional analyses were carried out by means of SEM-EDS and EPMA. The results show high variability of the main elements concentration, and some glasses could not be associated with any of the assessed glass type groups. Moreover, no continuity with Late Bronze Age glasses emerged, with a clear distinction of colouring agents (Polla et al. 2010).

15 turquoise blue and dark green beads found in Bologna (Trade Fair area) were analysed by means of EPMA, SEM-EDS, and ICP-MS (Arletti et al. 2011a) and the major elements showed different

compositional groups. Special attention was given to the cobalt source. Based on the trace elements content and their ratios, an "Eastern site" apart Egypt was proposed as a possible manufacturing site, but trace elements diagrams showed some heterogeneity of the set that would suggest different sources of the raw materials (Arletti et al. 2011a).

The results published for 12 vessels of Mediterranean group 2 is interesting because their chemical composition was similar to what is known for Mediterranean group 1, even though group 2 vessels were produced in 4th century BCE. Authors suggested a same provenance for these large groups of vessels even though EPMA and XRD analyses did not provide any information on trace elements content (Arletti et al. 2011b).

Some 23 objects from Verucchio were analysed by Angelini et al. (2015) with SEM-EDS, EPMA and XRD. High variability in their chemical composition and texture was noticed, and the role of transition metals in glass was discussed in this work. Based on "iron slags" presence in the glass matrix, the authors suggested that some of those objects were produced locally, although this conclusion is highly debatable.

A PhD thesis by Giulia Olmeda includes the study of 42 beads from the Piovego cemetery (Veneto) dated to the 6th to 4th century BCE. Raman, EPMA, SEM-EDS, XRD were used. These beads seem to be not so different from the ones found in Spina, Adria and Bagnolo de San Vito (Olmeda et al. 2015). They feature blue, yellow, "black" and white glass. The author argues that most of the samples belong to natron glasses and discusses the important questions of opacifiers and colorants that were present in the matrix, although no question on provenance was risen.

Some glasses relevant to this work were discussed in the study of the glass objects found in Southern Italy and Bologna by Conte and colleagues. 11 glass samples from the North of Italy (Bologna) were analysed by means of EPMA and ICP-MS (with Sr and Nd isotopic ratio determination for only Bologna glasses) and compared with the ones from the Cumae-Pozzuoli area (Southern Italy) and Chotin (Slovakia). The Italian glasses were identified as natron glasses. The research led to an interesting conclusion for black glasses, which featured FeO at 12 wt% as an average. To produce these glasses, the authors suggested the use of some specially selected "dark sands", although this seems less likely than an intentional addition of a chemically purer source of iron. The authors proposed an Egyptian origin for the Italian samples, based on composition and isotopic ratios. This statement also fits the theory that first natron glass production started there: as these samples are from the 9th to 5th century BCE, this set may include one of the earliest natron glasses found outside Egypt. It was clear, though, that different sands were used for the Bologna and Pozzuoli glasses, suggesting the existence of more than one centre of production. Other glasses from Southern Italy demonstrated different origin. They were divided on the compositional and chronological basis, which allowed to trace the change of glass recipes through time. Various technological and provenance inferences were made (Conte et al. 2016, 2018, 2019).

By reviewing the literature, it is evident that the history of archaeometric investigation of Etruscan glasses has some 25 years, and that glass from Central Italy was seldom in the focus of archaeological science. Among the tendencies, we can highlight the extensive use of EPMA, which is one of highly suitable and popular techniques for glass investigations, whereas XRF was used in only one study (Arletti el al. 2008). Most of the studies described in this section were using invasive approaches, and they were mainly focused on samples found in the northern Etruria, leaving southern part almost completely unstudied. Maybe the lack of archaeometric studies on the Early

Iron Age is related to the smaller number of finds from that period in general. Nevertheless, data from some of the papers mentioned in this section will be considered later in this thesis to discuss the data of the current study.

Conclusion. Glass owes its properties to its amorphous nature and is indeed a fascinating material. It takes a special place among ancient materials and requires a unique set of knowledge and skills in order to be produced and shaped. Ancient artisans proved to have a very practical notion of chemistry that allowed them to produce ever larger quantities and varieties of glass objects up to industrial scale in Roman times (Scott and Degryse 2014). The larger scale production started in the middle of the 2nd millennium BCE (Henderson 2013) and featured an already established set of raw materials: silica sources, fluxes, colourants and opacifiers. Mesopotamia, the Levant and Egypt were the lands where most of the glass was produced. The first half of the first millennium BCE brought a significant shift in fluxing source towards the natron. In this period, glass production and glass working started to be performed separately in space and time. The Greek and Phoenician trade networks allowed glass circulation on a wide area of the Mediterranean and beyond.

As for archaeological science, the last decade did not bring substantial innovation in the approaches for ancient glass studies. However, portable equipment is largely improving its performance, and new configurations appear for conventional techniques. Most studies on ancient glass use complementary techniques that allow comprehensive characterisation of the artefacts. Much of the attention is paid to the archaeological context of the finds. For archaeometry in general, there is the tendency to avoid invasive approaches and use the instruments, at least partially, on-site. Glass composition, along with its structure, is the essence of technology studies. It is a good practice to reconcile all the “pieces of the puzzle” from the glass matrix to the archaeological context. Provenance studies remain difficult since there are no straightforward proxies for precise attribution, with only rare exceptions. Nevertheless, provenance attribution to broad areas such as Egypt or Mesopotamia is considered a successful outcome of the archaeometric investigation on a specific set of samples.

CHAPTER 2. SOUTH ETRURIA AND LATIUM IN THE FIRST HALF OF FIRST MILLENNIUM BCE AND THE ARCHAEOLOGICAL CONTEXTS OF THE ANALYSED OBJECTS.

2.1. Trade development in the Mediterranean and the West-central Italy.

The famous French historian Fernand Braudel used to say that the sea can be a great link or a great divider (Braudel 1995), but as soon as people mastered navigation they turned the Mediterranean region into a unity of exchange of material items, knowledge and skills. In this section, the long-lasting system of links among some of the Mediterranean peoples and the outer regions, is outlined, keeping the focus on tendencies in Central Italy.

The Mediterranean basin in the first half of the 1st millennium BCE was one of the most developed and steadily growing macro-regions of the world, especially in its eastern part (Beaujard 2010). Two sailing peoples – the Greeks and the Phoenicians, developed complex trading networks that allowed uninterrupted flow of goods throughout this large area, with special interests in Italy and Etruria, and they traded the vast majority of the Mediterranean glass (Rehren and Freestone 2015).

To describe the Mediterranean in the first centuries of the Iron Age, one must bear in mind the series of events that happened mostly in the Eastern region of the sea and its surrounding areas and that are often called "the Bronze Age Collapse". Most scholars attribute this collapse to a combination of factors, such as an extensive disruption of the old trade routes, the decline of the old centres, the significant migrations of people and some climate changes. Disagreement persists on pinpointing the influence of each factor, and it is still difficult to building a reliable cause-consequence system of this "perfect storm", as data are scarce (Knapp and Van Dommelen 2015). The adoption of iron, which started the Iron Age in the 12th-11th century BCE in the Near East, was probably caused by that process (Erb-Satullo 2019). By the start of the first millennium BCE, iron was used by many peoples across the Eastern Mediterranean, and iron tools started to appear in the west, including Central Italy (Sestieri 1992).

In the first centuries of the 1st millennium BCE, a re-establishment of long-distance trade network occurred, mainly under Phoenician and Greek influence (Collis 2003). Both these powers were founding colonies in the west (Graham 2001). According to Andrew and Susan Sherratt (1993), this new system of trade had very characteristic features that included the leading role of private enterprises instead of the state trade, the increased role of city states that were flourishing by the middle of first Millennium all over the Mediterranean, the somewhat changed nature of slavery, the beginning of coinage, the development of new government structures and some changes in warfare.

The Phoenicians were dominating in the Mediterranean trade in the early first millennium BCE thanks to their innovations in ship construction and wide connections (Zalloua et al. 2008). Their cities skilfully turned the decline of the great powers, such as Hittite and Mycenaean states and the weakening of Egypt, to their own profit (McKenney 1975) as their geographical position was favourable for commerce with both the Near East and the East Mediterranean. Even though the written tradition is saying otherwise, the Phoenician merchants were not so prone to establish

permanent colonies until probably the 9th century BCE in Cyprus, and were soon outnumbered by the Greeks (Collis 2003, Nijboer 2008), to whom they appeared as skilful craftsmen and sailors (Hütwohl 2020; López-Ruiz 2021). On the other hand, Carthage had its own colonies in the Western Mediterranean: along the shores of Africa and Iberian Peninsula and settlements in Sardinia and Sicily (Carpenter 1958; Pilkington 2021).

In the first centuries of the 1st millennium BCE, The Phoenicians were actively trading with Greeks, and one of the earliest traded Phoenician goods that happened to be found in Greek burials was faience beads. Egyptian faience is generally considered to be traded more by Phoenicians than Greeks throughout the time-span considered here (Collis 2003).

The Phoenician cities had complicated relations and armed conflicts with the Assyrian empire, that ended with the complete incorporation of the first into the imperial structure (Oded 1974). By the end of the discussed period, they have fallen under the rule of the Achaemenid empire, where they constituted the most of these empires' navy force in the Mediterranean (Kelly 1992).

Money, i.e. one of the most important instruments of modern economy, appeared centuries before in the form of standardised pieces of metal, but coinage that started in Lydia in the 7th century BCE prevailed as both concept and technology in the later centuries (Balmuth 1975), reaching the west through Punic people in the 5th century (Delile et al. 2019).

During the Third Intermediate Period (roughly coincided with the Iron Age) Egypt was not in the best condition, having suffered from internal conflicts and external invasions (Taylor 2000) and lost significantly its influence in the Levant, as evident from the historical and archaeological record. This decline happened gradually in the course of few centuries. Phoenician traders played a significant role in the relations with Egypt (Evian 2011). Even in the 7th century BCE the Egyptians could possibly trade with Palestine (which is the closest geographically region) through the Levantine middlemen, probably Phoenicians (Maeir 2002).

The Early Iron Age period is often called the Dark Age of Greece. This is to signify a much less "exposed" period between the collapse of Mycenaean civilisation and Archaic Greece (Fagan 1996). After the period of Dark Ages, first Greek poleis appeared on a map in the 8th century BCE. The process of Greek colonisation of the Mediterranean and Black seas also started in that time (Broodbank 2013). It was a complex process that was stimulated by many factors, such as overpopulation, need for resources and land, trade establishment and political conflicts. With years the network included hundreds of settlements all around the Mediterranean area and the Black sea (White 1961; Graham 1999; Gagarin 2010). A well-accepted theory describes the foundation of a permanent colony as a quite stretched-in-time process. After the first contacts, a semi-permanent *emporion* was established, followed by turning it into an *apoikia* that was a permanent colony, a polis on its own (Tsetskhladze 1988; Roberts 2007).

The colony usually kept tight connections with Greece, as testified by the material culture. In Pithekoussai, imported Greek pottery from the 8th and 7th century, including Euboean (believed mother region) was quite abundant (Buchner 1966). Interestingly, sets of fibulae from the graves of presumably Greek settlers in Pithekoussai are identical to the ones found in Etruria and Latium, and do not have connections with the Greek ones (Hodos 1999). While intermarriage and mixing of population between the colonists and the native peoples was not evident for the early colonies, it is possible to assume such practice at Cumae. On the contrary, imported Etruscan and Italic fibulae

found in Sicily suggested an active trade that was using connections of local peoples rather than Greek newcomers (Hodos 1999).

The Greeks had intense trade with Egypt and even had a colony there in Naukratis (Villing and Schlotzhauer 2006). Later in time, the Greeks increased their presence in Southern Italy and Sicily. Greek trading posts on Etruscan shoreline were likely in the ports of Pyrgi and Gravisca, as suggested by the large quantity Greek pottery that was found there (Graham 1999; D'Ercole 2017).

Closer to the middle of the millennium, we can observe a differentiation process in North-West Mediterranean, that had implications on the international trade. For example, Etruscan imports in the 6th century BCE are very unevenly distributed with "sharp" borders, which might suggest some changes in the political relations (Briggs 2003).

In the context of this wide framework, it is appropriate to characterise the role of Central Italian population in the Mediterranean trade. It is crucial for this study to examine their international trade, especially the one with Phoenicians and Greeks. Celtic areas are also taken into consideration.

It is a widely accepted point of view that the Etruscans were powerful and skilled in the sea (Pomey 2017). Titus Livy calls them even more powerful in the sea than on land (Livy 1:23, 1912). However, it is hard to say how strong their power was before the 9th century BCE. Archaeological evidence of (undoubtedly) Etruscan ships is somewhat scarce, and shipwrecks dated to the 8th century or earlier have not been found so far. Most of what is known about Etruscan ships is based on iconography analysis (Turfa and Steinmayer 2001; Castello and Mandolesi 2009). The most famous shipwreck of Etruscan trade ship is probably Grand Ribaud F and it was attributed to the end of the 6th century BCE. It was a fairly large ship with 700 homogeneous amphorae on board (probably produced in Cerveteri) with a small addition of Greek pottery that allowed dating (Drap and Long 2001). It is a popular opinion that Etruscans had extensive maritime trade in Mediterranean Gaul at least before the foundation of Massalia (Graham 1999). On the other hand, there were not many finds of Etruscan pottery in Catalonia, and all of them were dated between the 7th to 5th century BCE, with a complete absence in the second half of the 5th century BCE layers onwards (Sanmarti et al. 2006). Etruscan ware was found even in the Black Sea Greek colonies (Graham 1999; Buiskich and Naso 2022).

Greeks and Phoenicians were likely to be very interested in trading with the people of the Italian peninsula, to whom they could bring rare and hence valuable oriental products (including glass and faience) and get natural resources (especially metals) and finished objects as the exchange (Sherratt and Sherratt 1993). The state of Urartu in Asia Minor, like the Etruscans, is famous for its bronze industry. Trade of bronze cauldrons reached Etruria as well as other regions of Mediterranean. Some stylistic details suggest that Urartian bronzes were copied by Greek and, perhaps, by the Etruscan artisans. It was proposed that seaborne trade was conducted by Greek merchants that were collecting these items in Al-Mina (Maxwell-Hyslop 1956; Pallottino 1958). Assyrian imports were probably also getting to Etruria on Greek or Phoenician ships. Trade with Carthage was intense since the Orientalizing period, as proved by pottery finds (Naso 2017c). Etruscan *bucchero* was famous overseas starting from the 7th century BCE, and the same goes for Etrusco-Corinthian ware that was found in Carthage. An interesting phenomenon of ancient trade was hospitality tokens and trademarks, that were evidence of international connections (D'Ercole 2017). Some Etruscan pots were found in South Mediterranean Greek colonies, including Naukratis in Egypt, that proves the link (might be indirect) between Etruria and Egypt (Naso 2006).

The Etruscans had a lively trade with lands across the Alps. Sometimes, especially for the Orientalizing period, it is interpreted by scholars as a trade between elites, implying that the commodities exchanged were destined for elite consumption. Trans-alpine trade was one of the ways of slave and perhaps, amber entry to Etruria. There was also an option to trade with Mediterranean Gaul by the Sea and then rivers to arrive deeper inland (Briggs 2003). Atlantic tin, an important raw material for bronze making, was in fact entering Italy through rivers and then the sea. Etruscan and Este textiles were appreciated in Gaul, and their production tended to increase with time (Briggs 2003).

Another direction of trans-alpine trade was to the east. The bronze urn from Veio AA1 grave is similar to ones found in middle Danube region and in northern Europe (Collis 2003). Amber trade with the Baltic region was conducted for the entire period discussed and it was probably carried out by Hallstatt populations, as amber was widely used not only by the Etruscans, but also by other Italic peoples of Northern Italy. This trade route from North to Italy was functioning from the Bronze Age to the Roman times with increasing scale of exchange of all kinds of goods (Briggs 2003; Bellintani 2014; Sanchez 2022). Instead, there is too little evidence of gold trade with the Celts north of the alps. The earliest golden objects attributed to Etruscan workshops date to the 7th-6th century BCE and are quite dispersed in transalpine Europe, particularly in modern Austria (Eluère 1989).

The regions of South Etruria and Latium were the most economically advanced ones within the Italian peninsula (Collis 2003). Together with that of Carthage, the Etruscan economy was competing with the Greek one for the economical influence on some European regions of the western Mediterranean (Sherratt and Sherratt 1993). The phases of thriving Etruscan international trade generally correspond to the main archaeological periods of Etruscan civilisation. For the Early Iron Age (950-720 BCE) the maritime trade network was starting to reappear, and occasional imports reached Etruria from the east. In the Orientalising period (720-580 BCE) we notice intensive trade that was at times called 'aristocratic' or elite trade. The scale of Greek trade of goods in other countries was massive. Etruscan export was reaching all the corners of the Mediterranean, but it played a crucial role in the Celtic lands. This integration in the Mediterranean system continued In the Archaic period (580-430 BCE). Etruria developed politically and economically, while experiencing the beginning of the decline for old urban centres. Nonetheless, it continued to be an important production and trade region of the Mediterranean basin.

2.2. Development of civilisation in the South Etruria and Latium.

The archaeological context in broader sense is a fundamental framework for the vitreous materials discussed in this work, as it serves as the basis for dating the objects and helps to understand what place glass was occupying in the every-day life. Below, there will be no holistic presentation about who populated nowadays Middle-Tyrrhenian Italy and how they lived, but rather a necessary minimum of information that is needed to discuss the glass use and perhaps even its production in these lands. For a more comprehensive discussion of the material cultures in this region one must refer to the works of Gierow (1966), Holloway (2014), Turfa (2014) and Naso (2017). Nevertheless, we must introduce the theoretical framework, periodisation and specific terms that are used throughout this dissertation. The section is divided according to three major periods that will be in focus, namely, Early Iron Age, Orientalising and Archaic.

The map of the Italian peninsula with the marked sites that are considered in the study is presented below (Figure 2.1). The majority of the sites lay in the present-day Lazio region of Italy. In the first millennium BCE, the area of interest was loosely divided into two parts: Etruria (only the southern part is considered in the study) and Latium. The former one was the first to enter the Iron Age with centres of development in South Etruria. Exclaves with similar material culture (Villanovan), like Verucchio in Emilia Romagna (14 on the map) also demonstrate early development (von Eles 2013).

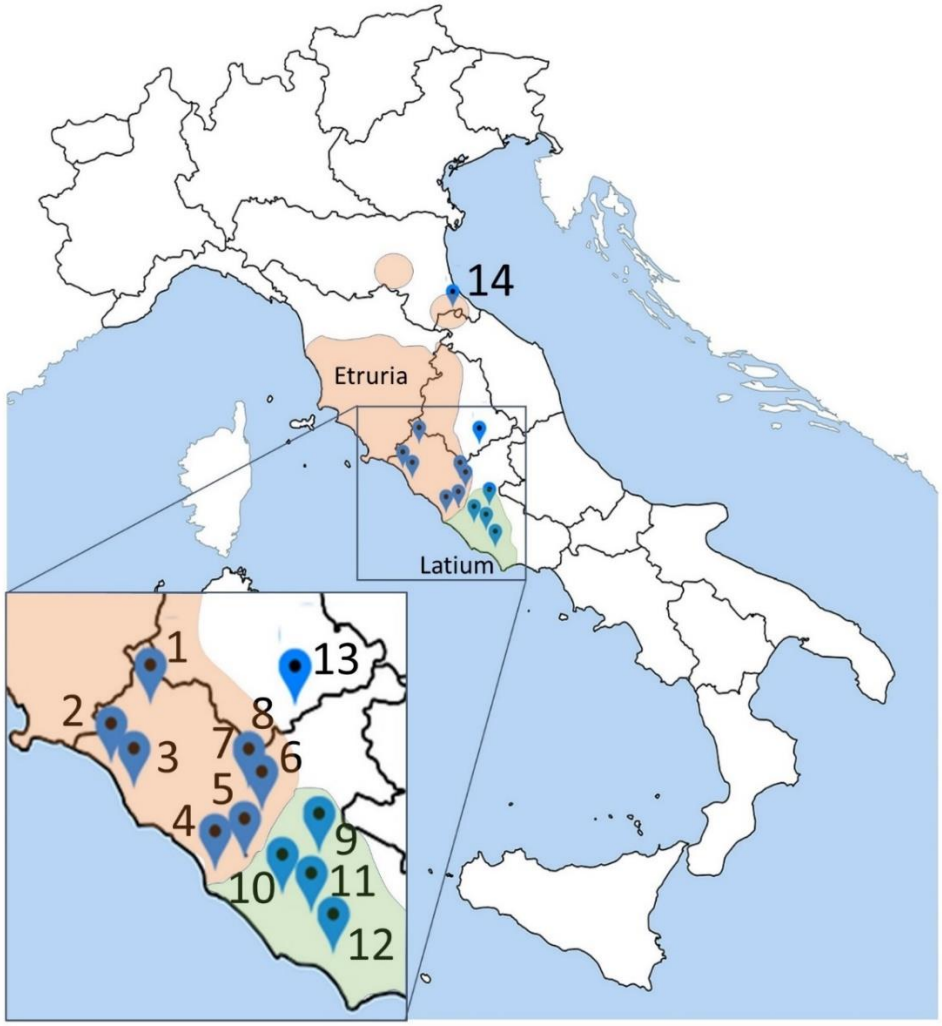

Figure 2.1. Map of modern administrative division of Italy with marked Etruria proper and Latium areas. Sites of origin of the materials involved in this study are marked with pins and assigned a number on the map: 1- Bisenzio; 2 - Vulci; 3 - Tarquinia; 4 – Cerveteri; 5 – Veio; 6 – Capena; 7 – Narce; 8 – Falerii; 9 – Tivoli; 10 – Osteria dell'Osa; 11 – Marino; 12 – Sermoneta; 13 – Terni; 14 – Verucchio.

Sites in Etruria proper considered in this study are those mentioned in the Figure 2.1: Bisenzio, Vulci, Tarquinia, Cerveteri, Veio, Capena, Narce and Falerii. The latter three were populated by Faliscans (Baccum 2009), though they always were organic part of South Etruria. Another group of

the archaeological sites considered in this work lay within Latium (Tivoli, Osteria dell'Osa, Marino and Sermoneta), that is a distinct historic region of Central Italy under certain influence from Etruria (Randall-MacIver 1924; Lulof 1996; Fulminante and Stoddart 2013; Holloway 2014).

These lands have a large percentage of good, arable land and some of them (exclusively some areas in Etruria) are rich in mineral resources including metal ores. Copper, iron, lead, silver, arsenic, tin, zinc and antimony deposits were known in central Italy (Giardino 2014) and used from ancient times, although apparently not simultaneously (Corretti and Benvenuti 2001). There was abundant water supply and wood to be use for building and as a fuel for craftspeople (Settis 1985).

2.2.1. The Early Iron Age period.

This period started in the 10th century BCE (Stoddart 2009). The Villanovan culture, which was associated with the Etruscan populations, is thought to be a continuation of development of the proto-Villanovan culture of the Bronze Age. The foundations of main Etruscan sites corresponded to a pattern established in the Late Bronze Age and was dated to the 10th century BCE (Cerveteri and Tarquinia at least), when urbanisation process started. In Etruria, it took the form of gathering of the populations of several villages on a single spacious plateau, that probably was already populated by some groups. In Latium, the process was somewhat different, with the predominant gradual growth of several proto-urban centres (Rassmusen et al. 2005; Fulminante and Stoddart 2013). The wattle and daub dwellings with a steep roof and some opening for the smoke were common for that period (McKay 1998). The first urban centres were surrounded by an agricultural hinterland, that included smaller settlements (Bonghi Jovino 2008; Pacciarelli 2016).

As their Bronze Age predecessors, the Villanovan and Latium people used cremation of the deceased and urns to contain their ashes (Hall 1996; Spivey 1997). The burial grounds were extensive, but the absence of any significant difference suggests that social differences were not pronounced yet (Pacciarelli 2016). Small groups of *pozzo* graves (a pit with the shaft where the urn was placed, often with the remains of the funeral pyre) were interpreted as family grounds (Amann 2017). Urns were typically hand-made *impasto* (coarse, low firing temperature) ceramic vessels with geometrical ornaments (Hall 1996; Spivey 1997). Another kind of urn was the one in the shape of a hut. These kinds of urns were particularly frequent in Latium, and more rarely found in South Etruria. Inhumations were found as well, depending on the zone (Seubers 2008): they are numerous in Latium, less common in South Etruria. Placement of urns into the carved tuff receptacles was also practiced (Iaia 1999). Burials that would suggest the high social rank of the buried individual started to appear in Southern Etruria first (Seubers 2008). Grave goods were not numerous, and included pottery, bronze razors, fibulae and jewellery (including glass) (McIver 1924; Hencken 1968; Iaia 1999). In a small group of male burials, high social rank was expressed by the placement of metal weapons, such as swords, spear heads and bronze helmets (Iaia 2013).

The metallurgy and metal working are some of the most remarkable features of Etruscan material culture. There was evidence of copper smelting in Early Iron Age in the area of Populonia (Mommersteeg 2011) and Tolfa mountains (Cerasuolo 2012). Production of a small metal artefacts such as razors, fibulae and buckles increased, as testified by the finds at the funerary contexts (Hencken 1968; Iaia 1999; Visco 2010). Very few bronze working facilities are known in Villanoval centres such as Bologna, Verucchio, Monfestino Monte Pezzola, Tarquinia Tivoli and Bolsena (Giardino 2014; Sagripanti 2022). Artisans were able to adjust the properties of the alloy by changing

its composition (Chiavari et al. 2007), tuning it with the function and desired appearance of the final object.

The Early Iron Age period is thought to end in the third quarter of 8th century BCE, shortly after the establishing of the first Greek emporia and proper colonies in mainland Italy, and the beginning of more evident and intensive interactions between the Etruscans and other Mediterranean people (Hodos 1999).

2.2.2. The orientalising period.

Urbanisation of the land continued with some South Etrurian cities occupying large areas: Cerveteri reached an area of 160 hectares, other large centres such as Tarquinia, Veio and Vulci had comparable or slightly smaller occupation areas of the urban settlement (Pacciarelli 2016). The economic growth was noticeable, as it is evident from the more diverse and sophisticated elements of the material culture and more substantial buildings in the cities (Izzet 2000). Moreover, the process of the differentiation of private and public spaces began (Pacciarelli 2017).

Imports from the Eastern Mediterranean were noted in various contexts mainly in south Etruria throughout and after the Bronze Age but in the end of the 8th century they reached a new level starting a process of penetration of selective elements from Eastern cultures with the indigenous one (Botto 2017). Greek art was also starting to flourish by this phase and Etruria underwent direct Phoenician and indirect Greek influence (Rathje 2010). For material culture and art, it meant not only import of goods, but also imitation of Eastern (including Greek) items and iconography. The adoption of the Euboean Greek alphabet happened in this period as well (Magness 2001). Stratification of the society and discrimination of the elites found their reflection in famous, so called, “princely” tombs (Curtis 1919; Winther 1997) that contained a variety of lavish imported or locally produced objects to highlight the social status of the buried. Cremations appeared alongside inhumations. Chamber structures of the tombs and mounds were adopted (Riva 2006). Some exotic materials appeared; for instance, it is common to find the ostrich eggs in the richer burials, but also ivory, faience and glass (Magness 2001). It is a subject of discussion what was the origin of those merchants who brought these items (Rathje 2010). It was not only imported luxury goods and objects of artistic and decorative value that accompanied the profound social changes, but also less traceable practices such as way of feasting (Tuck 1994), religious practices, hairdressing etc (Magness 2001). These changes could not have happened without direct presence of people of Near Eastern origin, for instance from Tyre, a city that was under pressure from the Assyrian empire (Magness 2001; Oded 1974). Latium seems to undergo a similar process, but since its economy was less diversified, it could not use all the benefits from the long-range trade available to the cities in Etruria. Penetration of Greek products was on fairly small scale compared to Etruria and South Italy. Rome started to gain influence in Latium in this period. (Smith 1994).

Original wheel-made Etruscan pottery called *Bucchero* started to be produced from the early 7th century onwards. Vessels were produced in a variety of shapes. Original manufacturing point is believed to be in Cerveteri, but soon this ware started to be produced in other centres of South Etruria (Stoddart 2009). In the second half of 7th century BCE, the imitation of Corinthian ware started to occur. Different types of impasto and bucchero vessels were produced in Latium, as well as in other several main production centres, as it can be seen from the fabric analyses (Attema et al. 2002).

Metallurgy and metalworking advanced significantly. Etruscan guilders started to use granulation for decorating fibulae and other objects (Parrini et al. 1982). Toreutics and repousse techniques became widespread, and the diversity of shapes increased (Zifferero 2017). Even though Etruria was rich in iron ores, the widespread evidence of iron working dates only to the 8th century BCE. We can say that production of weapons and tools from iron intensified in this period (Corretti and Benvenuti 2001; Iaia 2017). Nevertheless, bronze retained the position of the most popular metal used for production of many objects, from votive statues to cauldrons and tripods.

A network of roads, sometimes cut in tufa hills, appeared connecting cities. Major Etruscan settlements from now on could be differentiated as primary and secondary ones. Specialised craftsmen were, probably, connected to the "palatial" buildings, as evidenced form the excavation of the 7th century BCE workshop and palace at Murlo (Nielsen 1998).

2.2.3. Archaic period.

This period begun in the first decades of the 6th century BCE. It was characterised by the increased role of the cities, the growing of population and political and cultural development that already started in the Orientalising period. During the 6th century, the Etruscans expanded their influence and settlements in the Po valley and Campania. The cities started having more monumental fortifications (Rassmusen et al. 2005), the division between sacred, political and commercial spaces becomes clearer (Cerchiai 2017). In fact, a so-called Etruscan order was developed the architecture of sacred places, and several temples and sanctuaries of common features were built. Latium monumental buildings also used similar configuration and were encountered more often than in Etruria (Bispham and Smith 2014; Potts 2015). Houses were built on stone foundation and often had tiles with elaborated terracotta sculptures as roofing material (Winther 1997). The city planning became more evident, although most of the old cities retained their somewhat irregular system of streets. Latial cities also featured monumental buildings at the time, probably because of the redirection of wealth from the funerary practices (Smith 1994). It is important to notice the disappearance of graves in Latium in the Archaic period. So, the funerary contexts form Latium discussed in the present work are limited mostly to the EIA, and partly to the Orientalising period.

The population of West-central Italy is seen as people who were living and evolving within the cultural and technological trends of the larger region of the Mediterranean. They were able to adapt, incorporate new customs and contribute with their own know-hows especially in the field of metallurgy and metalworking. Regarding the glass production and working, Etruscans had all prerequisites to start the industry even in the Early Iron Age: silica sources that were present practically everywhere, wide abundance of halophytic plants and algae, and a trade networks for mineral source of flux, or of raw glass to be shaped into objects through heat; an easy access to most popular colorants and opacifiers used for glass from their own ores and through trade; abundance of fuel and the most important - practical knowledge of fire technology for (advanced) technical processes in metallurgy and pottery production.

2.3. Glass finds in South Etruria and Latium and the archaeological context of ones involved in this study.

This section discusses the diversity of glass finds in Central Italy and describes the archaeological contexts which, for the samples discussed in this work, are all funerary contexts. This section is meant to demonstrate the place of glass in the society of the first half of the first millennium BCE, although a complete and exhaustive list of objects found or associated with Etruscan and Latial context is not the aim here. The presentation is focused on the contexts available for the study in the two museums mentioned in the preface.

Chapter 1 already mentioned the fact that glass was not as an ubiquitous material as it was later, in Roman times, for example, when the glass blowing started to be broadly used (Tait 1992). Despite this fact, it was used in South Etruria and Latium throughout the whole period discussed here, as demonstrated by the diverse set of materials from necropolises near Veii (Koch 2011), probably imported by Phoenician merchants. When it comes to their shape and purpose, most of the objects fall within two distinct groups: jewellery elements and small vessels, as suggested by many scholars (De Marinis and Rapi 2005). Exceptions include the (not very numerous) finds of vitreous spindle whorls, as those conserved in the Bologna Museum, that topologically do not differ from large beads. It is therefore reasonable to subdivide this section into one part for jewellery and another for vessels, with the aim of overviewing the occurrences of the glass artefacts from the lands under Etruscan influence.

Jewellery (including the studied samples). In this category beads are the most common type of glass objects (Bell and Carpino 2016). They were found in a broad range of contexts throughout the timeline discussed in the current work as singletons or groups, and the former are usually bigger in size (Randall-MacIver 1924; Hencken 1968). One of the common ways of using glass beads was to decorate the bows of the fibulae, and glass objects shaped for this purpose were popular in the Early Iron Age period (Hencken 1968; Fusi 2021). Beads were also arranged in necklaces, as can be seen from materials found in burial grounds in Bologna, Vetulonia Tarquinia and Marino (Randall-MacIver 1924; Gierow 1964; Hencken 1968). Another way of using beads was as a decoration of clothes (Koch 2015), such as those found in the "Tomba dei Bronzetti Sardi" at Vulci (Arancio et al. 2010). Glasses from this tomb were studied within this work. These and other beads mentioned in this section are better described in Chapter 3.

Glass beads were usually found in female graves (Iaia 1999; Koch 2011) and the number of glass pieces can indicate the social status of the buried, which is obviously also related to the entire range of grave goods. For instance at Veii, in the Orientalising period, the "well equipped" female burials could contain no glass at all (Koch 2011). Children's graves also feature some glass beads. For children, at least in the Iron Age, glass seems to be one of the signs of social status distinction, together with the bracelets (Seubers 2008). It is difficult to interpret the purpose of glass beads and other objects in male graves. Materials for this study come from two collections: Museo Nazionale Etrusco di Villa Giulia and Museo delle Civiltà, featuring beads and other objects from burial contexts that demonstrate the diversity of the social status of the buried.

Several bead types, each made of differently coloured glass, were used in assortments making unique sets of artefacts and glass beads were used in combination with other materials such as amber. Some significant examples in the later Iron Age were reported by De Marinis and Rapi (2005). The

combination of glass with gold and semi-precious stones also supports the value of this material in the Orientalising period. A remarkable set of jewellery including a massive gold necklace with glass and stone elements of decoration is exhibited in the Metropolitan Museum of Art and a similar one can be seen in the Castellani collection (Villa Giulia museum in Rome), giving some indications on the appreciation of glass in Etruscan society and its usage for the representation of the social status of the buried person.

As for contexts, we will now introduce those that yielded beads and other jewellery objects included in this project, starting from South Etruria and then moving to Latium, the region immediately south of the river Tiber. A chronological division is applied per site. In this work, sites are large, mostly urban centres surrounded by necropolises, which are archaeological sites themselves; for sake of simplicity, the latter will be referred to as localities. The complete list of contexts with their dating is given in Appendix 1. The appearance of the beads is shown in the photographs reported in Appendix 2.

Samples from the middle-sized centre of **Bisenzio** were found in the so-called *pozzo* type graves, dated to the Early Iron Age II (EIA II) period (800-720 BCE). The vessels inside the tombs were of both local and imported types, and one of the graves (tomb 5) contained an iron spear and a sword (Delpino 1977).

Vulci was a proto-urban and, later, an urban centre surrounded by numerous necropolises. Beads that were studied here were found in contexts from the Early Iron Age I (10th-9th century BCE) to the Archaic period (6th century BCE). The earliest beads originate from the cemeteries of Cavalupo (*Tomba dei Bronzetti Sardi*) and Cuccumella (Tomb 83). Both tombs belong to the EIA I and were cremations with the urns and burial goods inserted in a stone receptacle. The "*Tomba dei Bronzetti Sardi*" (tomb of the Sardinian bronzes) at Cavalupo was a rich burial containing the remains of a female adult and a child. The cinerary urn was decorated with metal lamellae, and a set of bronze fibulae and a set of beads were accompanying the urn. Peculiar was the set of three bronze figurines of Nuragic type, which was suggestive of the Sardinian origin of the buried person (Arancio et al. 2010). Tomb 83 at Cuccumela contained a remarkable, but less rich, grave set which included an askoid jug of Sardinian type (Mangani 1995). The Early Orientalising tomb named as *6 settembre 1966* or *a fossa profonda* dates to ca. 700-690 BCE. Apart from some glass beads, it contained some exotic goods such as late geometric Euboean pottery and some West Phoenician goods. Iron objects, faience, amber jewellery, and silver fibulae, together with some spindle whorls, were also found (Moretti Sgubini 2001). The rest of the contexts belong to the beginning of the Late Archaic period (end of the 6th century BCE). They were glass buttons and a bracelet. The buttons were found together with Attic pottery and other imported tableware. Bronze and iron objects were also found in the same tomb (Falconi Amorelli 1967; Moretti Sgubini 2001). Glass buttons only started to be produced in the Archaic period. The oldest examples date to the 6th century BCE, but they become more common in the Hellenistic period (Eisen 1916), which is beyond the scope of this research.

Tarquinia is a major centre but the tombs that contained glass artefacts are not well represented in this study, and only two glass objects dated to the EIA I from the Villanovan Arcatelle necropolis (without grave context) could be analysed (Babbi 2005). The Tarquinia necropolises, in fact, yielded much more glass beads and some glass vessels (Hencken 1968). Glass beads, in combination with other precious materials such as bronze, electrum and amber were found in contexts such as the *fossa* with Bull-headed Staff (Seubers 2008).

Cerveteri (Caere) is another thriving proto-urban and then urban centre, represented by several burial grounds. The Cava della Pozzolana necropolis materials are not published yet, but this area mostly contained "Villanovan" or *pozzo* types of burials. Glass beads were found in tomb 27, that belongs to the EIA II (800-720 BCE). Tumulo del Colonnello is one of the biggest tumuli burials at the Banditaccia necropolis and was dated to the Orientalising period. It contains several burial chambers, the latest of which contained some vitreous beads that were identified as faience (Rizzi 1955). The late archaic period (520-430 BCE) is represented by the *Martiri Marescotti* tomb (n. 610) in the Monte Abatone necropolis. This rich burial contained more than 30 attic vessels and other items of significant artistic value (Ridgway 1968).

Caolino del Sasso di Furbara (Rome) was a minor centre in the immediate vicinity of Cerveteri. This locality featured only burials dated around the half of the 8th century BCE. These graves were *fossa* type featuring sometimes small cavities in one of the walls. The individuals were buried with fibulae and other decorative metal elements (rings and pendants, including silver and gold). Amber and some faience objects were also present in some graves. Out of the 5 tombs involved in this study, only one contained a ceramic vessel.

Veio was a major Etruscan centre a few kilometres north of Rome. The large number of objects included in this work originated from its necropolises. Quattro Fontanili was one of the largest and most important cemeteries. It contains two graves of EIA II period that belonged to a later stage of its use (earliest graves were dated to the 9th century BCE) and featured glass beads that were studied within this work. A *pozzo* grave belonged to a male warrior (*tomba di Guerriero AA1*) and contained an unusual double bead, which might be a part of a ceremonial weapon (Boitani 2004). Tomb HH11-13 was a fossa type grave for a woman, but the presence of a child was also suggested (Various authors *Notizie …*1965). In the same necropolis, there were more instances of glass finds (Koch 2011). For example, more than 1000 small beads were found in a single tomb in the other part of the necropolis (Pacciarelli 2017). Another necropolis with graves included in the study is Grotta Gramiccia. The two graves that contained studied glass items are very different one to the other. The 575 tomb (EIA II) is older and contained remains of a man in the urn covered with a crested helmet. The urn and grave goods were placed in a dolium. The Leoni Ruggenti tomb (Early Orientalising period) is a chamber tomb that contained several individuals. This grave was very rich, with numerous ceramic and metal objects, including imported ones. Amber decorations and weapons were found in both graves (Berardinetti and Drago 1997; Boitani 2010). The Vaccareccia necropolis featured *fossa* type graves that belonged to the time from the EIA II to the Middle Orientalising period. These graves contained brown *impasto* ware or different types. Some *bucchero* vessels were also documented. Fibulae were present in almost every grave. Decorations of noble metals (gold and silver) were not unusual within the grave set of those graves that also contained glass objects. Amber was also frequently found as a material for beads and fibulae decoration. Bronze items included fibulae, tubes, rings, bracelets, small vessels etc (Palm 1952).

Capena was a middle-size centre in the Tiber valley. Two graves with glass objects studied in this work were unearthed in Le Saliere necropolis. One of them was from EIA II period, the other one was from the Early Orientalising one (late 8th century BCE). Apart from the ceramic ware, the older grave (tomb 104) featured a bronze tripod and a bowl, while the more recent one (tomb 94) contained fibulae, distaff, amber (and glass) beads and other adornments made of bronze (Stefani 1912). Other glass objects from the Capena necropolises belonged to the Early and Middle Orientalising periods.

Three tombs, namely 60, 61 from San Martino and 100 from Monte Cornazzano, contained numerous ceramic vessels of black, brown and red *impasto*, red painted vessels and Greek type vessels with animalistic and geometric decorations. Tomb 60 was probably plundered, yet it still contained some bronze items; tomb 61 contained a bronze necklace (Paribeni 1906).

Narce was a small town in the Faliscan area, in South Etruria. It is represented in this work by a *pozzo* tomb 1 (EIA II) from the necropolis *i Tufi*. Glass beads found there were accompanied by a bronze belt and other adornments. The urn was covered with a decorated bowl.

Falerii, the main town of Faliscan area, is represented in this research by three tombs from the Montarano necropolis. Tomb 15 (XXVII) belongs to the late EIA II period and was a high rank woman *fossa* type burial. High social status of the buried person was highlighted by a tripod, a bronze censer, and a decorated distaff (Ligabue 2022). Tomb 17 (XXVI) is also a *fossa* burial of a woman. There was red impasto *holmos* and other ceramic ware. Weaving set, personal adornments and bronze cup finishes the list of grave goods. Tomb 10 also contained a *holmos* (Cozza and Pasqui 1981).

Tivoli was an important centre of the hinterland Latium Vetus. It is a less represented site with only one tomb involved in the study, an EIA II circular tomb of a woman that was buried with a small set of *impasto* vessels and bronze objects (CLP 1976).

Osteria dell'Osa, near Gabii (Rome), is the most extensively published Iron Age necropolis in Central Italy. Seven tombs that contained glass were studied within this project. They were all inhumations in fossa-graves, dating to the EIA I-II. Typical inventory included several *impasto* vessels and decorations like fibulae, rings, pieces of amber (beads and pendants), spindle whorls. Tomb 82 included more objects than the others considered in this research (Bietti Sestieri 1992; Koch 2018a).

At **Marino**, in the Alban Hills (Latium Vetus) three graves of the Orientalising period from Riserva del Truglio necropolis (Tombs 3, 21 and 30) were studied. Apart from glass beads, they contained significant number of amber pieces, sometimes used as fibulae decorations. Tomb 3 featured an iron spearhead. The rest of metallic objects were made of bronze. The most common ones were fibulae and rings. Tomb 30 contained more personal adornments made of bronze. Ceramic vessels were dark and red impasto and depurated fabric. Tomb 3 contained up to 10 vessels (Taloni 2013).

Sermoneta, in southern Latium, is represented by the Caracupa necropolis. It contained about a hundred graves, arranged in clusters, each grave usually positioned according to the terrain with heads of the buried being higher and legs lower. On the basis of the grave-goods, the necropolis was thought to be used between the 8th-7th century BCE. A foreign influence can be noticed in the shapes of the ceramic ware. The graves included here are dated to the EIA II period and apparently contained females . Tomb 89 featured a sword and a knife, and it was probably the only one attributed to a male individual that also included some glass objects. Tomb 48 was remarkable because of the position of the head of the deceased laid on a stone, the traces of wood casing and the unusual jewellery represented by a gold cylinder. Other graves also contained adornments with bronze fibulae prevailing in number. Amber was also found extensively. Lazio-type amphorae were found in tombs 8 and 57bis (Mengarelli and Savignoni 1903).

Terni was one of the most important pre-roman towns in Southern Umbria. One of the necropolises that were included in the study, which was in use from the late Bronze Age, is Acciaierie near Terni. All beads come from EIA I contexts, where inhumations prevail over cremations. Grave goods were similar to those already reported for the other sites, namely fibulae of different types and other bronze items, frequently found in the graves (Leonelli 2003).

Verucchio high status graves make one believe that such materials as glass and amber were rather more available there than in Etruria or Latium. The site was one of the most important in the early Iron Age in nowadays Emilia-Romagna and finds of glass from different burial grounds were frequent. Samples included in this study were found outside any tomb context at the Fondo Ripa necropolis, although they do not represent all the varieties of beads found in this site. A rather representative tomb in this regard, tomb 47 at Lippi necropolis, contained thousands of small glass and amber objects (Seubers 2008; Sestieri 1997), and it was associated with other burials with much fewer glass items inside. The typology of glass beads from Verucchio covers 18 different types, three of which are unique examples for the site. The most common type there is monochrome or decorated ring beads of different colours, which are counted on thousands: yellow, blue, dark (black appearance), white and turquoise with the number of blue and yellow ones prevailing. In addition, flattened spherical beads, usually less or not coloured at all, were also found. Among the ways of bead decoration, the most common were the eyes, garlands, scales or so-called herringbone ornament of mainly opaque yellow and white colours. In many cases, the bead itself was produced in dark, opaque glass (Koch 2015).

Vessels. Although these objects are not in the focus of the present research, they constitute an interesting and diverse class of objects that were used by Central Italian population. Below, an extremely synthetic overview on glass vessels is given, presenting the general frame beyond the specific samples that were included in this work.

Glass vessels started to appear in the beginning of the Orientalising period in the form of (most likely) imported objects from the Near East (Bonfante 1986). More than one hundred recognisable artefacts are presently known, although not all of them preserved their initial appearance and many are fragments (Sternini 2017). A dark blue glass bowl from the Bernardini tomb (Curtis 1919) at Palestrina is similar to the Nimrud ones, and there are more examples of the 7th century BCE Phoenician or Syrian glass bowls that could have been used in ritualised wine drinking (Naso 2017).

It was voiced by a considerable number of scholars that at least some *balsamari* (small vessels for precious substances) might be locally produced (Harden 1968). These claims were resting on the distribution of vessels, mostly *oinochoi*, decorated in a specific way with spikes all over the body. These vessels received many names in the literature: Hedgehog vases (Turfa 2005), Porcupine vases (Bonfante 1986), spiky vases (Cristensen 1997), etc. A frequently used term, even in publications written in English or Italian is the German *Stachelflaschen* (Towle and Henderson 2004). The oldest vessel of such shape was found in tomb 4 of Monte Abatone necropolis (Cerveteri) and was dated to the third quarter of the 7th century BCE. There are 5 more objects of this type (including 2 spiky ones) from the beginning of the 6th century (Banditaccia-Laghetto necropolis, tombs 365 and 445) (Giuntoli 1996).

The so-called Mediterranean group 1 was the prevailing typological group, among the core formed vessels, from the second half of the 6th to the first half of the 4th century (Blomme et al. 2016). Representatives if this type can be found all across the Mediterranean, and they appeared in Etruscan lands as well. Grose (1989) divided it into 8 classes, based on similarity of shape, colour and decoration. The most common shapes were the ones resembling Greek ceramic vessels, namely *alabastra* (tall vessels with a relatively small diameter and small handles, usually featuring linear decoration), kohl tubes, not so numerous *amforiskoi* and *aryballoi* (rather wider vessels with a narrow neck) and *oinochoi* (that have wavy necks and only one handle). Aryballoi are argued to be the last

shape appearing, because there were very few in the earlier contexts. On the other hand, the various classes of alabastra were the most represented shape of vessel. The main decoration technique was thread ornament (parallel lines, waves and zig-zags) of glass of a different colour from the one of the base glass, which was often opaque blue, brown, turquoise, white and yellow (appearing orange). Intense dark colours of the base glass often appear black as the final effect (Grose 1989).

Another type of elongated objects made from glass were called distaffs because of their strict association with glass spindle whorls, although it is still unclear if they were really used as spinning tools (Sternini 2017). Regarding the already mentioned vitreous spindle whorls, they were often confused with beads. They were made using a variety of colours (usually blue with white and yellow linear decorations) and most of them were from the Bologna-Este-Verucchio area. Their contexts were normally the rich female burials of 7th-6th century BCE, and glass distaffs with a metal core were found – although in small numbers - in Cerveteri, Campovalano, Marsiliana d'Albegna and Castelnuovo Bernardegna, and several more places (Gleba 2007).

Potential evidence of glass working was found in Cerveteri's craftsmen quarter, where waste materials, raw glass and glass paste was discovered (D'Ercole 2017) in a context dated to the Orientalising period. It was suggested that immigrant Near Eastern craftsmen were taking part in production in some way (Cerasuolo 2016). 12 pieces of vitreous material were then attributed to iron production (and not glass production) based on chemical analyses (Moretti Sgubini 2001). The workshops in Cerveteri were probably place of production of various range of objects made of different materials, mostly metals (Bellelli 2017). Another possible glass-working workshop could be the one at Murlo (Pogio Civitate) (Cristensen 1997), as the Piano del Tesoro lower building (second half of the 7th century) and the colonnaded workshop on the southern edge of the site featured some vitreous materials (Bell and Carpino 2016). Nielsen (1998) mentions some "vitreous slags" in the context of bronze making; therefore, it was apparent that a workshop of broad specialisation was active, but glass production was not attested there.

Many archaeologists agree that Etruscan glass working existed in the Orientalising period, mentioning peculiarly shaped artefacts (fibulae "*Glasbügelfibeln*" and vessels "*Stachelflaschen"*). It is popular opinion that the existence of glass industry could be the natural consequence of developed metallurgy and pottery making (testifying the mastering of fire technology) and the extensive trade connections with Egypt, Phoenician and Greek cities, which would support the import of skills and materials for a local glass production (Stoddart 2009).

Conclusion. The first half of the first millennium BCE was a period of profound changes in the economic and political life of Middle-Tyrrhenian Italy that introduced the re-establishment of long-range trade in the Mediterranean, mainly through Phoenician and Greek networks), development of crafts, urbanisation, social stratification. South Etruria seems a more developed and better-integrated region of Central Italy compared to Latium, with its own trajectory of development. It appears that glass production could have occurred in these lands as well as glass-working, the existence of which is presumed based on archaeological evidence. Glass beads discussed in the present work originated from diverse funerary contexts. The tombs that yielded glass objects and were mentioned in the text were of various types (*pozzo, fossa*, chamber tombs) and were different in terms of the grave goods sets: some contained dozens of imported ceramic vessels, others

contained very few, relatively simple items. Such differences are thought to reflect the different social positions of the buried people.

CHAPTER 3. MATERIALS: GLASS BEADS FROM SOUTH ETRURIA AND LATIUM IN THE FIRST HALF OF THE FIRST MILLENNIUM BCE.

3.1. Typologies of glass beads.

Making division based on the type of the object is beneficial when dealing with the large set of beads that have been considered in this research, because it allows for more precise characterisation of periods and places based on the variability in occurrences of the specific types of objects (DeCrose et al. 2003; Bar-Yosef Mayer 2013), given that a typological difference of artefacts between periods and/or places is indeed present.

Glass, thanks to its plasticity at high temperature, can be worked to produce an infinite variety of shapes, that can look even more different thanks to the ability of craftspeople to manipulate colour and translucency to achieve the desired appearance of the object. An attempt to systematise glass beads typology can be done if significant (i.e. non-random) attributes can be established. Whether the types originating from such an approach would mirror real groups of homogeneous beads, or if they are merely of practical use for archaeologists or art historians, is a matter of discussion (Hill and Evans 1972; Whittacker et al. 1998). Nevertheless, establishing criteria for grouping the artefacts that are considered in this research is certainly helpful for communicating and keeping the record of the data and the results of the archaeometric effort.

Despite the apparent lack of interest of the researchers for glass beads (Bar Yosef Meyer 2013), systematic typologies of glass beads for different parts of the world and time periods were produced for at least one hundred years. We can rely on these works for vocabulary of beads characterisation and a set of characteristic attributes that are crucial elements of any typological endeavour.

To the best of author's knowledge, the first attempt to systematically characterise archaeological glass beads was done by Gustavus Eisen in 1916. He worked with eye beads of various origin and characterised their appearance based on how the decoration was applied, with archaeological context playing a secondary role (Eisen 1916).

Horace Beck's work is the oldest, still widely cited (Sprincz and Beck 1981; Conn 1998; Beck 2006; Bar-Yosef Mayer 2013) typological study of archaeological beads and pendants. His work is not limited to glass and includes other types of materials. It was pioneering in establishing a system of features (attributes) that allowed for the differentiation of widely different beads. This work was done without any spatial or chronological considerations and featured mostly bead types inherent to Mediterranean and Northern-European production, starting from the Late Bronze Age.

Thea Elisabeth Haevernick's numerous works in *"Beiträge zur Geschichte des Antiken Glases"* – the yearly publication of the Römisch-Germanisches Zentralmuseum - RGZM (Haevernick 1959; 1960; 1961; 1962; 1965 and others) and monographs (Haevernick 1960, Haevernick et al. 1987) feature various types of glass objects (not limited to beads). Distribution patterns and chronological contexts of the types of the objects discussed were used to establish regions of production and present diachronic picture of glass circulation. Generalisations were possible through the systematic study of occurrences. A relevant role in discussion was played by the manner of producing and forming of beads and other objects.

Margaret Guido (1978) focused on the specific region of the British Isles, which allowed her to thoroughly systematise glass finds from specific areas and come up with quantifiable classes, for which the place and the manner of production were suggested. Her work is interesting because it highlights the difficulty of building typological frames. In her work, apart from the classes that were identified in a more strictly way, there were "groups" of objects that were joined together simply because they do not have enough characteristic features to make up a class. Despite similar appearance, these objects demonstrate certain variability. The need for chemical analyses was ascertained for these "groups" to make possible to break them down into classes, which is the type of insight this PhD thesis research attempted to provide, albeit for different assemblages of the analysed materials.

Particularly relevant for the present work are the typological considerations on the Iron Age beads found in Italy made by Leonie Koch (2011, 2015). Presence of decorations or, more simply, the parts of another colour, was made the highest order of division. This was an obvious first step in creating bead typology, with monochrome and polychrome glass beads being major groups of artefacts, with the latter ones having significantly larger number of sub-groups. Division by shape was made with the strict connection to manufacturing techniques used by artisans. Occurrences and distribution patterns are noted. This work and the following papers (Koch 2018a, 2018b, 2020 and others) feature types of beads considered in the present study.

Karlis Karklins' system of classification (2012) aims at unifying the approaches for the description of glass beads found in the Americas. It is based on the research of Kidd and Kidd (2012), who studied mostly trade beads from 16th-19th century CE. Such framework contains all important attributes of the beads and give indications for their concise documentation. In Karklins's work, the hierarchical system is used to divide the beads into large classes, each containing several types of beads. An even higher order of division is based on the manufacturing technique: winding or drawing. The colour is less prominent in this classification.

Normally typologies are created to include beads within a specific region and/or time (Alexeeva 1975; Sprincz and Beck 1981; Francis 1986; DeCrose et al. 2003; Karklins 2012; Bar-Yosef Mayer 2013; Then-Obłuska 2021 and references therein), making the task more feasible. In these cases, it is relevant to note that such typologies serve specific purpose, acting as an operative tool to support the overall research and the related outcomes. Despite the efforts of many scholars, a "universal" typology frame for glass beads is not available yet, and scholars continue creating case-specific divisions. Moving towards interdisciplinarity, it has proven on several occasions that the typological approach for ancient glass studies can take advantage from the chemical analyses (Panighello et al. 2012; Bandama et al. 2018; Neri et al. 2019). Such a combined approach will be adopted in this research project.

3.2. Defining a framework for typological grouping for this study.

To divide glass beads into "classes", "groups" and "types", the researchers mostly focus on shape and size, colour and translucency, number and qualities of the decorations (Guido 1978; Koch 2011, 2015; Kidd and Kidd 2012). In this project, a quantitative representation of the variability of these features within the investigated set of objects is employed. This quantitative representation is obtained by applying a single scale of measurement for each parameter to each of the objects within

this study. This approach gives the opportunity to build a classification system founded on defined rules, that could be readily replicated on a different assemblage.

Objects considered in this study were selected to represent all archaeological sites available within the museums' collections. In cases when many objects of similar appearance were available, several representative samples were selected in the way to cover both the geographical and chronological range of occurrence. Attention was also paid to cover possible variability among the groups of objects with similar appearance. In other words, if there was a slight variation of colour among similar beads then several objects were selected for the stage 1 to represent such variation (including the endmembers).

Below, in the designated sub-sections, the set of relevant parameters and the way of their measurement will be presented. Running ahead, we can say that measuring the parameters does not come without challenges. The system is built on the data collected from the objects that have kept their integrity and for which all the attributes could be reliably documented. Objects with chipped parts, those that demonstrate discolouration and degradation, fragmented ones - in short, those that have somehow their attributes changed - were largely excluded from the step in which the framework for typological grouping was build, and then assigned to specific types after the group division was assessed. To guide the reader within this process, images of individual objects can be found in the Appendix 2. The main aim of this subsection is not merely to divide the objects into groups, but to demonstrate how the documentation of the attributes was carried on and what is the extent of variability within the set. The process was performed in the museum, therefore specific constraints were present in some instances, for example with the objects arranged in showcases for exhibition purposes. These issues are also presented in the text. The parameters considered relevant for this study, with their values determined for each whole sample considered, can be found in the Appendix 3. The description of types that were distinguished is given in section 4 of this chapter.

In this section, the term "category" is used to mark the division within the single attribute as size (5 categories from very small to very large) or translucency (5 categories from opaque to clear). Samples that belong to the same category might not necessarily belong to the same typological group and vice versa.

3.2.1. Procedure for measuring the dimension and shape configuration of the beads.

Shape configuration indicates here the variability in ratios of diameter to width and to the aperture of the beads, as Non-beads are omitted in this discussion. This parameter can be used to divide glass beads into groups. The measurements of dimensions were performed in a standardised way: the two diameter measurements were taken at the widest direction of a cross section plane perpendicular to the aperture and the narrowest one. This variability occurs due to the imperfections or asymmetry of the beads as illustrated in Figure 3.1, which also reports the terminology used here to describe the beads. In case that same-looking beads were assembled on a necklace, the measurements that were documented are the biggest diameter of the group of beads and the smallest one. The larger diameter is noted as D1 in the Appendix 3 and the smaller one as D2. The width of the bead is a measurement along the direction of the aperture (Figure 3.1). When the two measures of width are taken (W1 and W2) that means that there are some irregularities in the shape,

or they represent the variation of largest and smallest measurement in the set of similar beads on a necklace. The aperture measurements - A1 and - in rare cases A2 - represent the diameter of the aperture, which sometimes is not the same for the two apexes.

The two ratios that are going to be the type determining attributes are the ratio of the diameter to the width (D/W) and the diameter to the aperture (D/A). To calculate those values, the average values between D1 and D2, W1 and W2, A1 and A2 were used, considering only the samples that kept their integrity. This procedure led to obtain values that were used as sample entries for typological definition. There are several kinds of result for each ratio: if the width is prevailing over the diameter by at least 10% (D/W ratio <0.9) the shape description of the beads would be “tubular” (this category would also include rare examples of barrel shaped beads); if the width and diameter are approximately equal (D/W – 0.9 – 1.1) such beads were described as “spherical”; if the D/W ratio is between 1.1 and 1.5, these beads were called “spherical-oblate”; from 1.5 to 2 – “oblate” and if the D/W ratio is more than 2 – “flat”.

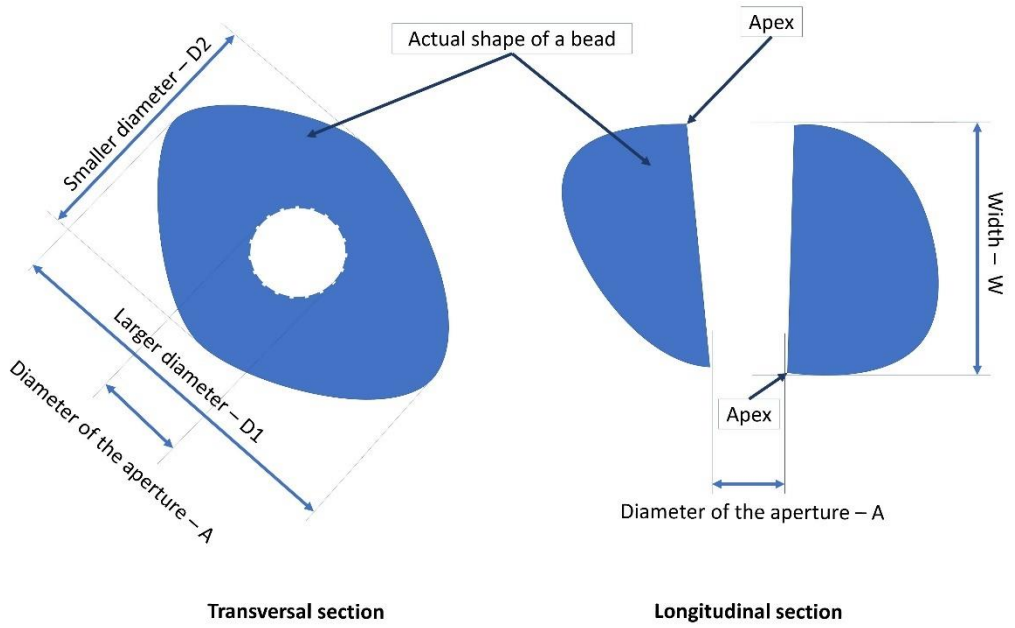

Figure 3.1. Explanation of the measurement directions and the dimensions of beads.

Figure 3.2 (a) shows the number of samples within each category: tubular beads make a small group of samples – 8 in total; spherical ones are also not so numerous – 17 samples; most of the samples are in two main categories – spherical-oblate – 93 samples and oblate – 75; flat beads are also not very numerous – 19 samples. It can be observed in Figure 3.2 (a) that there is a seeming gap between spherical-oblate and oblate categories of beads where the neighbouring slots next to the line of division seem to be less populated than the rest of the slots of the categories. Yet, this gap is not very pronounced.

The beads were divided into four categories based on their D/A ratio which reflects relative size of the aperture: large aperture (ring-beads) with the D/A ratio below 2.25; large-intermediate

group (D/A 2.25 – 3); small-intermediate (3 – 3.75) and beads with their D/A ratio above 3.75. The numbers of samples that belong to each category are shown in Figure 3.2 (b). Remarkable is that the most frequently found D/A ratio is 3 – 3.25 – lower margin of the small-intermediate beads. Intermediate beads appear to be the most frequently found groups.

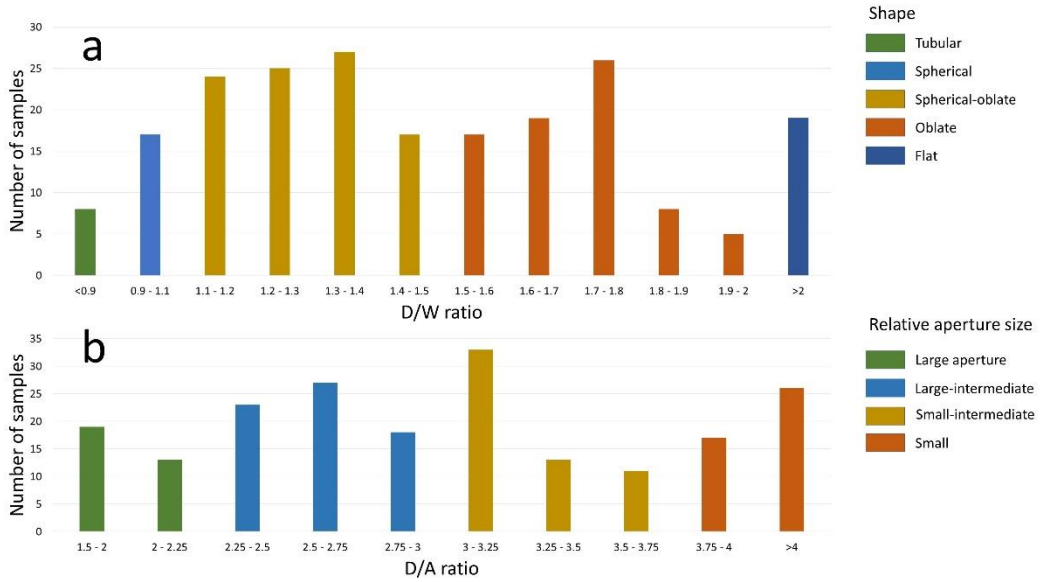

Figure 3.2. a – distribution of samples according to the ratio of diameter to the width (D/W ratio); b – ratio of the diameter of the beads to their apertures (D/A ratio).

These divisions reflect the various cross sections of the beads. Comparison of the cross sections is given in the Figure 3.3. The decrease of the width in comparison to the diameters is noticeable from tubular to flat beads. The difference in the aperture size influences cross sections in a considerable way. Beads considered within this study usually have spherical to oblate shape, which means that their longitudinal cross section would tend to be round or oval. This is not the case for a minor group of beads with cross sections that cannot be described as ovals. We use term “angular” to refer to the longitudinal cross sections of samples PG3, 64, 66, 90, 113, 162-164, VG17, 39-47, 64 and 81, which demonstrate rather square shapes of their longitudinal cross sections. Samples are termed “pear shaped” if the cross section parallel to the aperture is rather rhomboidal (biconical) or tend to be triangular (the largest diameter is not in the middle of the section, similar to VG81 in Figure 3.3. In this group, samples PG3, 64, 90, VG64 and 81 are included. Tubular samples that have D/W ratio less than 0.7 (PG66, 113, 162-164) are considered tall cylindric. The rest of the samples (VG17, 39-47) are considered short cylindric (they correspond, to but are not equal to, flat beads). The two cylindric groups have rectangular longitudinal cross sections.

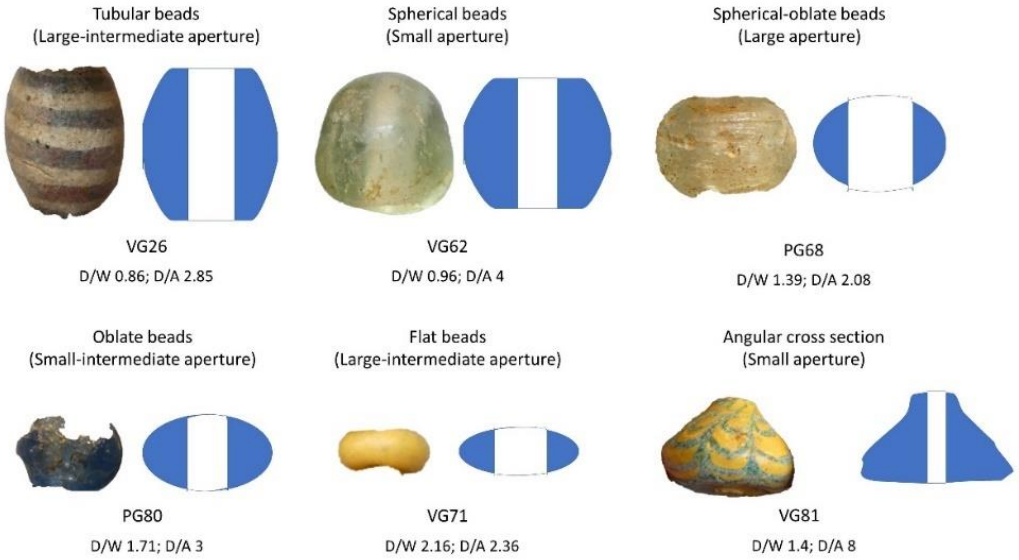

Figure 3.3. Comparison of different type of longitudinal cross sections within the set. Images of beads are not to scale.

Another important indicator that we use is the volume of the beads. It is hard to come up with a single formula for its calculation, because of the variety and irregularity of cross sections, or to measure precisely the volume of each individual bead. As a practical solution it was opted to use the volume of a circular cylinder circumscribing a bead and excluding the volume of the aperture by subtracting its diameter from the diameter of the bead. The formula of the volume of a cylinder was adjusted using the familiar measurements:

$$V_{bead} = 3.14 \times ((0.5 \times (D - A))^2 \times W$$

Values of volume in mm^3 do not reflect the true volume of the beads but simply help to divide them by size into categories. This formula provides less accurate volume estimation for spherical and pear-shaped bead categories. Figure 3.4 provides comparison of volume estimations within the set. It is possible to observe several categories of samples by size (distinguishable by the minima on the plot). Samples with less than 10 mm^3 are quite numerous – 26. Together with the ones below 50 mm^3 they are 58. Slot 40-50 mm^3 makes a regional minimum on the graph with just 6 samples. This category of samples is named “very small” samples. It is followed by “small” samples that includes 50 samples and is distinguished by the regional minimum at 90-100 mm^3. Medium sized beads (47 samples) have their volume estimations from 100 to 600 mm^3. Large beads are less frequent (34 samples) in the assemblage and their volume estimations are more evenly distributed over a larger range – 600 – 1600 mm^3. The rest of the beads (21 samples) are considered very large.

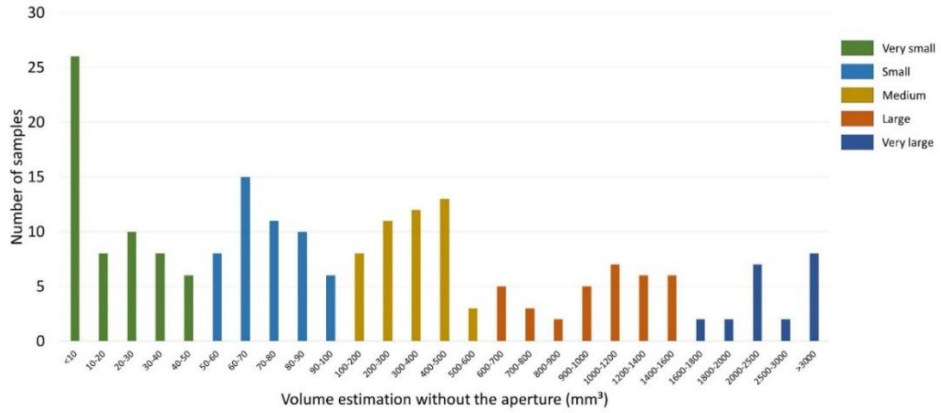

Figure 3.4. Distribution of sizes of beads according to the volume estimation. Volume estimation almost certainly overestimates real volume. Scale step increases with volume.

The division on categories by D/W and D/A ratios as well as the volume estimation demonstrate the significant variability in shapes and sizes among the beads from South Etruria and Latium.

3.2.2. Decorations.

By decorations we mean any shape and/or colour modification on the body (or base) of the bead, done deliberately to aesthetically enhance the appearance of the final product and to highlight morphological features. They presence or absence of any kind of decoration is crucial for distinguishing various types of beads. Reckoning of decorative elements was not straightforward for this assemblage, mostly because of the preservation state of the beads. On a number of cases, the decorations applied in different colours were lost in the course of centuries. In those cases, where we can find similar bead with a complete decoration, we assume that it was the same as for the bead with the lost decoration. For example, VG55 bead (Figure 3.5 a) has only traces of its former ring-eye decoration, unlike other similar beads one of which is shown in the Figure 3.5 (b). Sometimes the surface of a bead is altered, and the decorative part is not visible and/or detached. Typological assignment in these difficult cases must be done by the experts in the field.

Being cautious, it was determined that among all the beads that have kept their integrity 91 (almost a half) have some kind of decoration. The different decorative elements that were documented on the surface of the studied beads are counted in Figure 3.6, to which we will refer until the end of the paragraph. The majority of them, i.e. 61 beads, feature the so-called eye decoration: mostly ring eyes, but also spiral, horned and double ring eye decorations were noted. Wave decorations on the bead bodies were encountered 8 times and additional 2 times in combination with line decoration. Ribs, i.e. relief decoration along the aperture direction, were observed on 6 complete beads. The so-called herringbone pattern was observed 4 times. Same number of beads feature various spots on the surface. The rest of the decorations are unique for specific beads.

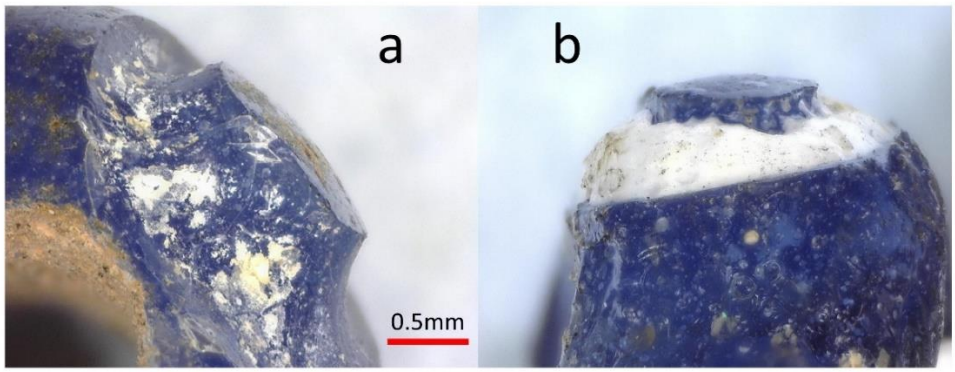

Figure 3.5. Groove of the detached decoration of sample VG55 (left) and the preserved decoration of similar bead (right) from Cerveteri, Sasso di Furbara. Scale bar is true for both images.

The above-mentioned decorations are not uniform across the samples, they are different by the manner of application, number of decorative elements per bead, etc. This variability is discussed below.

Eye decorations include several types of eyes. Most of the samples with this type of decoration have them as simple ring eyes (shown in the Figure 3.5 and Figure 3.7) made by a circle of differently coloured (opaque white or yellow) glass that does not rise above the surface. One sample – PG6 – has double ring eye decoration with concentric circles of lightly coloured glass. The number of eyes is usually 3 but for several specimens it is 2. The so-called "horned" stratified eyes influence the shape of a bead making its transversal section almost squared, as in the two samples that bear four of such eyes – PG84 and VG25. Another type of eye decoration is the spiral one. The spiral is created by twisting two coloured glasses (in this set, yellow and black appearing glass). PG166 is the only complete example within the set. A combination of spiral and horned eye decoration is also noted on PG122. All the types of eye decoration are included in Figure 3.7.

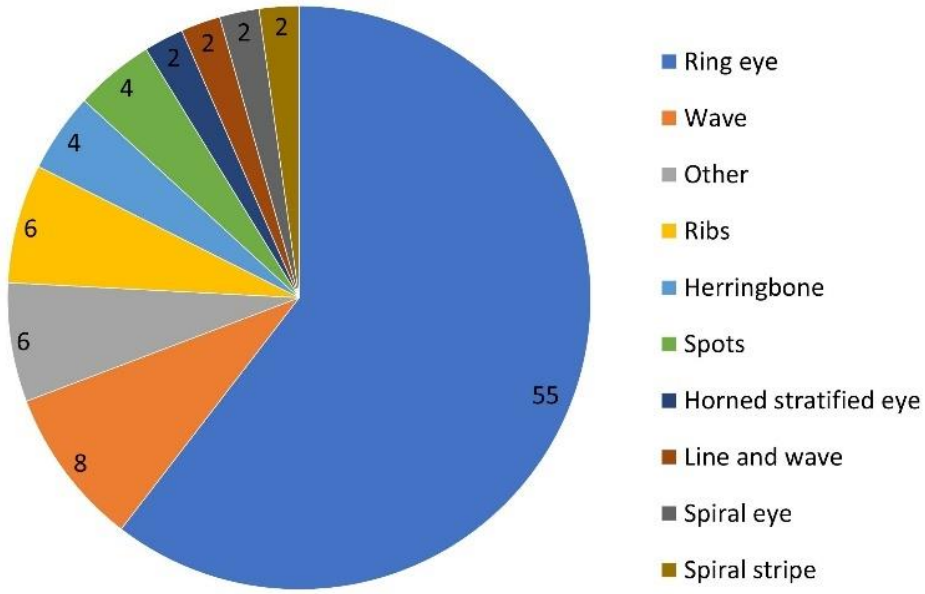

Figure 3.6. Number of occurrences of different types of decorations. "Other" includes double ring eye, double wave, horned spiral eye, line, protrusions and spiral stripe and spiral decorations that were encountered for a single object within the set of complete beads.

The wave decorations are usually applied in the middle of the width of the bead along the circumference. The number of periods of the wave depends on the circumference and it is usually from 3 for the smaller beads and up to 8 in larger ones. The number of wave decorations is usually 1 (Figure 3.7 VG37) but in cases of PG66 and VG30 they are 2 parallel waves. For some samples with angular cross sections (PG3 and 64) waves are combined with straight lines applied in the same direction (Figure 3.7).

Ribs are folds of glass mass that are made with a blunt tool to make relief decoration. They are parallel to the aperture. Axial sections of such beads remind a flower with 6-8 petals. All 6 complete samples with this type of decoration do not show traces of differently coloured glass application (Figure 3.7). Spiral decorations are mostly inherent to barrel shaped beads (Figure 3.7). Within the set of samples, the number of periods of revolutions depends on the width. Figure 3.7 presents an example of a bead that have spiral line with very few revolutions applied on a bead that is made in shape of a bird by making protrusions of glass in the shape of a head and a tail that are partially broken (VG88). The presence of different coloured areas visible on the surface of the bead, without any symmetric relation were identified as spot decorations. The spots (different number is present on each bead from 2 to 10) are usually coloured white or red. The only example of herringbone decoration on the bead's surface within this set is VG81 (Figure 3.7).

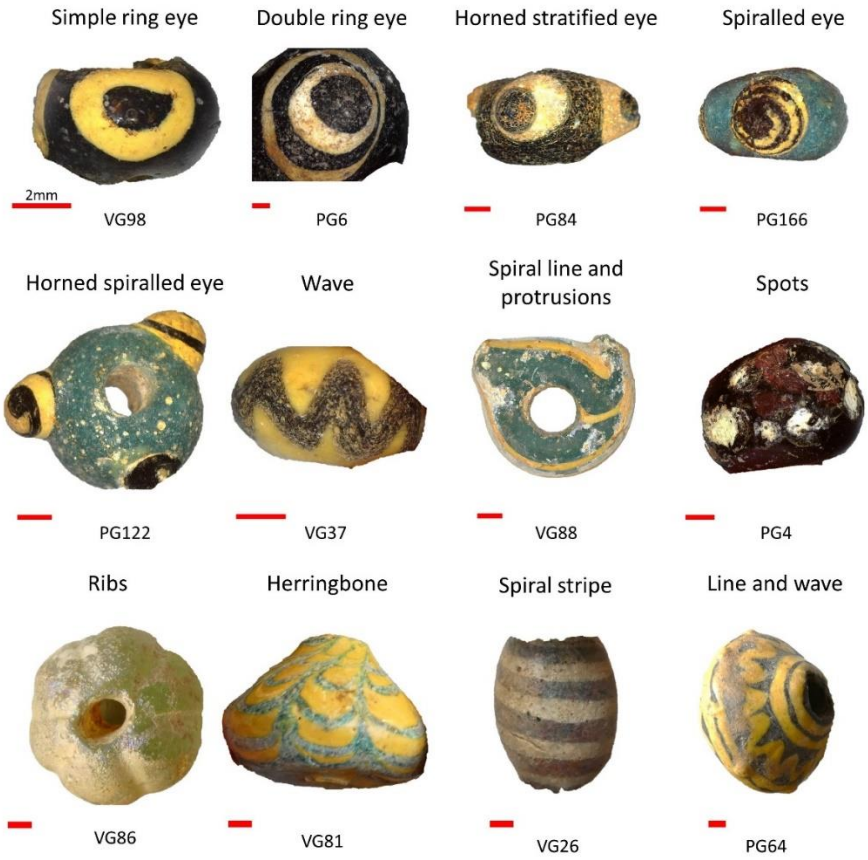

Figure 3.7. Representatives of samples with the most common kinds of polychrome decoration. Scale bar next to each image is 2mm.

3.2.3. Translucency and colour.

Colour is one of the most evident characteristics of ancient glass, which therefore usually plays a crucial role for the identification of specific categories of samples or types of glass. Together with translucency, colours reflect chemical composition features, unlike the previously discussed attributes, that mostly are the reflection of glass-working skills of ancient artisans. Yet, detection of colours has always been challenging (Gerharz et al. 1988; Ohta and Robertson 2006) and even more so for ancient glass, the colour of which can be affected with time (Abd-Allah 2009; Comite et al. 2020; Babini et al. 2022). Colour variation in ancient glasses is often observed within a same object, substantially complicating an "objective" evaluation of colour for typological purposes (Guido 1978; Karklins 2012). Nevertheless, colour documentation of glasses is possible with spectroscopic methods that operate in the visible light range and is widely used. If some favourable conditions are kept, it is also possible to assess the colour of ancient glasses (Babini et al. 2022 and references therein).

Glass beads are objects with oblique surface and those that are concerned in this study have rather small dimensions (most of the objects are less than 1 cm across). These factors make colour

estimation by means of spectroscopic techniques more difficult. In this study, both opaque and translucent glasses are considered. Translucency (diaphaneity) shall be considered as a separate characteristic for describing the appearance of glass, and therefore as a separate attribute for typology, but translucency can also change the perceived colour of glass. In this study, the translucency parameter was assessed by holding the bead by the apexes against the same light source and observing how much light passed through the body of a bead. The 5-step scale was adopted: 1 – there is no light transmitted through the bead – opaque; 2 – very small amount of light is passing through – semi-translucent; 3 – some light is passing through – translucent; 4 –much light is transmitted – semi-clear; 5 – nearly all the light is passing through with a possibility to distinguish darker and brighter areas behind the bead – clear. This simple assessment depends also on the size of the bead, size of its aperture and the state of the surface, which introduces biases. For the discussion of glass chemistry, the real and more fundamental division is the difference between opaque and translucent glasses. Figure 3.8 presents the distribution of samples according to their translucency values with some examples of beads with certain degree of translucency. It can be observed that almost half of all the objects considered can be described as opaque. Semi-translucent glasses, that are usually heavily coloured translucent glasses, make up almost quarter of all the beads considered. The share of translucent and clear objects is not the major one.

Colour measurements were done on the images by acquiring digital photographs in standardised conditions. Each bead was photographed with Panasonic DMC-TZ80 digital camera mounted on a tripod to take images of objects placed on the horizontal plane at the right angle from approximate height of 12 cm (subject to focusing for each session). Camera's white balance and exposure settings were adjusted for each photography session using X-Rite ColorChecker Passport reviewed by Myers (2010). This set of targets have white, grey and colour plates for setting up photographs. Photographs were acquired in RAW quality. Each sample was photographed in the natural light and artificial light conditions. Artificial light was supported by the 16 diode LED USB lamp directed at approximately 45°. The room was darkened to eliminate all external light. During the natural light photographs acquisitions, the settings were adjusted every several hours to offset the change in the room lighting due to the natural change in the angle of the sun. It was avoided to make photographs under the direct sunlight. In both settings, samples were placed on a grey paper to ensure same background of the photographs. Each session (change in settings of a camera) was started with the acquisition of ColorChecker photograph for creating session specific profiles for colour correction.

After the photographs were acquired, they were colour-corrected using the above-mentioned photographs of the colour target. Profiles were created in the Adobe Photoshop software with help of the DNG profile manager and ColorChecker camera calibration software from X-Rite. Batches of photographs of the objects were corrected using specific profiles and saved as JPEG files. RGB colour coordinates were extracted using ImageJ software from the representative areas of each coloured square of the ColorChecker (Figure 3.9, a), this procedure was repeated for all the corrected photographs of the target to assess reproducibility of the colour coordinates for each profile and setting.

Figure 3.8. Distribution of samples according to the translucency degree with typical representatives of each category.

The profiles were divided into two groups according to the lighting condition: the artificial light and the daylight ones. Their reproducibility was checked by the comparing the RGB data obtained for the different sessions on all the colour squares in the ColorChecker. Figure 3.9 presents such comparison of values in the tri-plots (b and c). Each square of the ColorChecker has specific number and colour in the Figure 3.9. The number of data points for each colour/square corresponds to the number of profiles prepared during the photographic campaign. It can be noted that the daylight profiles demonstrate higher consistency of the data – points of each colour are placed closer to one another with considerably fewer cases of the overlapping with other colours. This might be caused by the uneven lighting that illuminates certain region of the colour chart more than the other. Diffused sunlight seems to give more consistent lighting. That is why the decision was taken to extract RGB colour values from the images of objects acquired in the natural light conditions.

In the Figure 3.9 data of the squares 19 – 24 are falling into a small area approximately in the centre of the triangle. This is because these squares represent the grey scale from white to black, therefore their red, green and blue values are approximately equal for each square. The normalisation that is needed to make tri-plot equalises such values and makes them appear in the same spot, regardless the saturation. A different plot is needed to differentiate the light samples from the dark ones. An example of such plot is presented in Figure 3.10. There, the mean red, green and blue values of each of the 10 daylight profiles are grouped together by the square of the ColorChecker. Squares 19-24 are well separated, without any overlapping.

All the above-said substantiates two key statements: different colours of objects can be readily distinguished with the applied procedure using the images of such objects, and images taken on different days and/or camera settings provide reproducible information. This allows to use RGB values acquired from the images of the beads with the purpose of typological grouping.

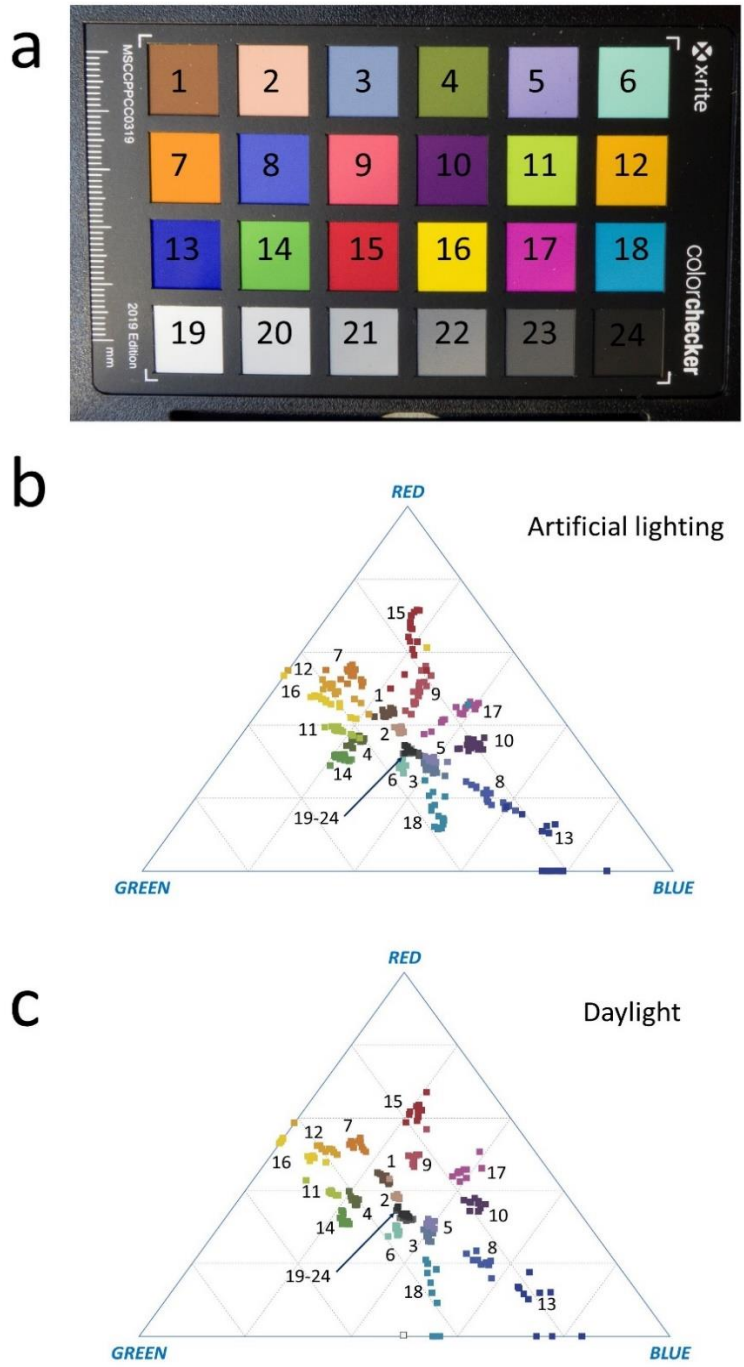

Figure 3.9. Colour palette of the X-Rite Passport ColorChecker (a) with numbers given to each colour. Tri-plot of colour coordinates (RGB colour space) acquired from the colour-corrected images of the ColorChecker in the artificial lighting conditions (b). Tri-plot of colour coordinates acquired from the colour-corrected images of the ColorChecker in the natural lighting conditions (c).

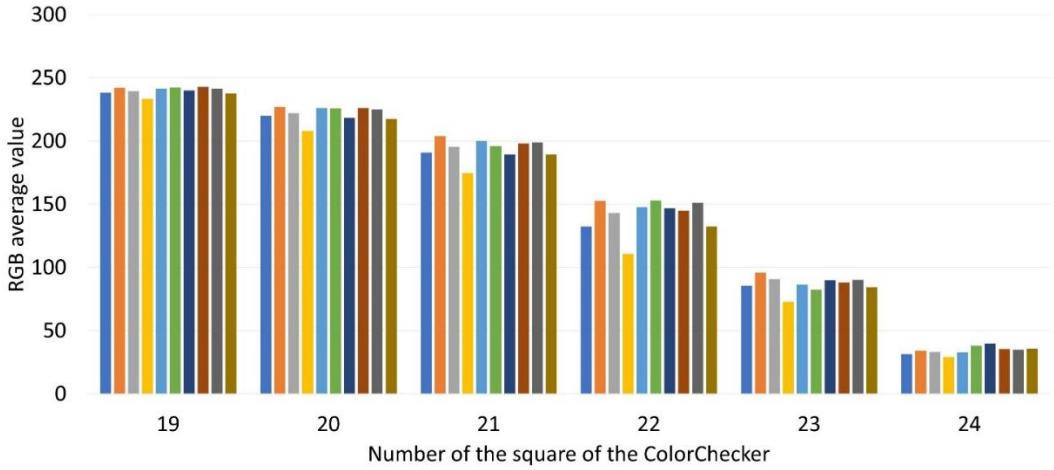

Figure 3.10. Mean RGB values of the daylight profiles (n.10) of the squares 19-24 of the ColorChecker.

Figure 3.11 presents the values of samples plotted in the similar way already presented for the data of ColorChecker. The average values for each square of the ColorChecker, calculated for the 10 profiles reported in Figure 3.9 and for the values reported in Figure 3.10 were inserted in the tri- and bar plots for reference. The tri-plot of the RGB values shows that the beads are mostly arranged along the Yellow-Blue axis with orange (square 12 of the ColorChecker) being the endmember on the yellow end and purplish (square 8) being the blue endmember. Some samples are deviating from the main trendline mostly in the bluish green-cyan direction (squares 6 and 18 respectively) (Figure 3.11, a). Several samples tend to be closer to brown-red zone (squares 1, 7, 9 and 15). Several groups of samples can be identified in the plot, they form densely packed groups in certain regions of the graph. Perhaps, they reflect types of differently coloured glass. The cloud of datapoints reaches its highest density near the centre of the tri-plot where data of the squares 19-24 are situated. The bar plot of Figure 3.11 (b) can bring clarity regarding the difference according to the grey scale. Mean value of R, B and G coordinates was calculated for each sample and the resulting values were sorted in the ascending order. Values of the squares 19-24 were inserted for reference. It can be observed that samples form a continuum with smooth transitions from darker to lighter colour. This way of presentation allows us to see in a dimension that cannot be presented by the tri-plot. Samples tend to be mostly dark, but their apparent “darkness” can be misleading. Brightly coloured samples would tend to have lower average values because only one or two coordinates would have high values while at least one has low ones. That is why attention should be paid to the position of a sample in the tri-plot – the further sample is from the centre – the less reliable is its position in the bar graph. These two plots will be presented together in the following chapters to discuss the colour properties of the beads.

The divisions considered in this section will serve as methodological basis for the division of the set into the typological groups of beads. Detailed documentation of the beads is present in the Appendix 3. It contains the samples used for establishing the categories in this section. Samples that

did not provide the opportunity to document all the attributes are omitted. It was demonstrated that measurable attributes of beads - if documented in according to a standardised procedure - can be used for description of individual beads and groups of beads.

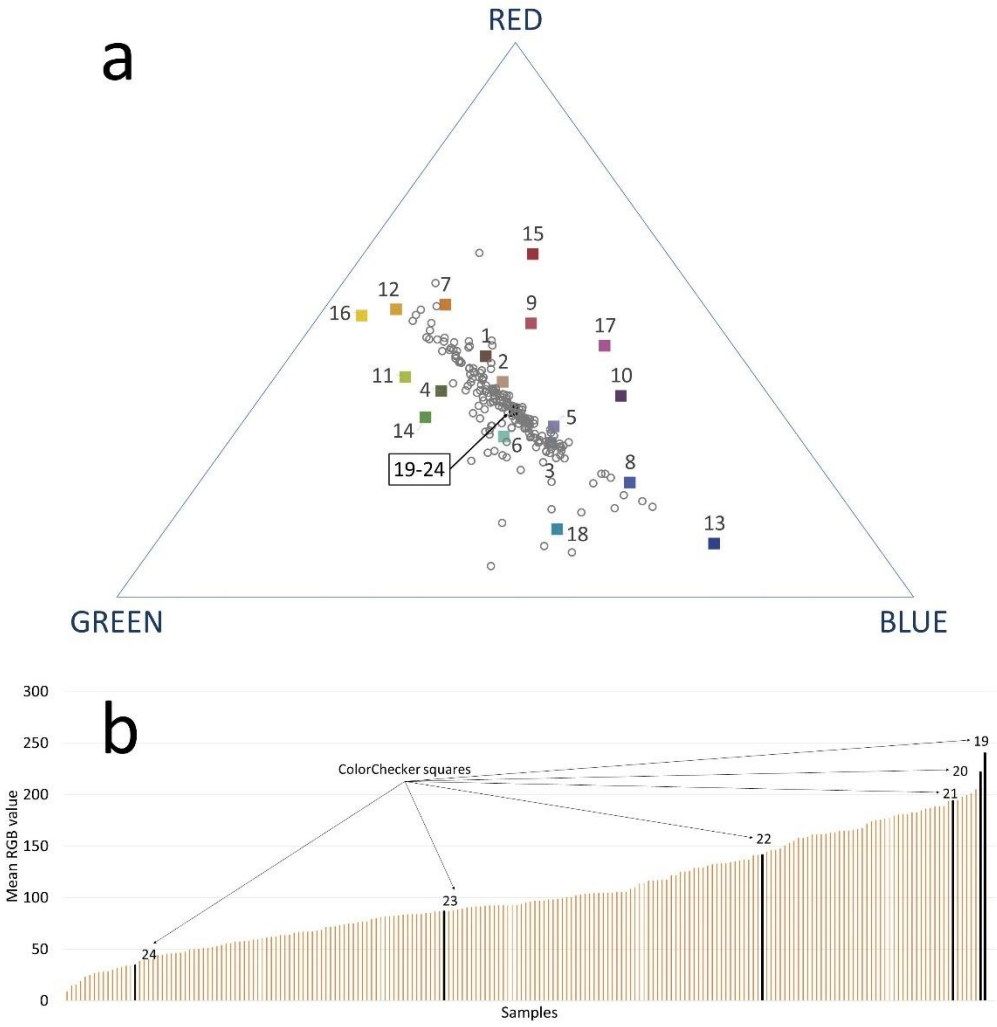

Figure 3.11. Tri-plot of RGB values of beads marked as grey circles (a) with ColorChecker RGB values places for the reference. Mean RGB values of same set of samples with ColorChecker squares 19-24 (white to black) set for the reference (b).

Table 3.1 provides verbal characteristics of the parameters along with their measurable meaning. Numerical measures are beneficial because they allow for direct comparison and for creating a system of robust indicators of certain typological features. RGB values did not provide defined categories of objects. Verbal, subjective indicators will be used to describe the beads, though individual RGB values of the samples will be used during analytical data presentation and statistical analysis of data.

Decorations parameter does not have numerical indicators except for the number of decorative elements. Types of the decorations were assigned arbitrary numbers to include them in the statistical analysis in the attempt to obtain a data-driven typology of the artefacts that would consider all the important attributes of the beads.

Table 3.1. The parameters of beads' visual characterisation and their scales that were applied to the description of types. Data on colour and the kind of decorations are not included due to the absence of scales.

Volume estimation	**V (mm^3)**	**Shape**	**D/W**	**Relative aperture size**	**D/A**	**Translucency**	**T**
Very small	<50	Tubular	<0.9	Small	>4	Opaque	1
Small	50-100	Spherical	0.9-1.1	Small-intermediate	3-3.75	Semi-translucent	2
Medium	100-600	Spherical-oblate	1.1-1.5	Large-intermediate	2.25-3	Translucent	3
Large	600-1600	Oblate	1.5-2	Large	1.5-2.25	Semi-clear	4
Very large	>1600	Flat	>2			Clear	5

3.3. Groups of glass beads included in this study.

The categories described in the previous section helped to divide the set into groups based on the attributes (characteristics) that were thought to be relevant for such division. The reason behind the grouping is to consider similar glasses together, but at the same time it will be important to see whether the particular configurations (or types) of the beads were made of chemically similar glass.

The beads were considered separately from Non-bead objects, that constitute a minor number of samples discussed in this work. The latter ones are presented in a following section.

As for the beads, their diversity was assessed, and 18 typological groups were created with differently-looking beads in each one. The higher order of division was by the colours and presence of the decorations (that usually were introducing other colours of their own). The colour division is aimed at facilitating the discussion of the analytical results, as differently coloured glasses are also compositionally different. That is why each group includes (with rare exceptions) similarly coloured glasses, even though the shape of the beads, which is one of the main typological criteria here, was the same.

The term "type" was avoided in order to avoid suggesting that groups of objects consist of objects of the same archaeological type, though in many instances this is the case.

In some instances, objects that could be considered as different types by archaeologists were considered together in the same group; or objects of the same type (by shape and way of manufacturing) but different by colour were divided by the colour characteristics into different groups. This was done to facilitate the discussion on colourants. Additionally to the 18 groups of beads, there were beads that could not be assigned to any group, having unique configuration and,

consequently, belonging to a different type. Each of those individual beads makes up a type of its own, therefore they are comprised here in the Other beads group. In the presentation of the results (Part II of the dissertation) the Other beads and the Non-beads are considered together with beads made of similar glass, i.e. certain number of Other beads and Non-beads is considered in almost every chapter of the results and discussion depending on the appearance of each object.

The division adopted in this study is schematically presented in Figure 3.12.

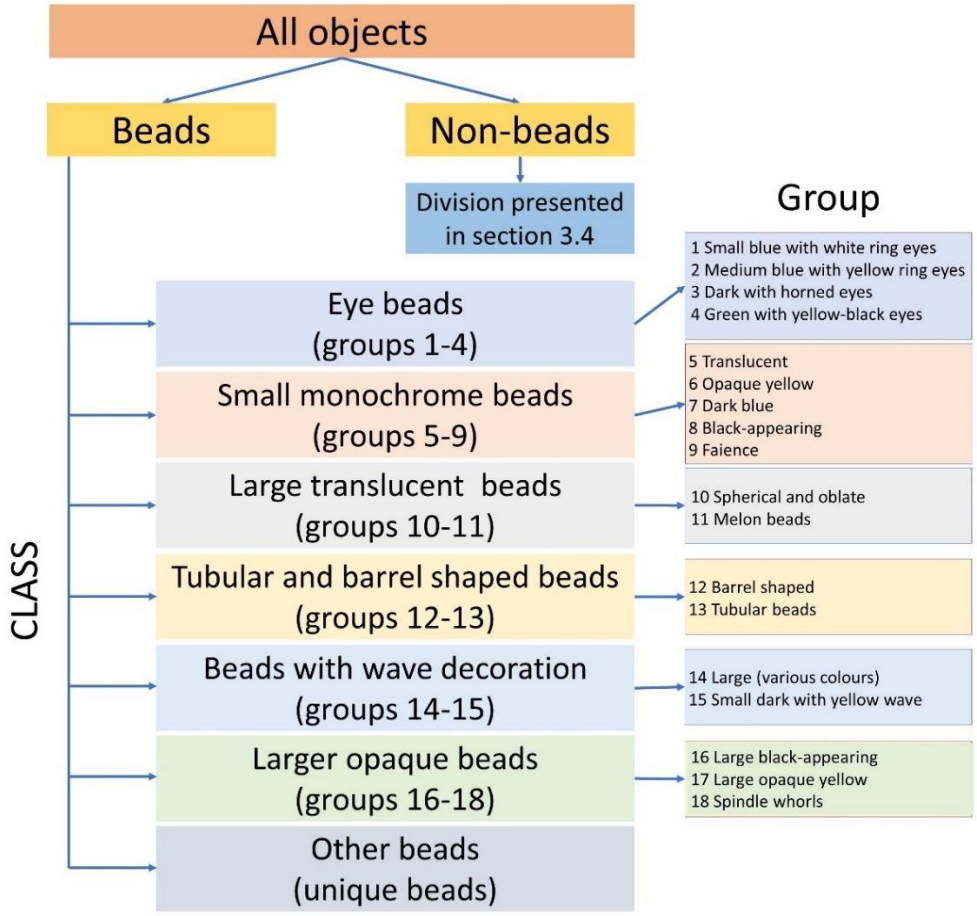

Figure 3.12. The major order of division of objects within this study.

Such division is arbitrary and was made solely for facilitating the navigation through the sample set within the scope of the present study. The first level of division is between beads and non-bead objects, that were studied alongside with the beads that make the bulk of the list of samples within this study. The bead objects can be divided in 7 classes: eye beads, small monochrome beads, large translucent, tubular and barrel shaped, beads with wave decoration, larger opaque beads and, finally, Other beads. Each class contains several groups of beads.

The division that was made by the visual examination of the beads was checked and displayed by Principal Component Analysis (PCA), which uses an algorithm for dimension reduction presenting variance of the datasets and finds countless applications, including glass studies (Baxter 1989; Renda

et al. 2019). In typological, or, at least morphological, studies, multivariate statistical analyses were also applied with a mixed success (Van Der Maaten et al. 2009; Buchanan and Collard 2010; Baxter 2015; Lucena et al. 2017; Garcia-Medrano et al. 2020). Recently, multivariate analyses in typology are not in high demand (Van Der Maaten et al. 2009) due to the issues pointed by Baxter (2015), who highlighted both methodological issues and argued on its general usefulness. In this study, the role of the PCA is in visualising the division and checking what attributes were most efficient for the distinction of groups.

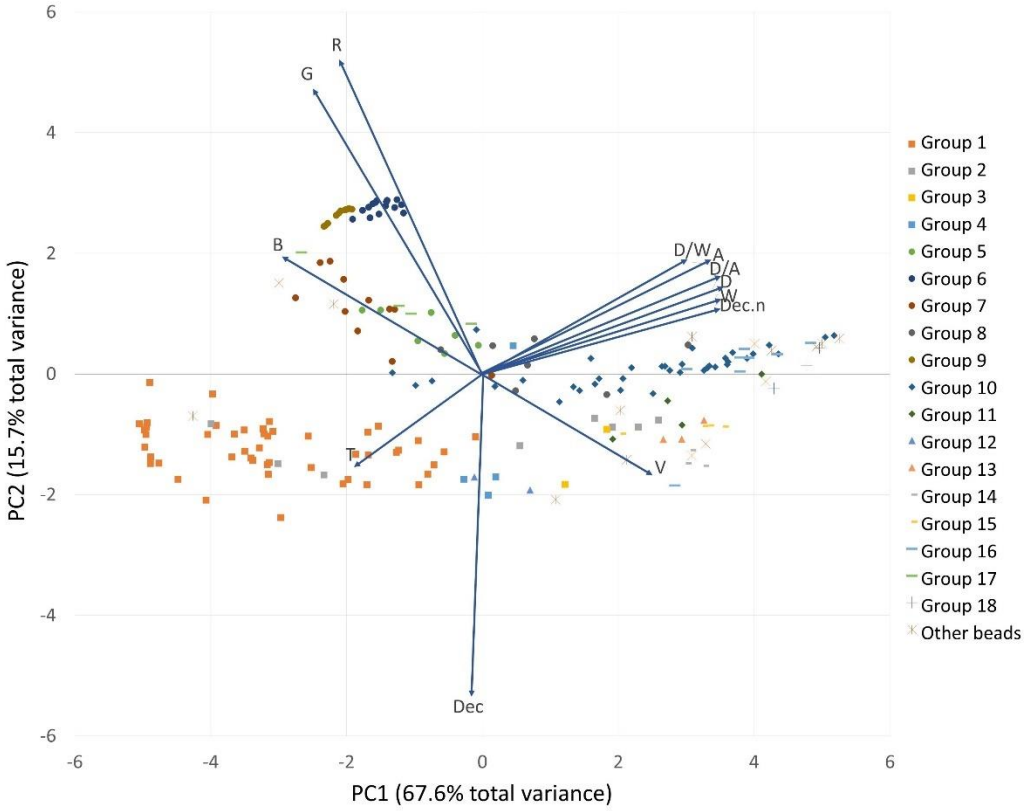

Figure 3.13. PCA results. PC1 vs PC2 binary plot. Scores and loadings are displayed in the same plot. Loadings were multiplied by 10 to improve legibility of the plot. Beads with eyes are marked by squares, small beads without decorative elements – by rounds, translucent beads of bigger size – by diamonds, tubular and barrel shaped beads by triangles, beads with wave decoration by short dashes, large opaque by longer dashes, pear shaped or spindle shaped beads by plusses, Other beads represent the beads that are unique within the set. Variables are: D – diameter of the bead; W – width; A – diameter of the aperture; D/W, D/A are derivative from the former three as well as V – volume; T – translucency; R, G and B – colour coordinates; Dec. – kind of decoration; Dec.n – number of decorative elements.

12 variables were selected for the analysis. Diameter (D), width (W), aperture diameter (A), D/W ratio, D/A ratio and volume (V) are the variables that represent the size and shape parameters.

The three latter ones are derived from the three former ones as described in section 3.2.1. Apart from these six, three – R, G and B represent colour coordinates of the bodies of the beads (excluding decorations). Translucency estimation (T) was also included in the list of variables. The last but not the least two variables that describe the decoration were added to represent the kind of decoration (Dec.) and the number of repeated decorations (Dec.n). It was crucial to make Dec. value somehow quantitative as decorations play prominent role for the glass identification. Each kind of decoration was assigned a number that was used in the computation.

The data were Standard Normal Variate (SNV) normalised before calculating principal components. PCA was done using Chemometrics Agile Tool (CAT) open-source software.

Seven principal components were calculated and represent 99.85% of total variance within the set, with the first two bearing most of it (67.47% and 15.43% respectively). Figure 3.13 shows the results of the PCA (loadings and scores are displayed together).

Figure 3.13 demonstrates that the division along PC1 is determined by variability of size and shape variables with colour and translucency ones. Variables related to the shape and size (D, W, A, D/W, D/A) appear correlated, but the volume (V) parameter is more independent. Samples of several groups are stretched along PC1 which is an indication of variability within the outlined types. PC2 is influenced by the type of decoration and colours. Several groups form B – V variables axis and are stretched along it.

We will refer to the results of the PCA in the discussion of individual groups below. Parameters of individual beads are in the Appendix 3.

Table 3.2 gathers the information about each group of objects. The table highlights common features for each group across all the parameters, therefore excluding the exceptions mentioned in the text below.

Table 3.2. Groups of glass beads description.

Group	Number of objects	V	D/W	D/A	T	Colour	Decoration	Comment
1	57	Very small, small	Spherical-oblate, oblate	Small-intermediate, large-intermediate	2	Blue	3 opaque white simple ring-eyes	PG112 might be different group
2	8	Small, Medium	Spherical, Spherical-oblate	Small-intermediate	2	Blue	3 opaque yellow simple ring-eyes	Can be subdivided by size
3	4	Medium, large	Spherical-oblate, oblate	Small-intermediate, Small	1	Dark-green, red	4 horned, stratified eyes of white and dark glass	
4	5	Medium	Variable	Variable	1	Green	Spiral, sometimes horned spiral eyes	

Group	Number of objects	V	D/W	D/A	T	Colour	Decoration	Comment
5	7	Very small, small	Spherical-oblate, oblate	Large, Large-intermediate	3	Variable	None	
6	28	Very small	Oblate	Large, large-intermediate	1	Yellow	None	
7	22	Very small	Spherical-oblate, oblate	Large, Large-intermediate	1	Blue, dark	None	
8	13	Very small	Spherical, spherical-oblate	Variable	1	Black	None	
9	10	Very small	Flat	Large intermediate	1	Blue, yellow	None	Rectangular cross-section
10	54	Large, very large	Spherical, Spherical-oblate	Small-intermediate, Small	3, 4	Variable	None	
11	6	Large, very large	Spherical, Spherical-oblate	Small-intermediate, Small	3, 4	Blue, yellow	Ribs	
12	2	Medium	Tubular	Small-intermediate, Large-intermediate	1	Red	Spiral stripe of opaque white colour	
13	3	Large, very large	Tubular	Large-intermediate	2	Dark blue-green	Herringbone pattern	
14	3	Medium	Oblate	Small-intermediate, Large-intermediate	1	Blue, yellow	Single wave of various colours	
15	4	Very small	Oblate	Large-intermediate	1	Brown	Yellow wave	
16	9	Medium-very large	Spherical, Spherical-oblate	Variable	1	Dark	Various	
17	4	Medium	Oblate	Small-intermediate	1	Yellow	None	
18	3	Very large	Pear, biconical	Small	1	Variable	Variable	

3.3.1. Eye beads.

Group 1 (small blue beads with rind eyes) includes very small to small sized (up to 100 mm^3 volume estimation) beads of spherical-oblate to oblate shape beads with intermediate apertures (comparing to the diameter) of similar appearance. They are blue with the appearance from opaque to semi-translucent (grades 1 – 2). Most of them are decorated with 3 simple ring-eyes of white glass, though in many cases the decoration glass has detached leaving a groove (seen in the Figure

3.5). These beads are contained within bottom left quadrant of the PCA plot (here and below Figure 3.13 is referred to when PCA is mentioned). The group representatives are stretched along the PC1 axis demonstrating the variability in size, shape and translucency outlined above. Such variability is determined by the difficulty to create small glass beads of exactly same size and colour by the winding method (section 1.3). 48 whole beads are present in the plot and used for visual characterisation of the group. 9 more fragments of the beads with similar appearance were added to this group. It must be noted that sample PG112 was only tentatively attributed to this group, as its fragmentary state prevented the straightforward recognition of the specific features of the decoration, which could be also interpreted as a spot decoration instead of the eye one. Photographs of the beads of this and subsequent groups can be found in Appendix 2.

Group 2 (medium, blue with yellow ring eyes) includes far fewer objects – 8 beads in total. Yet, this group of objects can be recognised by their size which is evident from the PCA plot. There are three (VG72, 98 and 99) beads that can be described as small, which would place them together with the group 1 beads, while the rest (VG59, 64, 65 and 91) are medium sized (grouped in bottom right quadrant). VG80 with the volume estimation of 635 mm^3, is actually classified as large, but this is because it has a smaller aperture compared to the diameter (D/A is 4). All these samples tend to have small-intermediate apertures and their shape can be termed as spherical to spherical-oblate. The features that keep them together are the semi-translucent appearance of the deep blue base glass and the 3 yellow ring-eye decoration.

Group 3 (dark with horned eyes) was defined here by only 2 objects – VG25 and PG84, both featuring horned eye decoration which holds them together in this group. They appear in fact quite separated in the bottom-right quadrant of the PCA plot. VG25 is large, spherical-oblate opaque bead with a small aperture. It has patches of red and green colour without precise boundaries. PG84 is an opaque, dark green, medium sized, oblate bead with small-intermediate aperture (seen in Figure 3.7). Similar to these two beads, that were used to define this group, other objects that lost their stratified eyes – PG87 and 167, were also included in this group.

Group 4 (green with yellow black eyes) refers to green-coloured, opaque, medium sized beads. They have different configuration of eyes that are spiral and can be levelled with the body surface of the bead or form protrusions or horns, so more than one type can be distinguished within this group. The beads have very different D/A and D/W ratios. In addition to the 3 objects considered to define the group, a further fragment (PG121) that demonstrates similar glass appearance was added and PG160 that might have lost its decoration, having spots of dark glass in the pits on a surface of the bead.

3.3.2. Small monochrome beads.

Group 5 (small translucent) is a set of differently coloured beads that includes semi-translucent and translucent beads of very small and small sizes, mostly spherical-oblate and oblate shape, though there are two flat beads as well. The apertures are predominantly large-intermediate, which allows to refer to these beads as ring-beads. No decoration is documented on these beads. Colours range from blue (PG69 and 70) to yellow (PG71, 72 and 154) and purple (PG75 and 76). The difference in colour and translucency is reflected in the PCA plot though the beads are all in top left quadrant situated along the B axis. Seven samples are included in this group.

Group 6 (opaque yellow) occupies small area in the PCA plot despite the large number of samples – 28 whole beads were considered. It is a very standardised set of very small beads of oblate shape with large to large-intermediate apertures – ring beads. They all are made with opaque yellow glass – hence the high position in the PCA along R and G variables.

Group 7 (dark blue) refers to twenty-two beads that have opaque dark blue and dark appearance. This group slightly overlaps with group 5 in the PCA plot. The reason for this is similar size and shape parameters except for smaller D/W ratio and smaller volume estimation in group 7 beads. Samples of this group exhibit narrower range of colours, though one of them (VG24) is dark red.

Group 8 (black-appearing) represents very small, mostly spherical to spherical-oblate beads that appear opaque black. They have large and intermediate apertures. Apart from seven whole objects, this group is supplemented by six beads in the fragmentary state. These samples are very scattered in the PCA plot, perhaps due to the relatively low scores on every parameter except D/A and D/W, that are very variable for these pieces.

Group 9 (faience) is composed of ten objects that might be faience. They are highly standardised very small, flat beads with rectangular frontal cross-sections. They have large intermediate aperture. The colours vary depending on the preservation state, but their original surface might be light blue. They are opaque. In the PCA plot they are situated close to the group 6, but they are skewed towards the B variable due to the difference in colour.

3.3.3. Large translucent beads.

Group 10 (spherical and oblate) consists of translucent beads. Their size ranges from medium (due to the large aperture) to very large, yet large and very large beads take 75% of total number of the whole beads of this group. The beads are mostly translucent and semi-clear but there are semi-translucent beads (PG1, 63, 104 and 140) as well, as the assessments of translucency might be compromised by surface degradation. The apertures are small-intermediate and small (exceptions PG11, 67, 68, VG53 and 90). The shape – spherical and spherical-oblate with exceptions of oblate and flat shape (PG11, 12, 33, 67, 104, VG14 and 48). The subdivision by colour is next: yellow to brown or so-called “honey” variety – 18 samples; beads with very weak colouring – 18; green tinge – 10; blue tinge – 8. Such division is arbitrary and somewhat subjective. There is no identifiable clustering of beads by colour but rather a spectrum of shades from yellow to dark blue. High variability is reflected in the PCA plot. These beads are stretched along the PC1, probably due to the size and colour difference.

Group 11 (melon beads) beads are characterised by the surface with ribbed or melon decoration that produces a flower-like transversal cross section. This is their only difference from typical representatives of group 10. In the PCA plot they follow parallel trends but are distinguishable precisely because of non-zero decoration scores. The samples are not numerous – 4 complete beads (PG39, 88, VG15 and 86) and 2 fragments (PG89 and 136).

3.3.4. Tubular and barrel shaped beads.

Group 12 (barrel shaped) apart for tubular (rather barrel) shape (D/W <0.9) the two beads (VG26 and VG29) included in this group are characterised by medium size, intermediate apertures,

and opaque red appearance. Spiral stripe of opaque white glass makes 3-5 overlaps around the beads' bodies (can be seen in Figure 3.3). In the PCA plot they are overlapping with group 4 probably due to the similarity in size and spiral decorations (group 4 has spirally formed eyes).

Group 13 (tubular) is represented by 3 exemplars – PG162, 163 and 164. They are the widest in the entire set reaching 7 cm between the apexes. Naturally, they are large or very large in size. Their apertures are large-intermediate. The narrow decorative spiral was wound around the bead body more than 20 times. It was fashioned into a herringbone pattern. The decoration was lost, but the residual grooves are visible. Samples are of semi-translucent, dark blue-green glass. The beads are well separated from the group 12 in the PCA plot being situated with a major part of group 2 (bottom right quadrant).

3.3.5. Beads with wave decoration.

Group 14 (large beads with wave) comprises larger specimens with wave decoration. They are 3 samples – VG33, 34 and 37. The first two have blue bases while the latter one is of yellow colour. They all are of similar size and shape, though, – medium size, intermediate apertures and oblate shape. The wave decoration makes 6-8 periods in the middle of the bead. The glass of decoration is yellow (VG33), white (VG34) and grey (VG37). This group is situated in the bottom right quadrant of the PCA plot.

Group 15 (small dark with wave) consists of four very small beads with wave decoration. They are oblate in shape and have large-intermediate apertures. Due to their size, the opaque yellow wave decoration only makes up to 3 periods. The bodies of these beads are dark in colour.

3.3.6. Larger opaque beads.

Group 16 (black-appearing) comprises beads of medium to large size with black appearance (9 samples in total). They do not always have decoration on them, but sometimes they have spots (PG4, 144, 173, 174 and VG50) of red and white colour. PG123 has hints of rib decoration similar to that of the samples of group 11 but kept in this group because of the glass appearance. Their apertures are variable in their relative sizes – from intermediate to small. Regarding the shape, they are spherical to spherical oblate.

Group 17 (opaque yellow), 4 beads are made of opaque yellow glass, although the texture would suggest they could be faience. They are medium sized beads, with the exception of VG19, which is small, of oblate shape and small-intermediate apertures. Unlike group 16, that on PCA plot is mostly overlapping with group 10 due to the similarity in size and shape, group 17 is overlapping with groups 5 and 7 – smaller beads of various appearances. These beads do not bear any decorative parts.

Group 18 (spindle whorls) includes three beads (or small spindle whorls) of pear and biconical shape (angular cross sections from Figure 3.3) samples. They are very large specimens with small apertures. The base glass is different in colour: PG3 is dark with groves of decoration without the signs that they were filled with differently coloured glass; PG64 has base of grey colour covered with opaque yellow wave and a straight-line decoration that are parallel to each other; VG81 (can be seen in Figure 3.3) has opaque yellow base (or at least is covered with such glass) and blue decoration

that forms a somewhat twisted herringbone pattern. It is evident that each sample in this group belongs to a different archaeological type.

3.3.7. Other beads within the list of studied objects.

Within this study, we also find a heterogeneous group of twenty beads that do not fit in any of the groups described above. They are described here following the same structure already used in Table 3.2 and sub-sections above. Although some similarities with the beads included in the previous groups can be recognised, the differences prevailed and therefore they were not included into any of them.

PG5 is a large black appearing bead with three parallel lines that go perpendicularly to the aperture. PG6 has double ring eyes on dark and opaque body. It is one of the largest beads in the whole assemblage. PG32 is a very small dark ring bead (spherical-oblate shape with large-intermediate aperture) which has two ring-eyes of white glass. It would fit group 7 if not for the decoration. PG58 has simple ring eyes. It is very large bead of spherical shape with small aperture. PG66 is a medium sized tubular bead of opaque, dark appearance. It is decorated with double white wave. It is different from the tubular beads that make up groups 12 and 13. PG90 could fit group 18 with its large size biconical shape and wave decoration except for the translucent colourless appearance. PG113 is a large tubular bead with very degraded surface that looks dark and opaque. It has spiral line decoration. PG114 is very large spherical-oblate bead with small aperture. It has three simple ring eyes. PG168 is a medium sized bead without any decoration. It is of spherical-oblate shape and could fit the group 10 beads except for its deep blue colour that is closer to group 14 representatives. PG169 has a shape of a pear but the size and colour are closer to group 4 beads. It does not have any group of decoration. PG170 is medium sized oblate bead of opaque blue glass that has unique shade for the dataset. PG172 is a bird bead (decoration demonstrated in Figure 3.7 as spiral line and protrusions. There is another example – VG88 but these two beads are realised in very different translucent glasses: while the former one is purple with green decoration, the latter one is green with yellow decoration. VG16's appearance reminds those of group 6, but its surface is severely degraded. VG18 is similar in shape to group 1, but the size of the aperture and the state of its degraded surface makes it impossible to assign it to any group. VG27 is probably a faience bead with opaque green appearance and rib decoration akin to the group 11 samples. VG28 and 38 are similar, large, opaque and dark appearing beads with severe alteration of the surface. VG54 is similar to group 1 but much larger and oblate shape. VG85 is almost spherical opaque white bead of medium size. Samples mentioned in this sub-section are presented in Figure 3.14.

Figure 3.14. Other beads that are unique to the studied assemblage. Objects are situated from left to right and from top to the bottom in the order of mentioning in the text.

3.4. Non-bead objects.

The non-bead objects are a group of samples that could not be characterised together with the beads due to the differences in configuration and shape. It is much more useful for the study and for their adequate perception to divide them by their use. These objects often lack the essential part of the bead – the aperture. In this way, the highest order of division is dictated to be drawn in the way that all the beads are in one group and the Non-beads are considered separately. Representatives of the non-beads group are divided in several subgroups described below, though here the system of description applied above is obviously not applicable.

The non-beads are mostly constituted by buttons or pinheads, bracelets and fibula decorations. The latter ones do have apertures, but the rods were never removed from them while still in function, sometimes these objects are called beads though. The buttons and pinheads are considered together because these objects are the only ones truly without an aperture, and they are impossible to distinguish if found without the object they were attached to.

Figure 3.15 presents the representatives of these subgroups of objects. The buttons and pinheads are the most numerous – 10 objects (VG1-7, 9, PG57 and PG135) where VG1-7 and 9 are very similar, except for the colour and translucency part where there are blue, yellow, white and clear glass objects of flattened shape, round in the biggest dimension plane (face of VG1 in Figure 3.15) and oval in the perpendicular cross section. Dimensions are: diameter – 16.5 – 20 mm; height – 9 – 10.5 mm. These objects have small pits (cavities) on the back side with the traces of iron in them (proofed by the XRF measurements). PG57 is very different, unique piece of irregular shape that somewhat resembles a flower. The rims of folds of black appearing glass are covered with opaque yellow glass. It is 10.5 mm across in the biggest dimension. The pit or cavity of attachment is not pronounced. PG135 is an object of a spherical shape 6 mm in diameter with a small pit.

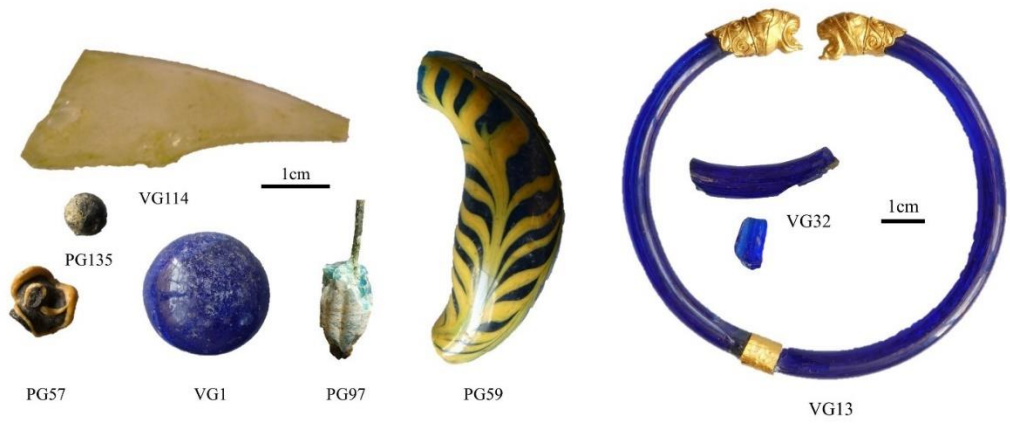

Figure 3.15. Non beads groups representatives. The buttons and pinheads (PG57 and VG1); Vessel fragment (VG114); Fibula bows and pendant (PG59 and PG97); Bracelets (VG13 and VG32). The scale on the left is to mark the size of former three groups of objects and the one on the right is the size reference of bracelet fragments.

VG114 is the only vessel fragment considered in this study. It was included into the sample set due to its archaeological relevance: it is one of the very few examples of mould-formed bowls in nowadays Italy (O'hea 2011). This fragment only allows us to conclude that the object was made of translucent glass with a yellow hue, with walls some 2.5 mm thick.

PG97 is a pendant with a metal core still inside. Despite its fragmented and degraded state, one can identify general elongated shape and a number of grooves applied along the aperture. VG56 also has a metal rod inside. The glass part consists of two beads of different diameters (19 and 14 mm) that are attached to each other and to the rod that makes their common axis. The rest of this group is comprised by the so-called fibula bows. They are decorative parts of fibulae made in glass, found mostly in the Italian peninsula (Koch 2010). The representatives of this type of objects are 6: PG59, 60, 61, 62, VG92 and VG93. They share the so-called "leech" shape being bent on the bow rod of the fibula. The herringbone decoration of yellow glass is applied on the semi-translucent blue (PG59 and PG60) or on opaque, black-appearing glass (PG61, PG62, VG92 and VG93). The straight measurement between the apexes is 39 – 46 mm, thickness in the middle – 11 – 15 mm.

The last type of objects considered in this sub-section is the bracelets. Among the entire set of samples selected for the study only two representatives appear: VG13 and VG32 (both in figure 3.15). They are rods of translucent blue glass (round in cross section) not more than 7.5 mm thick bent to form about 9 cm circle. VG13 has golden decorations in shape of lion heads.

All above mentioned 23 samples can be systematised in the way presented in Figure 3.16. This sub-set of samples demonstrates diversity that allows to readily divide it on the account of shape and consequently the manner of use.

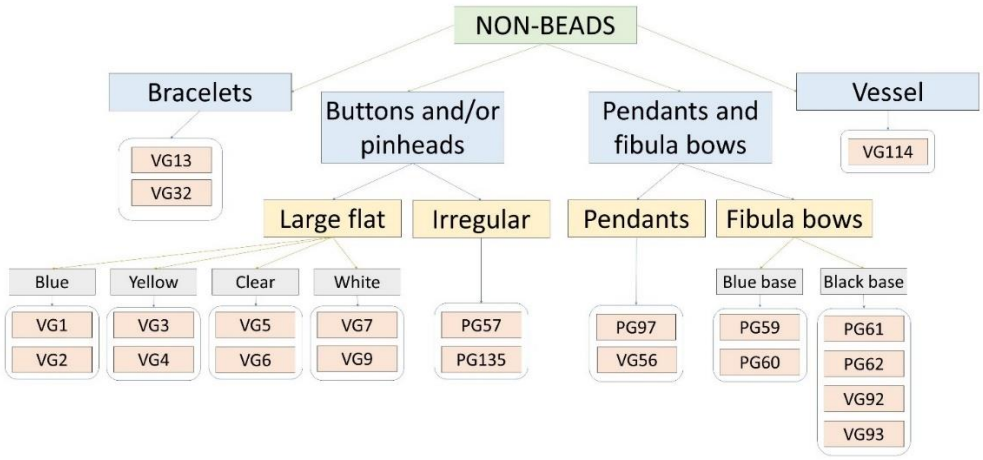

Figure 3.16. Schematic representation of the division of non-beads considered in this study.

3.5. Distribution of groups in space and time.

In this section we refer to the Appendix 3 where the information on archaeological contexts is gathered. Spatial distribution of glass objects was used by archaeologists to make suggestions on the places of glass production and, especially, working (Haevernick 1960; Harden 1968; Koch 2010), as

direct evidence is rarely encountered. As far as glass supply is concerned, the distribution patterns are important because on their basis it might be possible to reconstruct trade networks that existed in the past. Representativeness is the key to investigate the distribution. Since the set of samples discussed here does not cover all the glass collections within Middle-Tyrrhenian Italy that are dated to the Iron Age, the task of reconstruction of the exact distributions based on these data is foreknowingly futile. The purpose of outlining the distribution anyway is in the understanding and communicating the relationship among different groups of beads. The relevance of some of those groups will be discussed in the next section, connecting the types outlined above with the archaeological finds from literature and pondering whether the selected samples represent all of the Middle-Tyrrhenian Iron Age glass beads adequately. We start with the distribution of samples among the archaeological periods of the first half of the first millennium BCE – from the Early Iron Age I and II (EIA I and II) through the Early, Middle and Late Orientalising until the Archaic period. Another sub-section is dedicated to discussing how different types of objects are represented on each archaeological site in question.

3.5.1. Time frame of each group.

The period of time when a specific group of objects was deposited in the burials is discussed here. Such chronological distribution does not reflect all the instances of occurrence of similar objects on the other archaeological sites in South Etruria and Latium. Yet, the groups with numerous representatives (n. 1, 6, 7, 8 and 10) may reflect the actual distribution better as they belong to a bigger number of contexts. Figure 3.17 contains information on how many graves from the ones concerned in this study (mentioned in section 2.3 and Appendix 1) yielded particular groups of beads (upper numbers on the distribution chart). It can be seen that only beads included in group 1 and group 10 were found in more than 20 graves (21 each). The rest of the types were found in considerably fewer graves, and in many instances the beads included in one group were found in one or two graves (see Figure 3.17 for details), which cannot lead to any chronological conclusions without further comparative research. Consequently, in the latter case, the distribution bars are very short because they mirror the average date of the period that grave was assigned to. Figure 3.17 presents the chronological distribution of samples according to the archaeological periodisation for the region (discussed in section 2.2). It was pointed out in Chapter 2 that most of the glass beads involved in the study originate from EIA II and EO contexts. Figure 3.17 demonstrates that towards the end of the EIA II and beginning of EO period several types of beads cease to occur and other beads started being used in their stead. Types 1, 3, 4, 8, and 16 are more inherent to the EIA periods, while types 2, 6, 11, 15, and 18 tent to be assigned more frequently to the Orientalising periods.

Group 1 has only one representative in the grave that belongs to the EIA I (tomb 83 in Vulci-Cuccumella). Most of the group 1 beads (46 out of 57) belong to the EIA II period. 9 samples belong to different Orientalising periods, mostly Early Orientalising. Only one of them can be assigned to the Late Archaic making it a chronological outlier of the group. The blue beads with yellow eyes (group 2) in their mass are more recent than group 1 beads, though most of them are also from the EIA II period contexts. They are dated towards the end of it. There are also 2 representatives found in the graves of Orientalising period. Group 3 and 4 beads are mostly from contexts dated to the EIA

II period, with the exception of one bead in each group (that belong to the Bronzetti Sardi tomb from Vulci-Cavalupo and Terni-S.Agnese respectively).

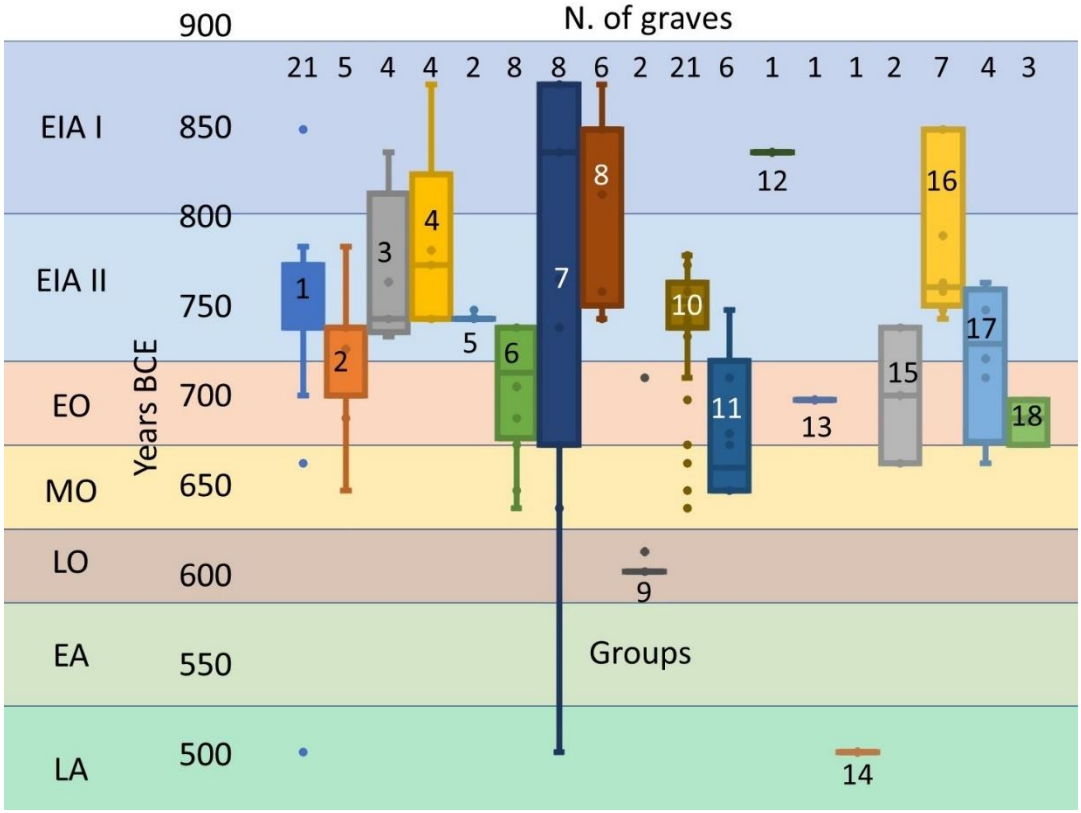

Figure 3.17. Distribution across time of different groups of beads. Spread bars were obtained from average value of the absolute dating window. Only the 18 main groups of beads are present (see section 3.3). Archaeological periods are outlined in colour of the background and on the left of the chart: EIA I and II - Early Iron Age I and II respectively; EO, MO, LO - Early, Middle and Late Orientalising respectively; EA and LA – Early and Late Orientalising respectively. Number on or below the spread bar is the number of the group. Number above the spread bar is the number of graves that yielded beads of specific group. Samples without grave context were adding 1 to the grave number if the site was the same, in case samples without context were from 2 or more sites they were counted as 2 or more.

Group 5 beads only originate from the EIA II contexts. Contexts in which Group 6 beads were found are spread between the end of the EIA II and Middle Orientalising period. The chronological distribution of group 7 beads is even wider – EIA I – Late Archaic (LA) period. Group 8 beads occur only in the EIA contexts. Light coloured flat beads (group 9) are represented only in the Orientalising period's contexts, mostly Late Orientalizing (LO).

Among the translucent beads, group 10 is the most numerous. They come from 21 grave, most of which are dated to the EIA II. Orientalising periods graves yielded minor number of objects that are included in this study. Interestingly enough, the beads with rib decoration (group 11) seem to be

deposited later in time – in Early and Middle Orientalising periods though one bead comes from EIA II context (tomb 26 of Cerveteri-Sasso di Furbara).

Tubular beads of groups 12 and 13 belong to two different graves that are distant from one another both in space and time. Group 12 beads belong to the EIA I context and group 13 to EO one.

Group 14 samples within this study were found only in one grave of LA context (Martiri Marescotti tomb (610) of Cerveteri-Monte Abatone necropolis). Group 15 beads are not numerous as well and belong to EIA II – Orientalising periods.

Group 16 beads are divided between two EIA periods which makes them coeval to other black appearing glasses (group 8). Group 17 beads seem to be more recent, represented by EIA II and Orientalising contexts. So are group 18 objects – all of them originate from EO contexts.

Among the "other groups" of beads that are represented within this study by a single sample the most ancient are PG5, 6, 113, 114, VG27 and 28. They all date to EIA I contexts. EIA II samples are PG66, 168-170, 172 and VG54. Samples PG32, 58, 90, VG16, 18, 85 and 88 were found in Early and Middle Orientalising contexts. Only one sample within this class of beads belong to the Archaic period – VG38.

The Non-Beads are the heterogeneous group of objects that mostly belong to the later periods concerned in this study – Orientalising and Archaic. For example, the bracelets and the large flat buttons belong to the LA period. The only representative of the EIA I period within this group of samples is PG135. EIA II is represented by the other sample of buttons/pinhead group – PG57. In addition, some of the fibula bow beads were found in this context (VG92 and 93). The rest of the fibula beads belong to the Orientalising context. PG97 also was found in the grave of the Orientalising period. Another pendant-like object VG56 can be assigned to the EIA II period. VG114 – the only vessel fragment is dated by the analogy to the similar bowls to the Orientalising period.

3.5.2. Areas of occurrence

The selection of samples for the analytical study proportionally reflects the presence of specific groups of beads within museum's collections. In this way, the distribution of groups of beads in time and space is representative of the collections that cover large number of archaeological sites in the Iron Age South Etruria and Latium. Despite the fact that such distributions cannot provide the full picture about occurrence of beads in all the concerned area, they are supposed to reflect general tendencies within the region.

Geographical distribution might give hints on possible production centres of specific groups of beads and/or the areas of circulation of certain groups of glass, which should reflect the trade network of the time. The number of the samples per site is uneven because of the uneven distribution of glass within the tombs of the sites and uneven representation of the sites within the archaeological collections involved in this study. Here we operate not by individual sites, though they will be mentioned in certain cases, but rather with areas that samples are originating from e.g. South Etruria and Latium. The sites of Terni and Verucchio are considered as the ones from the other regions as discussed in the previous chapter. The general distribution of samples by regions is presented in the Figure 3.18 (All beads).

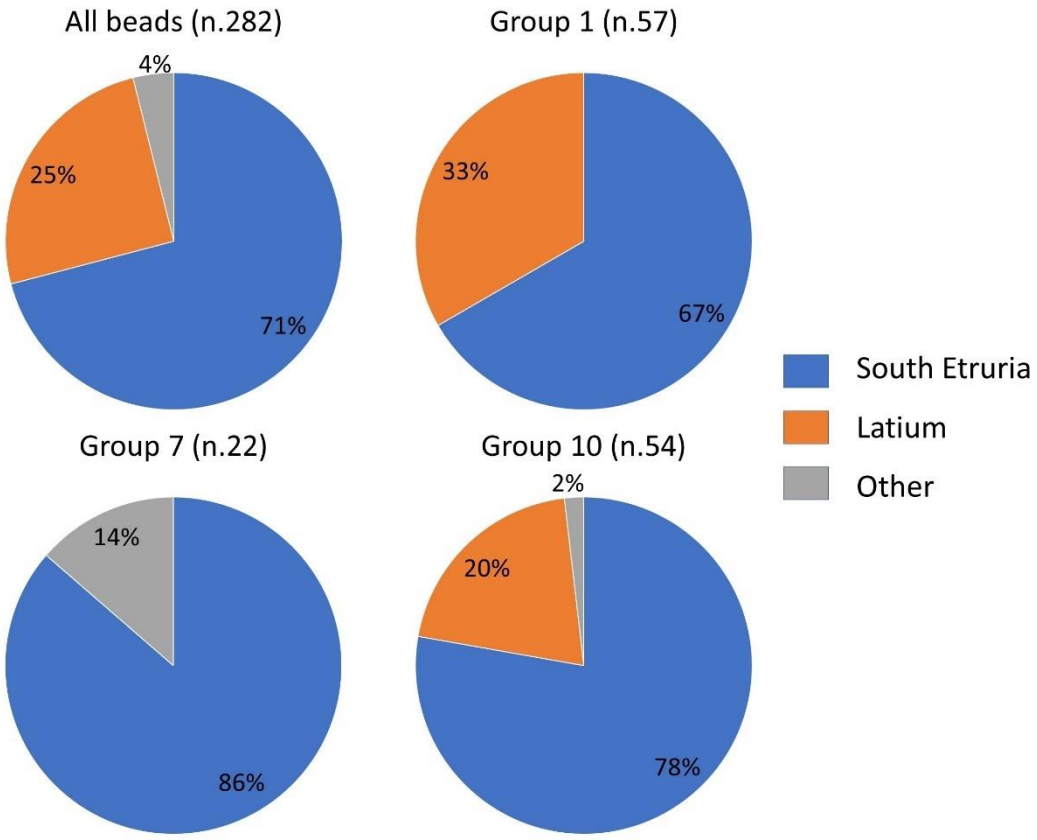

Figure 3.18. Spatial distribution of most represented groups of samples (n > 20) between South Etruria, Latium and Other refers to Terni and Verucchio sites that are located outside the main regions of Etruria and Latium.

It can be seen that samples of Etruscan contexts make up to 71% of all samples considered in this project. About a quarter of all samples originate from Latium contexts. 4% of all samples comes from outside Etruria and Latium.

If one descends on the level of individual groups then the distribution among the regions will be different, as can be seen from the Figure 3.18. For example, for group 1 an increase of share of Latium can be noted which makes the samples of this group more evenly distributed among the regions. Group 2 does not have so many representatives as group 1. They all come from just two sites in Etruria – Veio and Falerii. Group 3 and 4 samples on contrary mostly come from Latium and only one representative – VG25 of group 3, is from Etruria.

Small translucent ring beads (group 5) come mostly from a single grave in the Caracupa necropolis (tomb 48) and only one sample is from Cerveteri (Etruria). Group 6 beads come almost exclusively from Veio. Group 7 distribution is outlined in Figure 3.18. These beads mostly come from Etruria with the exception of three beads from Terni that are assigned to group 7 but have a slightly different appearance than the rest of the beads of same group. Group 8 beads except one all were

unearthed in Latium, the remaining one comes from Terni (Umbria). Group 9 objects involved in this study are from Cerveteri and Vulci (South Etruria).

The group 10 beads are distributed largely similarly to the general distribution of objects if the respective diagrams are compared. However, there is slight prevailing of occurrence in Etruria. Interestingly, translucent beads with rib decoration (group 11) only come from Etruria.

As already was mentioned, tubular beads of groups 12 and 13 come from distant locations: Vulci-Cavalupo for group 12 and Verucchio for group 13. Group 14 beads are all from a single tomb from Cerveteri-Monte Abatone (South Etruria). Beads of group 15 within this study are divided between two tombs from Falerii and Marino (Ager Faliscus (Etruria) and Latium respectively). Group 16 beads come predominantly from Latium contexts but on several occasions, they occur also in Etruria. Three out of four group 17 beads belong to sites in Etruria and one to Latium (Marino). Two of the group 18 beads come from Veio (Etruria) and the PG3 from Verucchio (Emilia-Romagna).

Regarding the other groups of beads, they, expectedly, come from several sites: PG5 and 6 – from Bisenzio, PG32 and 58 – from Veio, PG66 from Sermoneta, PG90 from Capena, PG113, 114, 168-170, 172 – from Osteria dell'Osa, VG16, 18, 27 and 28 – from Vulci, VG38 and 54 – from Cerveteri, VG85 and 88 – from Falerii. Similar division is noted for the Non-Beads: PG57, 59-62 and VG56 are coming from Veio, PG97 – Marino, PG135, VG1-7, 9, 13 – Vulci, VG32 – Cerveteri, VG92 and 93 – Falerii.

Indication of how many different objects came from each archaeological site discussed in the present work is given in Table 3.3. Total number of objects is 289. They were recovered from at least (some objects were found outside grave contexts) 66 graves located near 14 ancient settlements.

Table 3.3. Representation of sites among the contexts of samples selected during stage 1 of the study. Samples found outside grave context count as 1 in the number of graves.

Site	Number of graves	Groups	Number of samples (stage 1)	Chronological frame (BCE)
Bisenzio	3	10, 16	12	800-720
Capena	5	1, 10, 11, Other	17	800-625
Cerveteri	9	1, 7, 9, 10, 11, 14, 16, 17, Other, Non-beads	45	800-480
Falerii	3	1, 2, 6, 10, 11, 15, Other, Non-beads	20	800-600
Narce	1	1, 10	5	800-700
Tarquinia	1	10	2	900-700
Veio	14	1, 2, 6, 7, 10, 11, 16, 18, Other, Non-beads	73	770-630
Vulci	5	1, 3, 5, 9, 10, 11, 12, 17, Other, Non-beads	33	900-500
Marino	4	1, 10, 15, 17, Non-beads	10	730-600

Site	Number of graves	Groups	Number of samples (stage 1)	Chronological frame (BCE)
Osteria dell'Osa	7	1, 3, 4, 8, 10, 16, Other	36	900-720
Sermoneta	10	1, 3, 4, 5, 8, 10, 16, Other	25	770-720
Tivoli	1	8	1	770-720
Terni	2	4, 7, 8	5	900-800
Verucchio	1	10, 13, 18	5	800-600

3.6. Questions of representativeness.

This section discusses the occurrences of glasses similar to those considered in this research project that were found in other contexts. This will help to understand the place of the selected samples among the rest of the glass objects found in the Middle-Tyrrhenian Italy and beyond (if relevant for the research) and gives the idea on how they can represent the overall glass finds in the area. In several cases, comparison with literature helps to identify archaeometric case-studies that provided comparable chemical data for discussion in the following chapters, although both the archaeological and the archaeometric literature was reviewed. Below, each group of glass beads is associated with similar glasses presented in museum collections or excavation reports. This overview is not exhaustive, but rather helpful to give an idea on the presence of such beads in the wider context. Similar glass beads studied from the chemical point of view are also mentioned.

Group 1 is very well represented on many sites in both Etruria and Latium and it is found in many IA sites in the Italian peninsula from Verucchio (Koch 2015, group 6a) to its southernmost territories (Conte 2016). Eye decoration is one of the earliest used in bead-making since the LBA (Shortland et al. 2018) and continued to be one a popular choice to enhance the appearance of the beads throughout the IA and beyond (Guido 1978).

Group 2 beads are less frequent than Group 1 beads. They are also found (the smaller variety at least) in France (Gratuze and Picon 2005), whereas both groups 1 and 2 were found in modern Slovenia (Šmit et al. 2020).

Group 3 beads (with horned eye decoration) are actually more typical for the FBA period. They might have been produced of LMHK glass as such beads are documented in Frattesina and several more sites in the Po valley with a possibility of production also north from the Alps (Bellintani and Angelini 2020; Koch 2021). Naturally, such beads are scarce in the IA contexts.

Group 4 beads are also rare the IA contexts. All objects of this kind found in the collections were analysed.

Group 5 beads and all the ring beads of various colours (Groups 6 and 7) are very numerous, and their number in a same tomb normally suggest they were sufficient for assembling bracelets, necklaces and decoration of garments (Verucchio assemblage, for example, Koch 2015).

Group 5 objects are less common in the Iron Age than opaque beads, but they were also found in coeval Picenian contexts (nowadays Marche region of Italy). Chemical analyses of such beads are reported in Ferri et al. (2020) Similar objects were unearthed in the nowadays Poland (Purowski, 2016).

Group 6 is one of the most numerous among the objects examined in the collections. Large numbers of these beads were found in Verucchio (Koch 2015). Group 7 beads apparently were produced through a long period of time starting from the LBA (Varberg et al. 2015) and continued being produced throughout the Iron Age (Zlámalová Cílová et al. 2022, Olmeda 2015). These beads are frequently found in graves in large numbers (Koch 2015). Small black-appearing beads (Group 8) constitute a peculiar set of samples that might be one of the earliest examples of LMG in Central Italy (detailed discussion of occurrences that covers also Group 16 and some Other beads representatives is in Koch 2018a). Comparable glasses were studied using analytical chemistry methods (Conte et al. 2016).

Group 9 beads might be made of faience with is not a material of primary interest to this study. Faience is much more diverse in the Middle Tyrrhenian Italy than the objects discussed here and is considered an imported commodity (Nijboer 2008; Jackson-Tal 2019).

Group 10 is one of the more numerous groups among all samples, on a par with Group 1 samples, but in terms of presence in the collections it is less common than the beads of small size. This means that more Group 10 beads were studied with analytical methods per total available samples than beads of the Groups 1 or 6, for example. Such, mostly naturally coloured, beads have been produced throughout most of the entire history of glass production since the production of such beads does not require any excessive colourants and efforts dedicated to the decorative elements. Similar beads were found in various sites on Italian peninsula (Koch 2011; Olmeda 2015). Group 11 (rib decorated or melon) beads are less common in Etruscan contexts. There is a wide pool of compositional data for weakly coloured glasses from the first half of first millennium BCE Mediterranean (Reade 2021; Oikonomou et al. 2018).

Group 12 beads remind of LBA beads from Fattesina site (Bellintani and Angelini 2020). Such glasses are expected to have different composition from the IA glasses. The only difference between these beads and the FBA finds is the colour – beads considered here are red. This might not be intentional though.

Group 13 is less common; these objects do not belong to the Middle-Tyrrhenian Italy. Apart from these three samples several similar ones were found (Koch 2015).

Group 14 makes a heterogeneous group of objects that might be considered separately. These objects seem to be more characteristic of the second half of the first millennium BCE (Agua et al. 2017; Zlámalová Cílová et al. 2022). Blue and white variety (VG34) is the most common one. Such beads are known from several sites in Etruria, but the presence of such beads in Hallstatt contexts North-East from the Italian peninsula is remarkable, which is also true for samples of Group 15 (Koch 2011).

Group 16 beads also demonstrate a little variability as demonstrated in Koch (2018a). Composition of such glasses was compared to samples from modern Slovakia (Conte et al. 2018). These analyses included samples that we put in the category of Other beads made of black appearing glass.

Group 17 objects are made of glass similar in appearance to Group 6 beads. These objects are known from several sites in Italian peninsula including the ones included in this study (Olmeda 2015). Group 18 objects are very different in appearance. Object similar to a spindle whorl PG64 is known from Bologna (Archaeological Museum of Bologna website). The appearance of glass is similar to Group 15 beads. We did not find parallels in literature for the PG63 and VG81.

Among the rest of the samples discussed we must mention several peculiar varieties of objects. One of the groups of objects that we mention here are the so-called bird beads. Such group of objects is represented within this study by two samples PG172 and VG88. Bird beads have a wide distribution, but the majority of these objects are concentrated in the central part of the Italian peninsula and the Aegean (Rhodes in particular). They can be linked with Rhodes glass-working centre of the Iron Age due to the concentration of finds (Koch 2018b and references therein).

Fibula bows are probably one of few verified examples of Etruscan glass-working. This assumption was supported by their distribution in the archaeological contexts, with the highest occurrence of these finds is the area around Verucchio and Bologna, though the objects included in this study have somewhat different shape, unique for Etruria (Koch 2020).

The overall set of samples considered for this research, which was selected among glasses of two important archaeological collections for the Central Italy material culture, represent the major part of the beads groups found in the area. Even though the coverage of the necropolises in which each group of beads was found is not exhaustive, it shall be noticed that the archaeological assemblages included in this work are among the most important ones for characterising the Southern Etruria and Latium material culture.

Also, there is a (relatively) limited number of samples from outside of Etruria and Latium. Nevertheless, these are of great relevance, as their chemical characterisation could give a significant contribution to the discussion of glass supply for a wider area.

Among the groups of glass beads the selection of samples for the analyses was not proportionate to the actual number of similar objects found in the tombs. Several Groups, namely 1 and 6, featured large number of beads found in the same tomb. In those cases, only a small fraction of the beads was analysed. As an example, we can mention tomb 104 from Capena (Saliere necropolis) that contained more than a hundred beads of Group 1, yet only 6 were analysed. On the contrary, tomb 16 in Veio-Vaccareccia contained only 10 beads of Group 1 but 4 of them were analysed. In general, the preference was made to cover as many burials as was possible within these collections, taking into consideration their dating and location. Every group of glass beads found in a single tomb was subjected at least to non-invasive stage of the analyses. Every group of differently appearing glass and shape (decoration) was included in the study. Conclusions on consumption of certain groups of beads can be made based on the archaeological evidence. The basic assumption here is that the compositional heterogeneity within the group (if any) will be somehow reflected in the present set.

Conclusion. This chapter is dedicated to the presentation of systematic observations on the objects involved in the present study. The system of criteria (attributes and their documentation) was developed in order to describe the glass beads and to create a classification that would reflect all the significant attributes of the beads that were considered. The descriptive system was adapted according to the information gathered from the collections, and the samples were grouped according to the following characteristics: size, shape, colour, translucency and, last but not least, the presence of decorative elements. Since the system was configured for the beads of regular shapes, the Non-bead objects were put aside, and a separate kind of division was applied for this group of objects. The beads were divided into 18 groups, and one further group gathers all the beads that did not fit into any group (unique beads for the collections). This division was made to facilitate the

presentation and discussion of the data within this study, and these groups sometimes contain objects that could be considered separately as representing different archaeological types as the pool of objects increases. Each group was characterised using the criteria developed for each attribute, and the range of values for each attribute was marked. Each group's distribution was traced in space (distribution by site) and time (distribution by period). A brief overview of the occurrences of the beads was provided to highlight the significance of the sample set and its relationship to other assemblages. The analytical data of similar beads from other regions of the Italian peninsula and the wider area were mentioned to be used as a basis for the comparative study that will be presented in the subsequent chapters.

CHAPTER 4. METHODS FOR THE ARCHAEOMETRIC INVESTIGATION.

4.1. General description of reasoning and stages.

It was stated in the preface that the study was built in three stages. Stage 1 results have been largely presented already by describing the archaeological contexts of the analysed objects (section 2.3) and their description (methods of documentation were described in section 3.2, the results of documentation are contained within sections 3.3 and 3.4 as well as in Appendix 2 and 3).

Practically same set of objects was subjected to the stage 2. During stage 2 of the study, the non-invasive archaeometric analyses of the objects were arranged and carried out inside the museums' premises (the Museo Nazionale Etrusco di Villa Giulia and the Museo delle Civiltà) using portable equipment without any sample preparation. The museums allowed the analyses with non-invasive methods of the objects that were selected in stage 1 and contributed to the research suitable working spaces and management of glass collections. Most of the work within the museums was accomplished during a period of strict COVID-19 limitations, that dictated limited time for each analytical session.

Objects were examined using a Dino-Lite digital microscope first. This was part of sample's documentation during the stage 1, but it also provided the information on samples integrity/suitability for the analyses and helped in the identification of the RoI on each sample.

p-XRF was used as a method of elemental analysis and FORS was chosen to obtain more information regarding chromophores in the glass.

These techniques, because of their ability to produce quick response without any harm to the samples, allowed for the analysis of practically all glass objects in the collections. As for the necklaces made of similar beads found in a same tomb, they were analysed by considering only several representatives in each necklace. After the quality control procedures mentioned below, the data were assessed in terms of homogeneity/heterogeneity of composition for each group. In this way the compositional homogeneity of similarly looking objects was assessed.

Results from stage 2 set the basis for the selection of samples for the analyses in the laboratory, with micro-invasive approaches (stage 3). The fragmentary beads and least precious objects were preferred, if typological and context attribution could be confidently assigned, and given the similarity of the composition with the other whole beads and more valuable objects. The goal of this selection was to retrieve most of the information for a large set of samples with a reasonable number of representatives. At the same time, the permission was inquired to analyse in the laboratory the maximum number of objects that have demonstrated some differences (morphological or compositional) from the rest of the beads confirmed in their respective groups through the non-invasive, on-site analyses. This compromise was dictated by the limited time and resources that was available from each institution involved in stage 2 and 3.

Another influential point during the analytical sessions was the fact that absolute majority of the objects that were analysed in the Villa Giulia Museum were permanently on display, which of course prevented the possibility that these objects could be included in stage 3 of the study. On the other hand, objects from the Museo delle Civiltà were mainly from the storehouse, which meant much higher flexibility of the museum in handling the logistical issues.

Stage 3 was designed as the study, by means of micro-invasive approaches, of the smaller set of samples selected during stage 2. Analysed samples maintained full integrity after analyses except

those fragments of beads that were prepared as polished cross sections for Scanning Electron Microscopy coupled to Energy Dispersive Spectrometry (SEM-EDS). In addition, micro–Raman Spectrometry and Laser Ablation Inductively Coupled Plasma Mass Spectrometry (LA-ICP-MS) employed in the laboratory for the samples selected for stage 3, did not require any sample preparation. Samples were returned to the museums without visible change in appearance. General outline of the study is schematically presented in Figure 4.1.

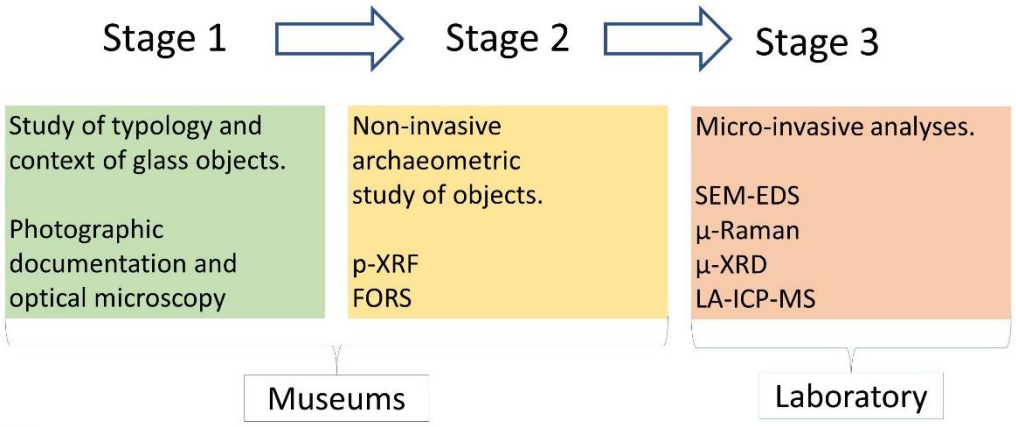

Figure 4.1. General outline of the study.

Appendix 4 contains details on what methods were used to analyse each sample. Somewhat generalised information on the quantity of samples analysed is contained in Table 4.1. The numbers in the table give the number of samples that underwent analyses, though not all of them provided meaningful result. Most of the samples were analysed with both FORS and p-XRF so there is no individual column for each method, unlike for stage 3 methods. Below, in the following sections, it is presented how each technique was utilised within this study together with quality assessment of the resulting compositional data of p-XRF, SEM-EDS and LA-ICP-MS. FORS, µ-Raman and µ-XRD were used here as qualitative methods of analysis to recognize chemical species by comparing our spectra/diffractograms with those available in databases for samples of known composition.

Table 4.1. Number of samples analysed during stage 2 and stage 3 per typological group. Methods applied during stage 3 have counts of their own. "-" – not represented.

Group	Number of samples stage 2	Number of samples stage 3	(VP)-SEM-EDS	µ-Raman	µ-XRD	LA-ICP-MS
1	56	19	5	19	2	19
2	8	1	1	1	1	1
3	4	2	-	2	-	2
4	5	2	1	2	1	2

Group	Number of samples stage 2	Number of samples stage 3	(VP)-SEM-EDS	μ-Raman	μ-XRD	LA-ICP-MS
5	7	2	-	2	-	2
6	28	6	3	6	2	6
7	22	7	1	7	1	7
8	13	4	2	4	-	4
9	10	4	4	4	4	4
10	54	19	9	19	-	19
11	6	3	3	3	1	3
12	2	-	-	-	-	-
13	3	-	-	-	-	-
14	3	-	-	-	-	-
15	4	1	-	1	-	1
16	7	7	-	7	-	7
17	4	-	-	-	-	-
18	3	2	-	2	-	2
Other beads	20	5	-	5	-	5
Non-beads	21	6	3	6	1	6
Total	280	90	32	90	13	90

4.2. Optical Microscopy.

Optical microscopy (OM) should be an initial step of any analytical study on archaeological materials. During the stage 1, a Dino-Lite AM4815ZT–Edge digital microscope was used for imaging all the samples at 20× magnification. Such photographs enhanced the thoroughness of the photographic documentation that was carried on during this stage. Subsequently, images on higher magnification (100×) were acquired to capture specific elements of the bead (or Non-bead) that might be characteristic for the production technique, e.g. they can give hints on how the glass was shaped into the final object. Texture of glass can be also useful in this way. Another purpose of this documentation was the examination of the preservation state of the bead by registering the surface depositions, cracking and bubbles, if visible on the surface. The microscope operated with the ring led light-set around the objective. In many cases, polarised light was used to remove reflections and improve the quality of the image. Also the use of light diffusing cups provided by the microscope producer, was useful to improve the images. Extended Depth of Field (EDOF) function allowed for making images where plains on different distance to the objective or oblique surfaces were equally focused. This function is invaluable for the bead examination and documentation.

For samples analysed in the laboratory (stage 3), Leica MZ95 stereomicroscope was used for documenting the prepared samples: Cross sections were photographed for reference when navigating them in the SEM.

µ-Raman, µ-XRD and LA-ICP-MS systems have their optical microscope systems for the selection of the spot for the analysis.

4.3. Fibre Optics Reflectance Spectrometry.

UV-Vis-NIR spectroscopy is used for detecting chromophores in archaeological glass (Weyl 1999). With the application of fibre optics, it became a flexible, simple, fast, non-invasive and relatively, low-cost method of analyses (Aceto et al. 2020; Micheletti et al. 2020). FORS analysis helps to understand the mechanism of colouring by identifying the chemical species (transition metal ions in particular), that give colour to the glass. The information from FORS can then be complemented/supported by elemental techniques of analysis. During the stage 2, the Ocean Insight HL-2000-HP-FHSA 20 W Tungsten halogen light source was used. The light was carried through a 2 m long fibre optics illumination/reflection bundle. The probe of 400 µm core diameter was finishing with a tip of 6.35 mm ferrule diameter. Measurements were carried out in the darkened rooms to avoid variation in lighting conditions.

In order to ensure desired positioning of the samples, it was opted to use plasticine to keep samples in the position, which allowed for flexible positioning. This plasticine stage was covered with polyethylene film to prevent adhesion of small portions of plasticine to the sample. The probe was positioned using the probe holder under 45° to the horizontal plane, in order to exclude reflected light from the source. Positioned samples were brought to the probe to keep the 45° angle. but on multiple occasions the angle was changed to capture characteristic features of the diffused light from the sample's surface. The analytical spot in this configuration was an oval, several mm across in the longer dimension. Its size was problematic for small-sized beads, which surface was curving away within this range, and this was another reason of making the incident angle more acute. The results for the decorative parts of some beads were compromised because the size of the decorative element was often smaller than the analytical spot. This is why some spectra of the decorations also contain less pronounced features of the main body of the bead.

The Ocean Insight QEPro CCD detector with HC1 grating was receiving the diffused light captured by the probe. Its operating range was set from 248 nm to 1038 nm with an optical resolution of 6,78 nm FWHM. A high reflectivity Spectralon reference was used to calibrate the instrument. Detector was integrating signal for at least 0.019 seconds (maximum 0.029 seconds) and minimum 40 scans were averaged to obtain a single spectrum. As a rule, at least 3 spectra were collected for each sample.

Differently coloured samples were producing widely different spectra in terms of relative reflection, with dark coloured samples returning sometimes less than 5% of what the Spectralon reference was returning. Translucent samples also did not reflect most of the incident light, transmitting it through the bulk. In order to maximise the features of each spectrum the values were normalised in a way that maxima of each spectrum were set to be equal to 100% and minima to 0%. This permitted to consider all spectra in the same frame of reference. It was noted that sometimes the features of different spectrum were pronounced differently on several spectra of a single sample. It seemed to depend on geometry of the measurement. This is why FORS spectra were considered strictly qualitatively. Normalisation of spectra was also useful to directly compare the absorption features of glasses with different colour saturation.

4.4. Portable X-Ray Fluorescence Spectrometry.

p-XRF is a well-established method of archaeological glass analysis (Janssens 2013; Scott et al. 2012; Micheletti et al. 2020; Abe et al. 2021, Yatsuk et al. 2023). This method is routinely used for checking the bulk composition of glass in various ways. Portability of equipment, simple measurement sequences, qualitative data availability in real time, reasonably broad range of elements that can be analysed and ability to detect some of them even in trace quantities are the important advantages of the method that earned its popularity among the users of different level of the expertise. One of methodologically challenging points of this study was the use of three different XRF spectrometers (approach discussed in Yatsuk et al. 2023). This was dictated by logistical issues, COVID-19 restrictions and sizes of objects supports that sometimes were attached to the beads and necklaces. In many applications (Koleini et al. 2017; Abe et al. 2018; Spencer et al. 2018; Bruni et al. 2020; Demisar Arli et al. 2020; Hein et al. 2021) XRF data are thought to be instrument-dependent, and various strategies are applied during the handling of data. Usually, such data are considered without the direct comparison with other datasets. In the case of the present study there was need to compare the data obtained with different spectrometers in the same frame of reference. It was necessary to assess the accuracy of the data by analysing same set of samples with known composition and compare whether different spectrometers would provide data of acceptable accuracy (i.e. quality) for pursuing the goals of the investigation.

4.4.1. Hardware and settings.

The three XRF units were: XGLab ELIO, produced by XGLab S.R.L. (Milan, Italy); Unisantis XMF-104, produced by Unisantis (Geneva, Switzerland); an in-house developed instrument called Frankie, produced by the Italian National Institute of Nuclear Physics – National Laboratories of Frascati (Frascati, Italy). Their hardware characteristics and acquisition parameters are presented in the Table 4.2. It is evident from the Table 4.1 that the three XRF units have very different features, and their respective spectra will be different in terms of count rate and the positions of the anode Rayleigh peaks.

Table 4.2. Description of the XRF units that and experimental setup used in this study.

ID	Hardware					Acquisition parameters				
Device	**Anode, V (max), I (max)**	**Beam focusing, focal spot**	**Detector: type, active area, thickness**	**Resolution at Mn Kα**	**CPU pulse processing channels**	**Spot focusing device(s)**	**Filter, thickness**	**Time**	**V**	**I**
ELIO	Rh 50 kV 50 μA	Pin hole 1.2 mm	SDD 25 mm^2 500μm	140 eV	2048	Laser + Camera	none	90 s	40 keV	40 μA
Unisantis	Mo, 50 kV 1000 μA	Polycapillary 80 μm	Si-PIN 7 mm^2 300 μm;	186 eV	2048	Laser + Microscope	none	150 s	50 keV	300 μA
Frankie	W 50kV 200 μA	Policapillary 300 μm	SDD 20 mm^2 450μm	173 eV	4096	Laser	none	200 s	40 keV	80 μA

Some preliminary work was done to optimise the acquisition parameters for the glass matrix using the ELIO unit. 9 combinations of acquisition time, voltage and current were tested on a set of materials with known composition. These settings combinations are outlined in Table 4.3.

Resulting spectra were compared by the parameters of counts obtained for K series peaks of major and minor elements, the Relative Standard Deviations of the peaks areas (in counts per second) and detection of some minor elements. Of particular interest was the question of the minimal time per acquisition still providing reliable data. It was observed that 90 s acquisitions and 120 s acquisitions were providing approximately same RSDs, whereas RSDs were higher for 60 s spectra. Based on this, it was decided to use 90 s per acquisition, that was enough time to accumulate counts even for minor elements. The voltage was kept at the maximum level of 40 keV to allow for detection of such elements as Sn and Sb, whose K lines are in the region after 20 keV. Higher current was causing more dead time for the detector without significant increase in count rate. This is how it was decided to use the combination 8 for the acquisition of data of samples of interest (Table 4.3). Using similar logic, the parameters of other XRF units were adjusted for optimal acquisition of signals from silica glass matrix.

Table 4.3. Test settings of ELIO p-XRF unit that were compared to select the most suitable one. The settings that were used are in the blue row.

Setting	Time (T, s)	Voltage (V, keV)	Current (A, μA)
1	90	40	80
2	60	40	80
3	120	20	80
4	120	40	40
5	120	20	40
6	90	20	40
7	60	20	40
8	90	40	40
9	60	40	40

4.4.2. Experiments and data treatment.

A set of reference materials that reflect expected archaeological glass compositions was comprised with three Corning Museum of Glass (CMOG) reference glasses – A, B and D (compositions provided by Adlington (2017)) and 5 archaeological glasses – CB36 (composition in Mirti et al. (2000)), CB65 (Mirti et al. 2003), VA08, VA27 (Mirti et al. 2008) and VA70 (Mirti et al. 2009). Their compositions are outlined in Table 4.4. These materials represent compositional range of Iron Age Mediterranean glasses better than commercially available CRMs. These samples were analysed as polished cross sections except for samples VA08 and VA27 that were analysed as chunks of glass, which provided us with opportunity to compare the data obtained on the flat and regular

surface with the ones from irregularly shaped pieces. Such comparison is important for assessing the bias caused by the irregular and curved surfaces of the beads that were studied within the museums.

Table 4.4. Compositions of the reference materials used to check accuracy of the p-XRF measurements. Number of significant digits reflects the precision of values. Composition of samples are published in: Adlington (2017) – CMOG reference glasses; Mirti et al. (2000) – CB36; Mirti et al. (2003) – CB65; Mirti et al. (2008) – VG08 and VA27; Mirti et al. (2008) – VA70. All values are in wt. %.

RMs	K	Ca	Ti	Mn	Fe	Co	Ni	Cu	Zn	Sr	Zr	Sn	Sb	Ba	Pb
CMOG_A	2.38	3.60	0.47	0.77	0.76	0.134	0.02	0.94	0.035	0.09	0.004	0.150	1.32	0.41	0.067
CMOG_B	0.83	6.12	0.053	0.194	0.238	0.036	0.078	2.13	0.153	0.016	0.019	0.019	0.346	0.069	0.57
CMOG_D	9.4	10.6	0.228	0.43	0.36	0.018	0.039	0.304	0.080	0.048	0.009	0.079	0.73	0.261	0.224
VA_08	2.70	3.64	0.066	0.026	0.48	N.D.	0.002	N.D.	N.D.	0.044	0.005	N.D.	N.D.	0.009	N.D.
VA_27	3.49	4.81	0.114	0.036	1.09	0.001	0.006	N.D.	N.D.	0.039	0.010	0.001	N.D.	0.010	N.D.
VA_70	2.19	4.90	0.019	0.209	0.182	N.D.	0.001	0.004	N.D.	0.041	N.D.	N.D.	N.D.	0.009	0.003
CB_65	1.06	5.1	0.072	0.42	2.11	N.D.	0.003	1.20	0.007	0.041	0.006	0.110	0.51	0.021	3.13
CB_36	0.51	4.80	0.060	0.71	1.53	0.004	N.D.	1.66	0.040	0.044	0.006	N.D.	0.075	0.029	0.139

Each reference material was analyses on various spots 3 times. In case of CMOG references, analysed by the ELIO unit, 10 spectra were acquired. For the beads, given their irregular shapes, the plasticine support covered with polyethylene film was used for precise positioning for the analysis. Samples were analysed 3 times, if another colour of glass was present as a decorative element, such decoration was analysed as if it was another independent sample. For the samples that are presented as a range of similar beads, each acquisition was done on a different, randomly selected bead within the same necklace. Appendix 4 contains information as to which specific unit provided data for each sample.

Resulting spectra were converted to conventional .spc, .spe or .mca formats and processed using PyMCA software (Solé et al. 2007), which was chosen because of its versatility. Compositions provided by the acquisition software of the instruments were in fact ignored. Instead, a Fundamental Parameters (FP) configuration file was prepared for each XRF unit to reflect the conditions and hardware of measurement, providing more accurate quantifications that were checked by adjusting the incident primary spectrum to obtain comparable-to-reference values compositional output of CMOG A reference glass spectrum. 15 elements were quantified: K, Ca, Ti, Mn, Fe, Co, Ni, Cu, Zn, Sr, Zr, Sn, Sb, Ba and Pb. Light elements such as Na, Mg, Si and Al were included in the FP models as part of the reference matrix composition, but not quantified due to the absence of reliable peaks. The configuration files were used to batch fit all the spectra including the spectra obtained from beads in the museums. A similar approach of quantitative p-XRF measurements, combining the FP models and standards for their improvement and assessment, was used by Heghinbotham et al. (2010; 2017; 2019).

4.4.3. Quality assurance and quality control of the data.

One of the first procedures that were aimed at ensuring reliability of data was establishing the Limits of Quantification (LOQ) for each element and XRF unit as they depend on the matrix. LOQs were estimated by calculating the gross area B under the peak of interest (for most of the elements Kα peaks were used except for Ba and Pb where Lα peaks were used for estimation) within the

spectra of CMOG A, B and D reference glasses using PyMCA software, then to this area was added the value of 10 square roots of B. The formula of the LOQs has next form:

$$LOQ = B + 10\sqrt{B}$$

This estimation was assumed to correspond to 30% uncertainty at the 99% confidence level (Keith et al. 1983). The maximum value of the LOQ among the three CMOG references was used as the general LOQ value for the specific element and unit of equipment. Figure 4.2 provides the information on the LOQs established by this procedure.

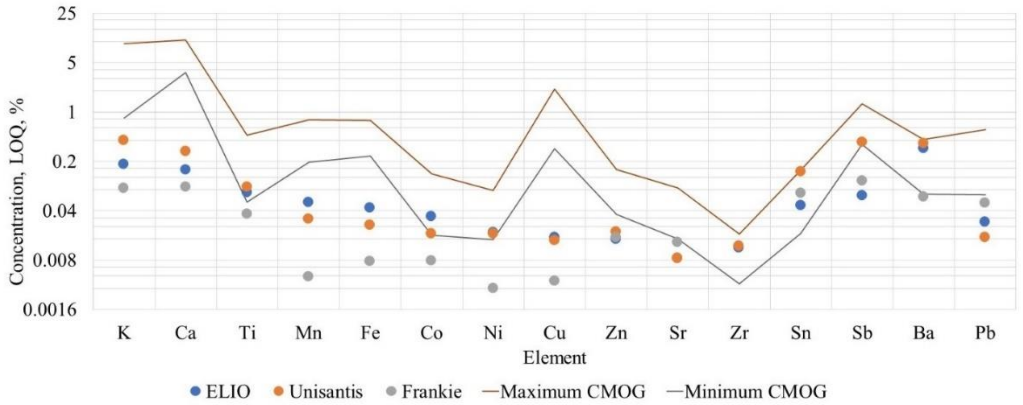

Figure 4.2. Limits of Quantification calculated for each element and XRF unit. Maximum and minimum concentrations in CMOG references are marked by continuous lines.

It can be noticed that for several elements, such as Ti, Ni, Zr, Sn and Ba, at least 2 instruments have their estimated LOQs above the minimum concentration in the CMOG references. This means that the datapoints available for precision and accuracy estimation were fewer for these units, in other words not every reference material could provide the concentration value for a specific element, as all the values lower than the respective LOQ were deemed unreliable and were discarded.

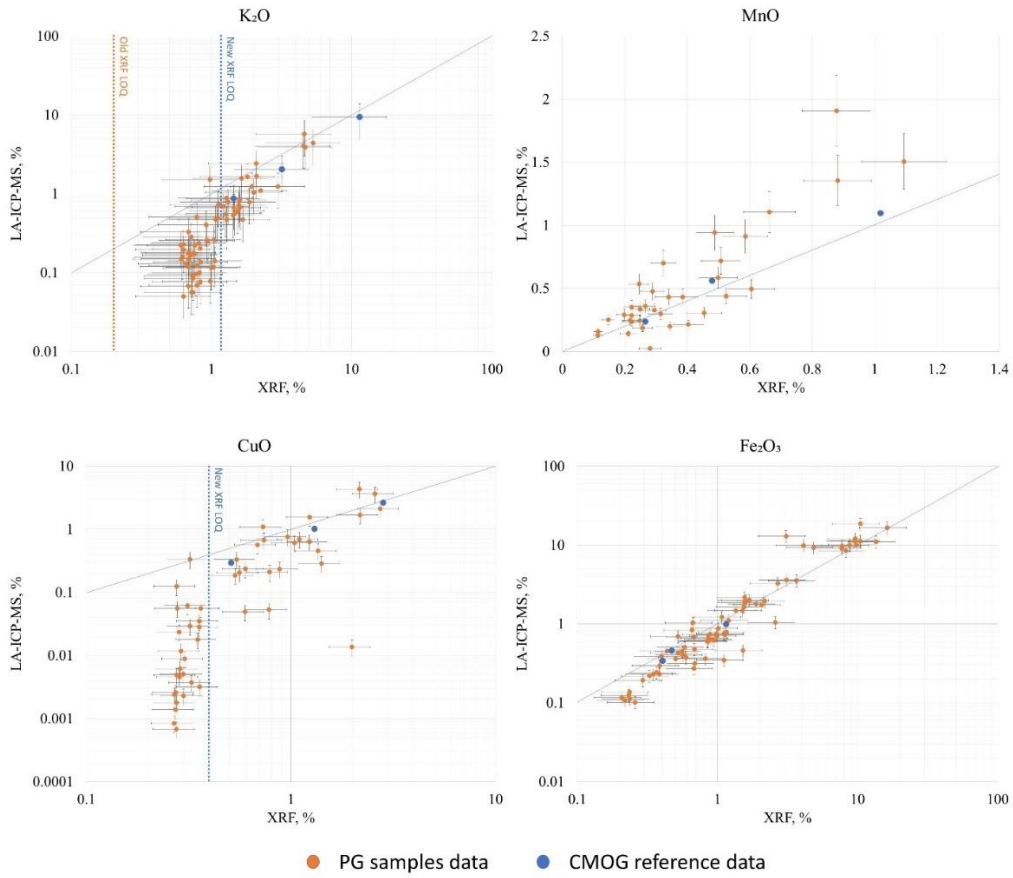

Figure 4.3. Comparison of ELIO p-XRF data with LA-ICP-MS ones. K_2O and CuO plots represent elements with deviation of p-XRF data from the 1:1 ratio (diagonal lines) at low elemental concentrations. In these situations, it was opted to raise the LOQ estimation (vertical blue dotted lines). MnO and Fe_2O_3 represent elements that show no bias with the change of concentration. CMOG reference glasses were inserted to represent the concentration range and be the reference of the overall accuracy if the data. Error bars represent relative error of the analyses determined on reference materials' measurements. All plots except MnO use logarithmic scale.

During the elaboration of the LA-ICP-MS data, the correspondence of the obtained concentrations was checked by plotting XRF concentrations of the samples included in this study against the ones obtained by LA-ICP-MS (for this technique, see section 4.7). This was done for the elements with a large number of the data points. Only the data of ELIO p-XRF unit were considered, as for the Unisantis and Frankie units there were much fewer datapoints available in the LA-ICP-MS block of data. The result of such comparison is presented in the Figure 4.3. K_2O and CuO binary plots demonstrate the tendency of data on several elements, namely K, Ti, Ni, Cu, Zn and Pb to have overestimated p-XRF concentration values when compared to the LA-ICP-MS data (that are supposed to have significantly lower LOQs (Trejos et al. 2013)). This problem might be mitigated by raising the LOQs for these elements up to the level where the concentrations of both datasets start to be similar

to each other. Since the quantification of the element concentration should be limited by the range of the calibration curve, it is worth noticing that such overestimation occurs only outside the CMOG references range (marked by blue points in the Figure 4.3).

Using this logic, it was decided to raise the LOQs for the ELIO p-XRF data to new values for the aforementioned elements: for K to 1.2%, for Ti to 0.26%, Ni – 0.06%, Cu – 0.4%, Zn – 0.03%, Pb – 0.09%. Data on Mn, Fe, Co and Sr did not show similar overestimation, so for these elements the LOQs remained unchanged (Figure 4.3 for Mn and Fe). Other elements did not provide significant number of data points during the p-XRF analyses to be considered in a similar way.

The analytical precision of the measurements was checked by calculating the Relative Standard Deviation (RSD) values of tri- and decaplicates. The mean RSD values were within the 25% limit, but in several cases RSD values for one or more reference materials could rise up to 50%. No systematic difference was detected when chunks and cross sections RSDs were compared. In this way it was concluded that spectra of irregularly shaped objects if obtained on a relatively flat surface do not introduce significant bias of measurement.

The accuracy of the compositions obtained by means of XRF analyses was checked by comparing the resulting compositions of the reference materials to the data in the Table 4.3. Unfortunately, for the majority of determined data points, the accuracy, calculated as double mean relative error, individual for each XRF unit and percentage deviation from the reference values was seldom lower than 15% through most of the values were within 50% of difference. Two ways of data correction were applied for different elements. For the elements that provided more than 4 data points for the calibration curve the correction was done using the following formula:

$$x_1 = x_0 b_0 + a_0$$

where x_1 is corrected value, x_0 is the initial value provided by PyMCA quantification, b_0 – the intercept of the initial linear regression function calculated for the reference values of given sample and their respective PyMCA values and a_0 – the slope of the same function. Such procedure is evaluated in greater detail in Rousseau et al. (1996).

For the elements that within the reference dataset provided less than 4 data points another formula was used:

$$x_1 = x_0 \frac{\left(\frac{A_{nom}}{A_{acq}}\right) + \left(\frac{B_{nom}}{B_{acq}}\right) + \left(\frac{D_{nom}}{D_{acq}}\right)}{3}$$

where x_1 is corrected value, x_0 is the initial value provided by PyMCA quantification, A_{nom}, B_{nom} and D_{nom} are the nominal, or reference concentrations (Table 4.2) of CMOG references A, B and D respectively and A_{acq}, B_{acq} and D_{acq} are the concentrations of element in the same reference glasses measured by p-XRF unit and quantified by PyMCA. Since the accuracy was measured as average relative error, it was not possible to provide adequate accuracy values for samples with very few datapoints. Consequently, the values of elements corrected by this method were considered as semi-quantitative.

The LOQs, accuracy and the way of correcting the initial XRF data is systematised in the Table 4.5. The values are individualised for each element and for each p-XRF unit. It can be seen that the processed data for most of the elements within each unit's dataset correlate strongly with the reference data from the Table 4.4 (values of 0.9 or higher).

The improvement in the accuracy from the initial PyMCA quantification reached by the application of corrections is demonstrated in the Figure 4.4. For initial quantification plots (Figure 4.4, left row) it is common to observe some data points outside the 20% accuracy interval. With the application of correction procedures, the data points tend to be closer to the nominal composition trend (Figure 4.4, central and right rows).

To assess general reproducibility, Principal Component Analysis and Hierarchical Cluster Analysis were used to check whether the data points will group by the name of the sample or by the XRF unit.

Table 4.5. Data on accuracy of the p-XRF measurement and the LOQs applied.

Element	ELIO				Unisantis				Frankie			
	LOQ (%)	type of correction	Pearson correlation	Relative Error 2σ, %	LOQ (%)	type of correction	Pearson correlation	Relative Error 2σ, %	LOQ (%)	type of correction	Pearson correlation	Relative Error 2σ, %
K	1.2	L[a]	0.990	54.5	0.4	L	0.996	27.4	0.08	L	0.998	34.0
Ca	0.15	L	0.946	15.8	0.28	L	0.987	13.2	0.09	L	0.932	19.7
Ti	0.26	L	0.994	32.1	0.09	R	0.983	N/A	0.04	L	0.995	24.3
Mn	0.05	L	0.993	12.4	0.04	L	0.978	15.5	0.005	L	0.988	36.7
Fe	0.04	L	0.986	33.6	0.03	L	0.989	6.5	0.008	L	0.994	27.4
Co	0.03	R[b]	0.989	N/A	0.02	R	0.992	N/A	0.008	R	0.999	N/A
Ni	0.06	R	0.986	N/A	0.02	R	0.983	N/A	0.003	L	0.998	12.0
Cu	0.4	L	0.970	22.7	0.02	L	0.965	49.6	0.004	L	0.989	11.5
Zn	0.03	L	0.969	22.7	0.02	L	0.998	6.6	0.02	L	0.998	11.9
Sr	0.008	L	0.969	33.0	0.008	L	0.965	11.8	0.01	L	0.868	17.6
Zr	0.01	R	N/A	N/A	0.01	R	N/A	N/A	N/A	N/A	N/A	N/A
Sn	0.05	R	0.876	N/A	0.15	R	N/A	N/A	0.07	R	0.846	N/A
Sb	0.07	L	0.983	100.0	0.37	R	0.914	N/A	0.1	L	0.736	64.1
Ba	0.3	R	N/A	N/A	0.36	R	N/A	N/A	0.06	R	0.999	N/A
Pb	0.09	L	1.000	33.4	0.02	L	0.999	26.4	0.05	L	0.995	98.0

[a]L – linear regression correction applied for the elements with 4 or more data points for each element;

[b]R – ratio coefficient correction applied for the elements with less than 4 data points.

PCA and HCA calculations were done using Standard Normal Variate (SNV) normalised data of the next set of elements: K, Ca, Ti, Mn, Fe, Co, Ni, Cu, Zn, Sr, Sn, Sb, and Pb. HCA calculations were done on Euclidian distances. All the data points that were below the LOQ estimation were set to the reference values (Table 4.4). Instant Clue data visualisation software was used for calculations (Nolte et al. 2018). VA27 results of the Unisantis XRF unit were discarded due to extremely high RSDs. Thanks to these calculations any systematic bias related to the equipment should be visible. Figure 4.5 presents the results of both PCA (a and b) and HCA (c).

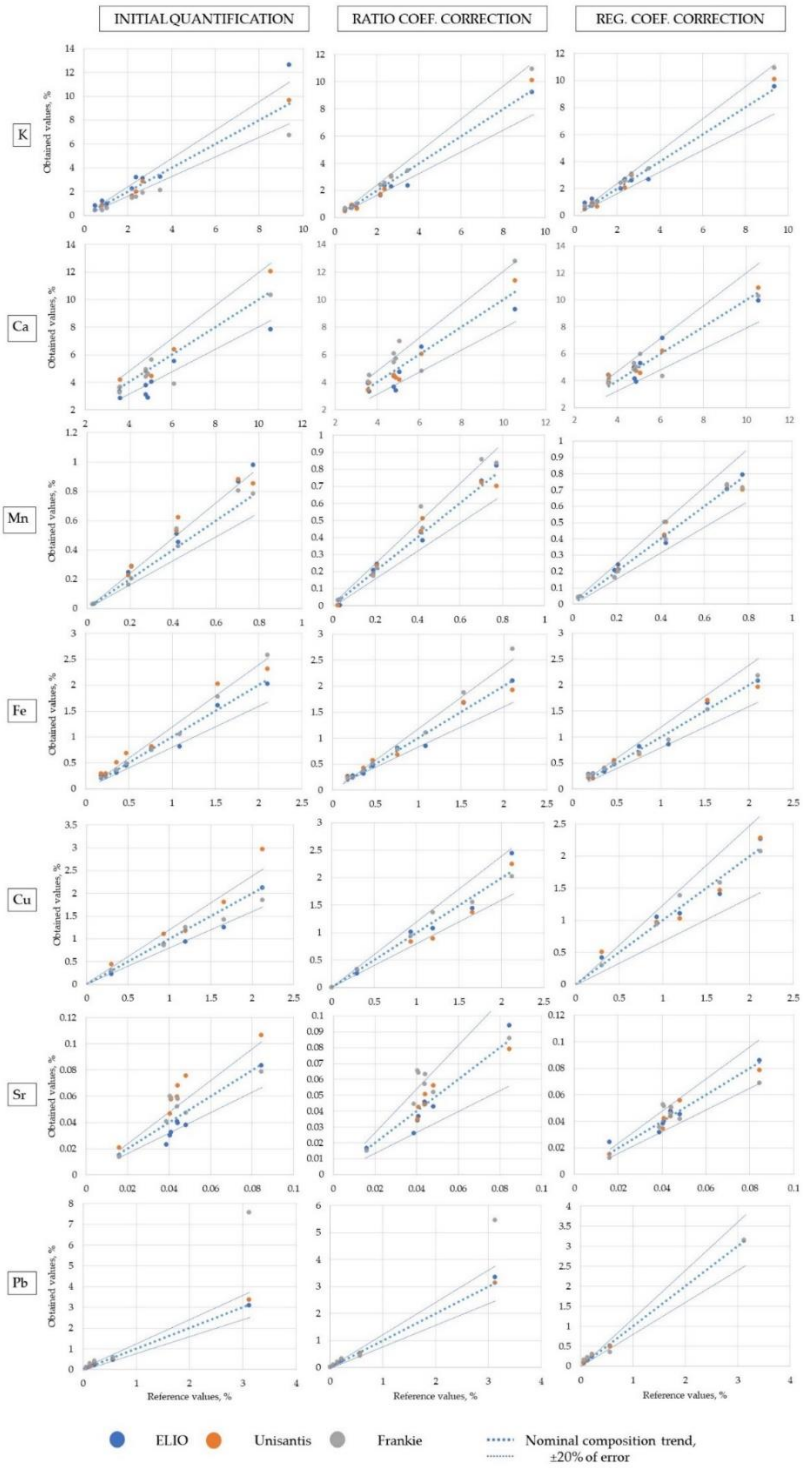

Figure 4.4. binary plots of reference compositions to the obtained ones during the Initial PyMCA quantification (left row), ratio coefficient correction (central row) and regression coefficients correction (right row). Only elements that have at least 5 data points are present.

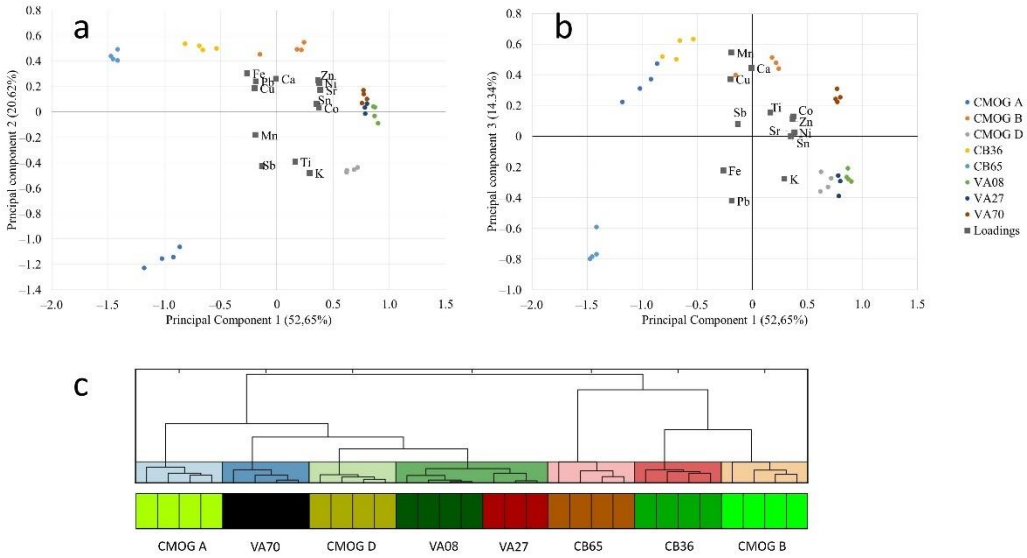

Figure 4.5. Results of the PCA and HCA for the data set of reference materials analysed with three XRF units. PCA results are represented by binary plots of PC1 vs PC2 (a) and PC1 vs PC3 (b). Scores and loadings of the specific PC are present in the same plot. Reference compositions are included in the scores. HCA dendrogram (c) includes values of different samples from three XRF units and the reference one for the sample. In all plots data from VA27 of Unisantis XRF unit were omitted.

Both PCA and HCA plots (Figure 4.5) show that data points obtained from the same sample tend to group together. CMOG reference glasses are located in different quadrants of the PCA plots and are separated by several orders of division in the HCA plot. This rightfully reflects their very different composition. VG08 and VA27, on contrary, are barely separated from one another in both PCA and HCA plots. This can be explained by the similarity of their composition observed in Table 4.4.

Based on this evidence, one can conclude that p-XRF analysis using 3 different XRF units provides data which accuracy is sufficient to effectively distinguish between glasses of different compositional groups. Procedures tested on a set of samples with known composition are useful in improving the overall accuracy of data and provide a framework of quality control.

4.4.4. Sample-dependent sources of bias.

The shape and roughness of the sample surface can influence the resulting XRF spectra. This issue was already addressed in the previous subsection. Another problematic methodological issue was the information that could be recovered from the decorations. Bias in the decorations analysis was suspected based on the width of some of the most common decorative elements and their thickness. The former source of bias is supposed to be inherent to the ELIO unit with the analytical spot of 1.2 mm. Some of the Group 1 samples with simple ring-eyes decorations, for example, do not have sufficient width of the white glass coil that often is less than 1 mm wide. Results of the

white parts analyses in those cases are bound to cover some of the blue base glass as well, introducing error in the determination of the white glass composition. Similarly, interference from base glass composition in the determination of the composition of the decorative parts can be linked to the low thickness of the decoration. Using type 1 beads as an example (most common decorated samples within the study), it is evident that the thickness of the white ring does not exceed 0.5mm for most of the beads examined (some photographs in the Appendix 2 give an idea of the decoration's thickness) often being much thinner. In these conditions, white decorations might not be "infinitely thick" for at least several of the measured elements (the heaviest ones) because the more energetic fluorescence X-rays that reach the detector can be produced at a greater depth (de Vries and Vrebos 2001).

These issues may be the reason why certain elements related to colour, in this case Co in the blue and Sb in the white parts of the same bead, were detected in the spectra of the other coloured part (but of lower intensity/concentration than in the part where it was expected). In this study, spectra of inclusions were considered in a strictly qualitative way, always together with their respective base glass spectra. We focused on the difference between the spectrum obtained from a decorative part from the one of the base glasses to note how the colour of the decoration was achieved.

It was presented in the previous section that some of the analysed samples have higher concentrations of certain elements than the calibration range applied to quantify the data in this study. It chiefly applies to glasses high in Fe and Pb vaguely corresponding to Groups 8 and 16 for the former and Groups 6 and 17 for the latter element. Matter interacts with the X-rays in a way that depends on the composition of the analyte. FP models applied for quantification of compositional data from the spectra were built on the reference materials that were sodium/potassium-lime-silica glasses. Presence of heavier elements in high concentrations can alter the primary and secondary absorption values resulting in lower accuracy for the values of some elements (Markowicz 2001; Adlington et al. 2020). The most evident case of the influence of the presence of one element on the apparent concentration of another would be Fe/Co correlations. It was noted during the XRF/LA-ICP-MS data reproducibility checks. The binary plot in the Figure 4.6 demonstrates the reproducibility of the data for cobalt.

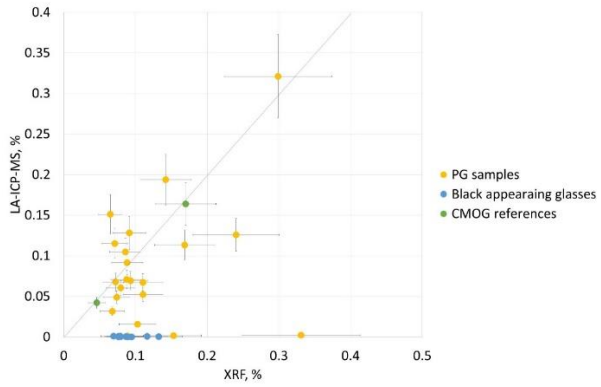

Figure 4.6. Cobalt XRF/LA-ICP-MS reproducibility plot. Diagonal line shows 1:1 ratio. Error bars indicate relative error of the measurements.

It can be observed that the Group of black appearing glasses (Groups 8, 16 and some Other beads and Non-beads) have overestimated p-XRF Co values. Coincidentally, these glasses contain 8.5 – 18.5% of Fe_2O_3 (LA-ICP-MS estimation). Reference materials that were used for FP models validation and corrections of the quantification contain maximum of 2.5% of Fe_2O_3. This makes the p-XRF results for such high Fe glasses unreliable (at least for Fe and elements of similar energy of fluorescence such as Co). Since Co Kα line has approximately same energy as Fe Kβ one, significant increase of Fe concentration, unaccounted by the FP model can result in overestimation of Co concentrations within this model. That is why it becomes important to validate the data by other means. In case of Co it might be done by FORS and/or LA-ICP-MS. It is also beneficial to consider glasses coloured in different way separately. This consideration has influence on the structure of presentation of the results of this study (Part II).

4.5. Scanning Electron Microscopy coupled to Energy Dispersive Spectrometry.

This technique is widely used in ancient glass studies, especially when invasive procedures are permitted (Lahlil et al. 2011; Conventi et al. 2012; Zacharias et al. 2018; Oikonomou et al. 2021). SEM-EDS analyses were carried out on a smaller number of samples (the list of samples can be found in the Appendix 4). These analyses marked the start of stage 3 of the project. Most of the samples that were authorised to be analysed with this method were prepared as polished cross sections. They were exclusively small fragments of glass that were non-compoundable with other fragments, e.g. could not be reconstructed into beads. Such fragments were embedded into the epoxy resin and wet-polished manually using deionised water and several kinds of abrasive paper with the increasingly higher grit number from 500 through 1200, 2400 and 4000. Polishing of samples was finished with 1µm diamond paste on the corresponding polishing substrate. Before the analyses, the cross sections were carbon-coated. Samples that were not authorised to be embedded in resin were analysed in the Variable Pressure (VP) mode without any sample preparation.

The microscope in use was a JEOL (Akishima, Japan) JSM-IT300LV coupled to an Energy Dispersive Spectrometer with SDD detector (Oxford Instruments, Abingdon, UK). Samples were observed and measured using the working distance of 10 mm. The EDS spectra were obtained using 15 kV excitation voltage for 40 s. The system was calibrated and checked in the beginning of every session with Co standard target. Under these conditions spectra of standard reference materials (NIST620, SGT7, 10, CMOG A, B, C and D) were acquired. Spectra of areas at 100×, 200×, 500× and 5000× were acquired. Accuracy at each magnification was assessed by comparing of the acquired values to the reference ones. Assessment has shown that spectra obtained under the highest (5000×) magnification have shown the best repeatability. Hence, it was decided to acquire all the spectra of the samples as approximately square area 10 µm in size at 5000×. To check the dispersion of measurement and potential heterogeneity of the bulk composition, at least 5 EDS spectra were obtained in different places of each sample. The output was calibrated using a built-in INCA software to either NIST620 (for major elements) values or default calibration (minor elements). Calibration counted in the effect of carbon-coating. All compositions were presented as oxides and normalised to 100%. Standard deviation was calculated to serve as precision indicator. The Limit of Detection was set to be 0.1% across the energy range.

Inclusions (if detected) were analysed in the point analysis mode using same settings but more suitable magnifications. Data on inclusions were treated as qualitative. Samples in VP mode were analysed at 50 Pa. Their EDS spectra were acquired at various magnifications. Same reference materials were used to determine the accuracy of measurements but instead of graphitised cross sections, the polished chunks of CRMs were used.

Accuracy of measurements was determined as average relative error of the measurement in both high vacuum and VP modes. Average relative errors, individual for each element detected, are displayed in Figure 4.7. It can be observed that VP accuracy is usually somewhat lower than such for the carbon-coated cross sections. For transition metals, the error values are higher than for alkali, alkali-earth elements and silicon. K and Cu values for both modes of acquisition are very high (42% and 53% in high vacuum mode respectively). Heavier elements do not demonstrate good agreement of the measured values with the certified ones. Data on the elements that show higher than 20% mean relative errors in the high vacuum mode – K, Ti, Cu, Sb, Ba and Pb, are considered qualitative.

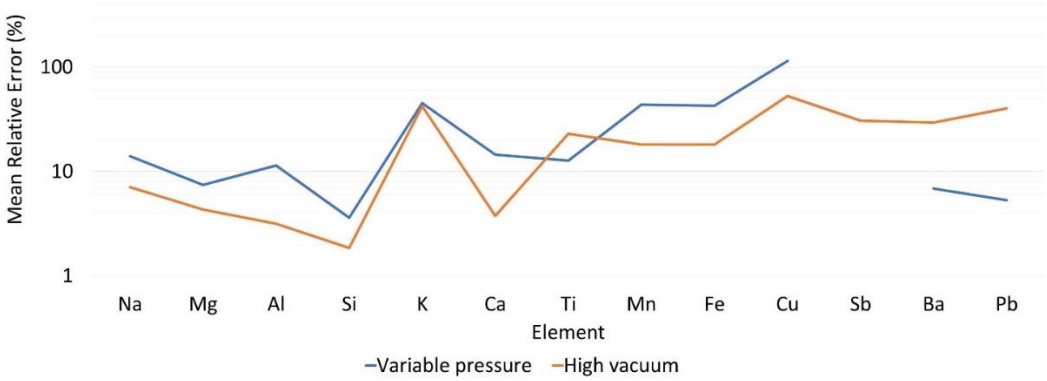

Figure 4.7. Average relative errors calculated for each element in high vacuum and variable pressure modes. Logarithmic scale.

The accuracy of measurement in VP mode, besides being lower than in high vacuum mode suffers from another major issue: glass alteration. With time, glass surface undergoes alkali leaching that changes its composition which changes the composition of the surface (Melcher and Schreiner 2006; Gulmini et al. 2009; Melcher et al. 2010; Hellman 2021). Such alteration was observed in samples discussed in this study. Figure 4.8 contains data on Na_2O levels of samples that were analysed without polishing by VP-SEM-EDS and the data obtained by LA-ICP-MS (from under the altered surface). VP sodium concentrations are at least three times lower than the ones obtained by LA-ICP-MS on the same sample. Cross-section of one of the glass samples confirms the presence of altered layer on the glass surface. This layer is poor in Na (for soda-lime-silica glasses). As a consequence, no accurate compositional information on the pristine glass of such samples can be obtained with SEM-EDS analysis. Apparent compositions of samples analysed in VP mode are considered in a qualitative discussion in this study.

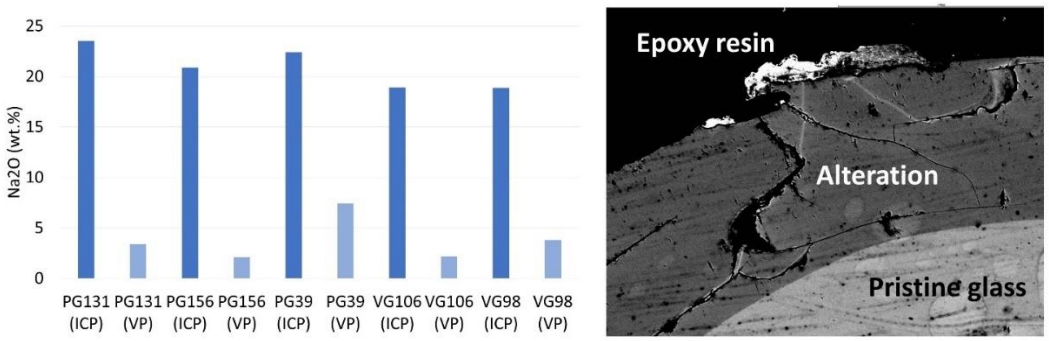

Figure 4.8. Sodium oxide levels of samples analysed without surface treatment by SEM-EDS (VP data) and LA-ICP-MS (ICP data). PG142 cross-section demonstrates the alteration of the surface that prevents obtaining accurate compositions from the sample's surface.

Ca concentrations obtained by the p-XRF analyses were used for LA-ICP-MS quantification as internal standard. In order to re-check the accuracy of the p-XRF Ca results, such concentrations were plotted against Ca concentrations of high vacuum SEM-EDS. Figure 4.9 demonstrates the result of this comparison. As can be seen from the graph, most of the samples are within 20% deviation of p-XRF to SEM-EDS data. The differences between values of two methods can be explained by surface alteration, Ca-rich surface depositions (in case of samples that are above the 1:1 ratio line) or heterogeneity of the samples themselves.

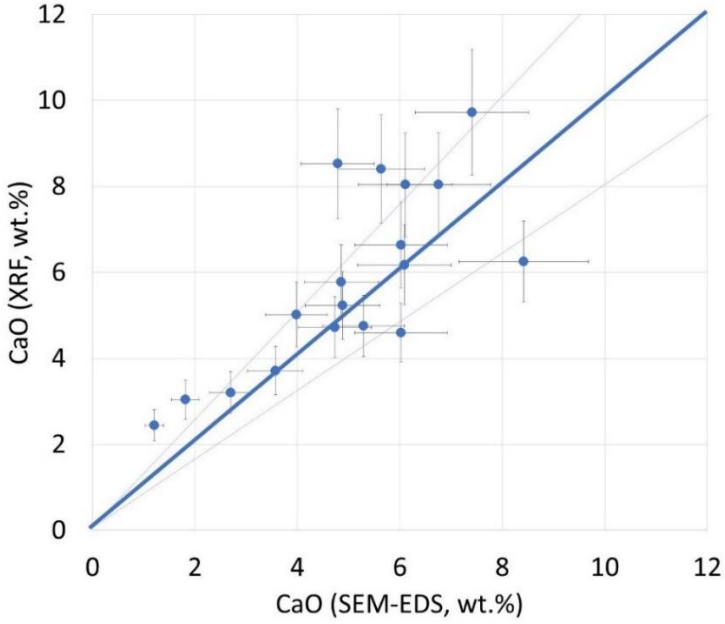

Figure 4.9. Correspondence of SEM-EDS CaO values to p-XRF ones. Diagonal line stands for 1:1 ratio. Thin dotted lines on each side mark 20% deviation. Error bars mark estimated accuracy of p-XRF analyses.

4.6. Micro-Raman Spectroscopy.

Micro-Raman spectroscopy is becoming increasingly well-established technique for the characterisation of glass objects. Raman spectra can be useful for the compositional group attribution, determination of the working range of glass (linked to the compositional group) and the detection of crystalline inclusions suspended in the glass matrix (Colomban 2003, 2008; De Ferri et al. 2012; Vandenabeele et al. 2014; Costa et al. 2019).

Raman shift spectra were acquired using LabRAMHR Evolution (Horiba, Kyoto, Japan) spectrometer. It is equipped with a Peltier-cooled charge-coupled device (CCD) detector. That allowed for the spectral resolution of about 1 cm^{-1}. Measurements were carried out using a He-Ne (633 nm) and an Ar (488-514 nm) lasers. Specifics about what laser was used on what sample are in the Appendix 4. Thanks to its ultra-low wavenumber module, it was possible to acquire spectroscopic information below 100 cm^{-1}. The system was calibrated before each session with a Si (111) standard (520.5 cm^{-1}).

Samples were positioned on the moving stage for focusing. Plasticine was used for positioning the beads. Analytical spot of 1 µm was selected using Leica DMLM microscope with four objectives: 20×, 50× and 100× that were used to focus the beam onto the surface of the cross sections and 50× long working distance objective (Olympus (Japan) to focus the beam on the whole beads surface (to ensure the safety for the objects under analysis).

Several tests were conducted to adjust the power of the laser in order to avoid any damage of glass objects. It was decided to operate at 25% (514 nm laser) and 75% of power for (633 nm laser). All spectra were acquired using 1800 gr/mm grating. Spectral range was set to be 60 – 1560 cm^{-1}. Accumulation of signal parameters were selected to achieve acceptable signal to noise ratio: 3-5 s for 50-450 readings.

At least 3 spectra were obtained for each sample (in case of polychrome glasses for each colour). Some samples did not produce meaningful spectra due to florescence or noise; they are omitted in the discussion. Spectra were smoothened and underwent the background subtraction within LabSpec6 software. It was opted to make linear background subtraction using anchors at ca. 60, 300, 700, 800 and 1300 cm^{-1} in order to bring the bending and stretching silica massifs to the baseline. The massifs' deconvolution was done using Fityk (Wojdyr, 2010) software.

4.7. Laser Ablation Inductive Coupled Plasma Mass Spectrometry.

ICP-MS analyses of vitreous materials push our knowledge of glass making to the new levels due to reliable bulk composition data, even for the elements that in archaeological glass are usually in trace concentrations. Laser ablation became one of the most popular choices for sample introduction when the integrity of the objects is of primary concern, allowing micro-sized amount of matter being extracted from below the altered surface of archaeological glass. This makes LA-ICP-MS one of the best suited methods for ancient glass characterisation (Dussubieux et al. 2009; Panighello et al. 2012; Cagno et al. 2016; Giachet 2019; Hodgkinson and Frick 2020).

Table 4.6. LA-ICP-MS settings.

Laser settings:	
Type	213 nm Nd:YAG
Energy at the sample (For 100 µm spot and 20 Hz)	3.2 mJ
Mode	Continuous pulse
Energy	80%
Repetition rate	20 Hz
Spot size	80 µm
Ablation time	60 s
Gas flow	He, 1L/min
ICP-MS settings:	
Nebuliser gas	Ar, 0.7 L/min
Auxilary gas	Ar, 1.2 L/min
Plasma gas	Ar, 15 L/min
RF power	1550 W
Acqusition mode	Peak hopping
Dwell time for the detector	5 ms for ^{23}Na, ^{27}Al, ^{28}Si and ^{44}Ca; the rest of the masses - 20 ms
n. of detector readings per acquisition	40

NexION 300×Perkin-Elmer (Waltham, USA) ICP single quadrupole mass spectrometer coupled to an ESI NWR 213 laser ablation system (ESI New Wave Research Co., Cambridge, UK) was used for the analyses of glasses. Table 4.6 provides an exhaustive list of settings for both LA system and the way measurements were carried out.

The full list of masses that were measured is present in the Table 4.7. Masses of 38 isotopes were included for the measurements and subsequent determination of concentrations. Table 4.7 also includes the precision (as RSDs of replicate measurements of the CRMs) and accuracy of the measurement (as average recovery values for each element). Settings reported in the Table 4.6 ensured the highest sensitivity of the measurements while being also efficient in preventing the formation of double charged ions and interatomic interferences. These settings were established after several test sessions, where different combinations of power and gas flows were used. Better count rates across the list of masses and better repeatability of measurements were achieved with increased sample depth parameter (the distance between the plasma torch and the interface cones). Optimisation procedures and quality control corresponded to the ones presented in D'Oriano et al. (2008).

Table 4.7. Average recoveries and relative standard deviations (n=69) of QC standards during LA-ICP-MS sessions: CMOG A for major and minor elements, NIST614 for trace elements.

	CMOG A Average recovery, %	**CMOG A RSD, %**		**NIST614 Average recovery, %**	**NIST614 RSD, %**
^{23}Na	97	2.2	^{85}Rb	99	5.2
^{24}Mg	100	5.9	^{88}Sr	98	0.3
^{27}Al	88	3.1	^{90}Zr	97	3.4
^{28}Si	92	3.2	^{133}Cs	97	1.6
^{39}K	80	22.9	^{138}Ba	102	3.4
^{48}Ti	102	8.6	^{139}La	87	8.2
^{51}V	99	1.3	^{140}Ce	99	6.1
^{55}Mn	115	7.6	^{144}Nd	97	9.2
^{57}Fe	91	6.4	^{147}Sm	107	5.2
^{59}Co	96	0.7	^{153}Eu	78	0.1
^{60}Ni	111	1.2	^{158}Gd	107	4.8
^{63}Cu	74	36.8	^{159}Tb	100	3.4
^{64}Zn	103	9.6	^{163}Dy	98	3.2
^{75}As	86	2.4	^{166}Er	112	12.4
^{118}Sn	87	8.3	^{174}Yb	109	6.4
^{121}Sb	96	10.6	^{175}Lu	105	4.7
^{208}Pb	85	4.8	^{177}Hf	101	0.6
			^{205}Tl	98	1.0
			^{232}Th	95	6.3
			^{238}U	100	0.7

Using the settings listed above, each session started by acquisitions of CRMs (CMOG A and NIST612) and blank values (collection of signals from the plasma without ablation). Acquisitions of CRMs were repeated every 4-6 samples to check for eventual instrumental drift and stability of the signal. Other CRMs were also ablated frequently, among them NIST614, CMOG B, C and D. 3–5-point acquisitions were made for each sample to have more representative compositions. During each acquisition, first 10 seconds of ablation were discarded manually by delaying the signal collection after the ablation started. This was done to discard the effect of the initial spark of the signal and to acquire the composition of pristine glass below the altered surface. Penetration through the altered layer was tracked in real time by the counts of ^{23}Na that were increasing comparatively to ^{28}Si ones with time/depth and usually stabilised after first 10 s of ablation. Same way of assessing the validity of results was applied for analyses of the decorative parts. In this case the signals of elements that were suspected to influence the colour of beads were tracked. In case of Group 1 beads the counts of ^{121}Sb for white decorations and ^{59}Co for blue bulk of the beads were tracked in real time. Tests have shown the systematic decrease of ^{121}Sb and simultaneous increase of ^{59}Co at various points

during the ablation. This was interpreted as penetration through the white decoration glass and hence the acquisitions of decorative elements were assumed to be compromised by presence of bulk glass in the ablated sample. In this way only qualitative interpretation of the decoration's data, inseparably from the bulk glass data is possible.

For calibration, NIST612 was used as primary standard. CMOG A (major and minor elements) and NIST614 (trace elements) were used as QC standards. ^{44}Ca was selected as internal standard during quantification procedure, as mentioned in section 4.5. p-XRF values of Ca were used to quantify the concentrations of elements obtained during the LA-ICP-MS analyses. After quantification the data of replicate analyses were averaged, major and minor elements were converted to respective oxides and the final result was normalised to 100%. It was noticed that Mg, K and Ti values were systematically under- or overestimated based on the CRMs output, so it was decided to "correct" their values using the coefficients that were calculated as average ratio of certified to acquired concentration in the CMOG glasses. All values of Mg were divided by 1.29, K by 0.82 and Ti by 0.68. Table 4.7 presents the recoveries of already corrected values for these elements. Limits of Quantification were calculated as 10× deviations of the background counts individually for each sample and element. As a rule, the LOQs do not exceed 2 ppm for trace elements being significantly higher for the major ones (but still being much lower than the concentrations of these elements in samples). Data for a few samples were discarded due to the low or extremely high total ppm values (monitored before normalisation).

4.8. X-Ray Diffraction.

Only 13 samples were analysed by the μ-XRD (Appendix 4). XRD studies of vitreous materials are targeted, expectedly, at the eventual crystalline phases that enter the batch and withstand glass-making processes or are formed on cooling (Lahlil et al. 2008; Costa et al. 2019; Emami et al. 2020). As a rule, one diffractogram was acquired for each sample, except for the cases where the peaks were not pronounced, or the Bremsstrahlung precluded their registration. SMARTLAB XE - Rigaku diffractometer was used. Configuration of the instrument was adjusted to operate in micro-diffraction mode. Cu Kα source radiation (wavelength - 1.5406 Å) was passing through 2 mm slit. The 2θ range was fixed at 3-70° with angular increment of 0.02° and speed of 0.5°/min. HyPix-3000 HPC detector with an active area of about 3000 mm^2 was used to capture reflected X-Rays in 1D scan mode. The resulting diffractograms were studied with DIFFRAC PLUS, EVA Application 7.0.0.1' (2001) by comparing the peaks with JCPDS-ICCD, ICSD and PCPDFWIN diffractogram databases and data available in the literature on XRD analysed of vitreous materials.

Conclusion. In addition to presenting the experimental procedures and equipment used in this study, this chapter includes an evaluation of the performance of the selected methods. The methods used here are well-established in the studies of ancient vitreous materials, but several methodological and logistical constraints are unique to this study. It was, therefore, essential to have both portable and high-performance laboratory equipment to address the archaeological questions posed in this study. Another critical issue presented and discussed here is the reproducibility of the results. The analytical accuracy of compositional analysis methods has been calculated, and their performance has been compared. The limitations of the chosen methodology were clarified by

establishing the accuracy and limits of quantification. The two-stage approach, with the last stage involving a smaller number of samples studied in the laboratory, made the overall research logistically simpler and rationalised the use of equipment and time while maintaining good representability of the final results. The use of several compositional (p-XRF, SEM-EDS and LA-ICP-MS) and structural (OM, FORS, μ-Raman and μ-XRD) methods of analysis allowed cross-checking of the data and more robust conclusions based on information from multiple sources.

PART II. RESULTS AND DISCUSSION.

This part of the thesis consists of 7 chapters in which the results of the analytical study are presented together with their interpretation. The typological classification discussed in Chapter 3 has been maintained throughout Part II and the compositional data are discussed within this typological framework. The overall chemical data obtained for the whole set of glass objects have been divided into six chapters, namely Chapters 5 to 9, each of which considers several typological groups, either as a whole or as selected objects.

The decision as to which group (or which objects of a particular group) should be included in each chapter was dictated by the glass's colour and its general appearance. p-XRF analyses gave further reasons to implement the subdivision of the archaeological finds into chapters within this dissertation. Indeed, the p-XRF study allowed us to identify the colouring elements and gather preliminary information on the raw materials. At the same time, Chapter 4 highlighted that the concentration of certain elements (which incidentally affected the colour/opacity) was above the calibration range of the p-XRF equipment, thus affecting the accuracy of the p-XRF results; it was opted to keep these objects in separate chapters.

Chapters 5-9 have a similar structure. Each of them consists of two main sections: one with the results obtained by each method/technique used for the analyses and the other one with their discussion. The results include a description of the most evident morphological features observed with the naked eye and under the portable microscope. The discussion is structured around the research questions: sources of silica, flux and stabiliser sources, colourants, and technical aspects related to the production of glass objects. Each research question is approached by combining/cross-checking the results obtained from the different methods employed for the analysis.

Chapter 10 is somewhat separated from the general discussion. It concerns all the faience objects included in the overall sample set. They were mainly studied non-invasively. Data were limited, and faience as a material was not presented in Chapter 1; therefore, Chapter 10 is almost self-consistent, relying on Part I only to describe the analytical methods.

Chapter 11, which concludes Part II of the dissertation, is a synthetic review of the technological and provenance aspects discussed in Chapters 5-9. It is aimed to compare typological groups and to provide a broader view of the glass supply by combining compositional, typological, chronological and spatial (in terms of distribution and provenance) aspects, making it possible to highlight the evolution of the glass supply in South Etruria and Latium during the first half of the first millennium BCE and to provide the basis for the conclusions of the whole research.

Part II

CHAPTER 5	Group 1; Group 2; Group 7; Group 14: VG33 and 34; Other beads: PG168 VG54; Non-beads: VG1, 2, 13, 32.
CHAPTER 6	Group 3; Group 4; Group 12; Group 13; Other beads: PG169, 170 VG28 and 38; Non-beads: PG59, 60.
CHAPTER 7	Group 5; Group 10; Group 11; Other beads: PG90, 172 VG88; Non-beads: PG97, VG5, 6, 56, 114.
CHAPTER 8	Group 6; Group 17; Group 18: VG81; Other beads: VG85; Non-beads: VG3, 4, 7, 9.
CHAPTER 9	Group 8; Group 14: VG37; Group 15; Group 16; Group 18: PG3 and 64; Other beads: PG5, 6, 32, 58, 66, 113, 114, VG18; Non-beads: PG57, 61, 62, 135, VG92, 93.
CHAPTER 10	Group 9 Other beads: VG16, 27.

Figure II. Distribution of samples by chapters of part two.

CHAPTER 5. COBALT-COLOURED GLASSES.

The following archaeological objects are discussed in this chapter:

- **Group 1: all;**
- **Group 2: all;**
- **Group 7: all;**
- **Group 14: VG33 and 34;**
- **Other beads: PG168 and VG54;**
- **Non-beads: VG1, 2, 13, 32.**

5.1. Results of the analyses.

5.1.1. Visual observation and Optical Microscopy.

Close observation with the naked eye and optical microscopy supported by digital imaging highlighted and documented the variability of the texture, the preservation state of the surfaces, the decorations and other details that can be useful to describe the present state of the archaeological object considered in this work. For some beads, morphological features and/or texture are typical of their Group. Visual documentation done with optical microscope is systematised below.

The beads of Group 1 feature various degree of preservation of their white-coloured decorative parts. On some beads, such as PG44, 100, 109, VG97 and VG113, the white decorations are fully preserved, whereas on the others the white parts are partially or completely lost (Figure 5.1). Beads with white glass preserved (Figure 5.1 a and b) show small cracks and surface depositions at the interface between the blue and white glass. Coils of white glass have various width and depth. Sometimes the ends of the coil do not meet. Sometimes the ends overlap forming wider side of the resulting ring as can be seen in Figure 5.1 d, where two groves are visible next to each other, which were left by the lost white decoration. Microphotographs include objects of the same type as those in Group 1, that were not studied with analytical methods and do not have any “laboratory name” assigned. For those beads, the archaeological context is used for their identification in the caption.

The shape of the majority of the beads of this Group is not regular. It can be seen in the images in the Appendix 2 that many beads of Group 1 feature protrusions at one of the apexes (Figure 5.1e), which may be related to the forming process of the bead. The internal surface of the aperture is usually covered in a brown residue of variable thickness (Figure 5.1 e and f). In several beads, some material other than glass is present inside the apertures. As a significant example, in the aperture of PG109 (Figure 5.1 f) a piece of (apparently) copper or bronze is visible, which could be a residue of the original wire passing through the apertures. Bubbles inside the glass matrix are often visible (Figure 5.1): they are small, round and not numerous. Surface of the better-preserved beads is smooth, but signs of alteration (iridescence, cracking or indentations) can be observed on every item in this Group.

Group 2 beads are similar to those of Group 1 (Figure 5.2). Sample VG64 (Figure 5.2 a) has a pear shape, that might be unintentional because of its asymmetry. On one of the sides, the yellow coil is of smaller span and does not close the circle (Figure 5.2 a). On contrary, VG65 features a ring eye with overlapping coil. Samples of Group 2 exhibit larger bubbles than those in samples of Group

1 (see Figure 5.1 b and Figure 5.2 c), though their sizes are variable. No advanced signs of detachment of the decoration glass were noted.

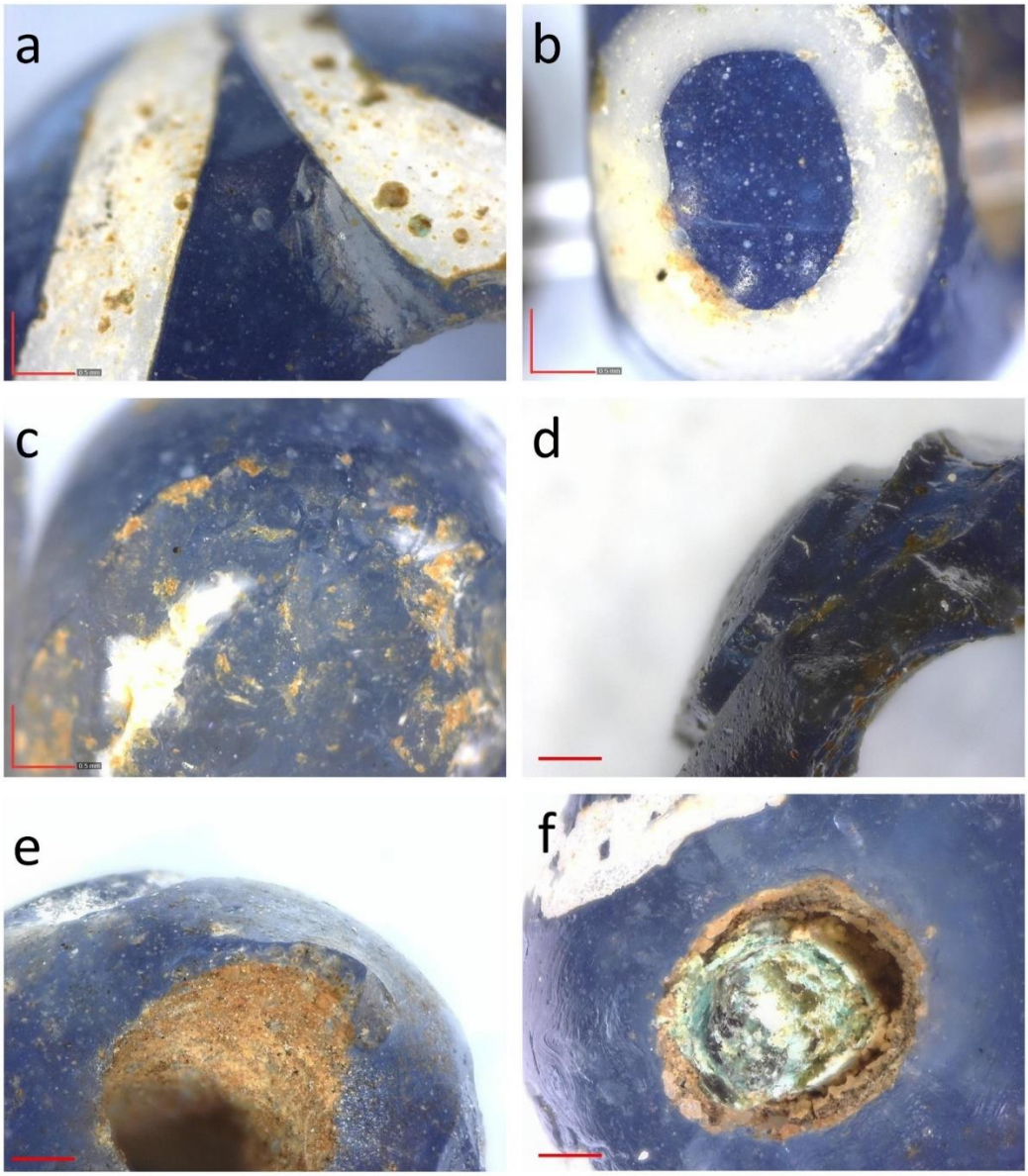

Figure 5.1. Microphotographs of Group 1 samples: a – eye decoration fragment of PG111; b – eye decoration of a bead from tomb 94 of Le Saliere necropolis near Capena site; c – deteriorated eye decoration of a bead from tomb 16 of Vaccareccia necropolis near Veio site; d – profile of eye decoration of PG86, where the white part is lost; e – protrusion near one of the apexes of VG20 and the surface of the aperture; f – aperture of the PG109 with some material inside. Scale bar is equal to 0.5 mm.

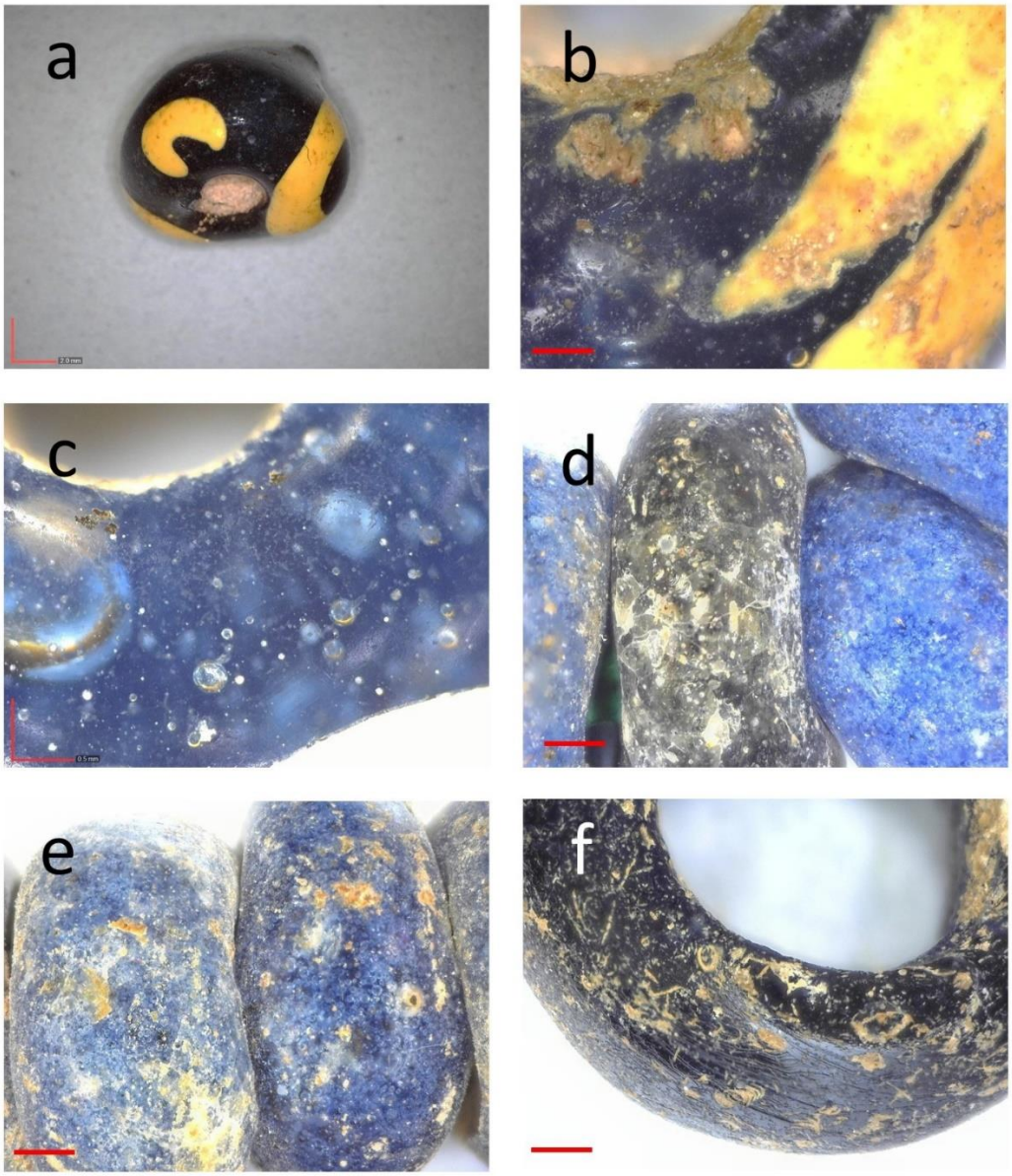

Figure 5.2. Dinolite images of samples of Groups 2 and 7: a – VG64 with the incomplete coil; b – overlapping of the coil on the surface of VG65; c – bubbles inside the VG80 bulk; d – different shades of samples of tomb 13 in Vaccareccia necropolis near Veio site and the bubbles suspended in the glass matrix; e – samples from tomb 20 in Vaccareccia necropolis near Veio site; f – surface of PG158 covered by cracks and round indentations. Scale bar in image a is 2 mm long while in the rest of the images it is 0.5 mm.

Samples of Group 7 are somewhat diverse in appearance. The beads within this Group have different texture and colour (see section 3.3). PG158 and PG159 have linear and circular indentations spread across their surface (Figure 5.2 f). Many beads within this Group seem to have small cracks and collapsed bubbles on the surface filled with brown residue. Small (100 µm or smaller) bubbles

are visible under the surface of blue variant of type 7 samples (Figure 5.2 d and e). Samples of type 7 seem to have similar protrusions near the apexes, that add some asymmetry. Samples of type 8 have more rounded apexes, but similar protrusions appear on some specimens.

VG33 and VG34 (Group 14) surface features are similar to those of Group 2 ones, with larger bubbles visible under the surface (some 200-300 µm across, but smaller ones are also present), smooth surface and wave decoration imperfections: in VG33 the ends do not meet, while in VG34 they overlap. Yellow glass shows the mixture of brighter and darker parts of the glass. It is also noticeable that the state of white decorative part on beads of Group 1 is worse than that of the yellow decoration on beads of Group 2, featuring numerous cracks. Figure 5.3 a and b demonstrate the differences discussed above for white and yellow glass, and also show the blue bases for these beads.

The remaining seven samples that are considered in this chapter (PG168, VG1, 2, 13, 32 and 54) demonstrate better preserved surfaces if compared with VG33 and VG34. Yet, under magnification, it is possible to see crizzled areas and iridescent spots (Figure 5.3 c, d). VG54 has areas of detached decoration that appear to be similar to Group 1 beads.

Round bubbles of various sizes were noticed in PG168, VG1, 2 and 54. For the bracelets (VG13 and 32), the bubbles are instead elongated (Figure 5.3 d lighter spots under the surface), which points to the stretching of a glass cylinder to form the object.

Buttons (VG1 and 2) have dark and brown residue in the pit for attachment.

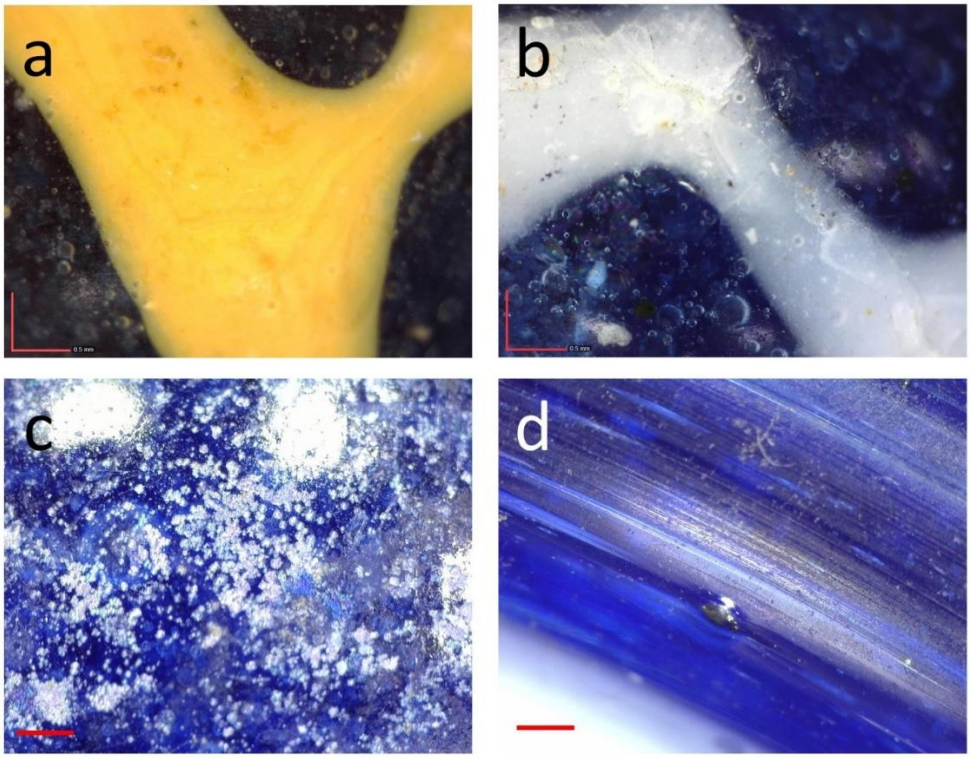

Figure 5.3. Dinolite images of decorations of Group 14 samples (a - VG33, b - VG34) and surfaces of VG1 (c) and VG13 (d). The scale bar is equal to 0.5 mm on all the images.

5.1.2. Apparent colours and Fibre Optics Reflection Spectroscopy.

This section presents the results of the colour documentation. Colour was measured by means of RBG data of the images taken during the photographic sessions within the museums, following the procedure that is detailed in section 3.2.3. RGB data are considered here together with the results of FORS. This allows to present the values of the apparent colours by distinguishing the influence of the specific chromophores (detected by FORS) from the influence of other physical factors - such as bubbles inside the bulk of glass, size/thickness of the sample, glass degradation - which can influence the colour that is captured by the camera.

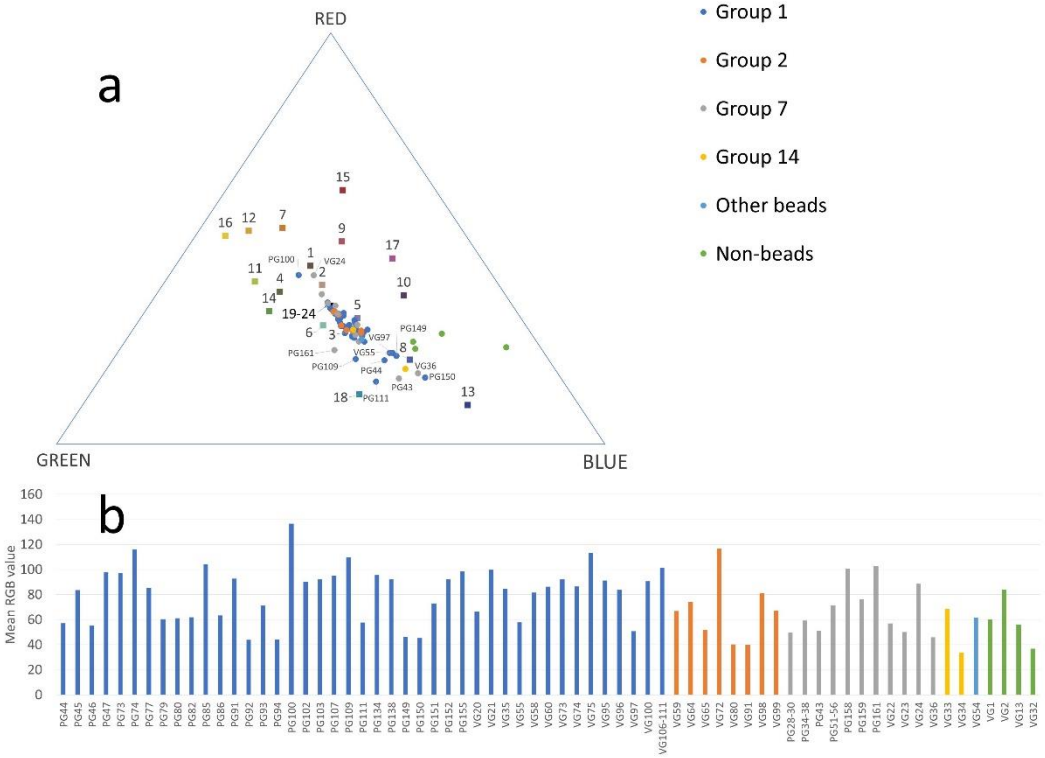

Figure 5.4. RGB values of the samples in each Group considered in this chapter. a - RGB normalised tri-plot with indicated coordinates of the ColorChecker (numbered squares), introduced in Chapter 3. The colours of the squares correspond to the colours of the references. Squares 19-24 are the grey scale (white to black) positioned in the centre of the tri-plot. b - mean of the RGB values of each sample; these values are a raw estimation of the lightness of the colour, with lighter colours having higher mean values and darker colour featuring lower mean values.

The RGB colour data are reported in Appendix 3 for all the beads already presented in Chapter 3. For the samples considered in this chapter RGB values are plotted in Figure 5.4. Fragmentary beads are omitted, as they might introduce some bias into the dataset due to their higher translucency connected to low thickness. For some beads, for example PG168, it was not possible to guarantee the standardised conditions needed for photographic acquisition, and were therefore not included

in the RGB set. The RGB values obtained from the photos of Non-bead objects were added as a separate Group. It can be seen in Figure 5.4(a) that samples are mostly stretched from the centre of the tri-plot to its blue side (the vector from squares 19-24 to 8 of the ColorChecker). Some samples are skewed on the green side and Non-beads are skewed to the purple side (closer to square 10). Bar graph of the grey scale (Figure 5.4b) demonstrates variability in the average RGB values within every Group though Group 1 samples are lighter on average.

FORS spectra provide information on the chromophores. A summary of spectral features detected for the beads in this study is reported as a table in Appendix 5. Figure 5.5 gathers the typical spectra obtained from the samples considered in this chapter; their interpretation is based on Micheletti et al. (2020) and the references therein, which report characteristic bands of the chromophores in glass. Absolute majority of the samples produced similar spectra, featuring Fe^{3+} bands in the UV-blue region of the spectrum (at about 380, 420 and 440 nm). Incidentally, these bands might also indicate the presence of Mn^{2+} dissolved in glass and compositional analysis will confirm or disprove its presence. Spectra in this region might have varying normalised relative reflectance levels demonstrated by samples PG109 and 155 (high violet reflectance) and VG58 (low violet reflectance). Co^{2+} bands, centred at approx. 540, 600 and 640 nm are also present. Absorption in the NIR region of the spectra, that increases towards the end of the spectral range, indicates the presence of Fe^{2+}. This latter band is present with a great variation from sample to sample. Other samples absorb NIR light in the range of 725 to 875 nm, which is the sign of Cu^{2+} presence (see sample PG109 in Figure 5.5).

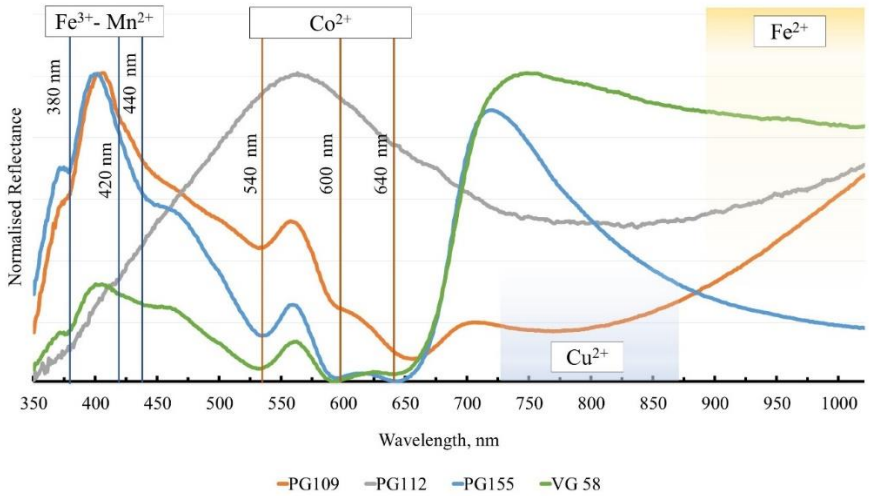

Figure 5.5. Representative FORS spectra of samples with the positions of bands marked by either vertical lines (Fe^{3+}, Co^{2+} bands) or by areas (Cu^{2+} and Fe^{2+} broad bands).

The list of samples that feature Cu^{2+} band in their FORS spectra includes: PG109, 110_1, 111, 112, 138, 151, and VG73 (Group 1) and PG158, 161 (Group 7). Moreover, PG112 and 161 do not show any Co^{2+} in their respective spectra. PG112 demonstrates Cu^{2+} and weak Fe^{3+} band, representing this type of spectrum in Figure 5.5. PG109, 111 and 161 are the samples that were skewed to the green zone in the tri-plot in Figure 5.4. FORS maximum of PG112 and 161 is shifted to the green region (495-570nm). The rest of the samples that demonstrated the Cu^{2+} signals have their

respective FORS reflection maxima in the blue region, and repeat the profile of most of the samples, as shown by PG109 in Figure 5.5. Sample VG24 is a single example within this chapter that features a pronounced band at 560 nm, that corresponds to the presence of Cu^0.

Dark coloured samples, in several cases, did not produce meaningful FORS spectra.

5.1.3. Portable X-Ray Fluorescence spectrometry.

p-XRF analyses, carried out using three different XRF units, provide the compositional data that allowed comparison of samples within and between the Groups. Compositional data obtained by p-XRF supported the selection of the samples for further analyses in the laboratory. Consequently, p-XRF data were used to link the composition of the objects analysed in the laboratory with the composition of those beads that could not leave the museum. Appendix 6 reports composition determined by p-XRF for all the samples considered in this study.

Principal Component Analysis (PCA) is the first approach to visualise the p-XRF data in order to highlight general compositional trends (Figure 5.6). Only the compositions of the base glass (i.e. excluding decorations) are considered, whereas the p-XRF results for the decorative parts are briefly discussed at the end of this sub-section.

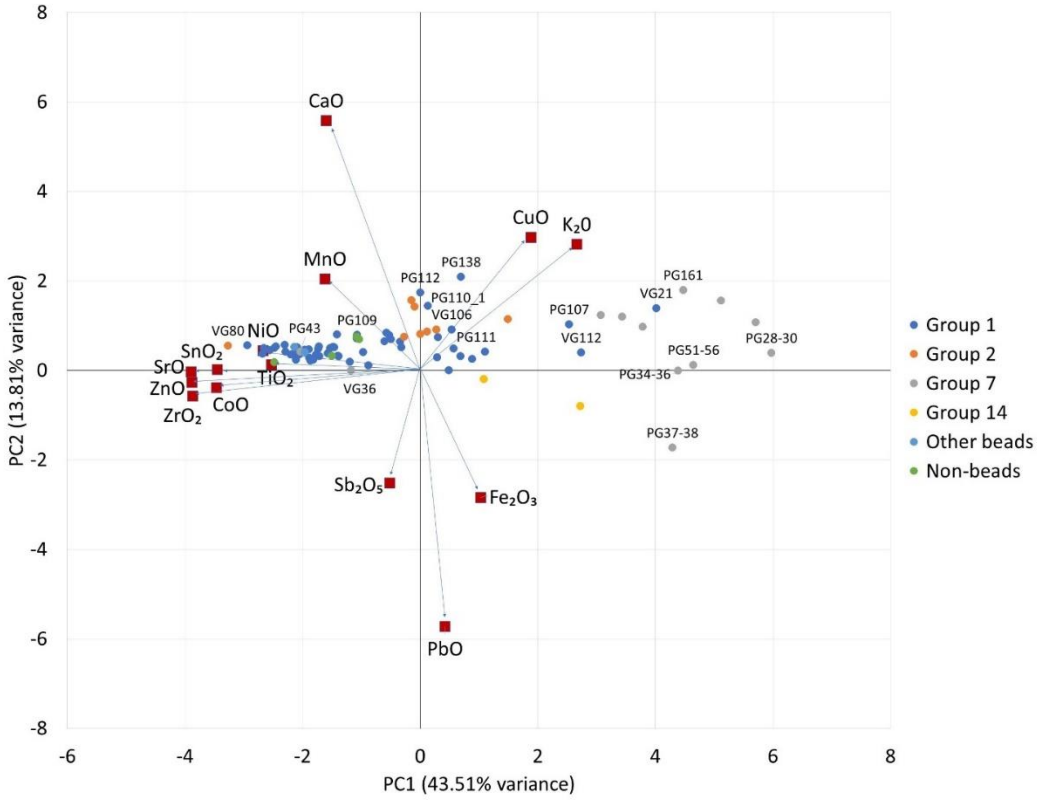

Figure 5.6. Results of the Principal Component Analysis performed on the samples included in Chapter 5. Scores and loadings are situated in the same plot. Loadings values were multiplied by 10 to increase legibility of the plot.

The first two PCs account for 57% of explained variance. Yet the main division of samples only appears along the PC1. The PCA plot shows the difference of Group 7 from the majority of the samples attributed to other Groups, with K and Cu playing the major role in this separation.

Samples of Group 7 feature higher values of PC1 and they contain more K_2O than the rest of the samples (some more than 5%). PG43 and VG36, which also feature a different shape than majority of the other beads of Group 7, stand out of this general picture. The samples of the other Groups contain less than 1% of K_2O, except for VG21 (which is also evident from the Figure 5.6) that contains 2.4% K_2O.

CuO levels detected by p-XRF are variable, but the samples that demonstrated Cu^{2+} bands in their FORS spectra also have Cu confirmed by p-XRF. It is evident in the PCA plot that PG107, 109, 110_1, 111, 112, 138 and VG106 are slightly elevated along the PC2 axis and are outside the centre of distribution of the Group 1 samples. Group 2 samples also seem to be divided by the Cu content: Cu is not detected in VG59, 80, 91, whereas VG64 has the lowest detected Cu concentration (0.15%). These samples are included in the larger variety of the Group 2. The rest of the Group 2 samples feature CuO between 0.34 and 0.75%. Samples of Group 7, as well as those of Group 14 and the Non-bead objects, also contain minor amounts of CuO, with the exception of PG34-38 and PG43. No Cu was detected in PG168 and VG54.

Minor elements such as Ti, Co, Ni, Zn, Sr, Zr, and Sn strongly influence PC1 too. Most of the samples considered here show negative PC1 values, determined by the presence of one or more of this set of elements. Ca and Fe strongly influence the distribution of the samples along PC2. To better highlight the grouping or trends based on compositional data, several scatter plots are presented in Figure 5.7.

Cobalt appears to be positively correlated with Ni and Zn in a majority of samples (Figure 5.7 a, b), with two noticeable exceptions: of most of the samples in Group 7 and the Non-beads. For most of the samples of Group 1, Co demonstrates a strong positive correlation with both Ni and Zn. Several samples already mentioned above for their elevated Cu contents do not contain detectable amount of Ni and Zn, and this compositional trait separate them from the rest of the samples.

Group 2 is divided in these plots – while the samples VG59, 64, 65 and 91 are following the trend set up by majority of the samples of Group 1, the rest of the beads have very little (if any detectable) quantities of these elements.

Also Group 7 samples do not remain together in the plots. Group 14 is not always consistent with the general compositional trend: while VG33 and 34 appear to have proportional concentrations of Co and Ni, they lack in Zn. VG54, from the Other beads Group, does not have Co detected. On contrary, PG168 stays together with the majority of the beads in these plots. The Non-beads mostly lack Ni and Zn values.

K_2O vs CaO plot (Figure 5.7 c) highlights a division within the samples of Group 7 based on three K_2O levels: PG43 and VG36 – below detection limit, PG28-30, 34-38, 51-56 and VG22 – 1–2%, and PG158, 159, 161, VG23, 24 – more than 3%. The rest of the samples seldom contain more than 1%. Exceptional, within the Group 1 is the VG21 that contains 2.4% K_2O. Remarkable is the outstanding quantity of CaO in samples of Group 14 and in the Non-beads, which is even more evident in the CaO vs SrO plot (Figure 5.7 d). In this plot, most of the samples are clustered and show some positive relationship between the elements. Separate trends might be noted for Group 2 and

part of Group 7, but the precision of the data, showed in the Appendix 6, does not allow to speculate on whether or not this division is significant.

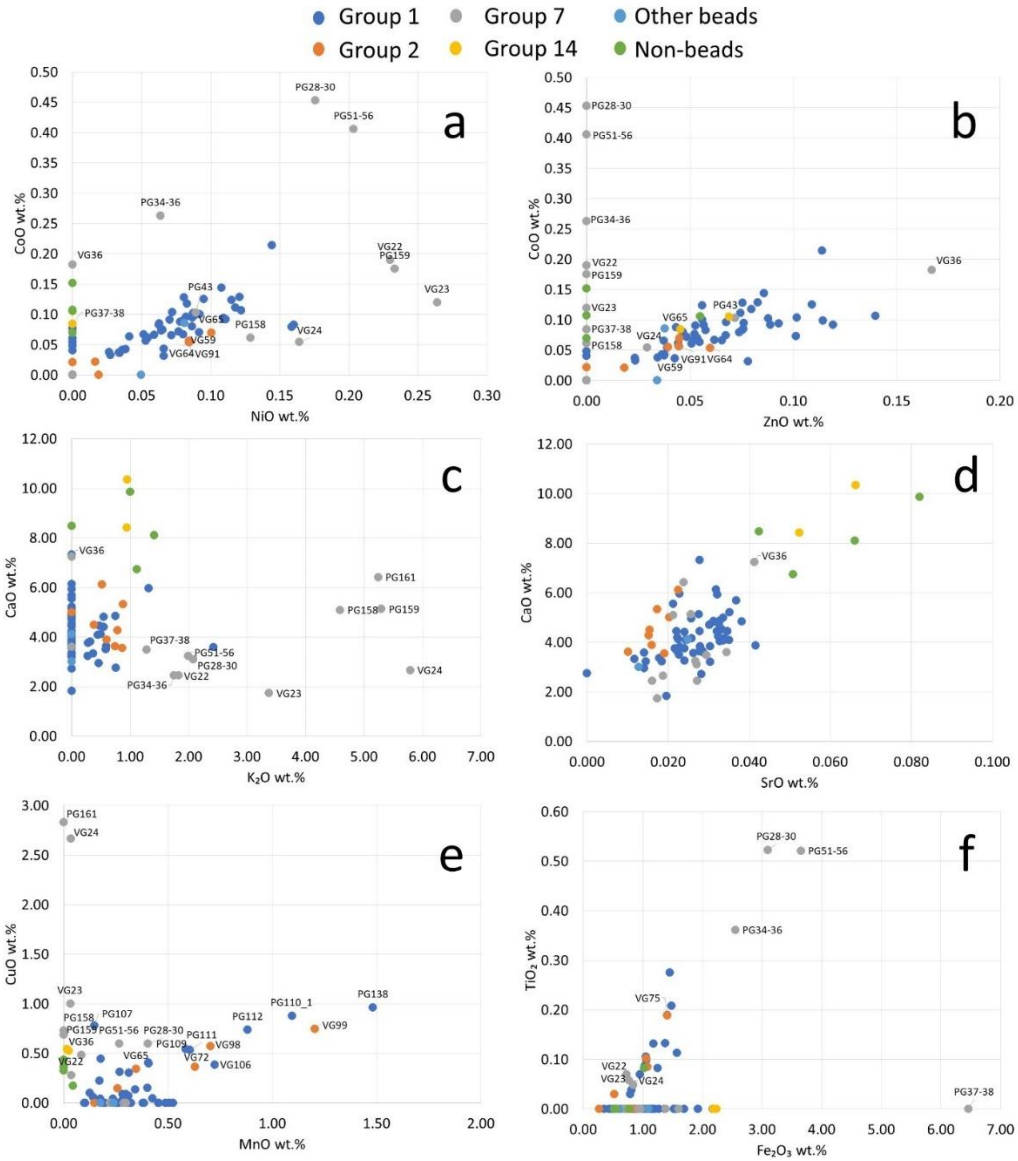

Figure 5.7. p-XRF results. Binary plots of selected oxides: a – CoO vs ZnO; b – CoO vs NiO; c – K_2O vs CaO; d – MnO vs CuO; e - SrO vs CaO; f – Fe_2O_3 vs TiO_2. Values that are below the LOQ are set to 0.

MnO vs CuO binary plot (Figure 5.7 e) demonstrates a positively correlated Group of samples formed by the representatives of Group 1 (PG109, 110_1, 111, 112, 138 and VG106) and a small variant within Group 2 samples (VG72, 98 and 99). Group7 mostly takes a high-Cu-low-Mn trend, with the exception of PG28-30 and 51-56. Groups 14 and Non-beads only have trace amount of Mn,

in their composition, coinciding with a minor concentration of CuO (below 0.5%). The rest of the beads are kept within of 0.5% of each element.

Ti appears to be positively correlated with Fe if the LOQ permits the detection of the former element (Figure 5.7 d). Samples PG37-38 contain 6.47% of Fe_2O_3 without proportional gain in TiO_2 similar to other samples of Group 7. Another feature of interest of several Group 7 samples is detectable Zr levels, above 180 ppm in samples PG28-30, 34-36, 51-56. Zr was also detected in PG168.

Regarding the decorative parts of these samples, the p-XRF data must be discussed taking into consideration the composition of their respective base glass. Figure 5.8 presents such comparison for the white decorations of Group 1 (a) and yellow decorations of Group 2 with VG33 from Group 14 (b). Ca and Sb levels in white decorations of Group 1 are generally higher than those in the blue bases. A same systematic difference is observed for both Sb and Pb concentrations, which are higher in the yellow decorations of Group 2 in respect to their blue glass bases. This qualitative difference is fundamental for establishing the colouring and opacifying agents in the decorations.

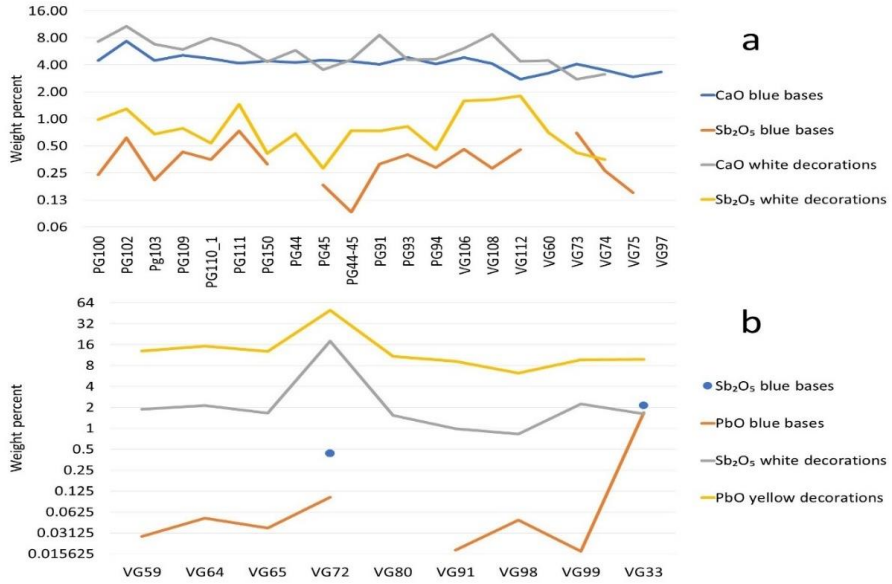

Figure 5.8. p-XRF data. Linear plots of concentrations of selected oxides per each sample in the bases' glass and their respective decorative parts. a – blue bases' values of CaO and Sb_2O_5 compared with those observed in white decorations of Group 1; b – blue bases' values of Sb_2O_5 and PbO compared with those observed in yellow decorations of Group 2 and VG33 (Group 14). Values below LOQs are omitted in the plots. Logarithmic scale.

A majority of the samples discussed in this chapter could not be transported to the laboratory. It is reasonable to assume that the results obtained with the analytical techniques employed in the laboratory (i.e. SEM-EDS, µ-Raman, µ-XRD and LA-ICP-MS) can be extrapolated for the samples that were analysed in the museums by FORS and p-XRF on the basis of the similarity highlighted by these latter techniques. In this way, the content of light and trace elements of the samples of Other beads Group that were not taken to the laboratory is assumed to be similar to the main sub-Group for

Group 1 samples. Group 14 samples are assumed to be similar to Non-beads and particularly VG32 – the only Non-beads Group representative that was analysed in the laboratory. Smaller variety of Group 2 samples is assumed to be similar to VG98 and the Cu-Mn rich sub-Group within Group 1. The larger variety of Group 2 is assumed to be similar with the major part of Group 1 samples. Group 7 samples appear to be heterogeneous. VG36 is assumed to be similar to the Group 14 and non-beads, PG43 to main sub-Group of Group 1, whereas the samples of the high K and high Fe varieties are all represented in the sample subset that reached the laboratory facilities.

5.1.4. Scanning Electron Microscopy coupled with Energy Dispersive spectrometry.

Eight samples were analysed with SEM-EDS: four were prepared as polished sections and analysed in high vacuum mode (PG110_1, 110_2, 139 and VG32) and four were analysed without any preparation in variable pressure mode (PG156, VG22, 98 and 106). Compositions of the bulk analyses are presented in the Table 5.1. Samples analysed as cross sections are soda-lime-silica glasses. Samples analysed without any preparation seem to lack sodium, but appear to have more K_2O (up to 2.5%), which can be a consequence of glass alteration (Gulmini et al. 2009), that lead the surface to be deplete in Na_2O. Altered layers of glass were in fact observed under the SEM-EDS on the surface of the samples prepared as cross sections, and these altered parts were not included in the determination of the bulk composition of the glass. Figure 5.9 represents the data from Table 5.1 in the form of a bar graph of normalised (100%) values to visualise the difference among samples.

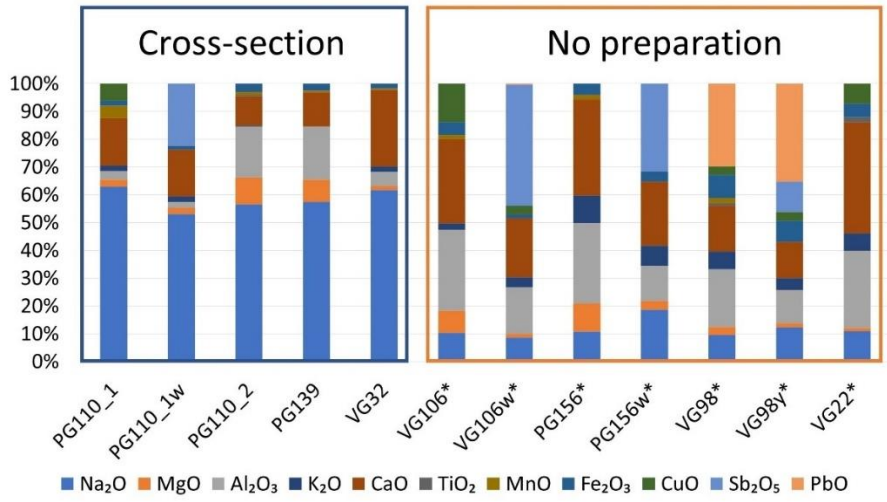

*Figure 5.9. Normalised to 100% totals SEM-EDS data of some oxides from Table 5.1. Results are divided into those obtained from the polished surfaces of the samples (left) and the surfaces that were not prepared in any way. *samples analysed in the VP mode without any sample preparation. VG98 belongs to the Group 2, VG22 to Group 7, VG32 to the Non-bead objects. The rest of the samples represent Group 1.*

The main component of all samples – SiO_2 - is omitted to magnify the difference in other components. The biggest difference among the samples is the Na_2O depletion of the samples that

were analysed without any preparation. Apart from PG110_1, MgO and Al_2O_3 are abundant in samples of Group 1. Al_2O_3 alone is also present in the samples of Groups 2 and 7 (VG98 and VG22 respectively). VG22 and VG32 have more CaO than the rest of the samples. PG110_1 has much more MnO than the rest of the samples which in addition to elevated CuO concentration corresponds to p-XRF data. Cu was detected also in VG22, 98 and 106. FeO level is elevated in VG98 (Group 2 representative). Sb rich inclusions were detected in Group 1 white decorations glass (Figure 5.10 a and b). Pb rich inclusions were detected in VG98 – the only representative of Group 2 analysed with SEM-EDS. These differences in composition are consistent with the p-XRF data (Figure 5.8). Fe and Cu rich inclusions were among the most frequently detected in the blue bases of this sample set.

*Table 5.1. Results of the EDS analyses. Values represent averaged bulk compositions with the standard deviations of the replicate analyses placed beneath the composition data. *data obtained in the VP mode on the untreated surfaces.*

Group	Sample/ st.dev.	Na_2O	MgO	Al_2O_3	SiO_2	SO_3	Cl	K_2O	CaO	TiO_2	MnO	Fe_2O_3	CuO	Sb_2O_5	PbO	Inclusions and trace occurences
1	PG110_1	17.48	0.74	0.85	71.00	0.38	1.29	0.53	4.73	<LOD	1.25	0.48	1.71	<LOD	<LOD	Cu
	st.dev.	*0.20*	*0.01*	*0.07*	*0.66*	*0.07*	*0.04*	*0.07*	*0.09*	-	*0.06*	*0.02*	*0.20*	-	-	
1	PG110_1w	16.53	0.73	0.67	68.29	0.81	0.71	0.60	5.26	<LOD	<LOD	0.44	<LOD	6.93	<LOD	Sb, Cu
	st.dev.	*0.06*	*0.06*	*0.05*	*0.64*	*0.11*	*0.01*	*0.11*	*0.11*	-	-	*0.03*	-	*0.56*	-	
1	PG110_2	19.23	3.30	6.24	64.89	0.58	0.67	0.12	3.58	0.19	0.34	0.99	<LOD	<LOD	<LOD	Cu, Fe, Ni, Cr
	st.dev.	*0.21*	*0.05*	*0.06*	*0.25*	*0.05*	*0.02*	*0.05*	*0.09*	*0.01*	*0.06*	*0.06*	-	-	-	
1	PG139	18.60	2.61	6.19	66.40	0.84	0.63	<LOD	3.98	<LOD	0.16	0.81	<LOD	<LOD	<LOD	Ca, Fe, Cr
	st.den.	*0.39*	*0.02*	*0.08*	*0.38*	*0.03*	*0.02*	-	*0.04*	-	*0.03*	*0.06*	-	-	-	
Non-beads	VG32	18.53	0.47	1.48	68.63	0.35	1.37	0.58	8.24	<LOD	0.21	0.50	<LOD	<LOD	<LOD	Ca, Fe, Co
	st.dev.	*0.09*	*0.03*	*0.05*	*0.17*	*0.05*	*0.04*	*0.06*	*0.23*	-	-	*0.10*	-	-	-	
1	VG106*	2.19	1.68	6.08	77.29	1.67	0.24	0.47	6.36	<LOD	0.33	0.96	2.89	<LOD	<LOD	
	st.dev.	*0.15*	*0.11*	*0.12*	*3.31*	*0.27*	*0.05*	*0.18*	*0.39*	-	*0.08*	*0.12*	*3.25*	-	-	
1	VG106w*	2.80	0.46	5.35	66.07	3.63	0.29	1.16	6.86	<LOD	<LOD	0.44	1.02	13.97	0.12	Sb
	st.dev.	*0.43*	*0.09*	*0.62*	*9.41*	*1.22*	*0.11*	*0.17*	*2.95*	-	-	*0.13*	*0.35*	*7.53*	-	
1	PG156*	2.10	1.99	5.66	79.06	0.96	0.52	1.93	6.73	<LOD	0.33	0.77	<LOD	<LOD	<LOD	Fe, Ti, Pb
	st.dev.	*0.25*	*0.35*	*0.32*	*1.56*	*0.04*	*0.07*	*1.14*	*0.93*	-	*0.09*	*0.26*	-	-	-	
1	PG156w*	6.50	1.09	4.36	62.94	2.68	0.92	2.49	8.00	<LOD	<LOD	1.27	<LOD	10.93	<LOD	Sb, Fe
	st.dev.	*1.54*	*0.17*	*1.58*	*7.90*	*0.90*	*0.18*	*0.55*	*0.61*	-	-	*0.46*	-	*4.84*	-	
2	VG98*	3.78	1.09	8.16	67.32	3.11	1.17	2.54	6.48	0.34	0.69	3.32	1.14	<LOD	11.70	Fe, P
	st.dev.	*1.76*	*0.06*	*4.43*	*9.38*	*1.77*	*0.26*	*1.00*	*1.38*	*0.09*	*0.19*	*1.69*	*0.34*	-	-	
2	VG98y*	4.49	0.52	4.35	60.99	3.66	1.26	1.55	4.74	<LOD	<LOD	2.74	1.16	3.95	12.78	Sb, Pb
	st.dev.	*0.78*	*0.06*	*0.98*	*2.13*	*0.84*	*0.36*	*0.11*	*0.41*	-	-	*0.64*	-	*0.27*	*2.08*	
7	VG22*	3.31	0.37	8.41	61.24	7.57	1.02	1.86	12.13	0.54	<LOD	1.44	2.18	<LOD	<LOD	P, Zn, Ba, A, I, Pb, Fe, Cu, Ni
	st.dev.	*0.32*	*0.15*	*0.69*	*9.60*	*3.04*	*0.41*	*0.37*	*4.29*	*0.31*	-	*0.73*	*0.54*	-	-	

Distribution, sizes and concentration of Sb-rich and Sb-Pb-rich inclusions are highlighted by BSE images of PG110_1, 156 and VG98 reported in Figure 5.10. Inclusions of several μm in size are densely distributed in the matrix of white (Figure 5.10 a and b) or yellow (Figure 5.10 c) glass. The difference with the blue base glass is evident in both surface images and cross sections. Surface of decoration glass is rougher than that of the base glass. VG22 surface is heterogeneous without regular distribution of specific inclusions. Instead, a diverse set of inclusions, rich in P, Zn, Ba, Al, I, Pb, Fe, Cu, Ni was detected on the surface of this sample (Figure 5.10 d). Inclusions cannot be attributed to any specific compound and, reasonably, constitute surface contamination from the soil.

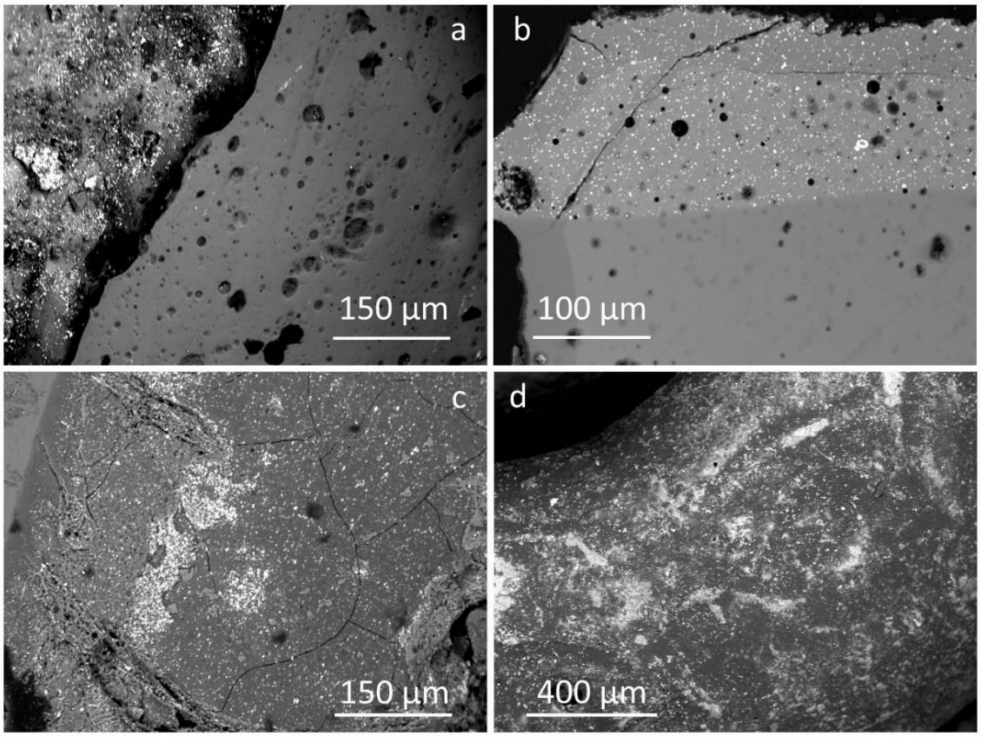

Figure 5.10. BSE images obtained during SEM-EDS analytical session. a – surface of PG156, white glass rich in Sb inclusions (left) and blue base glass (right); b – cross section of PG110_1, white part with Sb rich (top) and base (bottom); c – surface of the yellow decoration of the VG98 featuring Sb and Pb rich inclusions; d – surface of VG22 with compositionally heterogeneous polymetallic inclusions, rich in P, Zn, Ba, Al, I, Pb, Fe, Cu, Ni which might be soil contamination of the surface.

5.1.5. Laser Ablation Inductively Coupled Plasma Mass Spectrometry.

Compositional data obtained by means of LA-ICP-MS can be found in Appendix 7. In this chapter, the data obtained on 30 samples mostly from Group 1 (21 sample) and Group 7 (7 samples) are considered. In addition, VG98 represents Group 2 and VG32 represents the Non-beads.

To visualise the beads based on their elemental concentrations under a multivariate perspective, PCA was performed. A first set of data included major and minor elements (Appendix 7, table 1) and a second set was that of trace elements (Appendix 7, table 2). Major and minor elements expressed as oxides did not undergo any pre-treatment of data except autoscaling, while the trace elements expressed in ppm were subjected to Standard Normal Variate normalisation to avoid differentiation on account of general relative abundance/absence of REE as these elements are correlated among themselves in many cases. Figure 5.11 presents the results of the PCA analysis. Despite two different datasets for the same sample set, the trends highlighted by the two score plots are consistent.

PC1 of the major and minor oxides dataset is influenced mostly by the values of Na, Mg and Al on the positive direction and K, Cu, As and Sn on the negative side. The Groups 1 and 7 are divided by PC1 values and the divisions within these Groups occur along the PC2 and PC3 axes, influenced

by Si, Fe, and Pb for PC2 and Al, Ca, Mn, Ni, Co Zn and Sb for PC3. Previously observed divisions in the subsection 5.1.3 within the Group 1 occur also in the La-ICP-MS data distinguishing a small Group of samples (PG109, 110_1, 111, 112 and 151) that has more Mn and Cu. On the other hand, PG43 from Group 7 is detached from its Group and on all three plots finds itself among the samples of Group 1. VG98 is associated with the smaller number of samples in Group 1 that is consistent with the p-XRF data and, to some extent, with the SEM-EDS ones. VG32 seem to not belong to either of the aforementioned clusters within Group 1. Group 7 samples are scattered in the negative part of PC1. Their PC2 values differ greatly and can be both positive and negative (Figure 5.11 a and b).

Regarding the PCA of trace elements (Figure 5.11 c), it is important to highlight the importance of Rb and Ba that seem to be opposed to the rest of the elements. Ce, Nd, Dy, Gd and Sm values influence the PC2 values. Similar division observed in the other PCA plots can be observed with the exception of Group 7, being rather tightly clustered in the upper right quadrant of the plot. PG73 appears to be an outlier, being situated on a bigger distance from every other sample. This sample has low Sr values.

Several binary plots that include key major and minor elements for understanding the difference within the dataset are included in Figure 5.12. Cobalt is normally associated with Nickel and Zinc in samples of Group 1. These elements have similar concentrations in these glasses and Pearson correlation values of approx. 0.9. Cobalt also demonstrates weaker correlation with Mg, Al and Fe (r = 0.42-0.64). The tri-plot of Co Ni and Zn reveals similar division of Group 1 and 7 samples, with the latter ones having significantly less Zn, except for PG43 that remains together with Group 1 samples (Figure 5.12 a). Four samples, namely PG28, 37, 110_1 and 112, were not included in the plot because their CoO content was much lower than 100 ppm and probably means no intentional addition into the glass. VG98 (Group 2) joins the Group 1 samples in the centre of the plot, whereas VG32 (non-beads), by having relatively low Ni and Zn concentration, stays as an outlier near the top of the plot.

Group 7 is divided by the content of alkali oxides (Na_2O and K_2O). In Figure 5.12 b, it can be seen that PG158, 159 and VG22 contain major quantities of K_2O (more than 5% in each). In case of VG22 this result (10.43%) significantly differs from the p-XRF one (1.84%) though this sample appears heterogeneous in SEM-EDS. PG28 and PG51 also have higher K_2O levels in comparison to the rest of the samples, which usually do not contain more than 0.4%. Samples analysed by LA-ICP-MS can be divided by discrete MgO concentrations (Figure 5.12 c). PG109, 110_1, 112 from Group 1, together with the majority of Group 7 samples (except PG43) and VG32 and 98 contain less than 1.5% of MgO. The samples of Group 1 marked in Figure 5.12 c, and PG43, feature 2-3% MgO. The rest of Group 1 samples contain more than 3.5% of MgO.

As for the Al_2O_3 concentrations, reported in the same plot, they vary significantly (from 0.68% in PG110_1 to 9.67% in PG86) without producing any clustering among samples. Fe_2O_3 concentration in most of the samples is below 2%, with only a few samples of Group 7 abov this value: 13% in PG28, 9.9% in VG37 and 3.6% in PG51. These samples also feature high TiO_2 concentrations, although no strong correlation is revealed among them (Figure 5.12 d). Two trend lines can be suggested in the MnO vs TiO_2 plot (Figure 5.12 e). Samples of Group 7 – PG28, 37, 51 and 159 contain comparable quantities of both oxides up to 0.43%. Samples of Group 1 – PG73, 109, 110_1, 112, 151 have much higher MnO values.

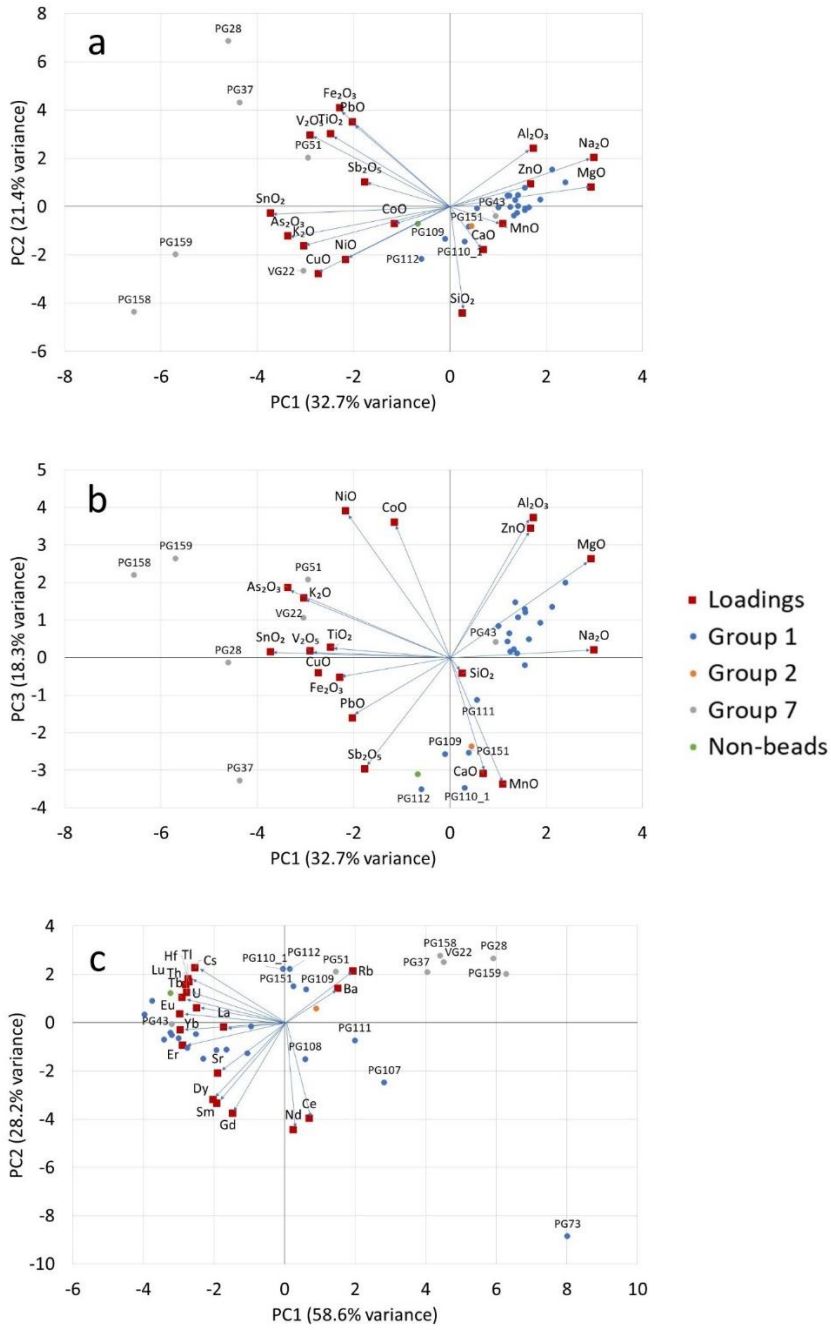

Figure 5.11. PCA of LA-ICP-MS data. a – PC1 vs PC2 of the major and minor oxides; b – PC1 vs PC3 of the major and minor oxides; c – PC1 and PC2 of the trace elements. Scores and loadings are placed in the same plot. Loadings values were multiplied by 10 to increase legibility of the plots.

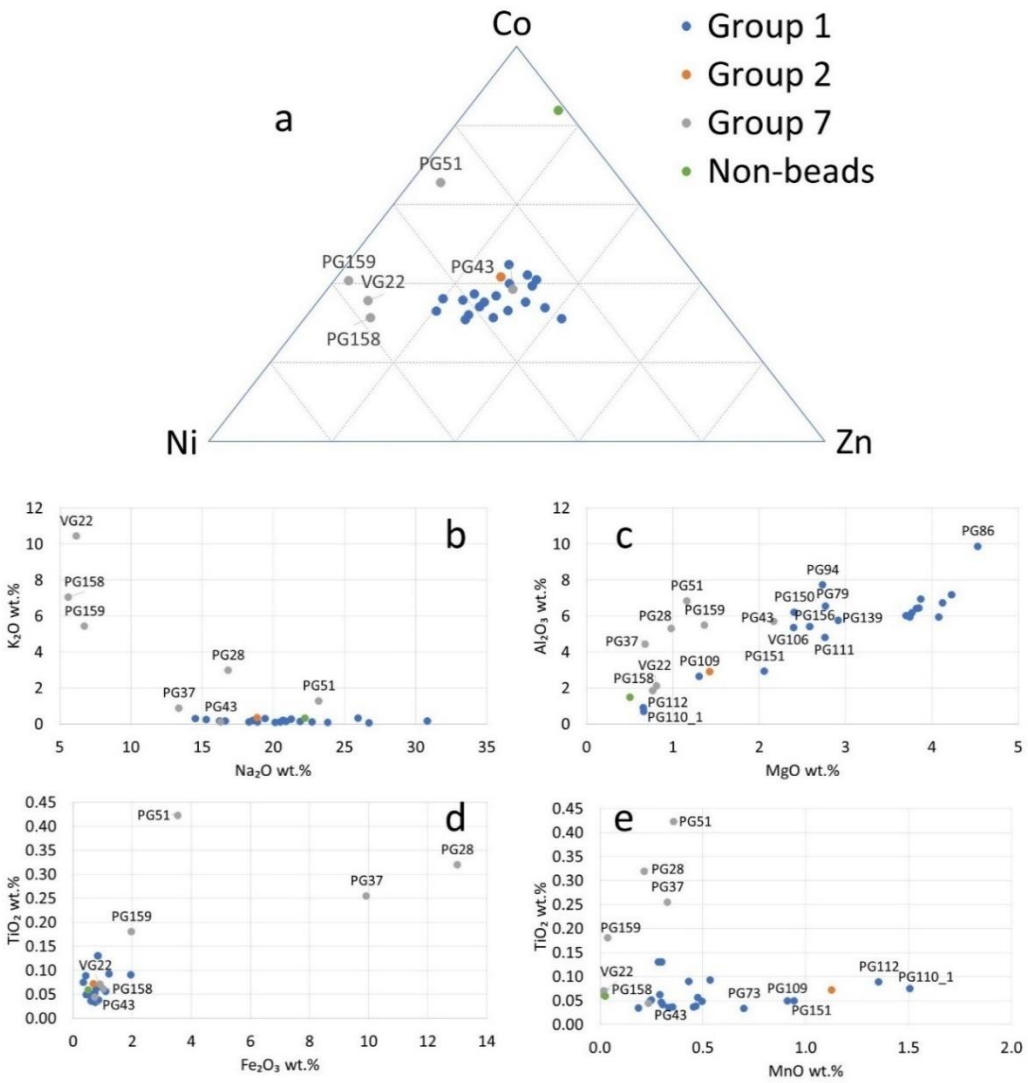

Figure 5.12. LA-ICP-MS data: a – tri-plot of Co, Ni and Zn values, only values with more than 100 ppm of CoO were included to count in only Co-coloured samples; b – Na2O vs K2O binary plot; c – MgO vs Al2O3 binary plot; d – Fe2O3 vs TiO2 binary plot; d – MnO vs TiO2 binary plot. The legend is true for all plots.

The differences in trace elements values among the samples is also reflected by concentration values normalised on the Upper Continental Crust (UCC) values (values of McLennan 2001), as reported in (Figure 5.13). Most of the Group 1 samples, including the PG73, 107, 108, 109, 111 and 151 (apparently separated in the PCA plot of Figure 5.11 c), but excluding PG110_1 and PG112, demonstrate similar profiles in Figure 5.13, which reports the relative abundance of trace elements including REE. Sr appears relatively abundant when compared to Rb and Cs, and relative abundance of mid-mass REE elements (Nd – Dy) together with U is evident for this Group. VG98, the only representative of Group 2, features a similar profile, but with an higher Ba concentration.

Group 7 samples, except PG43, are divided into two smaller sub-Groups by their trace elements concentrations. This division coincides with Fe and K concentrations observed in Figure 5.12. The high Fe sub-Group consists of PG28, 37 and 51 and, as a rule, has elevated Rb and Cs values (in case of 51 not so pronounced and also elevated Ba). The values of REE are more or less equally high, with elevated Hf level and relatively high U values. Mean RSD for this sub-Group is 34% with the maximum 116% for Rb values. The High K sub-Group averaged profile is "flatter" after Rb and Sr whose values are higher than those of the rest of the elements. The usual for other Groups relative U enrichment is absent. VG32 profile is similar to the Group 1 and 2 ones, but without enrichment in mid-mass REE elements. It is remarkable for its relative Sr abundance in comparison with Rb and Cs.

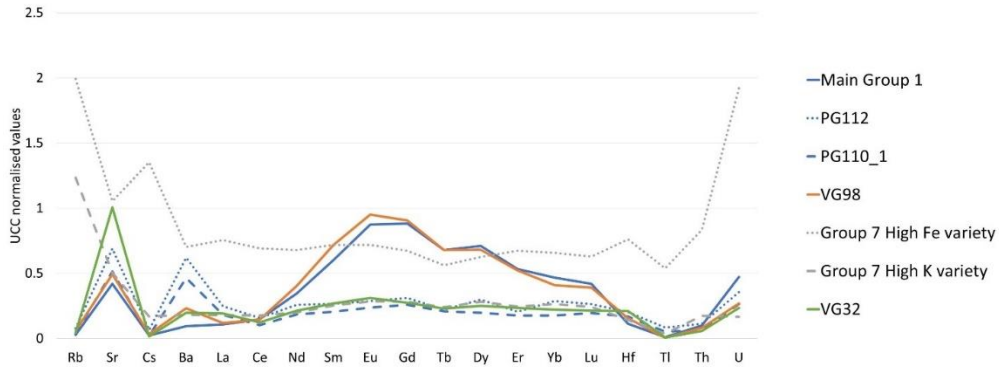

Figure 5.13. Upper Continental Crust normalised values of trace elements. ppm concentrations were normalised by values in McLennan 2001. Main Group 1 is averaged values of the Group 1 samples except PG110_1 and 112, it also includes PG43 from Group 7. Group 7 is divided into two varieties based on Fe and K content that have different profiles. The averaged values of these sub-Groups are presented in the plot separately.

5.1.6. Micro Raman Spectroscopy.

μ-Raman analyses provided two kinds of results: by comparison the bands of bending (300-700 cm^{-1}) and stretching (800-1200 cm^{-1}) of Si – O vibration modes, the glass compositional Group can be recognised, and the temperature range of the liquid melt can be suggested; another set of results is the detection of crystalline phases suspended in the glass matrix that usually are indicative of particular colour adjustments. The procedures that were followed according to established protocols to obtain the final data are described in section 4.6. Not all the samples that were exposed to the laser beam provided meaningful spectra, with clearly defined silica bands (or massifs). In this subsection we consider the spectra of 25 samples, with calculated areas of silica bands. A typical spectrum with this kind of feature is reported in Figure 5.14 a.

The area of Si-O bending and stretching massifs was calculated by the sum of areas of the fitting peaks as demonstrated in Figure 5.14 a. The ratio of these areas, termed as polymerisation index or A500/A1000 (according to Colomban 2003, 2008) varies in this sample set from 0.57 to 1.6, with the majority of the samples across all the Groups showing this value within the 0.7 – 1.3 interval. Exceptions are: PG112 – 0.57, PG79 – 1.37 and PG43 – 1.6. Certain division that might be indicative of the bulk glass composition can be observed in the binary plot of Si-O stretching maxima

wavenumbers and A500/1000 values (Figure 5.14 b). Most of the samples have their stretching maxima around 1100 cm^{-1}. This location coincides with CMOG A and B glass references' positions. Several samples from Group 1 (PG91, 112 and 151) and Group 7 (PG34 and PG37) have their respective maxima of Si-O stretching in the interval of 850-1000 cm^{-1}. According to Colomban (2008), these values correspond to Ca or Pb rich vitreous materials which is not in agreement with p-XRF and LA-ICP-MS results. These samples are in the vicinity of CMOG D reference glass (K rich) position. According to the LA-ICP-MS data, these glasses do not contain more than 0.88% of K_2O. This is why the results for these samples are taken with great caution, keeping in mind that they might be compromised by glass alteration or surface depositions.

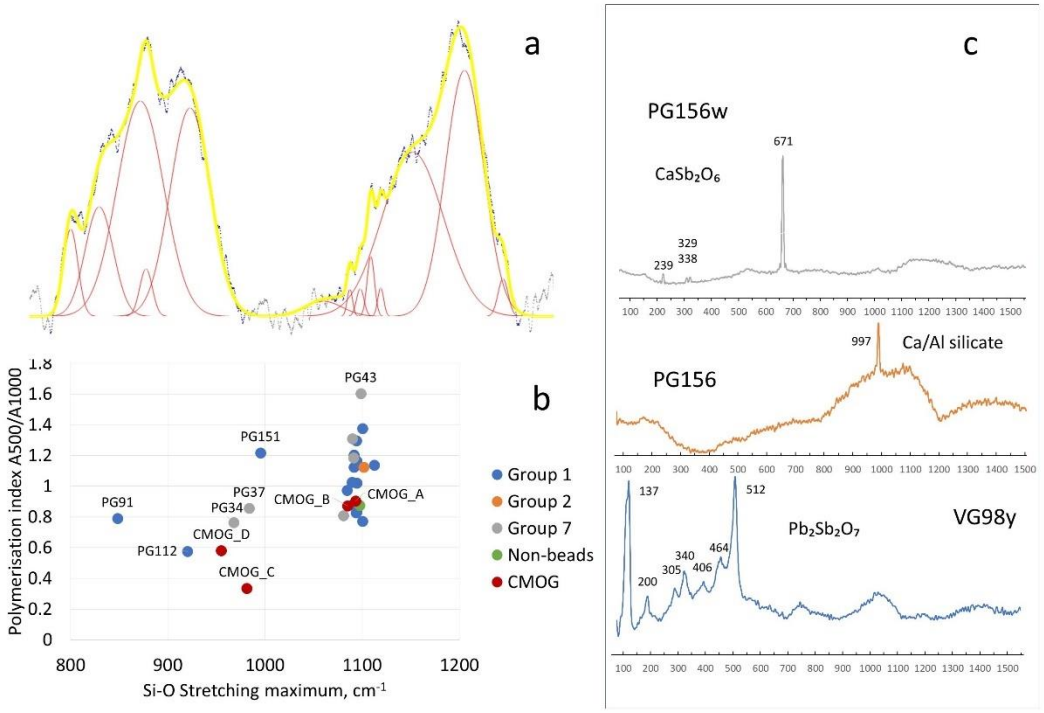

Figure 5.14. μ-Raman results. a – Si-O bending and stretching massifs pronounced in PG100's spectrum. The area of bands was calculated in Fityk software (Wojdyr, 2010) as the area of the fitting curve (yellow line) above the background; b – binary plot of Si-O stretching massif maxima of each sample against the polymerisation index (A500/A1000).

Spectra that revealed the presence of crystalline phases mostly feature the peaks of $CaSb_2O_6$, that was detected in the white decorative parts of Group 1 samples (Figure 5.14 c, top). Table 5.2 reports the complete list of the samples where it was detected. In the blue bases of Group 1 beads, the peak at 997 cm^{-1} frequently appears (Figure 5.14 c, middle), attributed to undefined Ca/Al silicates after Ricciardi et al. (2009). Anatase, with the main peak at 145, was detected in three samples: PG73, 151, 158. Calcite, with the main peak at 1087 cm^{-1} was detected in Group 7 samples (PG158 and PG159). These minerals are sometimes found in archaeological glass (Ricciardi et al. 2009), though it is possible that they do not represent actual matrix composition, but to surface

depositions, that are diagnostically irrelevant. Yellow decoration of VG98 exhibits peaks attributable to $Pb_2Sb_2O_7$, main ones being at 137 and 512 cm^{-1}. Several peaks remained without attribution, for example the one at 1450 cm^{-1}.

Table 5.2. Crystalline phases identified in the Raman spectra. Samples are sorted according to the Group and their names. In case two phases are identified, the wavenumber values of their peaks are separated by semicolon.

Group	Sample	Peaks (cm^{-1})	Phase
1	PG73	145; 996, 1450	Anatase, Ca/Al silicate
1	PG91w	238, 671	$CaSb_2O_6$
1	PG100w	237, 328, 337, 671	$CaSb_2O_6$
1	PG108w	241, 671	$CaSb_2O_6$
1	PG109w	237, 328, 337, 671	$CaSb_2O_6$
1	PG111w	237, 328, 337, 671	$CaSb_2O_6$
1	PG112	143, 673, 1044	$CaSb_2O_6$
1	PG139	997	Ca/Al silicate
1	PG150w	237, 328, 337, 671	$CaSb_2O_6$
1	PG151	146	Anatase
1	PG151w	241, 671; 1450	$CaSb_2O_6$, unidentified
1	PG156	997	Ca/Al silicate
1	PG156w	239, 329, 338, 671	$CaSb_2O_6$
1	PG94w	241, 328, 671	$CaSb_2O_6$
1	VG106	467, 617, 637, 996, 1080	Ca/Al silicate
1	VG106w	237, 328, 337, 671	$CaSb_2O_6$
2	VG98y	211, 275; 137, 200, 305, 340, 406, 464, 512	$Pb_2Sb_2O_7$, feldspar
7	PG158	148; 1087	Anatase, Calcite
7	PG159	1087	Calcite
7	VG22	839, 867, 1450	unidentified

5.1.7. Micro X-Ray Diffraction.

Five samples from this set were subjected to μ-XRD analyses. These were: PG10_1, PG156, VG22, VG98 and VG106. All of them, except VG22, were analysed on the decorative parts (white and yellow in case of VG98). Reference diffractograms are reported in Figure 5.15. Diffractograms of the white decorations of Group 1 samples (PG156 and VG106) revealed the presence of hexagonal $CaSb_2O_6$. Calcium antimonate was confirmed by comparison with the published XRD data on archaeological glasses (Arletti et al. 2006; Lahlil et al. 2010b; Drünert et al. 2018). Such form of calcium antimonate is cross checked by μ-Raman data. A barely detectable peak at about 26.5 2θ° would suggest the presence of quartz, although no other peaks of this phase have been detected.

For the white part of PG110_1, no peaks of $Ca_2Sb_2O_7$ and/or $CaSb_2O_6$ were registered, possibly due to the small size of the region of interest. Cristobalite was detected instead, it is likely in a

metastable state inside the glass matrix. Its formation is possible in glass making temperatures with addition (intentional or otherwise) of halite (Cultrone and Rosua 2020). In fact, Si rich inclusions in the matrix were observed in SEM.

$Pb_2Sb_2O_7$ was detected in yellow decorative elements of VG98, supporting the μ-Raman results. Its crystal arrangement corresponds to the naturally occurring mineral bindheimite, as demonstrated in the Figure 5.15. Diffractograms of VG22 do not contribute much of information.

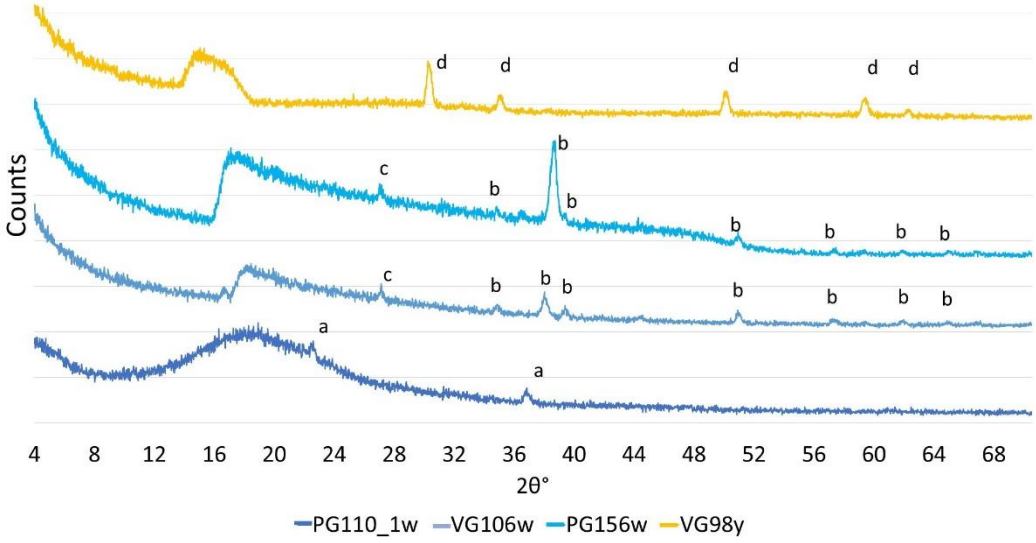

Figure 5.15. μ-XRD results. Diffractograms of samples with crystalline phases dispersed in the glass matrix: a – reflections of cristobalite; b - hexagonal $CaSb_2O_6$; c – quartz; d – bindheimite ($Pb_2Sb_2O_7$).

5.2. Discussion of the results.

5.2.1. Sources of silica.

Silica source in archaeological glasses is connected to glass provenance (Gratuze 2013), therefore the question of the sources of silica becomes the question of the primary glass provenance. General lack of archaeological records with attested Iron Age glass workshops makes the pinpointing of the precise places of production an almost futile task. Nevertheless, the compositional data obtained in this study can be comparted with the ones from chemical analyses of similar glasses from the literature, thus drawing some conclusions on glass provenance according to what is presently known on glass production in the Iron Age.

Chemical elements that are assumed to derive exclusively from the silica-rich natural raw material (sand or quartz pebbles) consist not only of silicon and oxygen but also of the so-called impurities, such as Al, Ti, Fe, Mn, Zr, Ba, REE, Hf, Th. They can be used as proxies for provenance determination (Brems and Degryse 2014), though it is important to not forget the potential impact of raw materials processing and the influence of other components of the batch on the final glass composition.

Samples of the Group 1 are divided into two sub-Groups – the main one including most of the samples (also representing the PG168 and VG54 from the Other beads Group and the larger variety of Group 2) and the small group of samples (PG109, 110_1, 111, 112, 138 and VG106) that had elevated Cu and Mn values across all the compositional kinds of analysis (p-XRF, SEM-EDS and LA-ICP-MS). Figure 5.13 demonstrated that from this small Group of samples, only PG110_1 and PG112 have different relative concentrations of REE and, in addition, elevated Ba values. The rest of the samples have their trace elements profile very similar to the main compositional sub-Group of the Group 1, with elevated Sm-Lu values. This would point to a same silica source for all the samples of Group 1, but for two of them.

The impact of the colourant raw materials on the trace elements and REE concentrations can be hypothesised, though the correlation of Eu, Gd, Tb, Dy with Co and associated elements never rise above 0.41 indicating a weak relationship (correlations between Co and Al, Fe, Ni, Zn were found and demonstrated in sections 5.1.3 and 5.1.5). The weak correlations most likely are due to the presence of certain amount of REE in both the silica and the Co source and to the heterogeneity of the Co-rich raw material, as reported by Shortland et al. (2006). On the other hand, the relation between Co and Al, Fe, Ni and Zn is known for LBA samples from Ancient Egypt (Hodgkinson and Frick 2020), Mycenian Greece (Walton et.al. 2009), IA glasses found in Villanovan sites in Italy (Arletti et al. 2011) and Nimrud (Reade 2021). All these glasses were attributed to production that involved Egyptian source of cobalt. Therefore, the trace elements profile of Group 1 and of the smaller variety of Group 2 is assumed to be influenced by the Co bearing raw material.

Some members of the Cu-Mn rich sub-Group of samples are appearing to stand apart from the rest of the samples of Group 1 in the Ba vs Ce binary plot (Figure 5.16). PG109, 110_1, 112 and 151 significantly differ from the other samples because of their high Ba content. Ba is strongly correlated with Mn not only in these samples, but throughout the Group 1 dataset. It is possible that at least PG110_1 and 112 were prepared using a different sand that contained wad (Brems and Degryse 2014). The rest of the Group 1 samples are grouping near Egyptian glasses of the LBA (Shortland et al. 2007). Coeval glasses found in Bologna (Arletti et al. 2011) are located in the same part of the plot, demonstrating same trend of Ce gain without the gain in Ba. Some of these samples are deviating in the same way as the minor sub-Group of Group 1 samples. Moreover, levels of Ti and Zr in the samples of Group 1 (for those samples in which these elements are above the instrumental detection limits) also correspond to the Egyptian glasses. On the basis of this evidence, an Egyptian provenance of the raw glass can be suggested for the main sub-Group of Group 1 and for VG98 (smaller variety of Group 2), the trace elements compositional pattern of which is consistent with the one of the majority of Group 1 samples, although this sample deviates for its high Ba concentration. A different, and undetermined, provenance is suggested instead for at least PG110_1 and PG112 but also, with weaker evidence, for PG109 and PG151 and VG98.

Trace elements divide Group 7 into two sub-Groups: the high Fe one – which includes PG28, 37 and 51, and the high K one with PG158, 159, VG22. In addition, as already mentioned above, PG43 clusters with the beads of the main sub-Group of Group 1. The two sub-Groups are distinguishable also in the content of their trace elements, as shown in Figure 5.13. The high-Fe sub-Group's concentrations of Ba and, especially, Ce are much higher than in the rest of the samples (Ba – 365-409 ppm and Ce – 28-57 ppm). Relative abundance of Hf might be indicative of the higher concentration of zircon in the silica source (Brems and Degryse 2014). Titania levels are higher in

PG51, despite the lower Fe_2O_3 content. Fe minerals might influence the trace elements profile of PG28 and 37, as its high content indicates a deliberate addition to the glass batch. High levels of K_2O (0.88-3%) coincide with the highest Rb concentration of the entire dataset, indicating the use of sands rich in K-feldspars. This is also supported by the high Al content. At the same time, PG51 data are somewhat different, demonstrating lower Rb light REE, Th and U content. Samples of high K sub-Group in the Figure 5.16 form a different trend line between the samples from Egypt (Amarna and Malkata) and the Greece (Pieria), though only PG159 is really separated from the rest of the samples. Their REE profile is fairly flat and low, though Rb concentrations are elevated, same as the high Fe sub-Group. High Rb corresponds to higher K values, but the different Al/K ratio does not support the attribution of K to the feldspar content of the sand. VG32 appears to fit well in the dataset of Pieria (Blomme et al. 2017 and Figure 5.16) that is attributed to a Levantine production, and its minor and trace elements composition suggests a relatively pure source of silica.

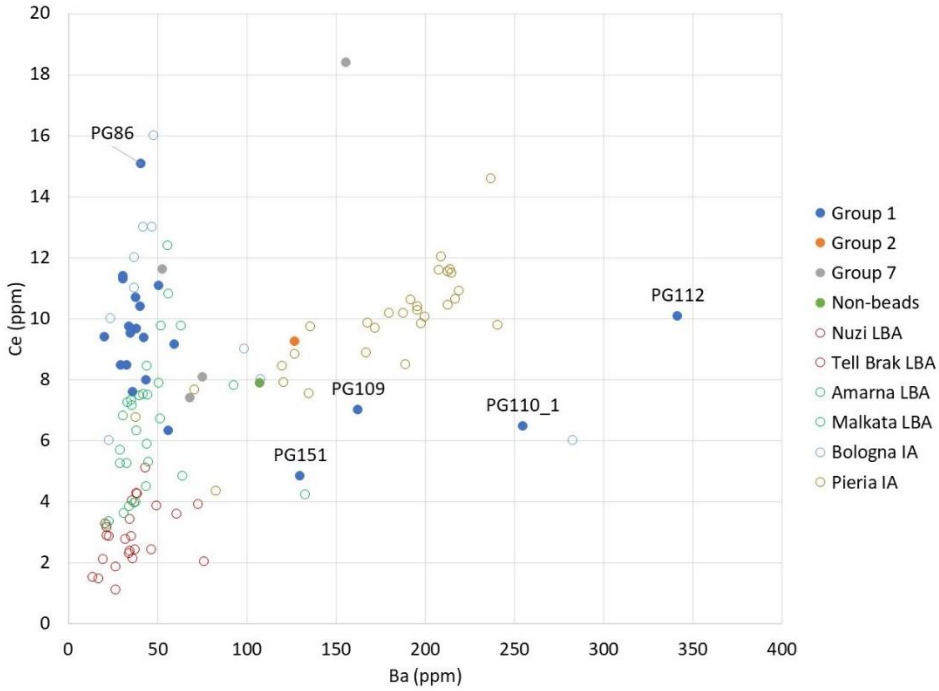

Figure 5.16. Binary plot of Ba and Ce values obtained within the present study compared with other published data. External data sources: Nuzi LBA, Tell Brak LBA, Amarna LBA and Malkata LBA are from Shortland et al. 2007; Bologna IA – Arletti et al. 2011; Pieria IA – Blomme et al. 2017. Samples PG28, 37 and 51 are omitted in the plot because of the high Ce (28-57 ppm) and Ba (365-409 ppm) values.

5.2.2. Fluxes and stabilisers.

Craftspeople that produced the primary glass employed for making the objects included in this set of samples exploited several fluxing agents, that left their compositional fingerprint in the

resulting glass. There are three major glass compositional groups that might occur in the period and areas covered by this study, namely HMG, LMG and LMHK, which reflects the use of different fluxes (Henderson 1988, 2013).

Figure 5.17 demonstrates the division of samples among the aforementioned glass compositional groups. Most of the samples of Group 1 tend to be outside of the boundaries of the compositional groups, having extremely low K_2O content, but high MgO one. The general distinctive feature of the LMG is that both K_2O and MgO do not exceed 1.5% (Rehren 2000; Genga et al. 2008; Schibille 2011; Verità et al. 2019). While K_2O levels fit in the LMG concentration, MgO content takes these samples to the levels of HMG. A possible explanation of such composition is the influence of the colouring raw materials, that will be discussed in the following subsection. In fact, samples that do not follow the general REE pattern of Group 1 (namely, PG109, 110_1, 112, 151) do fit in the LMG range. Na_2O concentrations are high in all samples of Group 1 (20.6% on average), which supports the hypothesis of the use of evaporitic Na-rich minerals (Henderson 1985) that was used for glass production in Egypt since 10th century BCE (Conte et al. 2016). Mineral source of flux can be suggested also for the Group 2, 14, and Non-beads, that exhibit similar ratios of the alkali oxides.

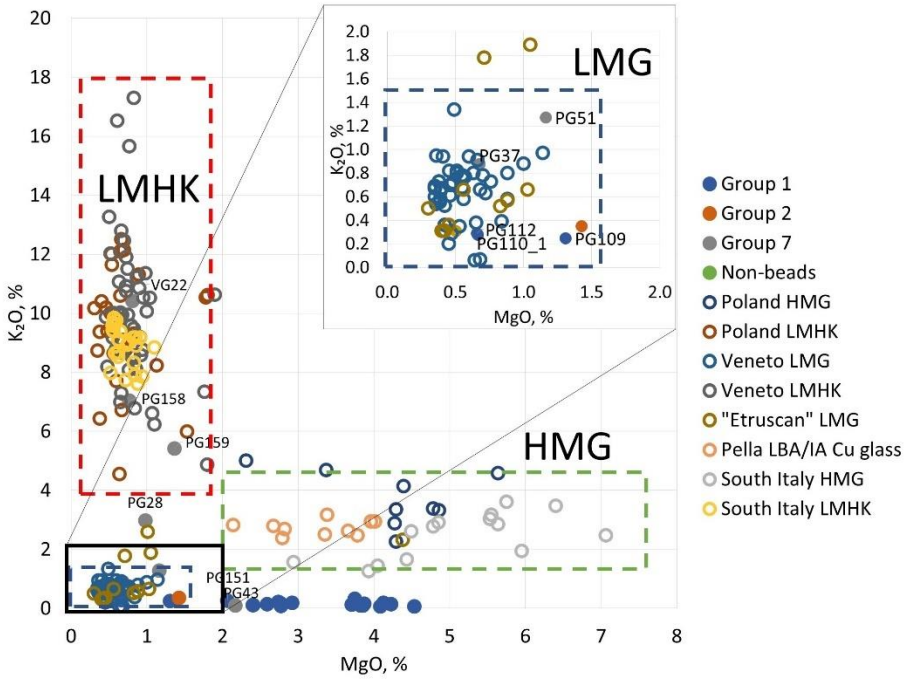

Figure 5.17. MgO vs K_2O plot of LA-ICP-MS data from this work and some external datasets: Poland HMG and Poland LMHK – Purowski et al. 2018; Veneto LMG and Veneto LMHK – Towle et al. 2001; "Etruscan" LMG – Towle and Henderson 2004; Pella LBA/IA Cu glass – Reade 2021; South Italy HMG and LMHK glass – Conte et al. 2019. The boundaries of major compositional groups of LBA/IA glass are marked with rectangles.

The picture appears more complex within Group 7 though. The levels of MgO and K_2O of the high-Fe sub-Group fall withing the concentration range of LMG, with the high content of K_2O in PG28 determined by feldspars (or other K containing minerals), as discussed in the previous subsection.

On the other hand, the high-K sub-Group demonstrates compositional features of LMHK glasses (relatively low MgO and high K_2O content) that were probably produced during the FBA in North Italy, though other places of production are possible within Western Europe. The nature of the fluxing materials for this glass production remains unclear (Henderson 1988; 2013; Towle et al. 2001; Paynter and Jackson 2022), however, such composition ultimately gives indication of the primary glass provenance.

Ca in the glass network makes it more stable to weathering. It could be added intentionally as independent component of the glass batch, or it can enter the glass together with the sand (in the form of carbonate from shell fragments or calcareous rocks), or as a constituent of the plant ash. Binary plots of the p-XRF data provide some information on this stabilising component (Figure 5.7 c and d). Group 14, the Non-Beads and VG36 show higher concentrations of Ca and Sr (> 6.5% CaO and >0.04% SrO) in comparison with all the other samples, and this suggests different recipes of the batch. Nevertheless, the raw material of Ca might be the same for all the samples though, since the same trend can be traced in the CaO vs SrO biplot.

5.2.3. Colourants and opacifiers.

Cobalt was detected in most of the samples by FORS in the form of tetrahedrally coordinated Co^{2+} ions, and also by means of p-XRF and LA-ICP-MS, with the highest concentration being 0.4% (weight oxide) and the mean CoO concentration 0.086%. p-XRF estimation is largely in agreement with LA-ICP-MS data. Such relatively small concentrations are sufficient to turn the glass blue and are typically measured in Co-blue glasses (Shortland and Tite 2000; Abe et al. 2012; Conte et al. 2016).

It was mentioned in the section 5.1.3 that Co in the samples of Group 1, 2 and Other beads is correlated with Ni (r = 0.76) and Zn (r = 0.8) based on the larger pool of p-XRF data. Weaker correlation was observed with Fe (r = 0.5). These relationships suggest that these elements entered the glass batch through the same raw material, though Fe probably also came in with the source of silica (Brems and Degryse 2014). For the same set of samples, correlation of CoO with Al_2O_3 is 0.64 and somewhat weaker with MgO – 0.4 (LA-ICP-MS data). Presence of these oxides in high quantities can be explained by the use of cobaltiferrous alums from Egypt that contain, apart from cobalt, the suite of mentioned elements in similar proportions (Shortland et al. 2006). These samples are situated in the same region of Co-Ni-Zn tri-plot as the other Egyptian cobalt glasses reported in Figure 5.18.

It was mentioned in section 5.1.5 that Group 1 samples can be divided into sub-Groups by their MgO content. In particular, three sub-Groups are identified with high (>3.5%), medium (2-3%) and low (<1.5%) MgO concentration. The correlation coefficient between CoO and MgO for the medium-MgO sub-Group is 0.56, which is higher than the one calculated for the high-MgO sub-Group. Also, CoO correlation with Al_2O_3 is high (0.85) for the medium-MgO sub-Group and low (0.13) for the high-MgO sub-Group. No additional Co or other Co-associated elements increase their values with the increase of MgO.

The MgO division can be connected to a different composition of cobalt bearing ore that was actually noticed in geological samples of close origin (Shortland et al. 2006), or different processing of the same raw material (Rehren 2001).

The high MgO sub-Group samples tend to have increased blue component of their RGB coordinates. This can be either due to their preservation state or because of a more efficient colouring.

The high Cu-Mn sub-Group in Group 1 and the small variety of Group 2 (size division within Group 2 was discussed in section 3.3) demonstrate gradual decrease of the Co values that are nevertheless correlated with Ni and Zn, with the exception of PG110_1 and PG112 that have very low concentration of CoO (5-6 ppm). The glass of these beads was Cu coloured, as they have high CuO concentrations registered by all the compositional techniques used in this study, but also Cu^{2+} ions, detected by FORS analysis, play a role in their final colour and these beads feature skewed-to-green RGB coordinates. In this way, PG110_1 and PG112 differ from the all the other samples of Group 1.

Group 7 samples are also different on account of their colorant origin. Sample PG43 demonstrates similarity with the Egyptian Co source. PG161 is an example of Cu coloured glass, as emerged by p-XRF and FORS data. VG36 lacks Zn and has high Cu concentration, which make it similar to the Group 14 and Non-beads samples. The high-Fe sub-Group is divided by the Co and Zn content. While PG29, 30, 34-36 and 51-56 are high in both Fe and Co (according to both p-XRF and LA-ICP-MS data), PG28 and 37-38 do not show any significant Co concentration (p-XRF data for high-Fe glass have overestimated Co levels). The latter samples are outliers in Figure 5.18. These samples are probably coloured by Fe, which is reflected in their darker blue colour. The former ones, underrepresented during the stage 3 and LA-ICP-MS analyses, are absent in Figure 5.18 because of the apparent absence of Zn. PG51 has relatively high Co compared to Ni and, especially, to Zn values and falls closer to the Co source that was used for LMHK glasses production in the LBA (Towle 2001). For this source, that probably lied in Europe, high As content is inherent (CoO/As_2O_3 r = 0.51). PG51 (according to LA-ICP-MS data) and other samples (according to their p-XRF spectra) contain only trace quantities of As, undetectable by p-XRF. These trace concentrations of As distinguish these glasses from the rest of the Co-containing ones.

As previously discussed in section 5.2.2, the high-K sub-Group of Group 7 samples belongs to LMHK glasses. Their Co-Ni-Zn relationship corresponds to other LMHK glasses from the FBA (Figure 5.18) also including association of Co with As. This piece of evidence further corroborates the hypothesis of separate provenance of the two sub-Groups of Group 7 samples. The surface of VG24 is unevenly coloured red by Cu^0 crystals suspended in the glass matrix. Another bead of similar appearance and provenance was studied by Angelini et al. (2004). Analyses revealed presence of 2-4 μm microcrystals of Cu concentrates at the surface of the blue-green base. Formation of such crystals is possible if specific (reducing) conditions are kept, if the concentration of Cu in the original glass is high enough to allow nucleation and growing of the crystals, and if some other favourable factors, such as presence of Fe and/or Sb (Bandiera et al. 2020) occurred. This bead, out of the set of three, has the highest CuO content (2.7%). For all of them, the presence of Fe and Sb is attested in the range of 0.7-0.9% and 0.2-0.4% respectively (weight oxide). Probably, all three beads had similar appearance, but due to the higher concentration of Cu, only this bead turned red, therefore it is possible that the red hue of this beads was not in the intentional design when the bead was formed.

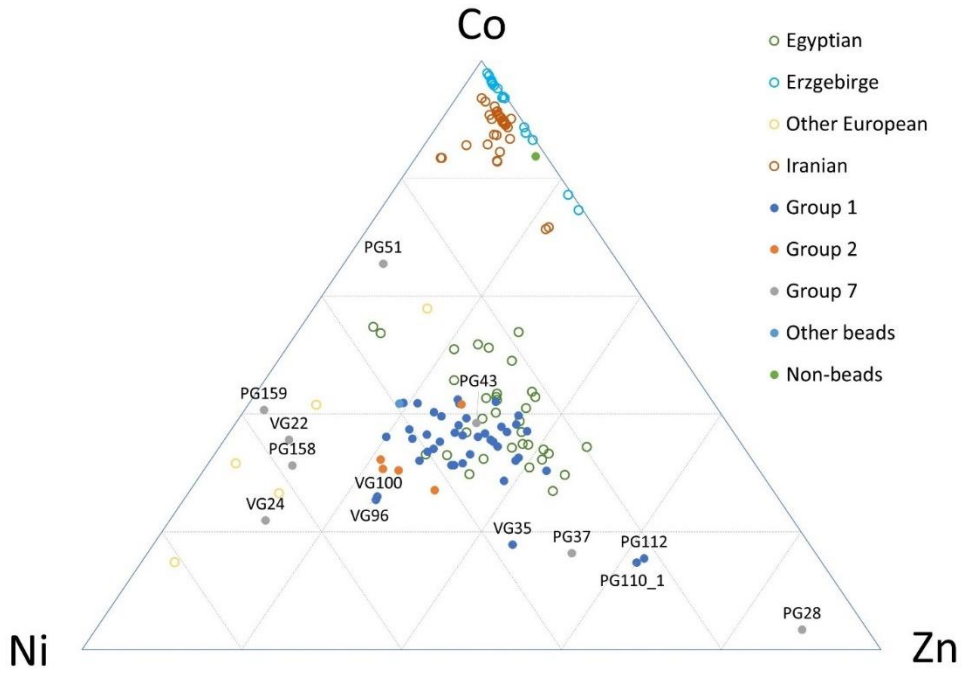

Figure 5.18. Co-Ni-Zn tri-plot. p-XRF values are displayed in case the sample was not considered for LA-ICP-MS analyses. Only samples for which all three elements were above the detection limits of the analytical procedure are displayed in the plot. External data sources mark the composition of the Cobalt blue glass of different origin: Egyptian from Conte et al. 2016 and Reade 2021; Erzgebirge from Costa et al. 2021; Other European sources from Towle et al. 2001; Iranian from Oikonomou et al. 2018.

Ni and Zn content in Group 14 and Non-beads is lower than LOQ of the p-XRF instruments, but LA-ICP-MS data showed that Zn is prevailing over Ni. These sample also do not have any As detected, except for several ppm in VG32 – the only sample that was analysed with LA-ICP-MS for this set of samples. According to compositional data obtained here, these samples might be coloured by Co from either the Erzgebirge/Krušnohoří mining region (Germany/Czechia) or the Iranian source that were suggested for the Phoenician and Hellenistic glasses (Oikonomou et al. 2018; Costa et al. 2021). This emerges from the fact that the Co-Ni-Zn ratio of VG32 is similar to these examples (Figure 5.18). Ores that were reported to occur in those regions are heterogeneous in the suite of associated elements, yet no elevated levels of minor and trace elements were noticed, except for Sb in the bracelet glasses (VG13 and VG32). In the buttons, there also might be minor concentration of Sb, but since the LOQ for the XRF unit that was used in their analyses is higher for this element, a quantitative information is not available. Sb was used as a decolourant of glasses (Silvestri et al. 2008; Biron and Chopinet 2013; Blomme et al. 2017), so we cannot exclude that Sb-decoloured glass could be used as a base to prepare the Co-coloured bracelet and, maybe buttons.

Antimony compounds were also used for glass opacification, and Sb was detected in the white decorative parts of Group 1 beads by means of both p-XRF and LA-ICP-MS. SEM-EDS analyses revealed Sb rich inclusions dispersed in the white parts of the beads. By means of μ-Raman and μ-XRD, it was established that the inclusions belong to the hexagonal $CaSb_2O_6$ phase, whereas no

orthorhombic ($Ca_2Sb_2O_7$) phase was detected. According to studies conducted by Lahlil et al. (2010a, 2010b) the opacification process of the glass used for decoration of Group 1 samples was closer to the one used by Roman glassmakers rather than Ancient Egyptian in the LBA. This can be assumed when the predominant phase (hexagonal), the size (<5µm) and shape (irregular and angular) are observed.

Lead antimonate $Pb_2Sb_2O_7$ was detected on the surface of VG98. Pb-rich composition of Group 2 decorative parts was established by p-XRF analyses. Such microcrystals were popular solution for making opaque yellow glass since the LBA in Egypt (Lahlil et al. 2011).

5.2.4. Production and forming techniques.

It was demonstrated in the subsections 5.2.1 and 5.2.2 that the batch for the glasses considered here was prepared in a variety of ways. The silica, probably in the form of sand, as suggested by the presence of impurities such as Al, Ti, Mn, Fe, Rb, Zr etc. (Silvestri et al. 2008; Brems et al. 2012) was mixed with the flux and, possibly, the stabiliser (if not already included in the flux or in the sand). Two distinct fluxes were used – the substance (maybe specific plant ash) that resulted in LMHK composition (for high K sub-Group of Group 7) and evaporitic deposit in the rest of the samples). There were two distinct proportions (Group 14, Non-beads and, maybe, VG36 vs the rest of the samples) of the stabiliser added to the mix. The main stabilising component – CaO - could enter the batch with the specifically selected sand containing useful amounts of shell/calcareous rocks or with addition of shell or limestone as separate components. Mg, that in majority of the samples came to the batch with Co bearing alum, can also act as a stabilising component, compensating the relatively low Ca content (Tite 2004). It is unclear what was the source of Ca in LMHK glasses (Henderson 2013). Cobalt source of the majority of the beads was alum, with minor concentrations of cobalt incorporated in it, which suggested that the relative quantity of alum in the batch should be quite high (Rehren 2001). It does not appear that other Co sources caused such significant impact on the bulk glass composition. Fe was added to the high Fe samples, though in case of PG51-56 it could have entered the batch together with silica. Sb, probably in the form of stibnite – the most common Sb ore, was used to make opaque white decorative glass of Group 1 samples, to decolour the Non-beads base glass and, together with Pb compounds, to produce opaque yellow glass of Group 2 decorations. The opacifying crystals of $CaSb_2O_6$ and $Pb_2Sb_2O_7$ were formed before adding them into the batch, which is evident from the size and shape of the crystals observed in SEM.

µ-Raman spectra where the bending and stretching Si-O vibrational modes were detected, showed that the polymerisation index across the glasses of all the Groups was mainly within 0.7-1.3 interval. This corresponds to 700-1000°C of processing temperature (Colomban 2003; Costa 2019). Composition of the LMG also corresponds to this range of temperatures (Rehren 2000). To ensure the formation of a homogeneous material, the batch was kept at this temperature for some time before cooling, but at least for the opaque white glasses this time was limited to about one day, since for longer heating time the thermodynamically more stable $Ca_2Sb_2O_7$ phase would have formed (Lahlil 2010b).

The redox conditions of the furnace to produce Co coloured glass should be reducing (Arletti et al. 2013; Hunault et al. 2016). Same is true for the dark, Fe-Co coloured beads. The more oxidised

conditions would be needed to create the Cu^{2+} blue-green glasses (PG110_1, 112, 161). Conditions where both Co^{2+} and Cu^{2+} are formed (parts of Group 1 and 2 samples) are probably more complex to investigate, but formation of these chromophores would also depend on the presence of other elements such as Mn and Fe. The red surface of VG24 could have been created by the intentional annealing of glass in the reduced conditions or, more likely, given its uneven coverage, as an effect of the cremation ritual, which was testified by the type of the grave where the bead was found.

The beadmaking process might have occurred in a different place, after the primary glass was cooled down and fashioned in rods or other shapes. Most of the beads considered here were formed by winding viscous glass around a metal or ceramic rod (or mandrel) of the same diameter of the aperture of the bead. Several beads could be made at the same time on the same mandrel. This can be deduced by the shape of the bead, which shows slight asymmetry in the direction parallel to the aperture, and by the presence of characteristic protrusions near one or, less common, both apexes (Figure 5.1 e). These are finishing or, in case of two, starting and finishing points, where the remaining glass was detached from the body of the formed bead (Sprague and Bowers, 1985; Koch, 2001; Bellintani, 2011). The D/W ratio (defined in section 3.2) depended on how much glass was actually allowed per each bead. The quantity of glass was probably a bit difficult to control, which resulted in the poor standardisation of the dimensions of the beads within each Group.

Both white and yellow eyes were applied as coils of white or yellow glass from a thin, coloured rod. The eye spot of these beads was formed by the base glass itself (Koch, 2001; Bellintani, 2011). Application of the coil was also a poorly standardised process, and numerous defects, for example, eyes overlapping, coils not meeting their ends, being too big or too small in comparison to the other ones on the same bead etc. were observed (Figures 5.1 and 5.2). There were no systematic traces that would suggest the production in different workshop. Wave decoration was applied in a same manner as eyes, but by spinning of the bead body so the white and yellow glass threads rocked above from side to side to form the wave. Apparently, it was not easy to calculate the amount of glass or the time needed to come the full circle, as the two ends of wave decorations of all the samples of Group 14 do not meet perfectly.

The Non-beads were formed in a different way. The bracelets are rods of blue glass that were stretched to achieve a suitable length and consequently - diameter. The stretching process is evidenced by the presence of the elongated bubbles in the glass matrix (Figure 5.3), caused by pulling the glass (Sprague and Bowers, 1985). It is reasonable to assume that the rod was bended in its final shape when the glass was less viscous. Buttons might have been made by rotating a bulb of viscous glass fixed on top of a mandrel so that the glass would flow to the sides from the centre of rotation by means of centrifugal force. They were attached to Fe harness, as confirmed by the XRF analysis of their attachment pit, that revealed Fe in great abundance.

Conclusion. This chapter presents and discusses the data on several groups of predominantly cobalt-coloured beads. The two elemental analytical techniques provided data that are mainly in agreement. Compositional information was supplemented by the insight into the chromophores (FORS) and crystalline inclusions (μ-Raman, μ-XRD and SEM-EDS). Based on all the gathered information, it was inferred that the cobalt ores employed to colour most of the samples discussed in this chapter were from Egyptian sources. However, some samples also contain Cu, which influences their colour too. Different cobalt sources are assumed for the Group 7, 14 and Non-bead

samples. Glasses were prepared using three distinct flux/stabiliser recipes: the LMG with high and low Ca content (section 5.2.2) and, only for several samples, a (still unknown) flux of LMHK glass.

Regarding the provenance, the raw materials point to Egypt for Groups 1 and 2 (except PG110 and 112), the LMHK glasses (high K part of Group 7) are of European, likely Italian origin, high Fe part of Group 7, Group 14 and Non-beads are of undetermined but possibly, Eastern Mediterranean origin. The beads were made by winding the glass around the mandrel and their decorations by inlaying coils of differently coloured glass, prepared with microcrystals of Ca and Pb antimonates (for white and yellow opaque glass, respectively).

CHAPTER 6. COPPER-COLOURED GLASSES.

The following archaeological objects are discussed in this chapter:

- **Group 3: all;**
- **Group 4: all;**
- **Group 12: all;**
- **Group 13: all;**
- **Other beads: PG169, 170 VG28 and 38;**
- **Non-beads: PG59, 60.**

6.1. Results of the analyses.

6.1.1. Visual observation and Optical Microscopy.

The groups of beads presented in this chapter differ among them in shape, decoration and also feature different textures. Their general appearance is reflected in the photographs within the Appendix 2.

The eye-beads of group 3 demonstrate different degrees of alteration. The surface of VG25 shows severe alteration and it is covered by a brownish crust with red stains, although the blue-green bulk glass is also visible (Figure 6.1 a). The other samples of this group do not show any red tinge on the surface. Only sample PG84 retained its eye decoration. The eyes have differences that are partially demonstrated in Figure 6.1 b. While one of the eyes does not seem to have complete white circle around the eye spot, another eye demonstrates certain mixing of white and dark glass in the shape of a whirl. The body of the beads is crizzled with a network of small cracks as shown in Figure 6.1 c. The three darker beads (PG84, 87 and 167) have this texture in common. These cracks are filled with brown-yellow residue. The eyespot glass, at least that of PG84 and VG25, appears to be the same as the body of the beads.

Group 4 samples' surfaces are rough, probably because of the many bubbles present throughout the matrix. The bubbles are varied in size and always spherical in shape (Figure 6.1 d), which excludes drawing as the forming technique. When observed as cross section, the glass appears translucent. Samples of this group feature different varieties of spiral eye decoration and, as it can be guessed by the remaining traces , other kind of (unidentified) decorations. Similarly to the body, the texture of the decorative parts is rough with many collapsed bubbles and dark coloured grains (Figure 6.1 e).

The surface of the samples of Group 12 is rather similar to that of VG25 (group 3) with areas stained dark or red, though the red surface is more abundant. The white decoration is levelled with the body surface (Figure 6.1 f) and is well preserved, as no signs of its detachment are observed.

Samples of group 13 exhibit pronounced surface pitting (Figure 6.2 a and b). The inner surface of these pits is covered in light coloured residues while the surface between them probably is of the initial bead colour. Tubular beads apexes do not have same shape: one end appears to be angular and even wider than the rest of the bead (Figure 6.2 a), another end is thinner and more round towards the aperture (Figure 6.2 b). There are spiral grooves observed on the surface without any signs of the decorative glass, that has detached completely.

Copper-coloured beads

The Other beads group is represented by four samples: PG169, 170, VG28 and 38. The first one is similar by the colour to the Group 4 beads, but its surface is much smoother, due to the smaller dimension of the bubbles that are visible at the surface. The lightly coloured areas swirl into more deeply coloured ones and it is covered in indentations (pits). PG170 is one of the best-preserved beads, as suggested by its smooth surface and vivid bright colour. Samples VG28 and 38, unfortunately, have their originally dark colour turned to a lighter one because of extensive pitting of the surface, as shown in Figure 6.2 c.

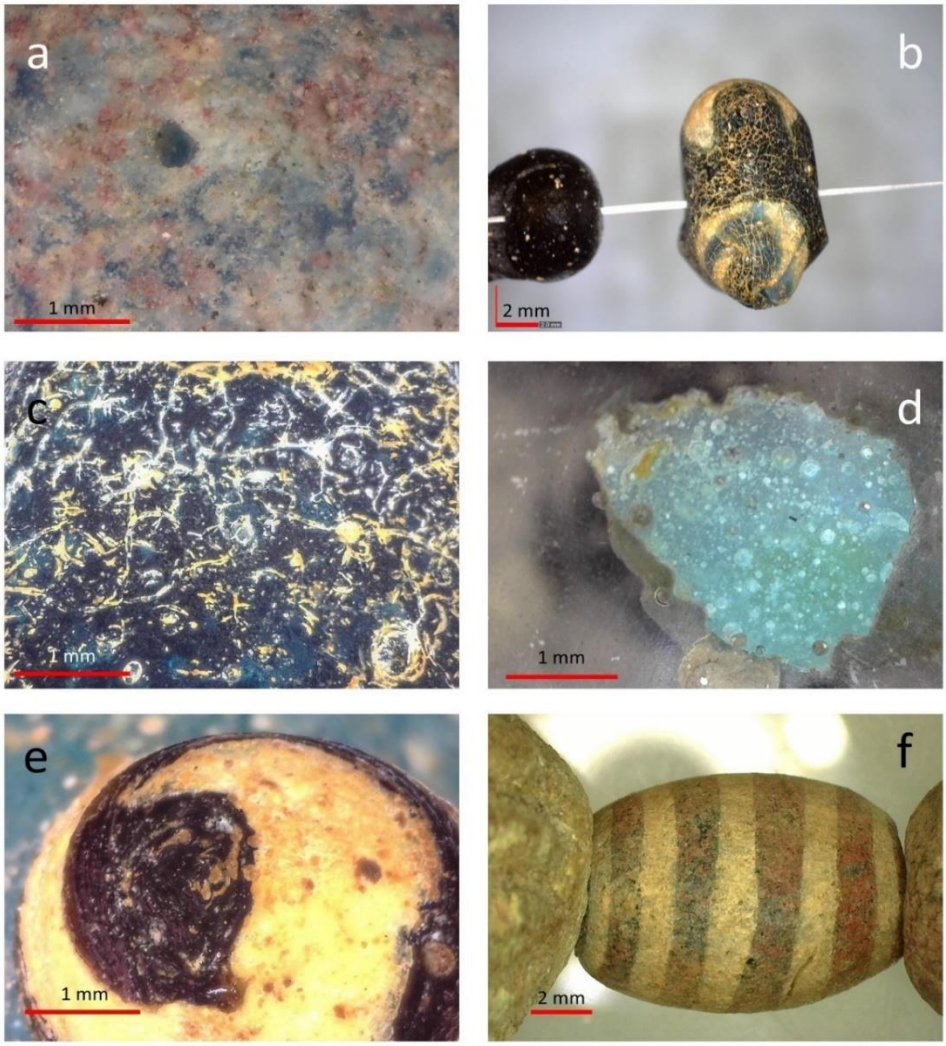

Figure 6.1. Microphotographs of the samples' surface in various magnifications: a – VG25 (group 3) showing areas of red colour on the surface and dark bulk; b – PG84 (group 3) differently formed eyes; c – PG87 (group 3) texture of the altered glass; d – PG121 (group 4) cross-section with many round bubbles; e – PG122 (group 4) the eye of the bead; f – VG26 (group 12) areas of dark and red glass.

The Non-beads PG59 and PG60 have a herringbone pattern of opaque yellow glass on the translucent blue body. In Figure 6.2 d the mixing of the two is demonstrated, showing the directions of glass flow. The yellow decoration also demonstrates similar pattern made by yellow glass with different colour intensity. Occasionally, some iridescence and brown residue is visible on the surface.

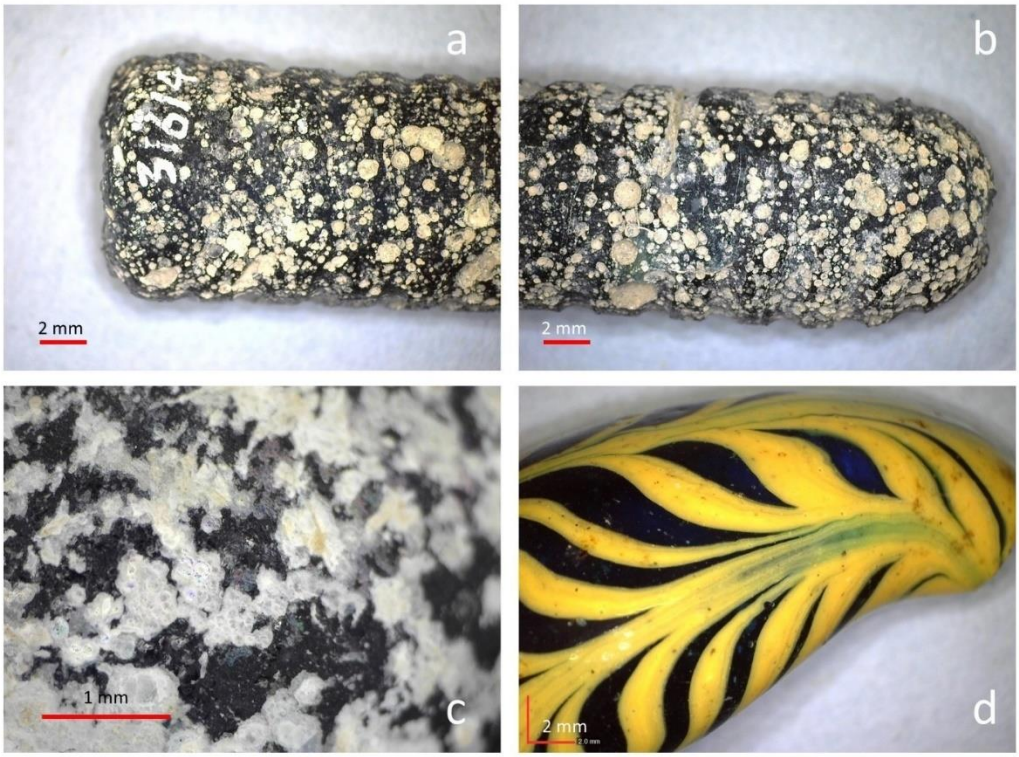

Figure 6.2. Microphotographs of the samples' surface. a and b – PG163's differently shaped apexes, general texture and grooves of decoration; c – VG38 dark bulk with white layer of altered glass on top; d – PG59 decoration pattern and mixing of blue and yellow glass.

6.1.2. Apparent colours and Fibre Optics Reflection Spectroscopy.

Colours of the samples, obtained as described in section 3.2, demonstrate a division among the groups, reported in Figure 6.3 a,b. The list of the samples from each group considered for colour evaluation can be retrieved in Figure 6.3 b. Group 3 samples are situated on the yellow side of the main yellow-blue trend, typical for the samples' distribution. Red and Green values for PG84 are higher than those of VG25, which may be the effect of alteration, as also suggested by the position in the graph of VG28 – a dark sample with a pronounced alteration. Nevertheless, these two samples are dramatically different on the grayscale plot reported in Figure 6.3 b. Group 4 samples are placed in small area near the square 6, which corresponds to green colour. Red coloured samples of group 12 are not very close to the red area of the Figure 6.3 a; they rather appear to be light grey, and they are placed very near VG25, which is the sample of similar colour and texture. Samples of Group 13 and the fibula bows (Non-beads) fall in the blue side of the main trend. The fibula bows show a

deeper colour, which correspond to the one of Group 1, discussed in Chapter 5. VG38 is placed in between those Groups, and it appears darker than VG28.

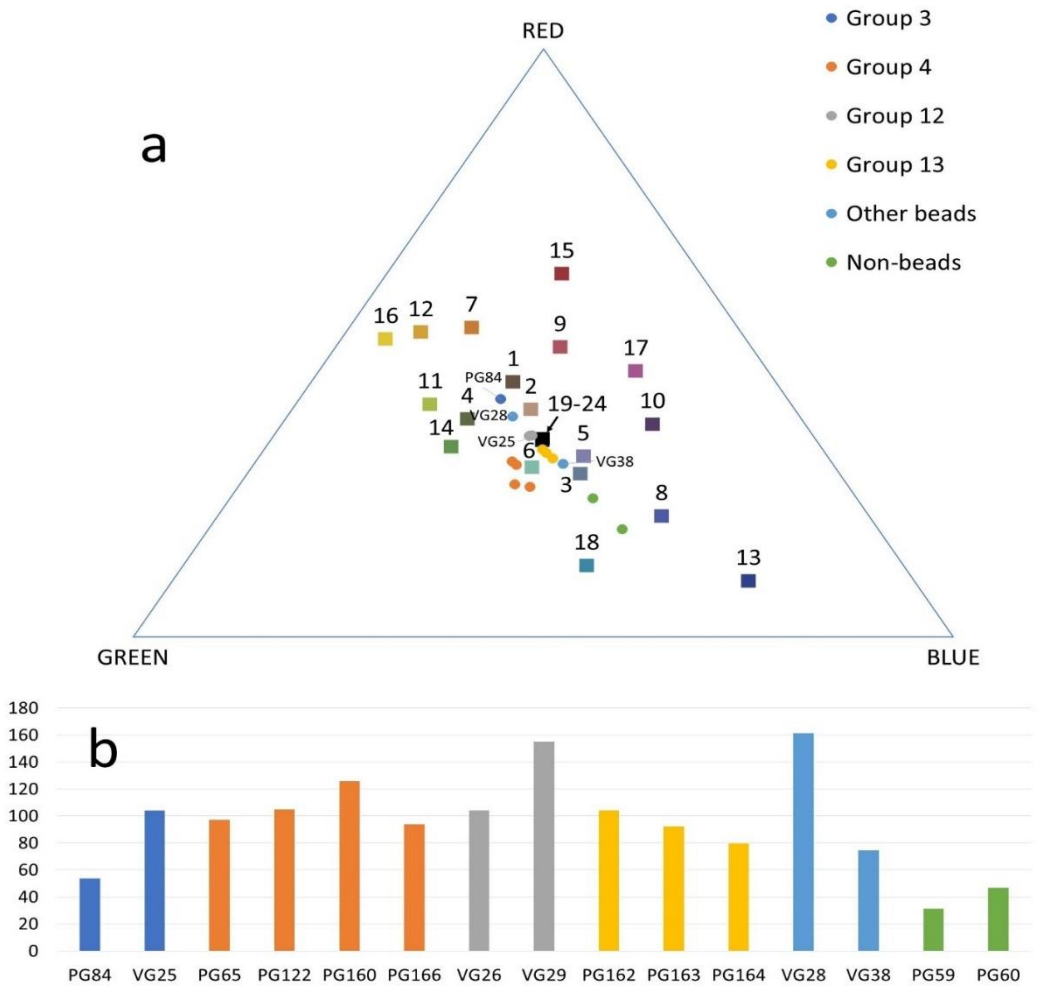

Figure 6.3. Plots of the RGB colour values. a – tri-plot of the RGB values of the base glass of the samples and the values of the Colorchecker (marked as squares with numbers); b – bar plot of the mean RGB values of the samples arranged by groups. The legend refers to both plots.

Most of the beads that produced meaningful FORS spectra yielded similar diffused reflectance patterns. These spectra feature a reflectance peak in the blue-green range of the spectrum and pronounced absorption in the 750-850 nm range which identifies to Cu^{2+}. Such spectra were produced by all the Group 3 samples (but VG25), Group 4, Group 13 (with one additional band), PG170 and by the Non-beads. They are presented in the Figure 6.4 (PG60, 122, 162, 167, 170). The maxima of reflectance for the blue coloured beads (PG60 and 170) are centred at approx. 475 nm, indicating the blue colour, PG162 spectrum maximum at about 550 nm making this sample green,

though such result can be caused by deposits on the surface. PG60 and all the samples of group 3 feature weak Fe^{3+} bands at 380 and/or 440 nm in addition to the main Cu^{2+} one.

Another marker of Cu presence is the Cu^0 band at 563 nm. This type of band is observed exclusively in red-coloured samples: VG25 and Group 12. On several spectra there is a gradual increase of absorption in the NIR part of the spectral range, which might be an indication of Fe^{2+} presence in the glass. Group 13 samples, in addition to the Cu^{2+} band, feature a sharper one at approx. 480 nm, that might be an indicator of Fe and Mn. Other beads stand out of this general frame. VG28 is one of the few samples that do not show any Cu bands. Instead, it has a pronounced absorption in the NIR region, that increases towards the end of the spectral range and can be interpreted as the absorption of Fe^{2+}, though the spectrum is not of ideal quality. The spectrum for PG170 has a maximum in the blue range and Cu^{2+} band in the NIR. Summary of FORS results for these (and other) samples is given in Appendix 5. The decorative parts on all the beads produced no meaningful spectra, except for weak Fe^{2+} band in the yellow part of the Non-beads.

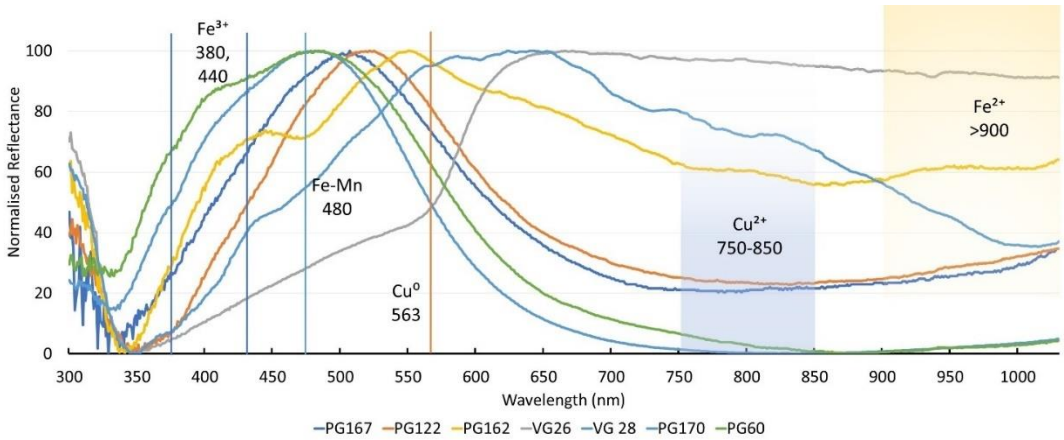

Figure 6.4. FORS representative spectra. Vertical lines represent the centring of the observed bands. $Cu^{2+}$and Fe^{2+} wide bands centring is marked by the range of values.

6.1.3. Portable X-Ray Fluorescence spectrometry.

The p-XRF data collected on the samples that are discussed in this chapter are presented in Appendix 6. Samples from Group 3 have 2.5-4.7% of K_2O. Such concentrations are matched only by Group 12 samples. The rest of the beads contain less than 2.8% (mean value 1.8%). Group 13, PG170, VG28 and VG38 have the lowest K_2O values within the set (all less than 1.6%). Group 4, Non-beads and PG169 have average values of 2.3%. CaO was detected in all the samples in a range of 1.8% (PG167) to 7.6% (PG65). Normally, Group 3 and 12 feature the lowest values (except for their decorative parts of white glass) and Group 4, 13 and Non-beads have their CaO concentration above 4%. The other beads are closer to the higher CaO subset. Group 4 samples show high concentrations of both Ti and Fe, i.e. between 0.26 and 0.41% TiO_2 and the latter between 1.5 and 2.6% Fe_2O_3. In the other samples, concentration of these elements is below the LOQ or below 0.15%. Group 13 is the only Group of samples with high MnO levels.

Co and Ni were detected in PG84 (Group 3) and VG29 (Group 12). PG28 also has its NiO concentration above the LOQ. CuO concentration reached the highest values in samples of Group 3 and Group 12 (from 2.6 to 5.1%). Zn and Zr were seldom detectable with values always near the LOQs. Sr is correlated with Ca (r=0.77) with the exception of VG28 and VG38, that have disproportionally high Sr concentrations when compared to those of Ca. Sn was mostly detected in samples of Group 3, 12 and Other beads. Sb and Pb seem to be connected to the yellow decorations, where they feature the highest concentrations and they are apparently less present in the body of the beads.

PCA was used to visualise the differences in composition detected by p-XRF (Figure 6.5). Part of the PCA results was already presented in Chapter 5 and two Groups (1 and 7) are included in Figure 6.5 for further reference. As for the samples discussed in this chapter, Figure 6.5 shows that two clusters are formed – the first includes Groups 3 and 12 and the second the rest of the samples. Both clusters are situated mostly in the first quadrant of the PCA plot, indicating high Cu and K_2O concentrations. Groups 3 and 12 join to Group 7 (see Chapter 5) especially to the high-K variety (established as LMHK glass), while the rest of the samples are in between Group 1 and 7. Group 13 is closer to the negative side of PC1 which can be explained by the higher MnO and CaO values.

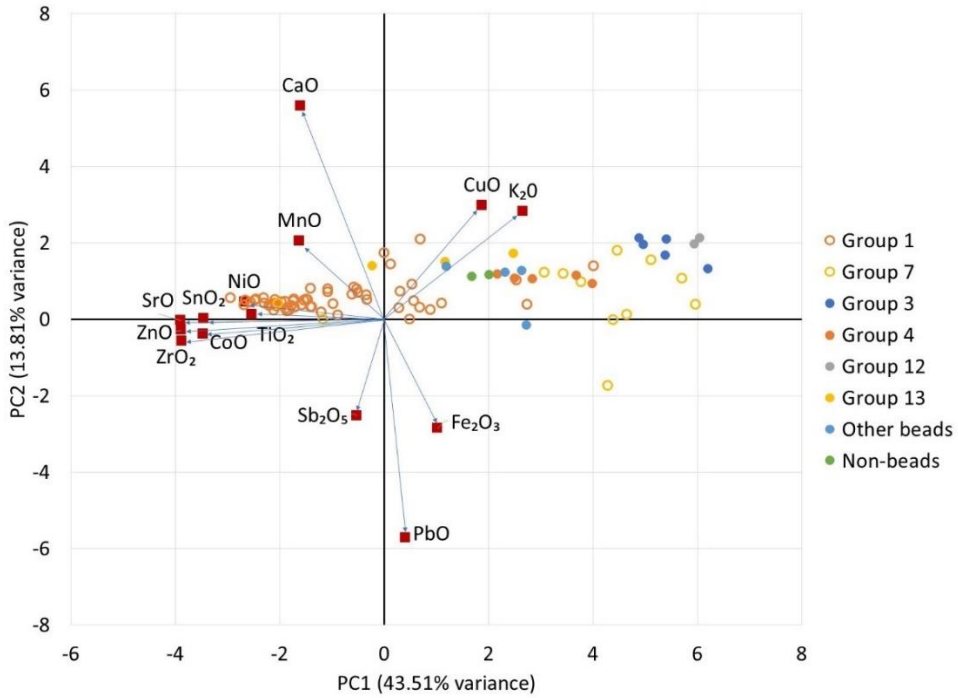

Figure 6.5. Results of the Principal Component Analysis performed on the p-XRF data. Samples from Group 1 and 7 marked as empty circles are added reference. Scores and loadings are situated in the same plot. Loadings values were multiplied by 10 to increase legibility of the plot.

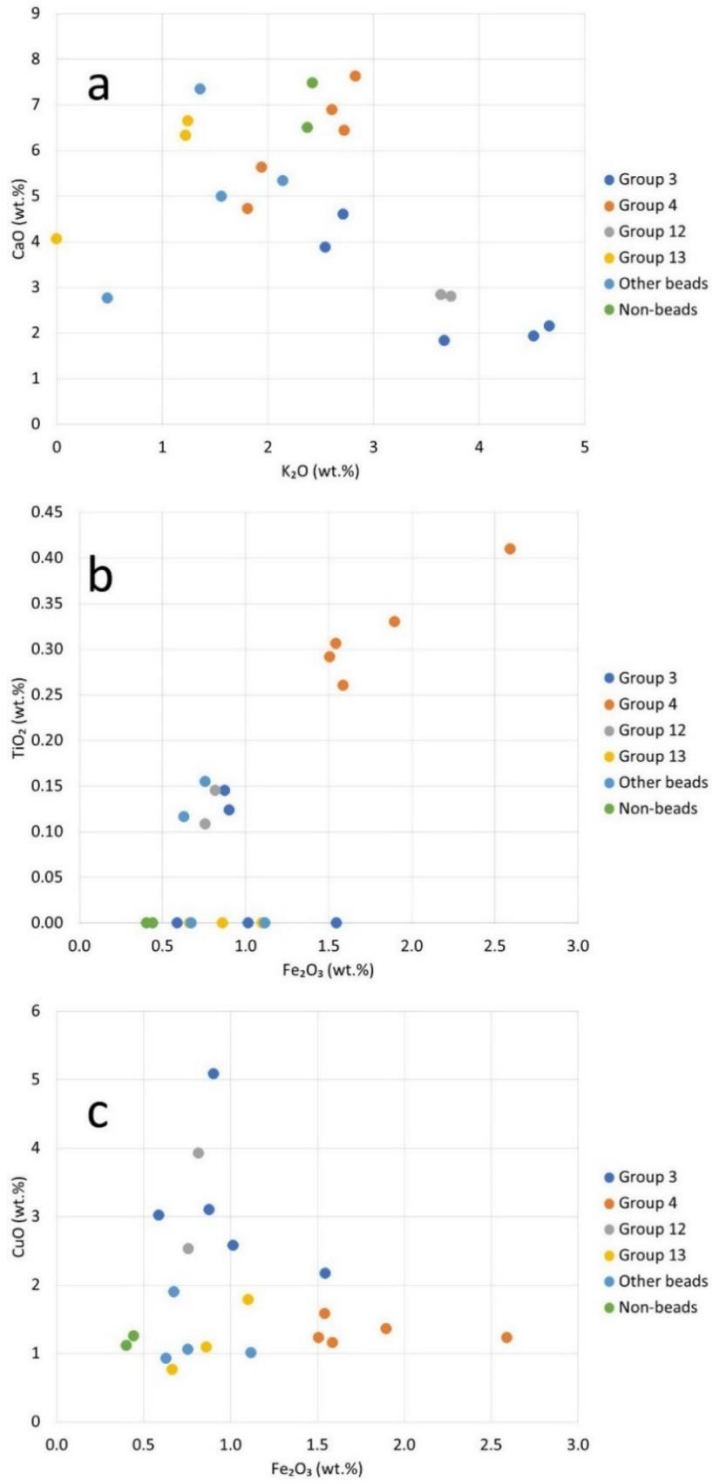

Figure 6.6. p-XRF data binary plots: a – K_2O vs CaO; b – Fe_2O_3 vs TiO_2; c – Fe_2O_3 vs CuO.

To go into details on the divisions among the Groups, several binary plots were prepared. The most important/informative ones are placed in Figure 6.6. The compositionally-determined Groups of samples are differentiated in the K_2O vs CaO binary plot (Figure 6.6 a). Samples from Groups 3 and 12 have higher K_2O values and demonstrate strong negative correlation with CaO values ($r = -0.86$). Instead, Group 4 and Non-beads, together with PG169 and VG38, demonstrate positive correlation ($r = 0.87$). Group 13 samples are not on the same trend. The difference in Fe_2O_3 and TiO_2 content already mentioned for Group 4 is evident in Figure 6.6 b, where this Group demonstrates strong positive correlation for these oxides. The rest of the samples hold either on the LOQ level, or below it. Samples are also different if Fe_2O_3 and CuO are considered (Figure 6.6 c). Most of the samples have more CuO than Fe_2O_3 with Groups 3 and 12 leading with average CuO to Fe_2O_3 ratio of 3.77. Group 4 on the other hand follows the high Fe trend and has the same ratio at 0.75. The rest of the samples have moderate values of this ratio – 0.9-2.83.

Decorative pieces of the beads show different composition. Group 3 and 12 white decorations have higher CaO content (with exception of PG84). The yellow decorations of Groups 4 and Non-beads demonstrate higher Sb and Pb concentrations in respect to their base glasses. Black elements of Group 4 samples' decorations tend not to be very different from the yellow parts, although a higher concentration emerge for Sb and Pb in the yellow decoration. As already discussed in section 4.4, p-XRF is not the ideal technique for the analysis of narrow and thin elements of the samples. Indeed, most of the fluorescence peaks in the spectra of black parts are comprised with the response of the yellow or green glass that lies around and below the surface.

From all the above said, it is apparent that samples of Group 3 and Group 12 were made of similar glass. This is an important piece of information: as samples of Group 12 were not analysed in the laboratory, we can reasonably assume that the conclusions drawn from the laboratory data of samples of Group 3 can be valid also for samples of Group 12.

Samples of Group 4 were made of glass of a peculiar composition, that is similar to the one of PG169 (Other beads). Group 13 is rather close to the Group 1 minor sub-Group of samples, that also have high Mn and Cu content (Figure 6.5). At the same time, their glass is similar to the fibula bows (Non-beads). Samples VG28 and VG38 make a separate group of beads. It is possible that, due to the alteration, the accurate composition of these samples would not be obtained with non-invasive methods. PG170 is remarkable by its high Sb content. These observations are essential to understand how the results of the laboratory analyses can be extrapolated on the beads that were not studied in the laboratory.

6.1.4. Scanning Electron Microscopy coupled with Energy Dispersive spectrometry.

One cross sectioned sample was analysed: PG121, which represents Group 4. The mean composition obtained after replicate analyses, together with the standard deviation, is reported in Table 6.1. SiO_2, Na_2O and CaO are the oxides that make up 87% of the total weight of the sample. MgO, Al_2O_3 and K_2O are minor oxides that are in a range of 2-3%. Fe_2O_3 value does not prevail over CuO as in case of the p-XRF results, but this might be because of poor accuracy for Cu as demonstrated in section 4.5. This sample does not contain any decorative part.

Table 6.1. SEM-EDS analyses result of the bulk of PG121.

Sample/st.dev.	Na_2O	MgO	Al_2O_3	SiO_2	SO_3	Cl	K_2O	CaO	TiO_2	Fe_2O_3	CuO
PG121	18.86	3.09	2.57	62.97	1.01	0.45	2.53	5.29	0.18	1.42	1.84
st.dev.	0.10	0.02	0.09	0.20	0.05	0.03	0.03	0.05	0.02	0.22	0.16

6.1.5. Laser Ablation Inductively Coupled Plasma Mass Spectrometry.

Only five samples were analysed: PG84, 87 (Group 3), 121, 122 (Group 4) and PG60 (Non-beads). The other samples are represented by either these or the samples discussed in Chapter 5, like in case of Group 13. The results of the analyses are presented in the Appendix 7 and visualised in Figure 6.7. The major elements content is somewhat different among the different Groups' representatives. Samples of Group 3 have the highest SiO_2 content – 74-82%, whereas concentration for other samples is in the range 51-64%. Figure 6.7(a) demonstrates relative abundance of other major oxides, set to 100% to amplify difference/similarity. Na_2O and CaO are less abundant in the Group 3 than in the rest of the samples, instead this Group contains more K_2O. Al_2O_3 values are comparable between Group 3 and 4, though the former one demonstrates higher abundance in the picture due to elevated SiO_2 values.

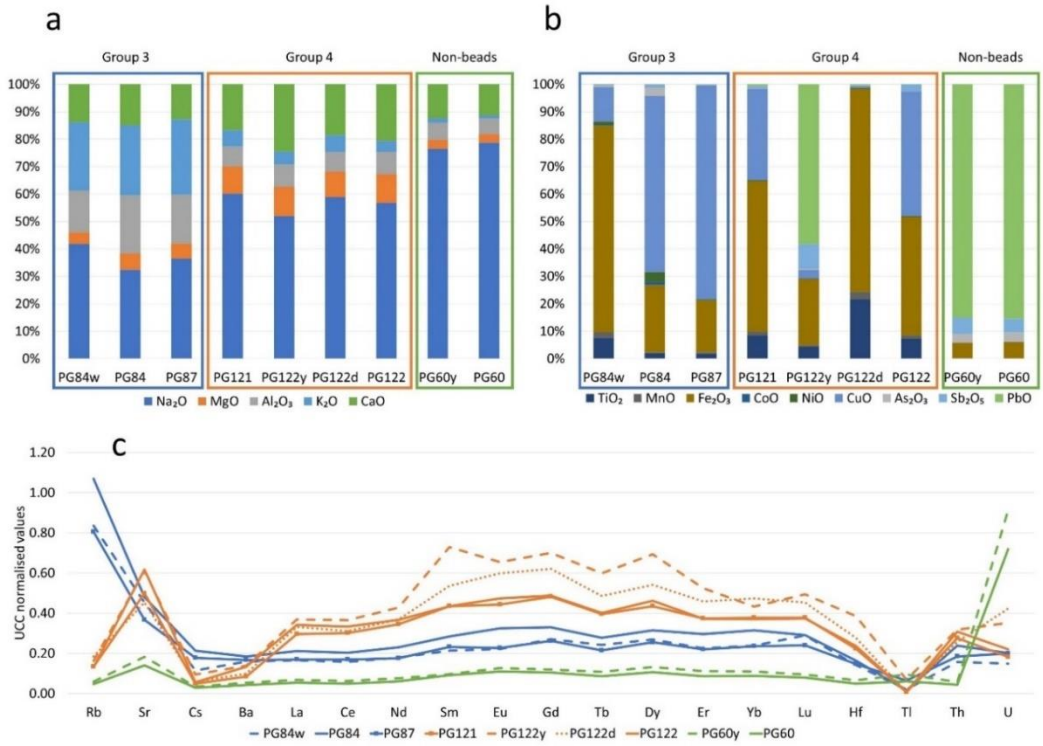

Figure 6.7. LA-ICP-MS results. a - normalised to 100% values of major oxides (except SiO_2); b - normalised to 100% values of some minor oxides; c - UCC normalised (after Mclennan 2001) values of trace elements. Groups of samples are marked by the rectangle of the corresponding colour (a and b) or by the colour of the lines and markers (c).

Group 4 samples have highest MgO and CaO content (3.2-4.1% of MgO and 5.6-9.3% of CaO). Their K_2O levels are lower than those of Group 3 (1.5-2.1% against 4.3-5% in Group 3), but not as low as in PG60 (Non-beads), in which only 0.2% K_2O was detected. Unfortunately, this last value is significantly lower than the one detected by p-XRF. Further comparison of compositions (Figure 6.7) showed that the results obtained on the (expected) blue glass of PG60 are very close to the ones obtained for the yellow glass and suggesting that the analyses of the blue glass might be compromised by the presence of some yellow glass under the surface or the blue one. This is supported by the trace elements data from supposed blue and yellow parts (Figure 6.7c), and would prevent us to draw robust conclusions for the type of blue glass of this sample; therefore the LA-ICP-MS results on the blue part of this sample were discarded.

Minor elements content is visualised in Figure 6.7(b). TiO_2 values are the highest in Group 4 samples (0.16-0.25%), though they are somewhat lower than the values determined by p-XRF. On the other hand, samples are not different in their V, Mn, and Fe concentrations. 40-800 ppm of Co were detected in PG84 of Group 3, in the base of this sample Co also coincides with elevated Ni and As concentrations. Cu values are prevailing over Fe in Group 3, but the opposite proportion is observed in samples of Group 4. The concentration of Cu drops drastically in the decorative parts, whereas high concentrations of Sb_2O_5 (0.5% in PG122, 2% in PG60) and PbO (3.5% in PG122, 30.1% in PG60) are observed. White decoration of PG84 is not enriched in Sb or any of the elements that could be interpreted as the presence of opacifier.

The trace elements concentrations, when normalised to the UCC values (concentrations of McLennan 2001), exhibit similar profile within each Group (Figure 6.7 c). Group 3 demonstrate higher Rb values (90-120 ppm) which is reflected in the plot. Apart from Sr values, the rest of the profile is flat, without significant anomalies. Group 4 samples have higher relative abundance of Sr than Rb and Cs and elevated REE concentrations. U is relatively less abundant than Th. PG60 (yellow) trace elements concentrations are lower that all the rest of the samples except for U values (2.5 ppm).

6.1.6. Micro Raman Spectroscopy.

Out of the samples that were studied in the laboratory, only PG121 did not produce any spectra meaningful for the investigation of the bending and stretching silica vibrational modes. In the rest of the samples, the values of polymerisation index are between 0.81 and 1.16. In the yellow decoration of PG122 (Group 4) this value is 0.21, which is close to the ratio of CMOG C reference glass. Black parts of the same sample show the bending massif towering over the stretching one, which resulted in the polymerisation index value of 11.6, which make any interpretation difficult.

Spectra of yellow decoration of PG60 did not show any silica massifs, peaks at 138, 205, 337, 460 and 509 cm^{-1} were observed instead (Figure 6.8) that were interpreted as $Pb_2Sb_2O_7$ in the mineral form of bindheimite (Ricciardi et al. 2009). Same series of peaks, but less pronounced, were detected in some spectra of the yellow decoration of PG122. The spectra obtained from the green glass of PG122 features a peak at 997 cm^{-1}, which can be assigned to Ca/Al silicate (Ricciardi et al. 2009). It is difficult to attribute a single peak at 154 cm^{-1} to any crystalline inclusions, as it could be related to several compounds.

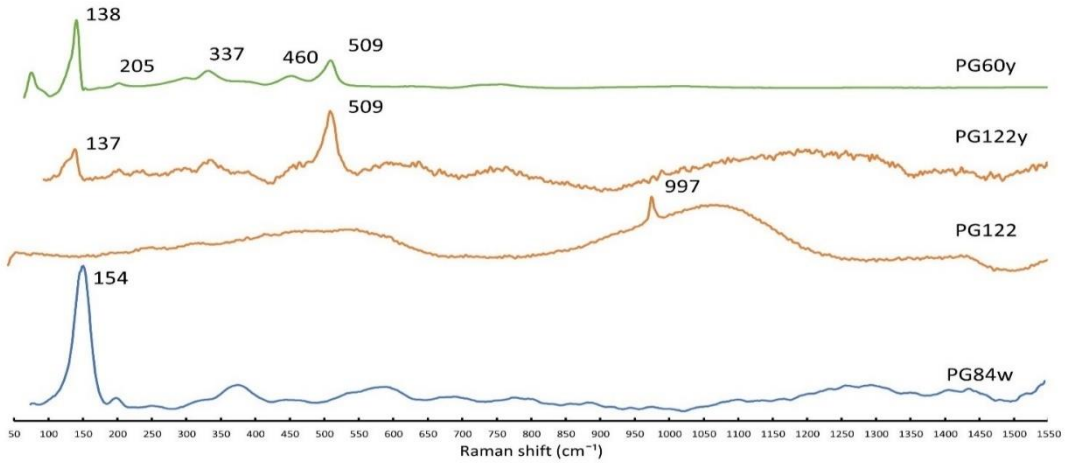

Figure 6.8. μ-Raman spectra of some crystalline inclusions found in the glass matrix. w – white, y – yellow.

6.2. Discussion of the results.

6.2.1. Sources of silica.

Concentrations of trace elements were used to deduce whether or not the objects discussed in this chapter were made from the same silica source. Figure 6.7(c) demonstrates differences among the Groups (or the samples) that were analysed with LA-ICP-MS, and their trace element pattern suggests different provenance of the silica source. Group 3 samples (and, by extent, Group 12), matches by the profile with the high-K sub-Group of Group 7, discussed in the Chapter 5 (Figure 5.13). Those beads were determined to be LMHK glasses and probably made in the FBA glass workshops of Frattesina or in vicinity (Henderson 1988; Towle et al. 2001). Such conclusion can be made by also comparing the trace elements profile of Group 3 samples with some LBA glass beads found on South Italian archaeological sites, particularly Roca Vecchia in the region of Puglia (Conte et al. 2019, several samples were included in Figure 6.9). They have matching Rb concentrations, but usually lower REE concentrations that, nevertheless, follow the same profile. Comparable Ba and La concentrations in these samples also put together Group 3 and the FBA glasses from South Italy in Figure 6.10. Similar values are observed in Mediterranean Group II and III samples found in Veneto region (Panighello et al. 2012) marked as Veneto IA in Figures 6.9 and 6.10. High relative abundance of Rb and low one of U are the features that can be used for discriminating the Mediterranean glass groups from the LMHK ones from the FBA, that can be interpreted as a difference in the fluxing materials, as these elements are likely to substitute the alkalis (Brems and Degryse 2014).

Group 4 has a distinct profile, that might have correspondence with some glasses from Villanovan site in Bologna (Italy). Yet, Sr, Ce and Hf concentrations in these glasses do not match with the Group 4 samples. Relative concentrations of the two latter elements are frequently used to discriminate among sediment sources (Owen 1987; Zhong et al. 2019; Barford et al. 2020). Nevertheless, significant difference in the relative content of these and other elements does not allow to assume a same provenance for the samples from Bologna and those in Group 4. The binary

plot of Ba vs La (Figure 6.10) sets these samples together with the small Group of samples from Bologna, and separates them from all other datasets included for sake of comparison. On these grounds, Group 4 attribution remains unknown. It is likely that these beads were made locally, away from major glass-making centres of Eastern Mediterranean, represented in the Figure 6.10 by datasets from, the literature. The influence of the colourant on the trace elements profile can be reasonably excluded because of the similar profile of green, yellow and black parts of these beads (Figure 6.7). One may assume same origin of PG169 – sample from the Other beads Group, though for this sample, consistently lower concentrations of Ti, Fe and Cu are detected.

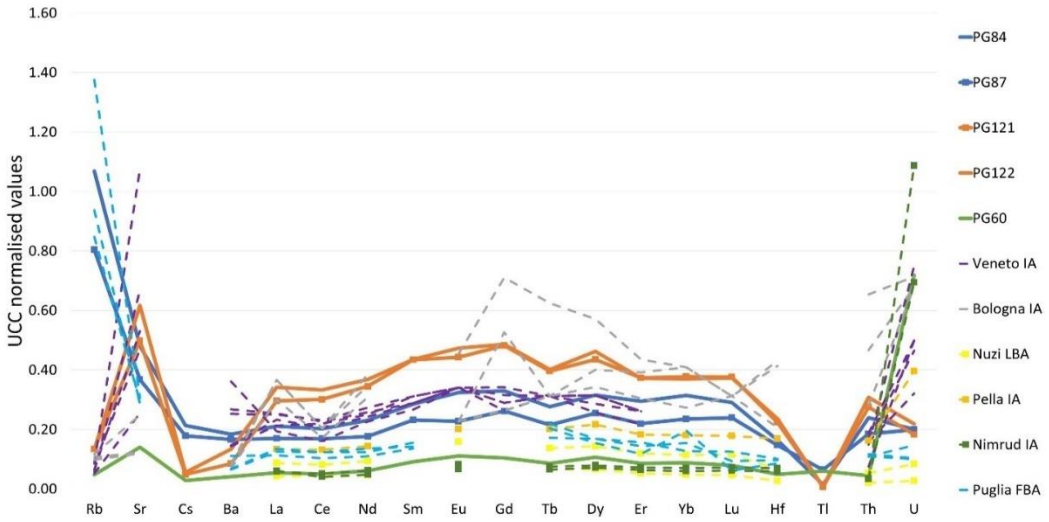

Figure 6.9. Trace elements concentrations normalised to UCC values (McLennan 2001), compared to published data: Veneto IA – values from Panighello et al. 2012; Nuzi LBA, Pella IA and Nimrud IA from Reade 2021; Puglia FBA – from Conte et al. 2019. Samples from the mentioned publications of data were selected for display on the basis of similarity with the studied sample set.

p-XRF analysis indicate that the samples of Group 13 are similar to the Cu-Mn sub-Group of Group 1, described in the Chapter 5. Glass of those samples was attributed to Egyptian production. Unfortunately, not much else can be said about the provenance of the raw glass for these beads and it is difficult to assign certain provenance for PG170, VG28 and VG38.

As already mentioned in the results section, the LA-ICP-MS results of PG60 probably provided the composition only of the yellow glass. Regarding this glass, several corresponding trace elements compositions were found among coeval glasses (Figure 6.9) and it can be connected to the Eastern Mediterranean production. As emerged from p-XRF data, K, Ca, Mn, Fe, Cu, and Sr content in the blue base glass is significantly and consistently different from the one in the yellow decoration (in addition to the Sb and Pb content that is probably related to the opacifier), which suggests that the provenance of the blue and the yellow glass may be different based on major and minor elements concentration.

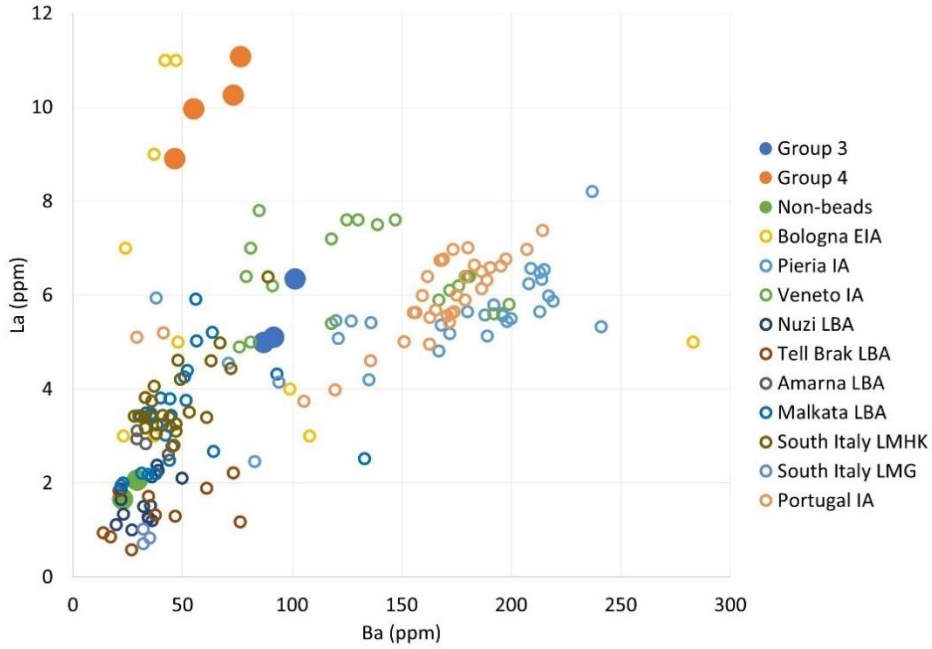

Figure 6.10. Binary plot of Ba vs La values. External sources: Bologna IA – Arletti et al. 2011; Pieria IA – Blomme et al. 2017; Veneto IA – Panighello et al. 2012; Nuzi, Tell Brak, Amarna, Malkata LBA – Shortland et al. 2007; South Italy LMHK, LMG – Conte et al. 2019; Portugal IA – Costa et al. 2021.

6.2.2. Fluxes and stabilisers.

It was mentioned in the previous subsection that Group 3 samples corresponded to the LMHK glasses as their composition in term of the major elements, and particularly their Mg and K content, fits the criteria for LMHK glasses. This is evident in Figure 6.11, where samples of Group 3 are set in the concentration range for this type of glass. This evidence links them to the high-K sub-group of Group 7 (discussed in Chapter 5).

Group 4 lays out of this frame, having less K_2O and more MgO. In the graph, samples of this group are set in the area of HMG, produced by using halophytic plant ash as flux (Henderson 1985; Rehren and Freestone 2015). Positive correlation of K_2O and CaO concentrations further supports the attribution. Given the difference of Group 4 from every other set of samples considered in this chapter demonstrated in the previous section, which might be the evidence of local glass-making, and the availability of the halophytic plants in the Italian peninsula (Sciandrello and Tomaselli 2014), one can assume that the local tradition of glass-making relied on plant ash as the flux to melt silica. Plant ashes have variable composition, that depends on both environment, geography, and species, and this intrinsic variability precludes the possibility of obtaining more details about the fluxing agents by speculating on compositional data (Henderson 2013).

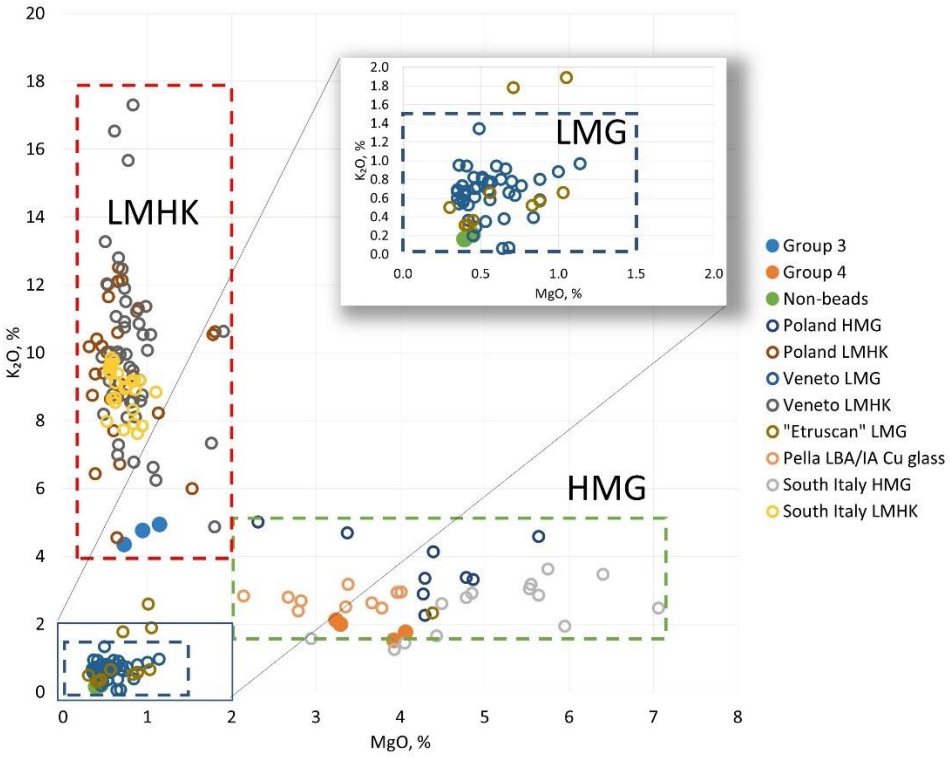

Figure 6.11. MgO vs K_2O binary plot. Poland HMG and Poland LMHK – Purowski et al. 2018; Veneto LMG and Veneto LMHK – Towle et al. 2001; "Etruscan" LMG – Towle and Henderson 2004; Pella LBA/IA Cu glass – Reade 2021; South Italy HMG and LMHK glass – Conte et al. 2019. The boundaries of major compositional Groups of LBA/IA glass are marked with rectangles.

Potassium levels were determined by p-XRF for the Other beads samples. PG169 is associated with Group 4 and has comparable concentration of K_2O and CaO, that support assigning this sample to the HMG. The concentration of K_2O is lower in PG170, (1.36%), which is near the LOQ of the p-XRF unit used for the analysis. Such a concentration is nevertheless lower than 1.5%, which is the accepted borderline between LMG and HMG (Rehren 2000; Genga et al. 2008; Schibille 2011; Verità et al. 2019) and sets PG170 in the LMG type. VG28 and 38 contain low amounts of K_2O and CaO, and it is difficult to assign them to a specific compositional Group, because it is possible that the heavily weathered surface prevented the pristine glass underneath to be analysed.

The Non-beads appear to be made of two distinct types of glass. The blue base fits the composition of HMG on account of the high K_2O concentrations established by p-XRF. The yellow part features less of K, as confirmed by LA-ICP-MS.

6.2.3. Colourants and opacifiers.

Cu is the element that influences the colour of most of the samples considered in this chapter. FORS spectra indicate that Cu is differently involved in the colour of these samples. VG25 is a peculiar

bead within Group 3, which feature both blue-green and red parts in the base glass, without any sharp boundary. FORS spectra indicated that the red colour is due to crystals of metallic copper. All these features suggest that the bead changed its colour after it was produced. It is likely that this bead was annealed in some reducing conditions, similarly to the red bead VG24 (already discussed in chapter 5), which comes from the same tomb. The CuO content for this bead, determined by the p-XRF analyses, was 3-5%, which is sufficient to form microcrystals of elemental copper on the glass surface, given the suitable temperature and redox conditions (Angelini et al. 2004; Bandiera et al. 2020). Group 12 samples, that come from the same context, were also coloured in the same way. The fact that all these beads come from the same tomb and are the only examples of red glass within the whole dataset, leads to conclude that their colour was not intentional and a change occurred in the funerary pyre, where the beads were placed.

The rest of the Group 3 samples were also coloured by Cu, but in these beads it is present as Cu^{2+}, as illustrated in subsection 6.1.2, though only PG167 produced a meaningful FORS spectrum. Significant quantity of Fe is also present in these beads (confirmed by both p-XRF and LA-ICP-MS). In fact, weak Fe^{3+} absorption was detected by FORS in PG167. Fe^{3+} in octahedral coordination would colour the glass yellow (Weyl 1999). Presence of Cu^{2+} and Fe^{3+} would result in overlapping of blue and yellow colour, resulting in the deep green colour that is observed in the majority of Group 3 samples. PG84 contains about 800 ppm of CoO. The absence of Co^{2+} bands in the FORS spectrum and its green colour indicate that Co^{2+} could be present in this sample with an octahedral coordination as a network modifier, acting as a weak chromophore without influencing the overall colour of the bead (Weyl 1999; Pollard and Heron 2005). Co in this bead is associated with Ni and As, same as with LMHK glasses form the Chapter 5, confirming the common provenance of this Group of beads.

It is difficult to determine the chromophore in the white parts of Group 3 and 12 samples based on the gathered data. The composition of white glass in PG84 analysed with LA-ICP-MS does not show major differences from the green part, except for lower Fe_2O_3, CoO and CuO contents. Red coloured samples tend to have higher CaO values in their white decorations. Ratio of CaO content in the white part and in the red-green one is 1.7 on average. The white decoration does not feature additional Sb or Sn, that would indicate crystalline inclusions. Apatite, obtained from bone ash, was suggested by Towle and Henderson (2004) as a white opacifier for some “Etruscan glasses”. Same colouring solution is proposed for the red coloured samples (VG25 and Group 12) but it was done only on account of CaO increase in the white parts, and more analyses are needed to clarify this question. PG84 does not have similar increase in CaO; in this case, crystalline silica or bubbles could be the agents that cause a colourless glass to appear opaque.

Group 4 samples are also coloured by Cu^{2+} in octahedral coordination (FORS data, Figure 6.4). Their colour is lighter and greenish in comparison to the one of Group 3 samples (Figure 6.3). Samples of Group 4 also feature lower concentration of Cu and higher concentration of Fe, that generate weak bands in FORS spectra as Fe^{3+}. Same formation of green colour is expected for this glass, but with increased yellow constituent. Under the optical microscope it was observed that the glass is fairly translucent, but it appears opaque because of the numerous bubbles suspended in the glass matrix. Indeed, the compositional analyses did not reveal any evidence of opacification with crystalline substances, as it was also evident for PG169.

In the yellow parts of Group 4 samples, both Pb and Sb are detected by p-XRF. This shall be interpreted as the presence of lead antimonate ($Pb_2Sb_2O_7$), which was in fact detected on the surface of PG122 with μ-Raman. This way of achieving opaque yellow glass is similar to the yellow decorations of Group 2 samples, discussed in Chapter 5 and described by Lahlil et al. (2011). It is difficult to deduce the use of particular chromophore for the dark coloured parts of Group 4 samples, as the compositional analyses provided very similar compositions for both the yellow and dark glasses, with the only difference of the presence of lead antimonate in the yellow parts.

Group 13 samples might also be coloured by copper in octahedral coordination. The amount of Fe is similar to the Group 3 samples. Fe-Mn complex band was observed in FORS spectra and the high Mn concentrations was confirmed by p-XRF analysis. Mn^{2+} is a weak chromophore and does not contribute to the colour (Bingham and Jackson 2008; Pollard and Heron 2015). Its concentrations, though, suggest intentional addition to the batch, where it could be used as a refining agent (Bingham and Jackson 2008). Yet, its correlation with Fe and Cu oxides might be the sign of its addition, deliberate or not, with one of the colouring components. Despite this Group of samples appeared to be similar to the Mn-Cu sub-group within Group 1 according to the PCA plot (Figure 6.5), p-XRF analysis did not detect any Co. Perhaps, same Cu bearing material was used to colour these and the Mn-Cu sub-group of Group 1.

Sn was detected in most of the samples of Groups 3 and 12. This may be suggestive of the use of bronze as the Cu-containing material added in the glass batch for colouring purpose. Typically, the Sn/Cu ratio in bronzes of Bronze and Iron Age is assumed to be 1:10 (Smirniou and Rehren 2013). In the samples of Groups 3 and 12 where Sn was detected, this ratio is 0.08 on average, which corresponds to some low Sn bronzes that were produced for specific purposes (Craddock 1977; Ingo et al. 2006). Yet, LA-ICP-MS composition estimates the Cu/Sn ratio in PG84 and PG87 at 0.02, which is much lower. In this way, it is difficult to assess whether or not bronze could be the source of copper in these samples, but the association between the Sn and Cu is evident. The rest of the samples, except PG169 and VG38, do not have Sn detected with p-XRF and it is unlikely that bronze was used to introduce Cu into their batch and a purer (at least on account of heavy elements) source of Cu is expected.

PG170 has a unique appearance within the set of samples and also shows elevated Cu and Sb concentrations. FORS analysis demonstrated that Cu^{2+} is responsible for the blue colour of the sample. In addition, the brightness and opacity of the bead is probably caused by the presence of calcium antimonate crystals (CaO values are one of the highest within the dataset, Sb is also present), which, as already discussed in Chapter 5, was a popular solution for bright white colour at the time. Unfortunately, the elemental data do not allow to identify whether it is $CaSb_2O_6$ or $Ca_2Sb_2O_7$.

VG28 and VG38 have altered surface and their FORS spectra are of poor quality. These samples might be coloured with Fe, as Fe^{2+} was detected. CuO in these samples has concentration of about 1%, yet it might be in its reduced form (Cu^{+}) and does not take part in the colouration.

The base glass of Non-beads is coloured by Cu^{2+}, with the lowest Fe_2O_3 concentrations within the dataset: p-XRF indicates it is some 0.4%, which is probably not enough to turn the glass green by the yellow colour of Fe^{3+}, as we observed in the rest of the samples. The yellow decoration is coloured by $Pb_2Sb_2O_7$. Remarkable is the amount of PbO, that reaches 30%. The stoichiometric ratio of Pb to Sb in the antimonate is approximately 1.7, whereas the ratio was estimated at 15.9 with LA-ICP-MS data obtained in PG59 and 60, highlighting an excess of Pb added to the batch.

6.2.4. Production and forming techniques.

The chemical composition and the appearance of the beads testify they were made using different raw materials and ways of their processing. The batch was formed with the silica source and the fluxing agent. In case of Groups 3 and 12 this was the LMHK type of flux. Group 4, Non-beads and PG169 were probably prepared by the addition of plant ash as the flux. Decorative glass of non-beads probably was natron based. Samples of Group 4 and the Other beads, with the exception of PG169, were also prepared with LMG, though in case of VG28 and 38 a reliable attribution is prevented due to extensive degradation. LMG samples glass would require source of Ca such as shells for stabilisation of the resulting glass.

Cu entered the batch probably as a relatively pure substance. Batches had different Fe to Cu ratio. Group 13 batch was prepared with addition of Mn containing material. To make opaque white glass of the decorations of Groups 3 and 12, probably, bone ash was added. It withstood the thermal processing of the batch to remain suspended in the matrix. For the opaque yellow glass of the decorations, previously prepared crystals of lead antimonite, with an excess Pb, were introduced instead of the Cu containing materials. Batch for Group 4 features the less pronounced excess of Pb, whereas the Non-beads had the highest excess. It is unclear whether the dark glass of Group 3 samples required addition of certain ingredients, or special processing step was required. Calcium antimonate was used to make PG170 glass together with Cu to manipulate the final appearance.

Forming temperatures indicator, i.e. the polymerisation index obtained by μ-Raman analyses, indicates 700-1000 °C range as the working temperature for these glasses. Oxidising conditions would be needed to prepare Cu^{2+} coloured glass for all the groups of objects discussed in this chapter. The difference in their colour can be attributed to the different relative concentrations of both Fe and Cu. Bubbles were used in the glass of Group 4 and PG169 to produce the opaque appearance.

Beads of Group 3 were formed by winding the base glass around a mandrel, similarly to the majority of beads already discussed in Chapter 5, but their eye decorations were obtained in different manner: by dropping white glass on the side of the bead. Both glasses should have been not too liquid, since the drop remained as a protrusion – or a horn – on the body of the bead. Then, a drop of the base glass was mounted on top of each horn. This makes this type of decoration a stratified eye, instead of ring eyes that are present in the beads discussed in Chapter 5.

Group 4 beads seem to be also formed by winding. Their decorations are different though. PG122 has three horned eyes formed by twisted and pre-fused rods of yellow and dark glass that were applied on the green glass surface (Koch 2011). In case of PG122, the protrusions suggests that glass was already having high viscosity. In case of PG166 such decoration is completely levelled with the green surface, which is a sign of post-heating and low glass viscosity. Decoration of Group 12 beads was applied as a thread of white glass that rotated 3 or 4 times around the body (or the other way around – the body was rotated on the mandrel).

Group 13 beads are of a particular tubular shape. The difference between their apexes might indicate the way they were produced (Figure 6.2): it is reasonable to assume that the glass was wound many times around the mandrel spirally, forming the long body; the difference between apexes might be caused by the way such beads were detached from the mandrel. On the bottom end, the flatter and thicker apex was formed, while the rounded and thinner one was formed on the other side. These beads can belong to drawn type (Kidd and Kidd 2012). Their decoration, which is

presently lost, was applied in the similar way to the beads from Group 12, but in case of Group 13 beads the thread made more than 20 rotations covering the whole length of the bead. After this, the decoration was “combed” in a herringbone pattern by perpendicular moves of a tool on the still somewhat liquid surface.

The Non-beads were made on already shaped bronze fibula bow. Rounded support was used to shape the fibula decoration from the bottom, and then the apexes were flattened by abrasion. Yellow decoration was applied on the blue base surface by winding the thread and “combed” several times into a herringbone pattern (Koch 2010). The surface was fairly viscous and the “combing” also affected the blue glass distribution (Figure 6.2).

Conclusion. Data gathered on predominantly Cu-coloured objects revealed complex relationships among types of objects, their bulk glass composition, and how the final appearance was achieved. Groups of objects discussed in this chapter were divided into LMHK, HMG and LMG compositional groups. They were, expectedly, of different provenance, which was confirmed by the trace elements' composition. Part of the objects belongs to the FBA production set in the north of the Italian peninsula (Groups 3 and 12). Another Group of samples (Group 4) featured a particular trace elements pattern that may identify it as an example of local primary glass making, and this compositional evidence combines with their unique appearance. Even though more data on similarly-looking beads should be collected, comparing their composition to local silica sources, this research gives some preliminary hints on this topic to shed more light on the question of local glass making. Compositional evidence suggested an Eastern Mediterranean origin for the rest of the beads discussed in this chapter.

CHAPTER 7. TRANSLUCENT GLASSES.

The following archaeological objects are discussed in this chapter:

- **Group 5: all;**
- **Group 10: all;**
- **Group 11: all;**
- **Other beads: PG90, 172 VG88;**
- **Non-beads: PG97, VG5, 6, 56, 114.**

7.1. Results of the analyses.

7.1.1. Visual observation and Optical Microscopy.

Translucency of the majority of objects considered in this chapter made their visual examination and documentation somewhat different from that of the other samples, as here it was possible to observe in transparency certain features such as bubbles and inclusions below the surface. Also capturing the colour was different in these translucent objects. Apparent colour in the photographs, taken both by the camera and the microscope, has two components: the light reflected from the surface and the light transmitted through the bulk from behind the object. This latter is influenced by the colour of the background. The apparent colour of translucent glass, as dictated by Beer-Lambert law, in part depends on the thickness of the measured samples (Capobianco et al. 2019). To minimise the influence of the background all the photographs, made both by camera and the microscope, were taken with identical sheet of grey paper as a background.

Group 5 consists of samples of several different colours, which are represented in Figure 7.1. Their texture appears to be similar to some of the beads that were discussed in the previous chapters, featuring certain degree of pitting (Figure 7.1 a-d). Bubbles in the bulk are more visible when translucency score rises. They appear to be round (Figure 7.1 b,d), though many of them caused the pronounced pitting of the surface. Sometimes, small parallel grooves in the direction perpendicular to the aperture can be seen (Figure 7.1 c).

Similar division by colour exists among the samples of Group 10, although the borders of such division are less defined (compare shades of several samples of Group 10 in Figure 7.1 e). The surface of Group 10 beads, which are larger in size than those of Group 5, is usually more regular with respect to those of Group 5, yet same features are present. Beads of these groups are well preserved, though some samples, as PG1, 63, 171, VG82, 90, 104, exhibit pronounced alteration in the form of crizzling, iridescence, pronounced deformation of the surface by grooves and extensive pitting (Appendix 2). Several samples within Group 10 have blunt grooves near one of the apexes, sometimes crossing the opening of the aperture itself (Figure 7.2 a). This is characteristic of PG95, 119, 146, 147, VG62. Some samples within this group have different diameter of the aperture at each apex (VG87, 89). In some beads, the bubbles are elongated (Figure 7.1 e, second from the left).

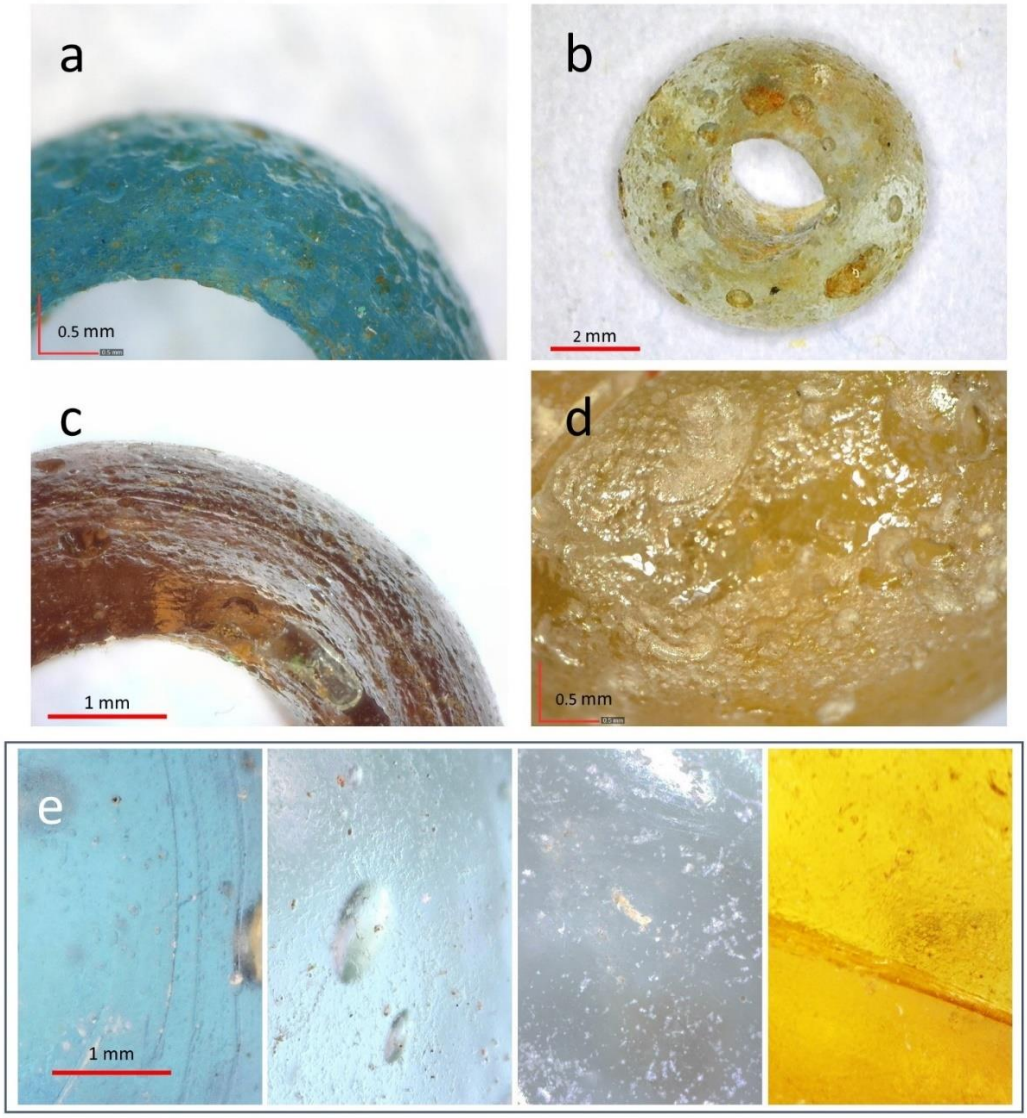

Figure 7.1. Microphotographs of samples: a - PG69; b - PG71; c - PG75; d - PG154; e - representatives of different colours within the set from left to right - PG9 (blue), PG95 (green), VG5 (clear), PG11 (yellow). Samples in a-d belong to Group 5, e – to Group 10, except VG5 (glass button in Non-beads group).

Group 11 samples are less preserved, but VG39 has its surface in better condition without pronounced surface alteration. The rest of the samples show signs of advanced decay (Figure 7.2 b, c). PG88, 89 and VG15 have white crusts on their surface, and similar crusts are present on PG88, and PG89, which are covered in grooves that are perpendicular to the aperture (Figure 7.2 b). The original blue colour can be seen only in some parts of the beads (Appendix 2). PG136 – a small bead fragment that does not carry any diagnostic features for typological assignment, was included in Group 11 based on the similarity of appearance of the glass with the blue samples within this group.

Original colour of VG15, observed in translucency under a source of light, appears similar to the one of VG86, the surface of which is marked with crizzling and patches of iridescence. Pitting similar to Group 10 samples is visible. Ribbed surface is created by blunt grooves that go parallel to the aperture (Figure 7.2 c).

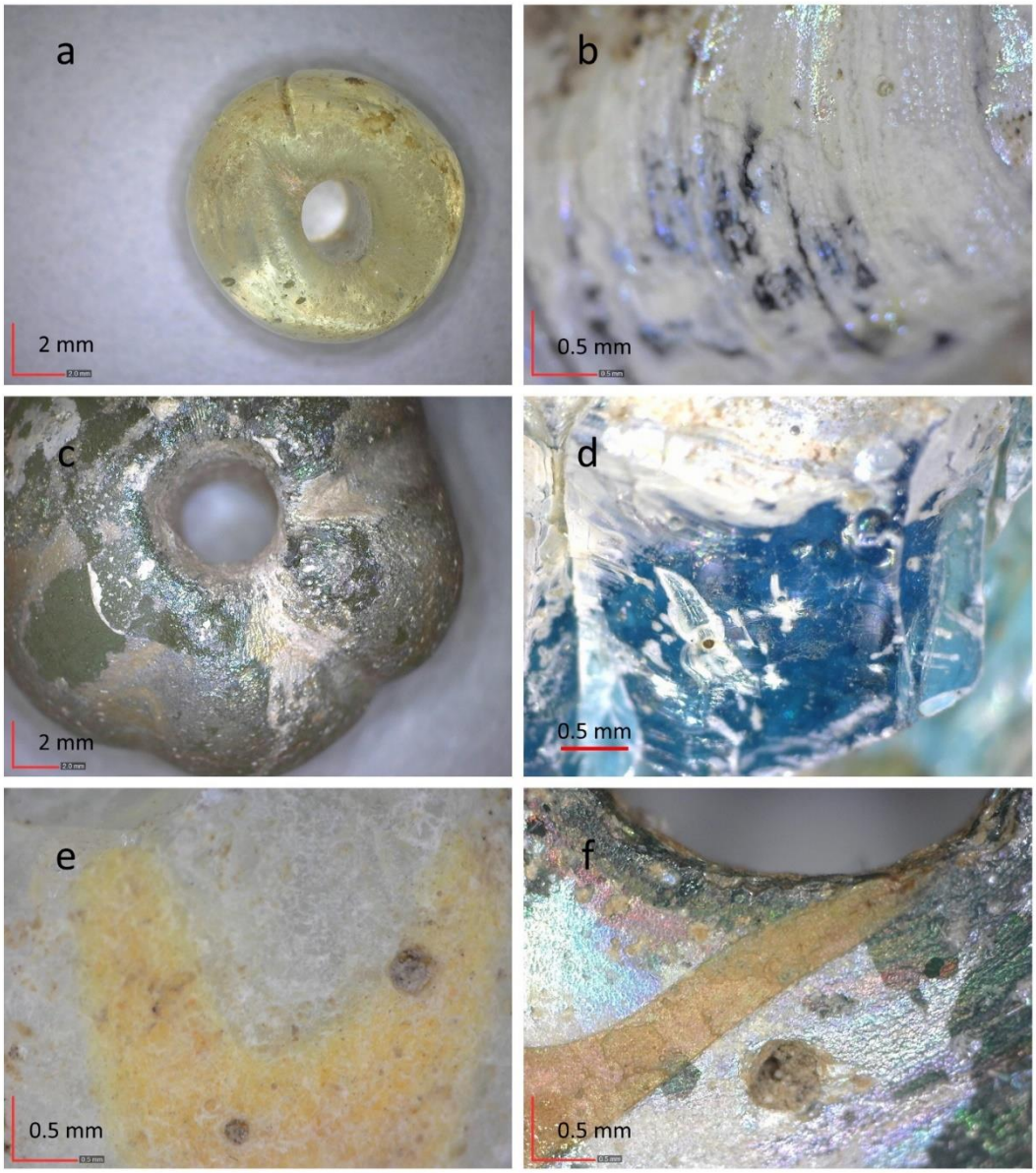

Figure 7.2. Microphotographs of samples: a - VG62 (Group 10); b - PG89 (Group 11); c - VG86 (Group 11); d - PG97 (Non-beads); e - PG90 (Other beads); f - VG88 (Other beads).

Similar type of shape is inherent to PG97 that belongs to the Non-beads group of samples. Remarkably similar type of alteration to the samples in Group 11 is observed on the surface of this sample (Figure 7.2 d in the top, original glass is below). VG5 and VG6 belong to the same group, but

they have different appearance, as the buttons of clear glass same as VG1 and 2 from Chapter 5. They are in good state of preservation, though some crizzling was observed (Figure 7.1 e, third from the left). VG56 consists of two clear aqua beads, which are among the best-preserved samples of the Non-bead group. VG114 features a crizzled surface with dark colour depositions on the surface.

The Other beads group of samples is represented by samples that are of unique shape for the entire sample set. PG90 is pear or spindle whorl shape with an opaque yellow wave decoration that is less noticeable due to the advanced crizzling of the entire surface (Figure 7.2 e). The other two samples within this group are the bird beads PG172 and VG88. They are different by the combination of base and decoration colour, as stated in Chapter 3. VG88 is less preserved, featuring iridescent crusts that seemingly do not extend on the yellow decoration surface (Figure 7.2 f). It is also noticeable that decorations on these samples are quite thin.

Compositional information obtained from the altered surface of some samples from all the above-mentioned groups should be taken with caution.

7.1.2. Apparent colours and Fibre Optics Reflectance Spectroscopy.

The difference in apparent colour was evident from the photographs reported in Appendix 2, and from Figures 7.1 and 7.2. Colour assessment adopted in this study further highlights division in the appearance of the samples. Figure 7.3 reports the RGB colour information which is available in the Appendix 3 for the majority of the beads discussed in this chapter. Similarly to what already presented for the previous chapters, samples in fragmentary state are omitted.

In the tri-plot of the RGB values (Figure 7.3 a), Group 5 is divided in the same way as was introduced in Chapter 3 and in section 7.1 of the present chapter. PG69 and PG70 occupy area near the square 18 of the ColorChecker (Cyan), PG71, PG72 are in the zone of clear glasses between green and brown squares (these samples also have the highest average RGB values within this group (Figure 7.3 b), PG75 and PG76 are close to the red zone of the triangle and - last but not the least – PG154 is situated in the orange-yellow zone, as expected.

Group 10 was preliminary divided into 4 sub-Groups: clear (PG12, 68, 119, 148, VG52, 53, 61, 104), yellow-honey (PG1, 2, 10, 11, 67, 104, 117, 140, 153, VG14, 89, 90, 102), green (PG7, 95, 165, VG48, 49, 57, 62, 63, 87, 105) and blue (PG8, 9, 33, 63, 116, VG103). The RGB values of these groups partially confirm the division, as in the tri-plot (Figure 7.3 a) the clear and green samples are not properly divided from one to another. Green samples, nevertheless are skewed to the green side. Several yellow-honey samples also have higher relative blue values, which makes them to overlap with clear and green samples.

Four samples from Group 11 were considered in the colour study (Figure 7.3). PG39, thanks to its clear surface, is placed in the Cyan zone. The rest of the samples are located near the centre of the tri-plot. They overlap with clear and green samples from Group 10. VG15 has higher average RGB values because of its light-coloured alteration crust. Other beads PG90 and VG88 overlap with green and clear samples, and PG90 has higher average RGB score, as expected. The Non-beads are situated in the blue-green area, with clear samples VG5 and 6 having their average RGB values at one of the highest levels.

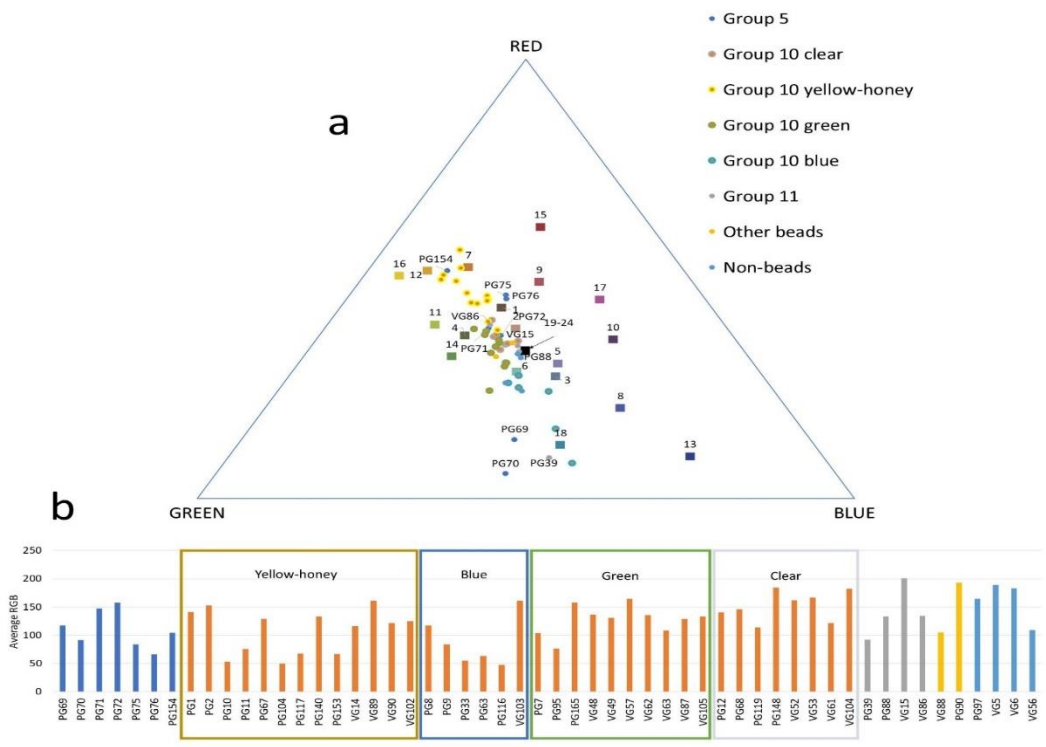

Figure 7.3. a - Tri-plot of RGB values of beads discussed in this chapter with ColorChecker RGB values placed for the reference (squares with numbers) b – average RGB values of samples divided on Groups. Group 10 is divided into four sub-Groups: clear, yellow-honey, green and blue, marked by rectangles within plot b.

Some correspondence of colour information with FORS is expected. Indeed, the shape of the FORS spectra of differently coloured glasses is slightly different among the previously-defined groups of yellow-honey, blue, clear and green glasses according to their place on the tri-plot in Figure 7.3 a. Such division can be observed in Figure 7.4, where representative spectra of each colour sub-group are displayed and certain variability is evident within each plot.

Yellow-honey glasses absorb in the purple-blue region of the spectrum (380-495 nm). Apart for the sub-group within Group 10, PG154 (Group 5) is included here. PG75 and PG76, though being slightly different (purplish) are also considered in the same plot (Figure 7.4 a). Their maxima are usually near 600 nm. In the 400-500 nm interval, several absorption bands occur in the majority of the spectra, and are recognised as Fe^{3+} bands, where Fe ions are arranged in a tetrahedral coordination in the glass network. It is evident from Figure 7.4 a that these bands appear in different places, usual centring being 410, 440 and 490 nm. Bands at 410 nm can be also interpreted as the absorption of the ferri-sulphide complex ($Fe^{3+} – S^{2-}$) (Schreurs and Brill 1984; Meulebroeck et al. 2010). This band appears in samples PG10, 14 and 67. Several samples (PG13, 75, 76, 140, 142) also feature a band placed between 470-510 nm, which might indicate Mn^{3+} presence (Micheletti et al. 2020), although the presence of Mn should be confirmed by elemental analysis. The NIR part of the

spectrum of these samples features increased absorption towards the end of the spectral range, which indicates Fe^{2+}.

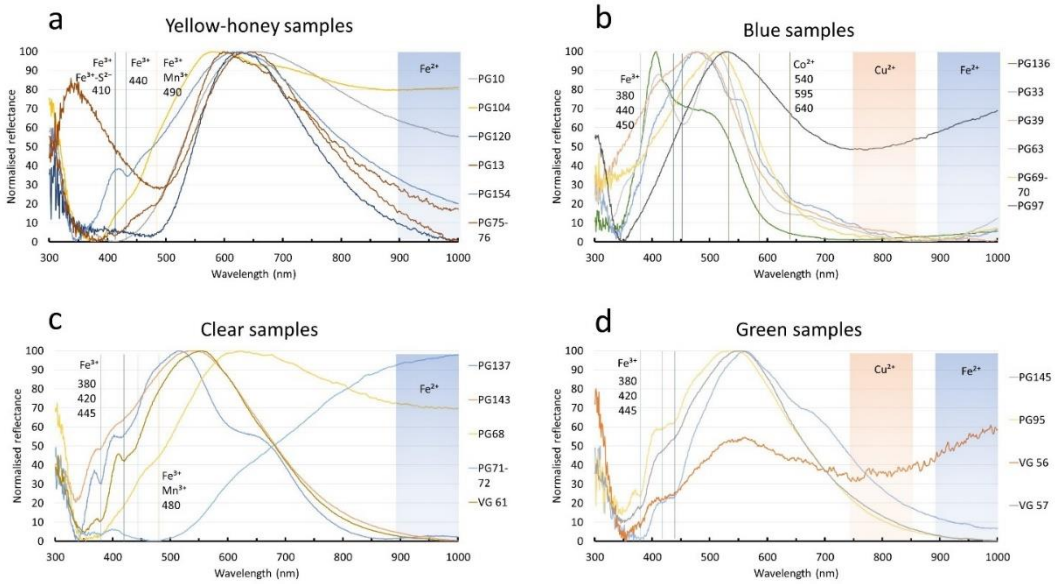

Figure 7.4. Representative spectra of FORS results: a - yellow-honey samples; b - blue samples; c - clear samples; d - green samples.

Blue samples, which include PG69, 70 (Group 5), PG39, 88, 89, 136 (Group 11) and PG97 (Non-beads) apart from the blue sub-Group of Group 10 samples, have their reflectance maxima shifted to the blue part of the spectral range (Figure 7.4 b). Usually, weak Fe^{3+} bands at 380 and 440 nm are present in the spectra, and also NIR absorptions are more pronounced. Several samples, namely PG69, 70 (Group 5), 33, 63, 116 (Group 10), 39, 89, 136 (Group 11) and PG97 (Non-beads) absorb also in 750-850 nm range, which indicate Cu^{2+} absorption. Fe^{2+} absorption is also present in the spectra of samples PG8, 9, 145 and VG103. PG33 also seem to contain Co^{2+} ions as evident from the weak triplet of bands at 540, 595 and 640 nm.

Figure 7.4 c presents the representative spectra of the clear or weakly coloured glasses. In addition to the corresponding part of Group 10, PG71, 72 (Group 5), VG5, 6 (Non-beads) are considered together with these samples. Clear samples have their respective peaks of reflectance in the green range. Both Fe^{3+} and Fe^{2+} bands are present in the majority of the spectra. Exceptional spectra are demonstrated by PG68, 71 and 72, which feature weak, or even none, of the Fe^{2+} band and possible weak Fe^{3+} or Mn^{3+} band centred at 480 nm. These two samples are more similar to the yellow-honey sub-group of samples.

Green samples, namely VG15, 86 (Group 11) and VG56 (Non-beads), yielded spectra that are very similar to the clear sub-group (compare Figure 7.4 c and 7.4 d). The only outlier within this Group is VG56, that apparently contains Cu^{2+} because of the presence of a broad band in the NIR region. Same spectrum contains pronounced Fe^{3+} bands (and no signals from Fe^{2+}).

20 samples (i.e. the 27% of the whole set considered in this chapter) did not produce meaningful FORS spectra and where therefore excluded from the discussion on FORS results. This issue could be connected to the translucency of the material, that led the FORS setup to catch too little diffused light, thus no signal. In addition, alteration of the glass, mentioned in section 7.1.1, also played a role in preventing the FORS investigation of some samples.

7.1.3. Portable X-Ray Fluorescence spectrometry.

p-XRF analyses revealed that the glasses considered in this chapter have very low contents of transition metals, with many elements near or below the LOQs. Therefore, it is difficult to trace any differences within the sample set. The compositions determined by p-XRF are reported in Appendix 6. The PCA, demonstrated in the previous chapters on predominantly Co and Cu coloured beads, did not differentiate the beads discussed here. The majority of the samples are placed in the same area of the plot with Group 1, stretched along the PC1 axis (Figure 6.5). When only these 75 objects were included in the PCA, most of the objects' scores remained in the same area of the plot (not reported) and several outliers are placed in various directions. Despite the apparent homogeneity of the set, it was decided to highlight any subtle differences among the groups by checking the sample set variable by variable.

It must be said in the beginning that VG148 (group 10) has a unique composition rich in silica, with Ni, Os and Bi peaks in its spectrum. This might be an example of rock crystal, and should be put aside.

Samples within Group 5 have K_2O levels below the LOQ (<1.2%). Their CaO values are average (Figure 7.5 a) within the set (mean value across the Group 6.37%). These beads contain low amount of transition metals, with the exception of Fe (Fe_2O_3 values contained in 0.63-0.92% range). PG75 and 76 have Mn in the matrix (0.9%), supporting FORS data, whereas PG69 and 70 featured elevated Cu content (1.3% on average).

Colour sub-groups within Group 10 do not show any systematic compositional difference. Individual samples show high concentrations of elements such as K, Mn, Cu and Sb. Indeed, across all colour sub-groups, some samples contain more than 1% of K_2O: PG2, 104, VG89 (yellow-honey sub-group), PG33, 63, 69, 145, VG82 (blue), all the green sub-group samples and PG12, 68, 119, VG53, 61, 62, 63, 84, 104 in the clear glasses. All the samples, but two, follow a similar trend line in the Ca and Sr graph, as demonstrated in Figure 7.5 a. Ti was detected in PG104. This sample has a peculiar composition, with elevated concentration of Mn, Fe and Zr. Apart from PG104 Ti concentrations were above the LOQs in VG52, 82, 83 and 84, though this should be on account of lower LOQ of the Frankie XRF unit in respect to ELIO and Unisantis units that were used to analyse all the other samples.

Mn was detected in minor quantities in many samples of Group 10 without any sub-group preference. Fe and Cu levels are demonstrated in Figure 7.5 b. It is evident that samples across all the groups usually contain 0.2-1.2% of Fe_2O_3. Average concentration across all the groups is 0.58%. Yellow-honey samples tend to have less Fe_2O_3 – 0.44% on average, while the green sub-Group have more – 0.66%, although this difference might not be significant because of dispersion of the data. Samples of the blue sub-group in Group 10 have elevated CuO levels, with the exception of PG8, 9, 145 and 171. CuO values above 0.5% were noted for PG69 and PG70 (Group 5), blue samples within

Group 11, bird beads PG172 and VG88 and PG97 of Non-beads. This corresponds to FORS data (Cu^{2+} was detected for these beads). Several samples contain still detectable but low amount of CuO (Figure 7.5b). They were analysed with Frankie and Unisantis XRF units for which the LOQ were set lower than for the ELIO unit.

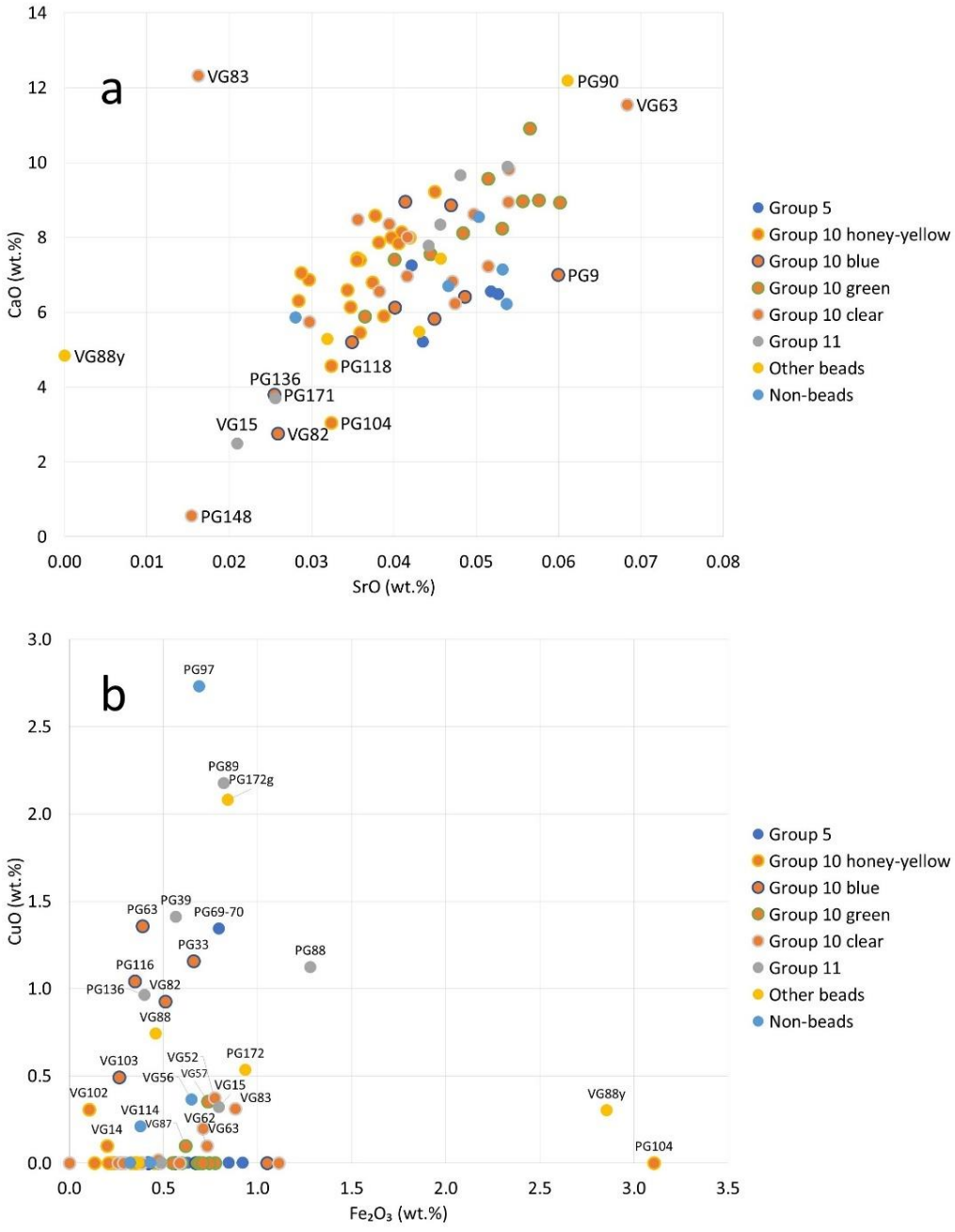

Figure 7.5. p-XRF data. Binary plots of SrO vs CaO (a) and Fe_2O_3 vs CuO (b).

PG171 contains detectable amount of Co, Ni and Zn. Co was also detected in VG15.

Sb, on the other hand, occurs more frequently and in more than trace amounts (>1000 ppm weight oxide). Samples within Group 10 that have detectable Sb_2O_5 concentrations: PG1, 2 (yellow-honey), 8, 145 (blue), 7, 95, 147, 165, VG57 (green), PG119, VG62, 83, 84 (clear).

Group 11 samples are remarkable by their Zr content. Samples that have higher Cu values (Figure 7.5 b) tend to have their ZrO content at 0.02-0.05% level, whereas in the rest of the samples, namely VG15 and VG86, this element is below the detection limit. Ca value of VG15 (2.5%) might be underestimated due to the surface alteration.

PG90 (other beads) has remarkable Sb_2O_5 content – 4%, in addition, its Zr concentration is also comparable with that of the blue samples from Group 11. The body of PG172 (bird bead) contains Mn (0.72%). Cu, Sb and Pb values could be influenced by the blue decorative thread, where these elements are in higher concentration than in the body of the bead. Another bird bead has higher CuO concentration in its body than in the decorative part. The yellow decoration is rich in Pb and Sb but also has higher Fe concentration. Both bird beads have elevated K_2O concentrations.

The Non-beads group contains glasses that have detectable amounts of K2O – 0.43-3%. Samples VG5, 6 and 114 have vestigial quantities of Sb and Pb as is evident from their spectra. VG56 and 114 contain minor amount of CuO (0.2-0.4%).

It is difficult to determine the order of the representativeness for the laboratory analyses. p-XRF data on elements such as K, Mn, Cu, Zr, Sb can be used. Their values are often near the LOQ, where lower reproducibility of XRF values was noted (section 4.4). No clear typological division is formed, i.e. samples from different groups can exhibit similar compositional features. Fortunately, one third of the total number of samples could be analysed in the laboratory by the LA-ICP-MS, ensuring that all groups and sub-groups discussed here had their representatives for the laboratory sessions. Bird beads (PG172, VG88) and glass buttons (VG5, 6) could not be transported. In this way the depth of insight to the technology of their production is limited the data presented so far.

7.1.4. Scanning Electron Microscopy coupled with Energy Dispersive Spectrometry.

Twelve samples were analysed by SEM-EDS, most of them as polished cross sections and only one (PG39) without any preparation in the variable pressure mode. Within this reduced set, eight samples represent Group 10, tree – Group 11 and one sample (VG114) is from the Non-beads. The results of the analyses are presented in the Table 7.1.

Silica concentrations vary from 68.3% to 77.1% and mean value of 73.7%. Sodium prevails over potassium in all the samples averaging at 16.3% weight oxide and very low dispersion of 1%. On the other hand, K_2O concentrations are under the LOD in all the samples but VG114, which contains 2.84% of K_2O. PG39, analysed in the variable pressure mode (not reported in Table 7.1), demonstrates the lowest Na_2O level, which may be the sign of glass surface alteration. Alkali-earth elements do not demonstrate much of variability neither, except of VG114 which has higher than the quantities of both MgO and CaO – 4 and 7.4% respectively, while the rest of the samples have

average MgO level at 0.47 and CaO at 5.5%. Relative abundance of some major and minor oxides is visualised in Figure 7.6. Al_2O_3, as can be seen from the Table 7.1 and Figure 7.6, is present in minor quantities that never exceed 0.68%.

Table 7.1. Results of the EDS analyses. Values represent averaged bulk compositions expressed as oxides with the standard deviations of the replicate analyses placed beneath the composition data. PG39 results are not reported (analysed without polishing)

Group	sample/st.dev.	Na_2O	MgO	Al_2O_3	SiO_2	SO_3	Cl	K_2O	CaO	MnO	Fe_2O_3	CuO
10	PG13	16.83	0.46	<LOD	75.62	0.47	0.60	<LOD	6.02	<LOD	0.21	<LOD
	st.dev.	*0.11*	*0.02*	-	*0.11*	*0.02*	*0.02*	-	*0.04*	-	*0.06*	-
10	PG15	16.06	0.58	0.24	76.66	0.64	0.92	<LOD	4.86	<LOD	0.24	<LOD
	st.dev.	*0.18*	*0.02*	*0.04*	*0.23*	*0.05*	*0.03*	-	*0.08*	-	*0.04*	-
10	PG96	16.42	0.44	<LOD	75.69	0.30	0.65	0.34	6.09	<LOD	0.23	<LOD
	st.dev.	*0.73*	*0.04*	-	*0.73*	*0.04*	*0.05*	*0.01*	*0.08*	-	-	-
10	PG116	15.70	0.51	0.33	74.61	0.83	0.92	<LOD	4.89	0.55	0.39	1.79
	st.dev.	*0.56*	*0.03*	*0.03*	*0.62*	*0.05*	*0.03*	-	*0.04*	*0.06*	-	*0.13*
10	PG118	17.40	0.54	0.37	74.22	0.46	0.85	<LOD	6.02	<LOD	0.32	<LOD
	st.dev.	*0.22*	*0.03*	*0.04*	*0.21*	*0.05*	*0.02*	-	*0.04*	-	*0.05*	-
10	PG137	15.65	0.36	0.11	77.07	0.92	0.52	<LOD	5.63	<LOD	0.23	<LOD
	st.dev.	*1.69*	*0.02*	*0.02*	*1.47*	*0.04*	*0.03*	-	*0.10*	-	-	-
10	PG142	18.11	0.38	<LOD	74.03	0.42	1.11	<LOD	6.11	<LOD	0.19	<LOD
	st.dev.	*0.37*	*0.04*	-	*0.28*	*0.03*	*0.02*	-	*0.02*	-	*0.02*	-
10	PG143	16.52	0.73	0.31	76.07	0.92	0.46	<LOD	4.79	<LOD	0.29	<LOD
	st.dev.	*0.28*	*0.05*	*0.02*	*0.32*	*0.05*	*0.01*	-	*0.04*	-	*0.05*	-
11	PG89	18.58	0.36	0.43	68.27	0.34	1.25	0.27	7.41	0.30	0.35	2.62
	st.dev.	*0.15*	*0.04*	*0.06*	*0.59*	*0.05*	*0.02*	*0.07*	*0.06*	*0.03*	*0.07*	*0.33*
11	PG136	17.50	0.38	0.37	74.06	0.88	0.97	<LOD	3.57	0.57	0.35	1.72
	st.dev.	*0.13*	*0.02*	*0.02*	*0.39*	*0.05*	*0.06*	-	*0.04*	*0.03*	*0.05*	*0.19*
Non-beads	VG114	15.24	3.95	0.68	68.76	0.43	0.20	2.84	7.42	<LOD	0.47	<LOD
	st.dev.	*0.08*	*0.03*	*0.04*	*0.25*	*0.06*	*0.02*	*0.05*	*0.04*	-	*0.05*	-

Transition metals are detected in minor quantities in concentrations that were observed in p-XRF data. MnO was detected in PG116 and Group 11 representatives (except PG39). Fe_2O_3 was detected in all the samples though in concentrations somewhat lower than those reported in p-XRF results. Cu was detected in PG116 and samples of Group 11. This results further corroborates p-XRF data.

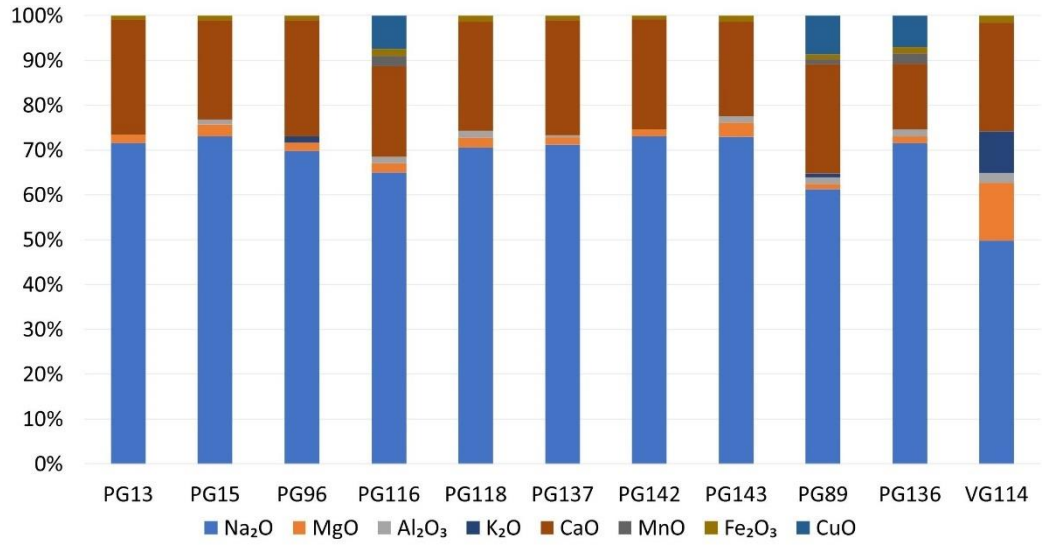

Figure 7.6. Normalised to 100% values of some major and minor oxides from the table 7.1.

7.1.5. Laser Ablation Inductively Coupled Plasma Mass Spectrometry.

Twenty-five samples were analysed. The results of the analyses are reported in Appendix 7. By the concentration of major, minor and trace elements, the analysed samples can be divided into three groups, that do not follow the typologically-established grouping. The first group consists of some samples of Group 5 (PG71 and PG75) and some of Group 10 (PG7, 9, 119 and 147). These samples are characterised by lower average Si and higher Mg and K concentrations (Figure 7.7 a, b). They also demonstrate higher Fe_2O_3/TiO_2 ratio (9.2 on average, st. dev. 0.4) which is visualised in Figure 7.7 c. For these samples, the expected positive correlation of Ca and Sr values is much weaker than for the entire set (0.18 against 0.7 for all samples), and they feature high Sr concentration (Figure 7.7 d).

As for trace elements, these samples have elevated Ba and Ce concentrations and demonstrate significant positive Ce anomaly (1.6 – 3.65, average 2.15), calculated on the UCC normalised values (McLennan 2001) of La and Nd using the formula: $Ce/Ce^*=3Ce_n/(2La_n+Nd_n)$, where $_n$ stands for normalised to UCC value of the element (Argentino et al. 2019). Within this group, PG75 has high MnO concentration (1.9%), which is higher than the one reported in section 7.3. In samples PG7, 119 and 147, Sb was above the detection limit and was quantified as 0.3 – 0.7% weight oxide.

Another group of samples includes representatives of Group 10 (PG15 and PG118), Group 11 (PG39 and 89), Other beads (PG90) and Non-beads (PG97). As reported in Figure 7.7 b, these samples have lower concentrations of MgO and K_2O: under 0.7 and 0.4% respectively. They also feature lower Fe_2O_3/TiO_2 ratio (3.8 on average, st. dev. 0.6), which is evident in Figure 7.7 c. They have very strong Ca/Sr correlation (0.95) and their Ce values are twice lower than those of the previous group, with slightly higher La values, that leads to weak negative Ce anomaly (0.64 – 0.74 with average of 0.7). Ba is less abundant in these sample, they have elevated Hf values instead (Figure 7.7 e), which corresponds to the elevated Zr values detected by p-XRF and proven for some samples at 60 – 280

ppm (compare to less than 50 ppm in other groups determined for some samples by LA-ICP-MS). Samples PG39, 89 and 97 have 0.3 – 2.1% of CuO. High Sb content in PG90 was confirmed by LA-ICP-MS analysis. The decorative part of this sample contains high amount of Pb (12.3% weight oxide).

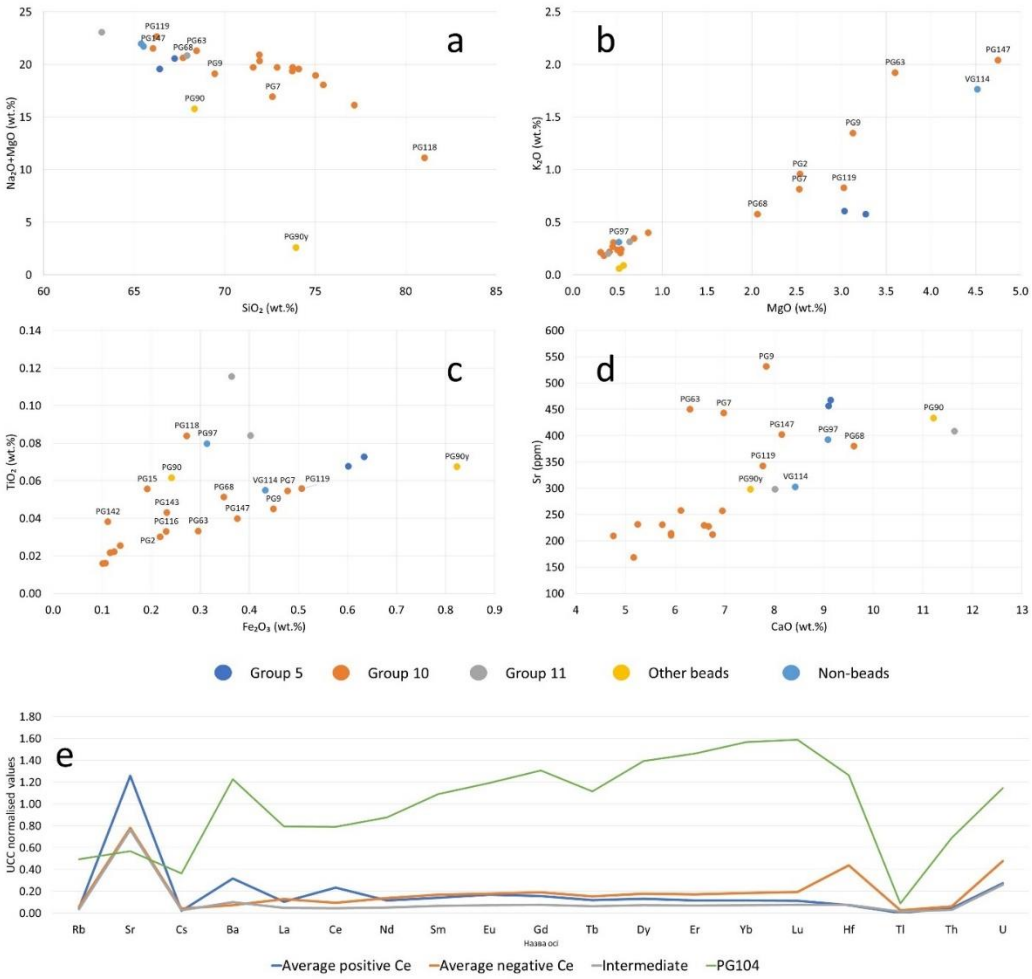

Figure 7.7. LA-ICP-MS data. Concentrations of several oxides displayed as binary plots: a - SiO_2 vs Na_2O+MgO; b - MgO vs K_2O; c - Fe_2O_3 vs TiO_2; d - CaO vs Sr. All values (except Sr) are in weight percent. Sr concentration is in ppm. e – average trace elements concentrations of the group of samples with positive, negative and no Ce anomaly including REE normalised to the UCC (values of McLennan 2001). PG104 is added individually due to its irregular profile.

The third group, that is called intermediate, is divided by MgO and K_2O content. Samples PG2, 63, 68 (Group 10) and VG114 (Non-beads) have higher concentrations of both, siding with the high Ba and Ce group, while the rest of the samples (PG10, 13, 14, 96, 116, 137, 142 and 143 all from Group 10) are closer to the high Zr and Hf group in this regard. Their minor and trace elements content is lower than in both above defined groups (Figure 7.7 c, e) which makes these samples somewhat separated from the rest. Samples PG2 and PG116 have elevated MnO concentration, with the exception of PG2, these samples also contain CuO in minor amount (approx. 0.5%), which seems

to be associated with Sn and Pb. PG2 and VG114 also have Sb at quantifiable levels (0.2 – 0.4% weight oxide). The REE profile of these samples is rather flat, without any anomalies (Figure 7.7 e).

PG104 (Group 10 honey variety) is different from all three above reported groups of samples, as it is significantly richer in Al (10.5% weight oxide) and poorer in Ca, with the Fe_2O_3 content that is the highest within the set – 3.6%. This sample has irregular UCC normalised trace elements profile due to high trace and REE content (Figure 7.7 e).

7.1.6. Micro Raman Spectroscopy.

Samples PG15, 39, 97, 118 and 142 did not produce meaningful spectra during µ-Raman analyses. The rest of the samples yielded well defined silica bending and stretching groups of peaks (massifs). Polymerisation indexes of glasses, calculated after Colomban (2003), demonstrated values from 0.5 to 2.1. Majority of the samples, though, is grouped within 0.7 – 1.3 interval (Figure 7.8) with few samples with lower (PG9, 75 and 104) and higher (PG10 and PG14) scores. In the binary plot of silica stretching maxima vs polymerisation index, most of the samples cluster around CMOG A glass, and occupy zone of soda-lime glass (Colomban 2008).

In PG7, 68, 148 (Group 10) and in the yellow part of PG90 from the Other beads group, Raman analyses revealed the presence of crystalline phases (Figure 7.9). Peak at 144 cm^{-1} detected in PG7 and PG68 is attributed to anatase, that might be a residual inclusion in the glass matrix or a surface deposition. PG148 yielded fine spectrum of quartz, which can be identified by the peaks at 128, 208, 266, 357, 399, 463, 701, 810 and 1165 cm^{-1}, in each replicate analysis. This sample also had unusual p-XRF spectrum rich in silicon. Bindheimite – lead antimonate compound ($Sb_2Pb_2O_7$), was detected in the yellow decoration of PG90.

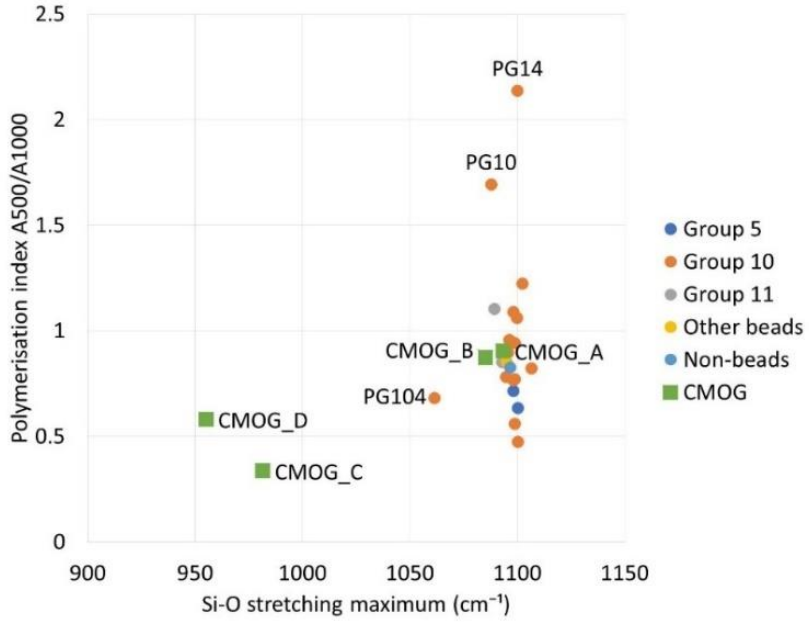

Figure 7.8. Binary plot of the Si-O stretching massif maximum on the µ-Raman spectra vs the Polymerisation index values. CMOG glasses scores are inserted for reference.

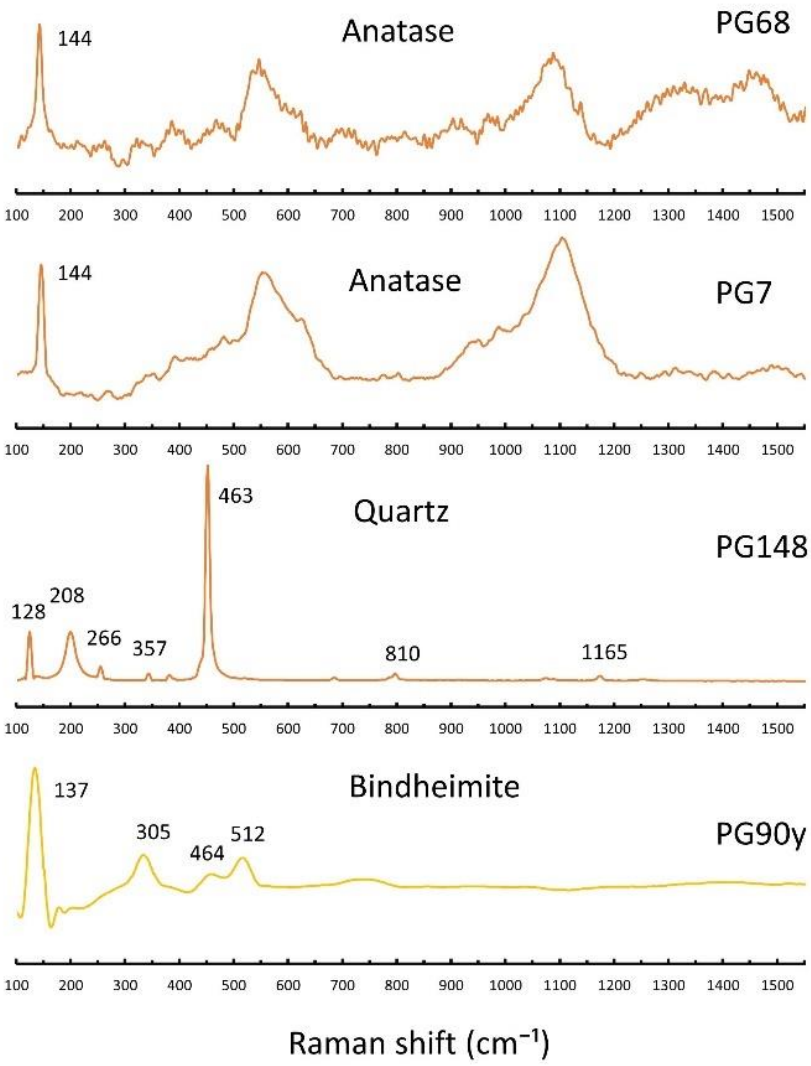

Figure 7.9. μ-Raman spectra of inclusion detected in the beads PG7, 68, 148 (Group 10) and in yellow decoration of PG90 (Other beads).

7.2. Discussion of the results.

7.2.1. Sources of silica.

PG148 is made of rock crystal based on the μ-Raman identification and p-XRF composition.

In section 7.1.5 samples analysed with LA-ICP-MS were divided into 3 groups based on their trace and REE elements content. Particularly remarkable is the group that demonstrated positive Ce anomaly and elevated Ba content. Its difference from some of the most representative assemblages of glasses from LBA and IA with determined Ce and La values is demonstrated in Figure 7.10 a.

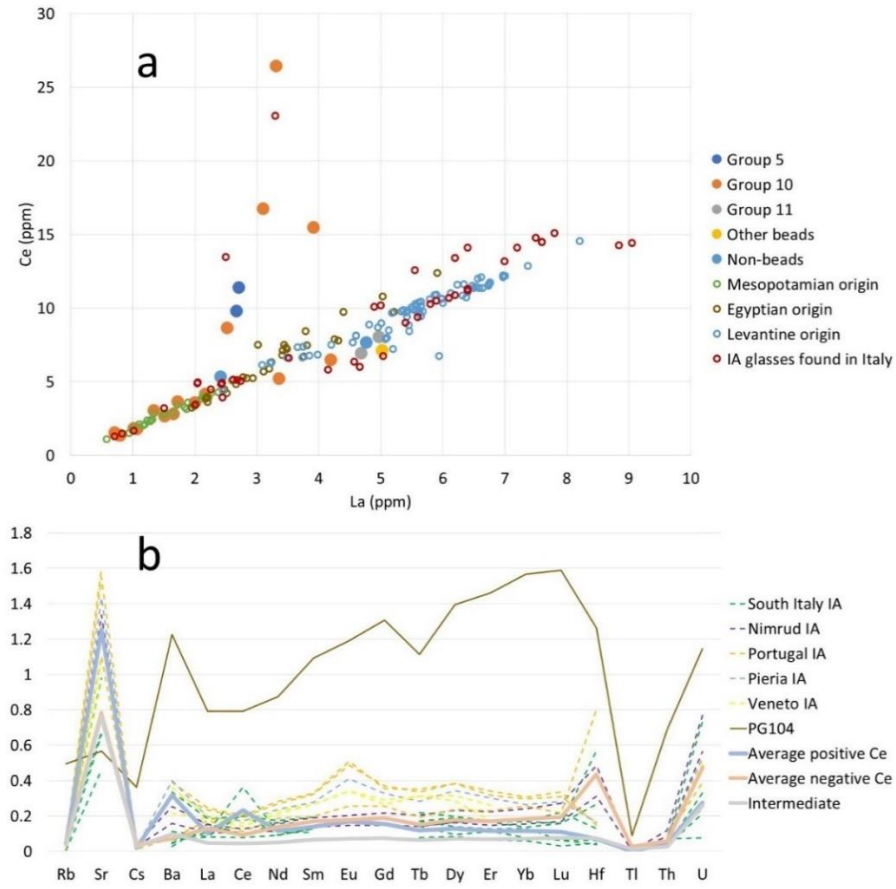

Figure 7.10. Comparison of values trace and RE elements of glasses considered in this chapter with data available from other IA and LBA contexts. a - binary plot of La vs Ce, external data on glasses of Mesopotamian and Egyptian origin are from Shortland et al. 2007, IA glasses of Levantine origin are from Blomme et al. 2017, Costa et al. 2021 and Reade 2021, IA glasses found on Italian peninsula are reported in Panighello et al. 2012 and Conte et al. 2019. b – linear plot of UCC normalised values of trace and REE of the previously mentioned groups of glasses (plus PG104) with positive Ce anomaly, negative Ce anomaly and samples without pronounced Ce anomaly (Intermediate), profiles of samples of external sources were selected on the basis of profile similarity. Data: South Italy IA – Conte et al. 2019; Nimrud IA – Reade 2021; Portugal IA – Costa et al. 2021; Pieria IA – Blomme et al. 2017; Veneto IA – Panighello et al. 2012;

The group of six samples from Groups 5 and 10 (detailed in section 7.1.5) has more Ce in respect to La than the majority of other glasses included in the plot. Interestingly, a same trend is featured by two samples from EIAII context in Francavilla Maritima reported by Conte et al. (2019) and presented in Figure 7.10a. The samples with negative Ce anomaly (some of Group 10 samples, all from Group 11, PG90 and PG97) follow the general trend set by the Mesopotamian, Egyptian and Levantine glasses (Figure 7.10 a). The Ce and La content in these glasses correspond to glasses of Egyptian and Levantine origin reported in Shortland et al. (2007), Panighello et al. (2012), Blomme

et al. (2017), Conte et al. (2019), Reade (2021), Costa et al. (2021). Samples from the intermediate group correspond more to the LBA glasses of Mesopotamian origin from Nuzi and Tell Brak (Shortland et al 2007).

Positive Ce anomalies are associated with anoxic and/or alkaline conditions of environment during the formation of various rocks due to its ability to exist in two valent states unlike the rest of the REE. On contrary negative Ce anomalies would mean oxic conditions (Möller and Bau 1993; Shields and Stille 1998; Shields-Zhou and Stille 2001; Trail et al. 2012; Argentino et al. 2019). Ce is in strong correlation with Si in positive Ce anomaly group (r=0.87), instead in other groups Ce is more associated with Ca (r = 0.52-0.60) which can mean that it entered the batch through different raw materials: sand in case of high Ba and Ce group and stabilising agent in case of high Hf and intermediate groups. In addition to the difference of Fe/Ti ratio mentioned in section 7.1.5 it can be concluded that different sands were used to produce glasses of these three groups. As for high Hf glass, it could be produced in Egypt as its average profile corresponds to glasses that were recognised as Egyptian (Conte et al. 2019; Costa et al. 2021). Production place of the glass for the rest of the samples is difficult to suggest. Perhaps, the glass for positive Ce group of samples could have been made locally, because the only correspondence for their composition was found with glasses found on the Italian peninsula. A more exhaustive comparison should be done in this regard.

Unfortunately, it is problematic to distinguish these three groups relying on p-XRF data, which would allow to suggest a provenance also for those samples that have not been analysed by LA-ICP-MS. Samples with high Ba and Ce contents features lower CaO/Sr ratio (188, st.dev. 27) than those with intermediate concentrations (252, st.dev. 40) and even more so for the high Hf group (275, st.dev. 29) according to the LA-ICP-MS data.

On the other hand, by considering p-XRF data, this same samples are not clearly distinguishable on compositional bases: high Ba and Ce samples have average CaO/Sr ratio at 163, st.dev. 27 and high Hf – 204 st. dev. 42. This might be due to poorer precision of p-XRF analyses. Most of the samples of Group 5 (but PG154) can be reasonably included into the high Ba and Ce group. Unfortunately, Fe_2O_3/TiO_2 ratio cannot be properly estimated due to the high LOQs for Ti, which lead the values very near or below the LOQ, preventing possibility to obtain accurate values for this ratio from p-XRF data.

In case of PG104, we can assume it was obtained from a clay-rich sediment, that can explain its exceptionally high Al content (Mermut and Cano 2001). In addition, this sample has elevated content of the elements associated with the heavy minerals fraction (Mn, Fe, Ba, Hf). It is unclear whether this can be attributed to an intentional addition of Fe-rich sediments or it could be a feature of a very peculiar network former. It is worth noting that high Al glasses reported in Purowski et al. (2012) and Conte et al. (2016) have similar major element compositions and UCC normalised REE profile. Such glasses were termed as Low Magnesium Medium Potassium (LMMK) and are thought to be made from an impure silica source.

To generalise on silicas origin, it can be said that the composition of these beads reveals at least 4 sources: a first one rich in Ce and with high Fe_2O_3/TiO_2 ratio (approx. 9.2). The first group (high Ba and Ce) could be viewed as locally produced glass due to the fact that the only coeval analogies were found in the present-day Italy. Their positive Ce anomaly could be used to narrow down the possible sand sources (Mongelli 1993; Whitehouse and Kamber 2002; Tostevin et al 2016). Second featured high Zr and Hf content and low Fe_2O_3/TiO_2 ratio (approx. 3.8). This group of samples might

be of Egyptian origin based on their trace elements profile, which is similar to some glasses that are thought to be made in Egypt (Conte et al. 2019; Figure 7.10 b). Values of Zr and other trace and RE elements are comparable with those found for Egyptian glasses in Shortland et al. (2007) and Lankton et al. (2022). The third has flat trace elements UCC normalised profile, comparatively low content of REE, and intermediate Fe_2O_3/TiO_2 ratio (approx. 6.3). Mesopotamian origin is suggested for glasses of the intermediate group based on their low REE values (Figure 7.10). Similar profile had samples PG110_1 and PG112 from Group 1 (discussed in Chapter 5) and yellow part of PG60 (discussed in Chapter 6). PG104 was made of less pure silica source, supposedly rich in clay minerals. It has common origin with LMMK glasses.

7.2.2. Fluxes and stabilisers.

By the content of MgO and K_2O, samples discussed in this chapter can be divided into those with higher amount of both these elements, and those that contain less than 1% of MgO and less than 0.5% of K_2O (Figure 7.7 b). The former compositional pattern, that is recurring in some glasses of all the groups, except for Group 11, allows to attribute these glasses to the HMG compositional group. HMG prepared with halophytic plant ashes is usually defined by concentrations of MgO above 2% and the K_2O above 0.5% (Sayre and Smith 1961; Rehren 2000; Mirti et al. 2008; Purowski et al. 2018; Angelini et al. 2019; Conte et al. 2019; Zlámalová Cílová et al. 2022). MgO and K_2O values in samples with elevated MgO content are correlated (r=0.77) meaning that these oxides were introduced into the batch through the same material: the plant ash. K values obtained during p-XRF analyses can be used as a marker of HMG within the larger set of samples for which MgO values could not be determined, though some of the HMG have their K_2O values as low as 0.58% - much below the LOQ of ELIO p-XRF unit. This makes the robust identification of HMG with p-XRF flawed. Nevertheless, samples with more than 1.5% of K_2O and more than 5% of CaO could be counted as HMG. Samples with lower K_2O values are likely to be LMG, but the possibility they are in fact the HMG type cannot be excluded.

Within Group 5, samples PG69-75 are recognised as HMG based on the LA-ICP-MS analyses of PG71 and PG75. These samples have similar composition and appearance, except for the elements that can be related to colour. PG154 remains undetermined. Group 10 samples demonstrated variable K_2O levels (section 7.1.3). Within this Group, the green beads variety is remarkable as all samples have elevated K concentrations and can be included in the HMG. Majority of colourless glasses can be included in this compositional group as well. The yellow-honey variety of samples is the one with the lower concentration of K_2O. This is partially confirmed by SEM-EDS data and LA-ICP-MS analyses, where only PG2 can be assigned to HMG. VG89 can be added to this list based on the p-XRF data. Despite the high K_2O concentrations, PG104 was assigned to LMMK glass with high Al content after Purowski et al. (2012) and Conte et al. (2016). Authors promote the idea that such glasses were made with soda rich flux and K_2O abundance is due to the impurities in silica source.

Group 11 samples, except VG86, remain in the LMG group, though alteration of VG15 precludes its attribution. The Other beads group is split in many sub-groups. PG90 belongs to the LMG according to LA-ICP-MS data, while the bird beads (PG172 and VG88) have elevated K_2O levels, which can be interpreted as the use of plant ash for making the glass. The K_2O concentrations are 1.5-2.1% - lower than LMHK glass encountered in Chapters 5 and 6, and their CaO concentrations

are above 5% - higher than typical LMHK representative (Towle et al. 2001). The glass buttons contain somewhat less than 1.5% of K_2O, same as their blue variety (discussed in Chapter 5). This makes their fluxing agent determination difficult, but positive correlation of K_2O and CaO in these four samples (r=0.64) would point towards the use of plant ash. The rest of the samples within the Non-beads group also have relatively high K_2O concentrations, which is consistent with HMG.

As for the stabilising agents, HMG samples were probably just two-component glasses, receiving their Ca and Mg from the plant ash (Henderson 2013). It was possible also for sands to have certain amount of Ca carbonate in form of crushed shell and/or limestone, which would enter the batch. The absence of pronounced Ca/Sr correlation (Figure 7.7 d) in the high Ba and Ce group (all HMG) suggests several Ca sources for the batches of HMG considered in this chapter, which probably resulted in additional intake of Sr, whose levels are generally higher than the average ones of the other groups. Or it would mean that the ashes were of heterogeneous composition with variable Ca and Sr concentrations (Tite et al. 2006).

Egyptian natron is the likely fluxing agent for making LMG, and it does not naturally contain high amounts of Ca, as do other sodium carbonate deposits (Devulder and Degryse 2014; Dardeniz 2015; Angelini et al. 2019). It is worth mentioning that CaO is negatively correlated with SiO_2 in all the three provenance groups (-0.69 – (-0.77)). Possibly sands with varying shell content were used in each case. CaO is positively correlated with Ba in the high Ba and Ce group and in the high Hf group, which further illustrates how these glasses were prepared using different raw materials (Ba in high Ba and Ce glasses likely derives from the ashes and Ba in high Hf group is likely to have geological origin) and are of different provenance. Variability in Sr content can be used as a proxy for determining the lime source in glass, but both shells and limestones can have different CaO/SrO ratios depending on the environment and time of deposition (Wedepohl et al. 2011; Brems et. al 2014) and the data obtained here do not allow to further differentiate among the sources of lime in these glasses.

7.2.3. Colourants, decolourants and opacifiers.

Most of the samples in this set owe their colours to the presence of iron. The presence of Fe^{2+} and Fe^{3+} was determined by FORS in the majority of samples that produced meaningful spectra (Appendix 5). In addition, several other elements influenced colours in specific samples.

Group 5 samples demonstrate a broad variety of colours. Cu^{2+} was detected in samples PG69 and 70 during FORS analyses and confirmed by p-XRF. This allows to suggest intentional addition of Cu to colour these beads. PG71 and 72 are weakly coloured, and a broad band centred at 480 would be an indication of Mn^{3+} presence. LA-ICP-MS analysis revealed that MnO content in PG71 is 0.1%. This quantity is not sufficient to influence the colour of the bead and might be interpreted as a sign of glass recycling, where some Mn coloured/decoloured glass was melted together with glass with no Mn, enhancing the concentration of the traces of Mn in the homogenised batch (Silvestri et al. 2008). At the same time, sands with MnO content as high as 0.2% were found in Italian peninsula (Brems and Degryse 2014). These samples share the shape and context with the purple coloured PG75 and PG76, that also exhibit Mn^{3+} band in FORS spectrum and contain more Mn than the PG71 and PG72. These quantities (1.9% determined by LA-ICP-MS) and oxidation state (Mn^{3+}) colour glass purple. PG154 is yellow in colour, apparently because of ferri-sulphide complex ($Fe^{3+} – S^{2-}$) presence,

even though the band at approx. 405 nm was not detected. The reason to assume its presence anyway is in the quite pronounced Fe^{2+} band, which would make this glass appear green together with Fe^{3+}. $Fe^{3+} – S^{2-}$ complex is created by reducing conditions attested by the Fe^{2+} presence and is a strong chromophore (Schreurs and Brill 1984; Meulebroeck et al. 2010).

Group 10 was divided into colour sub-groups and it is reasonable to follow same division in the present discussion. The redox state of Fe in glasses is customary expressed as $Fe^{2+}/\Sigma Fe$ – ferrous iron to total iron ratio (Schreurs and Brill 1984; Bingham and Jackson 2008; Ceglia et al. 2015). Unfortunately, the experimental setting did not allow to determine such ratio due to the absence of reference glasses with known Fe speciation. Based solely on the presence of Fe^{2+} and Fe^{3+} bands in the spectra of these samples, it can be reasonably concluded that, just like in case of PG154, the final colour of these samples was determined by the presence of ferri-sulphide complex, attested in samples PG10, 14 and 67.

Glasses with green tinge are also predominantly Fe coloured. These samples have more pronounced Fe^{2+} band than the ones in the previous sub-Group. One can assume the increase of the amount of Fe^{2+} in regard to total Fe content in these samples. Same can be said about clear or colourless glasses. Both sub-groups of samples include beads with noticeable Sb content. Sb was confirmed on the range of 0.3-0.7% in both samples of green colour analysed with LA-ICP-MS (PG7 and PG147). In quantities of less than 1% Sb_2O_5 was utilised for glass decolouring (Silvestri et al. 2008; Biron and Chopinet 2013; Bidegaray et al. 2019). The low Mn concentration in some of the colourless glasses would not support its use as a decolourant, although the concentration is sometimes higher than 0.2%, which is suggestive of glass recycling.

As for the glasses with neither Mn nor Sb detected, that nevertheless preserved their colourless appearance, it can be only said that the Fe redox state was managed slightly in favour of Fe^{3+} , as these glasses still contain up to 0.7% Fe_2O_3 (p-XRF estimation, Figure 7.5), though usually its content is lower.

Blue glasses within Group 10 can be divided into those coloured by Fe^{2+} and those coloured by Cu^{2+}, according to their FORS spectra. Cu in PG63 is associated with trace quantities of Sn in the ratio approaching 10:1, which might imply the use of bronze for colouring this bead (Costa et al. 2021). This sample can be associated with fibula bows discussed in Chapter 6 by their p-XRF composition. The rest of the samples do not have Sn detected in quantities higher than 75 ppm (weight oxide). Samples PG9, 33 and 171 have certain amounts of Co, which is associated with Ni and Zn in samples PG9 and 171. PG33 only presents Co^{2+} bands in its FORS spectrum, although p-XRF did not detect Co in this sample. Association with Ni and Zn points out towards the Egyptian source of the colourant (discussion in Chapter 5). In samples PG9 and PG33, Co concentration is not sufficient to be reflected in the colour variation (in PG9 Co content determined by LA-ICP-MS is at 37 ppm) and can be considered as a sign of recycling. Samples PG8, 9, 145 and VG103 are apparently coloured by Fe^{2+}.

Some of Group 11 beads are coloured by Cu^{2+}, as confirmed by both FORS and p-XRF. Within this Group, there are two samples that are rather green (VG15 and VG86), due to the presence of iron in both the oxidation states.

PG90 that is the Other beads group representative, and it features remarkable Sb content, which was probably used as a decoloriser, as its FORS spectrum features only weak Fe^{2+} band in the NIR region. Its yellow decoration is coloured and opacified by lead antimonate with the stoichiometric excess of Pb in the matrix.

Colours in the bird beads were achieved in different ways. PG172 body is coloured by Mn and its green decoration is Fe-Cu green with calcium antimonate opacification. The body of VG88 was coloured by Cu^{2+} and the decoration by lead antimonate with high Pb content (similarly to PG90 decoration except in VG88y there is more Fe).

By its colouring and other characteristics, PG97 is associated with Group 11 samples, where Cu was used to achieve the blue colour. VG5, 6 and 114 represent weakly coloured glasses that might have been decolourised with Sb, as suggested by the p-XRF data (K peaks of Sb are observed in all the spectra of these samples), though the amount of Sb is too low to be reliably quantified. Cu in VG114 is probably in its reduced state, that does not affect the colour. The amount of Fe below 0.5% suggest careful selection of the silica source. VG56 demonstrates weak Cu^{2+} band in the FORS spectrum, which corresponds to minor content of Cu detected by p-XRF. Fe ions should also participate in the colouring of this object.

7.2.4. Production and forming techniques.

Several receipts for making the glass batch were used to create objects within this set. For the glasses attributed to LMG, the batch would consist of the sands with certain amount of Fe (so there was no need in specific colourants). It was mixed with the mineral high-Na flux and probably some crushed shells as stabilising agent. The sands utilised for making the high Hf and intermediate glasses consisted mostly of silica, while sand for PG104 included large share of Al-rich impurities, such as clay, which is are reflected in the glass composition. Glasses for the HMG were prepared in a similar way, with the only difference in their fluxing agent (plant ash). Ca entered the batch through several materials, one of which was the plant ash utilised for fluxing. Same area of origin is suggested for HMG and LMG of intermediate group.

Most of the samples were made of glass with no additional colouring agents. Their natural Fe content and the conditions in the furnace were determining the final appearance of glass. In several cases, mostly in Group 11 samples, but also in the blue variety of Group 10 samples, Cu was added to give the resulting glass a blue tinge or even an intense blue appearance. Remarkable is the use of Sb for decolorising the glass. Mn could also be used for this purpose, but its concentrations are too low to produce the decolouring effect given the Fe abundance. It was undoubtedly used to produce purple glass (PG75, 76, 172) though. Several samples also feature Co in trace quantities (except PG171), associated with Egyptian cobaltiferous alum. Low concentrations of this element can be the sign of glass recycling, just like the trace quantities of Cu and Mn, suggesting that differently coloured glasses were added to uncoloured glass or to the new batch to facilitate the melting (Rehren and Freestone 2015; Deng et al. 2019).

The redox conditions were managed to produce differently coloured translucent glasses, though most of the samples (except the Cu coloured ones) were prepared in the reducing conditions. This can be assumed based on the Fe^{2+} bands that are present across all the sub-Groups of Fe coloured glasses and the total amount of Fe that would favour Fe^{2+} in tetrahedral coordination (Pollard and Heron 2015). Temperatures of melting and working range of glasses were generally in the expected temperature range of ancient furnaces, as emerged by the polymerisation index values calculated from μ-Raman data.

The beads of Group 5 were probably made in the same technique of winding thin thread of glass on a mandrel as Group 7 representatives, discussed in Chapter 5. Among the larger beads, some of them exhibit features of appearance of wound beads, like protrusions at apexes and direction of grooves perpendicular to the aperture (PG67 and 68). At the same time several beads within Group 10 (PG95, 119, 146, 147 and VG62) are similar to the beads prepared by folding the glass around the mandrel, that leaves characteristic groove next to the one of the apexes (Tamura and Oga 2016). Several beads have variable diameter of aperture at their apexes. This is the feature of somewhat conical shape of the mandrel. Different ratio of Diameter to the Width (D/W) is caused by the craftsperson's ability to control the glass blob and either letting it spread wider on the mandrel or occupy narrower space on it.

For the samples of Group 11, an additional step was taken to leave the grooves parallel to the aperture with a blunt tool. Decorations of Other beads group were made by applying thin thread of coloured and opacified glass on the side surface of the beads while it was on the mandrel. For the bird beads, the protrusions were made by pinching the glass in two places (making the head and the tail of a bird) after the decoration was applied.

The Non-beads objects were made differently from the beads. The pendant with the ribbed decoration (PG97) was formed in the same way of the fibula bows discussed in Chapter 6, with the sole difference that it was made on the straight rod and was not laid on a support. Its ribbed decoration is analogous to the decoration of Group 11 samples. The buttons (VG5 and 6) are of the same shape as those discussed in Chapter 5, and are assumed to be made in the same way. VG56 consists of two spherical beads attached by fixing them on the straight rod with flattened ends, perhaps some kind of adhesive material was used as well. VG114 is a fragment of a bowl that was probably mould formed in the way illustrated in Moorey (1999). Its chemical composition in terms of major elements is consistent with similar hemispherical bowls from Nimrud (Reade et al. 2009).

Conclusion. Primary glass for beads and other objects discussed in this chapter was made in at least four workshops. Compositional data gave some hints for possible provenance, suggesting Egypt and Mesopotamia. Another undetermined region is suggested for high Ba and Ce HMG, which could be the Italian peninsula, nevertheless connected to the Mediterranean glass-making tradition. A different workshop is suggested for LMMK high alumina glass.

Apart from HMG and one piece of LMMK, the LMG glass was also encountered. Glasses were naturally coloured by Fe, though in cases of the blue- and the purple-coloured beads, Cu^{2+} (Co^{2+} in case of PG171) and Mn^{3+} were used, respectively. The use of Sb as a decolourant in some samples is interesting, and the traces of glass recycling that emerged in other samples.

CHAPTER 8. LIGHT COLOURED OPAQUE OBJECTS.

The following archaeological objects are discussed in this chapter:

- **Group 6: all;**
- **Group 17: all;**
- **Group 18: VG81;**
- **Other beads: VG85;**
- **Non-beads: VG3, 4, 7, 9.**

8.1. Results of the analyses.

8.1.1. Visual observation and Optical Microscopy.

Photographs of the samples that are discussed here can be found in Appendix 2. Figure 8.1 and 8.2 present the texture and the features of the surface captured by the DinoLite microscope. Group 6 samples They are opaque, slightly asymmetrical, oblate beads that have similar protrusions near the apexes (Figure 8.1 a). Besides the colour, they are very similar to some beads of Group 7, already discussed in Chapter 5.

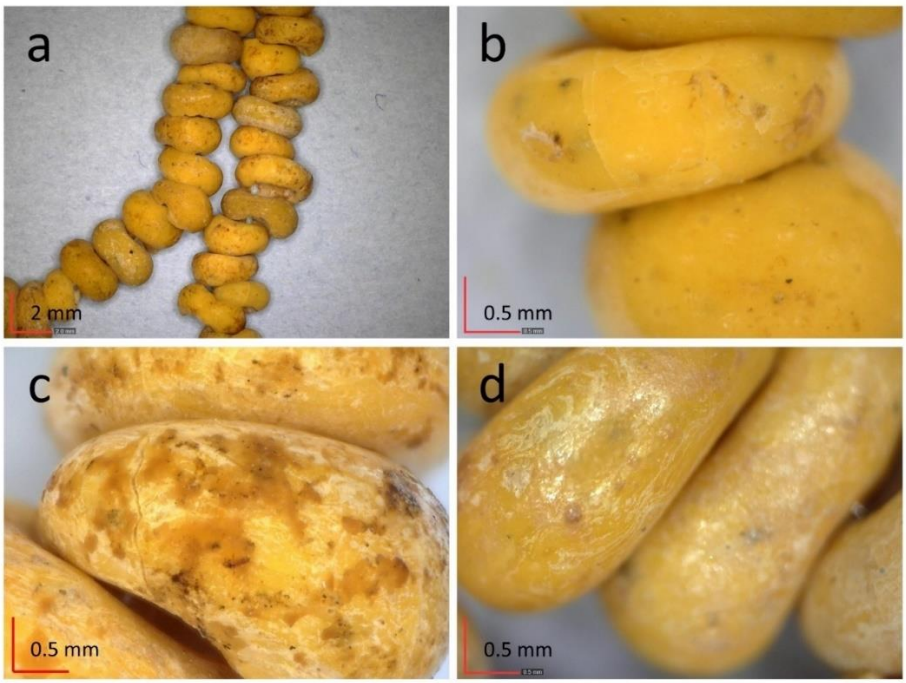

Figure 8.1. Microphotographs of beads represented by Group 6, all bead on the images were found in Veio (Vaccareccia): a – beads from tomb 6 on a string; b – tomb 1; c and d – tomb 2.

Their surface is relatively smooth, with dark inclusions sporadically distributed within the glass. Small cracks, sometimes joined in a dense network, are observed on the surface for the majority of beads (Figure 8.1 b, c). Many beads have darker spots on the surface, that might be related to glass

alteration. In some cases, they are subtle (Figure 8.1 b) but many beads demonstrate extensive darkening (Figure 8.1 c). Many beads of group 6 have signs of surface alteration that look like light colour deposits on the surface. (Figure 8.1 d). Despite the fact that the glass forming the bead is rather thin, most of these beads have retained their original shape.

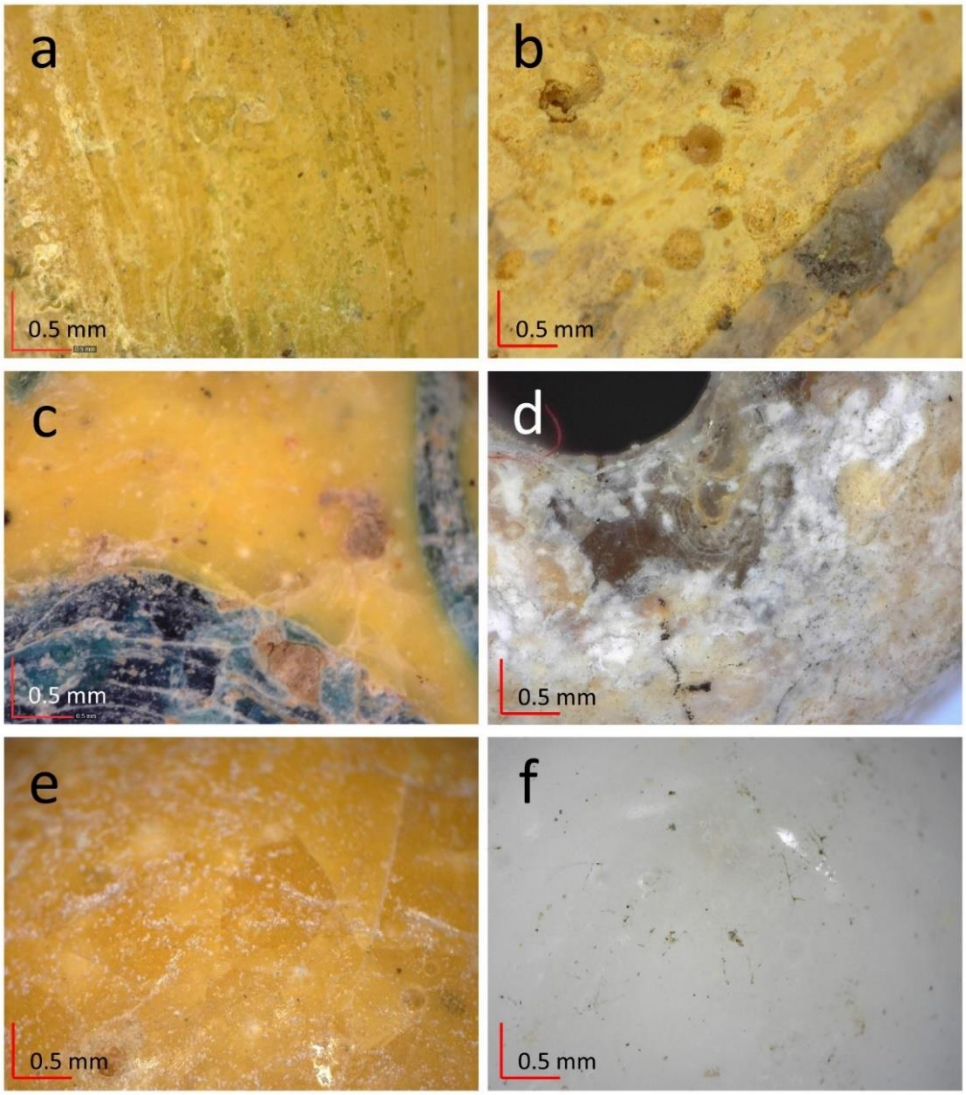

Figure 8.2. Microphotographs of samples considered in this chapter: a – surface of PG98 (Group 17); b – PG141 from the same Group; c – base surface of VG81 (Group 18) and decoration of green glass; d – surface of VG85 covered in white layer of altered glass with an opening to what might be original colour of this bead; e and f – surface of glass buttons (VG4 and VG7 respectively).

Each sample of Group 17 have its own texture and preservation state. This might be a consequence of their composition and/or of the conditions of the soil they were laying in for such a

long time. VG51 has similar appearance as Group 6 samples, with a smoother surface with respect to the other samples of this Group. It also resembles the beads of Group 6 for the similar dark spots and the superficial network of fine cracks. The surface of PG98 is rougher and it is covered in shallow grooves (Figure 8.2 a), similarly to those found on some translucent beads discussed in Chapter 7. PG141 and VG19 have a much rougher surface, with deep indentations and grooves (Figure 8.2 b), and the altered glass flakes during handling. A blue spot characterises VG19, indicating that this bead might have been covered, at least partially, with a blue vitreous layer.

The pear-shaped bead or spindle whorl VG81 has an opaque yellow surface similar to the smoother beads of Group 6 and 17, with a green decoration that was apparently added on top of that yellow glass. The glass of the decoration seems to have been originally translucent, but a dense network of cracks presently changes its appearance. Some brown residues fill in the pits on the surface of both base and decoration glasses, as shown in Figure 8.2 c.

VG85 appears as a light-coloured bead similar by texture to VG15, that was discussed in the previous chapter. VG85 was not included among the translucent beads of Chapter 7 as translucency is not evident. A dark spot, that looks like the opening to the inner glass observed for VG85 (Figure 8.2 d), shows a portion of the original glass, that actually reminds those of the yellow-honey sub-group of Group 10 (see Chapter 7); moreover, this sample also features a groove near the apex, which further resemble some samples discussed in Chapter 7. Besides this preliminary morphological evidence, compositional analysis will, hopefully, settle the attribution for this bead.

Glass buttons, in addition to the translucent blue and clear glass discussed in Chapter 7, were also produced from opaque yellow (VG3 and VG4) and white (VG7 and VG9) glass. Their surfaces are relatively well preserved (Figure 8.2 e and f). Yellow buttons surface is similar to the majority of yellow samples from Groups 6 and 17, while the white ones seem to have more bubbles in their bulk, though this interpretation may derive from the higher translucency of the white glass when compared to the yellow one. Certain degree of crizzling is observed.

8.1.2. Apparent colours and Fibre Optics Reflection Spectroscopy.

Samples can be divided, according to their macroscopic appearance, into yellow coloured and white coloured, and Figure 8.3 demonstrates the division by colour according to the RGB approach described in section 3.2.3. It can be seen in the tri-plot of the RGB values (Figure 8.3 a), that white samples (VG7, 9, 85) are closer to the centre of the tri-plot, demonstrating the highest average RGB values (Figure 8.3 b) starting from 194, whereas the highest mean RGB score of the yellow samples is 187. This difference is relatively small, but it increases when only Blue values are concerned: the yellow samples average B value is 95, while for the three white samples it is 192. As expected, the yellow samples (Group 6, 17, VG81 (without decoration), 3 and 4) are closer to the yellow and orange squares of the ColorChecker. Darkening demonstrated in the previous section might influence the RGB values and cause samples to produce lower and evener RGB values.

FORS analyses of yellow and white glasses did not yield informative spectra for the majority of the samples. The detailed summary of the detected bands is contained in Appendix 5. The spectra were similar to those of the yellow and white decorative parts on samples that were discussed in Chapters from 5 to 7, with little reflectance below 500 nm. In fact, a broad absorption is characteristic to these samples in the UV-blue region of the spectra. For Group 6, only weak Fe^{2+} absorption bands

in the NIR were detected. PG48-50 spectrum represents the entire Group 6 in Figure 8.4. In sample PG98 and, much more pronounced, in the green decoration of sample VG81, Cu^{2+} ions were detected by the band in the 700-850 nm range. These samples belong to Group 17 and 18 respectively, and their spectra have reflectance peaks in the green range. The spectrum, of another Group 17 representative – VG51, is similar to those obtained for Group 6 samples, with a weak Fe^{2+} band. Fe^{3+} bands at 380 and 440 nm were observed only in white buttons (VG7 and VG9). Spectrum of VG7 reflects evenly in the visible range (Figure 8.4).

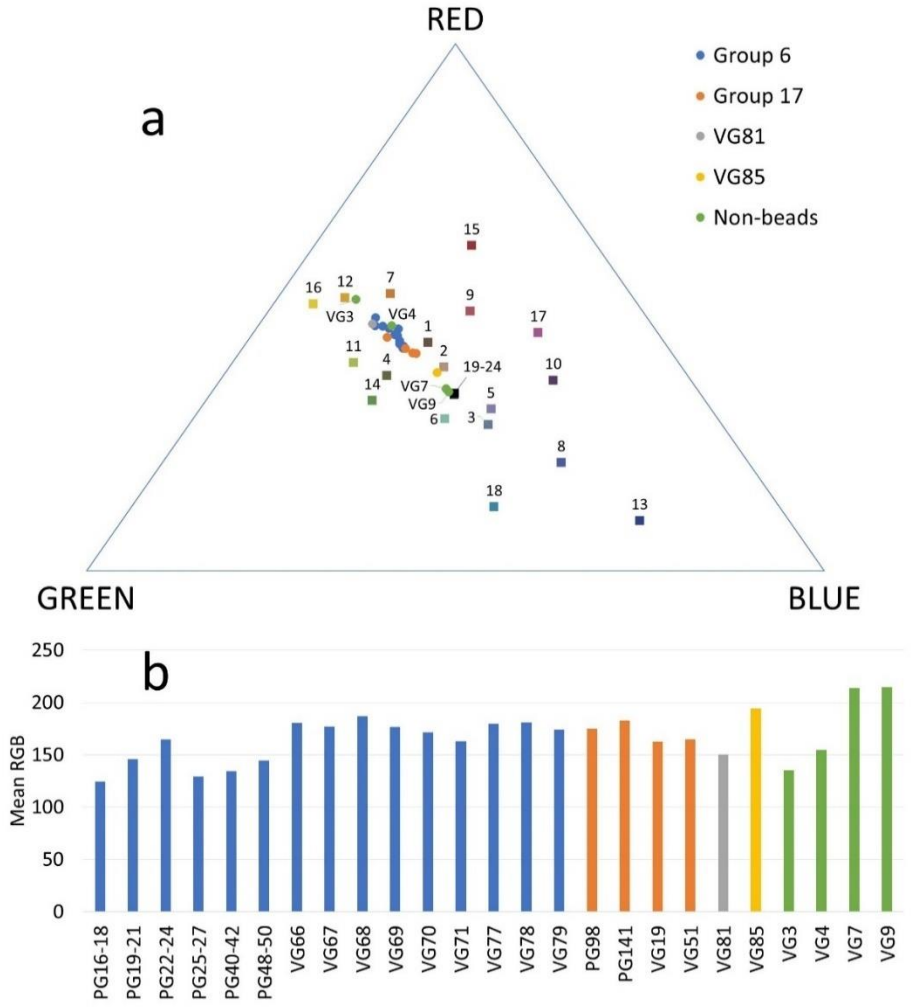

Figure 8.3. Visualisation of the colour information. a – tri-plot of the RGB values of samples compared to the ColorChecker values. b - mean RGB values of samples. The legend is true for both the plots.

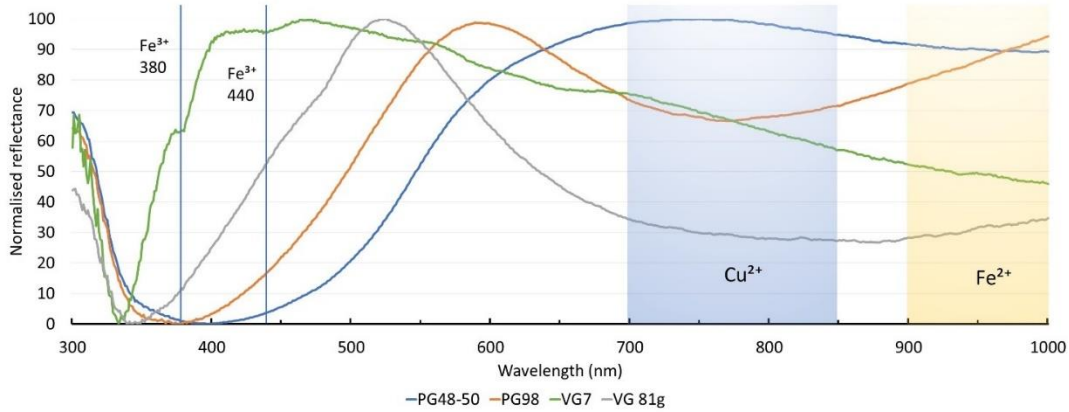

Figure 8.4. FORS results. Fe^{3+} bands are marked with vertical lines while broad Cu^{2+} and Fe^{2+} bands are marked with ranges.

8.1.3. Portable X-Ray Fluorescence spectrometry.

Most of the beads and buttons discussed in this chapter contain high concentrations of Pb. The issues related to p-XRF data for the beads with high Pb content has been explained in Chapter 4, and data for these samples need to be treated separately from those obtained from the other samples. First of all, Pb in these samples is outside of the available calibration range for the analysis. In this case, the matrix effects may interfere with the quantification of other elements of interest. Second, the thickness of the majority of the samples discussed here (Group 6) is not enough to support the assumption of an "infinitely thick material" for the p-XRF analyses. All this makes it a good call to consider the p-XRF data basically on qualitative or semi-quantitative basis.

Samples of Group 6 that are represented as ranges (analyses were conducted on several beads then averaged) do not demonstrate higher RSDs than the other samples included in this set (triplicates of analysis from a single bead averaged). PG samples from Group 6 have their mean RSD's (per row in Appendix 6) in the range of 10 – 34% across all the elements that consistently have their values above the LOQs (Ca, Fe, Sr, Sb, Pb) while the data on Group 17, VG81, VG85 and Non-beads discussed presently produce mean RSDs (per row in Appendix 6) in the range of 10 – 48%. These data indicate that Group 6 is a rather homogeneous set of samples from a compositional point of view. The set of elements that were detected by p-XRF is not wide, and consists of the already mentioned Ca, Fe, Sr, Sb and Pb. For the VG series of samples, this set is supplemented by Mn, Co and Cu values, that were detected due to the lower LOQs of the Unisantis XRF unit.

Sporadically, K was detected in concentrations less than 1% (again, only by the Unisantis spectrometer). Ti was detected only in VG66, 67 (Group 6) and 81 (Group 18). Mn was detected in all the samples of VG series and PG98 in quantities that border the LOQ, yet it is seemingly below LOQ in samples VG7, 9, 67 and 85. 450-700 ppm of Co (weight oxide) was detected in samples of Group 6 (VG series) except for VG66 and 67, VG19, 51, 81 and yellow buttons (VG3, and VG4). Cu was detected in minor quantities (less than 0.4% weight oxide) in the majority of the VG series samples. Higher quantities were attested in VG68 (1.5%) from Group 6, PG98 and VG19 from Group

17 (0.6 and 1.9% respectively) and VG81, where it prevails in the green decoration (7.1% weight oxide). Zn was detected in trace quantities in VG19 and VG81.

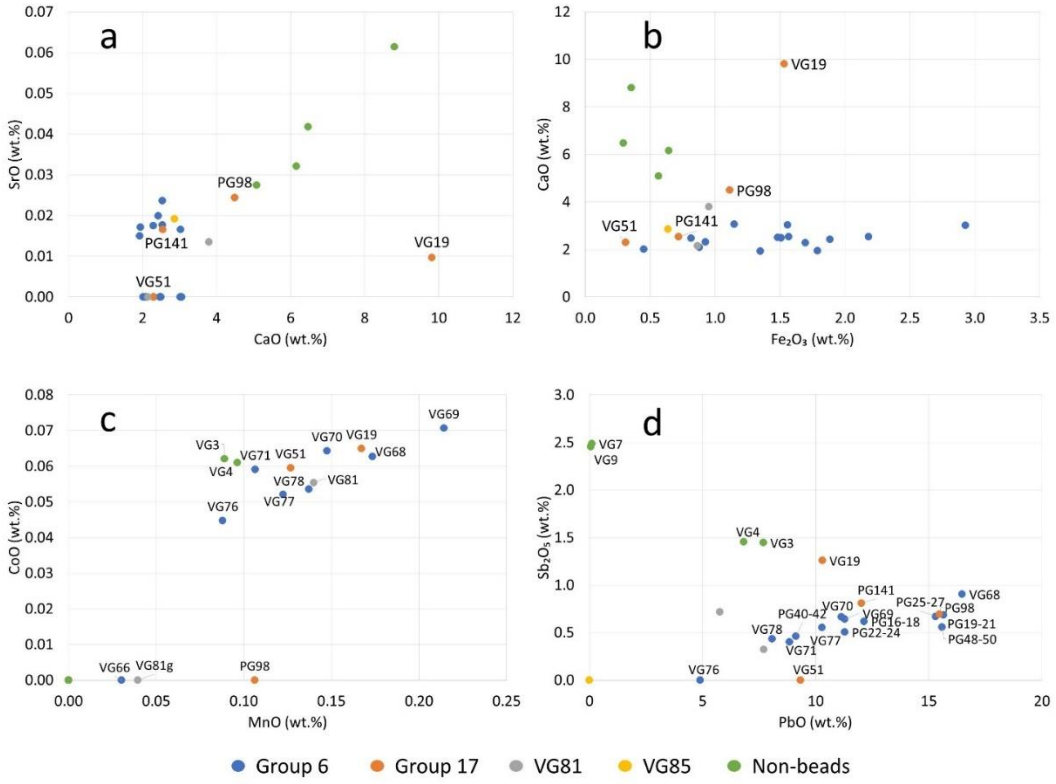

Figure 8.5. p-XRF results. Binary plots that demonstrate the relationships among several oxides: a – CaO vs SrO; b – Fe_2O_3 vs CaO; c – MnO vs CoO; d – PbO vs Sb_2O_5 (data for samples VG66 and VG67 are omitted due to incomparable concentrations of both PbO and Sb_2O_5). The legend is the same for all the plots.

The p-XRF data for several major and minor oxides are demonstrated in Figure 8.5. Group 6 samples appear to have less than 3% of CaO on average, with the mean value being 2.4% (Figure 8.5 a). This plot also demonstrates that these beads have low Sr content. Other samples, except for PG98, VG19 and buttons, have considerably more CaO: above 4%, while VG19 contains nearly 10% CaO. Positive CaO/SrO correlation characterises glass buttons and, tentatively, PG98. VG19, despite its highest CaO concentration within the set, does not demonstrate a proportional increase in SrO values. Certain VG series values have SrO concentrations below the LOQ. CaO vs Fe_2O_3 binary plot (Figure 8.5 b) further demonstrates that Group 6, Group 17 and glass buttons (Non-beads) may be produced from different glass. Within Group 17, each sample is somewhat different from the rest. Interesting is positive relationship (r=0.63) of MnO and CoO that was detected in some of the Group 6, 17, VG81 and the yellow buttons (Figure 8.5 c). Both elements are in concentrations near their respective LOQs, therefore LA-ICP-MS data are more suitable source of information on these elements.

PbO in concentrations 5 – 17% is present in all the samples but VG85, and the white buttons VG7 and VG9 (Figure 8.5 d). In samples VG66 and 67 concentrations of 29 and 34% were attested (omitted in Figure 8.5 d). Sb_2O_5 content does not usually exceed 1%. Exceptions are the glass buttons, where Sb_2O_5 prevails in white ones, and VG19. For Group 6, the correlation coefficient for PbO and Sb_2O_5 is 0.94, whereas Group 17 does not demonstrate any trend for the Sb and Pb content. VG19 is situated closer to yellow buttons and away from the trendline set by Group 6 samples. VG85 featured both oxides below the LOQs.

As Group 6 appears a homogeneous group of samples, it can be fully represented by the 6 beads that were analysed in the laboratory. PG141 and VG51 closely resemble Group 6 compositions, therefore they might be considered to be made of same glass and also represented by the beads of Group 6. For the rest of the samples, the conclusions on their technology can only be drawn from FORS and p-XRF data.

8.1.4. Scanning Electron Microscopy coupled with Energy Dispersive spectrometry.

Three samples from Group 6 were analysed by SEM-EDS: PG16, PG25 and VG76. All of them were processed to obtain polished cross sections and analysed in full vacuum mode. The results of bulk composition analyses are presented in Table 8.1. All samples contain 10-15% of Na_2O, 50-58% of SiO_2 and 21-31% of PbO. The minor oxides with concentrations above 1% are Al_2O_3 (0.7-1.4%), CaO (1.2-2%), Fe_2O_3 (1.7-3%), As_2O_3 (1.9% except VG76) and Sb_2O_5 (1.7-2%). All other oxides were below 1%. The data obtained with p-XRF are somewhat different from the ones in Table 8.1 – Fe, Sb and Pb concentrations are lower according to p-XRF estimation, probably due to thinness of the analysed samples and Pb concentration being outside of the calibration range of p-XRF.

Table 8.1. SEM-EDS results on bulk composition of samples with their respective standard deviations.

Sample/st.dev.	Na_2O	MgO	Al_2O_3	SiO_2	Cl	K_2O	CaO	TiO_2	Fe_2O_3	As_2O_3	Sb_2O_5	PbO
PG16	10.1	0.8	1.36	50	0.71	0.16	1.8	<LOD	3	1.9	1.67	30.7
st.dev.	0.3	0.2	0.03	0.7	0.03	-	0.1	-	0.1	0.3	0.03	0.4
PG25	13	<LOD	0.79	51.9	0.72	<LOD	1.21	<LOD	2.35	1.92	1.8	26.9
st.dev.	0.2	-	0.05	0.5	0.03	-	0.04	-	0.07	0.05	0.2	0.6
VG76	14.5	0.35	0.74	58	0.83	0.4	2	0.17	1.65	<LOD	1.9	21.2
st.dev.	0.5	0.04	0.06	0.8	0.08	0.1	0.2	-	0.2	-	0.2	0.5

The bulk of these samples is far from being homogeneous. Analysed surfaces feature densely distributed inclusions rich in Sb and Pb. They are usually several microns across, though sometimes they aggregate into larger ones (Figure 8.6). On average, Sb content is twice lower than Pb (ratio Sb/Pb is 0.51 with st. dev. of 0.06) in these inclusions. Mean composition of these inclusion was 21% of Sb_2O_5 (st. dev. 4.1%) and 41.3% of PbO (st. dev. 5.7%). Other inclusions consist mostly of silica

(darker spot in PG25 part of Figure 8.6). Another feature of these samples is the presence of bubbles of variable size and density of distribution.

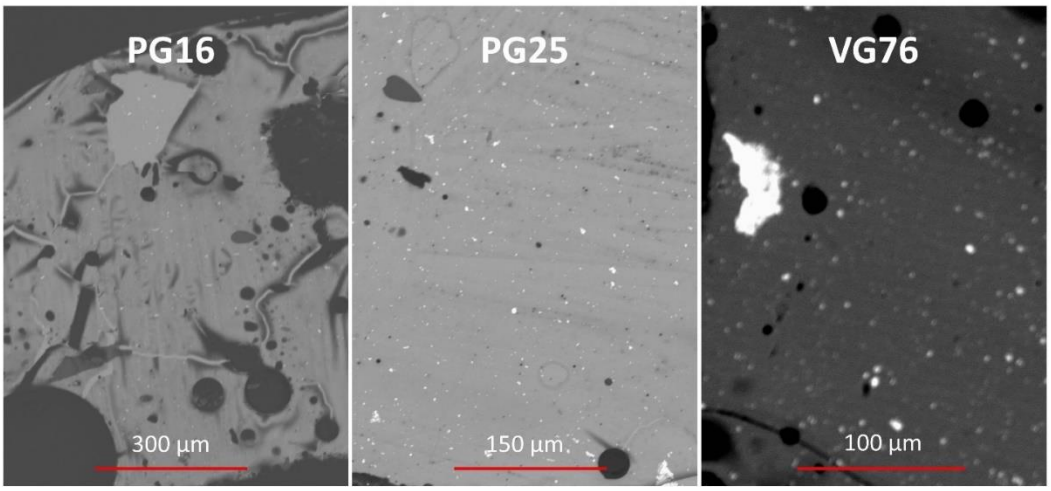

Figure 8.6. BSE images of (left to right) PG16, PG25 and VG76's surface. Light spots are Sb and Pb rich inclusions, the dark spot in PG25's bulk is a silica rich inclusion, round black areas are bubbles.

8.1.5. Laser Ablation Inductively Coupled Plasma Mass Spectrometry.

LA-ICP-MS analyses provided elemental composition of the analysed samples (PG16, 19, 25, 48 and VG76) with even higher Pb values than SEM-EDS and p-XRF. According to the composition in the Appendix 7 (LA-ICP-MS results), samples of Group 6 contain up to 43.2% percent of PbO (mean value 33.6%). Large share of Pb in these glasses makes the concentration of the other major elements appear lower (since the data are 100% normalised). It seems that although Pb is making at least one third of the total yellow glass mass, it is useful to calculate the composition of the base glass without lead. Major and minor oxides compositions normalised to 100% without PbO values are reported in Table 8.2.

Table 8.2. LA-ICP-MS values for major and minor elements (expressed as oxides) normalised to 100% without PbO (sample PG40 is omitted). Full compositions are in the Appendix 7.

Sample/st.dev.	Na_2O	MgO	Al_2O_3	SiO_2	K_2O	CaO	TiO_2	MnO	Fe_2O_3	CuO	As_2O_3	Sb_2O_5
PG16	14.2	1.0	2.1	69.6	0.2	2.9	0.10	0.03	3.4	0.05	2.24	4.1
PG19	11.3	0.4	0.9	77.3	0.1	1.9	0.10	0.02	3.4	0.21	0.11	4.2
PG25	16.8	0.4	1.1	71.5	0.2	1.9	0.05	0.02	2.6	0.03	2.22	3.2
PG48	20.1	0.5	1.1	69.8	0.2	2.7	0.14	0.13	2.6	0.08	0.02	2.6
VG76	15.7	0.6	1.3	73.6	0.2	3.4	0.14	0.03	2.2	0.02	0.06	2.7

It is evident that in the normalised compositions the prominent role is played by silica (70-77%) and Na_2O (11-20%). CaO is within the range of 2-3.4%, which is comparable with Fe_2O_3 and Sb_2O_5 values. As_2O_3, probably, has the most variable content of both. In PG16 and PG25 it is at 2.2% while

in the rest of the samples its value never goes higher than 0.1%. MgO and Al_2O_3 maintain the 0.5 ratio with concentrations of the former within 0.4-1% and the latter 0.9-2.1%. Elements like K, Ti, Mn and Cu are present in the very minor quantities (equal or below 0.2% weight oxide).

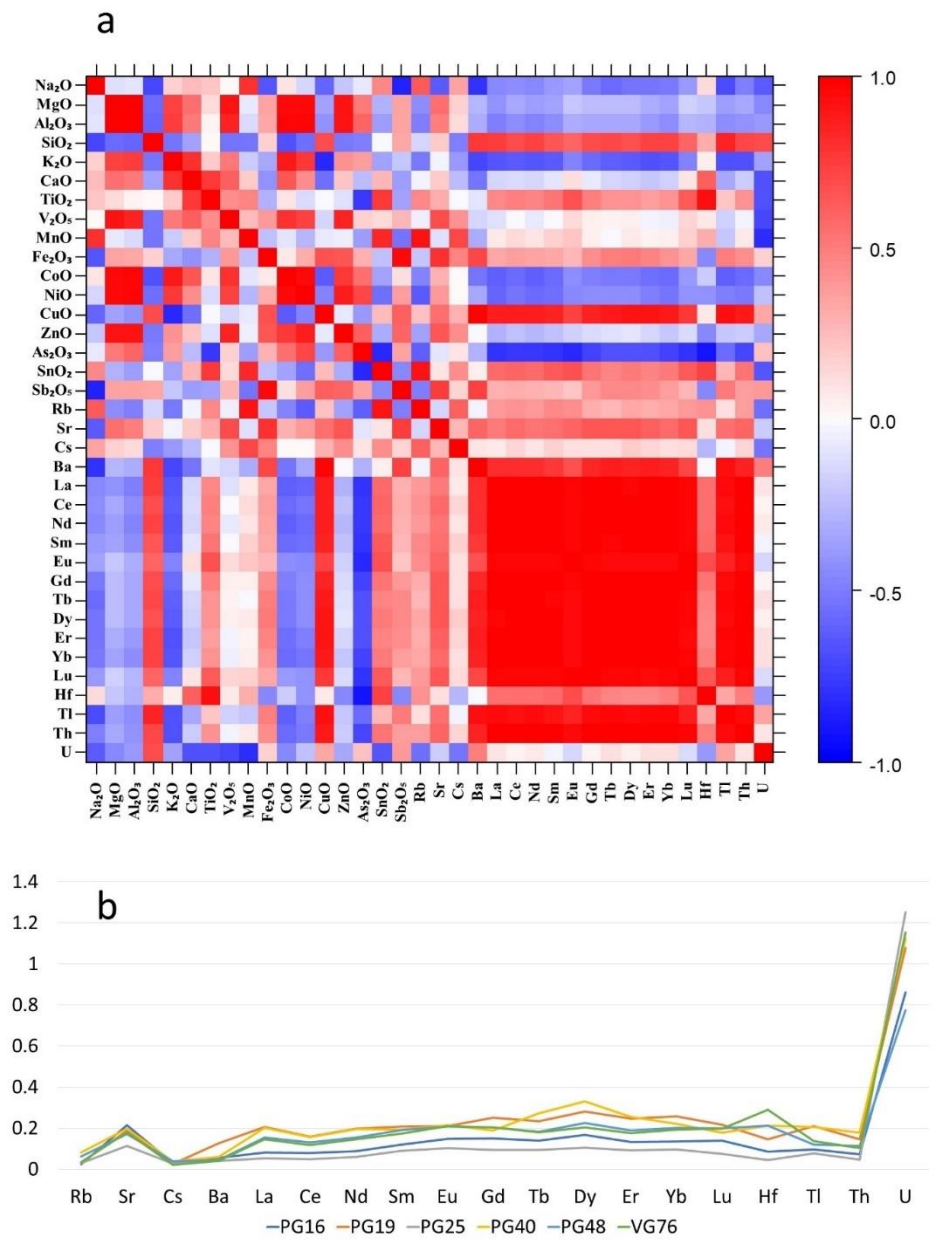

Figure 8.7. LA-ICP-MS results. A – correlation matrix of the reduced composition of Group 6; b – linear plot of the trace elements values normalised to the Upper Continental Crust UCC (values of McLennan 2001).

Figure 8.7 (a) reflects the relationship among the elements (oxides, lead excluded) of major, minor and trace levels in terms of values correlation. Although the number of samples is low, one

can notice the strong positive correlations of MgO, Al_2O_3, V_2O_5, CoO, NiO and ZnO; this group of elements is present in different concentrations with Co values being the lowest (several ppm). SiO_2 appears to be positively correlated with CuO, unlike with the rest of major and minor elements, for which a weak negative correlation is usually observed. These two oxides are positively correlated with the REE, that are also positively correlated among themselves and with TiO_2, Fe_2O_3, SnO_2, Sb_2O_5, and Sr, with which SiO_2 does not show any strong relationship. As_2O_3 seems to have strong negative correlation with TiO_2, SnO_2 and the REE. It is rather positively correlated with MgO, Al_2O_3, CoO, NiO and ZnO. Hf is highly associated with TiO_2. U is strongly correlated with silica.

Samples analysed with LA-ICP-MS have similar, rather flat UCC normalised trace elements profiles with elevated U values (Figure 8.7 b). The larger divergence is observed in Hf set of concentrations, where they are elevated relatively to Lu and Tl in PG48 and VG76, while the rest of the samples have lower relative concentrations. LA-ICP-MS data for Group 6 appears to be less homogeneous than the composition obtained by p-XRF. High As samples (PG16 and 25) have slightly lower concentrations of REE, although with a same profile.

8.1.6. Micro Raman Spectroscopy.

µ-Raman analyses of three samples (PG19, PG48 and VG76) yielded Si-O bending and stretching bands. After deconvolution, they produced very similar polymerisation index values (0.7 – 0.9). Positions of the maxima of the Si-O bands were similar for the stretching one (505 – 512 cm^{-1}) but somewhat different for the stretching one (989 – 1078 cm^{-1}). The polymerisation indexes of Group 6 samples correspond to CMOG A and B values, while the stretching maxima are in between CMOG B and CMOG C reference glass.

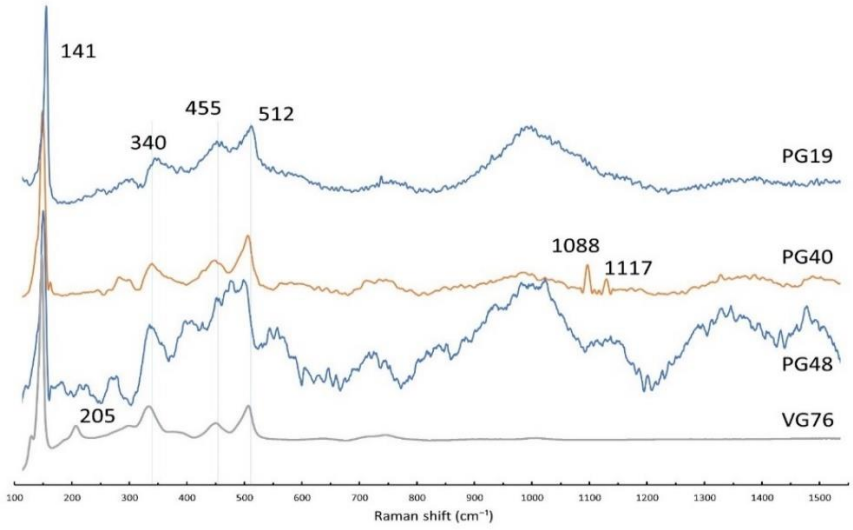

Figure 8.8. µ-Raman spectra of $Pb_2Sb_2O_7$ crystals suspended in the glass matrix observed in samples of Group 6. Additionally, calcite was detected in PG40 (peaks at 1088 and 1117 cm^{-1}.

Crystalline inclusions spectra were obtained from four samples: PG19, 40, 48 and VG76. They are displayed in Figure 8.8. All samples have their most prominent peak centred at 141 cm^{-1}. This and the minor peaks at 205 (only in VG76 spectrum), 340, 455 and 512 cm^{-1} are indicative of lead

antimonate compounds, such as bindheimite ($Pb_2Sb_2O_7$). This result also corresponds to bindheimite spectra of yellow decorations on samples from Group 2 and some other glasses (PG90, fibula bows). Slight variation of the peak positions might be determined by the presence of elements such as Fe, Zn and Sn (Lahlil et al. 2011). Among these elements, only Fe is present in major concentrations as shown by compositional analysis. Additionally, in PG40, two other peaks were identified – at 1088, 1117 cm^{-1}; they were attributed to calcite.

8.1.7. Micro X-Ray Diffraction.

Diffractograms of PG25 and VG76 can be observed in Figure 8.9. They feature peaks of bindheimite, hydrated crystal of chemical formula approx. $Pb_2Sb_2O_7$. This result confirms μ-Raman attribution and is corroborated by compositional data. Same inclusions were identified in yellow eye of V98 (Group 2), diffractogram is in Figure 5.15.

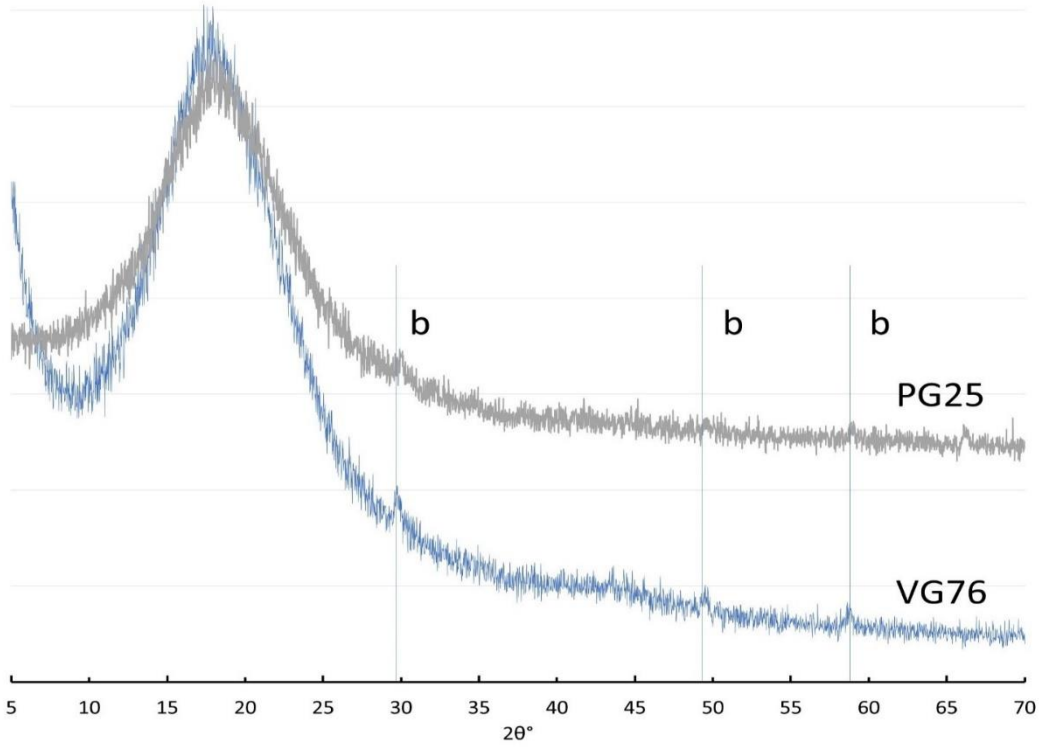

Figure 8.9. m-XRD results. Diffractograms of PG25 and VG76 with peaks of bindheimite marked with vertical lines.

8.2. Discussion of the results.

8.2.1. Sources of silica.

Lead added in significant quantities apparently did not influence the concentration of trace elements and REE, as the compositions calculated for Group 6 samples after having removed lead demonstrate strong positive correlations of trace and especially RE elements, with silica (Figure 8.7 a). This makes these elements proper candidates to be considered for the determination of the raw glass provenance, as already done in the previous chapters. Nevertheless, some trace elements, including REE, have also demonstrated weak positive correlation with PbO. Correlations might be a weak argument in this case, because they were calculated on the basis of only 5 samples. The UCC normalised profile of these samples was similar (except for negative Hf anomaly in high-As samples (Figure 8.7 b), so it was decided to present it as an average in Figure 8.10 (a), where comparison with other archaeological glasses is made. Regarding relatively low Hf in samples PG16 and PG25, it also coincided with lower Ti values and resulted in the same trendline (r=0.95) in the TiO_2 vs Hf binary plot (Figure 8.10 b). This might be the evidence that these glasses originated in the same place, but there was variability in the REE concentration in the silica source. In the end, Hf concentrations are not as high as in samples from high Hf group from Chapter 7 (PG90y and PG97 as representatives were included in Figure 8.10 a).

Figure 8.10 a contains representative samples from various sample sets that were attributed to Egyptian glass (namely Egypt LBA (Lankton et al. 2022), South Italy IA (Conte et al. 2019), Portugal IA (Costa et al. 2021)), Rhodian glass (Veneto IA (Panighello et al. 2012), though such attribution has been demonstrated to be potentially flawed (Blomme et al. 2016)) and Levantine glass (Greece IA (Blomme et al. 2017)). Samples from Group 6 have similarities with all these datasets, but they are more closely matched with the representatives of opaque yellow Egyptian glass. Certain glasses from Mediterranean group III found in Veneto have similar Sr content to Group 6, which is much lower than in the rest of the samples, but with different Eu and U relative abundance. Not all these elements are deriving from silica source though (Brems and Degryse 2014). Glasses from Iron Age Southern Italy have similar profile except for Sr and U. Glasses from Greece (Pieria) have comparable U values, but also have excess Ba. Despite its high Sr and low U content, which is likely related to different flux source, opaque yellow glasses from LBA contexts in Egypt have similar trace elements profiles. This might suggest Egyptian origin of the Group 6. Such conclusion is also supported by TiO_2 and Hf content that coincides with the aforementioned Egyptian glasses (Figure 8.10b). At the same time, similar TiO_2/Hf relationship is demonstrated by samples that are attributed to Levantine production (Greece IA), although grass from the Levant usually features higher Ba content.

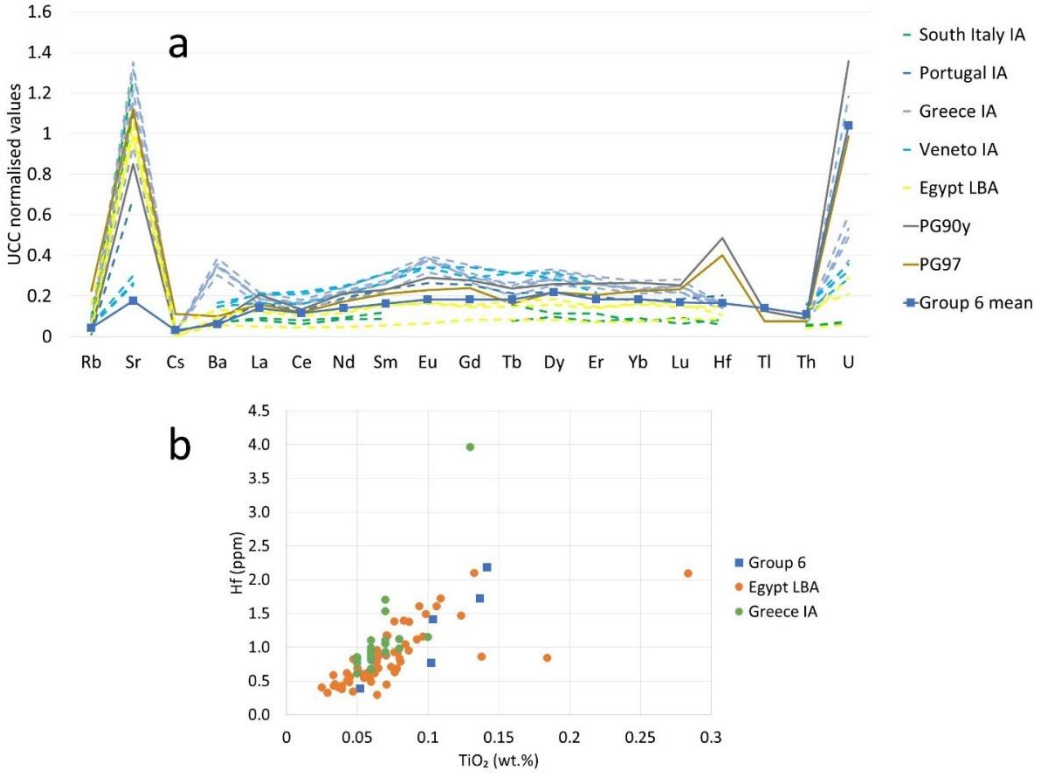

Figure 8.10. Comparison of trace elements data with other publications: a – linear plot of UCC normalised concentrations (values of McLennan 2001) of the Group 6 mean result with representative samples from Chapter 7 (PG90y and PG97) and external sources: South Italy IA – Conte et al. 2019; Portugal IA – Costa et al. 2021; Greece IA – Blomme et al. 2017; Veneto IA – Panighello et al. 2012; Egypt LBA – Lankton 2022. B – binary plot of TiO_2 values against Hf ones – Group 6 samples cannot be readily distinguished from Egyptian (Lankton et al. 2022) opaque yellow glasses.

8.2.2. Fluxes and stabilisers.

Alkali and alkali-earth content in the analysed samples, including data on K_2O gathered for a larger set of samples by p-XRF, points to the use of a mineral source for the flux. In the reduced composition calculated for samples of Group 6 with LA-ICP-MS data, Na_2O has concentrations 11.3 – 20%, which is comparable with the concentrations found in natron glasses (Phelps et al. 2016; Jackson et al. 2018). K_2O and MgO of the Group 6 samples analysed with LA-ICP-MS are both below 1 and 0.2% respectively (in the reduced composition, therefore excluding lead). U, which can be, at least partially, associated with natron (Brems and Degryse 2014) shows no evident correlation with Na in neither the reduced nor the full composition of Group 6 samples, yet it is present in much higher concentration than in other similar opaque yellow HMG from Egypt (Figure 8.10 a).

The low overall CaO content In samples of Group 6 suggests that the stabiliser was not intentionally added to the glass batch. Positive correlation of CaO with K_2O and Al_2O_3 is evident in the reduced composition, which is indicative of feldspars as one of the possible CaO source in the

sand. More than one source is likely because of absence of strong CaO/Sr correlation that can be interpreted as mixing of two or more different materials each with its own CaO/Sr ratio. For glass buttons and VG19, that differ from Group 6 and some of Group 17 samples because of a higher CaO content, the association with Sr is stronger (r=0.73). These glasses are similar in CaO content to those opaque yellow ones from LBA Egypt (Lahlil et al. 2011; Lankton et al. 2022) and the Ancient Roman ones (Lahlil et al. 2011). PbO found in high quantitates in Group 6 (but comparable amount of lead was found in other groups based on p-XRF data, that underestimated the concentration of PbO) may act as stabiliser in these glasses (Hynes and Jonson 1997; Eggert 1998) instead of Ca.

8.2.3. Colourants and opacifiers.

μ-Raman and μ-XRD analyses identified bindheimite – lead antimonate – $Pb_2Sb_2O_7$ as a crystalline phase inside the vitreous matrix. This compound was used to made glass opaque and yellow since the LBA and in subsequent historic periods (Mirti et al. 2002; Shortland 2002; Lahlil et al. 2008; Lahlil et al. 2011; Molina et al. 2014). The stoichiometric mass ratio of PbO and Sb_2O_5 in this compound is 1.38 (Shortland 2002). Based on p-XRF results, the ratio of PbO to Sb_2O_5 in Group 6 samples is 18.4 with st. dev. of 6.3. LA-ICP-MS results demonstrate similar ratio – approx. 15. Similarly, this value is 15.1 if p-XRF data of samples from Group 17 are considered. The yellow glass buttons demonstrate the lowest PbO/Sb_2O_5 ratio – 5 (p-XRF data). Values higher than the stoichiometric ratio mean that PbO is present in excess. This is also evident from the Figure 8.5(d). Addition of high Pb compounds apparently was a common practice in glassmaking (Shortland 2002; Lahlil et al. 2011; Molina et al. 2014; Van Ham-Meert et al. 2019; de Ferri et al. 2020). Different sizes of crystals and their angular shape (Figure 8.6) can be interpreted as addition of already synthetised lead antimonate into the glass and the positive correlation of PbO and Sb_2O_5 in Group 6 and majority of Group 17 samples (demonstrated in Figure 8.5 d) suggests that extra lead was added at this point together with the antimonate compound. The addition of extra lead would lower the softening temperature for the glass, and PbO/Sb_2O_5 ratio of 5 determines the formation of a eutectic mixture which melts at 850 °C (Shortland 2002).

Zn concentrations of maximum 30 ppm (LA-ICP-MS data, for p-XRF analyses almost exclusively <LOQ) allow to exclude the Pb source of Gebel Zeit in Egypt, that was actively used in lead supply for lead antimonate production (Shortland et al. 2000). Lead antimonate may be formed in antimonial litharge that derived from cupellation of silver ores (Mass et al. 1998, 2002), but such technology would need a careful selection and complex processing of raw materials to reach the compositions determined here, which were readily available as separate ores (galena and stibnite). These materials were treated according to already well-developed processes to achieve the yellow antimonate (Rehren 2003; Lahlil 2011). PbO in Group 6 glasses is associated with CuO (r=0.67). Fe is also found to be positively correlated with Pb within the p-XRF dataset (r=0.86). These features, however, do not allow pinpointing the source of lead for Group 6 glasses. Some Sb and Pb-rich objects found in Iron Age contexts in nowadays Armenia have similar compositional features, such as minor quantities of As (in variable concentrations) and trace levels of both Cu and Zn (Melikseitan et al. 2003), which would suggest the use of the same metal ores as those used to obtain the lead antimonate for Group 6 glasses. The region south of Caucasus mountains is known as a source of Sb ores since the LBA (Degryse et al. 2020).

Several samples in Group 17 have elevated Cu content. VG19 has a blue spot which was coloured by Cu^{2+} ions (FORS data). The state of the bead does not allow to speculate on whether or not this was an intentional decoration on the surface of the otherwise opaque yellow bead. Cu^{2+} is also responsible for the opaque green colour of the VG81 decoration. Green colour is apparently formed by $Pb_2Sb_2O_7$ that reflect in the yellow-red range and Cu^{2+} that reflects in blue-green range. On contrary to the yellow buttons, the white ones do not show comparable amount of Pb, instead they have somewhat higher concentration of Ca, therefore the use of calcium antimonate is suggested for these samples. Unfortunately, the data do not allow to indicate whether it is hexagonal or orthorhombic, as no XRD results are available for these samples. VG85 might not be originally opaque glass, as no Sb or other opacifier-related elements were detected by p-XRF.

8.2.4. Production and forming techniques.

Yellow opaque glasses from Group 6 were probably made in the same place using a siliceous sand poor in shell and rich in feldspars, as suggested by the correlation between Al, Ca and K in the reduced composition. Same hypothesis can be suggested for Group 17 samples, that have low Ca content. It cannot be confirmed that these Groups share the production place, but composition of PG141 and VG51 (obtained with p-XRF) is very similar to the one of Group 6.

Lead antimonate was probably prepared *ex situ* by heating lead (as metal or, perhaps, as litharge or galena) and smaller amount of stibnite. The yellow pigment was then added to the glass, that was prepared using mineral soda-rich flux. The use of lead-antimony anime suggested by Freestone and Stapleton (2015) is less likely in case of Group 6 samples, because their reduced composition is fully comparable to other LMG I terms of Na_2O and SiO_2. CaO amount in yellow buttons is also comparable with other buttons. White buttons underwent slightly different procedure of *in situ* formation of calcium antimonate crystals, where Sb was added to the glass batch.

Association of Mg, Al, Co, Ni and Zn as well as the presence of Cu in concentrations from 180 to 2100 ppm (weight oxide in reduced composition) is suggestive of some content of recycled glass inside the batch. Co is present in much lower concentration than Ni and Zn, which might mean poor quality of raw material. CuO is associated with SiO_2 (r=0.67 in reduced composition), but on the other hand it is also associated with PbO (r=0.66 in full composition). The latter association was attested for metal objects (Meliksetian et al 2003).

The polymerisation index of glasses from Group 6 is in the lower end of what was typically attested in glasses within the present work. Lower production temperatures are suggested for these glasses (starting from 800 °C). Pb presence probably made glass softer and extended its working range to lower temperatures (Hynes and Jonson 1997). Perhaps that is why the small yellow beads (Group 6) are somewhat asymmetrical and variable in the amount of glass in each bead.

The beads of Group 6 (and probably ones from Group 17 as well) were made by winding hot and soft glass around the mandrel as the majority of beads discussed up to now. This is evident from their shape and protrusions near apexes. Buttons were formed in the way that was already described in Chapter 5. VG81 is of a special shape and might be not entirely made of vitreous material. This can be deduced by sharp bottom edge and aperture outline. Its decorative part was applied on top of the yellow vitreous layer by first rotating and then by “combing” the glass to form a twisted herringbone decoration.

Conclusion. Light-coloured opaque objects discussed in this chapter owe their appearance to lead (yellow) and calcium (white) antimonates acting as opacifiers. These objects were made of soda-silica glass with little lime, except for the buttons (soda-lime-silica composition). Egyptian origin is suggested for Group 6 glasses, though this hypothesis shall be explored further by checking alternative production places. The use of Sb ores from the region of Caucasus is proposed for these objects. Unfortunately, only a limited set of samples was analysed in the laboratory, and data obtained with the non-invasive approach by FORS and p-XRF analyses do not allow obtaining a detailed composition of the base glass to trace the origin of colourants and opacifiers. One bead, namely VG85, although opaque, was originally translucent, as the opacifier was not evident on elemental bases.

CHAPTER 9. BEADS MADE OF DARK GLASS WITH HIGH IRON CONTENT.

The following archaeological objects are discussed in this chapter:

- **Group 8: all;**
- **Group 14: VG37;**
- **Group 15: all;**
- **Group 16: all;**
- **Group 18: PG3 and 64;**
- **Other beads: PG5, 6, 32, 58, 66, 113, 114, VG18;**
- **Non-beads: PG57, 61, 62, 135, VG92, 93.**

9.1. Results of the analyses.

9.1.1. Photography and Optical Microscopy.

Objects presented in this chapter have several main types of surface texture, as can be seen from the photographs reported in Appendix 2. Group 8 beads usually have smooth surface and light-coloured inclusions are visible in most of them (Figure 9.1 a–c). Asymmetries of the shape are evident near the apexes. On one occasion, two beads situated together on a string had corresponding protrusions and could be recomposed into a doublet of beads joined by the glass "bridge". This feature can be observed in Figure 9.1 a. It can be helpful in the reconstruction of the beadmaking process for this Group of beads. Figure 9.2(b) shows a fracture of PG133, which demonstrates that gas bubbles are present in the opaque-appearing matrix of the black glass, and that inclusions similar to those that were observed on the surface of beads of Group 8 are also dispersed in the glass under the surface. The surface of the Group 8 samples is covered with numerous but shallow grooves, that go around obstacles (inclusions, collapsed bubbles, some indentations). This type of texture can be seen in Figure 9.1 (c and d). Figure 9.1 d shows another relevant feature: protrusion near one of the apexes that is similar to those observed for Group 1, 6 and 7, discussed in the previous chapters. Some beads have brown residue on their surface. The thinnest elements of Group 8 beads, as well as some portions of glass surrounded by cracks, demonstrate slight yellow-brown tinge (Figure 9.1 b).

Group 15 samples and similar in glass appearance VG37 (Group 14), PG3 and 64 (Group 18) have rough surface of dark glass (Figure 9.1 e and f). This surface, though, is covered in subtle grooves that are stretched around the aperture. The dark glass surface appears altered, exhibiting relatively lightly coloured areas and more frequent indentations than Group 8 samples. Due to the small size of the beads in Group 15, their decorative elements cover a high percentage of their surface (Appendix 2). Larger beads from Group 14 and 18 are somewhat different. Visually similar glass was used to make VG37 (compare Figure 9.1 e with f) but instead of applying yellow decoration onto the dark coloured surface, the base was made of yellow opaque glass and the dark coloured wave decoration was applied onto that surface. As in case with all wave decorated beads, the alignment of the ends of the waves is not perfect. They are either not meeting (Figure 9.1 e) or overlapping. No residual decoration glass was observed in the microscope on the surface of PG3. These samples have a rougher texture than the samples of Group 15. On the other hand, PG64 is very similar by the glass

appearance to the samples of Group 15 and VG37. Only the shape and the decorative pattern differ. This sample has the area of pronounced degradation that can be seen in Appendix 2.

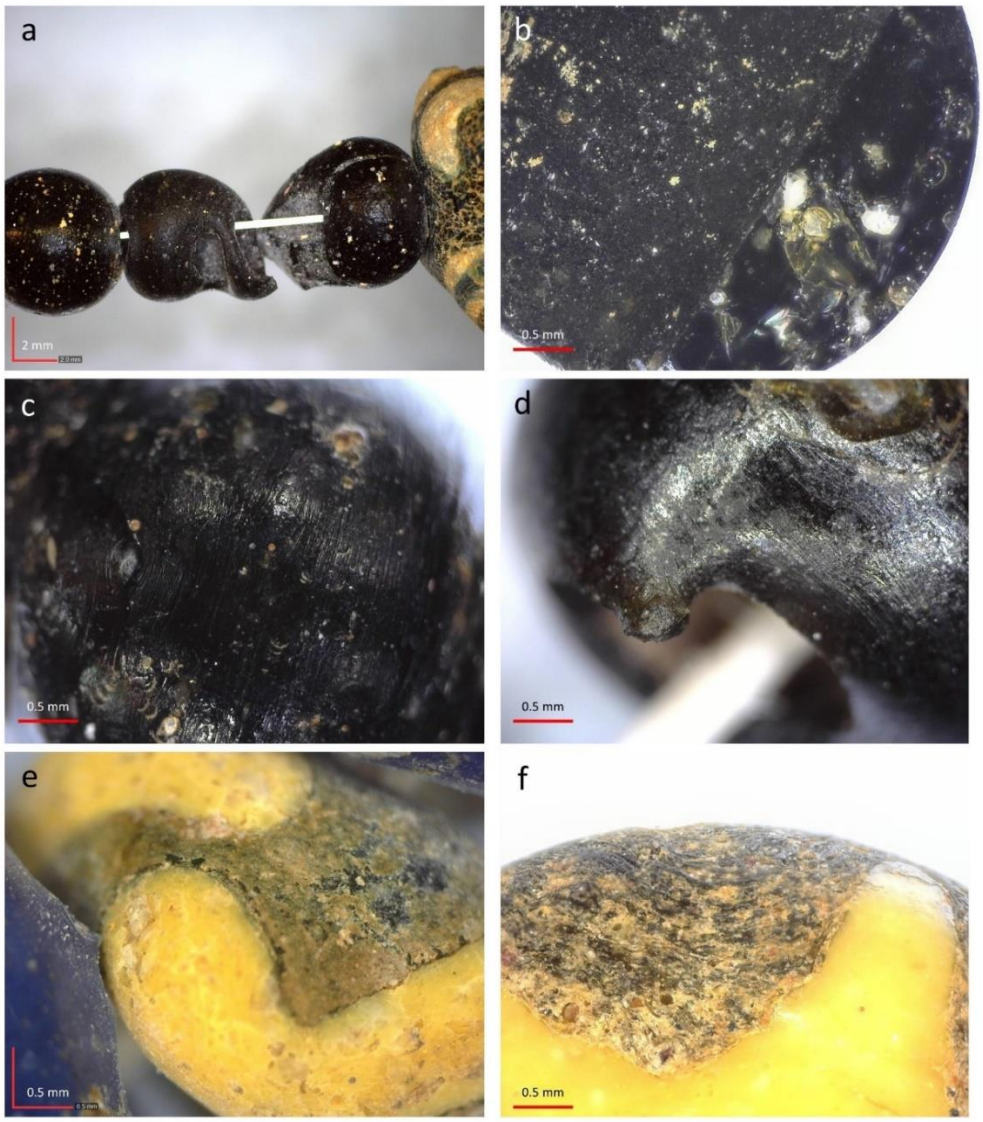

Figure 9.1. Microphotographs of beads: a - group of beads from tomb 57 bis unearthed at Sermoneta (Caracupa), beads seem to be joined once by the glass "bridge", they belong to the Group 8; b – sample PG133 observed form the broken side, light coloured inclusions are observed inside the matrix; c – surface texture of Group 8 beads represented by a bead from tomb 9 from Osteria dell'Osa necropolis; d – surface of Group 8 beads and the protrusion near the apex represented by a bead from tomb 15 from the Osteria dell'Osa necropolis; e – PG101 surface with dark coloured base and yellow wave decoration whose ends do not meet; f – VG37 surface with yellow base and dark wave decoration.

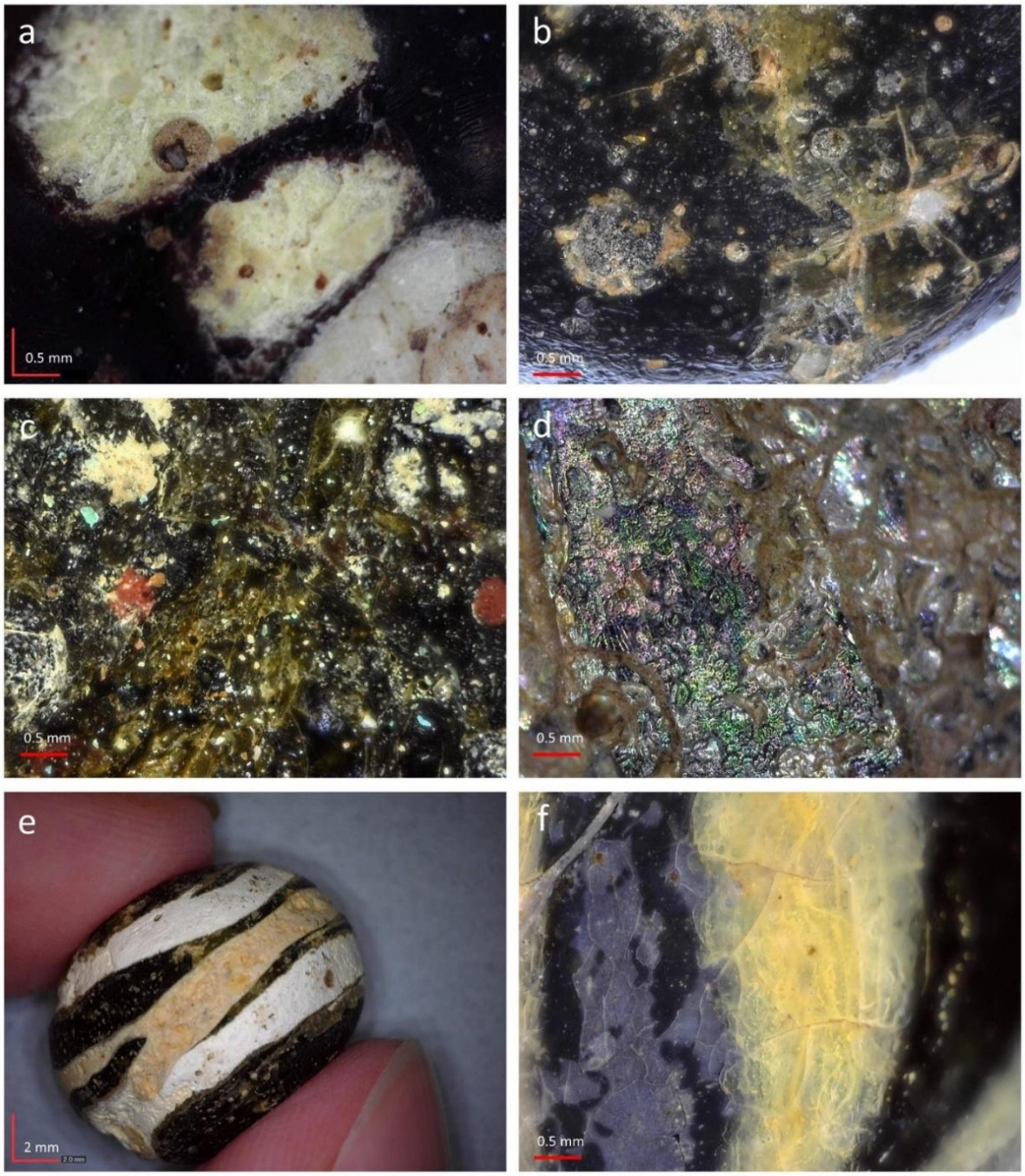

Figure 9.2. DinoLite images of samples: a – white spots on the surface of PG4; b – bubbles, cracks and indentations on the surface of PG124; c – texture of PG144 with spots of light and red colour; d – surface of PG113 featuring pronounced alteration and iridescence; e – PG5 decoration pattern, where yellow glass overlaps with the white; f – surface of PG61 with alteration crust and a network of fine cracks at the surface.

Beads of the Group 16 also are very dark in colour and appear opaque. Several samples have white, yellow or red spot decorations that do not appear to be organised in patterns. The light-coloured spots exhibit granular texture, sometimes containing inclusions (Figure 9.2 a). The dark glass appears more homogeneous, though indentations and grooves, similar to the ones found on

Group 8 samples, are visible. Bubbles suspended just beneath the surface are visible in some beads, thus demonstrating some translucency of the glass. Cracks that cross the surface of some beads make portions of the surface appear yellow-brown due to the reflection of light through a thin layer of glass from the reflective border of the crack (Figure 9.2 b). Roughness of some beads within this Group is a suitable substrate for surface depositions of various contaminants, as shown in Figure 9.2 c. The small red spots and yellow tinge of cracked glass are also visible on the surface of PG144 in the same figure. Macroscopic features of individual samples within this Group are the slightly asymmetric rib decoration of PG123, somewhat flattened surface in the widest part of PG127 and deep groove near one of the apexes of PG144. All mentioned features are presented in the photographs of the beads reported in Appendix 2.

Most of the beads presented in this chapter are relatively well preserved on a macroscopic scale, with sporadic indentations, cracks and surface depositions that do not preclude documentation of the original colour, translucency and decorative patterns. PG113 (Other beads) is an exception (together with VG18) as it is completely covered in an iridescent crust (Figure 9.2 d). This sample seems to have cylindrical shape and spiral decoration that probably was white in colour (small relicts are still visible in a groove). Light coloured decorations are the distinctive feature of the portion of Other beads discussed in this chapter. Depending on the sample, they are either white or yellow. PG5 is an exception here because it has line decorations made by both white and yellow stripes, with the yellow one overlapping the white ones (Figure 9.2 e). Part of the decoration is lost, leaving an empty groove. Among the Non-beads, PG135 is the only sample without any yellow decoration. It is covered in a light-coloured layer that can be tentatively attributed to alteration. Fibula beads appear to have two different types of texture. The PG61 and PG62 have smooth surface with a network of fine cracks and a thin, detached vitreous layer (Figure 9.2 f). This texture is similar to PG59 and PG60 that are similar objects coloured by copper (Chapter 6). The VG92 and VG93 feature grooves that are similar to rib decoration where the central axes of the herringbone pattern pass (Appendix 2). Their surface is rougher, which is an indicator of worse preservation state. PG57 (button or a pin head) is closer in this aspect to PG61 and PG62.

9.1.2. Apparent colours and Fibre Optics Reflection Spectroscopy.

Dark appearance of most of the beads is reflected in low RGB values. This makes the use of tri-plot of the RGB values not informative. Groups of beads can be divided into 2 major groups. Group 8 and 16 together with several Other beads (PG5, 6, 58 and 114) and Non-Beads (PG61, PG62 and VG93) have extremely low RGB values that do not rise above 60 (average – 34). This makes their colour close to N24 square of the ColorChecker – “Black 2”. Groups 15 together with VG37, PG3 and PG64, as well as several Other beads (PG32, 66, 113 and VG18) and Non-beads (PG57, 135 and VG92) have their average RGB values above 60 (average – 97), which corresponds to “Neutral 3.5” and “Neutral 5” squares of the grey scale on the ColorChecker (squares 22 and 23). RSDs among the RGB values of the single sample do not exceed 25% being 9.6% on average. Some samples were probably out of the “Black 2” cluster because of light-coloured depositions and/or alteration products of the original surface. PG101 is the lightest in colour (mean RGB value 188). It belongs to Group 15, all the samples of which have relatively high RGB values. This result might be caused at least partially by the influence of yellow decorative elements, which can be tracked by relatively low B values – a

pattern that only appears in samples with yellow decoration. In any case, base glass of Group 15 samples appears lighter in colour than the one of Group 8 and Group 16 samples. RGB values of Groups 8, 15, 16 and other beads are reported in Appendix 3.

FORS analyses dealt with the low reflectance that is expected for dark-coloured samples. Majority of the beads discussed in this chapter did not produce spectra with significant signals from the colourants (Appendix 5). The ones that featured some bands from dissolved ions of transition elements mostly showed the broad band of Fe^{2+} in the NIR region. Such spectra can be divided into two groups (Figure 9.3). One group of spectra features intense UV absorption and includes PG5 (reported in Figure 9.3) PG57, 61, 64, 81, 106, 113, 114, 131, 132 and VG93. Another group, represented in Figure 9.3 by the spectrum of PG127, includes PG127, PG4, 105, 123, 125 – 130, 157 and VG50, and does not feature absorption in the UV region. Many spectra do not have any bands except the strong absorption in the UV region, that might indicate the presence Fe^{3+} (spectrum of PG144), which is also highlighted by the slight shoulder between 380 to 500 nm. Five samples within the set demonstrate the Cu^{2+} band in the NIR part of the spectrum, similar to PG4 in Figure 9.3. Other samples with this band are PG6, 92, 115 and 133. PG3 is the only sample within this set for which Co^{2+} bands were detected (Figure 9.3).

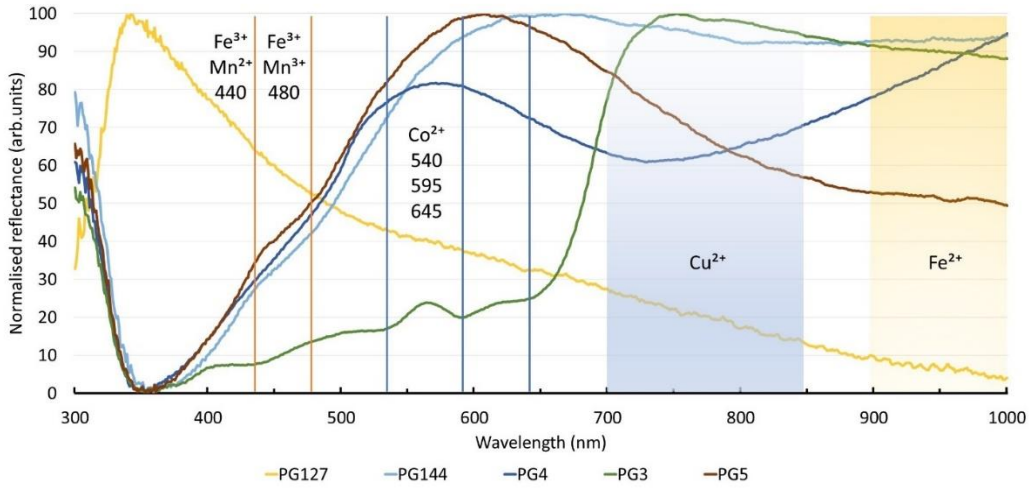

Figure 9.3. FORS results. Representative spectra of the samples discussed in Chapter 9. Fe^{3+} bands positions are marked by orange vertical lines, Co^{2+} bands positions are marked by blue vertical lines Cu^{2+} and Fe^{2+} broad bands positions are marked by blue and yellow areas respectively.

9.1.3. Portable X-Ray Fluorescence spectrometry.

Glasses included in this chapter have much higher iron content than the samples discussed in the previous chapters. According to p-XRF analyses, iron is at 8.6% (weight oxide) on average across all the Groups, with the highest concentration of Fe_2O_3 being 19.7% in PG128 (Group 8). This is much more than concentration range of Fe used for p-XRF calibration. Similarly to the beads discussed in the previous chapter, the p-XRF data for the high-Fe glasses considered here should be discussed as semi-quantitative information, as the matrix effects would be detrimental for an accurate estimation

of the concentrations of Fe and of the other elements in these samples. The most striking example of this issue is overestimation of Co values in these glasses, demonstrated in Chapter 4.

Compositional variability of samples could be presented through the results of PCA (Figure 9.4). When compared to the other groups of heavily coloured beads, discussed in Chapters 5 and 6, the present set is divided from those mainly along PC2, which is influenced by Ca, and Cu on one side and Fe, Sb and Pb on the other one. Dark glasses are situated in the lower quadrants of the plot, apart from VG94, 101 (Group 15), PG3 (Group 18) and VG18 (Other beads). These samples overlap with Co and Cu coloured glasses from Chapters 5 and 6 respectively. Along the PC1, the samples separate into two distinct clusters: samples from Group 8, VG37 (Group 14), majority of Group 16, PG64 and Other beads form relatively tight group stretched along the PC1; samples from Group 15, PG4 and PG123 (Group 16), PG3 (Group 18), PG5 and 58 (Other beads) and Non-beads are more scattered on the positive side of PC1 (influenced by K and Cu on one side and correlated variables of minor and trace transition metals on the other). PG3 appears to be an outlier within this loose cluster.

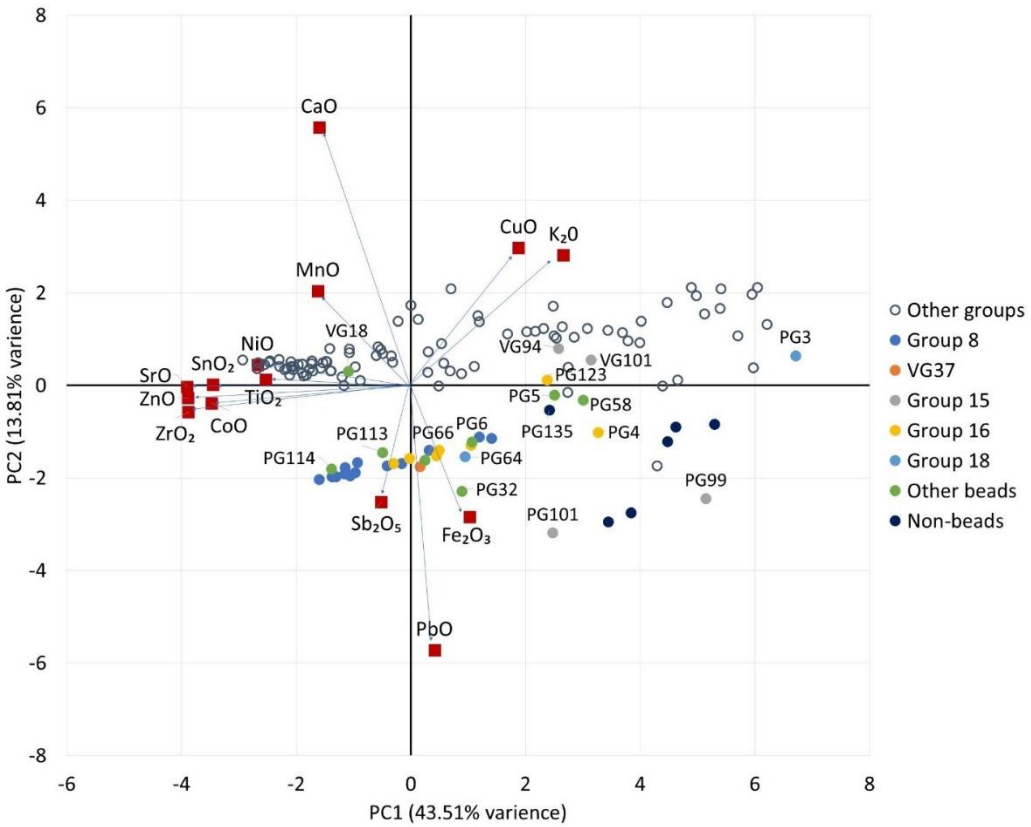

Figure 9.4. p-XRF data. PCA plot of PC1 against PC2. Other Groups represent the results of PCA for beads discussed in Chapters 5 and 6. Scores and loadings are situated in the same plot. Loadings values were multiplied by 10 to improve legibility of the plot.

PCA reflects general tendencies in dark glass compositions. K_2O concentrations that are above the LOQ for specific p-XRF unit are usually between 1 and 2% by weight (Appendix 6). Samples that have K_2O values below the LOQ have comparable K Kα peaks in their XRF spectra. This includes both PG and VG series samples. In several cases, K_2O concentrations are above 2%: PG58 (Other beads), 61, 62 (Non-beads), 83 and 125 (Group 8). CaO values are usually lower than 4%, although they are usually higher in samples of Group 15. VG18 is an outlier, featuring CaO concentration at 18.6%, which is unusual for ancient glasses. Due to it poor preservation state, it is impossible to assign this bead to any of the compositional groups; the concentration of Fe, Cu and Pb at about 1 – 2% oxide would exclude stone as a material for this bead.

Ti and Mn are elements that are detected only sporadically, in concentrations that are near their respective LOQs, although the latter is consistently present in the fibula beads. As already mentioned, Fe is always present in high quantities in the objects discussed in this chapter (Appendix 6) and its concentration determined by p-XRF is almost always above 4% (weight oxide). Exceptions that have less than 4% of Fe_2O_3 are following: VG94, 101 (Group 15), PG123 (Group 16), PG3 (Group 18), PG5 and VG18 (Other beads). Although accuracy is poor for Co concentration, 3 samples, namely PG3, VG94 and VG101, seem to have higher levels of Co without high Fe concentrations. For PG3 Co^{2+} bands were also detected by FORS. In these samples, Co is also associated with Ni and Cu. All samples of Group 15 seem to contain minor amounts of CuO. This element in lower concentrations was detected in fibula bows (in PG61 and 62, with peaks above LOD, but its concentration is below 0.4% that serves as the LOQ). CuO concentrations 0.5 – 2% are also determined for PG4, 127, 144 (Group 16), PG3 (Group 18), already mentioned VG18 and PG57 (Non-beads). Out of the 5 samples that feature the Cu^{2+} band in their FORS spectra, (see section 9.1.2) only PG4 confirms its copper content by p-XRF. Trace quantities of Zn were detected in the majority of the samples of Group 8, unlike in the rest of beads (with few exceptions).

Relationships among several oxides detected in these samples are demonstrated in Figure 9.5. Samples that have more than 2% of K_2O show positive correlation of this oxide with CaO (Figure 9.5 a). Group 8 and 18 samples tend to have lower CaO concentrations, and Group 15 and Non-beads tend to have slightly more CaO instead. The rest of the Groups appear scattered along the trend axis. This pattern is also noticeable in Figure 9.5 b, where the absolute majority of the datapoints are aligned in a positively correlated CaO/SrO trend. Samples PG101, 127, 133, VG50, 94 and 101 might form a parallel trend with slightly lower relative SrO values.

Two different trends are noticeable in TiO_2 vs ZrO_2 plot (Figure 9.5 c). PG6, 105 and 114 contain more Zr when compared to Ti than the rest of the samples. The latter one demonstrates a steep increase with the small increase of the former one. Samples PG3, 58, 64, 83, 125, 127, 144 are part of the opposite trend: Zr increases more slowly than Ti in their relative concentration ranges. For the rest of the samples, the concentration of these elements is below the LOQ, although they might feature either minor quantities of Ti or trace ones of Zr or none at all above the LOQs. No significant correlation between Zr with Fe concentrations emerged (Figure 9.5 d). Quantitative relations that emerged from the dispersion graphs are not Group-specific and PCA seems to be the best tool for Groups differentiation.

Decorations of beads demonstrate an increase of Ca and Sb values in the white decorations compared to those that are observed in the dark bodies of these samples, whereas yellow decorations are richer in Pb and Sb (Figure 9.5 e). For yellow decorations, the Pb/Sb ratio is 12.8 on

average, but values are broadly scattered, as mirrored by the value of the standard deviation: 6. Usually, lower concentration of Fe is detected in the glass of the decorations.

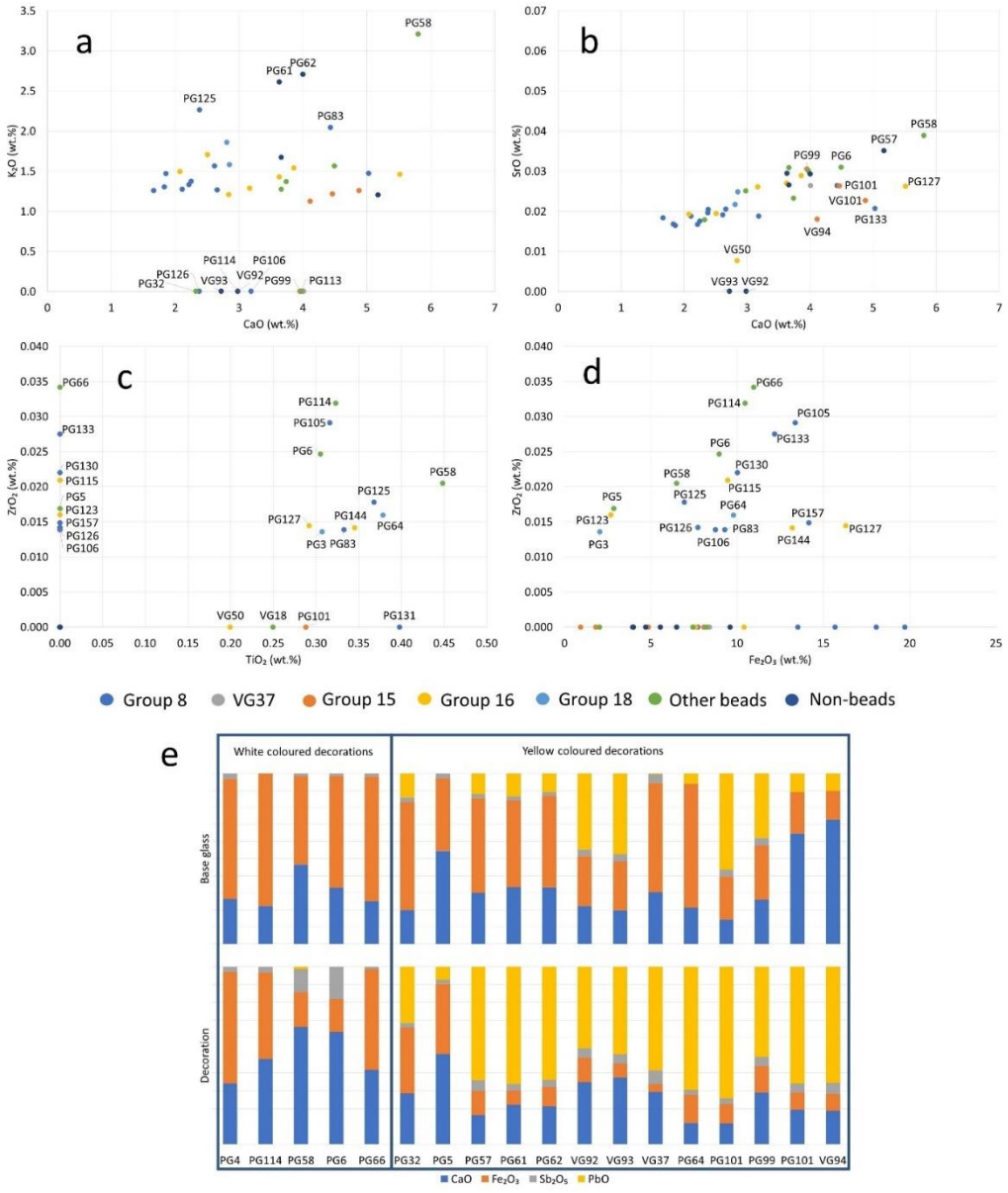

Figure 9.5. p-XRF data. Binary plots of selected oxides: a - CaO vs K_2O; b – CaO vs SrO; c – TiO_2 vs ZrO_2; d – Fe_2O_3 vs ZrO_2. Values below LOQs are substituted with 0. Legend is the same for all the plots. Plots that include CaO do not include VG18. e – comparison of relative abundance of certain oxides in the base glass (top graph) and glass of decorations (bottom graph). Samples are divided by the colour of the decorative part.

As a deliberate choice, almost a half of the discussed beads was analysed in the laboratory and LA-ICP-MS compositions are available for all Groups of objects (excluding VG37 from Group 14). It must be noted, however, that VG92 and VG93 seem to be different by their p-XRF compositions from PG61 and PG62 and cannot be represented by PG62 (analysed by LA-ICP-MS).

9.1.4. Scanning Electron Microscopy coupled with Energy Dispersive spectrometry.

Despite high number of samples analyses in the laboratory, only two of them could be analysed with SEM-EDS. PG106 was analysed as a polished cross section and PG131 without any surface preparation in the VP mode. Results of the bulk analyses are available in Table 9.1. The difference between the two in the Na_2O content can be explained by the surface alteration of PG131. The rest of the elements are similar, except Al and Ti concentrations. Particularly in PG131, EDS determined concentration of Al_2O_3 is 9%, which is one of the highest ones observed among all the beads analysed within this study. MgO concentrations are within 2%. S and Cl are contained within 1.5%. K values are slightly higher than p-XRF estimation, while Ca ones are closer. Cu is present in the concentration 0.8%. Such result does not correspond to the p-XRF estimation and should be re-checked by LA-ICP-MS, as Cu values do not have high accuracy when calculated from EDS spectra (Chapter 4). High-Zr inclusions were found in the matrix of PG106. On the surface of PG131, the electron beam detected the sporadic occurrence of heavy element particles, that might be attributed to surface depositions. Most often they were high-Fe particles, but several of such spots featured high concentrations of Ti, Cr, Sn and Bi.

*Table 9.1. SEM-EDS analyses results. All values are in per cent. *sample was analysed without surface preparation in the Variable Pressure mode.*

Sample/st.dev.	Na_2O	MgO	Al_2O_3	SiO_2	SO_3	Cl	K_2O	CaO	TiO_2	Fe_2O_3	CuO	Sporadic inclusions/surface depositons
PG106	18.1	1.95	2.05	59.6	0.50	1.10	2.60	2.70	0.18	11.8	0.8	Zr
st.dev.	*0.4*	*0.03*	*0.06*	*0.3*	*0.03*	*0.02*	*0.06*	*0.02*	-	*0.1*	*0.1*	
PG131*	3.4	1.4	9	69	1.4	0.8	2.1	2.7	0.6	10	0.8	Ca, Ti, Cr, Mn, Fe, Cu, Sn, Bi
st.dev.	*0.4*	*0.1*	*1*	*2*	*0.1*	*0.2*	*0.3*	*0.4*	*0.4*	*1*	*0.1*	

9.1.5. Laser Ablation Inductively Coupled Plasma Mass Spectrometry.

Analysed samples are mainly composed of silica, soda and iron oxide (Appendix 7). Other major oxides present in variable quantities are MgO (sometimes in minor concentrations), Al_2O_3, and CaO. K_2O is present in concentrations from 0.5 to 2%. Major concentrations of PbO and Sb_2O_5 were determined for yellow decorative parts. MgO content of samples that was previously used to distinguish sources of flux in beads demonstrates variable concentrations in the beads of the present set without strict typological division. MgO vs K_2O binary plot visualises such distribution of values (Figure 9.6 a). Three samples (PG4, 58 and 106) have elevated concentrations of both oxides. The

rest of the samples are situated along the X axis (no additional K_2O is observed with the increase of MgO).

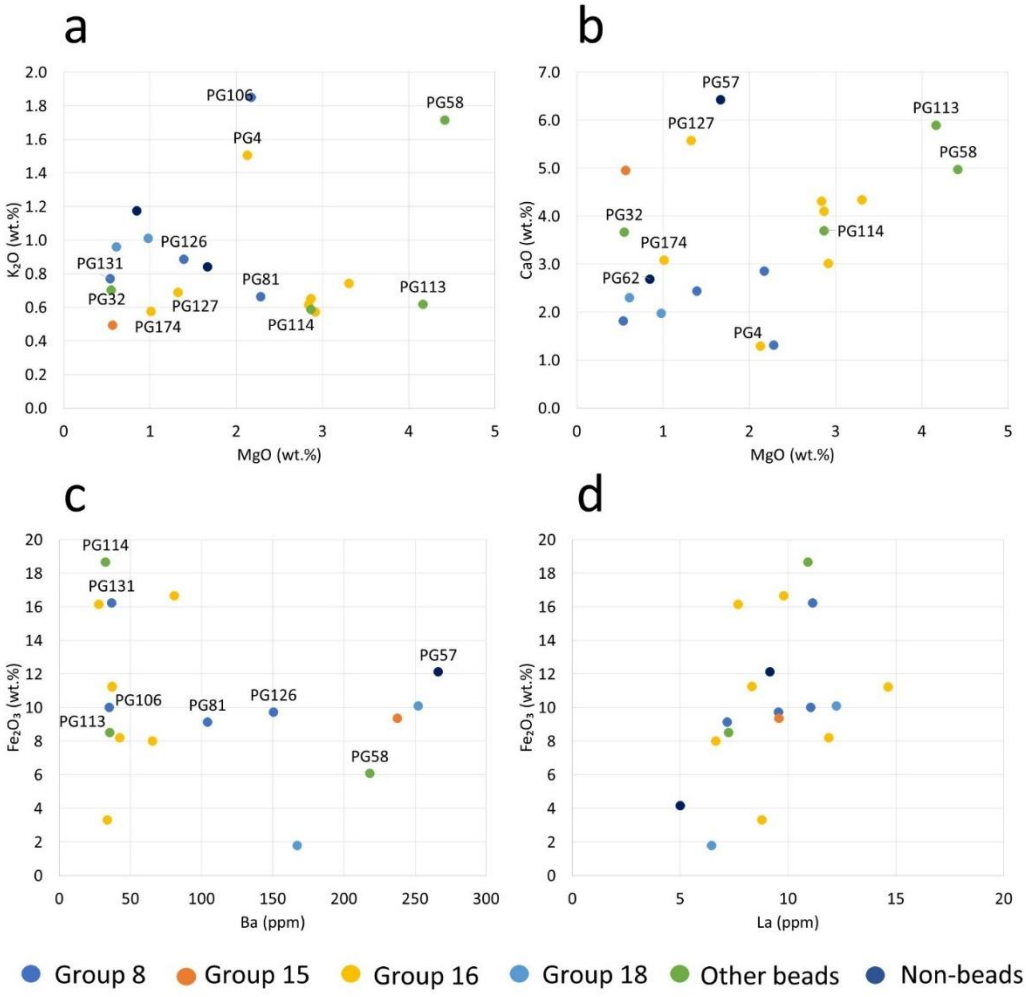

Figure 9.6. LA-ICP-MS data. Binary plots of selected oxides and trace elements: a - MgO vs K_2O; b - MgO vs CaO; Ba vs Fe_2O_3; d - La vs Fe_2O_3. PG32 is absent in the plots that involve Fe2O3 due to the extremely high concentration (54%). PG62 is absent in the plot c due to the high Ba concentration (540 ppm).

Figure 9.6 b, on contrary, demonstrates positive correlation of MgO and CaO values. Two parallel trends are observed. PG99, 127 and 57 that all belong to different Groups have more CaO than MgO. Most of the Group 16 and Other beads seem to have similar content of these oxides with the slight prevailing of the former one. Other samples are in between those trends. When divided by their Mg/CaO ratio, samples demonstrate three distinct groups: high Ca (ratio 0.11 – 0.32, medium 0.24) composed by samples PG3, 32, 99, 127, 131, 174 and Non-beads; low Ca (ratio 1.7) samples PG4 and PG81; medium Ca (ratio 0.5 – 0.97, mean 0.73) includes the rest of the samples (majority of Group 8, 16 and Other beads, plus PG64).

Fe content in the presently-discussed set of samples by LA-ICP-MS estimation is around 10% (weight oxide) on average. PG32, though, seem to contain some 55% Fe_2O_3 and is therefore excluded from the plots (Figure 9.6 c and d). As such value is way above the quantities usually registered in glasses the data on this bead were treated with caution. No evident correlation of this metal with any other of the determined element emerged, although several samples (namely Groups 15, 18, PG57 and 58, Figure 9.6 c) demonstrate a strong association between Fe and Ba. PG62 contains 540 ppm of Ba, but it's relation with iron is not evident. On the other hand, iron content does not show any relation with REE, as demonstrated by Fe_2O_3 vs La binary plot in Figure 9.6 d ($r = -0.05$). The same picture allows to distinguish three groups of samples by their Fe content. Boundaries of these groups determined as <5% for "low Fe" group (samples PG3, 62 and 123), >15% for "high Fe" group (samples PG32, 114, 127, 131 and 174). The rest of the samples have "medium" Fe content around 10% (weight oxide).

Other transition metals are contained in minor and trace quantities. MnO content is higher in samples of Group 15, 18 and Non-beads (0.1 to 0.5%). PG127 and PG32 from Group 16 and Other beads also contain elevated level of MnO. The rest of the samples do not contain more than 1000 ppm of MnO (usually not more than 200 ppm). Significant concentration of Co was (>1000 ppm) was confirmed for PG3, and also PG32 contains around 170 ppm of this metal, associated with the highest Ni, Cu and Sn amounts. Ni, Zn and As are on average present in concentrations of 200-300 ppm though their concentrations can be very different in each sample (from few tens to thousands of ppm), without any evident cluster (or trend) among themselves or with other transition metals.

Cu is present in somewhat higher amount on average. Samples PG3, 32, 99, 127 have more than 1800 ppm while the rest are contained within 500 ppm, with most of the samples being below 200 ppm (Appendix 7). PG3, 32 and 62 featured high concentrations of Sn (more than 200 ppm).

Yellow decorative parts reveal relatively high Pb, Sb, Cu and As content. Average PbO/Sb_2O_5 ratio is 8.8. In the white decorations Sb percentage is higher (though in PG114w still remains at trace levels) than in the dark base glass. Some red spots on PG4 and PG174 (sample that was only analysed by LA-ICP-MS and μ-Raman) that were analysed by this technique featured Cu signals, although the concentration of this element is contained within 1% (weight oxide).

In order to track the division of the samples on the level of trace elements, it was opted to use PCA. Several oxides (SiO_2, TiO_2 and V_2O_5) were added to the set of trace elements without Sr (these are mostly connected to the silica source). The data were SNV normalised prior to the PCA calculation. PCA plot (Figure 9.7 a) demonstrated the division of samples into two groups along the PC1, which is covering 85.4% of explained variance. Samples of Groups 8 (PG81 and PG126), 15, 18, PG32 (Other beads) and Non-beads have negative PC1 values. The rest of the samples (PG106 and PG131 from Group 8, Group 16 and most of the Other beads) have positive PC1 values. It is evident from the loadings that PC1 is influenced by the silica and light REE on one side and by the rest of REE together with Cs, Ba, Hf, Tl, TiO_2 and V_2O_5 on the other one. This difference is further visualised by the UCC normalised values of trace elements, placed into linear plots in Figure 9.7 (b and c), which keep the division observed in the PCA binary plot. Figure 9.7 b contains values of samples with positive PC1 values and Figure 9.7 c – those with negative PC1 values.

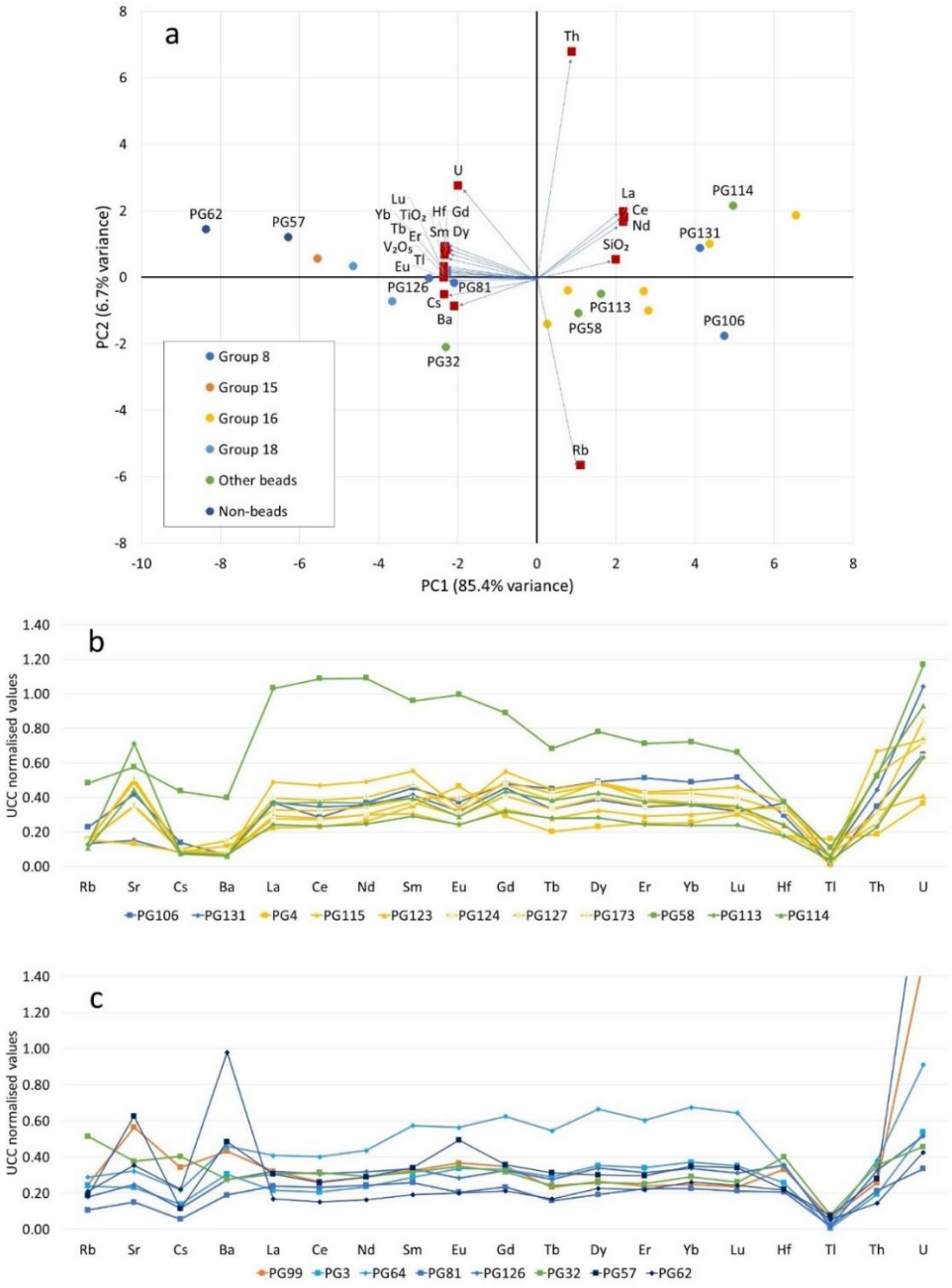

Figure 9.7. LA-ICP-MS results. a – PCA binary plot of PC1 vs PC2 that includes trace elements (without Sr) and some silica related oxides (SiO_2, TiO_2, V_2O_5). Scores and loadings are situated in the same plot. Loadings values were multiplied by 10 to increase legibility of the plot. Scores of samples are divided into those that have positive PC1 values and those with negative PC1 values. b – linear plot of UCC normalised values (McLennan 2001) of trace elements concentrations determined by LA-ICP-MS for samples that have positive PC1 values; c – same for samples with negative PC1 values.

Samples in Figure 9.7 b and 9.7 c differ mostly by the relative abundance of Ba (Figure 9.7 c), Eu anomalies and relative abundance of Hf. Samples in Figure 9.7 b tend to have elevated content of REE in respect to Ba and Hf on each side. Majority of the samples in Figure 9.7 b demonstrate negative Eu anomaly of the UCC normalised values (0.61 – 0.91). They are mostly Group 8 and 16 samples. PG99 (Group 15), PG4 (Group 16), Group 18, PG32, 58 and 62 (Other and Non-beads) do not have significant Eu anomaly (values within 0.9 – 1.1). Eu/Eu* anomaly calculated as follows: $Eu/Eu^*=2Eu_n/(Sm_n+Gd_n)$ after Pourret et al. (2022). PG58 and PG64 seem to be the outliers within the set by their trace elements profile.

9.1.6. Micro Raman Spectroscopy.

Seventeen samples have produced spectra of Si – O bending and stretching groups of bands taken from the surface of the base glass. Their bending and stretching massifs maxima were recorded and areas of these massifs calculated to provide the polymerisation index value as explained in section 4.6. Si – O stretching maximum positions and the polymerisation index values plotted against each other were also compared with CMOG reference glasses spectra (Figure 9.8 a). It can be seen that samples are largely divided into two groups: samples that have their silica stretching mode maxima in between 1070 and 1100 cm^{-1} and those that have their maxima at 950 – 1000 cm^{-1} interval. Sample PG58 is positioned in between these groups and PG64 – the only representative of Group 18 that produced useful data, has even lower stretching maximum, centred at 928 cm^{-1}. Incidentally, the first group with higher maxima is situated near CMOG A and B references and the second one is in the vicinity of CMOG C and D references. Interestingly, the second group of samples, according to LA-ICP-MS data contains more than 10% of Fe_2O_3. The stretching maxima across all samples considered are negatively correlated ($r = -0.5$) with the Fe content in the samples, confirming that high concentrations of Fe affect the region of Q_2/Q_3 stretching vibration of silica near 980 cm^{-1} (Baert et al. 2011).

Polymerisation index values, calculated after Colomban (2003), are contained within 0.6 and 1.1 (Figure 9.8 a). The only exceptions are samples PG32 (1.5) and PG123 (2.2). Assuming the shift of the stretching maxima of some samples to the high Fe content, it can be concluded that all the samples belong to soda-lime silica glasses (Colomban 2008).

Several crystalline phases were detected by μ-Raman analyses. In yellow decorative parts bindheimite (lead antimonate $Pb_2Sb_2O_7$), same phase that gave colour and opacity to the beads discussed in Chapter 8, was detected by its main peak at 142 cm^{-1} and minor peaks at 208, 340 455, 513 cm^{-1} in several samples with yellow decorations (Ricciardi et al. 2009). As this phase was detected in PG32, where yellow colour was not very evident, it was confirmed that this sample's decoration was in fact yellow by design. This phase is abundant in already mentioned PG32 but also in PG57, 62 and 64 (Figure 9.8 b). An undetermined Sb-O containing phase, was detected in white coloured parts of PG4 and PG114. It has main sharp peak centred at 656 cm^{-1} that corresponds to Sb-O bending (Bahfene and Frost 2010). Spectrum of PG4 features additional peaks of this or another crystalline phase at 85, 105, 152 and 763 cm^{-1}. On two occasions, crystalline phases were detected in the black appearing parts. One of the PG57 spectra features peaks of anatase (main at 145 and minor at 400, 513, 635 cm^{-1}). Peaks at 206 and 460 cm^{-1} that likely belong to quartz were noted in the spectrum of PG173.

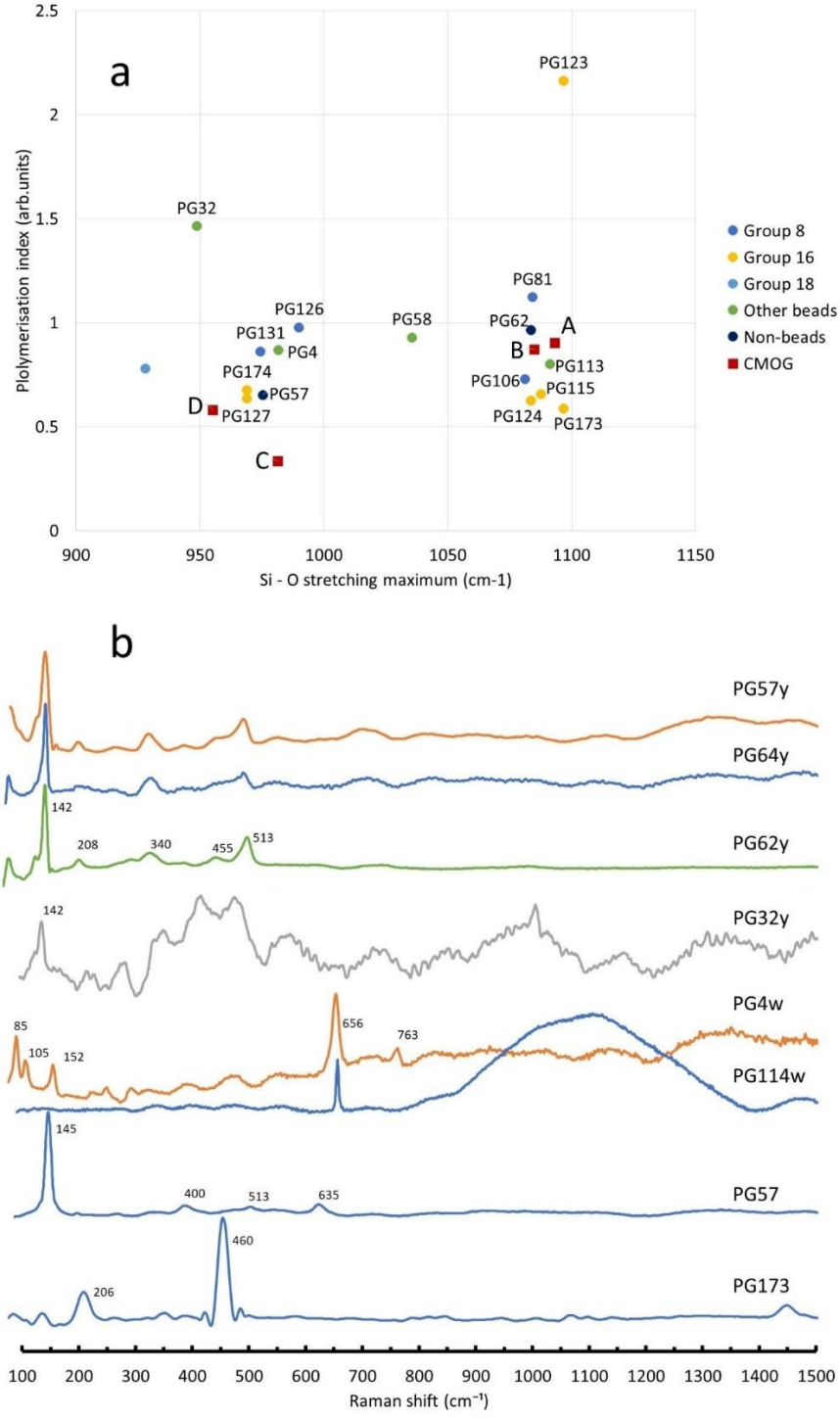

Figure 9.8. μ-Raman analyses results. a - binary plot of Si-O stretching massif maxima vs polymerisation index values calculated after Colomban 2003; b – spectra of crystalline inclusions found in the samples.

9.2. Discussion of the results.

9.2.1. Sources of silica.

Trace and REE seldom demonstrate correlation with Fe, therefore it can be reasonably assumed they are connected to the source of silica. In section 9.1.5 (LA-ICP-MS results), it was demonstrated that samples were divided by the Eu and Ba content into two groups: the one without pronounced (or positive) Eu anomaly and elevated Ba content and the one with negative Eu anomaly and lower Ba concentrations. Figure 9.9(a) visualises this division, and shows the samples analysed here with literature data, for the sake of comparison with other glass. Samples with neutral values of Eu anomaly, as a rule, contain at least 100 ppm of Ba. Also, samples with correlated values for Ba and Fe belong to this group. These samples follow the trend of the majority of the external datasets that were included for the comparison, which are mostly attributed to the Levantine origin (Panighello et al. 2012; Blomme et al. 2017; Costa et al. 2021). Samples with negative Eu anomaly values align well with the majority of dark-appearing samples unearthed in Pella (Jordan) and analysed by Reade et al. (2009, trace elements compositions published in Reade 2021).

In geological records, Eu primarily occurs in feldspars and its oxidation state is determined by the temperature and oxygen fugacity during magma cooling (Weill and Drake 1973; Gao and Wedepohl 1995). Its anomalies are important indicators of provenance but can be affected by sedimentation processes (McLennan et al. 1993; Götze 1998). In the present sample set, the correlation coefficient of Eu with Al is 0.87, strongly suggesting it originated from feldspars. Correlation coefficients calculated for two groups (the neutral Eu and the negative Eu) are still on the strong positive side, although somehow lower. Moreover, positive correlation of Eu and K was found within the negative Eu anomaly group of samples ($r = 0.65$), whereas a positive correlation of Eu with Ca emerged ($r = 0.88$) within the neutral Eu group. This might be suggestive of different kinds of feldspars within two sources of silica (K-feldspar for samples with negative Eu anomaly and plagioclase for the samples that exhibit no or slightly positive Eu anomaly).

Figure 9.9 b and c presents the averaged profile of the neutral Eu group (Figure 9.9 b) together with two outliers (PG58 and PG64). It can be noted that the selected representative samples from Mediterranean groups of vessels (Veneto IA – Panighello et al. 2012), glasses of Levantine origin from Greece (Pieria IA – Blomme et al. 2017) and Portugal (Costa et al. 2021) have similar UCC normalised values for REE elements and differ in Sr (which probably entered the batch with other components) and, to the lesser extent, Th concentration. This and Figure 9.9 a, where these samples are also on the same trend, suggest that samples in this group have same provenance. Sample PG64 demonstrates similar profile (enriched in the heavy REE) with the glasses found in the Iron Age Sardis (Van Ham-Meert et al. 2019), which can be also the place of production of such glass, as further suggested by its high Al content. Although PG58 is similar to the glass from Sardis if heavy REE content is considered, it is even more enriched in light REE, which makes this attribution weak, although it cannot be excluded that the trace element content could be influenced by the colourant.

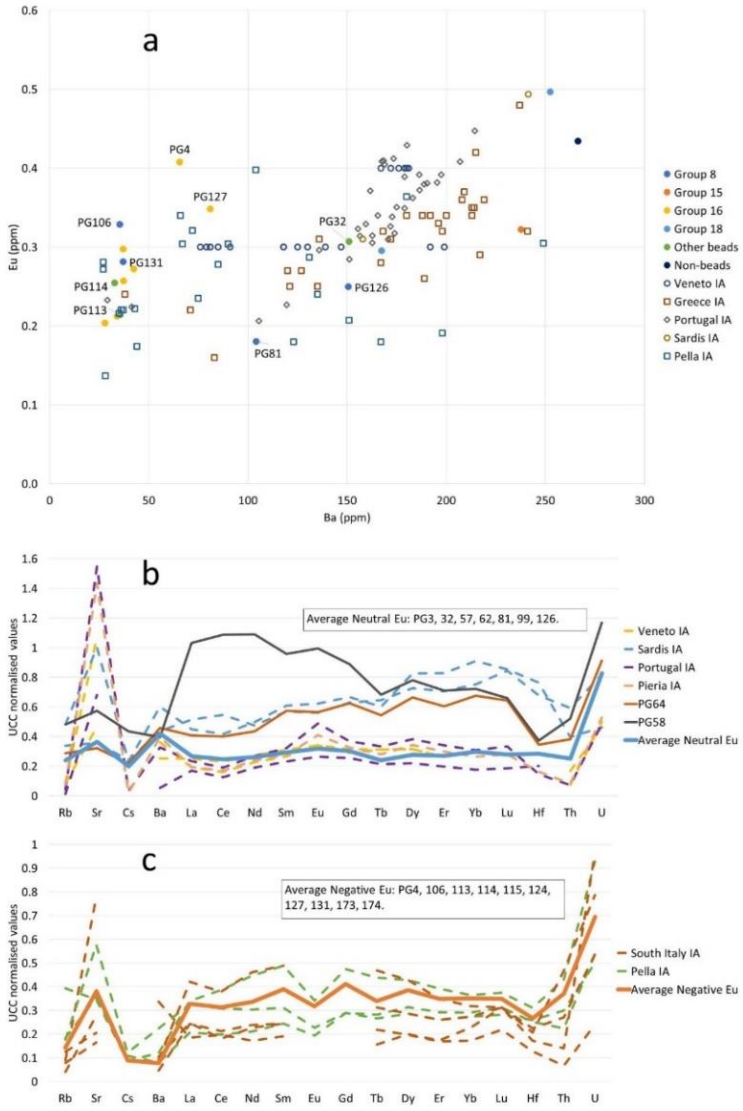

Figure 9.9. Comparison of trace elements concentrations of black appearing beads and published data. a - binary plot of Ba values against Eu ones. External data: Veneto IA – Panighello et al. 2012; Greece IA – Blomme et al. 2017; Portugal IA – Costa et al. 2021; Sardis IA – Van Ham-Meert et al. 2019; Pella IA – Reade 2021. Plot does not include PG62 and PG58 due to the high Ba and Eu content respectively. b – linear plot of UCC normalised (with values of McLennan 2001) values of trace elements for samples without pronounced Eu anomaly (Average Neutral Eu, the list of samples that were considered in in the box within the plot) and two outliers – PG58 and PG64 compared with selected samples data from literature: Veneto IA – Panighello et al. 2012; Sardis IA – Van Ham Meert et al. 2019; Portugal IA – Costa et al. 2021; Pieria IA – Blomme et al. 2017. c – similar plot that demonstrates averaged values of samples with pronounced negative Eu anomaly (list of samples is inside the box within the plot) compared with some dark glasses values from South Italy – Conte et al. (2016) and Pella – Reade (2021).

The negative Eu group average profile of trace and REE is presented in Figure 9.9 c. In case of these samples, trace element composition highlights a match with glasses found in Pella (Reade 2021) and in South Italy (with the suggested provenance in the Eastern Mediterranean, Conte et al. (2016)). Negative Eu anomaly is regularly noted in the sediments of granitic origin (Götze 1998). Unfortunately, data on Eu are not available for glasses from South Italy Iron Age contexts, which would be helpful to confirm the connection with the present set.

Iron that is almost certainly was present in the sand, was added to the batch as a separate raw material as well. This assumption is supported by the absence of any evident correlation and no elevated levels of elements that are frequently found in high-Fe sediments such as Al, Ti, V, Ba (except several mentioned samples) and REE (Tzifas et al. 2017). Despite this, high-Fe sands were suggested as a source of Fe in the similar black appearing glasses from South Italy by Conte et al. (2016) and for some Roman glasses (Cagno et al. 2014). The Ti/Zr division of samples observed in p-XRF block of data (Figure 9.5 c) cannot be confirmed or disproved by LA-ICP-MS, because not all samples were analysed and Zr values are available for only two samples (Appendix 7). Hf, which concentration can reflect the same trend as the one of Zr, cannot be used to discriminate samples in the same way, as both high and low Hf relative concentrations were observed in samples with neutral Eu and negative Eu anomaly samples.

Wrapping up, it can be stressed that at least three sources of silica can be suggested for the set of dark appearing glass: the first is relatively enriched in Ba with some plagioclase feldspar that does not have negative Eu anomaly (probably Levantine), the second one is Ba poor, with K-feldspar that adds negative Eu anomaly to the trace elements profile. PG64 was produced from a different silica source, similar to the one used to make dark-coloured glasses found in Sardis.

9.2.2. Fluxes and stabilisers.

All samples discussed in this chapter contain Na_2O at 17.1% (st. dev. 3.8%) average concentration. PG32 is the only sample that contains less than 10% (its Na_2O concentration is 5.6%). To distinguish between the use of a mineral source of flux and high soda plant ash it is possible to use the same criterion as in Chapter 7 (results and discussion of translucent glasses): plant ash glasses were recognised as those with MgO content above 2% and K_2O one above 0.5% (Rehren 2000; Mirti et al. 2008; Purowski et al. 2018; Angelini et al. 2019). The majority of samples of Group 16, Other beads and two beads form Group 8 (PG81 and PG106) fit this definition of HMG (Figure 9.6 a). On the other hand, in samples with high Mg content (>2% weight oxide), this element is positively correlated ($r = 0.85$) with Ca (Figure 9.6 b), and the MgO/CaO ratio is from 0.7 to 1.7 with average of 0.96. Both facts suggest the use of dolomitic rocks as the source of the stabiliser (Sperber et al. 1984). The same set of samples (except for PG81) consists of samples with negative Eu anomaly and for which K-feldspar was suggested as Eu bearing component. This would suggest that the slightly elevated K_2O levels should be attributed to feldspars. On contrary, samples with low MgO content are on a different Mg/Ca trend (Figure 9.6 b), they mostly belong to the samples for which sand containing plagioclase feldspar was suggested. These have much lower MgO/CaO ratios (0.1 – 0.6 and average 0.3).

If these K – Mg – Ca relationships are considered, it is evident that they are related to the silica source and do not reflect the composition of the flux. As the Na_2O concentrations are elevated, a

mineral source of flux can be suggested for all the samples discussed here, which shall therefore be recognized as LMG. Even in case of PG32 which has low concentrations of all major elements because of the outstanding Fe content (54%). In the reduced composition that excludes Fe the Na_2O value increases to 12.3%. With MgO and K_2O concentration of 1.2 and 1.5% respectively, PG32 can be also attributed to LMG.

Calcium – common stabilising component of silica glass (Tite 2004; Henderson 2013; Moretti and Hreglish 2013), is often present in black appearing glasses in concentrations that are less than 3% (weight oxide). In case of beads for which the high MgO content was attested, Mg also acts as important stabilising agent (Verità et al. 2009; Angelini et al. 2019). These two elements derive from dolomite in these samples and have slightly lower CaO/Sr ratio (243 with st.dev. of 21) than those with low MgO content (CaO/Sr = 316 with st. dev. of 118). The higher st. dev. of the CaO/Sr ratio can be caused by several sources of calcium. Ratios of CaO/Sr above 200 indicates an higher role of Ca-bearing minerals (carbonates, feldspars) in the total Ca budget (Wedepohl et al. 2011; Conte et al. 2016). This means that shell content in the sands that were used in production of these glasses was limited. Differences in the concentrations of stabiliser-related elements further supports the two different regions of provenance for these glasses. Ca and Mg in black appearing glasses are aided by Fe in their stabilising role, as iron can act as the stabiliser as well (Conte et al. 2016; Reade 2021).

9.2.3. Colourants and opacifiers.

Iron in sufficiently high concentrations, and given the appropriate thickness of glass, can make absorption of visible light intense enough for the glass to appear black and opaque (Möncke et al. 2014).

It was already stated that iron (in its bulk) did not enter the batch together with the silica source to make these glasses dark (so much so that they appear opaque) because of the absence of correlation of Fe with other elements that can be commonly found in sands. This means that Fe should have a separate source in the batch. No association of Fe with other transition metals (or even broader set of elements) was detected, except for the association with Ba in samples of Group 15 (PG99), 18 (PG3, PG64), samples PG57 and PG58 (from Non-beads and Other beads respectively). Barite was found to be associated with K-feldspars (feldspar was suggested to be the source of K in these samples) and iron minerals (Mathias and Rogers 1940; Sun et al. 1998; Hoffman et al. 2011). More research needs to be done to link this association to a specific source of iron. General lack of associations makes the use of Fe oxides or (by-)products of iron working to be the likely sources of Fe in the glass. Use of hammer scale or other by-products of iron working suggested for some black appearing glasses of Roman time (Cholakova et al. 2012; Cagno et al. 2014) is not supported by any visible evidence, such as prills or other types of inclusions, detected under high magnification. It shall be however considered that, for the presently discussed sample set, only one sample was examined in SEM-EDS as a polished cross-section, therefore this hypothesis cannot be discarded.

To understand the way of colouration it is useful to assess the redox balance of Fe in the matrix. Calculation of $Fe^{2+}/\Sigma Fe$ (Schreurs and Brill 1984; Bingham and Jackson 2008; Ceglia et al. 2015) was not possible here, just like in case of translucent beads from Chapter 7. Due to poor quality of the majority of FORS spectra, it is difficult to understand the oxidation state of Fe in these glasses. Fe^{2+} absorption in the NIR was recorded for the majority of samples in FORS spectra, but in the conditions

of poor reflectance (samples are black in colour) the bands, including the Fe^{3+} ones, were not pronounced, if present at all. The cracked surface of samples exhibits yellow-brown tinge (Figure 9.2 b and c) when observed in the optical microscope. These are the reasons to believe that these glasses were coloured by $Fe^{3+} – S^{2-}$ complex created in the reducing conditions (Schreurs and Brill 1984; Ceglia et al. 2014 and 2015). On another hand there was no pronounced band at around 405 nm that would confirm ferri-sulphide complex, though it could be superimposed with the pronounced absorption centred at 350-400 nm. μ-Raman analyses could contribute valuable information into the discussion of $Fe^{3+} – S^{2-}$ complex presence as it has a peak at 419 cm^{-1} (Ceglia et al. 2014). Unfortunately, this peak corresponds to a band in the Si – O bending massif and these cannot be told apart.

Cu^{2+} band was observed in PG4, 6, 92, 115 and 133. None of them was confirmed to have major amount of Cu. Data on PG4 are inconclusive (p-XRF and LA-ICP-MS data in different areas give different Cu concentrations, the highest one being in the red spot on the surface of the bead). Apart from red spots (also analysed on surface of PG174), Cu does not seem to play any role in the final colour of the samples. PG3 was confirmed to contain Co in concentration of 1260 ppm (weight oxide). At the same time the Fe_2O_3 content in this bead (or spindle whorl) is the lowest within the present sample set. As Co was found to be Co^{2+} (FORS data) this object can be counted as Fe-Co coloured.

The decoration glass can be divided into yellow and white, both of which have elevated Sb amount. Yellow glasses are coloured by $Pb_2Sb_2O_7$ crystals that were introduced to the batch after their preparation with an excess of lead similarly to the majority of beads discussed in Chapter 8. White decorations contain more Sb_2O_5 and CaO than the dark bases beneath them (Figure 9.5). The use of calcium antimonates can be reasonably assumed, although the low concentration of both antimony and calcium detected by LA-ICP-MS would make this attribution somehow problematic. The reason for low Ca and Sb concentrations in LA-ICP-MS can be the low thickness of the decorative parts, which is not as much of an obstacle for qualitative p-XRF analysis. On the other hand, characteristic peak of antimonate was detected by μ-Raman spectroscopy.

9.2.4. Production and forming techniques.

Two batch recipes can be reconstructed for the samples considered in this chapter, apart from PG64, which stands out of the general picture. In the first one, silica source would be mixed with dolomitic material (or dolomite was present in the sand already) and high Na mineral flux. Fe could be added at this stage. Lead antimonate would be prepared separately, for adding it to glass for decorations. In case of Group 15 samples, some of lead antimonate could be added to dark glass too. There were no beads with white decorations in the batches prepared in this way. Second recipe relied also on sand (of somewhat different composition) and Na bearing minerals, but a different source of stabiliser was used. It could be a mixture of Ca carbonate augmented by some plagioclase feldspar (again, could be naturally incorporated into sand). Iron was the main colouring agent, and it was added in significant quantities. Both lead antimonate and Ca antimonate were prepared. In addition, some high Cu glass was probably used in making these beads. They were all prepared in the reducing conditions. The same conditions are needed for the development of the ferri-sulphide complex.

Temperature range for the preparation of these glasses was within the 700 – 1000 °C, as suggested by polymerisation degree values calculated from Raman spectra (Colomban et al. 2008).

Beads of Group 8 and 15 were formed by winding a small portion of glass around the mandrel. These beads were made in series, where several beads were made with a single portion of glass on the same mandrel. This can be surmised by observing the protrusions near the apexes and especially in the case of double bead presented in Figure 9.1 a. In case of Group 15, a wave decoration was applied on top of dark coloured glass. Larger beads of Group 16 or Other beads might have been made in the same way, but more attention was given to make these more symmetric. PG144 could be made by the method of folding because of its characteristic groove near the apex (Tamura and Oga 2016).

There are signs of tooling on the surface of PG123 and PG127. The former one has grooves similar to rib decorated samples of Group 11. The latter one has somehow flattened surface in the widest part. Line, wave, ring-eyes, double ring-eyes or spot decorations were applied by dropping the decoration glass and rotating the bead in one direction (line) or just dropping and detaching the decoration glass in case of spot decoration or dropping and rotating the decoration glass rod in case of eye decorations. The eye of PG6 is not stratified, so two concentric rings were made by laying the rings on the surface of the bead.

Pear or biconical shape of Group 18 objects was obtained by shifting the centre of weight of the blob or tooling it to have an edge, though moulding was also an option. After the final shape was obtained a decoration applied in form of densely spaced line and wave decorations. Small protrusions on the edge of PG64 were applied with dropping yellow glass.

The fibula bows were made in the same way that the ones discussed in Chapter 6 except for the VG92 and VG93, for which the marks of a tool that was applied to make a herringbone pattern remained on the surface as grooves. This might mean that the herringbone pattern was made on a “stiffer” glass.

Glass button (pin head) PG57 was made by careful stretching of glass with the tool like tweezers from the centre of the blob. The yellow decoration was applied on the edge of the stretched parts.

Conclusion. Black glasses from South Etruria and Latium considered in this research have several places of origin and were prepared by mixing materials from different sources. Unfortunately, the typological division does not always reflect the compositional data and does not allow the attribution of the samples to a specific provenance group; therefore, samples that were not analysed in the laboratory are largely not attributed, although samples with the highest K concentrations could probably be included into the neutral Eu group detected by LA-ICP-MS. In any case, the glass seems to be imported from several glass-making centres of the Eastern Mediterranean. Iron, also from several sources, was used to colour these samples. Glass for decorative parts was prepared similarly, as demonstrated in the previous chapters.

CHAPTER 10. FAIENCE-LIKE OBJECTS.

The following archaeological objects are discussed in this chapter:

- **Group 9: all;**
- **Other beads: VG16, 27.**

Egyptian faience is not considered systematically within this work but as these samples were analysed on site, and very few of them could be analysed in the laboratory (VG39-42), it was decided to present the collected results and the preliminary conclusion as a separate chapter of this thesis. This part stands somewhat apart from the rest of the objects, which is reflected in the way the discussion is built.

10.1. Egyptian faience as a material and related literature.

Egyptian faience is a non-clay ceramic material that should be distinguished from the more recent tin-glazed clay ceramics that are still widely produced (Nicholson and Peltenburg 2000). Egyptian faience was made of silica base (crushed quartz pebbles or sand) which was shaped by adding water or binding agents and glazed with a coloured soda-lime-silica vitreous layer, though the exact composition of the glaze depended on the production technique (Mangone et al. 2011; Nicholson 2012; Angelini et al. 2019). Shapes of the objects made of this material could be made by hand, formed in the mould or on the core of other materials (Angelini et al. 2019).

The application of glaze could be done in three ways: efflorescence, application, and cementation (Nicholson and Peltenburg (2000) after the work of Vandiver).

The first one was done by mixing predominantly alkali salts like natron or the carbonates in the plant ash with quartz with addition of water and shaped into the desired form. On drying, the salts migrated leaving a layer of effloresce on the surface, which would act as the fluxing agent for the development of the vitreous glaze on firing.

The second one was based on preparing the slurry of raw or pre-fired mixture of silica, lime and alkali that were ground, mixed with water and applied onto quartz body with the subsequent firing.

The third method is the cementation, and it is still used in contemporary times by Qom artisans in Iran (Tite et al. 1983). According to this procedure, the shape is submerged in the powder of alkali and heated. The powder then reacted with the quartz body creating the glaze. The unreacted excess of the sintered powder is then removed.

There is an extensive scholarship on what macro and microscopic differences are diagnostic for the objects made by each of the abovementioned methods (Noble 1969; Kaczmarczyk and Hedges 1983; Tite et al. 1983, 2007; Tite and Bimson 1986; Vandiver 1998; Nicholson and Peltenburg 2000; Griffin 2002; Shortland and Tite 2005; Mangone et al. 2011; Read 2022 and some references therein). These studies do not demonstrate a unanimous confidence in the clear distinction between the manufacturing methods. Nevertheless, they provide a framework for material characterisation of faience based on such features as differences in stratigraphic layers and the ratio of their thickness, size and shape of particles, presence of voids and differences in chemical composition of each layer.

Egyptian faience objects appear to be covered with smooth, usually blue glaze. Underneath is the interface (contact) layer where vitreous phase is mixed with quartz grains. The bulk of the object

consists mostly of the quartz grains that are bound to each other by small quantity of interstitial glass (Tite et al. 1983; Shortland and Tite 2005).

Faience is known to be produced from the end of the 5th millennium BCE (Angelini et al. 2019) and by the time of EIA its production probably involved all the methods mentioned above and was spread among many regions in the Mediterranean (Nicholson and Peltenburg 2000; Angelini et al. 2019).

In the Iron Age, faience production is thought to be in decline and only small and relatively simple objects were being made. Though, orientalising culture of European Mediterranean kept certain demand for the Egyptian faience objects (Nicholson and Peltenburg 2000; Toffolo et al. 2013) and remains of several workshops attributable to the first millennium BCE were discovered (Nicholson and Peltenburg 2000; Angelini et al. 2019). For small objects such as beads, it was argued that cementation was the most suitable method of production. Based on experimental studies, such objects have thinner glaze and contact layer than those made by efflorescence, but this evidence should be treated with caution due to the presence of many variables such as weathering, firing time and chemical composition of the raw materials (Tite et al. 1983; Matin and Matin 2012; Costa et al. 2022).

Due to its complex structure, Egyptian faience is usually studied with invasive procedures to expose the inside of the object, with cross sections being among the most popular ways of samples preparation (Tite et al. 1983, 2007; Tite and Bimson 1986; Vandiver 1998; Mangone et al. 2011; Toffolo et al. 2013; Costa et al. 2022). The non-invasive methods for micro-structure characterisation open new opportunities for the researchers to study objects that cannot be altered (Liang et al. 2012; Targowski and Iwanicka 2012; Read et al. 2022). Chemical composition of each layer and phase is also in focus of the researchers, who try to suggest the raw materials that were used in making specific objects (Tite et al. 2007; Mangone et al. 2011; Matin and Matin 2012; Toffolo et al. 2013; Costa et al. 2022).

10.2. Results of the analyses of Egyptian faience beads.

Objects considered in this chapter are somewhat different in appearance. Within Group 9, VG17 has relatively smooth surface which has uneven colouring (Figure 10.1 a). It is covered in small and narrow cracks, but the bead keeps full integrity. The aperture is wider near the apexes, with the narrowest place near the middle of the width (all the beads of Group 9 are flat). The rest of the beads within this Group have rougher surface and have straight apertures.

The beads feature different colours, and three sub-Groups can be distinguished: the blue one, with dominant B colour value; the yellow one, with lower B values in respect to R and G ones, and the lightly coloured set of beads, for which the RGB values are set between those of the first two groups. The difference in colour of these samples is demonstrated in Figure 10.1 (b). Same image shows the difference in texture of the beads.

Yellow and lightly coloured beads tend to have rougher surface with grainy texture while the blue ones seem to be covered in smooth glaze, which appears cracked. Glaze covers most of the bead's surface.

Other beads that are considered have different appearance. Their preservation state is much worse than the beads discussed so far. VG27 (surface is shown in Figure 10.1 c) appears to be

unevenly coloured with green and brown patches. It is slightly deformed with rib decoration somewhat distorted. VG16 is an example of a very thin ring-bead that underwent severe alteration, result f which can be seen in Figure 10.1 (d).

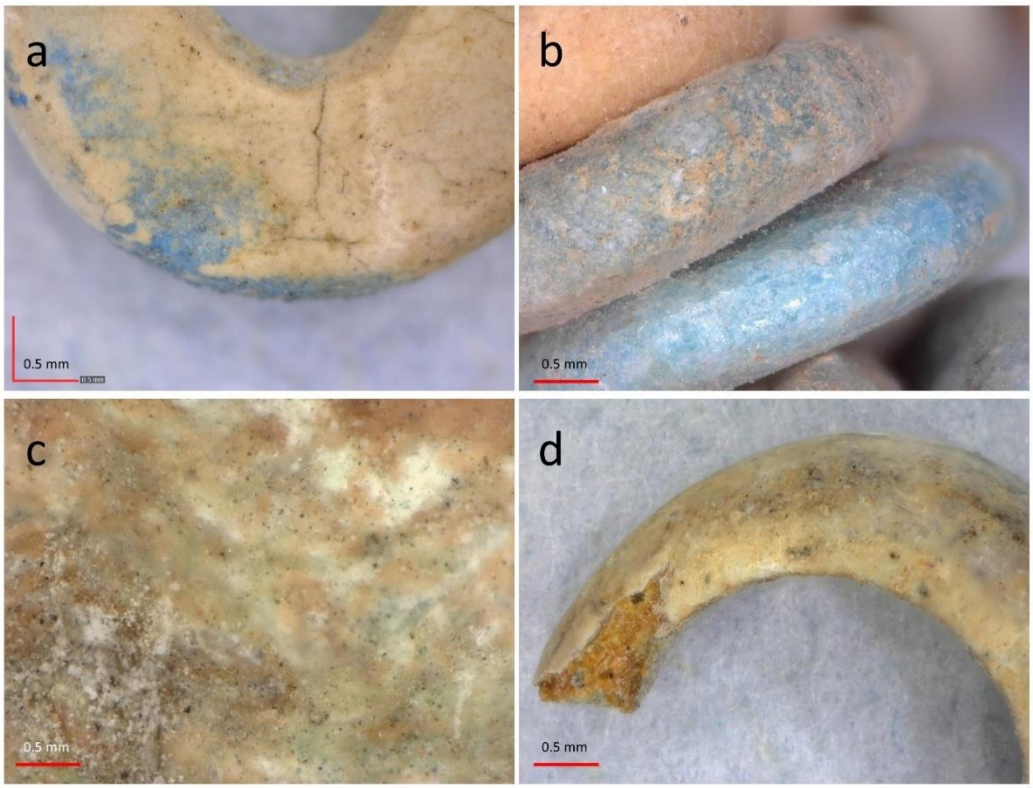

Figure 10.1. DinoLite images of beads: a - VG17; b - beads from tomb IV of the "Tumulo del Colonelo" at Cerveteri (Banditaccia) represented by samples VG39-47; c – surface of VG27; d – VG16.

Four beads (VG39-41_1) were studied in the laboratory but only VG39 was allowed to be prepared as cross section. Sample VG41_1 is an additional yellow bead from the same context as VG39-47 that was analysed in the laboratory, although it was excluded from the on-site analytical campaign. Both whole beads and the cross section of VG39 were studied by SEM-EDS, the former in the variable pressure mode, and the latter under high vacuum. Figure 10.2 includes the most informative BSE images obtained during the analyses, together with the stereomicroscope photograph of VG39 cross section (Figure 10.2 a). VG39 data are invaluable in characterisation of yellow variety of the Group 9 samples.

When polished, VG39 appears heterogeneous but does not demonstrate stratigraphic layers (Figure 10.2 a). SEM images of this sample demonstrate the differences near the surface. Alteration layer can be observed close to the initial surface of the bead (on the left side of the Figure 10.2 b). Deeper into the bead's bulk one can observe a somewhat lighter layer that has similar texture. At 50 µm a continuous vitreous phase appears to envelop the irregularly shaped and poorly sorted grains

that are 10 – 100 µm across. Among these, there are much smaller bright coloured inclusions made of heavier elements. These are sometimes aggregated to form larger structures that can reach 50 µm across.

Figure 10.2 (c) is a BSE image of the bulk of the bead. It is evident that vitreous matrix (lighter coloured material that surrounds darker grains) is continuous throughout the body of the beads. High atomic weight inclusions are present throughout the bulk. The surface of VG40-41_1 demonstrate certain degree of degradation, with surface deposits, roughness, and cracks. The surface of these beads is covered with particles of high atomic mean number (Figure 10.2 d).

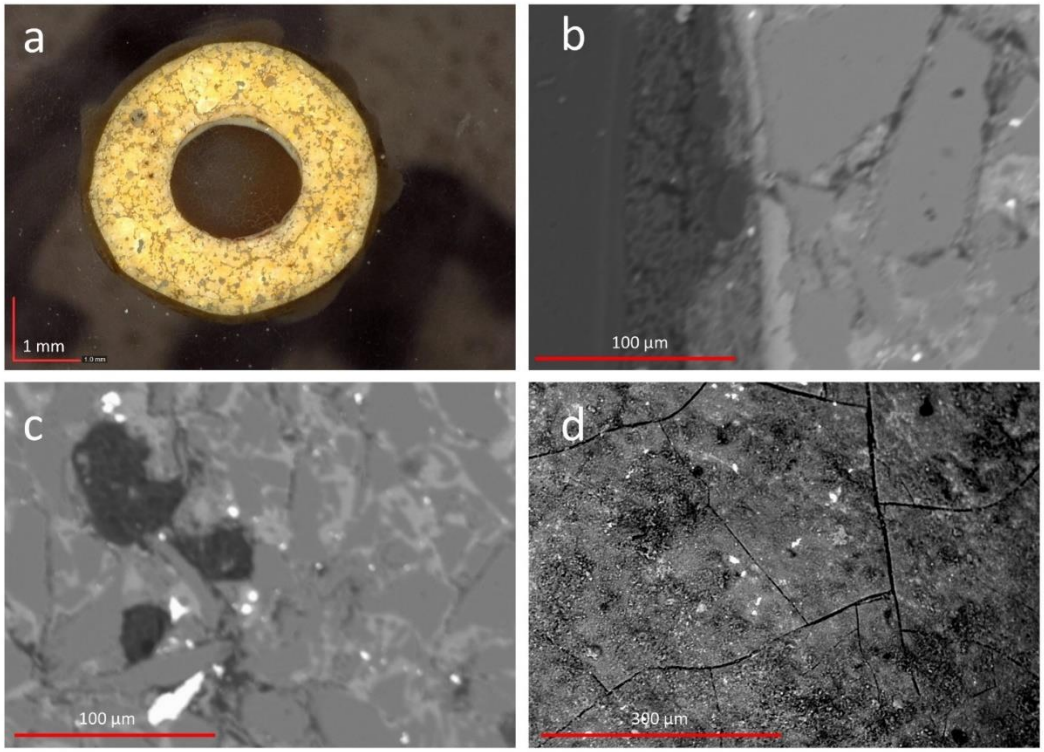

Figure 10.2. Images of samples that were studied in the laboratory: a - VG39 cross section as observed in DinoLite microscope; b - BSE image of the area of the same cross section where dark area on the left is the resin, alteration layer presents itself as cracked and rough looking area of darker and brighter colour, the bulk of the bead is on the right; c – another portion of the same cross section with the bulk of the bead in focus, dark areas are polishing agent (SiC) residue; d – surface of VG40 observed in SEM, no surface treatment was applied.

*Table 10.1. (VP)-SEM-EDS compositions obtained by analysis of different structural parts of samples: "grains" – darker grains inside the vitreous matrix; "incl." – heavy elements inclusions; "Vit" – vitreous matrix; "area" – spectra taken from the surfaces of VG40-41_1 that were not treated before the analyses; * - analysed in the Variable Pressure mode (VP); st.dev. – standard deviation of the replicate measurements.*

	Na_2O	MgO	Al_2O_3	SiO_2	P_2O_5	SO_3	Cl	K_2O	CaO	TiO_2	MnO	Fe_2O_3	NiO	CuO	Sb_2O_5	PbO
VG39 grains	0.18	<LOD	<LOD	99.95	<LOD	<LOD	<LOD	<LOD	<LOD	<LOD	<LOD	<LOD	<LOD	<LOD	<LOD	<LOD
st.dev.	0.03	-	-	0.07	-	-	-	-	-	-	-	-	-	-	-	-
VG39 incl.	0.7	0.3	0.30	34	<LOD	<LOD	0.54	<LOD	1.68	1.1	<LOD	3	<LOD	<LOD	27	37
st.dev.	1	0.2	0.02	23	-	-	-	-	-	0.5	-	1	-	-	13	12
VG39 vit.	<LOD	0.18	0.5	91	<LOD	<LOD	1.1	<LOD	1.2	<LOD	<LOD	0.7	<LOD	<LOD	1.02	6
st.dev.	-	0.02	0.3	2	-	-	0.5	-	0.4	-	-	0.3	-	-	-	1
VG40* area	1	0.7	6	75	4	0.78	0.4	1.6	9	0.26	0.3	2	<LOD	0.6	<LOD	0.2
st.dev.	0.2	0.1	1	6	1	0.06	0.1	0.7	2	0.09	0.1	0.6	-	0.1	-	0.1
VG40* incl.	0.8	0.6	4	70	4	0.69	0.4	1.3	10	0.82	8.95	2	<LOD	0.8	8	3
st.dev.	0.3	0.2	2	14	3	0.08	0.2	0.8	6	-	-	2	-	0.3	4	4
VG41* area	0.4	0.5	3	78	3	5	0.3	0.6	6	0.24	<LOD	4	<LOD	0.4	<LOD	4
st.dev.	0.1	0.1	1	16	2	4	0.2	0.5	4	0.06	-	7	-	0.2	-	4
VG41* incl.	0.5	0.8	4	61	1	4	0.4	1.4	6	1	1.1	10	<LOD	0.4	13	9
st.dev.	0.2	0.3	1	17	1	2	0.1	0.8	3	2	1	13	-	0.4	7	6
VG41_1* area	0.7	0.8	5	73	5	0.77	0.33	1.2	10	0.19	1.04	2.1	<LOD	0.48	6.59	2
st.dev.	0.1	0.1	1	12	3	0.08	0.06	0.6	6	0.01	0.08	0.9	-	0.03	-	2
VG41_1* incl.	1.2	0.8	5	56	2	1.17	0.5	1.5	6	0.40	0.43	5	<LOD	0.51	21	14
st.dev.	0.4	0.4	3	19	1	-	0.3	0.8	2	-	-	7	-	-	13	14

As for the nature of these structural parts, EDS spectra were acquired together information for revealing the material used in the manufacturing of these beads. The darker grains produce Si and O peaks that is suggestive of quartz. The vitreous part of the VG39 is also rich in Si and O (partly because of the possible excitation of the surrounding silica grains) but additionally major and minor quantities of Al, Cl, Ca, Fe, Sb and Pb also emerge, with the latter one prevailing (6% weight oxide while the rest of the elements have their respective concentrations around 1% or less). Heavy atomic weight particles across all the beads studied with SEM-EDS contain high percentages of Sb and particularly Pb. Additionally, major quantities of Al, Ca and Fe appear to be present. Ti and Cu are in minor quantities. As for the alkali and Mg, they appear in the minor quantities in the area scans including those made on the surface of the beads studied in the VP mode. Remarkable are the concentrations of P and S on the surface of VG40-41_1 (analysed without treatment). These elements were not detected in the cross section of VG39 was analysed. This can lead to conclusion that these elements are part of surface depositions that are observed in Figure 10.2 (d). Mn also seems to be present on the surface of the VG40-41_1 but not in the bulk of VG39. SEM-EDS compositions of each structural part of VG39 (vitreous matrix, silica grains and heavy elements

inclusions) as well as mean area and heavy elements inclusions compositions of samples VG40-41_1 are reported in Table 10.1. It can be observed that the standard deviations for all samples are high, mirroring the heterogeneity of the samples.

A wider set of samples was available to the p-XRF analyses. There are two methodological limitations that affect the final result though. First is the analytical spot of the analysis and focusing method of the hardware. Even though the XRF units used for acquisition of data were equipped with polycapillary optics, which allowed X-ray beam focusing on a spot of 300 µm (Frankie unit) or 80 µm (Unisantis unit), it was not possible to record data for grains, inclusions and vitreous part separately. Therefore, the p-XRF data represent the bulk composition of each analysed sample. Second limitation has to do with the difference of the analysed materials from glass that was used for calibrating the output. Similarly to the case of high Fe or high Pb glasses, p-XRF compositions of samples discussed in this chapter have to be treated in a semi-quantitative way. The table with the obtained concentration values can be found in the Appendix 6.

Group 9 samples (except VG17) appear to be similar in concentrations of K, Ca, Ti, Mn, Fe and Sr. All these elements, except for Ca in some of the samples are in minor to trace amounts (less than 1% weight oxide). Remarkable division is observed in the Co, Cu, Sb, and Pb oxides concentrations. Yellow samples (VG39-41) have higher Sb and Pb values while the blue and lightly coloured ones have higher Co and Cu values. Between blue and light coloured, Cu and Co values are higher in the blue ones. This division is visualised in Figure 10.3. Co seems to be associated with Ni and Zn in comparable amounts, though there are cases when Zn values are under the limit of quantification. It is evident from Figure 10.3 that relatively to Cu, the amount of Co is higher in the lightly coloured beads (VG42-44). In the yellow-coloured beads, the PbO/Sb_2O_5 ratio is 1.45 on average.

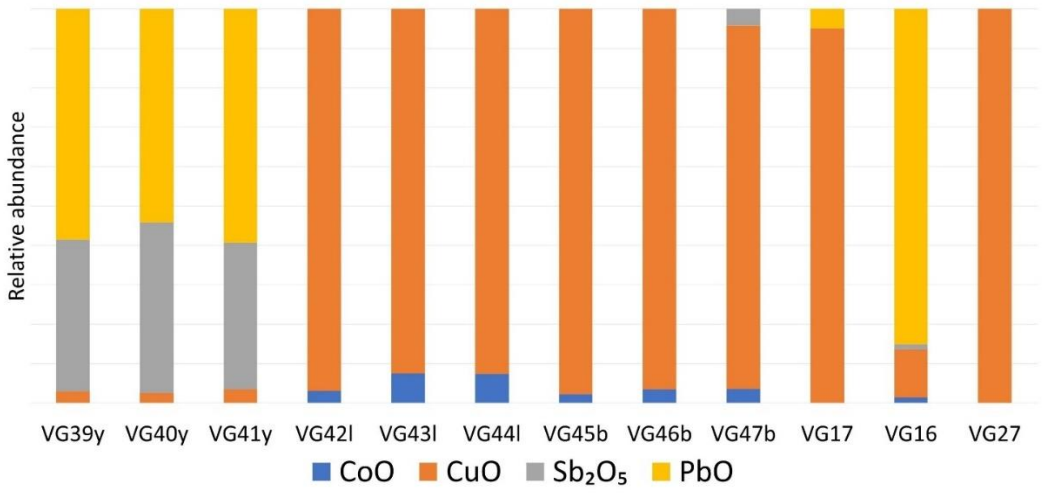

Figure 10.3. Relative abundance of certain oxides in the samples. "y" - yellow; "l" – light coloured; "b"- blue.

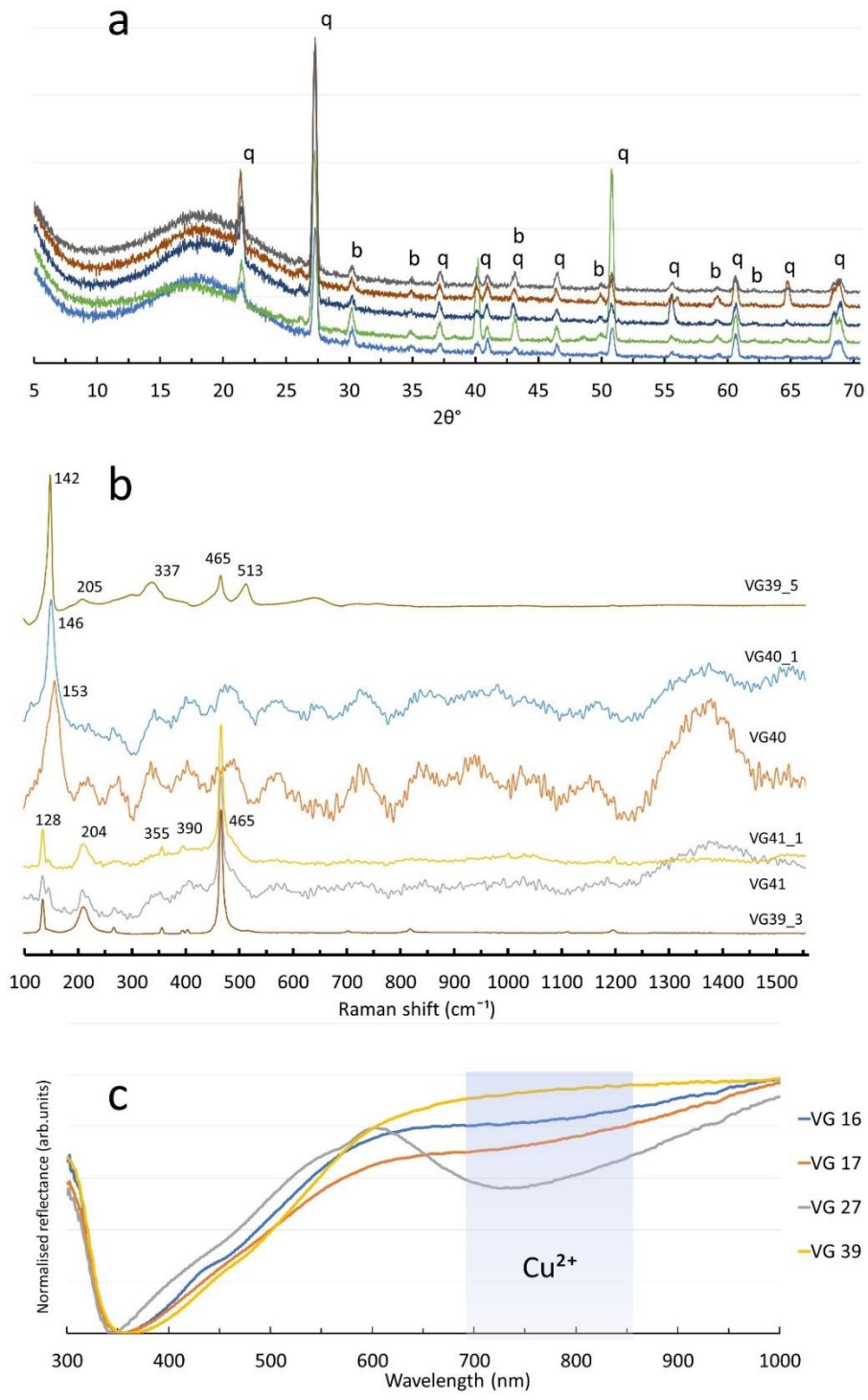

Figure 10.4. Structural analyses results: a - μ-XRD patterns of VG39 featuring quartz (q) and bindheimite (b); b - μ-Raman spectra of samples; c - selected FORS spectra.

VG17 is set aside within Group 9 because of its outstanding concentration of CaO – 46%. This sample seems to be made from different material, which might not be vitreous. This assumption is supported by the extremely low Fe_2O_3 concentration, that is bordering the LOQ and high SrO value that gives the CaO/SrO ratio of 217. Similarly to blue beads of the same Group, this sample contains 1.7% of CuO. Co was not detected in this sample, though.

The Other beads have slightly different composition from the majority of Group 9 samples. VG16 contains Fe, Cu and Pb in abundance (2.6, 1, 7.3% respectively). This sample appears to contain Co and Sb as well in nearly equal concentrations (0.11-0.12% weight oxide). VG27 has elevated levels of CuO but for the rest of the elements, the concentrations determined by p-XRF tend to be similar to the majority of the beads, or are below the LOQ.

LA-ICP-MS results are available only for two samples – VG39 and VG40. According to this type of analysis, which also presents rather bulk composition of the material, the main constituent of the beads is silica that accounts for more than 90% of total mass of the sample. Another major oxide is PbO (2-3 wt.%). The rest of the elements are present in minor or trace quantities (Appendix 7). The PbO/Sb_2O_5 ratio is bigger than the one observed in p-XRF data – 2.3 in VG39 and 5.2 in VG40. These samples have rather flat UCC normalised profiles. VG40 demonstrated positive Ce anomaly, both VG39 and VG40 have even bigger positive Tl anomaly.

µ-XRD analyses revealed the presence of quartz and bindheimite (hydrated form of lead antimonate $Pb_2Sb_2O_7$) as can be seen in Figure 10.4 (a). Diffractograms of VG39 that are present in the figure are representative of all analysed samples. Other diffractograms have lower intensity of peaks but those that are distinguishable are in the same 2θ° positions.

µ-Raman analyses yielded variable spectra of crystalline phases (Figure 10.4 b). Quartz signal is common among yellow beads of Group 9. It could be identified by the peaks at 128, 204, 355, 390, 465 cm^{-1} (Ricciardi et al. 2009). Bindheimite was also detected during Raman analyses in VG39. Spectra of samples VG40 feature only one peak with shifting Raman scattering peaks. This peak situated at 146-153 cm^{-1} can be also attributed to lead antimonate. Certain shifts of the main peak of bindheimite were observed for samples prepared in different way (Lahlil et al. 2011). On the other hand these peaks could be attributed to sporadic presence of anatase (Ricchiardi et al. 2009).

FORS did not yield many informative spectra. In fact, only three samples produced spectra with the more or less distinct band of Cu^{2+}, which is the only chromophore detected by FORS in these samples. It is a broad band in between 700 and 850 nm (Micheletti et al. 2020). This band was detected in VG16, VG17 and, is the most pronounced in VG27 (Figure 10.4 c). Spectrum of sample VG39 is inserted to demonstrate how the rest of the Group 9 samples were responding to the incident light beam. Samples tend to strongly reflect in the NIR and red part of the spectrum, while in the UV and blue part an absorption is usually observed.

10.3 Discussion of the results.

Due to the limitations of the compositional methods of analysis and the limited number of samples analysed in the most appropriate way (as a polished cross section), the obtained results cannot give a comprehensive material characterisation of this Group of samples. For the yellow variety of Group 9 samples some insight based on the information from the laboratory analyses was possible.

The outcomes of p-XRF analyses allow to assume some similarity among VG39-47 group of samples due to the similar concentrations of the elements not associated with possible colouring materials, namely, K, Ca, Mn and Fe (the two latter ones are known to be used as colourants but in the present case they are interpreted as unintentionally added elements). Of course, the set of the elements is very limited, therefore only major similarities can be possibly highlighted. Moreover, Sr concentrations were above the LOQ primarily for the light-coloured variety of Group 9 beads. The CaO/SrO ratio in these samples is from 47 to 59, which is different from the values observed in modern sea shells (Wedepohl et al. 2011). It can be assumed that Ca was entering into the bulk faience composition through a different material that contained more Sr than that of the rest of Group 9 samples, the other samples that contain measurable concentration of Sr have their CaO/SrO ratios at 106 (VG40), 126 (VG16) and 217 (VG17).

The blue and light-coloured varieties of Group 9 beads were probably prepared using similar colouring material. Yet the light-coloured objects demonstrate different CoO/CuO ratio – 0.06 in the blue ones and 0.03 in the lightly coloured ones. The amount of Co in blue samples is enough to cause the change of colour to turn the vitreous glaze blue (Smirniou and Rehren 2013; Gianini et al. 2017) but Co^{2+} bands were not detected in the FORS spectra. This might mean that the coordination of Co ions does not promote absorption of visible light. Its association with Ni and Zn in blue and partially in light coloured beads (in these beads Zn levels are below the LOQ) is an indicator of and Egyptian source of cobalt, as already discussed in Chapter 5. Cu^{2+} ions are assumed to be the only chromophore used for colouring of these samples. Cu is in lower concentration in light coloured beads, which might be suggestive of an intentional lower concentration in the pristine material or weathering of an originally more intensely coloured surface. Egyptian blue ($CaCuSi_4O_{10}$) can be excluded as the colouring substance because of the high CuO/CaO ratios in samples of blue variety (close to 5) and low CuO/CaO ratios in light coloured samples (close to 0.6), whereas the stoichiometric CuO/CaO ratio is 1.3. Moreover, this material would have strong absorption in the NIR region detectable by FORS (Accorsi et al. 2009). Unfortunately, it is impossible to make a further insight into the glaze composition of these samples based on just p-XRF and FORS data.

The yellow variety of Group 9 might belong to Type F by classification implemented by Lucas (1936). This type of Faience is prepared with lead glaze starting from second millennium BCE (Nicholson and Peltenburg 2000; Angelini et al. 2019). Only minor quantities of alkali were observed without any increase in the pristine surface of VG39's cross section. This recipe differs from the Ptolemaic time Egyptian alkali-lead glaze faience (Mao 2000). Major elements composition is similar to those found in Naucratis – ancient Greek trading post in the Nile delta (Meek et al. 2016). Colour of these beads was caused by the presence of lead antimonate ($Pb_2Sb_2O_7$) crystals that were detected by both μ-Raman and μ-XRD. This way of colouration was observed for other coeval or earlier examples of faience objects (Clark and Gibbs 1997; Middleton 2009; Meek et al. 2016). The PbO/Sb_2O_5 ratio is different than in the yellow beads that were discussed in Chapter 8, which means less excessive (if any at all) Pb was added to the mixture.

Beads VG39-47 were formed on the rod after mixing silica with colouring materials with addition of water. Certain type of flux would be needed in manufacturing blue and lightly coloured beads, but our limited data cannot clarify its nature. In yellow samples, the addition of Pb would also promote the development of liquid phases during firing, making it easier to partly fuse the material (Pollard and Heron 2015). There was no evident distinction observed in the cross section of VG39

between glaze, contact layer. The bead is slim (less than 2 mm wide) so these differences might not be very evident (similar situation was observed by Tite et al. (2007)). These beads could have been made by mixing quartz grains (and other sand constituents) with bindheimite without glazing the surface of the bead, so the material would be homogeneous all throughout. Beads were then formed on a rod that left an aperture and fired (Xia 2014).

VG17 appears to be made of Ca-based material and does not belong with the rest of Group 9 samples. Structural analysis (like XRD) could shed light onto the nature of the material. This bead is covered in Cu rich layer that induces blue colouration on outer side of the bead, which is evident from FORS and mainly from p-XRF analyses. As for the technique of production, the shape of the aperture can be of help. The bead could be made by pressing the raw material into the mould with the protrusion that was narrowing to the top. The inverted biconical shape of the aperture was finished by flipping the bead and pressing it again in the same mould with subsequent covering in the coloured, probably vitreous, material

VG16 is a sample of unclear nature. It has the highest Ca (except for VG17), Fe and Pb concentrations within the set (p-XRF data). It is the only sample for which both Co and Pb were detected in measurable quantities by p-XRF. At the same time, it exhibits a very weak band of Cu^{2+} in the FORS spectrum, that could be the cause of the initial blue colour. Unfortunately, it is not clear if the material is glass or faience. Forming around the mandrel seems to be a reasonable suggestion for the technique of production, as this sample is much thinner when compared to the other samples discussed in this chapter.

VG27 is a bead of large size. Unfortunately, only the colouring agent, which is Cu^{2+}, can be inferred by the analytical sessions. This bead could be made using the mould, but hand shaping cannot be excluded (Xia 2014).

Conclusion. Egyptian faience beads discussed in this chapter were all made by mixing quartz with a flux and the colouring compounds. Exceptions are VG17, which was made of some high-Ca material, and VG16, which nature needs to be clarified.

Copper was used for the blue-green colouring of the majority of objects. Co derived from an Egyptian source also was detected. The yellow variety of the beads was coloured by lead antimonate. Their composition corresponds to the coeval beads from Naucratis. Egyptian provenance can be tentatively suggested for the beads of Group 9. However, further characterisation of the materials in the laboratory on a more significant number of objects would be necessary to substantiate this hypothesis.

CHAPTER 11: GENERAL VIEW ON GLASS SUPPLY IN SOUTH ETRURIA AND LATIUM IN THE FIRST HALF OF THE FIRST MILLENNIUM BCE.

The objects discussed in this thesis represent many types of glass beads used in the first half of the first millennium BCE in South Etruria and Latium. These artefacts primarily reflect the content of the collections of the two museums that were involved in the project, the kind of beads and their quantity in the burials from archaeological sites. The collections of Museo Nazionale Etrusco di Villa Giulia and Museo delle Civiltà are crucial for studying the Iron Age in the region and cover some of the most important archaeological sites in the region. Returning to Chapter 3, the distribution of finds in space and time does not cover all South Etruria and Latium evenly. There are better and worse represented sites. If one takes a look at the chronological distribution of samples, it will become apparent that the Early Iron Age II period (800-720 BCE) is by far the best represented (by the number of beads and the diversity of contexts) within the set and conclusions drawn for this period benefit from the larger amount of data. At the same time, glass studied from the other periods of West-Central Italian protohistory is less represented, and conclusions regarding these samples must not be extrapolated (at least in a quantitative manner) on the entire period based on a smaller number of glasses. This being said, some thoughts must be voiced to conclude the discussion within this work, and they deal precisely with the chronology and spatial distribution of the groups of objects discussed in Chapters 5-10.

11.1. On the glass compositional types.

Chapter 3 (section 3.4.1) gave an overview of the chronological distribution of the typological groups of samples (Figure 3.17). It became apparent then that the different groups were not continuously represented in the sets of grave goods throughout all the studied periods. In Chapters 5 to 10, it was demonstrated that almost every group of beads was produced using a specific fluxing agent, which led to the assignment of each group to a specific compositional glass type: with a few exceptions, all samples within a specific group were assigned either to LMG, HMG or LMHK glasses. For several groups, there is a division of samples by the use of the fluxing agents. This section will highlight any spatial, chronological, or other contextual differences among the broad set of the discussed objects.

To start this discussion, it would be helpful to recap which, among the extended set of samples, were assigned to each compositional group of glass.

LMG is the most represented compositional group. It is made out of typological Groups 1 (small blue ring eye beads), 2 (medium blue ring eye beads), 6 (small yellow ring beads), part of type 7 (small blue ring beads, low-K sub-Group), type 8 (small black beads), part of type 10 (large translucent beads, particularly yellow variety), 11 (translucent beads with rib decoration), 13 (tubular beads), 15 (small beads with wave decoration), 16 (large black beads), 17 (large opaque yellow beads) and 18 (pear-shaped or spindle whorl beads). On top of this set, most of the Other beads and Non-beads can be counted in this glass type.

Far fewer samples were assigned to the HMG type. They consist of representatives of types 4 (green eye beads), 5 (small translucent beads), and some of the beads from type 10 (primarily green

and colourless varieties). Several more samples can be counted as HMG: bird beads, bodies of the blue fibulae bows, pin head PG135, double bead VG56 and the bowl fragment VG114.

Only 12 objects could be assigned to the LMHK glass: all the samples in type 3 (large horned eye beads), the high-K sub-Group in type 7 (small blue ring beads) and samples in type 12 (barrel beads with spiral decoration).

Figure 11.1 presents the chronological distribution of the analysed beads (Group 9, Other beads and Non-beads excluded) according to glass type.

LMG seem to be the most abundant compositional "family" throughout all the periods included in this research. This conclusion is, of course, made on the beads available for analysis. In the EIAI period, LMG showed the least convincing majority (12 out of 22 objects considered). Only one object of HMG appeared among the beads of EIAI. The number of LMHK glasses is relatively higher than in the other periods (9 objects out of 22). However, these numbers cannot represent the entire region (LMHK glasses, for example, come from very few contexts – *"Tomba dei Bronzetti Sardi"*, Acciaierie necropolis near Terni, and two Latial burials). The numbers agree with the generally accepted view that LMG was gradually substituting HMG (and in the case of Italian territory, also LMHK glass) starting from the 10th century BCE in the Mediterranean (Shortland et al. 2006; Dardeniz 2015; Conte et al. 2019). LMG is the most abundant type of glass in the subsequent periods. Instead, LMHK glass has almost disappeared in the EIAII, and only three objects were attested out of the 133 considered here from that period. HMG glass is actually better represented in EIAII and Orientalising period.

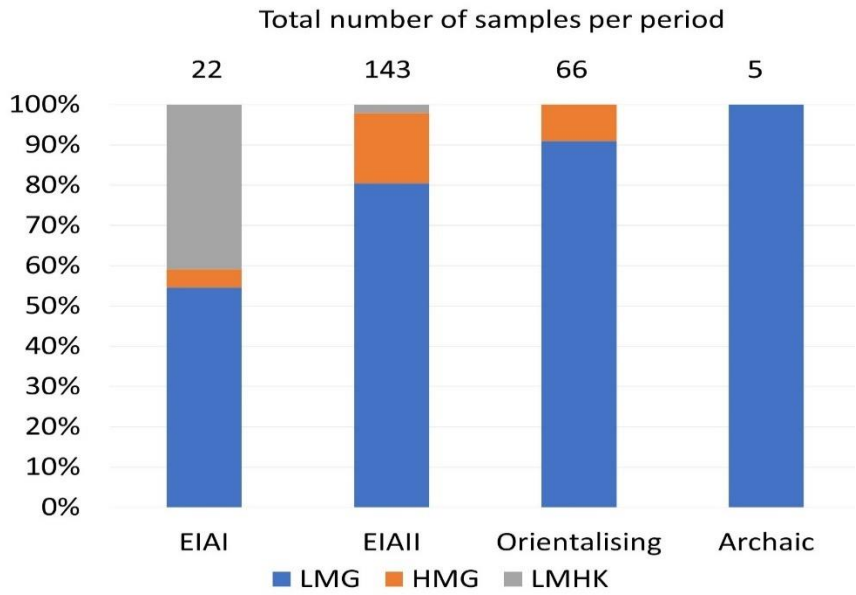

Figure 11.1. Distribution in time of the main compositional groups considered in this study. Only data from major Groups (1-18 except the 9 (faience)) are considered.

Objects from contexts in South Etruria and Latium indicated that HMG was not a popular choice for bead-making in the first half of the first millennium BCE, though its presence is traced throughout all the periods discussed. One shall remember that the attribution to HMG was obtained for some samples relying, among other evidence, on p-XRF data for K content. The elemental data showed, in fact, that it was reasonable to assume a correspondence between a larger set of samples featuring high K concentration with the smaller number of samples attributed to HMG based on LA-ICP-MS data. This might entail some errors in the final number of samples assigned to HMG, which is valid for the other compositional types. This is especially true for the Group 10 samples, which were divided into HMG and LMG based on their K content since no data on Mg were available for many samples. A detailed discussion on this topic can be found in Chapter 7.

The LMHK glass is usually found in LBA contexts (Brill 1992; Towle et al. 2001; Bellintani and Angelini 2020). This composition's highest density of finds is in the area of the Frattesina site, where evidence of glass-working was found. The archaeological records indicated that the site was in severe decline by the beginning of the Iron Age (Bietti-Sestieri et al. 2015). Incidentally, the frequency of LMHK finds in the Iron Age falls dramatically, though they are still found in archaeological contexts dated as late as the 7th century BCE (Henderson 1988). Within this frame, remarkable is the chronological evolution that occurred within Group 7. The high-K (LMHK) beads belong to EIAI, while the low-K (LMG) beads to EIAII and later periods. In this way, the occurrences of LMHK glass in the archaeological context can be viewed as evidence of the use of objects made significantly before they reached the tombs in which the archaeologists recovered them. More precisely, in the context of the *Tomba dei Bronzetti Sardi,* dated to the third quarter of the 9th century BCE (Arancio et al. 2010), the use of the set of beads (6 objects of Groups 3, 7 and 12) could have been well longer than a century. In the case of the horned eye beads (Group 3) found in a Latial tomb dated to the middle of the 8th century BCE (Mengarelli and Savignoni 1903; Gierow 1964; Bietti Sestieri 1992), the use of the beads should have lasted for some two centuries. The mentioned examples demonstrate that these objects were found in South Etruria, Latium and Umbria (in the case of Terni LMHK beads) without evidence of concentration in a specific place.

The HMG objects make a diverse and exciting list despite their small number (32 beads within Groups 1-18 and probably at least ten objects within the Other beads and Non-beads group mentioned at the beginning of this section). All the beads of Group 4 discussed in this work originated from the territory of Latium. They were primarily noted in EIAII contexts, as most of the HMG glasses. Aggregated data allow us to distinguish at least two types of HMG by their K concentrations. Group 4 samples and most of the Other and Non-beads made of HMG (bodies of blue fibulae, vessel fragment, double beads and bird beads) tend to have more K than the rest of the HMG and are closer to plant ash glasses found in LBA and IA contexts in the Eastern Mediterranean (Reade et al. 2009; Walton et al. 2012; Zacharias et al. 2018). Another group of samples, mainly consisting of translucent glasses (Groups 5 and 10), sometimes contained less than 1% of K_2O, with considerably higher MgO concentrations. Plant ash of different compositions, which would mean different choices of plants and/or processing, would have been employed when making those glasses. These beads also demonstrate distinct trace element profiles that point to a different provenance. More on the topic of provenance will be presented in section 11.3.

Translucent glasses truly appear only in the EIAII period (translucency score three or higher). They are both LMG and HMG without evident chronological or spatial speciation; they were spread throughout South Etruria and Latium.

The fibula bows (Non-beads) apparently were made from three different glasses. The blue fibulae bodies were made with HMG, but their decorations seem to be LMG. The black-appearing glass of four other samples was LMG. As discussed in Chapters 2 and 3, these objects were made on the Italian peninsula based on some archaeological evidence. On the other hand, compositional data revealed that the glass itself was not produced on the same spot, as two different raw glasses were employed to obtain the fibula bow. This evidence indicates that the workshop(s) that produced the objects were collecting glass (at least partially) from elsewhere. This entails the differentiation of primary and secondary workshops also in the Iron Age. The vessel fragment VG114 is similar to the HMG composition of the other hemispherical bowls of the Iron Age (Reade et al. 2009a).

As for the bird beads (PG172 and VG88), which were also obtained by assembling two differently coloured glasses, it was apparent that both of them were HMG, at least by the K and Ca contents, as they were not analysed in the laboratory. They were probably made in the same workshop out of differently coloured glass that nevertheless contained minor content of copper. These beads are somewhat compositionally different from the beads of Group 4 (green eye beads) and from other HMG translucent glasses (Groups 5 and 10), as indicated by their Ca, Ti and Sr content. As these beads are frequently found on Rhodes, it was suggested that the ones found in Italy might also be from there (Koch 2018b). Indeed, coeval HMG glasses from Rhodes (Oikonomou et al. 2012) match closely with the bird beads from this study by their (K, Ca, Fe and Sr content) which might suggest their similar provenance. A more targeted study could bring more clarity to the discussion.

LMG was produced in the 10th century BCE in either Egypt or Mesopotamia (Shortland et al. 2006b; Kaparou and Oikonomou 2022). The oldest LMG glasses found in Central Italy date to the 9th century BCE and appear as the dark-coloured beads from Latium, frequently reported in Osteria dell'Osa necropolis. They indeed proved to be LMG, as suggested by visual comparison with the other pieces analysed elsewhere (Koch 2018a). Most of the LMG samples analysed in this study were dated to EIAII and subsequent periods. When only three principal oxides for LMG are concerned (SiO2, Na2O and CaO), the base glass composition appears relatively uniform (Figure 11.2).

Regardless of their compositional group, most samples have a similar base glass if the reduced composition is considered: 70-80% SiO_2, 15-25% Na_2O and 2-8% CaO. The only noticeable differences are in the seemingly higher average content of Na_2O and lower SiO_2 in Group 1 samples (due to several outliers) and Group 6 with lower N_2O and higher SiO_2. These Groups consist of Co and $Pb_2Sb_2O_7$ coloured glasses, respectively. Colouring materials, as discussed in Chapters 5 and 8, respectively, introduce a significant share of other elements by mass. Heavily coloured dark Groups (high Fe content) seem to have less Ca and more Na than translucent glasses. Perhaps the batch formula was adjusted to address these challenges and ensure the total fusion of the mixture, though discrimination between these Groups is very weak. Another possibility is that partial fusion of the heavy-coloured glass batches occurred (Rehren 2000). Only the fused part of the batch (with more or less standardised composition of the principal oxides) was given further processing and used in bead making.

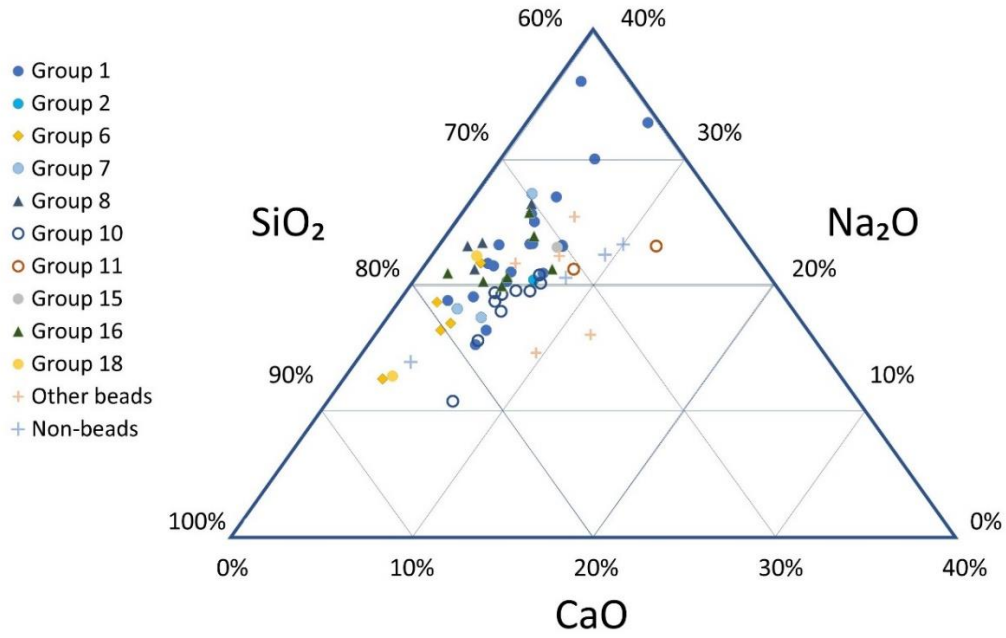

Figure 11.2. Tri-plot of major oxides including data of LMG samples obtained with LA-ICP-MS. Groups 7 and 10 are represented partially because they also contain HMG and LMHK glasses that were excluded from the plot.

Several sources of CaO were mentioned in the discussion of data in Chapters 5-9. For the HMG and LMHK glasses, lime could be assumed to come mainly from the ash, although some Ca can also enter the batch with the source of silica (as naturally present shell fragments). In the dark glasses, the sources of Ca might have a geological origin, such as dolomite or plagioclase feldspars, depending on the sample, but without strict typological division. This was established on the basis of correlation and ratios of Ca, Al, Mg and CaO/SrO ratios (Chapter 9). Most of the LMG glasses seem to contain Ca from shells, as evidenced by their CaO/SrO correlations and ratios (Wedepohl et al. 2011).

Concentrations of lime are the most scattered among the three primary LMG components (Figure 11.2). Samples that belong to the Archaic period tend to have a higher quantity of CaO (for example, the glass buttons or samples of Group 14 discussed in Chapter 5 (not included in Figure 11.2 due to the lack of LA-ICP-MS data). 7-10% of CaO observed in those samples is the range of values that is closer to LMG in some of the Archaic and Hellenistic glasses (Reade et al. 2009a; Arletti et al. 2011; Panighello et al. 2012; Oikonomou et al. 2018; Venclová et al. 2018).

As for the glass buttons, it is worth noting that, despite compositional differences for the elements that give colour, their base glass composition determined with p-XRF is similar. It can be suggested (without having a “full” composition) that the primary glass for this set of objects was produced in the same workshop. Since all of these objects ended up in the same grave and have similar compositional traits, it is likely that the colouring was done in the same place too. Whether or not the place for these processes was the same, it is difficult to say.

Already-mentioned Figure 3.17 also highlighted that a significant shift in the set of types of glass beads consumption occurred in the middle of the 8th century BCE. On the basis of the studied collections, it is apparent that EIA was the time when the most popular types of glass beads were those comprising Groups 1, 8, 10 (low-K ones) and 16 composed of LMG, Groups 3, 7 (high-K sub-Group) and 12 composed of LMHK glass and Groups 4, 5, 10 (high-K ones). At the end of the EIAII, new types of beads started to occur; they were mostly LMG and belonged to Groups 2, 6, 7 (low K-sub-Group), 10 (low K ones), 13, 14, 15, 17 and 18; HMG is represented only by some beads of Group 10. These new types reflect the establishment of ever-broader trade with the Eastern Mediterranean (Graham 1999; D'Ercole 2017). The selection of Latial contexts does not allow for gathering a good picture of the diversity of glass beads in the Orientalising period. Within this work, only the Marino contexts allow this insight for Latium. So, most of the Orientalising beads in this work are from South Etruria. Since the appearance (i.e. the type) of the beads changes simultaneously with the type of glass (with the notable exception of Group 10 large translucent beads), one can argue that the ideas or fashion from the East started to spread before the beginnings of the Orientalising period (ca 730 BCE), with glass being one of the first commodities to make this path. This conclusion is reached on the assumption that funerary contexts present contemporary trends in "fashion". However, we cannot exclude that the offerings were related to the trends that existed during the life of the buried individual.

The simultaneous occurrence of several compositional types of glass in the Early Iron Age periods leads to the assumption of several supply sources. The fact that the compositionally different glasses are, as a rule, grouped also typologically supports the picture of many workshops, each making a specific type of glass and specific type(s) of beads. It appears likely that a specific type of glass was produced and worked into beads and other objects in a single workshop. A notable exception is the fibula bows, which were documented as local "Etruscan" glass working and the beads in Groups 7 and 10. Group 7, sub-Groups are divided in time and can be discriminated by somewhat different shades. The specialisation of workshops and, perhaps, their different geographic location would entail a choice of specific raw materials other than fluxes by the workshops, so it is important to see if this is the case.

11.2. On the colourants and opacifiers.

The diversity of glass appearance was explained with details according to bead groups in Chapters 5-9 (Chapter 10 dealt with the colourants for the faience objects). This section gives a broader look at the region in general, focussing on chronological changes that emerged in the analysed materials due to the use of different colouring mechanisms.

Cobalt-coloured beads and other blue objects make up a large part of the sample set. Most of the blue objects were discussed in Chapter 5. Deep blue cobalt colouration of glass was very appreciated in ancient societies since the LBA, up to the restrictions of production and use (Barag 2009; Hodgkinson 2019; Schenkel 2019). The discussion of this colourant's source revealed interesting, although partially expected, results. In LMHK glasses, Co is associated with Ni and As, which indicates a separate provenance for the cobalt source, confirming data that other researchers previously obtained (Towle et al. 2001).

In the majority of LMG, Co is associated with much higher quantities of Al and Mg and comparable quantities of Ni and Zn, which was already recognised as a sign of Egyptian provenance of the colourant (Abe et al. 2012). These glasses include Group 1, which comes mainly from EIAII period contexts. This period corresponds in Egypt to a period known as the Third Intermediate Period (1085-715 BCE), which is characterised by the diminishing of glass and faience production compared to LBA, up to the disappearance of the evidence for Co coloured glass and faience production (Nicholson and Peltenburg 2000; Reade 2021 and references therein). Nevertheless, some Co-coloured glasses in the wider Mediterranean, dated to the 9th-8th centuries BCE, contained Egyptian Co (Gratuze and Picon 2005; Conte et al. 2016; Reade 2021), including the Group 1 ones. An alternative place of production could be Nimrud (Reade 2021). This would imply that raw materials such as natron and cobaltiferous alum were transported long distances before being turned into glass. Unfortunately, it is difficult to establish the provenance of the silica source in these glasses on a compositional basis because of the impact of the colouring material on the distribution of mid-REE. However, for the land of Central Italy, this means the long-range trade of glass existed as early as the 9th century BCE (one single bead is dated to EIAI in this study, but more examples are known). It was more intense in the EIAII and following periods.

In the Archaic period, a new source of the Co colourant appeared, and in Group 14, buttons and bracelets from this period might have been coloured with Co from a different, yet undetermined, source. Remarkably, no Co-coloured glasses were found among the samples assigned to HMG. It may mean that HMG makers did not have access to this colourant or could not make Co-coloured objects, though the number of objects assigned to HMG is too small to assume robust conclusions on this point.

The transition of the Co sources can be summarised as follows:

- FBA: use of a European Co source in the production of LMHK glasses;
- EIA: Egyptian Co coloured glass entered Central Italy and remained as the only Co source until the Archaic period;
- Archaic period: glasses were coloured with Co from another undetermined source.

Cu-coloured glasses sometimes also happened to contain Co. This is the case for both LMHK and LMG. In the latter ones, Co concentrations are low, meaning glass recycling or "conditioning" of the glass colour to obtain a colour similar to the Co-blue glass (examples from Groups 1 and 2). The association of Cu with Mn in some glasses remains unexplained.

Cu is the choice of blue-green colourant for the HMG. Particularly interesting is its use for colouring the samples of Group 4, as discussed in Chapter 6. In this case, Cu^{2+} and Fe^{3+} adsorb light to create green glass, and fine bubbles inside the glass matrix lead to the opacification effect. The contribution of bubbles to opacification is reported in archaeological glass from later periods (Mirti et al. 2002), and it is possible that the presence of bubbles was not intentional. Local, small-scale production was suggested for these samples, for which it is possible to assume that refining of glass at high temperature in the furnace was not accomplished thoroughly (low temperature or short time, or both), and bubbles did not escape the viscous glass mass (Zhou et al. 2019). The heterogeneous distribution of the bubbles was noted, thus supporting the hypothesis that this could be some "experimental" glass.

The translucent Cu-coloured glasses are much more homogeneous (in terms of structure). Among those, LMG (Groups 11, 13 and some of Group 10 samples) and HMG (Group 5, some of the

10 and blue fibula bows) were recognised on compositional bases. It was difficult to trace the origin of the raw material used for the colourant introduction. The possible use of bronze was examined, although the Cu/Sn ratio would exclude that bronze was systematically used as the source of copper. Cu, however, was found as an impurity in the lead antimonate mixture added to the glass, although its presence did not show any evident influence on the colour of the opaque yellow samples. No evident chronological distribution emerged regarding the composition of a possible Cu source and the abundance of Cu itself among Cu-coloured glasses. Most of the samples discussed belong to the EIA period, but this can be a consequence of the fact that EIA is better represented in the total number of samples.

Fe-coloured glasses exhibit a broad spectrum of hues. Among the translucent ones, the specialisation of workshops is evident for the green variety of samples of Group 10 and for the small translucent rings from Group 5 (all are likely HMG). However, they do not have any chronological speciation, being found from EIAII to the Orientalising period. In general, no chronological or geographical discrimination emerged for the translucent glasses from Group 10 since they started to appear in the EIAII (Chapter 7).

The hues of lightly coloured samples totally depend on the redox conditions inside the furnace, and different hues were obtained through the technological process rather than by the selection of specific raw materials. Sb was often detected in the green variety of beads. Its use for glass decolourising was documented in Roman times (Jackson 2005; Silvestri et al. 2008). It was also used for this purpose starting from the 7th century BCE (Biron and Chopinet 2013; Abd-Allah 2022).

Some glasses investigated in this work showed an Sb_2O_5 content of up to 1%, and they were found as early as the EIAII period. This might be one of the earliest examples of Sb decolourised glass encountered so far. The fact that these samples are seldom assigned to clear glasses, for the present case, might mean unintentional Sb presence. This is quite unlikely, as Sb is not abundant in the Earth's crust (Degryse et al. 2020); we shall therefore consider its addition for refining purposes (Möncke et al. 2014; Singkiburin et al. 2020). This could be the case for the green beads with minor Sb content.

The melon beads (Group 11) and pendants with similar decoration all come from the Orientalising period contexts though such shapes were known from LBA (Kaparou and Oikonomou 2022).

As for the black-appearing glass (Groups 8 and 16 mostly, Chapter 9), similar glasses with a consistent way of colouration (at least similar Fe and, possibly, related elements concentrations) were found in Eastern Mediterranean. The direction of trade is likely to be from East to West (more on this in the next section), so it means that glass arrived in Latium (the predominant area of occurrence of such glasses in this work) already coloured, if not in the form of already made beads.

Mn-coloured glass is scarce in the discussed contexts. Only three samples from EIAII Latium were coloured purple. These are the early examples of Mn-coloured glass in the region, though such glasses were also reported in the LBA (Shortland 2002; Arletti et al. 2008; Kemp et al. 2022). Interestingly, all these samples were HMG.

Opaque glasses were used to make the whole beads or their decorative elements. They also appear to spread in South Etruria and Latium throughout the discussed periods. The opaque glass was exclusively LMG (Chapter 8 for the high Pb beads like Group 6, for example) except for the decorative elements in LMHK glasses that were produced differently (Chapter 6). It is challenging to assess the similarity of Group 6 and 17 samples with the decorative elements of Groups 2, 4, 14, 15,

18, and Other beads and Non-beads due to the semi-quantitative nature of the data that were collected on these decorative elements. Nevertheless, considering the probable bias determined in the data from the opaque decorations by the base glass, it is reasonable to assume that the apparent compositions of the yellow decorations would be similar to those of beads in Groups 6 and 17. Given the established theory that this glass was used in the forming of Fibula bows and Group 4 beads (probably made locally), one can suggest that the place of production of Group 6 beads could be located in Central Italy.

The samples of Group 6 originate mainly from Veian contexts, just like some of the fibula bows. Therefore, it would be reasonable to suggest that a glass-working workshop was located in that area, and it was active from the end of EIAII to the Early Orientalising period using imported opaque yellow glass. In the Archaic period, the composition of the opaque yellow glass changed, as can be demonstrated by the data on glass buttons, which were excavated from a tomb in the same area.

If the glass type is considered, the following picture emerges for glass colour:

· LMHK glasses were coloured by Cu, Fe, Co (from a European source) and a crystalline opacifier (or bubbles) composed of light elements (for the white decorations);

· for HMG: Cu, Fe and Mn;

· for LMG: Co (Egyptian source), Cu, Fe, $CaSb_2O_6$ and $Pb_2Sb_2O_7$ micro-crystals dispersed in the glass matrix.

This further substantiates the hypothesis that glass was already coloured on its arrival in Etruria and Latium. On the other hand, besides several specific cases, compositional data could not help to clarify whether the glass arrived as chunks of raw glass to be shaped in Italy or if the finished objects were imported.

11.3. On the origin and trade of glass.

The quest of provenance was intentionally put in the end (unlike in Chapters 5-9, where it opened the discussion on the compositional data) to demonstrate that different origin of glass in the Iron Age contexts can be inferred by considering all the compositional information, from fluxing and silica sources to the colour palette of the objects. Most of the provenance discussion in those chapters was based on the trace elements data, particularly REE. It is beneficial to consider all the different groups of objects, as they were not compared in the previous chapters of this thesis.

Figure 11.3 shows such a comparison based on average values of previously-determined groups of samples. Samples with unique trace element patterns (i.e. outliers) were not included, although they also contributed to the knowledge of the distribution of glass production in the Mediterranean. For example, a connection to the glasses recovered in Sardis was highlighted in Chapter 9 (Group 18), and one sample of LMMK composition (with the corresponding trace elements profile) was initially set among Group 10 discussed in Chapter 7. These examples demonstrate the diversity of compositions encountered among the finds from Central Italy. However, some compositional profiles occur more frequently and are considered here as representative of a specific type of object.

Groups 1 and 2 have profiles that were probably affected by the intake of Co-bearing alum in the batch, as discussed in Chapter 5 (Walton et al. 2009; Hodgkinson and Frick 2020). This is the only evident case of colourant influence on the REE pattern within the set. Even though REE do not reflect

their content in silica material, the origin of at least one component is known – Egypt. Whether or not such glass was produced in Egypt or Assyria (as discussed above), this would mean it was imported to Central Italy. Many parallels were found for these glasses in the Iron Age (Gratuze and Picon 2005; Conte et al. 2016; Reade 2021), and the fact that Egyptian Co-coloured objects are among the best-represented kinds within this study makes an argument that this production was relatively substantial and established for some time, or at least that it continued in the Orientalising period. The Nimrud origin of glass is supported by the presence of Co-Cu coloured glasses with (relatively) high Mn concentrations. If this can be taken, as pure speculation, as the search for an alternative way to colour glass in the circumstances of the eventual limited supply from Egypt. Further analyses of similar glasses in the future should consider this possibility.

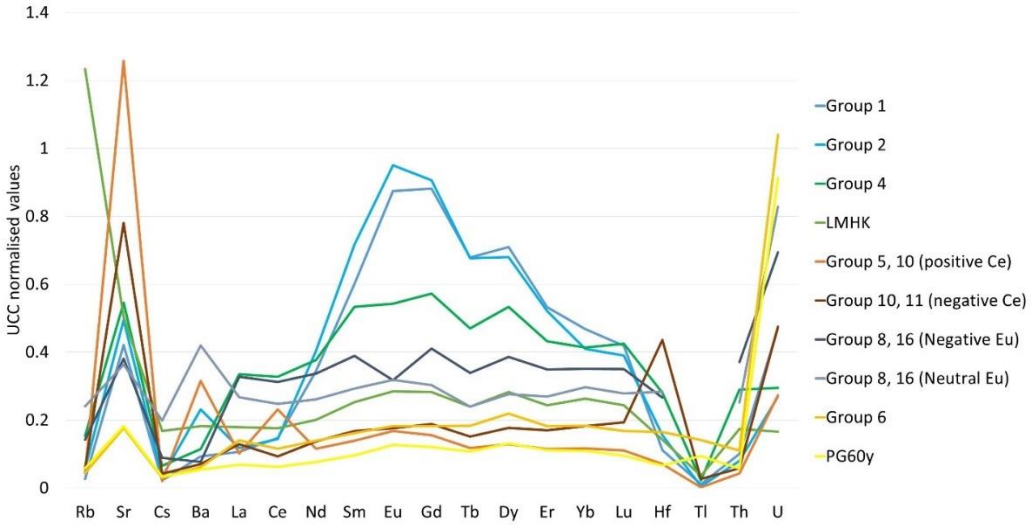

Figure 11.3. UCC normalised (values of McLennan 2001) average values of some groups of glasses that were analysed with LA-ICP-MS and mentioned in previous chapters. Samples with unique trace elements patterns were omitted.

LMHK glasses were assumed to be produced in the Po Valley (Towle et al. 2001). In Chapter 6, it was argued (by the absence of foreign parallels and similarity in Si-related trace elements with the supposedly local LMHK glasses) that Group 4 glass was made locally. Such a hypothesis stimulates several notions. First, the LMHK tradition was not revived, meaning artisans might not know about that technology. Second, the artisans used glass-making technology borrowed from the Near East and Egypt and known from the LBA. This means that the knowledge and the know-how had to travel somehow to be applied in the local circumstances, so artisans (local or foreign) probably travelled to distant lands. Halophytic plants are abundant on the Italian coasts, whereas mineral deposits of high-alkali carbonates were not known; therefore, raw materials for producing HMG are available in Italy, but not so much for the flux for LMG. As said in Chapter 2, Etruscans knew glass-working, metallurgy and other heat processes; therefore, it is not strange that they could have produced their own glass. The REE concentrations difference of Group 4 glass with LMHK can be explained by the use of less pure sources of silica. It is still reasonable to assume, on a compositional basis, that the silica source

has the same origin as the one employed for LMHK glass, assuming that the trace element differences (Rb, Sr, Ba) could be attributed to the different flux sources.

Another peculiar Group of HMG is the one with a positive Ce anomaly and a relatively high Ba content. In this case, it is challenging to suggest local production because the trace elements profile is not similar to that of "local" LMHK glasses. Nevertheless, it could not be excluded that sand with variable trace elements content can be found in different parts of Italy (Brems and Degryse 2014).

The high Ce and Ba glasses were found only in the EIA contexts, mixed with other objects of the same Group but with LMG composition and high Hf content. On the other hand, some HMG from the translucent groups does not show the same high Ce and Ba profile. They fall into the category of those intermediate glasses that do not have pronounced trace element content (apart from Sr, although this element is among the minor elements). Keeping all this information together, it emerged that HMG was produced in at least three different workshops: the one presumably on the Italian peninsula, another perhaps in the Levant (as discussed in Chapter 7) and the third one without regional association so far. More examples of such glass should be identified elsewhere to gather more information leading to some suggestions on their provenance.

Some LMG glasses tend to have higher Zr(Hf) values, and their trace element profiles are consistent with Egyptian glasses (part of Groups 10 and 11). Zr(Hf) content is believed to be higher in sands from Egypt than in Mesopotamia (Shortland et al. 2007).

Black-appearing glass could mainly be attributed to two primary workshops that probably were both in the Near East, with parallels with glasses from Pella (Reade 2021) and Levantine glass from Greece (Blomme et al. 2017). Both workshops were using less (if any at all) raw materials for stabilisation. It is likely that lime (a major stabilising component) entered the batch with the source of silica. Both workshops coloured glass in the same way. No connection of higher relative abundance of the REE was found with the colourant (Fe), which excludes the use of specific high Fe sands with abundant heavy minerals fraction were used. Instead, a more chemically pure source of Fe is proposed for these beads.

Lastly, to demonstrate the similarity among the high Pb opaque yellow beads and decorative elements on other beads, the mean Group 6 trace element profile and the fibula decoration were compared in Figure 11.3. Their profiles appear to be very similar, from which a conclusion can be drawn that these glasses are from the same source and that source is related to that of the intermediate beads of Group 10, if the relative abundance of the REE is considered.

As a general picture, it was noted that the bulk of the glasses (mainly LMG) was imported from the Eastern Mediterranean. This agrees with the generally accepted vision of the main glass-producing regions at the time (Rehren and Freestone 2015; Reade 2021). The present work adds some details to this general picture, such as the division among the several workshops that were operating to supply glass to South Etruria and Latium.

For the LMG, at least five different types of sands (probably from the same number of different localities) were identified. This number does not include the silica source for the glasses coloured with Egyptian cobalt. There is no sharp boundary for the time during which these workshops were active. They seem to operate more or less contemporarily, using specialised colourants. It is also reasonable to conclude that in the Archaic period, glass buttons and other objects were made using different batch formulas and were probably, made in a different place.

The LMHK glasses are unusual in the EIA contexts and consistent with the FBA compositions, so those beads should be taken not as a continuation of the production but as relics of previous production.

For the HMG glass, at least three main producing regions were supplying glass to South Etruria and Latium during the EIA (on a small scale). The instances of HMG occurrences in the Orientalising contexts are scarce, although small-scale local HMG glass production cannot be excluded. HMG glasses have different trace element profiles and also differ by colourant in terms of quantity and quality of the colouring species. It is unlikely that a workshop in the same place changed its production from plant ash to natron glass at some point in time, as there is no evidence of HMG and LMG glasses within objects of the same type (except the most generic shapes of objects).

The glass industry of the Iron Age in the Mediterranean seems to be decentralised. South Etruria and Latium benefited from long-distance trade with the Eastern Mediterranean on account of glass supply. LMG glasses entered these lands in large numbers soon after the technology was established, which must mean the existence of long-distance trade networks even in the EIAI period. Local glass-working and, perhaps, small-scale raw glass production occurred in the EIAII and the Orientalising period. Glasses from the Archaic period appear to be different from the earlier examples. Such compositional change is also reflected in the typology of the objects, giving a material representation of the development of glass technology in later periods.

CONCLUSIONS AND FUTURE WORK.

The study of glass objects (mostly beads) from the South Etruria and Latium dated to the first half of the first millennium BCE was conducted in three stages. During the first one, the archaeological context of the finds was studied, and extensive documentation was undertaken to "measure the appearance" of glass beads. In the documentation framework, several variables related to the shape, size, colour and translucency of beads and the presence of any decoration were measured in the standardised way presented in detail within this thesis. Some aspects of the process and/or criteria for describing the beads can be used in other glass beads studies. The ability to fully link the analytical information about the glass to the appearance of the final objects was paramount throughout this study.

The second stage was the application of non-invasive analytical methods in the museum setting with the use of portable equipment. This was done to make a broad coverage of objects. Particularly interesting and methodologically challenging was the use of the data from three different p-XRF units in the same frame of reference. Although the procedure is laborious, we demonstrated that obtaining quantitative data of acceptable accuracy and reproducibility is possible. The way of data treatment allowed to fully exploit the potential of the analysis. The initial non-invasive screening was used to identify compositionally similar glasses in order to select representative samples for the laboratory study (stage 3). It was also evident that differently coloured glasses posed quantification challenges, which partially determined the structure of the presentation of the results.

A smaller number of samples was allowed to be transported and studied in the laboratory. After the analyses were finished for these beads and other objects, there were several compositional blocks of data (from p-XRF, SEM-EDS and LA-ICP-MS) and structural ones (FORS, μ-Raman, μ-XRD) were available for these artefacts. Strictly micro-invasive protocols were implemented so that the beads could keep their integrity. Data from several sources were compared, and more robust conclusions could be drawn on their basis.

The data were used to make an insight into the glass technology and supply in South Etruria and Latium during the Iron Age. The outcomes of the study in this regard are largely defined in Chapter 11, and only a short summary is presented here to highlight the most relevant points.

Glass found in predominantly EIAII (800-720 BCE) burials appeared chemically comparable with other examples of glass found in the Mediterranean from the broader period (FBA – Archaic period). Glass production presents itself as decentralised. High Silica raw materials from several origins were used to make glass in several ways that were known for the time. In some instances, a region of provenance could be suggested. Glasses produced in Egypt, the Levant and the Italian peninsula were identified. However, these conclusions should be taken cautiously in the absence of actual glass-making evidence and large-scale provenance screenings.

Several sources of fluxing compounds were identified. Glasses made with mineral flux (LMG) are dominant within the set. In many cases, a flux source could also be suggested for samples not studied in the laboratory through their link with the representative samples that underwent a complete set of analyses. It was noted that glasses prepared with specific flux also originated from different places of glass production. The data support the view that there were several regions of

glass-making, each of whom had a special glass-making "tradition". Remarkable is the limited use of the stabiliser in the earliest LMG. This can be interpreted as a period of soda-silica glasses that were stabilised by compounds other than lime from the shell or calcareous rocks. The stabilising components in colourant-related material or a mineral source could be naturally mixed with silica.

Locally made glasses were noted on the base of the compositional similarity to the Italian glass and to glasses of another compositional group identified as a local attempt at glass-making. These samples do not comprise a large share of the samples considered in this research, but their compositional features are the most fascinating.

Each glass-making workshop, and this is true for both imported and locally made glasses, had produced glass of particular colour and perhaps beads were made on the glass-making site. This further supports the decentralised production view of the glass industry in the Iron Age. Nevertheless, local glass-working was also attested, so the beads could have been made closer to the places of deposition.

Based on the abovesaid, we can conclude that the selected methodology allowed to achieve the depth of insight that was needed to answer research questions of the study. Glass supply and glass-making technology in two small regions on the Italian peninsula – South Etruria and Latium, was investigated and the primary raw materials, colourants/opacifiers were identified. When compared in terms of the glass found there, these regions are not opposing each other though certain regional differences were noted. This comparison is limited by the representativity issues highlighted in Chapter 11.

This study is scalable, and widening the scope of the materials can be beneficial to check/supplement/compare the data presented within this thesis. Among the directions of further research, some targeted studies can be suggested. For example, isotopic ratio analyses of previously identified provenance groups could bring more clarity to the questions of sample attribution and relations among the workshops. Local glass production could be further explored by involving some geological materials in the discussion. Colourants can be better studied with replication experiments and the use of invasive procedures for their identification to obtain better insight into glass-making technology.

Appendixes to this thesis provide exhaustive information on the samples involved in this study, and the use of that information can be facilitated by creating a database. Instead of organising information by its kind/source, like it was done in the Appendixes, data can be organised around individual samples. Such a way of organisation could make it easier for archaeologists to access and use the data and make the research results more accessible in general.

Disclaimer

This project has received funding from the European Union's Horizon 2020 research and innovation program under the Marie Skłodowska-Curie grant agreement No 754511. The contents of this paper are the sole responsibility of the authors and do not necessarily reflect the opinion of the European Union.

UNIVERSITÀ DI TORINO

References

Abd-Allah, R. (2009). Solarization behavior of manganese-containing glass: an experimental and analytical study. Mediterranean Archaeology and Archaeometry, 9(1), 37-53.

Abd-Allah, R. (2022). From Decolorization to Solarization of Historical Glass: A review. Advanced Research in Conservation Science, 3(1), 30-41.

Abe, Y., Harimoto, R., Kikugawa, T., Yazawa, K., Nishisaka, A., Kawai, N., Yoshimura, S., & Nakai, I. (2012). Transition in the use of cobalt-blue colorant in the New Kingdom of Egypt. Journal of Archaeological Science, 39(6), 1793-1808

Abe, Y., Shikaku, R., & Nakai, I. (2018). Ancient glassware travelled the Silk Road: Nondestructive X-ray fluorescence analysis of tiny glass fragments believed to be sampled from glassware excavated from Niizawa Senzuka Tumulus No. 126, Japan. Journal of Archaeological Science: Reports, 17, 212-219.

Abe, Y., Shikaku, R., Murakushi, M., Fukushima, M., & Nakai, I. (2021). Did ancient glassware travel the Silk Road? X-ray fluorescence analysis of a Sasanian glass vessel from Okinoshima Island, Japan. Journal of Archaeological Science: Reports, 40, 103195.

Accorsi, G., Verri, G., Bolognesi, M., Armaroli, N., Clementi, C., Miliani, C., & Romani, A. (2009). The exceptional near-infrared luminescence properties of cuprorivaite (Egyptian blue). Chemical Communications, (23), 3392-3394.

Aceto, M., Fenoglio, G., Labate, M., Picollo, M., Bacci, M., & Agostino, A. (2020). A fast non-invasive method for preliminary authentication of mediaeval glass enamels using UV–visible–NIR diffuse reflectance spectrophotometry. Journal of Cultural Heritage, 45, 33-40.

Adlington, L. W. (2017). The Corning archaeological reference glasses: new values for" old" compositions. Papers from the Institute of Archaeology, 27(1).

Adlington, L. W., Gratuze, B., & Schibille, N. (2020). Comparison of pXRF and LA-ICP-MS analysis of lead-rich glass mosaic tesserae. Journal of Archaeological Science: Reports, 34, 102603.

Aerts, A., Janssens, K., Adams, F., & Wouters, H. (1999). Trace-level microanalysis of Roman glass from Khirbet Qumran, Israel. Journal of Archaeological Science, 26(8), 883-891.

Aerts, A., Velde, B., Janssens, K., & Dijkman, W. (2003). Change in silica sources in Roman and post-Roman glass. Spectrochimica Acta Part B: Atomic Spectroscopy, 58(4), 659-667.

Agua, F., Conde, J. F., Kobylińska, U., Kobyliński, Z., García-Heras, M., & Villegas, M. Á. (2017). Chemical–physical characterisation of Early Iron Age glass beads from Central Europe. Boletín de la Sociedad Española de Cerámica y Vidrio, 56(3), 119-130.

Amann, P. (2017) Society. In: Naso, A. (Ed.) Etruscology. Walter de Gruyter GmbH & Co KG. pp. 179-194.

References

Angelini, I., Artioli, G., Bellintani, P., Diella, V., Gemmi, M., Polla, A., & Rossi, A. (2004). Chemical analyses of Bronze Age glasses from Frattesina di Rovigo, northern Italy. Journal of Archaeological Science, 31(8), 1175-1184.

Angelini, I., Gratuze, B., & Artioli, G. (2019). Glass and other vitreous materials through history. EMU notes in Mineralogy, 20, 87-150.

Angelini, I., Vandini, M., Chinni, T., Koch, L.C., Von Eles, P., Molin, G. (2015) The glass of the early Etruscans: archaeometric investigation of beads from Verucchio. 20e Congrès de l'Association Internationale pour l'Histoire du Verre. 37.

Arancio, M. L., Moretti Sgubini, A. M., & Pellegrini, E. (2010). Corredi funerari femminili di rango a Vulci nella prima età del ferro: il caso della Tomba dei Bronzetti sardi. Preistoria e Protostoria in Etruria. In: Negroni Catacchio, N.[ed.] L'alba dell'Etruria. Fenomeni di continuità e trasformazione nei secoli XII-VIII aC Ricerche e scavi. Atti del IX Incontro di studi (Valentano-Pitigliano, 12-14 settembre 2008), Milano: Centro di Studi di Preistoria e Archeologia, pp. 169-213.

Archaeological Museum of Bologna web site:
http://www.museibologna.it/archeologicoen/percorsi/66288/id/74583/oggetto/74567/ [last access 14/12/2022].

Argentino, C., Lugli, F., Cipriani, A., Conti, S., & Fontana, D. (2019). A deep fluid source of radiogenic Sr and highly dynamic seepage conditions recorded in Miocene seep carbonates of the northern Apennines (Italy). Chemical Geology, 522, 135-147.

Arletti, R., Ciarallo, A., Quartieri, S., Sabatino, G. & Vezzalini, G. (2006). Archaeometric analyses of game counters from Pompeii. Geological Society, London, Special Publications. 257. 175-186. 10.1144/GSL.SP.2006.257.01.14.

Arletti, R., Vezzalini, G., Quartieri, S., Ferrari, D., Merlini, M. & Cotte, M. (2008). Polychrome glass from Etruscan sites: first non-destructive characterization with synchrotron μ-XRF, μ-XANES and XRPD. Applied Physics A, 92, 127-135.

Arletti, R., Maiorano, C., Ferrari, D., Vezzalini, G. & Quartieri, S. (2010). The first archaeometric data on polychrome Iron Age glass from sites located in northern Italy. Journal of Archaeological Science, 37(4), 703-712.

Arletti, R., Bertoni, E., Vezzalini, G. & Mengoli, D. (2011a). Glass beads from Villanovian excavations in Bologna (Italy): an archaeometrical investigation. European Journal of Mineralogy, 23(6), 959-968.

Arletti, R., Rivi, L., Ferrari, D. & Vezzalini, G. (2011b). The Mediterranean Group II: analyses of vessels from Etruscan contexts in northern Italy. Journal of archaeological science, 38(9), 2094-2100.

Arletti, R., Quartieri, S., & Freestone, I. C. (2013). A XANES study of chromophores in archaeological glass. Applied Physics A,111(1), 99-108.

Attema, P. A. J., Beijer, A. J., Kleibrink, M., Nijboer, A. J., & Van Oortmerssen, G. J. M. (2002). Pottery Classifications: Ceramics from Satricum and Lazio, Italy, 900-300 BC. Palaeohistoria, 321-396.

References

Babalola, A. B., Dussubieux, L., McIntosh, S. K., & Rehren, T. (2018). Chemical analysis of glass beads from Igbo Olokun, Ile-Ife (SW Nigeria): New light on raw materials, production, and interregional interactions. Journal of Archaeological Science, 90, 92-105.

Babbi, A. (2005). Reperti della necropoli delle Arcatelle, BPI 93-94 (2002-2003), pp.115-154.

Babini, A., Green, P., George, S., & Hardeberg, J. Y. (2022). Comparison of Hyperspectral Imaging and Fiber-Optic Reflectance Spectroscopy for Reflectance and Transmittance Measurements of Colored Glass. Heritage, 5(3), 1401-1418.

Bacci, M., & Picollo, M. (1996). Non-destructive spectroscopic detection of cobalt (II) in paintings and glass. Studies in Conservation, 41(3), 136-144.

Bacci, M., Corallini, A., Orlando, A., Picollo, M., & Radicati, B. (2007). The ancient stained windows by Nicolò di Pietro Gerini in Florence. A novel diagnostic tool for non-invasive in situ diagnosis. Journal of cultural heritage, 8(3), 235-241.

Baert, K., Meulebroeck, W., Wouters, H., Cosyns, P., Nys, K., Thienpont, H., & Terryn, H. (2011). Using Raman spectroscopy as a tool for the detection of iron in glass. Journal of Raman Spectroscopy, 42(9), 1789-1795.

Bahfenne, S., & Frost, R. L. (2010). Raman spectroscopic study of the antimonate mineral lewisite $(Ca,Fe,Na)_2$ $(Sb,Ti)_2O_6$ $(O,OH)_7$. Radiation Effects & Defects in Solids: Incorporating Plasma Science & Plasma Technology, 165(1), 46-53.

Bakkum, G. C. (2009). The Latin dialect of the Ager Faliscus: 150 years of scholarship (Vol. 1). Amsterdam University Press. Language Arts & Disciplines, 678 p.

Balmuth, M. S. (1975). The critical moment: the transition from currency to coinage in the eastern Mediterranean. World Archaeology, 6(3), 293-298.

Balvanović, R., & Šmit, Ž. (2020). Sixth-century AD glassware from Jelica, Serbia—an increasingly complex picture of late antiquity glass composition. Archaeological and Anthropological Sciences, 12, 1-17.

Bandama, F., Chirikure, S., Hall, S., & Tinguely, C. (2018). Measly but motley and manifest: The typological and chemical characterisations of glass beads from the Southern Waterberg, Limpopo Province of South Africa. Journal of Archaeological Science: Reports, 18, 90-99.

Bandiera, M., Verità, M., Lehuédé, P., & Vilarigues, M. (2020). The technology of copper-based red glass sectilia from the 2nd century AD Lucius Verus villa in Rome. Minerals, 10(10), 875.

Barag, D. P. (2009). Socio-economic observations on the history of ancient glass. In: K.Janssens, P. Degryse, P. Cosyns, J. Caen, L. Van't Dack [eds.] Annales du 17e Congr`es de l'Association Internationale pour l'Histoire du Verre, Antwerp, 3-10.

Barber, D. J., & Freestone, I. C. (1990). An investigation of the origin of the colour of the Lycurgus Cup by analytical transmission electron microscopy. Archaeometry, 32(1), 33-45.

Barfod, G. H., Freestone, I. C., Lesher, C. E., Lichtenberger, A., & Raja, R. (2020). 'Alexandrian' glass confirmed by hafnium isotopes. Scientific reports, 10(1), 11322.

References

Bar-Yosef Mayer, D. E. (2013). Towards a typology of stone beads in the Neolithic Levant. Journal of Field Archaeology, *38*(2), 129-142.

Baxter, M. J. (1989). Multivariate analysis of data on glass compositions: a methodological note. Archaeometry, 31(1), 45-53.

Baxter, M. J. (2015). Exploratory multivariate analysis in archaeology. ISD LLC. 330p.

Beaujard, P. (2010). From three possible Iron-Age world-systems to a single Afro-Eurasian world-system. Journal of World History, 1-43.

Beck, H. C. (1928). I.—Classification and nomenclature of beads and pendants. Archaeologia, 77, 1-76.

Beck, H. C. (2006). Classification and Nomenclature of Beads and Pendants. BEADS: Journal of the Society of Bead Researchers, 18(1), 1-76.

Bell, S., & Carpino, A. A. (Eds.). (2016). A Companion to the Etruscans. John Wiley & Sons.

Bellelli, V. (2009). Etrusco-Corinthian notes. A class of pottery and its socio-economic context in two centuries of scholarship. In: C. Isler-Kerényi, V. Nørskov, L. Hannestad, S. Lewis [eds.] The World of Greek Vases, Analecta Romana Instituti Danici. Supplementa, 41, 77-87.

Bellelli, V. (2017). La città che produce: appunti per una ricerca di archeologia della produzione a Cerveteri in età arcaica. Scienze dell'Antichità 23(2), Roma: Edizioni Quasar, 201-213.

Bellintani, P. (2011). Progetto Materiali vetrosi della protostoria italiana: aggiornamenti e stato della ricerca. Progetto Materiali vetrosi della protostoria italiana: aggiornamenti e stato della ricerca, 257-282.

Bellintani, P. (2014). Baltic amber, alpine copper and glass beads from the Po Plain: amber trade at the time of Campestrin and Frattesina. Baltic amber, alpine copper and glass beads from the Po plain: Amber trade at the time of Campestrin and Frattesina, 111-140.

Bellintani P, Angelini I. (2020) I vetri di Frattesina. Caratterizzazione crono-tipologica, archeometria e confronti nell'ambito della tarda età del Bronzo dell'Europa centro-orientale e del Mediterraneo. PADUSA Bollettino del Centro. 311, 71-118.

Berardinetti, A., Drago L. (1997). La necropoli di Grotta Gramiccia, in Gilda Bartoloni, a cura di, Le necropoli arcaiche di Veio. Giornata di studio in memoria di Massimo Pallottino, Università degli Studi di Roma "La Sapienza", 39-61.

Bidegaray, A. I., Cosyns, P., Gratuze, B., Terryn, H., Godet, S., Nys, K., & Ceglia, A. (2019a). On the making, mixing and trading of glass from the Roman military fort at Oudenburg (Belgium). Archaeological and Anthropological Sciences, 11, 2385-2405.

Bidegaray, A. I., Godet, S., Bogaerts, M., Cosyns, P., Nys, K., Terryn, H., & Ceglia, A. (2019b). To be purple or not to be purple? How different production parameters influence colour and redox in manganese containing glass. Journal of Archaeological Science: Reports, 27, 101975.

Bietti Sestieri, A. M., Bellintani, P., Salzani, L., Angelini, I., & Chiaffoni, B. (2015). Frattesina: un centro internazionale di produzione e di scambio nell'Età del bronzo del Veneto. in “Preistoria e protostoria del Veneto”. Firenze – Padova: Istituto italiano di preistoria e protostoria, Soprintendenza per i beni archeologici del Veneto, Università degli studi di Padova, 427-436.

Bietti Sestieri, A.M. (1992) La necropoli laziale di Osteria dell’Osa. Quasar.

Bingham, P. A., & Jackson, C. M. (2008). Roman blue-green bottle glass: chemical–optical analysis and high temperature viscosity modelling. Journal of Archaeological Science, 35(2), 302-309.

Biron, I., & Chopinet, M. H. (2013). Colouring, decolouring and opacifying of glass. In: Janssens, K. (Ed.) Modern methods for analysing archaeological and historical glass, John Wiley & Sons, Ltd, Vol. 1, 49-65.

Bispham, E., & Smith, C. (2014). Religion in archaic and republican Rome and Italy: evidence and experience. Routledge, 216.

Blomme, A., Elsen, J., Brems, D., Shortland, A., Dotsika, E., & Degryse, P. (2016). Tracing the primary production location of core-formed glass vessels, Mediterranean Group I. Journal of Archaeological Science: Reports, 5, 1-9.

Blomme, A., Degryse, P., Dotsika, E., Ignatiadou, D., Longinelli, A., & Silvestri, A. (2017). Provenance of polychrome and colourless 8th–4th century BC glass from Pieria, Greece: a chemical and isotopic approach. Journal of Archaeological Science, 78, 134-146.

Boitani, F. (2004). La tomba di guerriero AA1 dalla necropoli dei Quattro Fontanili di Veio. AM Moretti Sgubini (a cura di), Scavo nello scavo. Gli Etruschi non visti, Roma, 128-149.

Boitani, F. (2010). Veio, la Tomba dei Leoni Ruggenti: dati preliminari. Archeologia nella Tuscia. Atti dell'Incontro di Studi (Viterbo 2007). Viterbo: Università degli Studi della Tuscia. Daidalos, 10, 23-48.

Bonfante, L. (Ed.). (1986). Etruscan life and afterlife: a handbook of Etruscan studies. Wayne State University Press, 289.

Bonghi Jovino, M. (2008). Tarquinia etrusca: Tarconte e il primato della città. In: A. M. Sgubini-Moretti [ed.] Tarquinia etrusca. Soprintendenza archeologica per l'Etruria meridionale, 1-52.

Botto, M. (2017). The diffusion of Near Eastern cultures. In: A. Naso (ed.) Etruscology, De Gruyter, 581-616.

Braudel, F. (1995). The Mediterranean and the Mediterranean World in the Age of Philip II: Volume II (Vol. 2). Univ of California Press. 1375.

Brems, D., Ganio, M., Latruwe, K., Balcaen, L., Carremans, M., Gimeno, D., ... & Degryse, P. (2013). Isotopes on the beach, part 2: neodymium isotopic analysis for the provenancing of Roman glass-making. Archaeometry, 55(3), 449-464.

Brems, D., & Degryse, P. (2014a). Trace Element Analysis in Provenancing Roman Glass-Making. Archaeometry, 56, 116-136.

Brems, D., & Degryse, P. (2014b). Trace elements in sand raw materials. Glass making in the Greco-Roman World. Results of the ARCHGLASS project, Leuven, 69-85.

Brems, D., Ganio, M., & Degryse, P. (2014). The Sr-Nd isotopic fingerprint of sand raw materials. Glass making in the Greco-Roman world. Studies in Archaeological Sciences, 4, 31-67.

Briggs, D. N. (2003). Metals, salt, and slaves: economic links between Gaul and Italy from the eighth to the late sixth centuries BC. Oxford Journal of Archaeology, 22(3), 243-259.

Brill, R. H. (1963). Ancient glass. Scientific American, 209(5), 120-131.

Brill, R. H. (1992). Chemical analyses of some glasses from Frattesina. Journal of Glass Studies, 11-22.

Brill, R. H., & Cahill, N. D. (1988). A red opaque glass from Sardis and some thoughts on red opaques in general. Journal of Glass Studies, 16-27.

Brill, R. H., & Moll, S. (1961). The electron-beam probe microanalysis of ancient glass. Studies in Conservation, 6(sup1), 145-151.

Brill, R. M. (1999). Chemical Analysis of Early Glasses: The Catalogue. Corning Museum of Glass. 335.

Broodbank, C. (2013). The Making of the Middle Sea: A History of the Mediterranean from the Beginning to the Emergence of the Classical World. Thames & Hudson, 672.

Bruni, Y., Hatert, F., George, P., & Strivay, D. (2020). The Reliquary bust of Saint Lambert from the Liège cathedral, Belgium: gemstones and glass beads analysis by pXRF and Raman spectroscopy. Archaeometry, 62(2), 297-313.

Buchanan, B., & Collard, M. (2010). A geometric morphometrics-based assessment of blade shape differences among Paleoindian projectile point types from western North America. Journal of Archaeological Science, 37(2), 350-359.

Buchner, G. (1966). Pithekoussai, oldest Greek colony in the West. Expedition, 8(4), 4.

Buiskikh, A. V., & Naso, A. (2022). Etruscan Bucchero Pottery in the Northern Black Sea Littoral. Ancient Civilizations from Scythia to Siberia, 28(1), 1-22.

Cable, M. (2001). The Art of Glass by Antonio Neri. Translated into English by Christopher Merrett.

Cagno, S., Cosyns, P., Izmer, A., Vanhaecke, F., Nys, K., & Janssens, K. (2014). Deeply colored and black-appearing Roman glass: a continued research. Journal of archaeological science, 42, 128-139.

Cagno, S., Hellemans, K., & Janssens, K. (2016). The Role of LA-ICP-MS in the Investigation of Archaeological Glass. In Recent Advances in Laser Ablation ICP-MS for Archaeology, Springer, Berlin, Heidelberg, 163-178.

Capobianco, N., Hunault, M. O., Balcon-Berry, S., Galoisy, L., Sandron, D., & Calas, G. (2019). The Grande Rose of the Reims Cathedral: an eight-century perspective on the colour management of medieval stained glass. Scientific Reports, 9(1), 3287.

Carpenter, R. (1958). Phoenicians in the West. American Journal of Archaeology, 62(1), 35-53.

Castello, C., & Mandolesi, A. (2009). Modellini di navi tirrenico-villanoviane da Tarquinia. Modellini di navi tirrenico-villanoviane da Tarquinia, 1000-1020.

Cecere, F., Carraro, A., Ferro, D., & Visco, G. (2008). Individuation of characteristic parameters of "glass paste" of Meridional Etruria by the use of scientific methodologies. Microchemical Journal, 88(2), 130-135.

Ceglia, A., Meulebroeck, W., Cosyns, P., Nys, K., Terryn, H., & Thienpont, H. (2013). Colour and Chemistry of the glass finds in the Roman villa of Treignes, Belgium. Procedia Chemistry, 8, 55-64.

Ceglia, A., Nuyts, G., Cagno, S., Meulebroeck, W., Baert, K., Cosyns, P., ... & Terryn, H. (2014). A XANES study of chromophores: the case of black glass. Analytical methods, 6(8), 2662-2671.

Ceglia, A., Nuyts, G., Meulebroeck, W., Cagno, S., Silvestri, A., Zoleo, A., ... & Terryn, H. (2015). Iron speciation in soda-lime-silica glass: a comparison of XANES and UV-vis-NIR spectroscopy. Journal of Analytical Atomic Spectrometry, 30(7), 1552-1561.

Cerasuolo, O. (2008). All'origine di Caere: Contributo alla conoscenza del processo formativo protourbano in un settore dell'Etruria meridionale. Preistoria e protostoria in Etruria. Paesaggi reali e paesaggi mentali. Ricerche e scavi. Atti dellVIII Incontro di Studi, Valentano-Pitigliano 2006, 683-694.

Cerasuolo, O. (2016). Chapter 3 The Orientalizing Period Material and Cultural Connection. In Caere (pp. 27-40). University of Texas Press.

Cerchiai, L. (2017). Urban Civilization. In: Naso A. (Ed.) Etruscology. Walter de Gruyter GmbH & Co KG. V.1, pp. 617-644.

Chang, Q., Kimura, J. I., & Vaglarov, B. S. (2015). In situ Sr isotope measurement of small glass samples using multiple-Faraday collector inductively coupled plasma mass spectrometry with 10 12 Ω resistor high gain Faraday amplifiers. Journal of Analytical Atomic Spectrometry, 30(2), 515-524.

Chiavari, C., Degli Esposti, M., Garagnani, G. L., Martini, C., Prandstraller, D., & Trocchi, T. (2007). Bronze archaeological finds from the Villanovan Necropolis of Orto Granara (BO): study of manufacturing technologies and evaluation of the conservation state. la metallurgia italiana.

Cholakova, A., Rehren, T., Scott, R., Braekmans, D., Carremans, M., & Degryse, P. (2012). Producing black glass during the Roman period-notes on a crucible fragment from Serdica, Bulgaria. In Proceedings of the 39th International Symposium for Archaeometry, Leuven, Belgium (Vol. 28).

Clark, R. J., & Gibbs, P. J. (1997). Non-Destructive In Situ Study of Ancient Egyptian Faience by Raman Microscopy. Journal of Raman Spectroscopy, 28(2-3), 99-103.

Clarke, F. W., & Washington, H. S. (1924). The composition of the earth's crust (Vol. 127). US Government Printing Office.

CLP, Various authors (1976) Civiltà del Lazio Primitivo. Multigrafica Editrice 394p.

Collis, J. (2003). The European Iron Age. Routledge.

Colomban, P. (2003). Polymerization degree and Raman identification of ancient glasses used for jewelry, ceramic enamels and mosaics. Journal of Non-Crystalline Solids, 323(1-3), 180-187.

Colomban, P., Tournie, A., & Bellot-Gurlet, L. (2006). Raman identification of glassy silicates used in ceramics, glass and jewellery: a tentative differentiation guide. Journal of Raman Spectroscopy, 37(8), 841-852.

Colomban, P., & Tournié, A. (2007). On-site Raman identification and dating of ancient/modern stained glasses at the Sainte-Chapelle, Paris. Journal of Cultural Heritage, 8(3), 242-256.

Colomban, P. (2008). On-site Raman identification and dating of ancient glasses: A review of procedures and tools. Journal of Cultural Heritage, 9, e55-e60.

Colomban, P. (2013). Non–destructive Raman analysis of ancient glasses and glazes. Modern methods for analysing archaeological and historical glass, 1, 275-300.

Comite, V., Andreoli, M., Atzei, D., Barca, D., Fantauzzi, M., La Russa, M. F., ... & Fermo, P. (2020). Degradation products on Byzantine glasses from Northern Tunisia. Applied Sciences, 10(21), 7523.

Conn, R. G. (1998). Progress and Problems in Recent Trade Bead Research. BEADS: Journal of the Society of Bead Researchers, 10(1), 63-66.

Conradt, R. (2019). Thermodynamics and Kinetics of Glass. In: Musgraves, J. D., Hu, J., & Calvez, L. (Eds.) Springer handbook of glass (No. Part A). Cham: Springer, 51-77.

Conte, S., Arletti, R., Mermati, F., Gratuze, B., 2016. Unravelling the Iron Age glass trade in southern Italy: the first trace-element analyses. Eur. J. Mineral. 28 (2), 409–433.

Conte, S., Arletti, R., Henderson, J., Degryse, P., & Blomme, A. (2018). Different glassmaking technologies in the production of Iron Age black glass from Italy and Slovakia. Archaeological and Anthropological Sciences, 10(3), 503-521.

Conte, S., Matarese, I., Vezzalini, G., Pacciarelli, M., Scarano, T., Vanzetti, A., ... & Arletti, R. (2019). How much is known about glassy materials in Bronze and Iron Age Italy? New data and general overview. Archaeological and Anthropological Sciences, 11, 1813-1841.

Conventi, A., Neri, E., & Verità, M. (2012). SEM-EDS analysis of ancient gold leaf glass mosaic tesserae. A contribution to the dating of the materials. In IOP Conference Series: Materials Science and Engineering (Vol. 32, No. 1, p. 012007). IOP Publishing.

Corretti, A., & Benvenuti, M. (2001). The Beginning of Iron Metallurgy in Tuscany, with Special Reference to" Etruria Mineraria". Mediterranean Archaeology, 127-145.

Costa, M., Arruda, A. M., Barbosa, R., Barrulas, P., Vandenabeele, P., & Mirão, J. (2019a). A micro-analytical study of the scarabs of the Necropolis of Vinha das Caliças (Portugal). Microscopy and Microanalysis, 25(1), 214-220.

Costa, M., Arruda, A. M., Dias, L., Barbosa, R., Mirão, J., & Vandenabeele, P. (2019b). The combined use of Raman and micro-X-ray diffraction analysis in the study of archaeological glass beads. Journal of Raman Spectroscopy, 50(2), 250-261.

References

Costa, M., Barrulas, P., Arruda, A. M., Dias, L., Barbosa, R., Vandenabeele, P., & Mirão, J. (2021). An insight into the provenance of the Phoenician-Punic glass beads of the necropolis of Vinha das Caliças (Beja, Portugal). Archaeological and Anthropological Sciences, 13(9), 149.

Costa, M., Barrulas, P., Arruda, A. M., Barbosa, R., Vandenabeele, P., & Mirao, J. (2022). New approaches for the study of faience using beads from Southern Portugal. Journal of Archaeological Science: Reports, 46, 103703.

Cosyns, P., Warmenbol, E., Bourgeois, J., & Degryse, P. (2003). Pre-Roman glass beads in Belgium. Annales du 16ème Congrès de l'Association Internationale pour l'Histoire du Verre, London, 326-330.

Cozza, A., Pasqui, A. (1981). Carta archeologica d'Italia (1881-1897): materiali per l'agro falisco: lavoro pubblicato con il contributo del Consiglio nazionale delle ricerche. LS Olschki.

Craddock, P. T. (1977). The composition of the copper alloys used by the Greek, Etruscan and Roman civilisations: 2. the Archaic, Classical and Hellenistic Greeks. Journal of archaeological science, *4*(2), 103-123.

Cristensen, A. (1997). Glass finds from Poggio Civitate (Murlo) In: Bonfante, L., Rallo, A., Rowe, P., Edlund-Berry, I., Hall, J., Whitehead, J., ... & Curry, J. The Etruscans Revisited: A Symposium. Etruscan Studies, 4(1), 13.

Cultrone, G., & Rosua, F. J. C. (2020). Growth of metastable phases during brick firing: Mineralogical and microtextural changes induced by the composition of the raw material and the presence of additives. Applied Clay Science, *185*, 105419.

D'Ercole, M. C. (2017). Economy and trade. In: Naso A. (Ed.) Etruscology, De Gruyter, V.*1*, 143-164.

D'Oriano, C., Da Pelo, S., Podda, F., & Cioni, R. (2008). Laser-ablation inductively coupled plasma mass spectrometry (LA-ICP-MS): setting operating conditions and instrumental performance. Periodico di mineralogia, 77(3), 65-74.

Dardeniz, G. (2015). Was Ancient Egypt the Only Supplier of Natron?: New Research Reveals Major Anatolian Deposits. Anatolica, 41, 191-202.

de Ferri, L., Bersani, D., Colomban, P., Lottici, P. P., Simon, G., & Vezzalini, G. (2012). Raman study of model glass with medieval compositions: artificial weathering and comparison with ancient samples. Journal of Raman Spectroscopy, 43(11), 1817-1823.

de Ferri, L., Mezzadri, F., Falcone, R., Quagliani, V., Milazzo, F., & Pojana, G. (2020). A non-destructive approach for the characterization of glass artefacts: The case of glass beads from the Iron Age Picene necropolises of Novilara and Crocefisso-Matelica (Italy). Journal of Archaeological Science: Reports, *29*, 102124.

De Marinis, R. C., & Rapi, M. (2005). L'abitato etrusco del Forcello di Bagnolo S. Vito (Mantova): le fasi arcaiche, Comune di Bagnolo San Vito, 311.

Debenedetti, P. G., & Stillinger, F. H. (2001). Supercooled liquids and the glass transition. Nature, 410(6825), 259-267.

DeCorse, C. R., Richard, F. G., & Thiaw, I. (2003). Toward a systematic bead description system: a view from the Lower Falemme, Senegal. Journal of African Archaeology, 1(1), 77-109.

Degryse, P., & Schneider, J. (2008). Pliny the Elder and Sr–Nd isotopes: tracing the provenance of raw materials for Roman glass production. Journal of Archaeological Science, 35(7), 1993-2000.

Degryse, P., & Shortland, A. J. (2009). Trace elements in provenancing raw materials for Roman glass production (an inaugural lecture to the society). Geologica Belgica, 12(3-4), 135-143.

Degryse, P., Boyce, A., Erb-Satullo, N., Eremin, K., Kirk, S., Scott, R., ... & Walton, M. (2010). Isotopic discriminants between late Bronze Age glasses from Egypt and the Near East. Archaeometry, 52(3), 380-388.

Degryse, P., Shortland, A. J., Dillis, S., van Ham-Meert, A., Vanhaecke, F., & Leeming, P. (2020). Isotopic evidence for the use of Caucasian antimony in Late Bronze Age glass making. Journal of Archaeological Science, 120, 105195.

Delile, H., Pleuger, E., Blichert-Toft, J., Goiran, J. P., Fagel, N., Gadhoum, A., ... & Wilson, A. I. (2019). Economic resilience of Carthage during the Punic Wars: Insights from sediments of the Medjerda delta around Utica (Tunisia). Proceedings of the National Academy of Sciences, 116(20), 9764-9769.

Delpino, F. (1977). La prima éta del ferro a Bisenzio, divisione in fasi ed interpretazione culturale.(Le 1 Age du Fer à B., subdivisions chronologiques et interprétation culturelle). Studi Etruschi Firenze, 45, 39-49.

Demirsar Arli, B., Simsek Franci, G., Kaya, S., Arli, H., & Colomban, P. (2020). Portable X-ray Fluorescence (p-XRF) uncertainty estimation for glazed ceramic analysis: Case of Iznik Tiles. Heritage, 3(4), 1302-1329.

Deng, W., Wright, R., Boden-Hook, C., & Bingham, P. A. (2019). Melting behavior of waste glass cullet briquettes in soda-lime-silica container glass batch. International Journal of Applied Glass Science, 10(1), 125-137.

Devulder, V., & Degryse, P. (2014). The sources of Natron. Glass Making in the Greco-Roman World: Results of the ARCHGLASS project. Leuven University Press, Leuven, 87-95.

Docter, R., & Sonneveld, J. (2009). Punic glass from Carthaginian settlement excavations. Carthage Studies, 3, 125-146.

Drap, P., & Long, L. (2001). Towards a digital excavation data management system: the "Grand Ribaud f" estruscan deep-water wreck. In: D. Arnold, A. Chalmers, D. Fellner [eds.] Proceedings of the 2001 conference on Virtual reality, archeology, and cultural heritage, Association for Computing Machinery, 17-26.

Drünert, F., Palamara, E., Zacharias, N., Wondraczek, L., & Möncke, D. (2018). Ancient Roman nano-technology: Insight into the manufacture of mosaic tesserae opacified by calcium antimonate. Journal of the European Ceramic Society, 38(14), 4799-4805.

Duckworth, C. N., Henderson, J., Rutten, F. J., & Nikita, K. (2012). Opacifiers in Late Bronze Age glasses: the use of ToF-SIMS to identify raw ingredients and production techniques. Journal of Archaeological Science, 39(7), 2143-2152.

Dussubieux, L., Robertshaw, P., & Glascock, M. D. (2009). LA-ICP-MS analysis of African glass beads: laboratory inter-comparison with an emphasis on the impact of corrosion on data interpretation. International Journal of Mass Spectrometry, 284(1-3), 152-161.

Eggert, G. (1998). The identification of high-lead glass using simple methods. The conservator, 22(1), 12-16.

Eisen, G. (1916a). Button Beads—with Special Reference to those of the Etruscan and Roman Periods. American Journal of Archaeology, 20(3), 299-307.

Eisen, G. (1916b). The Characteristics of Eye Beads from the Earliest Times to the Present. American Journal of Archaeology, Vol. 20 (1), 1-27.

Eluère, C. (1989). A 'Gold connection' between the etruscans and early celts? Gold Bulletin, 22(2), 48-55.

Emami, M., Rozatian, A. S. H., Vallcorba, O., Anghelone, M., Hadian Dehkordi, M., Pritzel, C., & Trettin, R. (2020). Synchrotron micro-XRD study, the way toward a deeper characterizing the early prehistoric Iranian glass cylinders from Late Bronze Age (1280 BC). The European Physical Journal Plus, 135(6), 1-14.

Erb-Satullo, N. L. (2019). The innovation and adoption of iron in the ancient Near East. Journal of Archaeological Research, 27, 557-607.

Eremin, K., Degryse, P., Erb-Satullo, N., Ganio, M., Greene, J., Shortland, A., ... & Stager, L. (2012). Iron Age glass beads from Carthage. In: N. Meeks, C. Cartwright, A. Meek, A. Mongiatti [eds.] Historical technology, materials and conservation: SEM and microanalysis.

Evian, S. B. D. (2011). Egypt and the levant in the iron age I–IIA: the ceramic evidence. Tel Aviv, 38(1), 94-119.

Fagan, B. M. (Ed.). (1996). The Oxford companion to archaeology. Oxford University Press, Oxford, 1507.

Falconi Amorelli, M.T. (1967). Corredo di una tomba etrusca arcaica di Monte Aùto, Arch Class, XIX, pp.306-312.

Figueiredo, M. O. (2012). Synchrotron radiation (SR) in materials science: a brief retrospective on first approaches towards the use of SR at European research facilities. Ciência & Tecnologia dos Materiais.

Frahm, E. (2014). Scanning electron microscopy (SEM): Applications in archaeology. In: C. Smith [ed.] Encyclopedia of global archaeology, 6487-6495.

Frahm, E., & Doonan, R. C. (2013). The technological versus methodological revolution of portable XRF in archaeology. Journal of Archaeological Science, 40(2), 1425-1434.

Francis, P. (1986). Collar beads: A new typology and a new perspective on ancient Indian beadmaking. Bulletin of the Deccan College Research Institute, 45, 117-121.

Freestone, I. C. (1992). Theophilus and the composition of medieval glass. MRS Online Proceedings Library (OPL), 267, 739.

Freestone, I. C., Ponting, M., & Hughes, M. J. (2002). The origins of byzantine glass from Maroni Petrera, Cyprus. Archaeometry, 44(2), 257-272.

Freestone, I. C., Leslie, K. A., Thirlwall, M., & Gorin-Rosen, Y. (2003). Strontium isotopes in the investigation of early glass production: Byzantine and early Islamic glass from the Near East. Archaeometry, 45(1), 19-32.

Freestone, I. C., Wolf, S., & Thirlwall, M. (2009). Isotopic composition of glass from the Levant and south-eastern Mediterranean Region. Isotopes in vitreous materials, 1, 31.

Freestone, I., & Stapleton, C. P. (2015). Composition technology and production of coloured glasses from Roman mosaic vessels. In: Bayley, J and Freestone, I and Jackson, C, [eds.] Glass of the Roman World. Oxford, Oxbow, 61-76.

Fudall, R. F. (1981). The major element chemistry of Libyan Desert Glass and the mineralogy of its precursor. Meteoritics, 16(3), 247-259.

Fulminante, F., & Stoddart, S. (2013). Indigenous political dynamics and identity from a comparative perspective: Etruria and Latium Vetus. In Alberti, ME. [Ed.] Exchange Networks and Local Transformations Interaction and Local Change in Europe and the Mediterranean from the Bronze Age to the Iron Age. Oxbow Books Limited. 117-133.

Fusi, G. D. T. M. (2021). I Reperti In Vetro Del Museo Guarnacci Di Volterra. Velathri Volaterrae: La città etrusca e il municipio romano, 64, 409.

Gagarin, M. (Ed.). (2010). The Oxford encyclopedia of ancient Greece and Rome (Vol. 1). Oxford University Press. 251-256.

Gallo, F., Marcante, A., Silvestri, A., & Molin, G. (2014). The glass of the “Casa delle Bestie Ferite”: a first systematic archaeometric study on Late Roman vessels from Aquileia. Journal of Archaeological Science, 41, 7-20.

Gallo, F., Silvestri, A., Degryse, P., Ganio, M., Longinelli, A., & Molin, G. (2015). Roman and late-Roman glass from north-eastern Italy: The isotopic perspective to provenance its raw materials. Journal of Archaeological Science, 62, 55-65.

Ganio, M., Boyen, S., Fenn, T., Scott, R., Vanhoutte, S., Gimeno, D., & Degryse, P. (2012). Roman glass across the Empire: an elemental and isotopic characterization. Journal of Analytical Atomic Spectrometry, 27(5), 743-753.

García-Medrano, P., Maldonado-Garrido, E., Ashton, N., & Ollé, A. (2020). Objectifying processes: The use of geometric morphometrics and multivariate analyses on Acheulean tools. Journal of Lithic Studies, 7(1), 1-16.

Genga, A., Siciliano, M., Tepore, A., Mangone, A., Traini, A., & Laganara, C. (2008). An archaeometric approach about the study of medieval glass from Siponto (Foggia, Italy). Microchemical Journal, 90(1), 56-62.

Gerharz, R. R., Lantermann, R., & Spennemann, D. R. (1988). Munsell color charts: a necessity for archaeologists? The Australian Journal of Historical Archaeology, 6, 88-95.

Getty Trust Art and Architecture Thesaurus [http://vocab.getty.edu/page/aat/300010797] last accessed 12/04/2022.

Giachet, M. T., Gratuze, B., Ozainne, S., Mayor, A., & Huysecom, E. (2019). A Phoenician glass eye bead from 7th–5th c. cal BCE Nin-Bèrè 3, Mali: compositional characterisation by LA–ICP–MS. Journal of Archaeological Science: Reports, 24, 748-758.

Giannini, R., Freestone, I. C., & Shortland, A. J. (2017). European cobalt sources identified in the production of Chinese famille rose porcelain. Journal of Archaeological Science, 80, 27-36.

Giardino, C. (2014). Villanovan and Etruscan mining and metallurgy. In Turfa J.M. [Ed.] The Etruscan World, Routledge, 769-785.

Gierow, P. G. (1964). The Iron Age culture of Latium. 2, Excavations and finds: 1. The Alban hills. (Vol.22) CWK, Gleerup, 418.

Gierow, P. G. (1966). The Iron Age Culture of Latium: Classification and Analysis (Vol. 24). CWK, Gleerup, 418.

Giuntoli, S. (1996). Balsamari etruschi in vetro di età orientalizzante e arcaica. I Quaderni del Giornale Economico: Il vetro dall'antichita all'eta contemporanea, 13-16.

Gleba, M. (2007). Textile Production in Proto-historic Italy: from Specialists to Workshops. In: I. C. Gillis, & M-L. Nosch [ed.], Ancient Textiles: Production, Craft and Society. Left Coast Press. ancient textiles series, 1, 71-76.

Goffer, Z. (2006). Archaeological chemistry. John Wiley & Sons, 656.

González-Ruibal, A. (2004). Facing two seas: Mediterranean and Atlantic contacts in the north-west of Iberia in the first millennium BC. Oxford Journal of Archaeology, 23(3), 287-317.

Götze, J. (1998). Geochemistry and provenance of the Altendorf feldspathic sandstone in the Middle Bunter of the Thuringian basin (Germany). Chemical geology, 150(1-2), 43-61.

Graham, A. J. (1999). Colony and mother city in ancient Greece. Manchester university press, 259.

Graham, A. J. (2001). Collected papers on Greek colonization. Brill, vol. 214, 432.

Gratuze, B., & Janssens, K. (2004). Provenance analysis of glass artefacts. In: K. Janssens and R. Van Grieken [eds.] Comprehensive Analytical Chemistry. Elsevier. 42, 663-712.

Gratuze, B., & Picon, M. (2005). Utilisation par l'industrie verri`ere des sels d'aluns des oasis ´egyptiennes au d´ebut du premier mill´enaire avant notre `ere. In Borgard, P., Brun, J., & Picon, M. (Eds.), L'alun de M´editerran´ee. Publications du Centre Jean B´erard. 269-276.

Gratuze, B. (2013). Provenance analysis of glass artefacts. In: K. Janssens [ed.] Modern methods for analysing archaeological and historical glass, John Wiley & Sons, 1, 311-343.

Griffin, P. S. (2002). Reconstructing the materials and technology of Egyptian faience and frit. MRS Online Proceedings Library (OPL), 712, II4-2.

Grose, D. F. (1989). Early ancient glass: core-formed, rod-formed, and cast vessels and objects from the late Bronze Age to the early Roman Empire, 1600 BC to AD 50. New York: Hudson Hills Press in association with the Toledo Museum of Art, 453.

Guido, M. (1978). The glass beads of the prehistoric and Roman periods in Britain and Ireland. Society of Antiquaries of London, 294.

Gulmini, M., Pace, M., Ivaldi, G., Ponzi, M. N., & Mirti, P. (2009). Morphological and chemical characterization of weathering products on buried Sasanian glass from central Iraq. Journal of non-crystalline solids, 355(31-33), 1613-1621.

Haevernick, T. E. (1959). Beiträge zur Geschichte des antiken Glases. Jahrbuch des Römisch-Germanischen Zentralmuseums Mainz, 6, 57-65.

Haevernick, T. E. (1960a) Beiträge zur Geschichte des Antiken Glases. III Mykenisches Glas. Jahrbuch des Römisch-Germanischen Zentralmuseums Mainz, 7, 36-50.

Haevernick, T. E. (1960b) Die Glasarmringe und Ringperlen der Mittel-und Spätlatènezeit auf dem europäischen Festland. Römisch-Germanische Kommission Des Deutschen Archäologischen Instituts Zu Frankfurt A.M, 10, 302-337.

Haevernick, T. E. (1961) Beiträge zur Geschichte des antiken Glases. Die Aggryperlen – Chevron Pattern Beads – Rosettaperlen – Star-Beads. Jahrbuch Des Romisch-Germanischen Zentralmuseums Mainz, 8, 121-137.

Haevernick, T. E. (1962). Beiträge zur Geschichte des antiken Glases. Jahrbuch des Römisch-Germanischen Zentralmuseums Mainz, 9, 58-67.

Haevernick, T. E. (1965). Beiträge zur Geschichte des antiken Glases. XIII. Nuzi-Perlen. Ein Versuch. Jahrbuch des Römisch-Germanischen Zentralmuseums Mainz, 12, 35-40.

Haevernick, T. E., Dobiat, C., Matthäus, H., Raftery, B., & Henderson, J. (Eds.). (1987). Glasperlen der vorrömischen Eisenzeit: Ringaugenperlen und verwandte Perlengruppen. Dr. Wolfram Hitzeroth Verlag, 167.

Hall, J. F. (Ed.). (1996). Etruscan Italy: Etruscan influences on the civilizations of Italy from antiquity to the modern era. Indiana University Press, 411.

Harden, D. B. (1968). Ancient Glass, I: Pre-Roman. Archaeological Journal, 125(1), 46-72.

Harden, D. B., & Tatton-Brown, V. A. (1981). Catalogue of Greek and Roman glass in the British Museum. Vol 1. Core-and rod-formed vessels and pendants and Mycenaean cast objects.

Heginbotham, A., Bezur, A., Bouchard, M., Davis, J. M., Eremin, K., Frantz, J. H., ... & Speakman, R. J. (2010). An evaluation of inter-laboratory reproducibility for quantitative XRF of historic copper alloys.

In: Metal 2010: International Conference on Metal Conservation, Interim Meeting of the International Council of Museums Committee for Conservation Metal Working Group, October 11-15, 2010, Charleston, South Carolina, USA. Clemson University.

Heginbotham, A., & Solé, V. A. (2017). CHARMed PyMca, Part I: A Protocol for Improved Inter-laboratory Reproducibility in the Quantitative ED-XRF Analysis of Copper Alloys. Archaeometry, 59(4), 714-730.

Heginbotham, A., Bourgarit, D., Day, J., Dorscheid, J., Godla, J., Lee, L., ... & Robcis, D. (2019). CHARMed PyMca, Part II: An evaluation of interlaboratory reproducibility for ED-XRF analysis of copper alloys. Archaeometry, 61(6), 1333-1352.

Heimann, R. B. (2018). Weathering of ancient and medieval glasses—potential proxy for nuclear fuel waste glasses. A perennial challenge revisited. International Journal of Applied Glass Science, 9(1), 29-41.

Hein, A., Dobosz, A., Day, P. M., & Kilikoglou, V. (2021). Portable ED-XRF as a tool for optimizing sampling strategy: The case study of a Hellenistic amphora assemblage from Paphos (Cyprus). Journal of Archaeological Science, 133, 105436.

Hellmann, R. (2021). Mechanisms of Glass Corrosion by Aqueous Solutions. Encyclopedia of Glass Science, Technology, History, and Culture, 1, 647-662.

Hencken, H. (1968) Tarquinia, Villanovans and Early Etruscans. American school of Prehistoric research, Harvard University. Vol. I and II 719.

Henderson, J. (1985). The raw materials of early glass production. Oxford Journal of Archaeology, 4(3), 267-291.

Henderson, J. (1988a). Electron probe microanalysis of mixed-alkali glasses. Archaeometry, 30(1), 77-91.

Henderson, J. (1988b). Glass production and Bronze Age Europe. Antiquity, 62(236), 435-451.

Henderson, J. (2013). Ancient glass: an interdisciplinary exploration. Cambridge University Press.

Henderson, J., Chenery, S., Omura, S., Matsumura, K., & Faber, E. (2018). Hittite and Early Iron Age Glass from Kaman-Kalehöyük and Büklükale, Turkey: Evidence for Local Production and Continuity?. Journal of Anatolian Archaeology, 21, 1-15.

Henderson, J., Evans, J. A., Sloane, H. J., Leng, M. J., & Doherty, C. (2005). The use of oxygen, strontium and lead isotopes to provenance ancient glasses in the Middle East. Journal of Archaeological Science, 32(5), 665-673.

Henderson, J., Ma, H., & Evans, J. (2020). Glass production for the Silk Road? Provenance and trade of Islamic glasses using isotopic and chemical analyses in a geological context. Journal of Archaeological Science, 119, 105164.

Hill, J & Evans, R, (1972) A model for classification and typology. In: A. Clarke, L. David, Models in archaeology, Oxford: Methuen, 231-273.

Hodgkinson, A. K. (2019). Manufacturing colourful glass objects in New Kingdom Egypt: a spatial and statistical analysis. In: Warburton, D. and Thavapalan, S. [eds.], Value of Colour. Material and Economic Aspects in the Ancient World, Berlin. Edition Topoi, 125-175.

Hodgkinson, A. K., & Frick, D. A. (2020). Identification of cobalt-coloured Egyptian glass objects by la-icp-ms: a case study from the 18th dynasty workshops at Amarna, Egypt. Mediterranean Archaeology and Archaeometry, 20(1), 45-57.

Hodos, T. (1999). Intermarriage in the western Greek colonies. Oxford Journal of Archaeology, 18(1), 61-78.

Hoffman, P. F., Macdonald, F. A., & Halverson, G. P. (2011). Chemical sediments associated with Neoproterozoic glaciation: iron formation, cap carbonate, barite and phosphorite. Geological Society, London, Memoirs, 36(1), 67-80.

Holloway, R. R. (2014). The archaeology of early Rome and Latium. Routledge, 228.

Hughes-Brock, H. (1999). Mycenaean beads: gender and social contexts. Oxford journal of archaeology, 18(3), 277-296.

Hunault, M., Bauchau, F., Loisel, C., Hérold, M., Galoisy, L., Newville, M., & Calas, G. (2016). Spectroscopic investigation of the coloration and fabrication conditions of medieval blue glasses. Journal of the American Ceramic Society, 99(1), 89-97.

Hütwohl, D. J. (2020). Herodotus' Phoenicians: mediators of cultural exchange in the Mediterranean. Rivista di studi fenici: XLVIII, Roma: Edizioni Quasar, 107-120.

Hynes, M. J., & Jonson, B. (1997). Lead, glass and the environment. Chemical Society Reviews, 26(2), 133-146.

Iaia, C. (1999). Simbolismo funerario e ideologia alle origini di una civiltà urbana. Forme rituali nelle sepolture" villanoviane" a Tarquinia e Vulci, e nel loro entroterra (Vol. 3, pp. 0-156). All'insegna del giglio.

Iaia, C. (2013). Metalwork, rituals and the making of elite identity in central Italy at the Bronze Age-Iron Age transition. In: M. E. Alberti, S. Sabatini, Exchange Networks and Local Transformation, Oxbow books, 102-116.

Iaia, C. (2017). Handicraft (Early Iron Age). In: A. Naso [ed.] Etruscology. Walter de Gruyter, 739-757.

Ingo, G. M., De Caro, T., Riccucci, C., Angelini, E., Grassini, S., Balbi, S., ... & Vassiliou, P. (2006). Large scale investigation of chemical composition, structure and corrosion mechanism of bronze archeological artefacts from Mediterranean basin. Applied Physics A, 83, 513-520.

Izzet, V. E. (2000). The Etruscan sanctuary at Cerveteri, Sant'Antonio: preliminary report of excavations 1995–8. Papers of the British School at Rome, 68, 321-335.

Jackson, C. M. (2005). Making colourless glass in the Roman period. Archaeometry, 47(4), 763-780.

Jackson, C. M., & Nicholson, P. T. (2010). The provenance of some glass ingots from the Uluburun shipwreck. Journal of Archaeological Science, 37(2), 295-301.

Jackson, C. M., Booth, C. A., & Smedley, J. W. (2005). Glass by design? Raw materials, recipes and compositional data. Archaeometry, 47(4), 781-795.

Jackson, C. M., Paynter, S., Nenna, M. D., & Degryse, P. (2018). Glassmaking using natron from el-Barnugi (Egypt); Pliny and the Roman glass industry. Archaeological and Anthropological Sciences, 10, 1179-1191.

Jackson-Tal, R. E. (2019). The faience finds. In: Stern, I. [Ed.] Excavations at Maresha Subterranean Complex 169: Final Report. Seasons 2000-2016, Jerusalem: Hebrew Union College, 263-271.

Janssens, K. (2013). X–Ray Based Methods of Analysis. In: Janssens, K. [Ed.] Modern methods for analysing archaeological and historical glass, 1, pp. 79-128.

Janssens, K. [Ed.]. (2013). Modern methods for analysing archaeological and historical glass (Vol. 1). John Wiley & Sons, 768.

Janssens, K., Vincze, L., Vekemans, B., Aerts, A., Adams, F., Jones, K. W. & Knöchel, A. (1996). Synchrotron Radiation Induced X-Ray Microfluorescence Analysis. In: Benoit, D., Bresse, JF., Van't dack, L., Werner, H., Wernisch, J. [eds.] Microbeam and Nanobeam Analysis. Microchimica Acta Supplement, Springer, Vienna, 13, 87-115.

Jones, J. D. (1995). Classical and Hellenistic core-formed vessels from Gordion. Journal of Glass Studies, 37, 21-33.

Kaczmarczyk, A., and Hedges R. E. M.. (1983). Ancient Egyptian faience: An analytical survey of Egyptian faience from predynastic to Roman times. Warminster, England: Aris & Phillips, 587.

Kaparou, M., & Oikonomou, A. (2022). Mycenaean through Hellenistic glass in Greece: where have we got to?. Archaeological and Anthropological Sciences, 14(5), 92.

Karklins, K. (2012). Guide to the description and classification of glass beads found in the Americas. Beads: Journal of the Society of Bead Researchers, 24(1), 62-90.

Keith, L.H., Crummett, W., Deegan Jr., J., Libby, R.A., Taylor, J.K. and Wentler, G. (1983) Principles of Environmental Analysis. Analytical Chemistry, 55, 2210-2218.

Kelly, T. (1992). The Assyrians, the Persians, and the Sea. Mediterranean. Hist. Rev. 7, 5–28.

Kemp, V., Brownscombe, W., & Shortland, A. (2022). The investigation and provenance of glass vessel fragments attributed to the Tomb of Amenhotep II, KV35, Valley of the Kings. Archaeometry, 64(1), 147-160.

Kidd, K. E., & Kidd, M. A. (2012). A classification system for glass beads for the use of field archaeologists. Beads: Journal of the Society of Bead Researchers, 24(1), 39-61.

Knaf, A. C. S., Koornneef, J. M., & Davies, G. R. (2017). "Non-invasive" portable laser ablation sampling of art and archaeological materials with subsequent Sr–Nd isotope analysis by TIMS using 10 13 Ω amplifiers. Journal of Analytical Atomic Spectrometry, 32(11), 2210-2216.

Knapp, A. B., & Van Dommelen, P. (Eds.). (2015). The Cambridge Prehistory of the Bronze and Iron Age Mediterranean. Cambridge University Press.

References

Koch, L. C. (2010). Die Glasbügelfibeln des 8. und 7. Jahrhunderts aus Etrurien. Ein Beitrag zur eisenzeitlichen Glastechnik und zu den Bestattungssitten des Orientalizzante. Univforsch. Prähist. Arch, 190.

Koch, L. C. (2011). Früheisenzeitliches Glas und Glasfunde Mittelitaliens: eine Übersicht von der Villanovazeit bis zum Orientalizzante und eine Analyse der Glasperlen als Grabbeigabe des Gräberfeldes Quattro Fontanili in Veji. Leidorf, 262.

Koch, L. C. (2015). Le Perle di Vetro a Verucchio. In: von Eles, P., Bentini, L., Poli, P., & Rodriguez, E. [Eds.]. Immagini di uomini e di donne dalle necropoli villanoviane di Verucchio. All'Insegna del Giglio, 1-34.

Koch, L. C. (2018a). Die schwarzen Perlen in Osteria dell'Osa (Rom, Italien): Ein Beitrag zu den ersten Glasperlen der frühen Eisenzeit in Latium. Bericht der Römisch-Germanischen Kommission, 99, 5-82.

Koch, L. C. (2018b). Report on the Vitreous Bird Beads (Vogelperlen). ARIMNESTOS Ricerche di Protostoria Mediterranea 1/2018, 1, 227.

Koch, L. C. (2020). The Large Glass Beads of Leech Fibulae from Iron Age Necropoli in Northern Italy. BEADS: Journal of the Society of Bead Researchers 32, 3-14.

Koch, L. C. (2021). Glas und glasartiges Material in Italien zur Bronze-und Früheisenzeit–Forschungsstand und Perspektiven. In: Klimscha F., Karlsen HJ., Hansen S., Renn L. [Eds.] Vom künstlichen Stein zum durchsichtigen Massenprodukt. Innovationen in der Glastechnik und ihre sozialen Folgen zwischen Bronzezeit. Berliner Studien zur Antiken Welt Berlin, 67–103.

Koleini, F., Pikirayi, I., & Colomban, P. (2017). Revisiting Baranda: a multi-analytical approach in classifying sixteenth/seventeenth-century glass beads from northern Zimbabwe. Antiquity, 91(357), 751-764.

Koleini, F., Colomban, P., Pikirayi, I., & Prinsloo, L. C. (2019). Glass beads, markers of ancient trade in Sub-Saharan Africa: Methodology, state of the art and perspectives. Heritage, 2(3), 2343-2369.

Kolesnychenko, A., & Yatsuk, O. (2021). Glass production or glass-working? Yahorlyk settlement in the light of the new studies. (Виробництво скла чи його обробка? Ягорлицьке поселення у світлі нових досліджень). Eminak: Scientific Quarterly Journal, 1, 33, 144-156.

Lafuente, B., Downs, R. T., Yang, H., & Stone, N. (2015). The power of databases: The RRUFF project. In: T. Armbruster and R. M. Danisi [eds.] Highlights in mineralogical crystallography. De Gruyter, 1-30.

Lahlil, S., Biron, I., Galoisy, L., & Morin, G. (2008). Rediscovering ancient glass technologies through the examination of opacifier crystals. Applied Physics A, 92(1), 109-116.

Lahlil, S., Biron, I., Cotte, M., Susini, J., & Menguy, N. (2010a). Synthesis of calcium antimonate nano-crystals by the 18th dynasty Egyptian glassmakers. Applied Physics A, 98, 1-8.

Lahlil, S., Biron, I., Cotte, M., & Susini, J. (2010b). New insight on the in situ crystallization of calcium antimonate opacified glass during the Roman period. Applied Physics A, 100, 683-692.

Lahlil, S., Cotte, M., Biron, I., Szlachetko, J., Menguy, N., & Susini, J. (2011). Synthesizing lead antimonate in ancient and modern opaque glass. Journal of Analytical Atomic Spectrometry, 26(5), 1040-1050.

Lankton, J. W., Pulak, C., & Gratuze, B. (2022). Glass ingots from the Uluburun shipwreck: Glass by the batch in the Late Bronze Age. Journal of Archaeological Science: Reports, 42, 103354.

Le Losq, C., Cicconi, M.R., Greaves, G.N., Neuville, D.R. (2019). Silicate Glasses. In: Musgraves, J.D., Hu, J., Calvez, L. [eds.] Springer Handbook of Glass. Springer Handbooks. Springer, 441-503.

Leonelli, V. (2003) La necropoli della prima età del ferro delle acciaierie a Terni : contributi per un'edizione critica. Firenze: All'insegna del giglio, 347.

Levey, M. (1955). Chemical furnaces of ancient Mesopotamia and Palestine. Journal of Chemical Education, 32(7), 356.

Liang, H., Sax, M., Saunders, D., & Tite, M. (2012). Optical Coherence Tomography for the non-invasive investigation of the microstructure of ancient Egyptian faience. Journal of Archaeological Science, 39(12), 3683-3690.

Ligabue, G. (2022). Falerii Veteres. Il sepolcreto di Montarano. Scavi, materiali e contesti. Monumenti antichi. 28. 1150.

Liritzis, I., & Zacharias, N. (2011). Portable XRF of archaeological artifacts: current research, potentials and limitations. In: S.H. Shackley [ed.] X-ray fluorescence spectrometry (XRF) in geoarchaeology, Springer, New York, 109-142.

Liu, S., Li, Q. H., Gan, F., Zhang, P., & Lankton, J. W. (2012). Silk Road glass in Xinjiang, China: chemical compositional analysis and interpretation using a high-resolution portable XRF spectrometer. Journal of Archaeological Science, 39(7), 2128-2142.

Liu, Y., Hu, Z., Gao, S., Günther, D., Xu, J., Gao, C., & Chen, H. (2008). In situ analysis of major and trace elements of anhydrous minerals by LA-ICP-MS without applying an internal standard. Chemical Geology, 257(1-2), 34-43.

Livy. (1912) History of Rome. English Translation by. Rev. Canon Roberts. New York, New York. E. P. Dutton and Co 1:23.

Lončarić, V., & Costa, M. (2023). Known Glass Compositions in Iron Age Europe—Current Synthesis and Emerging Questions. Heritage, 6(5), 3835-3863.

López-Ruiz, C. (2021). Phoenicians and the Making of the Mediterranean. Harvard University Press, 440.

Lucena, M., Fuertes, J. M., Martínez-Carrillo, A. L., Ruiz, A., & Carrascosa, F. (2017). Classification of archaeological pottery profiles using modal analysis. Multimedia Tools and Applications, 76(20), 21565-21577.

Lulof, P.S., (1996). The Ridge-Pole Statues from the Late Archaic Temple at Satricum. Michigan University, Amsterdam, 250.

Maeir, A. M. (2002). The relations between Egypt and the Southern Levant during the Late Iron Age: the material evidence from Egypt. Ägypten und Levante/Egypt and the Levant, 12, 235-246.

Magness, J. (2001). A Near Eastern ethnic element among the Etruscan elite?. Etruscan Studies, 8(1), 79-118.

Maltoni, S., & Silvestri, A. (2018). Innovation and tradition in the fourth century mosaic of the Casa delle Bestie Ferite in Aquileia, Italy: archaeometric characterisation of the glass tesserae. Archaeological and Anthropological Sciences, 10(2), 415-429.

Maltoni, S., Chinni, T., Vandini, M., Cirelli, E., Silvestri, A., & Molin, G. (2015). Archaeological and archaeometric study of the glass finds from the ancient harbour of Classe (Ravenna-Italy): new evidence. Heritage Science, 3(1), 1-19.

Mangani, E. (1995). Corredi vulcenti degli scavi Gsell al Museo Pigorini. Bullettino di Paletnologia Italiana, 86, 373-428.

Mangone, A., De Benedetto, G. E., Fico, D., Giannossa, L. C., Laviano, R., Sabbatini, L., ... & Traini, A. (2011). A multianalytical study of archaeological faience from the Vesuvian area as a valid tool to investigate provenance and technological features. New Journal of Chemistry, 35(12), 2860-2868.

Mao, Y. (2000). Lead-alkaline glazed Egyptian faience: Preliminary technical investigation of Ptolemaic period faience vessels in the collection of the Walters Art Gallery. Journal of the American Institute for Conservation, 39(2), 185-204.

Margaret O'hea (2011) Another Look at the Origins of Iron Age II Cast Glass Vessels in the Levant, Levant, 43:2, 153-172.

Markowicz A.A. (2001) X-ray Physics. In: Van Grieken, R., & Markowicz, A. (Eds.) Handbook of X-ray Spectrometry. CRC press, Taylor and Frencis, 1016.

Mass, J. L., Stone, R. E., & Wypyski, M. T. (1998). The mineralogical and metallurgical origins of Roman opaque colored glasses. In: P. McCray [ed.] The prehistory and history of glassmaking technology, American ceramic society, University of Michigan, 8, 121-144.

Mass, J. L., Wypyski, M. T., & Stone, R. E. (2002). Malkata and Lisht glassmaking technologies: towards a specific link between second millennium BC. Archaeometry, 44(1), 67-82.

Mathias, M., & Rogers, A. W. (1940). The occurrence of barite in an iron ore deposit in Namaqualand. Transactions of the Royal Society of South Africa, 28(3), 207-217.

Matin, M. (2019). Tin-based opacifiers in archaeological glass and ceramic glazes: a review and new perspectives. Archaeological and Anthropological Sciences, 11, 1155-1167.

Matin, M., & Matin, M. (2012). Egyptian faience glazing by the cementation method part 1: an investigation of the glazing powder composition and glazing mechanism. Journal of Archaeological Science, 39(3), 763-776.

Maxwell-Hyslop, K. R. (1956). Urartian bronzes in Etruscan tombs. Iraq, 18(2), 150-167.

McKay, A. G. (1998). Houses, villas, and palaces in the Roman world. JHU Press. 288.

McKenney, M. (1975). The Phoenician Peace. Peace Research, 7(1), 25-30.

McLennan, S. M. (2001). Relationships between the trace element composition of sedimentary rocks and upper continental crust. Geochemistry, Geophysics, Geosystems, 2(4) 2000GC000109.

McLennan, S. M., Hemming, S., McDaniel, D. K., & Hanson, G. N. (1993). Geochemical approaches to sedimentation, provenance, and tectonics. In: M. J. Johnsson, A. Basu Processes Controlling the Composition of Clastic Sediments, Geological Society of America, 284, 21-21.

Meek, A., Bouquillon, A., Lehuédé, P., Masson, A., Villing, A., Pierrat-Bonnefois, G., & Webb, V. (2016). Discerning differences: Ion beam analysis of ancient faience from Naukratis and Rhodes. Technè. La science au service de l'histoire de l'art et de la préservation des biens culturels, (43), 94-101.

Melcher, M., & Schreiner, M. (2006). Leaching studies on naturally weathered potash-lime–silica glasses. Journal of Non-Crystalline Solids, 352(5), 368-379.

Melcher, M., Wiesinger, R., & Schreiner, M. (2010). Degradation of glass artifacts: application of modern surface analytical techniques. Accounts of chemical research, 43(6), 916-926.

Meliksetian, K., Pernicka, E., Avetissyan, P., & Simonyan, H. (2003). Chemical and lead isotope characterisation of Middle Bronze Age bronzes and some Iron Age antimony objects (Armenia). Archaeometallurgy in Europe, 2, 311-318.

Mengarelli, L., Savignoni, R. (1903). La necropoli arcaica di Caracupa tra Norba e Sermoneta, in Notizie degli Scavi 1903, 289-344.

Mermut, A. R., & Cano, A. F. (2001). Baseline studies of the clay minerals society source clays: chemical analyses of major elements. Clays and Clay Minerals, 49(5), 381-386.

Meulebroeck, W., Baert, K., Wouters, H., Cosyns, P., Ceglia, A., Cagno, S., ... & Thienpont, H. (2010). The identification of chromophores in ancient glass by the use of UV-VIS-NIR spectroscopy. In Optical Sensing and Detection, 7726, 97-108.

Micheletti, F., Orsilli, J., Melada, J., Gargano, M., Ludwig, N., & Bonizzoni, L. (2020). The role of IRT in the archaeometric study of ancient glass through XRF and FORS. Microchemical Journal, 153, 104388.

Middleton, A. P. (2009). Beads beyond number: faience from the 'Isis Tomb'at Vulci, Italy. From mine to microscope: advances in the study of ancient technology. Oxbow Books, Oxford, 69-78.

Mirti, P., Ferrari, R. P., Laurenti, E., & Casoli, A. (1993). A study of Roman glass by reflectance and electron paramagnetic resonance spectroscopies. Spectrochimica Acta Part A: Molecular Spectroscopy, 49(9), 1361-1371.

Mirti, P., Lepora, A., & Sagui, L. (2000). Scientific analysis of seventh-century glass fragments from the Crypta Balbi in Rome. Archaeometry, 42(2), 359-374.

Mirti, P., Davit, P., Gulmini, M., & Saguì, L. (2001). Glass fragments from the Crypta Balbi in Rome: the composition of eighth-century fragments. Archaeometry, 43(4), 491-502.

Mirti, P., Davit, P., & Gulmini, M. (2002). Colourants and opacifiers in seventh and eighth century glass investigated by spectroscopic techniques. Analytical and bioanalytical chemistry, 372(1), 221-229.

Mirti, P., Pace, M., Negro Ponzi, M. M., & Aceto, M. (2008). ICP–MS Analysis of Glass Fragments of Parthian and Sasanian Epoch from Seleucia and Veh Ardašir (Central Iraq). Archaeometry, 50(3), 429-450.

Mirti, P., Pace, M., Malandrino, M., & Ponzi, M. N. (2009). Sasanian glass from Veh Ardašīr: new evidences by ICP-MS analysis. Journal of Archaeological Science, 36(4), 1061-1069.

Molina, G., Odin, G. P., Pradell, T., Shortland, A. J., & Tite, M. S. (2014). Production technology and replication of lead antimonate yellow glass from New Kingdom Egypt and the Roman Empire. Journal of Archaeological Science, 41, 171-184.

Möller, P., & Bau, M. (1993). Rare-earth patterns with positive cerium anomaly in alkaline waters from Lake Van, Turkey. Earth and Planetary Science Letters, 117(3-4), 671-676.

Mommersteeg, P. W. (2011). Metallurgy and the development of Etruscan civilisation (Doctoral dissertation, UCL (University College London)), 148.

Möncke, D., Papageorgiou, M., Winterstein-Beckmann, A., & Zacharias, N. (2014). Roman glasses coloured by dissolved transition metal ions: redox-reactions, optical spectroscopy and ligand field theory. Journal of Archaeological Science, 46, 23-36.

Mongelli, G. (1993). REE and other trace elements in a granitic weathering profile from “Serre”, southern Italy. Chemical Geology, 103(1-4), 17-25.

Moorey, P. R. S. (1999). Ancient Mesopotamian materials and industries: the archaeological evidence. Eisenbrauns, 415 p.

Moretti, C., & Hreglich, S. (2013). Raw materials, recipes and procedures used for glass making. Modern methods for analysing archaeological and historical glass, 1, 23-47.

Morrison, G. H., & Kl, C. (1979). General Aspects Of Trace Analytical Methods. In: Recommendations For Nomenclature, Standard Procedures And Reporting Of Experimental Data For Surface Analysis Techniques. Pure and Applied Chemistry, 51, 11, 2243-2250.

Murai, S., Fujita, K., & Tanaka, K. (2013). New Glasses for Photonics. In: S. Somiya [ed.] Handbook of Advanced Ceramics. Elsevier Inc, 1258.

Myers, R. D. (2010). Colorchecker passport technical review. Robin Myers Imaging (www. rmimaging. com), 3.

Naso, A. (2006). Etruscan and Italic Finds in North Africa, 7th-2nd century BC. British Museum Research Publications, 162, 187.

Naso, A. (Ed.). (2017a). Etruscology (Vol. 1). Walter de Gruyter GmbH & Co KG. 1844.

Naso, A. (2017b). Death and Burial. In: Naso, A. (Ed.) Etruscology. Walter de Gruyter GmbH & Co KG. V.1, 317-340.

Naso, A. (2017c) North Africa. In: Naso, A. (Ed.) Etruscology. Walter de Gruyter GmbH & Co KG. pp. 1695-1708.

Neri, E., Gratuze, B. & Schibille, N. The trade of glass beads in early medieval Illyricum: towards an Islamic monopoly. Archaeol Anthropol Sci 11, 1107–1122 (2019).

Nicholson, P. T. (2012). Stone... that flows: faience and glass as man-made stones in Egypt. Journal of Glass Studies, 11-23.

Nicholson, P. T., & Peltenburg, E. J. (2000). Faience. In Ogden, J., Nicholson, P. T., & Shaw, I. (2000). Ancient Egyptian materials and technology. Camrbidge University press, Cambridge, 702.

Nielsen, E. (1998). Bronze Production at Poggio Civitate (Murlo). Etruscan Studies, 5(1), 95-108.

Nijboer, A. J. (2008a). Italy and the Levant during the Late Bronze and Iron Age (1200-750/700 BC.). Beyond the Homeland: Markers in Phoenician Chronology, 28, 423-460.

Nijboer, A. J. (2008b). A Phoenician family tomb, Lefkandi, Huelva and the tenth century BC in the Mediterranean. Peeters. pp. 365-377.

Nikita, K., & Henderson, J. (2006). Glass analyses from Mycenaean Thebes and Elateia: compositional evidence for a Mycenaean glass industry. Journal of Glass Studies, 71-120.

Noble, J. V. (1969). The technique of Egyptian faience. American journal of archaeology, 73(4), 435-439.

Nolte, H., MacVicar, T. D., Tellkamp, F., & Krüger, M. (2018). Instant clue: a software suite for interactive data visualization and analysis. Scientific reports, 8(1), 1-8.

O'Hea, M. (2005). Late Hellenistic glass from some military and civilian sites in the Levant: Jebel Khalid, Pella and Jerusalem. Ann AIHV, 16, 44-48.

Oded, B. (1974). The Phoenician cities and the Assyrian Empire in the time of Tiglath-Pileser III. Zeitschrift des Deutschen Palästina-Vereins (1953-), (H. 1), 38-49.

Ohta, N., & Robertson, A. (2006). Colorimetry: fundamentals and applications. John Wiley & Sons, 334.

Oikonomou, A., Beltsios, K., Zacharias, N., & Triantafyllidis, P. (2012). Technological and provenance study of archaic glassy materials from Rhodes island, Greece using p-XRF and SEM/EDX analysis. In Proceedings of the 39th International Symposium for Archaeometry.

Oikonomou, A., & Triantafyllidis, P. (2018a). An archaeometric study of Archaic glass from Rhodes, Greece: Technological and provenance issues. Journal of Archaeological Science: Reports, 22, 493-505.

Oikonomou, A., Henderson, J., Gnade, M., Chenery, S., & Zacharias, N. (2018b). An archaeometric study of Hellenistic glass vessels: evidence for multiple sources. Archaeological and Anthropological Sciences, 10, 97-110.

Oikonomou, A., Henderson, J., & Chenery, S. (2020). Provenance and technology of fourth–second century BC glass from three sites in ancient Thesprotia, Greece. Archaeological and Anthropological Sciences, 12, 1-15.

Oikonomou, A., Rehren, T., & Fiolitaki, A. (2021). An early Byzantine glass workshop at Argyroupolis, Crete: Insights into complex glass supply networks. Journal of Archaeological Science: Reports, 35, 102766.

Oikonomou, A., Kaparou, M., Šelih, V. S., van Elteren, J. T., Zacharias, N., Chenery, S., & Henderson, J. (2023). Theban Glass Traditions in the 1st Millennium BCE, Greece: New LA-ICP-MS Data and Their Archaeological Implications. Heritage, 6(1), 705-723.

Olmeda, G. (2015) Evolution of ornamental vitreous materials in Italy from the Middle Bronze Age to the Iron Age: case studies from Lipari and from the Veneto region. PhD thesis, University of Padova, 238.

Olmeda, G., Prosdocimi, B., Angelini, I., Cupitò, M., & Molin, G. (2015). Archeologia e archeometria delle perle in vetro della necropoli patavina del CUS-Piovego (VI-IV secolo aC): osservazioni sulla tecnologia del vetro in Veneto nella piena Età del ferro. In: G. Leonardi e V. Tiné [eds.] Preistoria e Protostoria del Veneto, 549-557.

Oppenheim, A. L. (1973). Towards a history of glass in the ancient Near East. Journal of the American Oriental Society, 93(3), 259-266.

Owen, M. R. (1987). Hafnium content of detrital zircons, a new tool for provenance study. Journal of Sedimentary Research, 57(5), 824-830.

Pacciarelli, M. (2016). The Earliest Processes Toward City-States, Political Power and Social Stratification in Middle Tyrrhenian Italy. Origini, 39, 169-207.

Pacciarelli, M. (2017). Society, 10th Cent.-730 BCE. In: Naso A. (Ed.) Etruscology, Walter de Gruyter GmbH & Co KG. V.1, 759-778.

Palavestra, A. (1997). Prehistoric amber and glass beads from Kosovo. Balcanica, (28), 15-43.

Pallottino, M. (1958). Urartu, Greece and Etruria. East and West, 9(1/2), 29-52.

Palm, J. (1952). Veiian tomb groups in the Museo Preistorico, Rome, in Opuscula Archaeologica VII, p.70, n. 25.

Panighello, S., Orsega, E. F., van Elteren, J. T., & Šelih, V. S. (2012). Analysis of polychrome Iron Age glass vessels from Mediterranean I, II and III groups by LA-ICP-MS. Journal of archaeological science, 39(9), 2945-2955.

Paribeni, R. (1906) Necropoli del territorio capenate. Monumenti Antichi dei Lincei 16, 277-490.

Parrini, P., Formigli, E., & Mello, E. (1982). Etruscan granulation: Analysis of orientalizing jewelry from Marsiliana d'Albegna. American Journal of Archaeology, 86(1), 118-121.

Paul, A. (1989). Chemistry of glasses. Springer Science & Business Media, 368.

References

Paynter, S., & Jackson, C. M. (2022). Investigating Late Bronze Age Glass Beads from Stotfold, Bedfordshire, UK. Heritage, 5(2), 634-645.

Pelletier, J. M., & Qiao, J. (2019). Metallic glasses. Springer Handbook of Glass, 617-643.

Phelps, M., Freestone, I. C., Gorin-Rosen, Y., & Gratuze, B. (2016). Natron glass production and supply in the late antique and early medieval Near East: The effect of the Byzantine-Islamic transition. Journal of Archaeological Science, 75, 57-71.

Phelps, M., Freestone, I., Gorin-Rosen, Y., Gratuze, B., & Langton, J. (2015). Technological change and provenance of glass in Early Islamic Palestine. In 20th Congress of the International Association for the History of Glass, Friborg-Romont, Switzerland, 157.

Picollo, M., Aceto, M., & Vitorino, T. (2018). UV-Vis spectroscopy. Physical sciences reviews, 4(4), 20180008.

Pilkington, N. (2019). The Carthaginian Empire: 550–202 BCE. Lexington Books, 226.

Pliny the Elder (1855). The Natural History. J. Bostock [Ed.], M.D., F.R.S. H.T. Riley, Esq., B.A. London. Taylor and Francis, Red Lion Court, Fleet Street. 245.

Polikreti, K., Murphy, J. M., Kantarelou, V., & Karydas, A. G. (2011). XRF analysis of glass beads from the Mycenaean palace of Nestor at Pylos, Peloponnesus, Greece: new insight into the LBA glass trade. Journal of Archaeological Science, 38(11), 2889-2896.

Polla, A., Angelini, I., Artioli, G., Bellintani, P., & Dore, A. (2011). Archaeometric investigation of early Iron Age glasses from Bologna. In Proceedings of the 37 th International Symposium on Archaeometry, 13th-16th May 2008, Siena, Italy. Springer Berlin Heidelberg, 139-144.

Pollard, A. M., & Heron, C. (2015). Archaeological chemistry. Royal Society of Chemistry Publishing, 456.

Pomey, P. (2017). Ships and Shipping. In: Naso A. (Ed.) Etruscology, De Gryuter, V.1, 371-390.

Potts, C. R. (2015). Religious architecture in Latium and Etruria, c. 900-500 BC. Oxford University Press, 178.

Pourret, O., van Der Ent, A., Hursthouse, A., Irawan, D. E., Liu, H., & Wiche, O. (2022). The 'europium anomaly'in plants: facts and fiction. Plant and Soil, 1-8.

Purowski, T., Dzierżanowski, P., Bulska, E., Wagner, B., & Nowak, A. (2012). A study of glass beads from the Hallstatt C–D from southwestern Poland: implications for glass technology and provenance. Archaeometry, 54(1), 144-166.

Purowski, T., Kępa, L., & Wagner, B. (2018). Glass on the Amber Road: the chemical composition of glass beads from the Bronze Age in Poland. Archaeological and Anthropological Sciences, 10, 1283-1302.

Qin, Y., Wang, Y., Chen, X., Li, H., Xu, Y., & Li, X. (2016). The research of burning ancient Chinese lead-barium glass by using mineral raw materials. Journal of Cultural Heritage, 21, 796-801.

Quartieri, S., & Arletti, R. (2013). The use of X–ray absorption spectroscopy in historical glass research. Modern methods for analysing archaeological and historical glass, 1, 301-309.

Randall-MacIver, D. (1924). Villanovans and early Etruscans: a study of the early Iron Age in Italy as it is seen near Bologna, in Etruria and in Latium. Clarendon Press, 270.

Rao, K. J. (2002). Structural chemistry of glasses. Elsevier Science, 584.

Rasmussen, S. C. (2012). How glass changed the world: The history and chemistry of glass from antiquity to the 13th century. Springer Science & Business Media, 85.

Rasmussen, T., Osborne, R., & Cunliffe, B. (2005). Etruscan urbanisation. In Mediterranean Urbanization 800-600 BC. Oxford University Press, 71-90.

Rathje, A. (2010). Tracking down the Orientalizing. Bollettino di Archeologia on line, 23, 30.

Read, M., Cheung, C. S., Liang, H., Meek, A., & Korenberg, C. (2022). A non-invasive investigation of Egyptian faience using Long Wavelength Optical Coherence Tomography (OCT) at 2 µm. Studies in Conservation, 67(3), 168-175.

Reade, W. J., Jones, J. D., & Privat, K. (2009a). Iron Age and Hellenistic monochrome glasses from Gordion. Iron Age, 1, 1-19.

Reade, W., Freestone, I. C., & Bourke, S. (2009b). Innovation and continuity in Bronze and Iron Age glass from Pella in Jordan. Iron Age, 38(16.69), 3-91.

Reade, W. (2021). The First Thousand Years of Glass-Making in the Ancient Near East: Compositional Analyses of Late Bronze and Iron Age Glasses. Archaeopress. 273.

Rehren, T. (2000). Rationales in Old World base glass compositions. Journal of Archaeological science, 27(12), 1225-1234.

Rehren, T. (2001). Aspects of the production of cobalt-blue glass in Egypt. Archaeometry, 43(4), 483-489.

Rehren, T. (2003). COMMENTS I. Archaeometry, 45(1), 185-190.

Rehren, T., & Freestone, I. C. (2015). Ancient glass: from kaleidoscope to crystal ball. Journal of Archaeological Science, 56, 233-241.

Rehren, T. (2021). The origin of glass and the first glass industries. Ancient Glass of South Asia: Archaeology, Ethnography and Global Connections, 3-20.

Renda, V., Nardo, V. M., Anastasio, G., Caponetti, E., Vasi, C. S., Saladino, M. L., ... & Ponterio, R. C. (2019). A multivariate statistical approach of X-ray fluorescence characterization of a large collection of reverse glass paintings. Spectrochimica Acta Part B: Atomic Spectroscopy, 159, 105655.

Ricciardi, P., Colomban, P., Tournié, A., Macchiarola, M., & Ayed, N. (2009). A non-invasive study of Roman Age mosaic glass tesserae by means of Raman spectroscopy. Journal of Archaeological Science, 36(11), 2551-2559.

Ridgway, D. (1968). Archaeology in Central Italy and Etruria, 1962–67. Archaeological Reports, 14, 29-48.

Riemer, H. (2007). Mapping the movement of pastro-foragers: The spread of desert glass and other objects in the eastern Sahara during the Holocene “humid phase”, 30-33.

Riva, C. (2006). The Orientalizing period in Etruria: sophisticated communities. Debating orientalization: multidisciplinary approaches to change in the ancient Mediterranean, 110-134.

Roberts, J. (2007) Oxford dictionary of classical world. Oxford University press, 858.

Robino, M.T.A. (2016) La necropoli del Canal Bianco di Adria (RO): problemi e prospettive a settant’anni dallo scavo, in Digging Up Excavations. In: P. Rondini e L. Zamboni [eds.] Processi di ricontestualizzazione di “vecchi” scavi archeologici: esperienze, problemi, prospettive, Roma, 91-101.

Rousseau, R. M., Willis, J. P., & Duncan, A. R. (1996). Practical XRF calibration procedures for major and trace elements. X-Ray Spectrometry, 25(4), 179-189.

Rubert, D. G. I., & Alonso, F. G. (2011). Phoenician Trade in the North-East of the Iberian Peninsula: a Historiographical Problem. Oxford Journal of Archaeology, 30(1), 33-56.

Rutten, F. J. M., Roe, M. J., Henderson, J., & Briggs, D. (2006). Surface analysis of ancient glass artefacts with ToF-SIMS: A novel tool for provenancing?. Applied surface science, 252(19), 7124-7127.

Sagripanti, L. (2022). Fingere ex argilla: gli indicatori di produzione di miniaturistici nel contesto votivo di Tivoli, Loc. Acquoria, Scienze dell’Antichita V. 28, 515-520.

Sanchez, C. (2022). Trading networks in Transalpine Gaul before and after the conquest in 125 BCE.

Sanmartí, J., Martín, M. A., & Asensio, D. (2006). Etruscan imports in the indigenous sites of Catalonia, Istituti editoriali e poligrafici internazionali, 202.

Sayre, E. V. (1964). Some ancient glass specimens with compositions of particular archaeological significance (No. BNL-879). Brookhaven National Lab., Upton, NY.

Sayre, E. V., & Smith, R. W. (1961). Compositional categories of ancient glass. Science, 133(3467), 1824-1826.

Schenkel, W. (2019). Colours as viewed by the Ancient Egyptians and the explanation of this view as seen by academics studying colour. In Warburton, D. and Thavapalan, S. [eds.], Value of Colour. Material and Economic Aspects in the Ancient World, Berlin. Edition Topoi, 35-55.

Schibille, N. (2011). Late Byzantine mineral soda high alumina glasses from Asia Minor: a new primary glass production group. PLoS One, 6(4), e18970.

Schibille, N., Sterrett-Krause, A., & Freestone, I. C. (2017). Glass groups, glass supply and recycling in late Roman Carthage. Archaeological and Anthropological Sciences, 9, 1223-1241.

Schmidt, K. (2019). Glass and glass production in the Near East during the Iron Age: evidence from objects, texts and chemical analysis. Archaeopress Publishing Ltd.

Schreurs, J. W., & Brill, R. H. (1984). Iron and sulfur related colors in ancient glasses. Archaeometry, 26(2), 199-209.

Sciandrello, S., & Tomaselli, V. (2014). Coastal salt-marshes plant communities of the Salicornietea fruticosae class in Apulia (Italy). Biologia, 69, 53-69.

Scott, R. B., Shortland, A. J., Degryse, P., Power, M., Domoney, K., Boyen, S., & Braekmans, D. (2012). In situ analysis of ancient glass: 17th century painted glass from Christ Church Cathedral, Oxford and Roman glass vessels. Glass Technology-European Journal of Glass Science and Technology Part A, 53(2), 65-73.

Scott, R. B., & Degryse, P. (2014). The archaeology and archaeometry of natron glass making. Glass Making in the Greco-Roman World: Results of the ARCHGLASS Project, 15-26.

Sestieri, A. M. B. (1992). The Iron Age community of Osteria dell'Osa: a study of socio-political development in central Tyrrhenian Italy. CUP Archive, 271.

Sestieri, A. M. B. (1997). Italy in Europe in the Early Iron Age. In Proceedings of the Prehistoric Society Cambridge University Press, 63, 371-402.

Settis, S. (1985). The land of the Etruscans: from prehistory to the Middle Ages. Scala. 96.

Seubers, J. F. (2008). A Key to the Coffin: A model to assess social change in Villanovan tombs from Veii, Tarquinia and Verucchio (950 to 700 BC). Babesch, 83, 1-16.

Sherratt, S., & Sherratt, A. (1993). The growth of the Mediterranean economy in the early first millennium BC. World Archaeology, 24(3), 361-378.

Shields, G., & Stille, P. (1998). Stratigraphic trends in cerium anomaly in authigenic marine carbonates and phosphates: diagenetic alteration or seawater signal. Goldschmidt Conference, 1387-1388.

Shields, G., & Stille, P. (2001). Diagenetic constraints on the use of cerium anomalies as palaeoseawater redox proxies: an isotopic and REE study of Cambrian phosphorites. Chemical Geology, 175(1-2), 29-48.

Shortland, A. J., Nicholson, P. T., & Jackson, C. M. (2000). Lead isotopic analysis of eighteenth-dynasty Egyptian eyepaints and lead antimonate colourants. Archaeometry, 42(1), 153-157.

Shortland, A. J., & Tite, M. S. (2000). Raw materials of glass from Amarna and implications for the origins of Egyptian glass. Archaeometry, 42(1), 141-151.

Shortland, A. J. (2002). The use and origin of antimonate colorants in early Egyptian glass. Archaeometry, 44(4), 517-530.

Shortland, A. J., & Tite, M. S. (2005). Technological study of Ptolemaic–early Roman faience from Memphis, Egypt. Archaeometry, 47(1), 31-46.

Shortland, A. J., Tite, M. S., & Ewart, I. (2006a). Ancient exploitation and use of cobalt alums from the Western Oases of Egypt. Archaeometry, 48(1), 153-168.

Shortland, A., Schachner, L., Freestone, I., & Tite, M. (2006b). Natron as a flux in the early vitreous materials industry: sources, beginnings and reasons for decline. Journal of Archaeological Science, 33(4), 521-530.

Shortland, A., Rogers, N., & Eremin, K. (2007). Trace element discriminants between Egyptian and Mesopotamian late Bronze Age glasses. Journal of Archaeological Science, 34(5), 781-789.

Shortland, A. J., & Schroeder, H. (2009). Analysis of first millennium BC glass vessels and beads from the Pichvnari necropolis, Georgia. Archaeometry, 51(6), 947-965.

Shortland, A. J., Kirk, S., Eremin, K., Degryse, P., & Walton, M. (2018). The analysis of Late Bronze Age glass from Nuzi and the question of the origin of glass-making. Archaeometry, 60(4), 764-783.

Shortland, A. J., & Degryse, P. (2021). Ancient Glass, Late Bronze Age. Encyclopedia of Glass Science, Technology, History, and Culture, 2, 1249-1259.

Shugar, A., & Rehren, T. (2002). Formation and composition of glass as a function of firing temperature. Glass Technology, 43, 145-150.

Silvestri, A., Molin, G., & Salviulo, G. (2008). The colourless glass of Iulia Felix. Journal of archaeological science, 35(2), 331-341.

Silvestri, A., & Marcante, A. (2011). The glass of Nogara (Verona): a “window” on production technology of mid-Medieval times in Northern Italy. Journal of Archaeological Science, 38(10), 2509-2522.

Singkiburin, N., Srisittipokakun, N., & Keawkhao, J. (2020). Effect of antimony (III) oxide on reduction of bubbles from glass melting process. In Journal of Physics: Conference Series, IOP Publishing 1428, 1, 012030.

Smirniou, M., & Rehren, T. (2013). Shades of blue–cobalt-copper coloured blue glass from New Kingdom Egypt and the Mycenaean world: a matter of production or colourant source?. Journal of Archaeological Science, 40(12), 4731-4743.

Šmit, Ž., Janssens, K., Bulska, E., Wagner, B., Kos, M., & Lazar, I. (2005). Trace element fingerprinting of façon-de-Venise glass. Nuclear Instruments and Methods in Physics Research Section B: Beam Interactions with Materials and Atoms, 239(1-2), 94-99.

Šmit, Ž., Laharnar, B., & Turk, P. (2020). Analysis of prehistoric glass from Slovenia. Journal of Archaeological Science: Reports, 29, 102114.

Smith, C. J. (1994). A review of archaeological studies on Iron-Age and archaic Latium. Journal of Roman Archaeology, 7, 285-302.

Solé, V. A., Papillon, E., Cotte, M., Walter, P., & Susini, J. (2007). A multiplatform code for the analysis of energy-dispersive X-ray fluorescence spectra. Spectrochimica Acta Part B: Atomic Spectroscopy, 62(1), 63-68.

Sosman, R. B. (1927). The Properties of Silica: An introduction to the properties of substances in the solid non-conducting state. Book Department, The Chemical Catalog Company, Inc. 37.

Spencer, H. M., Murdoch, K. R., Buckman, J., Forster, A. M., & Kennedy, C. J. (2018). Compositional Analysis by p-XRF and SEM–EDX of Medieval Window Glass from Elgin Cathedral, Northern Scotland. Archaeometry, 60(5), 1018-1035.

Sperber, C. M., Wilkinson, B. H., & Peacor, D. R. (1984). Rock composition, dolomite stoichiometry, and rock/water reactions in dolomitic carbonate rocks. The Journal of Geology, 92(6), 609-622.

Spivey, N. J. (1997). Etruscan art. Thames & Hudson. 216.

Sprague, R., & Bowers, A. W. (1985). Glass trade beads: A progress report. Historical Archaeology, 19(2), 87-105.

Sprincz, E., & Beck, C. W. (1981). Classification of the amber beads of the Hungarian Bronze Age. Journal of field archaeology, 8(4), 469-485.

Stefaní, E. (1912). Scoperte archeologiche nell'Agro Capenate. Bollettino di Paletnologia Italiana, 38, 147-158.

Stern, E. M. (1995). Roman mold-blown glass: the first through sixth centuries. L'Erma di Bretschneider, Toledo Museum of Art, 388.

Stern, E. M. (1999). Ancient glass in Athenian temple treasures. Journal of Glass Studies, 41, 19-50.

Stern, E. M. (2007). Ancient glass in a philological context. Mnemosyne, 60(3), 341-406.

Sternini, M. (2017). La lavorazione del vetro nel mondo antico. In Pretiosa vitrea: l'arte vetraria antica nei musei e nelle collezioni private della Toscana. 5continents. 14-21.

Stoddart, S. K. (2009). Historical dictionary of the Etruscans. Scarecrow Press. 24, 105.

Sun, H., Wu, J., Yu, P., & Li, J. (1998). Geology, geochemistry and sulfur isotope composition of the Late Proterozoic Jingtieshan (Superior-type) hematite-jasper-barite iron ore deposits associated with stratabound Cu mineralization in the Gansu Province, China. Mineralium Deposita, 34, 102-112.

Tait, H. (1991). Glass, 5,000 years. H. Tait [ed.]. New York: H.N. Abrams. 256.

Taloni, M (2013). Le tombe da Riserva del Truglio al Museo Pigorini di Roma, Officina Etruscologia, 8, Rome, 437.

Tamura, T., & Oga, K. (2016). Archaeometrical investigation of natron glass excavated in Japan. Microchemical Journal, 126, 7-17.

Taniichi, T. (1992). Spacer Glass Beads in the Second Millennium BC. Orient, 28, 132-146.

Targowski, P., & Iwanicka, M. (2012). Optical coherence tomography: its role in the non-invasive structural examination and conservation of cultural heritage objects—a review. Applied Physics A, 106, 265-277.

Taylor, J. (2000). The third intermediate period. In: Ian Shaw (ed.) Oxford History of Ancient Egypt. Oxford: Oxford University Press, 324-364.

Then-Obłuska, J. (2021). Typology of Glass Beads: Techniques, Shapes, Colours and Dimensions. In: Kanungo, A.K., Dussubieux, L. [eds.] Ancient Glass of South Asia. Springer, Singapore, 211-224.

Tite, M. S. (2004). Glass and related vitreous materials. In Physics Methods in Archaeometry, IOS Press 369-376.

Tite, M. S., & Bimson, M. (1986). Faience: an investigation of the microstructures associated with the different methods of glazing. Archaeometry, 28(1), 69-78.

Tite, M. S., Freestone, I. C., & Bimson, M. (1983). Egyptian faience--an investigation of the methods of production. Archaeometry, 25(1), 17-27.

Tite, M. S., Manti, P., & Shortland, A. J. (2007). A technological study of ancient faience from Egypt. Journal of archaeological science, 34(10), 1568-1583.

Tite, M. S., Shortland, A., Maniatis, Y., Kavoussanaki, D., & Harris, S. A. (2006). The composition of the soda-rich and mixed alkali plant ashes used in the production of glass. Journal of Archaeological Science, 33(9), 1284-1292.

Toffolo, M. B., Klein, E., Elbaum, R., Aja, A. J., Master, D. M., & Boaretto, E. (2013). An early Iron Age assemblage of faience beads from Ashkelon, Israel: chemical composition and manufacturing process. Journal of archaeological science, 40(10), 3626-3635.

Tostevin, R., Shields, G. A., Tarbuck, G. M., He, T., Clarkson, M. O., & Wood, R. A. (2016). Effective use of cerium anomalies as a redox proxy in carbonate-dominated marine settings. Chemical Geology, 438, 146-162.

Towle, A., Gambacurta, G., Bellintani, P., & Henderson, J. (2001). Frattesina and Adria: report of scientific analysis of early glass from the Veneto. Frattesina and Adria: report of scientific analysis of early glass from the Veneto, Padusa: bollettino del centro polesano di studi storici archeologici ed etnografici: XXXVII, 37,1-62.

Towle, A., & Henderson, J. (2004). The glass bead game: archaeometric evidence for the existence of an Etruscan glass industry. Etruscan Studies, 10(1), 47-66.

Trail, D., Watson, E. B., & Tailby, N. D. (2012). Ce and Eu anomalies in zircon as proxies for the oxidation state of magmas. Geochimica et Cosmochimica Acta, 97, 70-87.

Tsetskhladze, G. R. (1998). Greek colonisation of the Black Sea area: stages, models, and native population. Historia. Einzelschriften, (121), 7-330.

Tuck, A. S. (1994). The Etruscan seated banquet: Villanovan ritual and Etruscan iconography. American Journal of Archaeology, 98(4), 617-628.

Turfa, J. M. (2005). Catalogue of the Etruscan gallery of the University of Pennsylvania Museum of Archaeology and Anthropology. UPenn press, Museum of Archaeology, 816.

Turfa, J. M. [Ed.]. (2014). The Etruscan World. Routledge, 1216.

Turfa, J. M., & Steinmayer Jr, A. G. (2001). Swen hulls and self-defense. The International Journal of Nautical Archaeology, 30(1), 122-127.

Turner, W. E. S. (1954). Studies of ancient glass and glassmaking processes. Crucibles and melting temperatures employed in ancient Egypt at about 1370 BC. J. Soc. Glass Technol, 38, 436-44.

Turner, W. E. S. (1956). Ancient glasses and glassmaking processes. The chronology of the glassmaking constituents. J. Soc. Glass Technol, 40, 39-52.

Turner, W. E. S. (1959). Studies in ancient glasses and glassmaking processes. The composition and physical characteristics of the glasses of the Portland Vase. Journal of the Society of Glass Technology, 43, 262-284.

Tzankova, N., & Mihaylov, P. (2019). Chemical characterization of glass beads from the necropolis of Dren-Delyan (6th–4th century BC), Southwest Bulgaria. Geol. Balc, 48, 31-50.

Tzifas, I. T., Misaelides, P., Godelitsas, A., Gamaletsos, P. N., Nomikou, P., Karydas, A. G., ... & Papadopoulos, A. (2017). Geochemistry of coastal sands of Eastern Mediterranean: The case of Nisyros volcanic materials. Geochemistry, 77(3), 487-501.

Van Der Maaten, L., Lange, G., & Boon, P. (2009). Visualization and Automatic Typology Construction of Pottery Profiles. Pattern Recognition Letters, 2614, 2174-2186.

Van Ham-Meert, A., Dillis, S., Blomme, A., Cahill, N., Claeys, P., Elsen, J., ... & Degryse, P. (2019). A unique recipe for glass beads at Iron Age Sardis. Journal of Archaeological Science, 108, 104974.

Vandenabeele, P., Edwards, H. G. M., & Jehlička, J. (2014). The role of mobile instrumentation in novel applications of Raman spectroscopy: archaeometry, geosciences, and forensics. Chemical Society Reviews, 43(8), 2628-2649.

Vandiver, P. B. (1998). A review and proposal of new criteria for production technologies of Egyptian faience, La couleur dans la peinture et l'émaillage de l'Egypte ancienne: actes de la table ronde, Ravello, 20-22 mars 1997, Bari, Edipuglia, 121-139.

Varberg, J., Gratuze, B., & Kaul, F. (2015). Between Egypt, Mesopotamia and Scandinavia: Late Bronze Age glass beads found in Denmark. Journal of Archaeological Science, 54, 168-181.

Various Authors (1965) Veio - Isola Farnese. Scavi di una necropoli villanoviana in località „Quattro Fontanili". Notizie degli Scavi (8), 123-138.

Venclová, N., Hulínský, V., Henderson, J., Chenery, S., Šulová, L., & Hložek, J. (2011). Late Bronze Age mixed-alkali glasses from Bohemia. Archeologické rozhledy, 63(4), 559-585.

Venclová, N., Křížová, Š., Dillingerová, V., & Vaculovič, T. (2018). Hellenistic cast monochrome glass vessels from Staré Hradisko, 2nd–1st cent. BCE. Journal of Archaeological Science: Reports, 22, 540-549.

Verheijen, O.S., Hubert, M. (2019). Batch Chemistry and Reactions. In: Musgraves, J.D., Hu, J., Calvez, L. (eds) Springer Handbook of Glass. Springer Handbooks. Springer, Cham, 1233-1258.

Verità, M., James, L., Freestone, I., Henderson, J., Nenna, M. D., & Schibille, N. (2009). Glossary of mosaic glass terms. humanities, 1273, 678001.

Verità, M., Lazzarini, L., Tesser, E., & Antonelli, F. (2019). Villa del Casale (Piazza Armerina, Sicily): stone and glass tesserae in the baths floor mosaics. Archaeological and Anthropological Sciences, 11, 373-385.

Villing, A., Schlotzhauer U. [Ed.] (2006). Naukratis: Greek Diversity in Egypt. Trustees of the British Museum, 245.

Visco, G., Ridolfi, S., Plattner, S. H., & Gigante, G. E. (2010). Razors, horse bits or axes; search of the different composition in common use bronze Villanovan objects (VIII-VII century BC, Italy) by multivariate analysis. Current Analytical Chemistry, 6(1), 11-18.

von Eles, P. (2013). Research in Villanovan necropoleis of Verucchio, 9th to 7th century BC. Research into Pre-Roman Burial Grounds in Italy, Caeculus: Papers on Mediterranean Archaeology & Greek Roman Studies, (8), 83-102.

von Eles, P., Bentini, L., Poli, P., & Rodriguez, E. [Eds.]. (2015). Immagini di uomini e di donne dalle necropoli villanoviane di Verucchio. All'Insegna del Giglio. 34, 224.

Vries, de J.L. and Vrebos, B.A.R. (2001) Quantification of Infinitely Thick Specimens by XRF Analysis. In: Van Grieken, R., & Markowicz, A. (Eds.) Handbook of X-ray Spectrometry. CRC press, 341-406.

Walton, M. S., Shortland, A., Kirk, S., & Degryse, P. (2009). Evidence for the trade of Mesopotamian and Egyptian glass to Mycenaean Greece. *Journal of Archaeological Science*, *36*(7), 1496-1503.

Walton, M., Eremin, K., Shortland, A., Degryse, P., & Kirk, S. (2012). Analysis of Late Bronze Age glass axes from Nippur—A new cobalt colourant. *Archaeometry*, *54*(5), 835-852.

Wang, K. W., Iizuka, Y., & Jackson, C. (2022). The production technology of mineral soda alumina glass: A perspective from microstructural analysis of glass beads in Iron Age Taiwan. Plos one, 17(2), e0263986.

Wedepohl, K. H., Simon, K., & Kronz, A. (2011). Data on 61 chemical elements for the characterization of three major glass compositions in Late Antiquity and the Middle Ages. *Archaeometry*, *53*(1), 81-102.

Weill, D. F., & Drake, M. J. (1973). Europium anomaly in plagioclase feldspar: experimental results and semiquantitative model. *Science*, *180*(4090), 1059-1060.

Weyl, W. (1999). Coloured glasses. W. A. Weyl. Monographs on glass technology (Sheffield, Eng., Society of Glass Technology). Sheffield, UK, Society of Glass Technology, 542.

White, M. E. (1961). Greek colonization. The journal of economic history, 21(4), 443-454.

Whitehouse, M. J., & Kamber, B. S. (2002). On the overabundance of light rare earth elements in terrestrial zircons and its implication for Earth's earliest magmatic differentiation. *Earth and Planetary Science Letters*, *204*(3-4), 333-346.

Whittaker, J. C., Caulkins, D., & Kamp, K. A. (1998). Evaluating consistency in typology and classification. *Journal of Archaeological Method and Theory*, *5*(2), 129-164.

Winther, H. C. (1997). Princely tombs of the orientalizing period in Etruria and Latium Vetus. Urbanization in the Mediterranean in the 9th to 6th Centuries BC, 7, 423.

Wojdyr, M. (2010). Fityk: a general-purpose peak fitting program. *Journal of Applied Crystallography*, *43*(5-1), 1126-1128.

References

Won-in, K., Thongkam, Y., Pongkrapan, S., Intarasiri, S., Thongleurm, C., Kamwanna, T., ... & Dararutana, P. (2011). Raman spectroscopic study on archaeological glasses in Thailand: ancient Thai glass. Spectrochimica Acta Part A: Molecular and Biomolecular Spectroscopy, 83(1), 231-235.

Xia, N. (2014). Ancient Egyptian Beads. Berlin: Springer, 173.

Yatsuk, O., Ferretti, M., Gorghinian, A., Fiocco, G., Malagodi, M., Agostino, A., & Gulmini, M. (2022). Data from Multiple Portable XRF Units and Their Significance for Ancient Glass Studies. Molecules, 27(18), 6068.

Zacharias, N., Kaparou, M., Oikonomou, A., & Kasztovszky, Z. (2018). Mycenaean glass from the Argolid, Peloponnese, Greece: A technological and provenance study. Microchemical Journal, *141*, 404-417.

Zachariasen, W. H. (1932). The atomic arrangement in glass. Journal of the American Chemical Society, 54(10), 3841-3851.

Zalloua, P. A., Platt, D. E., El Sibai, M., Khalife, J., Makhoul, N., Haber, M., ... & Tyler-Smith, C. (2008). Identifying genetic traces of historical expansions: Phoenician footprints in the Mediterranean. The American Journal of Human Genetics, 83(5), 633-642.

Zhong, S., Seltmann, R., Qu, H., & Song, Y. (2019). Characterization of the zircon Ce anomaly for estimation of oxidation state of magmas: a revised Ce/Ce* method. Mineralogy and Petrology, *113*, 755-763.

Zhou, Y., Jin, Y., Wang, K., Sun, J., Cui, Y., & Hu, D. (2019). Opaque ancient K2O–PbO–SiO2 glass of the Southern Song Dynasty with fluorite dendrites and its fabrication. Heritage Science, *7*(1), 1-9.

Zifferero, A. (2017). Mines and Metal Working. In: Naso A. Etruscology, Walter de Gruyter GmbH & Co KG. V.1, 425 -444.

Zlámalová Cílová, Z., Čisťakova, V., Kozáková, R., & Lapčák, L. (2022). Chemistry and Production Technology of Hallstatt Period Glass Beads from Bohemia. Materials, *15*(16), 5740.

APPENDIX 1. ARCHAEOLOGICAL CONTEXTS OF THE SAMPLES INVOLVED IN THE INGOT-EL PROJECT.

The table below presents samples discussed in the study in their numerical order. The PG series precedes the VG series. Data on contexts are structured on topographical (grave-site-locality) and chronological (period and absolute dates) levels. By the site we mean larger area where the artifacts were found. For example, Cerveteri site is represented by several burial sites or necropolis: Cava della Pozzolana, Monte Abatone, Banditaccia, Sasso di Furbara that are separate archaeological sites around the main ancient settlement. The necropoli are named as “localities” in the table. Samples that were found outside of graves are marked as those without precise context. Dates of the graves are provided with the indication of the relative period. In cases where it was possible for archaeologists to narrow down the absolute date such date is provided in the table, in all other cases the absolute dates refer to the absolute dates of the period the graves are assigned to. References are supplied as a source of information on specific graves but also about the whole necropolis.

Sample name	Grave	Site	Locality	Absolute date	Relative date	Reference
VG1	Kottabos tomb	Vulci	Osteria	520-500 BCE	Late Archaic	Moretti Sgubini, A.M., 2001
VG2						
VG3						
VG4						
VG5						
VG6						
VG7						
VG9						
VG13	Tomb "a camera"	Vulci	Monte Auto	520-510 BCE	Late Archaic	Falconi Amorelli, M.T., 1967

Sample name	Grave	Site	Locality	Absolute date	Relative date	Reference
VG14	Tomb "a fossa profonda"	Vulci	Poggio Maremma	725-700 BCE	Early Orientalising	Moretti Sgubini, A. M., 2001
VG15						
VG16						
VG17						
VG18						
VG19						
VG20						
VG21						
VG22	Bronzetti Sardi tomb	Vulci	Cavalupo	850-825 BCE	EIA I	Arancio M.L. et al., 2010
VG23						
VG24						
VG25						
VG26						
VG27						
VG28						
VG29						
VG32	Martiri Marescotti Tomb (610)	Cerveteri	Monte Abatone	530-480 BCE	Late Archaic	Ridgway, D., 1968
VG33						
VG34						
VG35						
VG36						
VG37						
VG38	Tomb ad est del Laghetto	Cerveteri	Banditaccia	550-510 BCE	Early Archaic	Unpublished

Sample name	Grave	Site	Locality	Absolute date	Relative date	Reference
VG39	Tumulo del Colonello, Tomb IV	Cerveteri	Banditaccia	630-580 BCE	Late Orientalising	Ricci, G., 1955
VG40						
VG41						
VG42						
VG43						
VG44						
VG45						
VG46						
VG47						
VG48	Tomb XXVII	Cerveteri	Cava Della Pozzolana	800-730 BCE	EIA II	Unpublished
VG49						
VG50						
VG51						
VG52						
VG53						
VG54						
VG55						
VG56	Tomb AA1	Veio	Quattro Fontanili	770-730 BCE	EIA II	Boitani, F., 2004
VG57	Tomb HH 11-12	Veio	Quattro Fontanili	750-730 BCE	EIA II	Various authors, 1965
VG58						
VG59						
VG60						
VG61						
VG62						
VG63						
VG64						
VG65						

Sample name	Grave	Site	Locality	Absolute date	Relative date	Reference
VG66	Tomb HH 11-13	Veio	Quattro Fontanili	750-730 BCE	EIA II	Various authors, 1965
VG67						
VG68						
VG69						
VG70						
VG71						
VG72	Tomb 575	Veio	Grotta Gramiccia	800-770 BCE	EIA II	Berardinetti, A. and Drago L., 1997
VG73						
VG74						
VG75						
VG76	Leoni Ruggenti tomb	Veio	Grotta Gramiccia	710-670 BCE	Early Orientalising	Boitani, F., 2010
VG77						
VG78						
VG79						
VG80						
VG81						
VG82	Tomb 1	Narce	Necropoli dei Tufi	800-720 BCE	EIA II	Tabolli, J., 2013
VG83						
VG84						
VG85	Tomb 17 (XXVI)	Falerii	Montarano	700-600BCE	Orientalising	Cozza, A. and Pasqui, A., 1981
VG86						
VG87						
VG88						
VG89						
VG90						
VG91						

Sample name	Grave	Site	Locality	Absolute date	Relative date	Reference
VG92	Tomb 15 (XXVII)	Falerii	Montarano	750-730 BCE	EIA II	Ligabue, G., 2022
VG93						
VG94						
VG95						
VG96						
VG97						
VG98						
VG99						
VG100						
VG101						
VG102	Tomb 104	Capena	Saliere	800-750 BCE	EIA II	Stefani, E., 1912
VG103						
VG104						
VG105						
VG106						
VG107						
VG108						
VG109						
VG110						
VG111						
VG112	Tomb 1	Narce	Necropoli dei Tufi	800-730 BCE	EIA II	Tabolli, J., 2013
VG113						
VG114	No context			720-630 BCE	Orientalising	Unpublished
PG1	No context	Tarquinia	Arcatelle	900-720 BCE	EIA	Babbi, A., 2005
PG2						
PG3	No context	Verucchio	Fondo Ripa	800-600 BCE	EIA II/Oriantalising	Brizio, E., 1898

Sample name	Grave	Site	Locality	Absolute date	Relative date	Reference
PG4	Tomb 3	Bisenzio	Polledrara	900-800 BCE	EIA I	Delpino, F., 1977
PG5						
PG6	Tomb 5	Bisenzio	Polledrara	900-800 BCE	EIA I	Delpino, F., 1977
PG7	Tomb 11	Bisenzio	Polledrara	800-720 BCE	EIA II	Delpino, F., 1977
PG8						
PG9						
PG10						
PG11						
PG12						
PG13						
PG14						
PG15						
PG16-18	Tomb 10	Falerii	Montarano	720-580 BCE	Orientalising	Cozza, A. and Pasqui, A., 1981
PG19-21	Tomb 1	Veio	Vaccareccia	700-650 BCE	Early Orientalising	Palm, J., 1952
PG22-24	Tomb 2	Veio	Vaccareccia	700-650 BCE	Early Orientalising	Palm, J., 1952
PG25-27	Tomb 6	Veio	Vaccareccia	650-630 BCE	Middle Orientalising	Palm, J., 1952
PG28-30						
PG31						
PG32						
PG34-38	Tomb 13	Veio	Vaccareccia	750-730 BCE	EIA II	Palm, J., 1952
PG33						
PG39	Tomb 14	Veio	Vaccareccia	700-650 BCE	Early Orientalising	Palm, J., 1952
PG40-42	Tomb 15	Veio	Vaccareccia	750-730 BCE	EIA II	Palm, J., 1952
PG43						

Sample name	Grave	Site	Locality	Absolute date	Relative date	Reference
PG44	Tomb 16	Veio	Vaccareccia	750-730 BCE	EIA II	Palm, J., 1952
PG45						
PG46						
PG47						
PG48-50						
PG51-56	Tomb 20	Veio	Vaccareccia	700-650 BCE	Early/Middle Orientalising	Palm, J., 1952
PG57						
PG58	Tomb 23	Veio	Vaccareccia	650-630 BCE	Middle Orientalising	Palm, J., 1952
PG59	Tomb 24	Veio	Vaccareccia	700-650 BCE	Early/Middle Orientalising	Palm, J., 1952
PG60						
PG61						
PG62						
PG63						
PG64						
PG65	Tomb 8	Sermoneta	Caracupa	770-720 BCE	EIA II	Mengarelli, L. and Savignoni, R., 1903
PG66	Tomb 16	Sermoneta	Caracupa	770-720 BCE	EIA II	Mengarelli, L. and Savignoni, R., 1903
PG67	Tomb 48	Sermoneta	Caracupa	770-720 BCE	EIA II	Mengarelli, L. and Savignoni, R., 1903
PG68						
PG69						
PG70						
PG71						
PG72						
PG73						
PG74						
PG75						
PG76						

Sample name	Grave	Site	Locality	Absolute date	Relative date	Reference
PG77	Tomb 53	Sermoneta	Caracupa	770-720 BCE	EIA II	Mengarelli, L. and Savignoni, R., 1903
PG78	Tomb 57	Sermoneta	Caracupa	770-720 BCE	EIA II	Mengarelli, L. and Savignoni, R., 1903
PG79						
PG80						
PG81	Tomb 57 bis	Sermoneta	Caracupa	770-720 BCE	EIA II	Mengarelli, L. and Savignoni, R., 1903
PG82						
PG83						
PG84						
PG85	Tomb 89	Sermoneta	Caracupa	770-720 BCE	EIA II	Gierow, P. G., 1964
PG86						
PG87	Tomb 90	Sermoneta	Caracupa	770-720 BCE	EIA II	Gierow, P. G., 1964
PG88	Tomb 61	Capena	S. Martino	675-625 BCE	Middle Orientalising	Paribeni, R., 1906
PG89	Tomb 60	Capena	S. Martino	675-625 BCE	Middle Orientalising	Paribeni, R., 1906
PG90	Tomb 100	Capena	Monte Cornazzano	730-675 BCE	Early Orientalising	Paribeni, R., 1906
PG91	Tomb 94	Capena	Contrada Le Saliere	730-675 BCE	Early Orientalising	Stefaní, E., 1912
PG92						
PG93						
PG94						
PG95	Tomb 3	Marino	Riserva del Truglio	730-600 BCE	Orientalising	Taloni, M., 2013
PG96						
PG97	Tomb 21	Marino	Riserva del Truglio	730-600 BCE	Orientalising	Taloni, M., 2013
PG98	Tomb 30	Marino	Riserva del Truglio	730-600 BCE	Orientalising	Taloni, M., 2013
PG99						
PG100						
PG101						
PG102						
PG103						

Sample name	Grave	Site	Locality	Absolute date	Relative date	Reference
PG104	No context	Marino	Riserva del Truglio	730-600 BCE	Orientalising	Taloni, M., 2013
PG105	Tomb 9	Roma	Osteria dell'Osa	900-800 BCE	EIA I	Bietti Sestieri, A.M., 1992
PG106						
PG113	Tomb 5	Roma	Osteria dell'Osa	900-800 BCE	EIA I	Bietti Sestieri, A.M. 1992
PG114						
PG115						
PG107	Tomb 10	Roma	Osteria dell'Osa	800-750 BCE	EIA II	Bietti Sestieri, A.M., 1992
PG108						
PG109						
PG110_1						
PG110_2						
PG111						
PG112						
PG116						
PG117						
PG118						
PG119						
PG120						
PG121						
PG122						
PG123	Tomb 13	Roma	Osteria dell'Osa	800-720 BCE	EIA II	Bietti Sestieri, A.M., 1992
PG124						
PG125	Tomb 15	Roma	Osteria dell'Osa	800-720 BCE	EIA II	Bietti Sestieri, A.M., 1992
PG126						

Sample name	Grave	Site	Locality	Absolute date	Relative date	Reference
PG127	Tomb 22	Roma	Osteria dell'Osa	900-800 BCE	EIA I	Bietti Sestieri, A.M., 1992
PG128						
PG129						
PG130						
PG131						
PG132						
PG133	Tomb 6	Tivoli	Rocca Pia	770-720 BCE	EIA II	Various authors (1976)
PG134	Tomb 83	Vulci	Cuccumella	900-800 BCE	EIA I	Mangani, E., 1995
PG135						
PG136	Tomb 26	Cerveteri	Sasso di Furbara, Caolino	770-730 BCE	EIA II	Brusadin Laplace, D. et al., 1992
PG137	Tomb 29	Cerveteri	Sasso di Furbara, Caolino	770-730 BCE	EIA II	Brusadin Laplace, D. et al., 1992
PG138						
PG139						
PG140	Tomb 34	Cerveteri	Sasso di Furbara, Caolino	770-730 BCE	EIA II	Brusadin Laplace, D. et al., 1992
PG141						
PG142						
PG143						
PG144						
PG145	Tomb 40	Cerveteri	Sasso di Furbara, Caolino	770-730 BCE	EIA II	Brusadin Laplace, D. et al., 1992
PG146						
PG147						
PG148						
PG149						
PG150						
PG151						
PG152						
PG153						

Sample name	Grave	Site	Locality	Absolute date	Relative date	Reference
PG154	Tomb 41	Cerveteri	Sasso di Furbara, Caolino	770-730 BCE	EIA II	Brusadin Laplace, D. et al., 1992
PG155						
PG156						
PG157	No context	Terni	S. Agnese, Acciaierie	950-800 BCE	EIA I	Leonelli, V., 2003
PG158	Tomb 91	Terni	S. Agnese, Acciaierie	950-800 BCE	EIA I	Leonelli, V., 2003
PG159						
PG160	No context	Terni	S. Agnese, Acciaierie	950-800 BCE	EIA I	Leonelli, V., 2003
PG161	Tomb 91	Terni	S. Agnese, Acciaierie	950-800 BCE	EIA I	Leonelli, V., 2003
PG162	No context	Verucchio	Fondo Ripa	800-600 BCE	EIA II/Oriantalising	Brizio, E., 1898
PG163	No context	Verucchio	Fondo Ripa	800-600 BCE	EIA II/Oriantalising	Brizio, E., 1898
PG164	No context	Verucchio	Fondo Ripa	800-600 BCE	EIA II/Oriantalising	Brizio, E., 1898
PG165	No context	Verucchio	Fondo Ripa	800-600 BCE	EIA II/Oriantalising	Brizio, E., 1898
PG166	Tomb 91	Sermoneta	Caracupa	770-720 BCE	EIA II	Gierow, P.G., 1964
PG167	Tomb 82	Roma	Osteria dell'Osa	750-720 BCE	EIA II	Bietti Sestieri, A.M. 1992
PG168						
PG169						
PG170						
PG171						
PG172						
PG173	Tomb 94	Sermoneta	Caracupa	770-720 BCE	EIA II	Gierow, P.G., 1964
PG174	Tomb 15	Roma	Osteria dell'Osa	800-720 BCE	EIA II	Bietti Sestieri, A.M., 1992

REFERENCES FROM THE TABLE

Arancio M.L., Moretti Sgubini A. M., Pellegrini E. (2010). Corredi funerari femminili di rango a Vulci nella prima età del ferro: il caso della Tomba dei Bronzetti sardi. In: *Atti del Nono Incontro di Studi Valentano (Vt) - Pitigliano (Gr), 12-14 Settembre 2008. L'alba dell'Etruria. Fenomeni di continuità e trasformazione nei secoli XII-VIII a. C. Ricerche e scavi;* Negroni Catacchio, N. Ed. Milano; pp. 169–214.

Babbi, A. (2005). Reperti della necropoli delle Arcatelle, BPI 93-94 (2002-2003), pp.115-154

Berardinetti, A., Drago L. (1997). La necropoli di Grotta Gramiccia, in Gilda Bartoloni, a cura di, Le necropoli arcaiche di Veio. Giornata di studio in memoria di Massimo Pallottino, Università degli Studi di Roma «La Sapienza. pp.39-61

Bietti Sestieri, A.M. (1992) La necropoli laziale di Osteria dell'Osa. Quasar.

Boitani, F. (2004). La tomba di guerriero AA1 dalla necropoli dei Quattro Fontanili di Veio. *AM Moretti Sgubini (a cura di), Scavo nello scavo. Gli Etruschi non visti, Roma*, 128-149.

Boitani, F. (2010). Veio, la Tomba dei Leoni Ruggenti: dati preliminari. *Archeologia nella Tuscia. Atti dell'Incontro di Studi (Viterbo 2007). Viterbo: Università degli Studi della Tuscia. Daidalos*, *10*, 23-48.

Brizio, E. (1898). Verucchio. Scoperta di sepolcreti tipo Villanova. *Notizie degli Scavi. Italia*, 343-390.

Brusadin Laplace, D., Patrizi-Montoro, G., & Patrizi-Montoro, S. (1992). Le necropoli protostoriche del Sasso di Furbara III. Caolino e altri sepolcreti villanoviani. *Origini*, *16*, 221-294.

Cozza, A., Pasqui, A. (1981). *Carta archeologica d'Italia (1881-1897): materiali per l'agro falisco: lavoro pubblicato con il contributo del Consiglio nazionale delle ricerche*. LS Olschki.

Delpino, F. (1977). La prima éta del ferro a Bisenzio, divisione in fasi ed interpretazione culturale.(Le 1 Age du Fer à B., subdivisions chronologiques et interprétation culturelle). *Studi Etruschi Firenze*, *45*, 39-49.

Falconi Amorelli, M.T. (1967). Corredo di una tomba etrusca arcaica di Monte Aùto, *Arch Class*, XIX, pp.306-312.

Gierow, P. G. (1964). The Iron Age culture of Latium. 2, Excavations and finds: 1. The Alban hills. Gleerup.

Leonelli, V. La necropoli della prima età del ferro delle acciaierie a Terni : contributi per un'edizione critica Firenze : All'insegna del giglio, 2003, 347p.

Ligabue, G. (2022). Falerii Veteres. Il sepolcreto di Montarano. Scavi, materiali e contesti. *Monumenti antichi*. 28. 1150p.

Mangani, E. (1995). Corredi vulcenti dagli scavi Gsell al Museo Pigorini, BPI, p. 374.

Mengarelli, L., Savignoni, R. (1903). La necropoli arcaica di Caracupa tra Norba e Sermoneta, in *Notizie degli Scavi 1903*, pp. 289-344.

Moretti, A. M. S. (Ed.). (2001). *Veio, Cerveteri, Vulci: città d'Etruria a confronto: Roma, Museo nazionale etrusco di Villa Giulia, Villa Poniatowski, 1 ottobre-30 dicembre 2001* (Vol. 32). L'Erma di Bretschneider.

Palm, J. (1952). Veiian tomb groups in the Museo Preistorico, Rome, in *Opuscula Archaeologica* VII, p.70, n. 25.

Paribeni, R. (1906) Necropoli del territorio capenate. *Monumenti Antichi dei Lincei* 16, pp. 277-490.

Ricci, G. (1955). Necropoli della Banditaccia, zona A'del recinto'--Caere. *Monumenti Antichi, XLII,*coll. 201-1047

Ridgway, D. (1968). Archaeology in Central Italy and Etruria, 1962–67. *Archaeological Reports*, 14, 29-48.

Stefaní, E. (1912). Scoperte archeologiche nell'Agro Capenate. *Bollettino di Paletnologia Italiana*, 38, pp. 147-158.

Tabolli, J. (2013). Narce tra la prima età del Ferro e l'Orientalizzante antico. L'abitato, I Tufi e La Petrina. Mediterranea, suppl. 9.

Taloni, M (2013). Le tombe da Riserva del Truglio al Museo Pigorini di Roma, *Officina Etruscologia*, 8, Rome.

Various Authors (1965) Veio - Isola Farnese. Scavi di una necropoli villanoviana in località „Quattro Fontanili". *Notizie degli Scavi* (8), pp. 123-138.

Various Authors (1976). Civiltà del Lazio Primitivo. Multigrafica Editrice 394p.

APPENDIX 2. PHOTOGRAPHS OF OBJECTS WITHIN THE DISCUSSION.

Objects under study are grouped by their groups as described in the Chapter 3, section 3. The scale bars are true throughout the group but change from one group to another to ensure the rational use of space. Samples are presented in numerical order. PG series precedes the VG series.

GROUP 1 SAMPLES

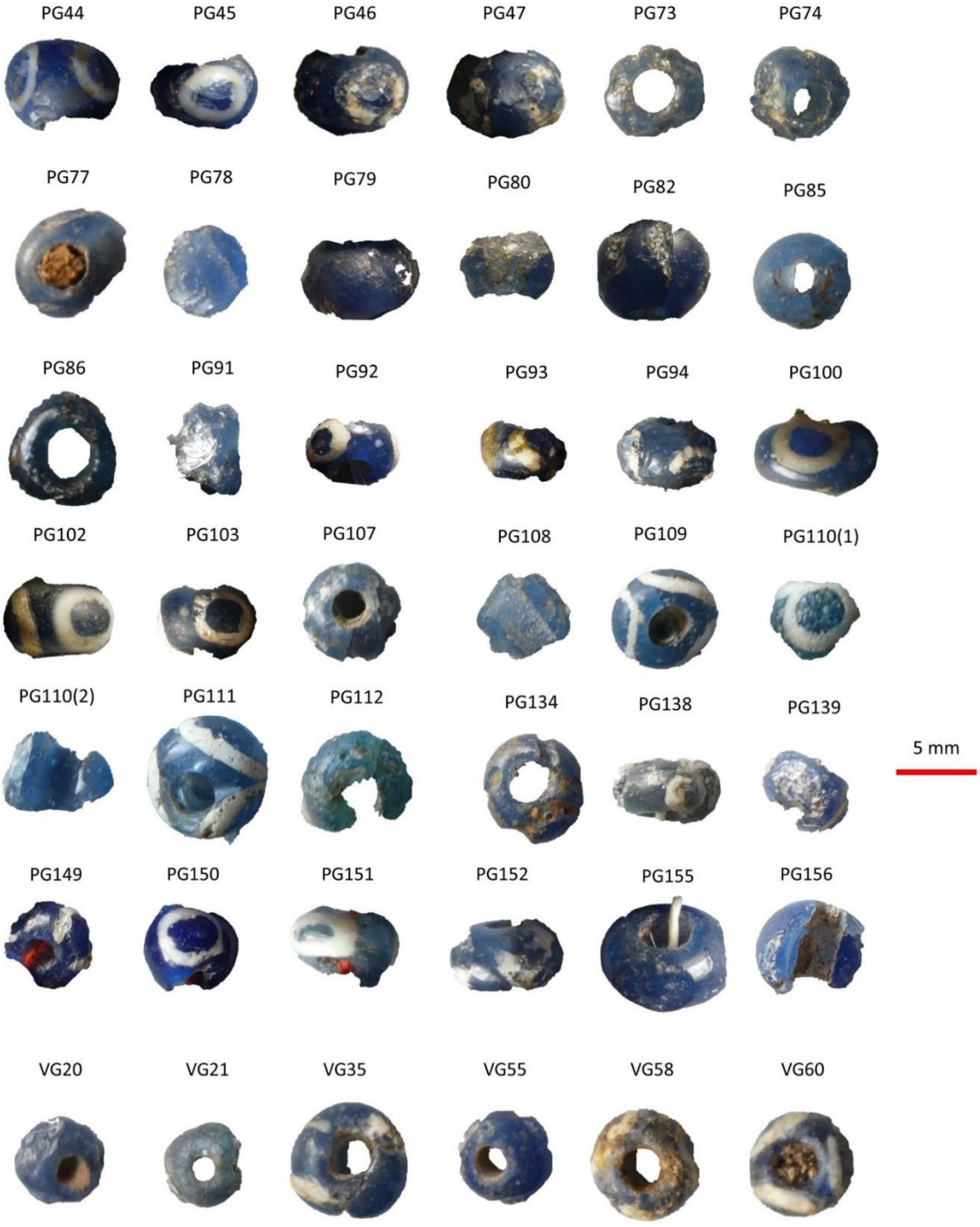

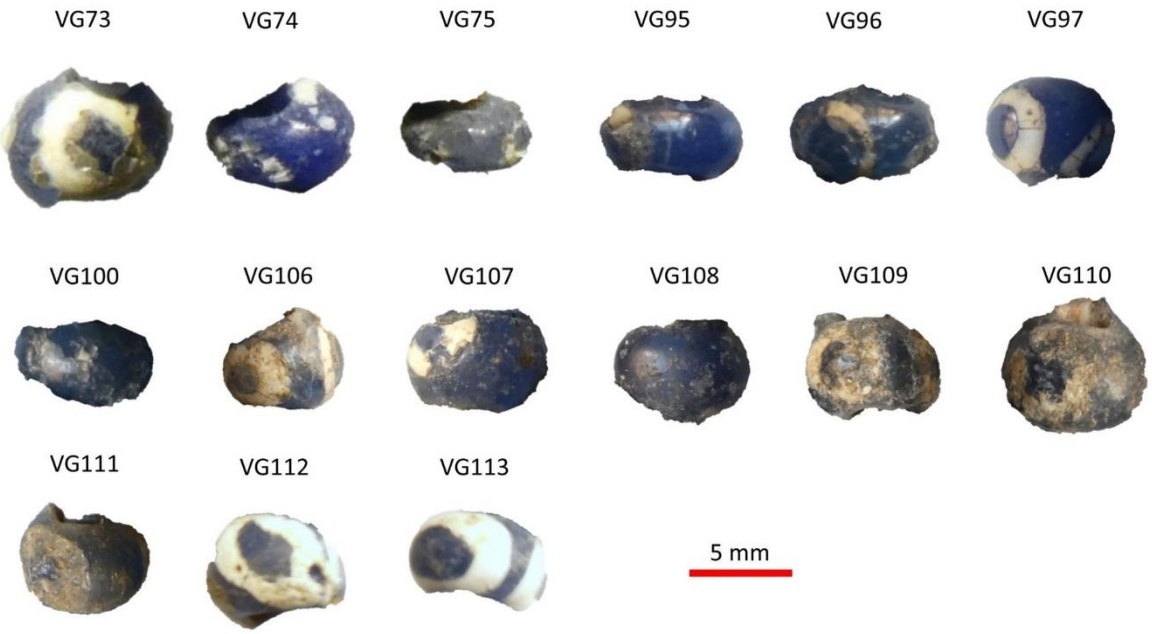

GROUP 2 SAMPLES

GROUP 3 SAMPLES

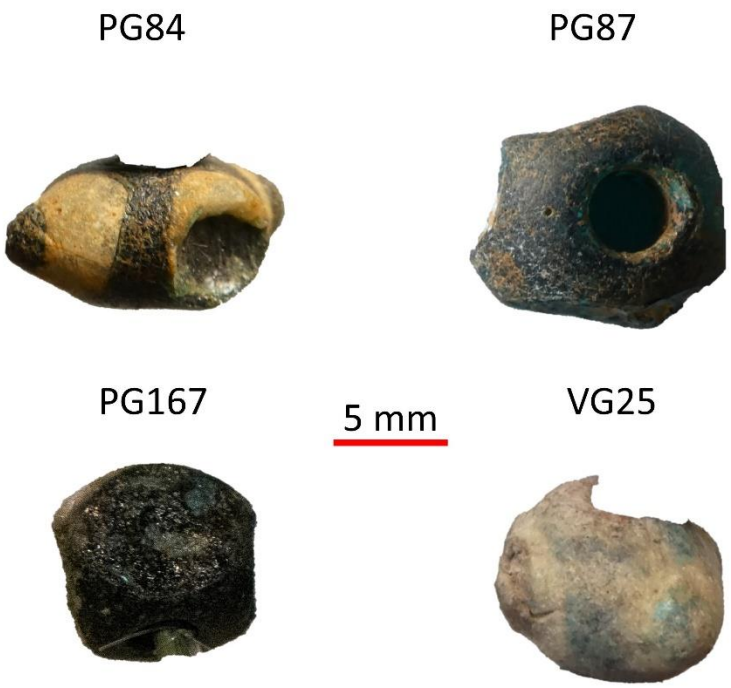

GROUP 4 SAMPLES

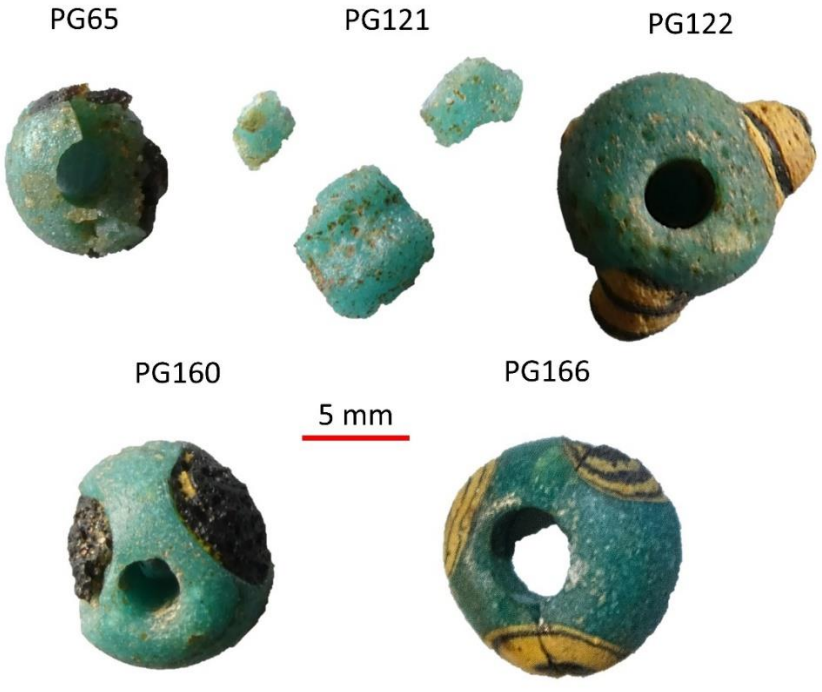

GROUP 5 SAMPLES

GROUP 6 SAMPLES

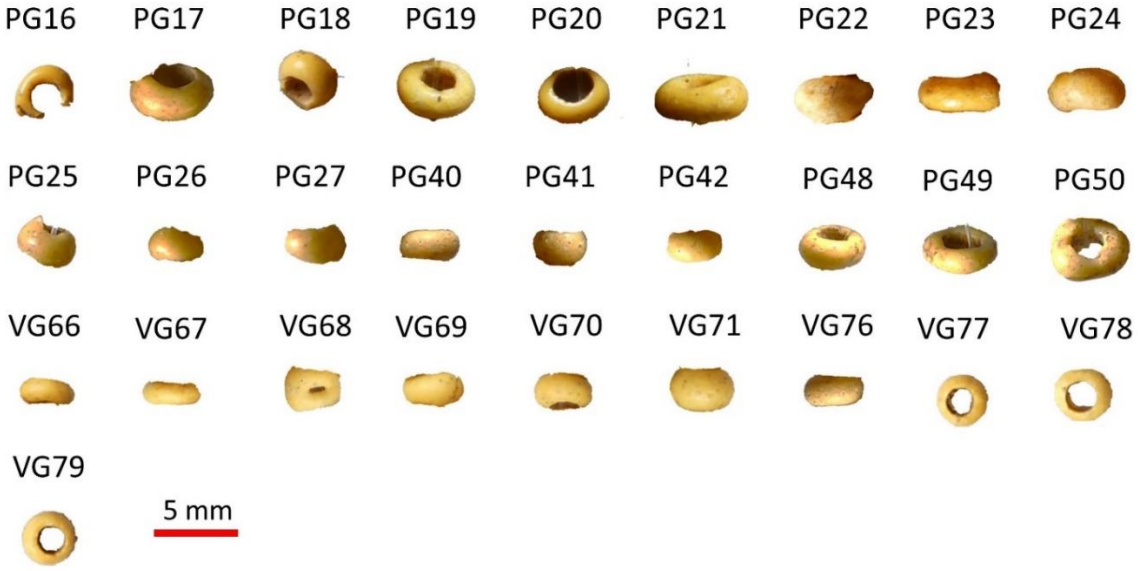

GROUP 7 SAMPLES

GROUP 8 SAMPLES

GROUP 9 SAMPLES

GROUP 10 SAMPLES

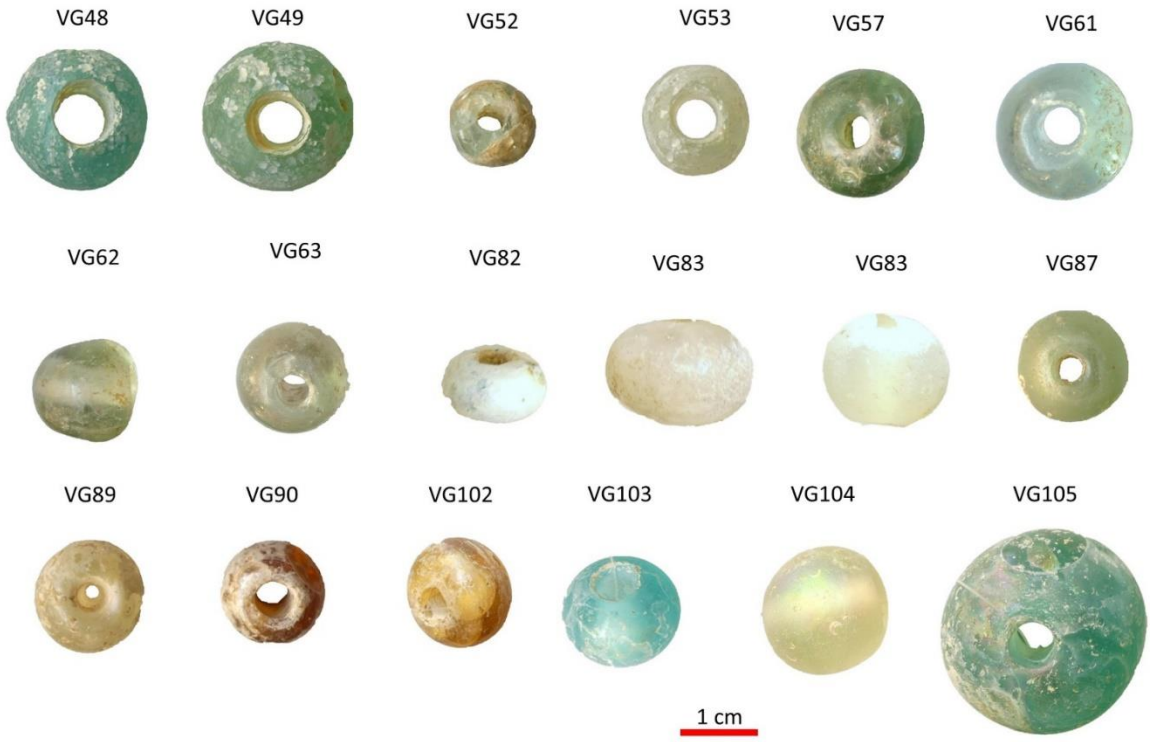

GROUP 11 SAMPLES

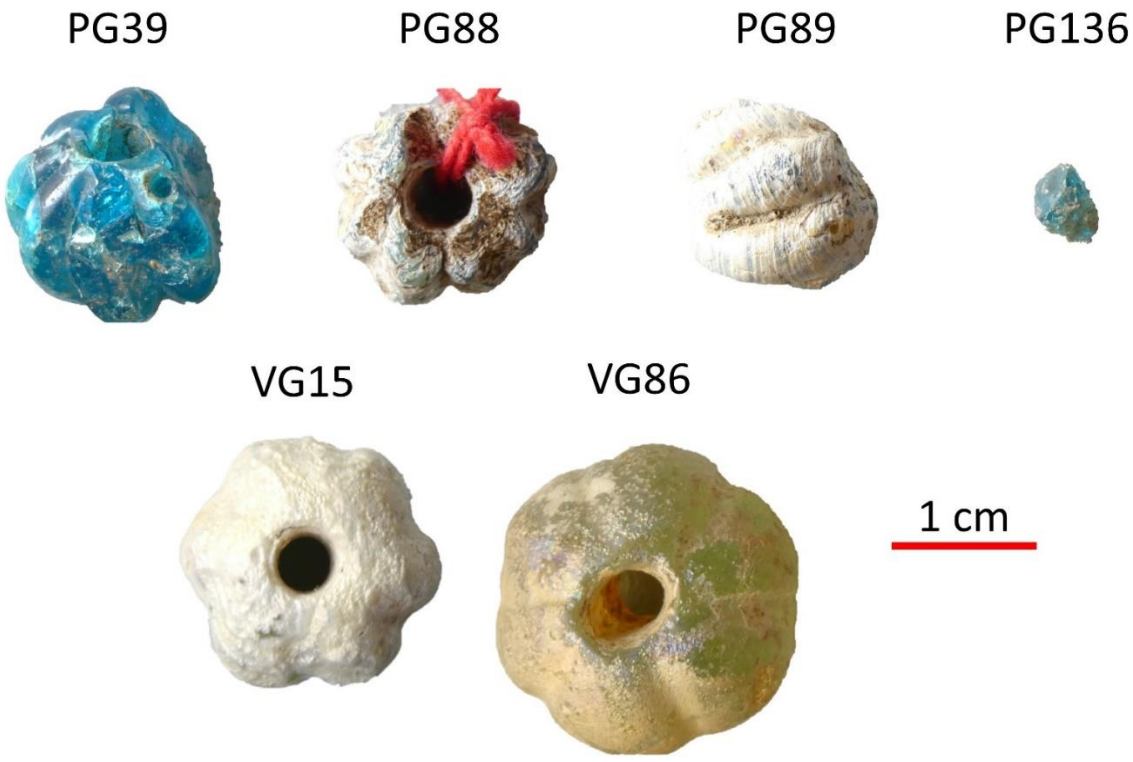

GROUP 12 SAMPLES

GROUP 13 SAMPLES

GROUP 14 SAMPLES

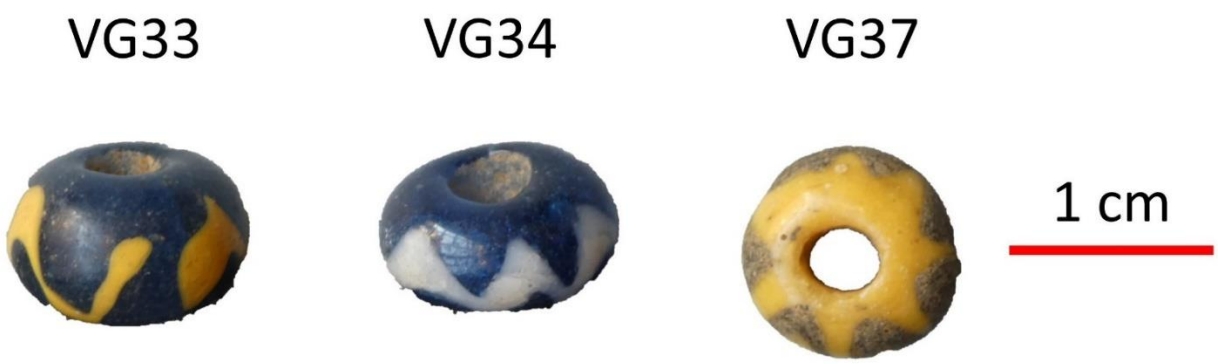

GROUP 15 SAMPLES

GROUP 16 SAMPLES

GROUP 17 SAMPLES

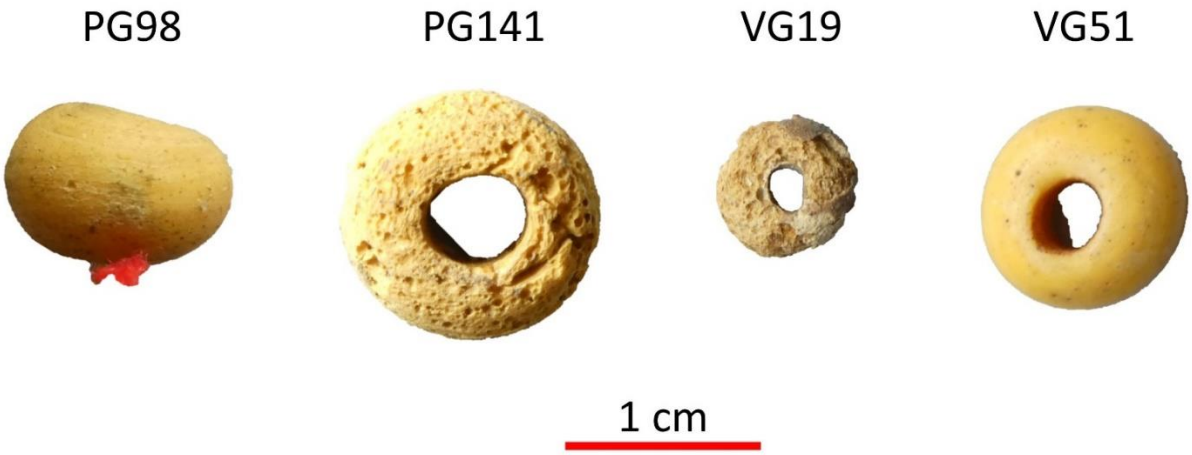

GROUP 18 SAMPLES

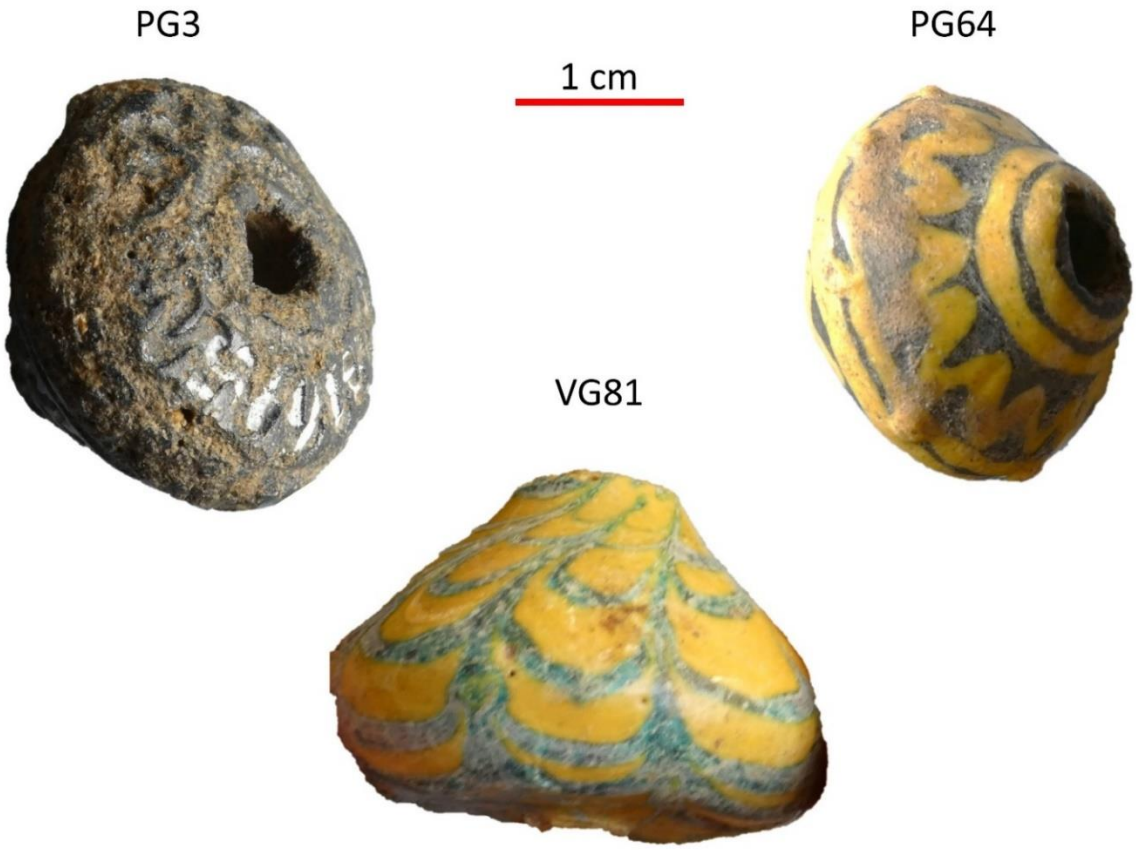

OTHER BEADS


PG5
PG6
PG32
PG58
PG66
PG90
PG113
PG114
5 mm
PG168
PG169
PG170
PG172
VG28
VG38
VG88
VG16
VG18
VG27
VG54
VG85

NON-BEAD OBJECTS

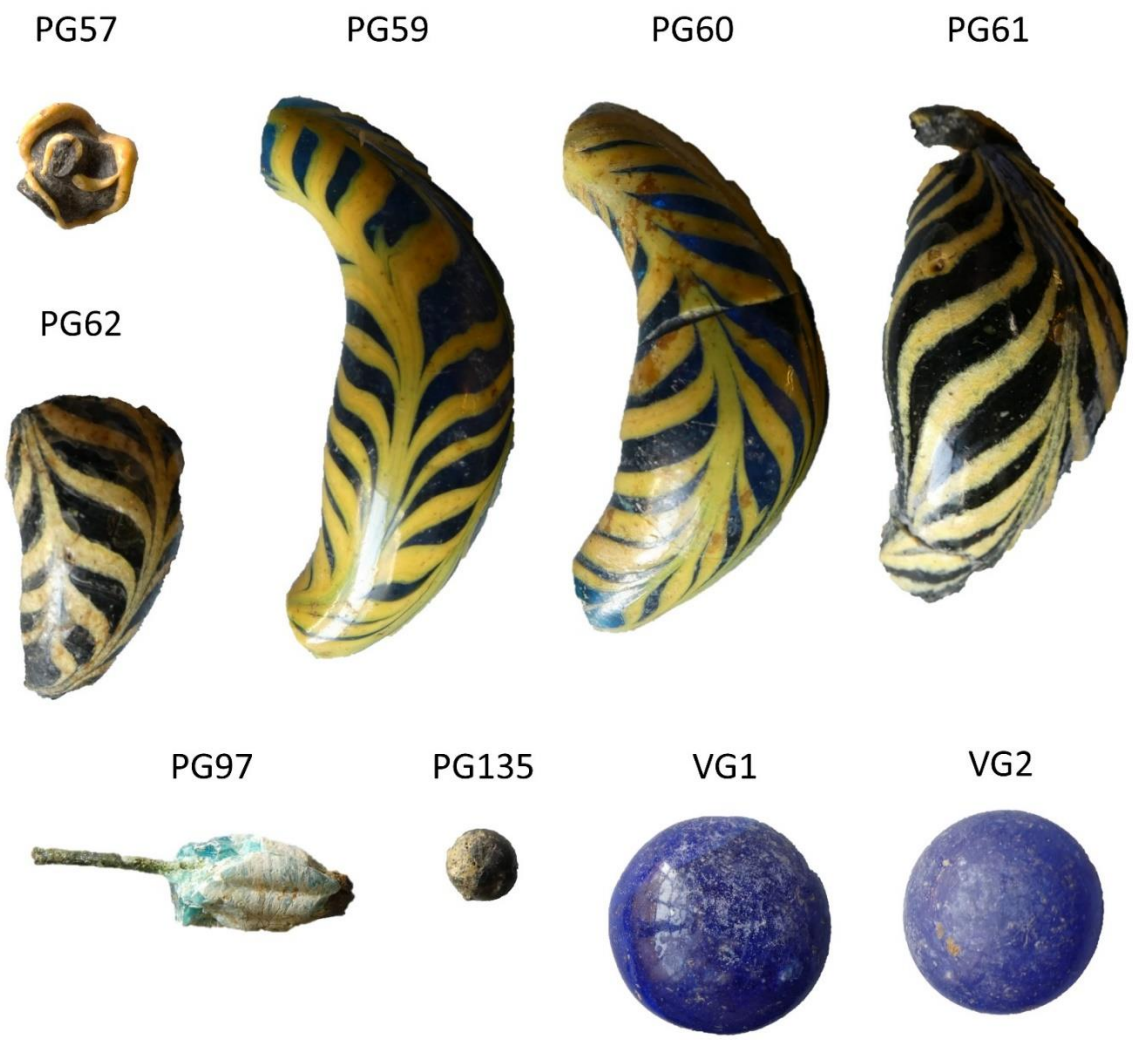

VG3

VG4

VG5

VG6

VG7

VG9

VG32

VG56

VG92

VG93

VG114

1 cm

VG13

APPENDIX 3. THE DOCUMENTED ATTRIBUTES OF BEADS DISCUSSED IN THE STUDY.

The table below contains the description of the beads sorted by typological groups established in Chapter 3. Only the samples that could provide all the values in the controlled way are included. Samples in fragmented state, or the ones whose colour parameters could not be retrieved are omitted in this table. The meaning of columns is following: groups – typological groups of the beads from 1 to 18 established in Chapter 3, section 3, Other beads means that this sample cannot be attributed to any of the types and makes a type of their own within the set; Sample name – name of the bead, PG means the bead is from Museo delle Civita, VG – from Museo Nazionale Etrusco di Villa Giulia, ranges like PG16-18 mean that the parameters are averaged values of samples on a sting that share similar appearance and context (typical for samples of groups 6 and 7); D – diameter of the bead in mm; W – width of a bead in mm; A – diameter of the aperture of the bead in mm; D/W – diameter to width ratio; D/A diameter of the bead to diameter of the aperture ratio; V – volume estimation in mm^3; R, G, B – colour coordinates in the RGB space; T – translucency estimation on the scale from 1 to 5; Decoration – description of decorative elements (if any); Dec.n. – number of such elements. This table with modified translucency and decoration parameters (converted in numbers) was used for the PCA analysis presented in Chapter 3, section 3.

Group	Sample name	D	W	A	D/W	D/A	V	R	G	B	T	Decoration	Dec.n.
1	PG44	6.00	5.00	3.00	1.20	2.00	35.31	35.03	51.36	84.92	2	Ring eye	3
1	PG45	6.00	5.00	3.00	1.20	2.00	35.31	62.51	78.55	109.45	2	Ring eye	3
1	PG46	6.00	5.00	3.00	1.20	2.00	35.31	48.18	53.36	64.56	2	Ring eye	3
1	PG47	6.00	5.00	3.00	1.20	2.00	35.31	90.11	96.93	106.84	2	Ring eye	3
1	PG73	7.00	3.50	3.00	2.00	2.33	43.96	83.84	97.27	110.49	2	Ring eye	3
1	PG74	7.00	4.00	2.00	1.75	3.50	78.50	103.00	107.00	138.00	2	Ring eye	3
1	PG77	7.00	4.50	2.00	1.56	3.50	88.31	69.44	80.42	105.71	2	Ring eye	3
1	PG79	7.50	6.00	3.00	1.25	2.50	95.38	51.96	60.30	69.38	2	Ring eye	3
1	PG80	6.00	3.50	2.00	1.71	3.00	43.96	48.27	56.97	78.07	2	Ring eye	3
1	PG82	7.00	5.50	2.00	1.27	3.50	107.94	52.28	58.54	74.72	2	Ring eye	3

Group	Sample name	D	W	A	D/W	D/A	V	R	G	B	T	Decoration	Dec.n.
1	PG85	6.50	5.50	3.00	1.18	2.17	52.89	81.89	103.44	127.71	2	Ring eye	2
1	PG86	7.00	4.00	3.00	1.75	2.33	50.24	60.33	63.31	66.29	2	Ring eye	3
1	PG91	7.00	5.00	2.50	1.40	2.80	79.48	77.73	92.00	108.63	3	Ring eye	2
1	PG92	7.50	5.00	2.50	1.50	3.00	98.13	39.79	40.32	51.83	2	Ring eye	3
1	PG93	7.00	5.00	2.50	1.40	2.80	79.48	63.05	71.52	78.86	2	Ring eye	3
1	PG94	6.00	4.00	2.00	1.50	3.00	50.24	36.92	38.94	56.73	2	Ring eye	3
1	PG100	7.50	5.00	3.00	1.50	2.50	79.48	168.55	144.26	96.64	2	Ring eye	3
1	PG102	7.25	5.00	3.00	1.45	2.42	70.90	89.04	90.67	91.07	2	Ring eye	3
1	PG103	6.50	4.00	2.50	1.63	2.60	50.24	83.90	91.61	100.78	2	Ring eye	3
1	PG107	6.00	5.00	2.50	1.20	2.40	48.08	77.21	96.80	111.83	2	Ring eye	3
1	PG109	6.75	5.00	2.50	1.35	2.70	70.90	68.18	115.53	145.47	2	Ring eye	3
1	PG111	7.25	6.00	2.50	1.21	2.90	106.27	26.36	59.02	87.66	2	Ring eye	3
1	PG134	7.00	4.00	2.00	1.75	3.50	78.50	75.54	94.56	116.98	2	Ring eye	3
1	PG138	6.25	4.00	2.50	1.56	2.50	44.16	87.33	91.72	97.83	2	Ring eye	3
1	PG149	5.50	3.00	2.00	1.83	2.75	28.85	29.85	37.95	71.25	2	Ring eye	3
1	PG150	6.00	5.00	2.00	1.20	3.00	62.80	22.14	33.64	80.66	2	Ring eye	3
1	PG151	7.25	5.00	2.50	1.45	2.90	88.56	63.02	73.96	82.09	3	Ring eye	3
1	PG152	6.50	5.00	2.50	1.30	2.60	62.80	71.78	90.57	114.46	3	Ring eye	3
1	PG155	8.00	5.00	3.00	1.60	2.67	98.13	83.46	97.05	115.08	2	Ring eye	3
1	VG20	6.00	5.00	1.25	1.20	4.80	88.56	53.69	61.39	84.47	2	Ring eye	3
1	VG21	5.25	4.00	1.00	1.31	5.25	56.72	91.15	100.22	108.52	2	Ring eye	2
1	VG35	7.50	5.00	2.00	1.50	3.75	118.73	69.91	81.18	102.98	2	Ring eye	2
1	VG55	6.00	5.00	2.00	1.20	3.00	62.80	38.57	48.88	86.37	3	Ring eye	3
1	VG58	7.00	4.00	2.50	1.75	2.80	63.59	77.95	77.42	89.16	2	Ring eye	3
1	VG60	7.00	4.00	2.00	1.75	3.50	78.50	81.02	83.05	95.18	2	Ring eye	3
1	VG73	6.75	4.75	2.50	1.42	2.70	67.35	86.49	90.78	99.72	2	Ring eye	3

Group	Sample name	D	W	A	D/W	D/A	V	R	G	B	T	Decoration	Dec.n.
1	VG74	6.75	4.75	2.50	1.42	2.70	67.35	81.24	84.52	93.80	2	Ring eye	3
1	VG75	6.75	4.75	2.50	1.42	2.70	67.35	112.78	113.92	113.67	2	Ring eye	3
1	VG95	7.50	4.50	2.50	1.67	3.00	88.31	74.52	83.01	116.17	2	Ring eye	2
1	VG96	7.50	4.50	2.50	1.67	3.00	88.31	79.78	82.17	89.69	2	Ring eye	3
1	VG97	7.50	4.50	2.50	1.67	3.00	88.31	33.85	42.14	76.56	2	Ring eye	3
1	VG100	7.50	4.50	2.50	1.67	3.00	88.31	84.48	88.79	98.62	2	Ring eye	3
1	VG106-111	6.25	4.75	2.00	1.32	3.13	67.35	104.71	101.16	97.83	2	Ring eye	3
2	VG59	10.75	7.00	2.50	1.54	4.30	374.00	63.00	65.74	71.73	2	Ring eye	3
2	VG64	11.75	9.00	3.00	1.31	3.92	540.91	64.01	74.53	83.22	2	Ring eye	3
2	VG65	11.75	8.00	3.00	1.47	3.92	480.81	43.23	51.70	60.68	2	Ring eye	3
2	VG72	6.75	4.75	2.50	1.42	2.70	67.35	112.63	116.86	120.42	2	Ring eye	3
2	VG80	12.00	10.00	3.00	1.20	4.00	635.85	32.64	37.16	50.69	3	Ring eye	3
2	VG91	11.75	8.00	3.00	1.47	3.92	480.81	32.92	36.47	49.73	2	Ring eye	3
2	VG98	7.50	4.50	2.50	1.67	3.00	88.31	78.56	80.52	84.17	2	Ring eye	3
2	VG99	7.50	4.50	2.50	1.67	3.00	88.31	55.45	64.77	80.88	2	Ring eye	3
3	PG84	12.50	6.50	4.00	1.92	3.13	368.66	65.05	56.32	39.69	1	Horned stratified eye	4
3	VG25	13.75	9.00	3.50	1.53	3.93	742.27	106.59	108.10	97.74	1	Horned stratified eye	4
4	PG65	8.00	6.00	3.00	1.33	2.67	117.75	75.42	117.68	97.53	1	Spiral eye	3
4	PG122	11.50	8.00	3.00	1.44	3.83	453.73	93.60	122.10	98.37	1	Horned spiral eye	3
4	PG160	9.50	9.00	2.00	1.06	4.75	397.41	110.36	145.72	121.15	1	None	None
4	PG166	11.50	7.00	3.50	1.64	3.29	351.68	71.62	109.12	100.02	1	Spiral eye	3
5	PG69	6.75	5.00	2.50	1.35	2.70	70.89	46.87	158.04	146.39	3	None	None
5	PG70	7.00	4.00	2.50	1.75	2.80	63.59	15.20	137.92	121.12	3	None	None
5	PG71	7.00	3.00	2.50	2.33	2.80	47.69	171.18	160.33	110.79	3	None	None
5	PG72	7.00	4.00	3.00	1.75	2.33	50.24	175.16	166.84	131.12	3	None	None
5	PG75	6.00	3.50	3.00	1.71	2.00	24.73	116.00	75.00	60.00	2	None	None

Group	Sample name	D	W	A	D/W	D/A	V	R	G	B	T	Decoration	Dec.n.
5	PG76	6.25	5.00	2.00	1.25	3.13	70.90	89.48	59.65	48.27	2	None	None
5	PG154	8.00	5.00	3.00	1.60	2.67	98.13	162.42	112.99	38.43	3	None	None
6	PG16-18	4.50	3.00	3.00	1.50	1.50	5.29	179.73	137.40	56.98	1	None	None
6	PG19-21	3.75	2.00	2.00	1.87	1.87	4.80	203.56	164.46	69.86	1	None	None
6	PG22-24	4.00	3.00	2.00	1.33	2.00	9.42	226.97	171.63	95.62	1	None	None
6	PG25-27	3.25	2.00	2.00	1.62	1.62	2.45	168.18	138.67	80.42	1	None	None
6	PG40-42	3.50	2.00	2.00	1.75	1.75	3.53	180.55	143.79	78.22	1	None	None
6	PG48-50	4.00	2.00	2.00	2.00	2.00	6.28	201.28	158.69	73.54	1	None	None
6	VG66	3.50	2.00	1.75	1.75	2.00	4.81	229.91	193.74	117.93	1	None	None
6	VG67	3.50	2.00	1.75	1.75	2.00	4.81	224.14	189.56	117.41	1	None	None
6	VG68	3.50	2.00	1.75	1.75	2.00	4.81	237.08	201.32	122.22	1	None	None
6	VG69	5.75	3.00	3.00	1.92	1.92	17.81	228.09	190.94	111.26	1	None	None
6	VG70	5.75	3.00	3.00	1.92	1.92	17.81	219.16	183.50	111.78	1	None	None
6	VG71	6.50	3.00	2.75	2.17	2.36	33.12	213.44	174.53	101.22	1	None	None
6	VG77	4.00	2.00	1.50	2.00	2.67	9.81	241.91	191.62	105.07	1	None	None
6	VG78	3.50	2.00	1.50	1.75	2.33	6.28	242.00	192.53	107.95	1	None	None
6	VG79	3.50	2.00	1.50	1.75	2.33	6.28	240.11	187.66	93.97	1	None	None
7	PG28-30	3.50	2.00	1.50	1.75	2.33	6.28	39.65	48.01	61.46	1	None	None
7	PG34-38	4.00	2.00	2.00	2.00	2.00	6.27	44.39	57.39	75.58	1	None	None
7	PG43	6.75	5.00	2.50	1.35	2.70	70.83	24.40	45.20	83.28	2	None	None
7	PG51-56	3.50	2.00	2.00	1.75	1.75	3.53	67.81	70.49	75.85	1	None	None
7	PG158	5.00	2.00	2.50	2.50	2.00	9.81	87.62	92.40	121.79	2	None	None
7	PG159	6.00	3.50	2.50	1.71	2.40	33.66	83.80	76.51	69.22	1	None	None
7	PG161	6.50	2.00	3.50	3.25	1.86	14.13	70.34	116.55	120.80	1	None	None
7	VG22	6.00	4.50	3.50	1.33	1.71	22.08	58.54	57.13	55.51	1	None	None
7	VG23	6.25	5.00	3.50	1.25	1.79	29.68	50.61	48.44	50.96	1	None	None

Group	Sample name	D	W	A	D/W	D/A	V	R	G	B	T	Decoration	Dec.n.
7	VG24	5.50	3.00	3.00	1.83	1.83	14.72	109.13	86.39	70.09	1	None	None
7	VG36	5.00	4.50	1.50	1.11	3.33	43.27	23.83	35.07	79.04	1	None	None
8	PG81	6.50	6.00	2.00	1.08	3.25	95.38	30.99	28.61	23.67	1	None	None
8	PG105	6.50	5.00	2.00	1.30	3.25	79.48	14.59	13.66	14.43	1	None	None
8	PG125	5.00	4.50	3.00	1.11	1.67	14.13	11.09	8.40	6.80	1	None	None
8	PG128	6.00	3.00	2.50	2.00	2.40	28.85	32.67	33.38	36.02	1	None	None
8	PG129	5.00	3.00	2.00	1.67	2.50	21.20	27.47	28.72	28.05	1	None	None
8	PG130	4.00	4.00	2.00	1.00	2.00	12.56	23.72	24.00	25.82	1	None	None
8	PG133	6.00	5.00	3.00	1.20	2.00	35.33	23.45	23.08	21.62	1	None	None
9	VG17	5.50	1.00	2.00	5.50	2.75	9.62	215.29	195.51	153.72	1	None	None
9	VG39	4.50	2.00	2.00	2.25	2.25	9.81	221.41	191.26	146.40	1	None	None
9	VG40	4.50	2.00	2.00	2.25	2.25	9.81	222.45	201.66	167.95	1	None	None
9	VG41	4.50	2.00	2.00	2.25	2.25	9.81	221.74	203.78	172.36	1	None	None
9	VG42	4.50	2.00	2.00	2.25	2.25	9.81	201.94	196.99	166.65	1	None	None
9	VG43	4.50	2.00	2.00	2.25	2.25	9.81	212.10	214.29	188.84	1	None	None
9	VG44	4.50	2.00	2.00	2.25	2.25	9.81	190.68	191.01	160.31	1	None	None
9	VG45	4.50	2.00	2.00	2.25	2.25	9.81	149.21	172.17	155.74	1	None	None
9	VG46	4.50	2.00	2.00	2.25	2.25	9.81	160.41	185.37	180.17	1	None	None
9	VG47	4.50	2.00	2.00	2.25	2.25	9.81	152.95	177.15	172.20	1	None	None
10	PG1	15.50	13.00	5.00	1.19	3.10	1125.10	188.82	152.64	82.48	2	None	None
10	PG2	19.50	16.00	5.00	1.22	3.90	2640.74	175.33	161.37	121.89	3	None	None
10	PG7	15.00	14.00	4.00	1.07	3.75	1329.79	119.50	119.72	71.08	4	None	None
10	PG8	15.00	13.00	3.00	1.15	4.99	1468.54	92.42	138.94	120.40	4	None	None
10	PG9	15.00	11.00	4.00	1.36	3.75	1044.84	63.35	96.96	91.48	3	None	None
10	PG10	12.00	8.00	4.00	1.50	3.00	401.92	89.62	50.28	18.55	3	None	None
10	PG11	14.50	8.00	6.00	1.81	2.42	453.73	115.59	84.34	27.53	3	None	None

Group	Sample name	D	W	A	D/W	D/A	V	R	G	B	T	Decoration	Dec.n.
10	PG12	11.25	7.00	3.00	1.61	3.75	374.00	155.41	153.95	113.15	3	None	None
10	PG33	11.00	6.00	3.50	1.83	3.14	264.94	26.19	62.38	77.47	3	None	None
10	PG63	23.75	20.00	5.00	1.19	4.75	5519.53	46.17	65.43	78.62	2	None	None
10	PG67	10.50	6.00	6.00	1.75	1.75	95.38	192.21	146.87	47.26	4	None	None
10	PG68	12.50	9.00	6.00	1.39	2.08	298.50	178.07	153.03	107.60	3	None	None
10	PG95	17.00	15.00	3.00	1.13	5.67	2307.90	56.28	99.30	73.93	4	None	None
10	PG104	18.00	7.00	5.50	2.57	3.27	858.59	65.64	52.15	30.42	2	None	None
10	PG116	12.00	8.00	3.00	1.50	4.00	508.68	11.37	55.34	75.51	3	None	None
10	PG117	15.00	10.00	4.00	1.50	3.75	949.85	106.48	68.37	28.21	3	None	None
10	PG119	15.50	16.00	4.00	0.97	3.88	1661.06	115.60	126.29	99.88	4	None	None
10	PG140	12.00	10.00	3.00	1.20	4.00	635.85	183.81	130.66	84.19	2	None	None
10	PG148	18.75	15.00	4.50	1.25	4.17	2391.06	198.46	184.07	171.15	5	None	None
10	PG153	15.00	11.00	4.00	1.36	3.75	1044.84	99.15	72.03	29.59	3	None	None
10	PG165	16.50	14.00	5.00	1.18	3.30	1453.43	167.44	171.51	133.90	4	None	None
10	VG14	15.00	8.00	5.00	1.88	3.00	628.00	157.17	115.14	75.54	4	None	None
10	VG48	15.50	10.00	4.50	1.55	3.44	949.85	122.88	156.59	130.06	4	None	None
10	VG49	19.00	17.00	6.00	1.12	3.17	2255.31	129.92	152.08	110.45	4	None	None
10	VG52	11.00	8.50	3.50	1.29	3.14	375.33	170.00	172.56	142.46	4	None	None
10	VG53	13.50	12.00	5.50	1.13	2.45	602.88	175.79	175.52	147.92	4	None	None
10	VG57	15.50	13.00	4.00	1.19	3.88	1349.61	169.98	184.14	138.88	4	None	None
10	VG61	17.00	14.00	5.00	1.21	3.40	1582.56	112.68	137.32	115.07	5	None	None
10	VG62	12.00	12.50	3.00	0.96	4.00	794.81	146.56	147.25	113.84	5	None	None
10	VG63	14.00	13.00	3.50	1.08	4.00	1125.10	123.40	119.92	81.14	4	None	None
10	VG87	13.75	13.00	3.00	1.06	4.58	1179.32	143.99	145.46	97.19	4	None	None
10	VG89	13.75	12.00	2.00	1.15	6.88	1300.55	193.92	171.89	117.02	4	None	None
10	VG90	13.25	9.00	5.00	1.47	2.65	480.86	163.80	121.67	78.75	3	None	None

Group	Sample name	D	W	A	D/W	D/A	V	R	G	B	T	Decoration	Dec.n.
10	VG102	14.00	10.50	4.00	1.33	3.50	824.25	175.03	133.23	66.55	3	None	None
10	VG103	15.50	11.00	5.00	1.41	3.10	952.01	134.93	179.26	168.64	4	None	None
10	VG104	16.50	15.50	2.75	1.06	6.00	2300.42	203.66	196.08	147.34	4	None	None
10	VG105	26.00	24.00	5.25	1.08	4.95	8111.80	123.34	149.99	126.45	4	None	None
11	PG39	15.50	14.00	3.50	1.11	4.42	1581.77	25.44	115.75	135.85	3	Ribs	8
11	PG88	14.50	11.50	4.00	1.26	3.63	995.28	133.16	136.99	129.35	1	Ribs	8
11	VG15	17.00	14.50	4.00	1.17	4.25	1923.64	208.56	203.94	190.03	2	Ribs	6
11	VG86	20.50	18.50	5.00	1.11	4.10	3489.03	159.15	144.35	100.72	3	Ribs	6
12	VG26	10.00	13.00	3.50	0.77	2.86	431.16	106.59	108.10	97.74	1	Spiral stripe	1
12	VG29	11.00	12.50	3.50	0.88	3.14	551.95	159.22	159.08	146.95	1	Spiral stripe	1
13	PG162	8.00	68.00	3.00	0.12	2.67	1334.50	99.18	106.30	106.03	2	Herringbone	1
13	PG163	9.00	60.00	3.00	0.15	3.00	1695.60	83.85	93.08	99.46	2	Herringbone	1
13	PG164	8.00	68.00	3.00	0.12	2.67	1334.50	74.69	81.13	83.15	2	Herringbone	1
14	VG33	12.00	7.00	3.50	1.71	3.43	397.01	57.23	65.63	82.60	1	Wave	1
14	VG34	11.50	6.50	4.00	1.77	2.88	287.02	18.44	27.46	54.88	2	Wave	1
14	VG37	10.75	6.00	3.50	1.79	3.07	247.57	100.79	85.52	63.35	1	Wave	1
15	PG99	5.00	3.00	2.00	1.67	2.50	21.20	115.61	101.50	77.04	1	Wave	1
15	PG101	5.25	3.00	2.00	1.75	2.63	24.87	223.27	195.99	145.08	2	Wave	1
15	VG94	5.25	3.00	2.50	1.75	2.10	17.81	108.08	103.66	103.85	1	Wave	1
15	VG101	5.25	3.00	2.50	1.75	2.10	17.81	78.29	77.39	80.88	1	Wave	1
16	PG4	11.00	9.00	4.00	1.22	2.75	346.19	21.19	20.11	16.28	1	Spots	4
16	PG115	13.00	9.00	5.00	1.44	2.60	452.16	27.27	27.43	30.17	1	None	None
16	PG123	12.00	11.50	5.00	1.04	2.40	442.35	15.54	15.00	15.44	1	Ribs	7
16	PG124	12.75	8.50	4.50	1.50	2.83	454.15	30.98	32.59	33.77	1	None	None
16	PG127	9.50	9.00	3.00	1.06	3.17	298.50	34.12	30.90	28.83	1	None	None
16	PG144	13.50	11.00	4.00	1.23	3.38	779.31	66.53	65.01	59.16	1	Spots	1

Group	Sample name	D	W	A	D/W	D/A	V	R	G	B	T	Decoration	Dec.n.
16	PG173	14.00	12.50	3.00	1.12	4.67	1187.31	32.72	30.26	26.17	1	Spots	1
16	VG50	12.00	10.00	3.00	1.20	4.00	635.85	25.64	25.70	28.61	1	Spots	2
17	PG98	11.00	7.50	3.50	1.47	3.14	331.17	221.48	187.02	116.24	1	None	None
17	PG141	13.00	7.00	4.00	1.86	3.25	445.10	225.82	189.67	132.16	1	None	None
17	VG19	7.00	4.50	2.00	1.56	3.50	88.31	201.77	171.47	115.18	1	None	None
17	VG51	10.75	6.00	3.00	1.79	3.58	282.89	218.99	182.96	92.12	1	None	None
18	PG3	23.50	28.00	4.50	0.84	5.22	7934.78	92.38	88.55	79.02	1	Line and wave	8
18	PG64	23.00	18.00	5.00	1.28	4.60	4578.12	96.88	93.34	87.19	1	Line and wave	8
18	VG81	28.00	20.00	3.50	1.40	8.00	9423.93	211.18	170.31	69.60	1	Herringbone	8
Other Beads	PG5	15.00	12.00	3.00	1.25	5.00	1356.48	68.94	61.03	46.49	1	Line	3
Other Beads	PG6	26.00	20.00	5.00	1.30	5.20	6923.70	42.11	39.95	33.65	1	Double ring eye	3
Other Beads	PG32	5.00	4.00	2.00	1.25	2.50	28.26	92.22	90.75	78.42	1	Ring eye	2
Other Beads	PG58	18.00	19.00	4.50	0.95	4.00	2718.26	51.48	46.55	39.04	1	Ring eye	3
Other Beads	PG66	7.00	11.00	2.50	0.64	2.80	174.86	77.65	75.66	71.76	1	Double wave	4
Other Beads	PG90	16.75	14.50	4.00	1.16	4.19	1850.37	204.56	199.04	176.23	2	Wave	1
Other Beads	PG113	12.50	20.00	3.00	0.63	4.17	1416.93	100.04	82.83	62.22	1	Spiral stripe	4
Other Beads	PG114	19.00	14.00	5.00	1.36	3.80	2154.04	43.53	39.16	37.30	1	Ring eye	3
Other Beads	VG18	8.00	5.00	2.00	1.60	4.00	141.30	185.16	170.29	142.18	1	None	None
Other Beads	VG27	17.50	14.50	3.00	1.21	5.83	2393.17	90.07	81.91	74.93	1	Ribs	8
Other Beads	VG28	15.00	11.50	4.00	1.30	3.75	1092.33	181.23	169.25	133.48	1	None	None
Other Beads	VG38	15.50	10.00	4.50	1.55	3.44	949.85	65.67	73.52	84.47	1	None	None
Other Beads	VG54	12.00	8.00	3.50	1.50	3.43	453.73	47.26	58.51	79.37	1	Ring eye	3
Other Beads	VG85	9.00	8.00	2.50	1.13	3.60	265.33	219.38	196.05	167.49	1	None	None
Other Beads	VG88	11.25	7.00	3.50	1.61	3.21	330.04	101.64	121.12	93.05	3	Protrusions and spiral stripe	1

APPENDIX 4. TYPES OF ANALYSES USED TO ANALYSE EACH SAMPLE.

Table below contains the list of samples analysed during stage 2 and 3 with an indication of methods used. The division on types is kept throughout the table. PG series of samples precedes the VG series within each type. The legend for the marks in the methods' cells is provided below. Samples in the Variable pressure mode of SEM-EDS were analysed without sample preparation, for the rest of the samples a graphitised cross section was analysed. Both Raman and XRD were operated in the micro analysis mode.

- – not analysed;
+ – analysed;
E – ELIO p-XRF unit;
F – Frankie p-XRF unit;
U – Unisantis XRF unit;
(VP) – variable pressure mode;
514 nm and 633 nm – respective wavelengths of Raman laser.

Group	Sample name	FORS	XRF	(VP)-SEM-EDS	LA-ICP-MS	Raman	XRD
10	PG1	+	+ E	-	-	-	-
10	PG2	+	+ E	-	+	+ 514nm	-
18	PG3	+	+ E	-	+	+ 514nm	-
16	PG4	+	+ E	-	+	+ 514nm	-
Other Beads	PG5	+	+ E	-	-	-	-
Other Beads	PG6	+	+ E	-	-	-	-
10	PG7	+	+ E	-	+	+ 514nm	-
10	PG8	+	+ E	-	-	-	-
10	PG9	+	+ E	-	+	+ 514nm	-
10	PG10	+	+ E	-	+	+ 514nm	-
10	PG11	+	+ E	-	-	-	-
10	PG12	+	+ E	-	-	-	-
10	PG13	+	+ E	+	+	+ 633nm	-
10	PG14	+	+ E	+	+	+ 633nm	-
10	PG15	+	+ E	+	+	+ 633nm	-
6	PG16-18	+	+ E	+	+	+ 633nm	-
6	PG19-21	+	+ E	-	+	+ 514nm	-
6	PG22-24	+	+ E	-	-	-	-
6	PG25-27	+	+ E	+	+	+ 633nm	+
7	PG28-30	+	+ E	-	+	+ 514nm	-
10	PG31	+	+ E	-	-	-	-
Other Beads	PG32	+	+ E	-	+	+ 514nm	-
10	PG33	+	+ E	-	-	-	-
7	PG34-38	+	+ E	-	+	+ 514nm	-
11	PG39	+	+ E	+ (VP)	+	+ 633nm	+

Group	Sample name	FORS	XRF	(VP)-SEM-EDS	LA-ICP-MS	Raman	XRD
6	PG40-42	+	+ E	-	+	+ 514nm	-
7	PG43	+	+ E	-	+	+ 514nm	-
1	PG44	+	+ E	-	-	-	-
1	PG45	+	+ E	-	-	-	-
1	PG46	+	+ E	-	+	+ 514nm	-
1	PG47	+	+ E	-	+	+ 514nm	-
6	PG48-50	+	+ E	-	+	+ 514nm	-
7	PG51-56	+	+ E	-	+	+ 514nm	-
Non-beads	PG57	+	+ E	-	+	+ 514nm	-
Other Beads	PG58	+	+ E	-	+	+ 514nm	-
Non-beads	PG59	+	+ E	-	-	-	-
Non-beads	PG60	+	+ E	-	+	+ 514nm	-
Non-beads	PG61	+	+ E	-	-	-	-
Non-beads	PG62	+	+ E	-	+	+ 514nm	-
10	PG63	+	+ E	-	+	+ 514nm	-
18	PG64	+	+ E	-	+	+ 514nm	-
4	PG65	+	+ E	-	-	-	-
Other Beads	PG66	+	+ E	-	-	-	-
10	PG67	+	+ E	-	-	-	-
10	PG68	+	+ E	-	+	+ 514nm	-
5	PG69	+	+ E	-	-	-	-
5	PG70	+	+ E	-	-	-	-
5	PG71	+	+ E	-	+	+ 514nm	-
5	PG72	+	+ E	-	-	-	-
1	PG73	+	+ E	-	+	+ 514nm	-
1	PG74	+	+ E	-	-	-	-
5	PG75	+	+ E	-	+	+ 514nm	-
5	PG76	+	+ E	-	-	-	-
1	PG77	+	+ E	-	-	-	-
1	PG78	+	+ E	-	+	+ 514nm	-
1	PG79	+	+ E	-	-	-	-
1	PG80	+	+ E	-	-	-	-
8	PG81	+	+ E	-	+	+ 514nm	-
1	PG82	+	+ E	-	-	-	-
8	PG83	+	+ E	-	-	-	-
3	PG84	+	+ E	-	+	+ 514nm	-
1	PG85	+	+ E	-	+	+ 514nm	-
1	PG86	+	+ E	-	+	+ 514nm	-
3	PG87	+	+ E	-	+	+ 514nm	-
11	PG88	+	+ E	-	-	-	-
11	PG89	+	+ E	+	+	+ 633nm	-
Other Beads	PG90	+	+ E	-	+	+ 514nm	-

Group	Sample name	FORS	XRF	(VP)-SEM-EDS	LA-ICP-MS	Raman	XRD
1	PG91	+	+ E	-	+	+ 514nm	-
1	PG92	+	+ E	-	-	-	-
1	PG93	+	+ E	-	-	-	-
1	PG94	+	+ E	-	+	+ 514nm	-
10	PG95	+	+ E	-	-	-	-
10	PG96	+	+ E	+	+	+ 633nm	-
Non-beads	PG97	+	+ E	+	+	+ 633nm	+
17	PG98	+	+ E	-	-	-	-
15	PG99	+	+ E	-	+	+ 514nm	-
1	PG100	+	+ E	-	-	-	-
15	PG101	+	+ E	-	-	-	-
1	PG102	+	+ E	-	-	-	-
1	PG103	+	+ E	-	-	-	-
10	PG104	+	+ E	-	+	+ 514nm	-
8	PG105	+	+ E	-	-	-	-
8	PG106	+	+ E	+	+	+ 633nm	-
1	PG107	+	+ E	-	+	+ 514nm	-
1	PG108	+	+ E	-	+	+ 514nm	-
1	PG109	+	+ E	-	+	+ 514nm	-
1	PG110_1	+	+ E	+	+	+ 633nm	-
1	PG110_2	-	-	+	+	+ 633nm	-
1	PG111	+	+ E	-	+	+ 514nm	-
1	PG112	+	+ E	-	+	+ 514nm	-
Other Beads	PG113	+	+ E	-	+	+ 514nm	-
Other Beads	PG114	+	+ E	-	+	+ 514nm	-
16	PG115	+	+ E	-	+	+ 514nm	-
10	PG116	+	+ E	+	+	+ 633nm	-
10	PG117	+	+ E	-	-	-	-
10	PG118	+	+ E	+	+	+ 633nm	-
10	PG119	+	+ E	-	+	+ 514nm	-
10	PG120	+	+ E	-	-	-	-
4	PG121	+	+ E	+	+	+ 633nm	+
4	PG122	+	+ E	-	+	+ 514nm	-
16	PG123	+	+ E	-	+	+ 514nm	-
16	PG124	+	+ E	-	+	+ 514nm	-
8	PG125	+	+ E	-	-	-	-
8	PG126	+	+ E	-	+	+ 514nm	-
16	PG127	+	+ E	-	+	+ 514nm	-
8	PG128	+	+ E	-	-	-	-
8	PG129	+	+ E	-	-	-	-
8	PG130	+	+ E	-	-	-	-
8	PG131	+	+ E	+ (VP)	+	+ 633nm	-

Group	Sample name	FORS	XRF	(VP)-SEM-EDS	LA-ICP-MS	Raman	XRD
8	PG132	+	+ E	-	-	-	-
8	PG133	+	+ E	-	-	-	-
1	PG134	+	+ E	-	-	-	-
Non-beads	PG135	+	+ E	-	-	-	-
11	PG136	+	+ E	+	+	+ 633nm	-
10	PG137	+	+ E	+	+	+ 633nm	-
1	PG138	+	+ E	-	-	-	-
1	PG139	+	+ E	+	+	+ 633nm	-
10	PG140	+	+ E	-	-	-	-
17	PG141	+	+ E	-	-	-	-
10	PG142	+	+ E	+	+	+ 633nm	-
10	PG143	+	+ E	+	+	+ 633nm	-
16	PG144	+	+ E	-	-	-	-
10	PG145	+	+ E	-	-	-	-
10	PG146	+	+ E	-	-	-	-
10	PG147	+	+ E	-	+	+ 514nm	-
10	PG148	+	+ E	-	+	+ 514nm	-
1	PG149	+	+ E	-	-	-	-
1	PG150	+	+ E	-	+	+ 514nm	-
1	PG151	+	+ E	-	+	+ 514nm	-
1	PG152	+	+ E	-	-	-	-
10	PG153	+	+ E	-	-	-	-
5	PG154	+	+ E	-	-	-	-
1	PG155	+	+ E	-	-	-	-
1	PG156	+	+ E	+ (VP)	+	+ 633nm	+
8	PG157	+	+ E	-	-	-	-
7	PG158	+	+ E	-	+	+ 514nm	-
7	PG159	+	+ E	-	+	+ 514nm	-
4	PG160	+	+ E	-	-	-	-
7	PG161	+	+ E	-	-	-	-
13	PG162	+	+ E	-	-	-	-
13	PG163	+	+ E	-	-	-	-
13	PG164	+	+ E	-	-	-	-
10	PG165	+	+ E	-	-	-	-
4	PG166	+	+ E	-	-	-	-
3	PG167	+	+ E	-	-	-	-
Other Beads	PG168	+	+ E	-	-	-	-
Other Beads	PG169	+	+ E	-	-	-	-
Other Beads	PG170	+	+ E	-	-	-	-
10	PG171	+	+ E	-	-	-	-
Other Beads	PG172	-	+ E	-	-	-	-
16	PG173	-	-	-	+	+ 514nm	-

Group	Sample name	FORS	XRF	(VP)-SEM-EDS	LA-ICP-MS	Raman	XRD
16	PG174	-	-	-	+	+514nm	-
Non-beads	VG1	+	+ U	-	-	-	-
Non-beads	VG2	+	+ U	-	-	-	-
Non-beads	VG3	+	+ U	-	-	-	-
Non-beads	VG4	+	+ U	-	-	-	-
Non-beads	VG5	+	+ U	-	-	-	-
Non-beads	VG6	+	+ U	-	-	-	-
Non-beads	VG7	+	+ U	-	-	-	-
Non-beads	VG9	+	+ U	-	-	-	-
Non-beads	VG13	+	+ F	-	-	-	-
10	VG14	+	+ U	-	-	-	-
11	VG15	+	+ U	-	-	-	-
Other Beads	VG16	+	+ U	-	-	-	-
9	VG17	+	+ U	-	-	-	-
Other Beads	VG18	+	+ U	-	-	-	-
17	VG19	+	+ U	-	-	-	-
1	VG20	+	+ U	-	-	-	-
1	VG21	+	+ U	-	-	-	-
7	VG22	+	+ F	+ (VP)	+	+ 514nm	+
7	VG23	+	+ F	-	-	-	-
7	VG24	+	+ F	-	-	-	-
3	VG25	+	+ F	-	-	-	-
12	VG26	+	+ F	-	-	-	-
Other Beads	VG27	+	+ F	-	-	-	-
Other Beads	VG28	+	+ F	-	-	-	-
12	VG29	+	+ F	-	-	-	-
Non-beads	VG32	+	+ U	+	+	+ 514nm	-
14	VG33	+	+ U	-	-	-	-
14	VG34	+	+ U	-	-	-	-
1	VG35	+	+ U	-	-	-	-
7	VG36	+	+ U	-	-	-	-
14	VG37	+	+ U	-	-	-	-
Other Beads	VG38	+	+ F	-	-	-	-
9	VG39	+	+ F	+	+	+ 514nm	+
9	VG40	+	+ F	+ (VP)	+	+ 514nm	+
9	VG41	+	+ F	+ (VP)	+	+ 514nm	+
9	VG42	+	+ F	+ (VP)	+	+ 514nm	+
9	VG43	+	+ F	-	-	-	-
9	VG44	+	+ F	-	-	-	-
9	VG45	+	+ F	-	-	-	-
9	VG46	+	+ F	-	-	-	-
9	VG47	+	+ F	-	-	-	-

Group	Sample name	FORS	XRF	(VP)-SEM-EDS	LA-ICP-MS	Raman	XRD
10	VG48	+	+ U	-	-	-	-
10	VG49	+	+ U	-	-	-	-
16	VG50	+	+ U	-	-	-	-
17	VG51	+	+ U	-	-	-	-
10	VG52	+	+ U	-	-	-	-
10	VG53	+	+ U	-	-	-	-
Other Beads	VG54	+	+ U	-	-	-	-
1	VG55	+	+ U	-	-	-	-
Non-beads	VG56	+	+ U	-	-	-	-
10	VG57	+	+ U	-	-	-	-
1	VG58	+	+ U	-	-	-	-
2	VG59	+	+ U	-	-	-	-
1	VG60	+	+ U	-	-	-	-
10	VG61	+	+ U	-	-	-	-
10	VG62	+	+ U	-	-	-	-
10	VG63	+	+ U	-	-	-	-
2	VG64	+	+ U	-	-	-	-
2	VG65	+	+ U	-	-	-	-
6	VG66	+	+ F	-	-	-	-
6	VG67	+	+ F	-	-	-	-
6	VG68	+	+ U	-	-	-	-
6	VG69	+	+ U	-	-	-	-
6	VG70	+	+ U	-	-	-	-
6	VG71	+	+ U	-	-	-	-
2	VG72	+	+ F	-	-	-	-
1	VG73	+	+ F	-	-	-	-
1	VG74	+	+ F	-	-	-	-
1	VG75	+	+ F	-	-	-	-
6	VG76	+	+ U	+	+	+ 514nm	+
6	VG77	+	+ U	-	-	-	-
6	VG78	+	+ U	-	-	-	-
6	VG79	+	+ U	-	-	-	-
2	VG80	+	+ U	-	-	-	-
18	VG81	+	+ U	-	-	-	-
10	VG82	+	+ F	-	-	-	-
10	VG83	+	+ F	-	-	-	-
10	VG84	+	+ F	-	-	-	-
Other Beads	VG85	+	+ U	-	-	-	-
11	VG86	+	+ U	-	-	-	-
10	VG87	+	+ U	-	-	-	-
Other Beads	VG88	+	+ U	-	-	-	-
10	VG89	+	+ U	-	-	-	-

Group	Sample name	FORS	XRF	(VP)-SEM-EDS	LA-ICP-MS	Raman	XRD
10	VG90	+	+ U	-	-	-	-
2	VG91	+	+ U	-	-	-	-
Non-beads	VG92	+	+ U	-	-	-	-
Non-beads	VG93	+	+ U	-	-	-	-
15	VG94	+	+ U	-	-	-	-
1	VG95	+	+ U	-	-	-	-
1	VG96	+	+ U	-	-	-	-
1	VG97	+	+ U	-	-	-	-
2	VG98	+	+ U	+ (VP)	+	+ 514nm	+
2	VG99	+	+ U	-	-	-	-
1	VG100	+	+ U	-	-	-	-
15	VG101	+	+ U	-	-	-	-
10	VG102	+	+ U	-	-	-	-
10	VG103	+	+ U	-	-	-	-
10	VG104	+	+ U	-	-	-	-
10	VG105	+	+ U	-	-	-	-
1	VG106	+	+ F	+ (VP)	+	+ 514nm	+
1	VG107	+	+ F	-	-	-	-
1	VG108	+	+ F	-	-	-	-
1	VG109	+	+ F	-	-	-	-
1	VG110	+	+ F	-	-	-	-
1	VG111	+	+ F	-	-	-	-
1	VG112	+	+ F	-	-	-	-
1	VG113	+	+ F	-	-	-	-
Non-beads	VG114	+	+ U	+	+	+ 514nm	-

APPENDIX 5. FIBRE OPTICS REFLECTION SPECTROSCOPY RESULTS.

Following table contains qualitative results of the interpretation of FORS spectra. The results are sorted by chapter of the thesis. Inside every chapter, the rows of each sample are sorted by type. Inside each type the samples are sorted by the number in ascending order. PG series of samples precedes the VG series of samples. The "Result" column indicates whether the spectra obtained by analysing the sample contained useful analytical information. In case no bands were obtained in any of the spectra of the sample, no result – "nr." Indication is inserted. Bands of various chromophores were evaluated using 3-level descriptive system: + – the band(s) is(are) weakly pronounced; ++ – is moderately pronounced; +++ – is strongly pronounced. "Other" is the space of indication of other chromophores that were detected.

Chapter	Group	Sample name	FORS	Co^{2+}	Cu^{2+}	Fe^{2+}	Fe^{3+}	Other
5	1	PG100	+	+++	-	+++	+++	-
5	1	PG102	+	+++	-	+++	+++	-
5	1	PG103	+	++	-	++	++	-
5	1	PG107	+	++	-	+	+	-
5	1	PG108	nr.	-	-	-	-	-
5	1	PG109	+	+++	++	-	+	-
5	1	PG110_1	nr.	-	-	-	-	-
5	1	PG110_2	+	+++	-	++	+	-
5	1	PG111	+	+++	+	-	++	-
5	1	PG112	+	-	++	-	-	-
5	1	PG134	+	+++	-	++	++	-
5	1	PG138	+	+++	++	-	+	-
5	1	PG139	+	+++	-	++	++	-
5	1	PG149	+	+++	-	++	++	-
5	1	PG150	+	+++	-	+++	++	-
5	1	PG151	+	+++	++	-	++	-
5	1	PG152	+	+++	-	++	++	-
5	1	PG155	+	+++	-	++	++	-
5	1	PG156	+	+++	-	++	++	-
5	1	PG44	+	+++	-	++	++	-
5	1	PG45	+	+++	-	++	++	-
5	1	PG46	+	++	-	++	++	-
5	1	PG47	+	++	-	++	++	-
5	1	PG73	+	+++	-	+++	++	-
5	1	PG74	+	+++	-	+++	++	-
5	1	PG77	+	+++	-	-	-	-
5	1	PG78	+	+++	-	++	+	-
5	1	PG79	+	+++	-	++	+	-
5	1	PG80	+	++	-	+	-	-
5	1	PG82	+	++	-	+	+	Mn^{2+}
5	1	PG85	+	++	-	++	+	-

Chapter	Group	Sample name	FORS	Co^{2+}	Cu^{2+}	Fe^{2+}	Fe^{3+}	Other
5	1	PG86	+	++	-	++	+	-
5	1	PG91	+	+++	-	-	+	-
5	1	PG92	+	+++	-	++	++	-
5	1	PG93	+	+++	-	-	+	-
5	1	PG94	+	+++	-	++	++	-
5	1	VG100	+	+++	-	++	+	-
5	1	VG106	+	+++	-	-	+	-
5	1	VG107	+	+++	-	-	+	-
5	1	VG108	+	+++	-	-	+	-
5	1	VG109	+	+++	-	+	+	-
5	1	VG110	+	+++	-	+	+	-
5	1	VG111	+	+++	-	+	+	-
5	1	VG112	+	+++	-	++	++	-
5	1	VG113	+	+++	-	+	++	-
5	1	VG20	+	+++	-	++	+	-
5	1	VG21	+	+++	-	++	+	-
5	1	VG35	+	+++	-	+++	+++	-
5	1	VG55	+	+++	-	++	+	-
5	1	VG58	+	+++	-	+	++	-
5	1	VG60	+	++	-	++	+	-
5	1	VG73	+	++	-	++	+	-
5	1	VG74	+	++	+	-	+	-
5	1	VG75	+	++	-	++	+	-
5	1	VG95	+	+++	-	++	+	-
5	1	VG96	+	+++	-	++	+	-
5	1	VG97	+	+++	-	++	+	-
5	2	VG59	+	+++	-	+++	+++	-
5	2	VG64	+	+++	-	+++	++	-
5	2	VG65	+	+++	-	+++	++	-
5	2	VG72	+	++	+	-	+	-
5	2	VG80	+	+++	-	++	++	-
5	2	VG91	+	+++	-	+++	+++	-
5	2	VG98	+	+++	-	++	+	-
5	2	VG99	+	+++	-	++	+	-
5	7	PG158	+	++	+	-	++	-
5	7	PG159	+	++	-	++	-	-
5	7	PG161	+	-	+++	-	-	-
5	7	PG28-30	+	+++	-	++	+	-
5	7	PG34-36	+	+++	-	+++	+	-
5	7	PG37-38	+	-	-	+++	+	-
5	7	PG43	+	+++	-	++	++	-
5	7	PG51-56	+	+++	-	++	+	-

Chapter	Group	Sample name	FORS	Co^{2+}	Cu^{2+}	Fe^{2+}	Fe^{3+}	Other
5	7	VG22	+	-	-	-	-	-
5	7	VG23	+	+++	-	++	+	-
5	7	VG24	+	-	-	-	-	Cu^{0}
5	7	VG36	+	+++	-	++	+	-
5	14	VG33	+	+++	-	++(y)	+	-
5	14	VG34	+	+++	-	++	-	-
5	Non-beads	VG1	+	+++	-	+++	+	-
5	Non-beads	VG13	+	+++	-	+++	+	-
5	Non-beads	VG2	+	++	-	+++	-	-
5	Non-beads	VG32	+	+++	-	+++	+	-
5	Other Beads	PG168	+	+++	-	+++	+++	-
5	Other Beads	VG54	+	+++	-	++	+	-
6	3	PG167	+	-	+++	-	-	-
6	3	PG84	nr.	-	-	-	-	-
6	3	PG87	nr.	-	-	-	-	-
6	3	VG25	+	-	-	-	-	Cu^{0}
6	4	PG121	+	-	+++	-	+	-
6	4	PG122	+	-	+++	-	+	-
6	4	PG160	+	-	+++	-	+	-
6	4	PG166	nr.	-	-	-	-	-
6	4	PG65	+	-	+++	-	+	-
6	12	VG26	+	-	-	-	-	Cu^{0}
6	12	VG29	+	-	-	-	-	Cu^{0}
6	13	PG162	+	-	+	-	-	-
6	13	PG163	+	-	+	-	-	-
6	13	PG164	nr.	-	-	-	-	-
6	Non-beads	PG59	+	-	-	+	-	-
6	Non-beads	PG60	+	-	+++	+(y)	+	-
6	Other Beads	PG169	+	-	++	+	-	Mn^{2+}
6	Other Beads	PG170	+	-	+++	-	+	-
6	Other Beads	VG28	+	-	-	++	-	-
6	Other Beads	VG38	+	-	-	++	-	-
7	5	PG154	+	-	-	++	++	-
7	5	PG69	+	-	+++	-	-	-
7	5	PG70	+	-	+++	-	-	-
7	5	PG71	+	-	-	-	+	-
7	5	PG72	+	-	-	-	+	Mn^{3+}
7	5	PG75	+	-	-	++	+	Mn^{3+}
7	5	PG76	+	-	-	++	+	Mn^{3+}
7	10	PG1	+	-	-	+++	-	-
7	10	PG10	+	-	-	+++	-	Fe-S complex
7	10	PG104	+	-	-	-	+	-

Chapter	Group	Sample name	FORS	Co^{2+}	Cu^{2+}	Fe^{2+}	Fe^{3+}	Other
7	10	PG11	+	-	-	++	-	-
7	10	PG116	+	-	+	-	+	-
7	10	PG117	nr.	-	-	-	-	-
7	10	PG118	nr.	-	-	-	-	-
7	10	PG119	+	-	-	++	++	-
7	10	PG12	nr.	-	-	-	-	-
7	10	PG120	+	-	-	+++	-	-
7	10	PG13	+	-	-	++	+++	Mn^{2+}
7	10	PG137	+	-	-	++	++	Mn^{2+}
7	10	PG14	+	-	-	+++	-	Fe-S complex
7	10	PG140	+	-	-	+++	-	Mn^{2+}
7	10	PG142	+	-	-	+++	-	Mn^{2+}
7	10	PG143	+	-	-	+++	+	-
7	10	PG145	+	-	-	+++	++	-
7	10	PG146	+	-	-	+++	++	-
7	10	PG147	+	-	-	+++	++	-
7	10	PG148	nr.	-	-	-	-	-
7	10	PG15	+	-	-	+++	++	-
7	10	PG153	+	-	-	++	+	-
7	10	PG165	nr.	-	-	-	-	-
7	10	PG171	nr.	-	-	-	-	-
7	10	PG2	+	-	-	+	-	-
7	10	PG31	+	-	-	++	-	-
7	10	PG33	+	++	+++	-	+	-
7	10	PG63	+	-	+++	-	-	Mn^{2+}
7	10	PG67	+	-	-	+++	-	Fe-S complex
7	10	PG68	+	-	-	++	-	-
7	10	PG7	+	-	-	+	-	-
7	10	PG8	+	-	-	++	++	-
7	10	PG9	+	-	-	+++	-	-
7	10	PG95	+	-	-	++	+++	-
7	10	PG96	+	-	-	++	-	-
7	10	VG102	+	-	-	+++	-	-
7	10	VG103	+	-	-	+++	-	-
7	10	VG104	+	-	-	++	-	-
7	10	VG105	+	-	-	+++	-	Mn^{2+}
7	10	VG14	+	-	-	+++	-	-
7	10	VG48	nr.	-	-	-	-	-
7	10	VG49	nr.	-	-	-	-	-
7	10	VG52	+	-	-	+++	+	-
7	10	VG53	nr.	-	-	-	-	-
7	10	VG57	+	-	-	+++	++	-

Chapter	Group	Sample name	FORS	Co^{2+}	Cu^{2+}	Fe^{2+}	Fe^{3+}	Other
7	10	VG61	+	-	-	+++	+++	-
7	10	VG62	nr.	-	-	-	-	-
7	10	VG63	nr.	-	-	-	-	-
7	10	VG82	nr.	-	-	-	-	-
7	10	VG83	+	-	-	+	-	-
7	10	VG84	+	-	-	+++	-	-
7	10	VG87	nr.	-	-	-	-	-
7	10	VG89	nr.	-	-	-	-	-
7	10	VG90	+	-	-	++	-	-
7	11	PG136	+	-	+++	-	++	-
7	11	PG39	+	+++	-	-	-	-
7	11	PG88	nr.	-	-	-	-	-
7	11	PG89	+	-	+++	-	-	-
7	11	VG15	+	-	+	-	-	-
7	11	VG86	+	-	-	++	-	-
7	Non-beads	PG97	+	-	+++	-	-	-
7	Non-beads	VG114	nr.	-	-	-	-	-
7	Non-beads	VG5	+	-	-	+++	++	-
7	Non-beads	VG56	+	-	+	-	-	Mn3+
7	Non-beads	VG6	nr.	-	-	-	-	-
7	Other Beads	PG172	nr.	-	-	-	-	-
7	Other Beads	PG90	+	-	-	+	-	-
7	Other Beads	VG88	+	-	+	-	-	-
8	6	PG16-18	+	-	-	+	-	-
8	6	PG19-21	+	-	-	+	-	-
8	6	PG22-24	nr.	-	-	-	-	-
8	6	PG25-27	nr.	-	-	-	-	-
8	6	PG40-42	nr.	-	-	-	-	-
8	6	PG48-50	+	-	-	+	-	-
8	6	VG66	+	-	-	+	-	-
8	6	VG67	nr.	-	-	-	-	-
8	6	VG68	+	-	-	+	-	-
8	6	VG69	nr.	-	-	-	-	-
8	6	VG70	+	-	-	+	-	-
8	6	VG71	nr.	-	-	-	-	-
8	6	VG76	+	-	-	+	-	-
8	6	VG77	nr.	-	-	-	-	-
8	6	VG78	nr.	-	-	-	-	-
8	6	VG79	nr.	-	-	-	-	-
8	14	VG37	nr.	-	-	-	-	-
8	15	PG101	nr.	-	-	-	-	-
8	15	PG99	nr.	-	-	-	-	-

Chapter	Group	Sample name	FORS	Co^{2+}	Cu^{2+}	Fe^{2+}	Fe^{3+}	Other
8	15	VG101	+	+++	-	++	+	-
8	15	VG94	+	+++	-	++	+	-
8	17	PG141	nr.	-	-	-	-	-
8	17	PG98	+	-	+++	-	-	-
8	17	VG19	nr.	-	-	-	-	-
8	17	VG51	+	-	-	+	-	-
8	18	PG3	+	+	-	++	+	-
8	18	PG64	+	-	-	+	-	-
8	18	VG81	+	-	+++	-	-	-
8	Non-beads	VG3	+	-	-	++	-	-
8	Non-beads	VG4	+	-	-	+	-	-
8	Non-beads	VG7	+	-	-	++	++	-
8	Non-beads	VG9	+	-	-	++	+	-
8	Other Beads	VG85	nr.	-	-	-	-	-
9	8	PG105	nr.	-	-	-	-	-
9	8	PG106	+	-	-	++	+	-
9	8	PG125	nr.	-	-	-	-	-
9	8	PG126	nr.	-	-	-	-	-
9	8	PG128	nr.	-	-	-	-	-
9	8	PG129	nr.	-	-	-	-	-
9	8	PG130	nr.	-	-	-	-	-
9	8	PG131	+	-	-	++	-	-
9	8	PG132	+	-	-	++	-	-
9	8	PG133	+	-	+	-	-	Mn^{2+}
9	8	PG157	nr.	-	-	-	-	-
9	8	PG81	+	-	-	++	+	-
9	8	PG83	+	-	-	-	-	Fe-S complex
9	16	PG115	+	-	+	-	-	-
9	16	PG123	nr.	-	-	-	-	-
9	16	PG124	nr.	-	-	-	-	-
9	16	PG127	nr.	-	-	-	-	-
9	16	PG144	nr.	-	-	-	-	-
9	16	PG173	nr.	-	-	-	-	-
9	16	PG4	+	+	-	-	-	-
9	16	VG50	+	-	-	++	-	-
9	Non-beads	PG135	nr.	-	-	-	-	-
9	Non-beads	PG57	+	-	-	-	-	Fe-S complex
9	Non-beads	PG61	+	-	-	+++	-	-
9	Non-beads	PG62	+	-	-	+++	-	-
9	Non-beads	VG92	+	-	+	-	-	-
9	Non-beads	VG93	+	-	-	+++	-	-
9	Other Beads	PG113	+	-	-	+	+	-

Chapter	Group	Sample name	FORS	Co^{2+}	Cu^{2+}	Fe^{2+}	Fe^{3+}	Other
9	Other Beads	PG114	+	-	-	++	++	Fe-S complex
9	Other Beads	PG32	+	-	-	++	-	-
9	Other Beads	PG5	+	-	-	++	+	Mn^{2+}
9	Other Beads	PG58	+	-	-	-	-	Mn^{2+}
9	Other Beads	PG6	+	-	+	+	+	-
9	Other Beads	PG66	nr.	-	-	-	-	-
9	Other Beads	VG18	nr.	-	-	-	-	-
10	9	VG17	+	-	+	-	-	-
10	9	VG39	nr.	-	-		-	-
10	9	VG40	nr.	-	-			-
10	9	VG41	nr.	-	-	-	-	-
10	9	VG42	nr.	-	-	-	-	-
10	9	VG43	nr.	-	-	-	-	-
10	9	VG44	nr.	-	-	-	-	-
10	9	VG45	nr.	-	-	-	-	-
10	9	VG46	nr.	-	-	-	-	-
10	9	VG47	nr.	-	-	-	-	-
10	Other Beads	VG16	+	-	+	-	-	-
10	Other Beads	VG27	+	-	+++	-	-	-

APPENDIX 6. PORTABLE X-RAY FLUORESCENCE SPECTROMETRY RESULTS.

Table below contains the results of the quantification of the p-XRF spectra. This quantification was performed using PyMCA software. Elemental concentrations were corrected, Limits of Quantification (LOQ) estimated and the values converted to the respective oxides in the way explained in the section 4.4 of the main text. The table presents mean concentrations of du- or triplicate analyses with their standard deviation values (in italic) for each element that was detected. Sporadic detection of other elements was noted but is not reflected in the content of the table. Values that were below the LOQ were discarded, "<" followed by the LOQ of element for the p-XRF unit used in the acquisition was placed in each. Some elements were detected only in one (of usually three) spectrum and, consequently, in these cases the mean value of this element concentration is below the LOQ estimation. Nevertheless, it is kept in the table to serve as a record of non-systematic detection. Column "XRF unit" is providing the information about what XRF unit was used to acquire spectra of each sample. "E" stands for ELIO, "U" for Unisantis, "F" for Frankie. The description of the hardware is provided in the section 4.4 of the main text. In case of polychrome beads, each colour was treated as separate spectrum. To distinguish between the base colour and the decoration one, the representative compositions of the colours of decorations are marked with a letter. "d" stands for dark, "g" stands for green, "r" – red, "y" – yellow, "w" – white colour. In cases the information on specific element was not recorded for a specific element with any of the p-XRF units, instead of the concentration value "N/A" was inserted. The absence of the standard deviation value (either because the concentrations were below the estimated LOQs or only one acquisition was done) is marked with "-". Samples are sorted by chapter of the thesis where the discussion of the results of specific group takes place. The next order of division is by the group in ascending order. The other beads and the non-beads groups are placed in the end of each chapter's section of the table. Within each group samples are sorted by the series (PG samples precede the VG samples) and number in ascending order.

Chapter	**Group**	**Sample name/st.dev.**	**XRF unit**	**K_20**	**CaO**	**TiO_2**	**MnO**	**Fe_2O_3**	**CoO**	**NiO**	**CuO**	**ZnO**	**SrO**	**ZrO_2**	**SnO_2**	**Sb_2O_5**	**PbO**
5	1	PG44	E	<1.2	4.24	<0.26	0.265	1.08	0.080	0.086	<0.4	0.047	0.032	<0.014	<0.064	<0.17	<0.09
		PG44 st.dev.	*E*	-	*0.49*	-	*0.016*	*0.02*	*0.014*	*0.007*	-	*0.006*	*0.001*	-	-	-	-
5	1	PG44-45w	E	<1.2	5.83	<0.26	0.077	0.49	<0.038	<0.06	<0.4	<0.037	0.035	<0.014	<0.064	0.69	<0.09
		PG44-45w st.dev.	*E*	-	*1.97*	-	*0.059*	*0.15*	-	-	-	-	*0.007*	-	-	*0.21*	-
5	1	PG45	E	<1.2	4.52	<0.26	0.287	1.12	0.090	0.080	<0.4	0.053	0.033	<0.014	<0.064	0.18	<0.09
		PG45 st.dev.	*E*	-	*0.08*	-	*0.032*	*0.01*	*0.006*	*0.020*	-	*0.001*	*0.002*	-	-	*0.01*	-
5	1	PG46	E	<1.2	4.16	<0.26	0.314	0.68	0.083	0.062	<0.4	0.058	0.034	<0.014	<0.064	0.28	<0.09
		PG46 st.dev.	*E*	-	*0.01*	-	*0.009*	*0.02*	*0.008*	*0.008*	-	*0.001*	*0.000*	-	-	*0.02*	-
5	1	PG47	E	<1.2	5.68	<0.26	0.454	0.99	0.128	0.081	<0.4	0.075	0.037	<0.014	<0.064	0.29	<0.09
		PG47 st.dev.	*E*	-	*0.54*	-	*0.024*	*0.02*	*0.002*	*0.001*	-	*0.005*	*0.003*	-	-	*0.08*	-

Chapter	Group	Sample name/st.dev.	XRF unit	K_20	CaO	TiO_2	MnO	Fe_2O_3	CoO	NiO	CuO	ZnO	SrO	ZrO_2	SnO_2	Sb_2O_5	PbO
5	1	PG73-74	E	<1.2	3.74	<0.26	0.324	1.11	0.100	0.092	<0.4	0.056	0.024	0.023	<0.064	<0.17	<0.09
		PG73-74 st.dev.	*E*	-	*1.45*	-	*0.083*	*0.26*	*0.034*	*0.008*	-	*0.020*	*0.005*	*0.017*	-	-	-
5	1	PG77	E	<1.2	3.56	<0.26	0.099	0.77	0.040	<0.06	<0.4	<0.037	0.026	<0.014	<0.064	<0.17	<0.09
		PG77 st.dev.	*E*	-	*0.21*	-	*0.004*	*0.07*	*0.003*	-	-	-	*0.003*	-	-	-	-
5	1	PG78	E	<1.2	3.59	<0.26	0.257	0.96	0.088	0.078	<0.4	0.043	0.029	<0.014	<0.064	<0.17	<0.09
		PG78 st.dev.	*E*	-	*0.24*	-	*0.017*	*0.06*	*0.008*	*0.005*	-	*0.004*	*0.002*	-	-	-	-
5	1	PG79	E	<1.2	4.88	<0.26	0.249	0.86	0.072	0.077	<0.4	0.048	0.033	<0.014	<0.064	<0.17	<0.09
		PG79 st.dev.	*E*	-	*0.68*	-	*0.067*	*0.15*	*0.018*	*0.021*	-	*0.009*	*0.004*	-	-	-	-
5	1	PG80	E	<1.2	3.66	<0.26	0.186	0.79	0.077	<0.06	<0.4	0.052	0.028	<0.014	<0.064	<0.17	<0.09
		PG80 st.dev.	*E*	-	*0.49*	-	*0.040*	*0.12*	*0.017*	-	-	*0.008*	*0.000*	-	-	-	-
5	1	PG82	E	<1.2	4.04	<0.26	0.380	1.18	0.124	0.115	<0.4	0.056	0.033	<0.014	<0.064	<0.17	<0.09
		PG82 st.dev.	*E*	-	*0.51*	-	*0.044*	*0.12*	*0.009*	*0.018*	-	*0.008*	*0.003*	-	-	-	-
5	1	PG85	E	<1.2	5.93	<0.26	0.248	0.87	0.066	0.071	<0.4	0.037	0.032	<0.014	<0.064	<0.17	<0.09
		PG85 st.dev.	*E*	-	*0.76*	-	*0.045*	*0.11*	*0.009*	*0.010*	-	*0.005*	*0.004*	-	-	-	-
5	1	PG86	E	<1.2	6.13	<0.26	0.385	2.17	0.129	0.121	<0.4	0.083	0.032	<0.014	<0.064	<0.17	<0.09
		PG86 st.dev.	*E*	-	*0.53*	-	*0.045*	*0.23*	*0.018*	*0.011*	-	*0.006*	*0.000*	-	-	-	-
5	1	PG91	E	<1.2	4.07	<0.26	0.222	0.66	0.075	0.065	<0.4	0.067	0.034	<0.014	<0.064	0.31	<0.09
		PG91 st.dev.	*E*	-	*1.33*	-	*0.057*	*0.16*	*0.019*	*0.016*	-	*0.017*	*0.005*	-	-	*0.01*	-
5	1	PG91w	E	<1.2	3.54	<0.26	0.095	0.37	<0.038	<0.06	<0.4	<0.037	0.025	<0.014	<0.064	0.28	<0.09
		PG91w st.dev.	*E*	-	*2.52*	-	*0.047*	*0.14*	-	-	-	-	*0.019*	-	-	*0.24*	-
5	1	PG92	E	<1.2	4.74	0.275	0.405	1.45	0.111	0.118	0.41	0.074	0.033	0.029	<0.064	<0.17	<0.09
		PG92 st.dev.	*E*	-	*0.64*	*0.052*	*0.043*	*0.22*	*0.021*	*0.018*	*0.03*	*0.013*	*0.002*	*0.003*	-	-	-
5	1	PG93	E	<1.2	4.84	<0.26	0.310	0.92	0.103	0.087	<0.4	0.088	0.038	<0.014	<0.064	0.40	<0.09
		PG93 st.dev.	*E*	-	*2.32*	-	*0.117*	*0.41*	*0.044*	*0.031*	-	*0.037*	*0.011*	-	-	*0.11*	-
5	1	PG93w	E	<1.2	4.53	<0.26	0.089	0.70	<0.038	<0.06	<0.4	<0.037	0.033	<0.014	<0.064	0.74	<0.09
		PG93w st.dev.	*E*	-	*1.68*	-	*0.065*	*0.53*	-	-	-	-	*0.005*	-	-	*0.02*	-
5	1	PG94	E	<1.2	4.10	<0.26	0.288	1.20	0.070	0.091	<0.4	0.053	0.035	<0.014	<0.064	0.29	<0.09
		PG94 st.dev.	*E*	-	*1.54*	-	*0.128*	*0.41*	*0.032*	*0.033*	-	*0.021*	*0.008*	-	-	*0.03*	-

Chapter	Group	Sample name/st.dev.	XRF unit	K_20	CaO	TiO_2	MnO	Fe_2O_3	CoO	NiO	CuO	ZnO	SrO	ZrO_2	SnO_2	Sb_2O_5	PbO
5	1	PG94w	E	<1.2	8.60	<0.26	0.131	0.73	<0.038	<0.06	0.81	<0.037	0.039	<0.014	<0.064	0.73	<0.09
		PG94w st.dev.	*E*	-	*1.27*	-	*0.045*	*0.16*	-	-	*0.33*	-	*0.006*	-	-	*0.16*	-
5	1	PG100	E	<1.2	4.45	<0.26	0.245	1.07	0.092	0.109	<0.4	0.119	0.028	<0.014	<0.064	0.24	<0.09
		PG100 st.dev.	*E*	-	*1.22*	-	*0.093*	*0.44*	*0.043*	*0.040*	-	*0.051*	*0.006*	-	-	*0.01*	-
5	1	PG100w	E	<1.2	7.30	<0.26	<0.065	0.63	<0.038	<0.06	<0.4	<0.037	0.033	<0.014	<0.064	0.98	<0.09
		PG100w st.dev.	*E*	-	*1.98*	-	-	*0.26*	-	-	-	-	*0.007*	-	-	*0.29*	-
5	1	PG102	E	<1.2	7.32	<0.26	0.179	0.72	0.061	<0.06	0.45	0.051	0.028	<0.014	<0.064	0.62	<0.09
		PG102 st.dev.	*E*	-	*0.96*	-	*0.030*	*0.04*	*0.010*	-	*0.03*	*0.005*	*0.001*	-	-	*0.35*	-
5	1	PG102w	E	<1.2	10.80	<0.26	0.133	0.58	0.039	<0.06	0.40	0.038	0.030	<0.014	<0.064	1.29	<0.09
		PG102w st.dev.	*E*	-	*2.55*	-	*0.030*	*0.10*	*0.007*	-	*0.02*	*0.008*	*0.005*	-	-	*0.30*	-
5	1	PG103	E	<1.2	4.45	<0.26	0.262	0.76	0.067	0.080	<0.4	0.052	0.032	<0.014	<0.064	0.21	<0.09
		PG103 st.dev.	*E*	-	*1.40*	-	*0.058*	*0.20*	*0.022*	*0.021*	-	*0.012*	*0.004*	-	-	*0.01*	-
5	1	PG103w	E	<1.2	6.82	<0.26	0.092	0.37	<0.038	<0.06	<0.4	<0.037	0.033	<0.014	<0.064	0.68	<0.09
		PG103w st.dev.	*E*	-	*2.49*	-	*0.069*	*0.22*	-	-	-	-	*0.006*	-	-	*0.16*	-
5	1	PG107	E	<1.2	1.82	<0.26	0.147	0.89	<0.038	<0.06	0.78	<0.037	0.020	<0.014	<0.064	<0.17	<0.09
		PG107 st.dev.	*E*	-	*0.39*	-	*0.062*	*0.17*	-	-	*0.44*	-	*0.002*	-	-	-	-
5	1	PG108	E	<1.2	3.27	<0.26	0.198	1.16	0.048	<0.06	<0.4	<0.037	0.024	<0.014	<0.064	0.18	<0.09
		PG108 st.dev.	*E*	-	*0.96*	-	*0.069*	*0.20*	*0.018*	-	-	-	*0.002*	-	-	*0.01*	-
5	1	PG109	E	<1.2	5.13	<0.26	0.586	0.44	<0.038	<0.06	0.54	<0.037	0.028	<0.014	<0.064	0.43	<0.09
		PG109 st.dev.	*E*	-	*1.22*	-	*0.069*	*0.05*	-	-	*0.01*	-	*0.002*	-	-	*0.08*	-
5	1	PG109w	E	<1.2	5.95	<0.26	0.240	0.40	<0.038	<0.06	0.44	<0.037	0.025	<0.014	0.088	0.79	<0.09
		PG109w st.dev.	*E*	-	*2.70*	-	*0.203*	*0.20*	-	-	*0.19*	-	*0.005*	-	*0.124*	*0.29*	-
5	1	PG110_1	E	<1.2	4.70	<0.26	1.094	0.50	<0.038	<0.06	0.88	<0.037	0.030	<0.014	<0.064	0.35	<0.09
		PG110_1 st.dev.	*E*	-	*1.00*	-	*0.268*	*0.11*	-	-	*0.15*	-	*0.004*	-	-	*0.07*	-
5	1	PG110_1w	E	<1.2	7.96	0.292	0.429	0.78	<0.038	<0.06	0.61	<0.037	0.032	<0.014	<0.064	0.54	<0.09
		PG110_1w st.dev.	*E*	-	*1.92*	*0.076*	*0.120*	*0.27*	-	-	*0.15*	-	*0.005*	-	-	*0.15*	-
5	1	PG110_2	nr.														
		PG110_2 st.dev.	*nr.*														

Chapter	Group	Sample name/st.dev.	XRF unit	K_20	CaO	TiO_2	MnO	Fe_2O_3	CoO	NiO	CuO	ZnO	SrO	ZrO_2	SnO_2	Sb_2O_5	PbO
5	1	PG111	E	<1.2	4.15	<0.26	0.605	0.85	0.043	0.066	0.53	0.038	0.026	<0.014	<0.064	0.73	<0.09
		PG111 st.dev.	*E*	-	*0.31*	-	*0.090*	*0.08*	*0.012*	*0.012*	*0.03*	*0.006*	*0.002*	-	-	*0.05*	-
5	1	PG111w	E	<1.2	6.51	<0.26	0.162	0.50	<0.038	<0.06	<0.4	<0.037	0.026	<0.014	<0.064	1.45	<0.09
		PG111w st.dev.	*E*	-	*1.38*	-	*0.064*	*0.10*	-	-	-	-	*0.002*	-	-	*0.07*	-
5	1	PG112	E	<1.2	3.63	<0.26	0.881	0.52	<0.038	<0.06	0.74	<0.037	0.028	<0.014	<0.064	<0.17	<0.09
		PG112 st.dev.	*E*	-	*2.13*	-	*0.603*	*0.33*	-	-	*0.35*	-	*0.009*	-	-	-	-
5	1	PG134	E	<1.2	2.72	<0.26	0.192	0.97	0.055	<0.06	<0.4	0.039	0.028	<0.014	<0.064	<0.17	<0.09
		PG134 st.dev.	*E*	-	*0.68*	-	*0.057*	*0.30*	*0.015*	-	-	*0.008*	*0.005*	-	-	-	-
5	1	PG138	E	<1.2	3.88	<0.26	1.483	0.35	<0.038	<0.06	0.96	<0.037	0.042	<0.014	<0.064	0.26	<0.09
		PG138 st.dev.	*E*	-	*1.15*	-	*0.557*	*0.11*	-	-	*0.28*	-	*0.009*	-	-	*0.09*	-
5	1	PG139	E	<1.2	4.99	<0.26	0.257	0.52	0.096	0.082	<0.4	0.067	0.034	<0.014	<0.064	0.27	<0.09
		PG139 st.dev.	*E*	-	*3.01*	-	*0.174*	*0.33*	*0.068*	*0.054*	-	*0.043*	*0.012*	-	-	*0.03*	-
5	1	PG149	E	<1.2	3.83	<0.26	0.259	0.64	0.144	0.108	<0.4	0.086	0.030	<0.014	0.075	<0.17	<0.09
		PG149 st.dev.	*E*	-	*0.30*	-	*0.029*	*0.03*	*0.007*	*0.006*	-	*0.002*	*0.002*	-	*0.034*	-	-
5	1	PG150	E	<1.2	4.44	<0.26	0.525	1.13	0.214	0.144	<0.4	0.114	0.035	<0.014	<0.064	0.31	<0.09
		PG150 st.dev.	*E*	-	*0.53*	-	*0.053*	*0.15*	*0.021*	*0.019*	-	*0.011*	*0.003*	-	-	*0.07*	-
5	1	PG150w	E	<1.2	4.35	<0.26	0.209	0.54	0.085	<0.06	<0.4	0.050	0.028	<0.014	<0.064	0.41	<0.09
		PG150w st.dev.	*E*	-	*0.97*	-	*0.034*	*0.04*	*0.008*	-	-	*0.004*	*0.003*	-	-	*0.02*	-
5	1	PG151	E	<1.2	4.72	<0.26	0.488	1.52	0.117	0.083	<0.4	0.080	0.030	0.038	<0.064	<0.17	<0.09
		PG151 st.dev.	*E*	-	*0.23*	-	*0.062*	*0.11*	*0.012*	*0.007*	-	*0.005*	*0.002*	*0.005*	-	-	-
5	1	PG152	E	<1.2	3.20	<0.26	0.252	0.79	0.092	0.070	<0.4	0.057	0.030	<0.014	<0.064	<0.17	<0.09
		PG152 st.dev.	*E*	-	*0.89*	-	*0.079*	*0.26*	*0.030*	*0.025*	-	*0.017*	*0.004*	-	-	-	-
5	1	PG155	E	<1.2	3.84	<0.26	0.253	1.27	0.106	0.122	<0.4	0.140	0.028	<0.014	<0.064	<0.17	<0.09
		PG155 st.dev.	*E*	-	*0.86*	-	*0.051*	*0.35*	*0.029*	*0.034*	-	*0.040*	*0.004*	-	-	-	-
5	1	PG156	E	<1.2	5.22	<0.26	0.222	0.94	0.095	0.087	<0.4	0.076	0.035	<0.014	<0.064	<0.17	<0.09
		PG156 st.dev.	*E*	-	*0.44*	-	*0.021*	*0.08*	*0.010*	*0.010*	-	*0.008*	*0.001*	-	-	-	-
5	1	VG20	U	0.32	3.81	<0.15	0.172	0.54	0.056	0.053	0.22	0.045	0.023	N/A	N/A	<0.5	<0.018
		VG20 st.dev.	*U*	*0.56*	*0.85*	-	*0.074*	*0.16*	*0.011*	*0.023*	*0.20*	*0.012*	*0.003*	*N/A*	*N/A*	-	-

Chapter	Group	Sample name/st.dev.	XRF unit	K_20	CaO	TiO_2	MnO	Fe_2O_3	CoO	NiO	CuO	ZnO	SrO	ZrO_2	SnO_2	Sb_2O_5	PbO
5	1	VG21	U	2.42	3.59	0.113	0.407	1.57	0.094	0.109	0.40	0.093	0.014	N/A	N/A	<0.5	<0.018
		VG21 st.dev.	*U*	*0.86*	*0.56*	*0.098*	*0.125*	*0.35*	*0.021*	*0.029*	*0.05*	*0.019*	*0.000*	*N/A*	*N/A*	-	-
5	1	VG35	U	0.28	3.23	<0.15	0.103	1.01	0.032	0.066	<0.02	0.078	0.015	N/A	N/A	<0.5	<0.018
		VG35 st.dev.	*U*	*0.48*	*0.36*	-	*0.035*	*0.30*	*0.027*	*0.013*	-	*0.015*	*0.002*	*N/A*	*N/A*	-	-
5	1	VG55	U	<0.48	3.36	<0.15	0.126	0.52	0.061	0.055	0.10	0.044	0.018	N/A	N/A	<0.5	<0.018
		VG55 st.dev.	*U*	-	*0.32*	-	*0.043*	*0.09*	*0.010*	*0.011*	*0.17*	*0.005*	*0.001*	*N/A*	*N/A*	-	-
5	1	VG58	U	0.28	3.75	<0.15	0.269	0.86	0.064	0.041	0.31	0.055	0.022	N/A	N/A	<0.5	<0.018
		VG58 st.dev.	*U*	*0.48*	*0.20*	-	*0.041*	*0.20*	*0.008*	*0.011*	*0.02*	*0.004*	*0.002*	*N/A*	*N/A*	-	-
5	1	VG60	U	<0.48	3.23	<0.15	0.314	1.93	0.099	0.089	0.31	0.114	0.018	N/A	N/A	<0.5	<0.018
		VG60 st.dev.	*U*	-	*0.08*	-	*0.110*	*0.14*	*0.029*	*0.022*	*0.01*	*0.016*	*0.002*	*N/A*	*N/A*	-	-
5	1	VG60w	U	<0.48	8.79	0.095	<0.039	0.66	<0.024	<0.024	0.31	<0.025	0.027	N/A	N/A	1.64	0.04
		VG60w st.dev.	*U*	-	*1.86*	*0.134*	-	*0.34*	-	-	*0.02*	-	*0.006*	*N/A*	*N/A*	*0.17*	*0.01*
5	1	VG73	F	0.45	4.09	0.088	0.236	1.04	0.033	0.027	0.04	0.024	0.024	N/A	<0.09	0.70	0.04
		VG73 st.dev.	*F*	*0.12*	*0.96*	*0.023*	*0.163*	*0.42*	*0.022*	*0.019*	*0.03*	*0.033*	*0.002*	*N/A*	-	*0.51*	*0.06*
5	1	VG73w	F	0.65	4.39	0.125	0.117	1.13	0.011	0.011	0.26	<0.02	0.028	N/A	<0.09	1.81	0.05
		VG73w st.dev.	*F*	*0.36*	*1.98*	*0.034*	*0.032*	*0.08*	*0.016*	*0.007*	*0.25*	-	*0.015*	*N/A*	-	*1.78*	*0.07*
5	1	VG74	F	0.59	3.50	0.132	0.241	1.38	0.073	0.064	0.02	0.101	0.023	N/A	<0.09	0.27	<0.05
		VG74 st.dev.	*F*	*0.06*	*1.57*	*0.061*	*0.037*	*0.13*	*0.023*	*0.015*	*0.00*	*0.032*	*0.004*	*N/A*	-	*0.05*	-
5	1	VG74w	F	0.34	4.46	0.093	0.048	0.71	0.012	0.009	0.09	0.013	0.021	N/A	<0.09	0.70	<0.05
		VG74w st.dev.	*F*	*0.01*	*0.54*	*0.019*	*0.003*	*0.03*	*0.000*	*0.001*	*0.03*	*0.019*	*0.001*	*N/A*	-	*0.09*	-
5	1	VG75	F	0.46	2.95	0.190	0.142	1.41	0.037	0.034	0.06	0.043	0.014	N/A	<0.09	0.15	<0.05
		VG75 st.dev.	*F*	*0.65*	*3.35*	*0.268*	*0.122*	*1.42*	*0.032*	*0.032*	*0.08*	*0.060*	*0.020*	*N/A*	-	*0.21*	-
5	1	VG75w	F	0.22	2.78	0.055	0.054	0.68	0.009	0.007	0.05	0.013	0.009	N/A	<0.09	0.42	<0.05
		VG75w st.dev.	*F*	*0.31*	*1.59*	*0.078*	*0.022*	*0.33*	*0.013*	*0.010*	*0.03*	*0.019*	*0.013*	*N/A*	-	*0.06*	-
5	1	VG95	U	<0.48	4.20	<0.15	0.319	0.87	0.092	0.111	<0.02	0.089	0.022	N/A	N/A	<0.5	<0.018
		VG95 st.dev.	*U*	-	*1.24*	-	*0.140*	*0.34*	*0.026*	*0.041*	-	*0.027*	*0.005*	*N/A*	*N/A*	-	-
5	1	VG96	U	<0.48	5.55	<0.15	0.506	1.69	0.080	0.159	<0.02	0.074	0.021	N/A	N/A	<0.5	<0.018
		VG96 st.dev.	*U*	-	*1.39*	-	*0.105*	*0.35*	*0.002*	*0.024*	-	*0.007*	*0.000*	*N/A*	*N/A*	-	-

Chapter	Group	Sample name/st.dev.	XRF unit	K_20	CaO	TiO_2	MnO	Fe_2O_3	CoO	NiO	CuO	ZnO	SrO	ZrO_2	SnO_2	Sb_2O_5	PbO
5	1	VG97	U	0.37	3.33	<0.15	0.402	1.36	0.125	0.095	0.15	0.109	0.012	N/A	N/A	<0.5	<0.018
		VG97 st.dev.	*U*	*0.52*	*0.68*	-	*0.180*	*0.40*	*0.038*	*0.031*	*0.21*	*0.033*	*0.003*	*N/A*	*N/A*	-	-
5	1	VG97w	U	<0.48	3.15	<0.15	<0.039	0.18	<0.024	<0.024	0.29	<0.025	0.005	N/A	N/A	0.35	0.02
		VG97w st.dev.	*U*	-	*0.65*	-	-	*0.07*	-	-	*0.00*	-	*0.008*	*N/A*	*N/A*	*0.00*	*0.02*
5	1	VG100	U	<0.48	4.96	<0.15	0.457	1.57	0.083	0.160	<0.02	0.075	0.026	N/A	N/A	<0.5	<0.018
		VG100 st.dev.	*U*	-	*1.16*	-	*0.162*	*0.52*	*0.023*	*0.054*	-	*0.022*	*0.005*	*N/A*	*N/A*	-	-
5	1	VG106	F	0.55	4.82	0.070	0.724	0.95	0.085	0.063	0.39	0.076	0.031	N/A	<0.09	0.46	<0.05
		VG106 st.dev.	*F*	*0.10*	*1.13*	*0.019*	*0.189*	*0.21*	*0.019*	*0.013*	*0.16*	*0.016*	*0.002*	*N/A*	-	*0.02*	-
5	1	VG106w	F	0.60	4.56	0.060	0.258	0.64	0.026	0.019	0.19	0.025	0.029	N/A	<0.09	0.82	0.05
		VG106w st.dev.	*F*	*0.33*	*0.82*	*0.010*	*0.265*	*0.20*	*0.036*	*0.026*	*0.07*	*0.035*	*0.004*	*N/A*	-	*0.43*	*0.07*
5	1	VG107	F	0.48	4.45	0.098	0.300	1.06	0.043	0.038	0.09	0.036	0.022	N/A	<0.09	0.28	<0.05
		VG107 st.dev.	*F*	*0.03*	*0.16*	*0.041*	*0.060*	*0.20*	*0.011*	*0.010*	*0.05*	*0.003*	*0.003*	*N/A*	-	*0.02*	-
5	1	VG108	F	0.50	4.12	0.030	0.343	0.79	0.067	0.051	0.13	0.062	0.023	N/A	<0.09	0.28	<0.05
		VG108 st.dev.	*F*	*0.09*	*1.03*	*0.042*	*0.076*	*0.12*	*0.015*	*0.012*	*0.02*	*0.012*	*0.001*	*N/A*	-	*0.03*	-
5	1	VG108w	F	0.55	4.63	0.120	0.181	0.93	0.042	0.026	1.42	0.040	0.028	N/A	<0.09	0.46	0.05
		VG108w st.dev.	*F*	*0.16*	*2.03*	*0.057*	*0.011*	*0.23*	*0.008*	*0.003*	*1.12*	*0.006*	*0.007*	*N/A*	-	*0.11*	*0.06*
5	1	VG109	F	0.59	3.63	0.208	0.283	1.48	0.037	0.033	0.09	0.023	0.022	N/A	<0.09	0.27	<0.05
		VG109 st.dev.	*F*	*0.27*	*1.24*	*0.195*	*0.147*	*1.06*	*0.010*	*0.012*	*0.08*	*0.033*	*0.004*	*N/A*	-	*0.07*	-
5	1	VG110	F	0.55	4.41	0.106	0.284	1.05	0.041	0.036	0.04	0.038	0.024	N/A	<0.09	0.10	<0.05
		VG110 st.dev.	*F*	*0.13*	*1.84*	*0.041*	*0.137*	*0.01*	*0.014*	*0.015*	*0.01*	*0.015*	*0.001*	*N/A*	-	*0.14*	-
5	1	VG111	F	0.75	4.85	0.132	0.310	1.18	0.066	0.059	0.07	0.065	0.031	N/A	<0.09	<0.14	<0.05
		VG111 st.dev.	*F*	*0.08*	*1.87*	*0.098*	*0.063*	*0.32*	*0.022*	*0.016*	*0.06*	*0.036*	*0.007*	*N/A*	-	-	-
5	1	VG112	F	0.76	2.76	0.082	0.427	1.25	0.104	0.072	0.05	0.102	<0.02	N/A	<0.09	0.45	<0.05
		VG112 st.dev.	*F*	*0.09*	*0.63*	*0.021*	*0.105*	*0.25*	*0.026*	*0.017*	*0.01*	*0.024*	-	*N/A*	-	*0.03*	-
5	1	VG112w	F	1.24	6.08	0.191	0.038	0.80	<0.01	<0.004	0.10	<0.02	0.027	N/A	<0.09	1.59	0.04
		VG112w st.dev.	*F*	*0.40*	*1.03*	*0.047*	*0.011*	*0.15*	-	-	*0.01*	-	*0.003*	*N/A*	-	*0.49*	*0.06*
5	1	VG113	F	1.32	5.96	0.038	0.175	0.81	0.038	0.026	0.04	0.034	0.023	N/A	<0.09	0.21	<0.05
		VG113 st.dev.	*F*	*0.40*	*2.54*	*0.033*	*0.077*	*0.17*	*0.020*	*0.015*	*0.01*	*0.031*	*0.005*	*N/A*	-	*0.06*	-

Chapter	Group	Sample name/st.dev.	XRF unit	K_20	CaO	TiO_2	MnO	Fe_2O_3	CoO	NiO	CuO	ZnO	SrO	ZrO_2	SnO_2	Sb_2O_5	PbO
5	2	VG59	U	0.79	4.27	0.085	0.238	1.08	0.055	0.085	<0.02	0.039	0.015	N/A	N/A	<0.5	0.03
		VG59 st.dev.	*U*	*0.10*	*0.59*	*0.121*	*0.053*	*0.12*	*0.005*	*0.010*	-	*0.003*	*0.001*	*N/A*	*N/A*	-	*0.04*
5	2	VG59y	U	<0.48	2.87	<0.15	0.165	0.62	0.077	<0.024	0.20	<0.025	<0.01	N/A	N/A	1.87	12.92
		VG59y st.dev.	*U*	-	*0.63*	-	*0.020*	*0.35*	*0.002*	-	*0.28*	-	-	*N/A*	*N/A*	*1.40*	*5.39*
5	2	VG64	U	0.60	3.89	0.102	0.258	1.05	0.054	0.084	0.15	0.060	0.016	N/A	N/A	<0.5	0.05
		VG64 st.dev.	*U*	*0.85*	*1.24*	*0.145*	*0.131*	*0.59*	*0.004*	*0.031*	*0.21*	*0.017*	*0.005*	*N/A*	*N/A*	-	*0.00*
5	2	VG64y	U	0.36	3.42	<0.15	0.184	0.64	0.084	<0.024	0.29	<0.025	<0.01	N/A	N/A	2.12	15.26
		VG64y st.dev.	*U*	*0.51*	*0.34*	-	*0.015*	*0.10*	*0.003*	-	*0.00*	-	-	*N/A*	*N/A*	*0.49*	*2.02*
5	2	VG65	U	0.88	5.33	0.188	0.347	1.41	0.070	0.100	0.34	0.045	0.017	N/A	N/A	<0.5	0.04
		VG65 st.dev.	*U*	*0.18*	*1.22*	*0.023*	*0.059*	*0.30*	*0.016*	*0.005*	*0.07*	*0.003*	*0.002*	*N/A*	*N/A*	-	*0.01*
5	2	VG65y	U	<0.48	2.86	<0.15	0.177	0.73	0.069	<0.024	0.69	<0.025	<0.01	N/A	N/A	1.66	12.71
		VG65y st.dev.	*U*	-	*0.71*	-	*0.058*	*0.52*	*0.001*	-	*0.45*	-	-	*N/A*	*N/A*	*0.55*	*4.06*
5	2	VG72	F	0.74	3.62	0.030	0.630	0.52	0.022	0.016	0.37	<0.02	0.010	N/A	0.219	0.44	0.10
		VG72 st.dev.	*F*	*0.02*	*0.68*	*0.043*	*0.114*	*0.04*	*0.005*	*0.004*	*0.06*	-	*0.014*	*N/A*	*0.019*	*0.06*	*0.01*
5	2	VG72y	F	1.15	5.95	0.348	0.051	3.13	<0.01	0.007	0.19	<0.02	0.023	N/A	5.752	17.96	49.69
		VG72y st.dev.	*F*	*0.06*	*2.05*	*0.100*	*0.072*	*0.71*	-	*0.001*	*0.01*	-	*0.033*	*N/A*	*0.542*	*6.14*	*16.40*
5	2	VG80	U	<0.48	5.00	<0.15	0.148	0.26	<0.024	0.019	<0.02	<0.025	0.020	N/A	N/A	<0.5	<0.018
		VG80 st.dev.	*U*	-	*0.59*	-	*0.022*	*0.04*	-	*0.027*	-	-	*0.001*	*N/A*	*N/A*	-	-
5	2	VG80y	U	0.45	4.12	<0.15	0.201	0.88	0.067	<0.024	0.15	<0.025	<0.01	N/A	N/A	1.53	10.85
		VG80y st.dev.	*U*	*0.63*	*2.33*	-	*0.097*	*0.54*	*0.021*	-	*0.21*	-	-	*N/A*	*N/A*	*0.96*	*5.40*
5	2	VG91	U	0.87	3.55	<0.15	0.225	0.84	0.057	0.084	<0.02	0.045	0.019	N/A	N/A	<0.5	0.02
		VG91 st.dev.	*U*	*0.14*	*0.26*	-	*0.013*	*0.06*	*0.002*	*0.012*	-	*0.005*	*0.002*	*N/A*	*N/A*	-	*0.02*
5	2	VG91y	U	0.82	3.20	<0.15	0.144	0.95	0.059	<0.024	0.15	<0.025	<0.01	N/A	N/A	0.99	9.22
		VG91y st.dev.	*U*	*0.02*	*1.23*	-	*0.048*	*0.46*	*0.012*	-	*0.21*	-	-	*N/A*	*N/A*	*0.55*	*4.67*
5	2	VG98	U	0.39	4.49	<0.15	0.705	0.56	<0.024	<0.024	0.57	<0.025	0.015	N/A	N/A	<0.5	0.05
		VG98 st.dev.	*U*	*0.55*	*1.30*	-	*0.237*	*0.36*	-	-	*0.09*	-	*0.003*	*N/A*	*N/A*	-	*0.02*
5	2	VG98y	U	<0.48	2.56	<0.15	0.151	0.46	0.057	<0.024	0.30	<0.025	<0.01	N/A	N/A	0.83	6.20
		VG98y st.dev.	*U*	-	*0.05*	-	*0.008*	*0.06*	*0.003*	-	*0.00*	-	-	*N/A*	*N/A*	*0.02*	*0.51*

Chapter	Group	Sample name/st.dev.	XRF unit	K_20	CaO	TiO_2	MnO	Fe_2O_3	CoO	NiO	CuO	ZnO	SrO	ZrO_2	SnO_2	Sb_2O_5	PbO
5	2	VG99	U	0.52	6.11	<0.15	1.204	0.73	0.021	<0.024	0.75	0.018	0.023	N/A	N/A	<0.5	0.02
		VG99 st.dev.	*U*	*0.74*	*1.55*	-	*0.501*	*0.33*	*0.030*	-	*0.19*	*0.026*	*0.005*	*N/A*	*N/A*	-	*0.02*
5	2	VG99y	U	<0.48	3.57	<0.15	0.113	0.71	0.061	<0.024	0.34	<0.025	<0.01	N/A	N/A	2.24	9.69
		VG99y st.dev.	*U*	-	*2.04*	-	*0.085*	*0.51*	*0.024*	-	*0.03*	-	-	*N/A*	*N/A*	*2.18*	*7.97*
5	7	PG28-30	E	2.08	3.10	0.523	0.403	3.10	0.453	0.176	0.60	<0.037	0.027	0.020	0.067	<0.17	0.82
		PG28-30 st.dev.	*E*	*0.35*	*0.53*	*0.123*	*0.046*	*0.74*	*0.177*	*0.089*	*0.24*	-	*0.003*	*0.006*	*0.077*	-	*0.35*
5	7	PG34-36	E	1.75	2.44	0.361	0.298	2.55	0.263	0.064	<0.4	<0.037	0.027	0.018	<0.064	0.18	0.28
		PG34-36 st.dev.	*E*	*0.08*	*0.12*	*0.023*	*0.041*	*0.19*	*0.025*	*0.006*	-	-	*0.001*	*0.009*	-	*0.01*	*0.01*
5	7	PG37-38	E	1.282	3.48	<0.26	0.289	6.46	0.084	<0.6	<0.4	<0.037	0.029	<0.014	<0.064	0.38	2.41
		PG34-38 st.dev.	*E*	0.312	0.84	-	0.091	1.85	0.042	-	-	-	0.006	-	-	0.06	0.81
5	7	PG43	E	<1.2	3.60	<0.26	0.222	0.97	0.103	0.089	<0.4	0.072	0.034	<0.014	<0.064	<0.17	<0.09
		PG43 st.dev.	*E*	-	*0.55*	-	*0.034*	*0.17*	*0.012*	*0.011*	-	*0.012*	*0.004*	-	-	-	-
5	7	PG51-56	E	1.99	3.24	0.521	0.266	3.65	0.406	0.203	0.60	<0.037	0.027	0.020	<0.064	0.21	0.18
		PG51-56 st.dev.	*E*	*0.28*	*0.39*	*0.116*	*0.071*	*0.73*	*0.085*	*0.043*	*0.09*	-	*0.003*	*0.005*	-	*0.02*	*0.05*
5	7	PG158	E	4.59	5.09	<0.26	<0.065	0.67	0.061	0.129	0.73	<0.037	0.021	<0.014	<0.064	0.20	0.11
		PG158 st.dev.	*E*	*2.60*	*1.47*	-	-	*0.27*	*0.039*	*0.079*	*0.27*	-	*0.004*	-	-	*0.02*	*0.04*
5	7	PG159	E	5.30	5.13	<0.26	<0.065	1.60	0.175	0.233	0.69	<0.037	0.026	<0.014	<0.064	<0.17	<0.09
		PG159 st.dev.	*E*	*2.05*	*1.47*	-	-	*0.67*	*0.086*	*0.118*	*0.22*	-	*0.005*	-	-	-	-
5	7	PG161	E	5.24	6.41	<0.26	<0.065	0.93	<0.038	<0.06	2.83	<0.037	0.024	<0.014	<0.064	<0.17	<0.09
		PG161 st.dev.	*E*	*2.02*	*1.03*	-	-	*0.29*	-	-	*1.09*	-	*0.004*	-	-	-	-
5	7	VG22	F	1.83	2.44	0.070	0.036	0.72	0.190	0.230	0.28	<0.02	0.016	N/A	<0.09	0.19	0.11
		VG22 st.dev.	*F*	-	-	-	-	-	-	-	-	-	-	*N/A*	-	-	-
5	7	VG23	F	3.38	1.73	0.049	0.032	0.84	0.120	0.264	1.00	<0.02	0.017	N/A	<0.09	0.35	0.12
		VG23 st.dev.	*F*	-	-	-	-	-	-	-	-	-	-	*N/A*	-	-	-
5	7	VG24	F	5.79	2.65	0.058	0.034	0.77	0.054	0.164	2.67	0.029	0.019	N/A	<0.09	0.22	0.11
		VG24 st.dev.	*F*	-	-	-	-	-	-	-	-	-	-	*N/A*	-	-	-
5	7	VG36	U	<0.48	7.24	<0.15	0.085	1.38	0.183	<0.024	0.48	0.167	0.041	N/A	N/A	0.72	0.21
		VG36 st.dev.	*U*	-	*1.01*	-	*0.050*	*0.13*	*0.024*	-	*0.02*	*0.002*	*0.003*	*N/A*	*N/A*	*0.15*	*0.03*

Chapter	Group	Sample name/st.dev.	XRF unit	K_20	CaO	TiO_2	MnO	Fe_2O_3	CoO	NiO	CuO	ZnO	SrO	ZrO_2	SnO_2	Sb_2O_5	PbO
5	14	VG33	U	0.94	8.42	<0.15	0.024	2.18	0.084	<0.024	0.53	0.045	0.052	N/A	N/A	2.12	1.67
		VG33 st.dev.	*U*	-	-	-	-	-	-	-	-	-	-	*N/A*	*N/A*	-	-
5	14	VG33y	U	<0.48	3.74	0.092	0.133	0.67	0.067	<0.024	0.32	<0.025	0.006	N/A	N/A	1.60	9.76
		VG33y st.dev.	*U*	-	*1.53*	*0.130*	*0.099*	*0.38*	*0.022*	-	*0.03*	-	*0.008*	*N/A*	*N/A*	*0.80*	*5.63*
5	14	VG34	U	0.95	10.35	<0.15	0.016	2.24	0.105	<0.024	0.54	0.069	0.066	N/A	N/A	1.15	1.69
		VG34 st.dev.	*U*	*0.07*	*1.16*	-	*0.016*	*0.34*	*0.019*	-	*0.05*	*0.007*	*0.011*	*N/A*	*N/A*	*0.12*	*0.37*
5	Other Beads	PG168	E	<1.2	4.11	<0.26	0.238	1.09	0.085	0.081	<0.4	0.038	0.025	0.032	<0.064	<0.17	<0.09
		PG168 st.dev.	*E*	-	*0.84*	-	*0.068*	*0.22*	*0.019*	*0.016*	-	*0.006*	*0.002*	*0.007*	-	-	-
5	Other Beads	PG170	E	1.36	7.34	<0.26	<0.065	0.67	<0.038	<0.06	1.90	<0.037	0.053	<0.014	<0.064	2.61	<0.09
		PG170 st.dev.	*E*	*0.14*	*1.59*	-	-	*0.12*	-	-	*0.43*	-	*0.010*	-	-	*0.36*	-
5	Other Beads	VG54	U	<0.48	3.01	<0.15	0.175	0.60	<0.024	0.050	<0.02	0.034	0.013	N/A	N/A	<0.5	<0.018
		VG54 st.dev.	*U*	-	*0.27*	-	*0.015*	*0.05*	-	*0.011*	-	*0.002*	*0.001*	*N/A*	*N/A*	-	-
5	Non-beads	VG1	U	1.41	8.10	<0.15	<0.039	0.77	0.108	<0.024	0.44	<0.025	0.066	N/A	N/A	<0.5	0.09
		VG1 st.dev.	*U*	*0.35*	*0.96*	-	-	*0.14*	*0.013*	-	*0.16*	-	*0.006*	*N/A*	*N/A*	-	*0.01*
5	Non-beads	VG2	U	1.11	6.74	<0.15	<0.039	0.52	0.070	<0.024	0.33	<0.025	0.051	N/A	N/A	<0.5	0.29
		VG2 st.dev.	*U*	*0.21*	*0.71*	-	-	*0.04*	*0.007*	-	*0.01*	-	*0.003*	*N/A*	*N/A*	-	*0.02*
5	Non-beads	VG13	F	1.00	9.86	0.083	0.044	1.02	0.106	<0.004	0.17	0.055	0.082	N/A	<0.09	0.64	0.14
		VG13 st.dev.	*F*	*0.12*	*2.04*	*0.033*	*0.005*	*0.24*	*0.007*	-	*0.02*	*0.004*	*0.017*	*N/A*	-	*0.10*	*0.02*
5	Non-beads	VG32	U	<0.48	8.48	<0.15	<0.039	0.55	0.152	<0.024	0.36	<0.025	0.042	N/A	N/A	0.66	0.04
		VG32 st.dev.	*U*	-	*0.14*	-	-	*0.01*	*0.004*	-	*0.00*	-	*0.001*	*N/A*	*N/A*	*0.02*	*0.00*
6	3	PG84	E	4.52	1.93	<0.26	<0.065	1.55	0.056	0.159	2.16	<0.037	0.024	<0.014	<0.064	0.19	<0.09
		PG84 st.dev.	*E*	*2.19*	*0.80*	-	-	*0.84*	*0.039*	*0.101*	*1.21*	-	*0.006*	-	-	*0.03*	-
6	3	PG84w	E	1.63	1.89	<0.26	<0.065	0.98	<0.038	<0.06	<0.4	<0.037	0.025	<0.014	<0.064	<0.17	<0.09
		PG84w st.dev.	*E*	*0.25*	*0.39*	-	-	*0.14*	-	-	-	-	*0.004*	-	-	-	-
6	3	PG87	E	4.66	2.15	<0.26	<0.065	1.02	<0.038	<0.06	2.58	<0.037	0.025	<0.014	0.141	<0.17	<0.09
		PG87 st.dev.	*E*	*1.18*	*0.04*	-	-	*0.08*	-	-	*0.19*	-	*0.002*	-	*0.004*	-	-
6	3	PG167	E	3.67	1.83	<0.26	<0.065	0.59	<0.038	<0.06	3.02	<0.037	0.021	<0.014	0.418	<0.17	<0.09
		PG167 st.dev.	*E*	*0.57*	*0.14*	-	-	*0.07*	-	-	*0.35*	-	*0.001*	-	*0.059*	-	-

Chapter	Group	Sample name/st.dev.	XRF unit	K_20	CaO	TiO_2	MnO	Fe_2O_3	CoO	NiO	CuO	ZnO	SrO	ZrO_2	SnO_2	Sb_2O_5	PbO
6	3	VG25g	F	2.72	4.60	0.124	0.039	0.90	<0.01	<0.004	5.08	<0.02	0.019	N/A	0.441	<0.14	0.10
		VG25g st.dev.	*F*	-	-	-	-	-	-	-	-	-	-	*N/A*	-	-	-
6	3	VG25r	F	2.54	3.88	0.145	0.041	0.88	<0.01	<0.004	3.10	0.027	0.017	N/A	0.314	<0.14	0.11
		VG25r st.dev.	*F*	-	-	-	-	-	-	-	-	-	-	*N/A*	-	-	-
6	3	VG25w	F	0.74	10.56	0.086	0.031	0.61	<0.01	<0.004	0.54	<0.02	0.028	N/A	0.201	<0.14	0.11
		VG25w st.dev.	*F*	-	-	-	-	-	-	-	-	-	-	*N/A*	-	-	-
6	4	PG65	E	2.83	7.63	0.330	<0.065	1.90	<0.038	<0.06	1.36	<0.037	0.037	0.016	<0.064	0.19	<0.09
		PG65 st.dev.	*E*	*0.56*	*1.73*	*0.087*	-	*0.63*	-	-	*0.44*	-	*0.006*	*0.005*	-	*0.03*	-
6	4	PG65d	E	2.07	4.96	0.301	<0.065	1.22	<0.038	<0.06	0.43	<0.037	0.030	0.015	<0.064	0.19	0.10
		PG65d st.dev.	*E*	*0.51*	*1.20*	*0.098*	-	*0.40*	-	-	*0.08*	-	*0.006*	*0.010*	-	*0.05*	*0.06*
6	4	PG121	E	1.81	4.73	0.410	<0.065	2.59	<0.038	<0.06	1.23	<0.037	0.034	0.014	<0.064	<0.17	<0.09
		PG121 st.dev.	*E*	*0.23*	*0.99*	*0.088*	-	*0.27*	-	-	*0.23*	-	*0.005*	*0.002*	-	-	-
6	4	PG122	E	1.94	5.63	0.292	<0.065	1.51	<0.038	<0.06	1.23	0.050	0.031	<0.014	<0.064	0.25	<0.09
		PG122 st.dev.	*E*	*0.08*	*0.28*	*0.049*	-	*0.11*	-	-	*0.05*	*0.001*	*0.000*	-	-	*0.02*	-
6	4	PG122d	E	2.86	5.65	0.293	<0.065	1.63	<0.038	<0.06	0.40	<0.037	0.028	<0.014	<0.064	0.69	1.19
		PG122d st.dev.	*E*	-	-	-	-	-	-	-	-	-	-	-	-	-	-
6	4	PG122y	E	1.83	4.50	0.317	<0.065	1.79	<0.038	<0.06	0.58	<0.037	0.026	0.015	<0.064	0.91	3.38
		PG122y st.dev.	*E*	*0.62*	*2.09*	*0.203*	-	*1.13*	-	-	*0.19*	-	*0.007*	*0.011*	-	*0.19*	*2.13*
6	4	PG160	E	2.61	6.89	0.260	<0.065	1.59	<0.038	<0.06	1.16	<0.037	0.037	<0.014	<0.064	<0.17	<0.09
		PG160 st.dev.	*E*	*0.76*	*1.97*	*0.082*	-	*0.49*	-	-	*0.31*	-	*0.008*	-	-	-	-
6	4	PG160d	E	2.58	4.81	<0.26	<0.065	1.02	<0.038	<0.06	<0.4	<0.037	0.027	<0.014	<0.064	0.20	0.17
		PG160d st.dev.	*E*	*0.09*	*0.23*	-	-	*0.17*	-	-	-	-	*0.001*	-	-	*0.05*	*0.06*
6	4	PG166	E	2.72	6.44	0.306	<0.065	1.54	<0.038	<0.06	1.58	<0.037	0.035	<0.014	<0.064	0.30	0.23
		PG166 st.dev.	*E*	*0.57*	*1.36*	*0.086*	-	*0.40*	-	-	*0.36*	-	*0.007*	-	-	*0.06*	*0.10*
6	4	PG166d	E	2.32	5.88	0.283	<0.065	1.08	<0.038	<0.06	<0.4	<0.037	0.025	<0.014	<0.064	0.93	1.59
		PG166d st.dev.	*E*	*0.13*	*0.65*	*0.059*	-	*0.12*	-	-	-	-	*0.001*	-	-	*0.08*	*0.35*
6	4	PG166y	E	2.05	7.20	0.341	<0.065	1.35	<0.038	<0.06	0.50	0.055	0.032	0.015	<0.064	1.41	5.12
		PG166y st.dev.	*E*	*0.16*	*0.73*	*0.042*	-	*0.12*	-	-	*0.04*	*0.014*	*0.006*	*0.005*	-	*0.44*	*1.23*

Chapter	Group	Sample name/st.dev.	XRF unit	K_20	CaO	TiO_2	MnO	Fe_2O_3	CoO	NiO	CuO	ZnO	SrO	ZrO_2	SnO_2	Sb_2O_5	PbO
6	12	VG26	F	3.64	2.84	0.145	0.038	0.82	<0.01	<0.004	3.92	<0.02	<0.02	N/A	<0.09	<0.14	<0.05
		VG26 st.dev.	*F*	-	-	-	-	-	-	-	-	-	-	*N/A*	-	-	-
6	12	VG26w	F	3.92	3.40	0.127	0.035	0.80	<0.01	<0.004	2.55	<0.02	0.026	N/A	<0.09	<0.14	<0.05
		VG26w st.dev.	*F*	-	-	-	-	-	-	-	-	-	-	*N/A*	-	-	-
6	12	VG29	F	3.73	2.79	0.108	0.035	0.76	0.018	0.031	2.53	<0.02	0.017	N/A	0.123	<0.14	0.12
		VG29 st.dev.	*F*	-	-	-	-	-	-	-	-	-	-	*N/A*	-	-	-
6	12	VG29w	F	4.05	8.33	0.159	0.040	0.87	<0.01	0.029	0.47	<0.02	0.079	N/A	0.144	<0.14	<0.05
		VG29w st.dev.	*F*	-	-	-	-	-	-	-	-	-	-	*N/A*	-	-	-
6	13	PG162	E	<1.2	4.06	<0.26	0.666	0.66	<0.038	<0.06	0.76	<0.037	0.027	<0.014	<0.064	<0.17	<0.09
		PG162 st.dev.	*E*	-	*0.65*	-	*0.077*	*0.17*	-	-	*0.07*	-	*0.002*	-	-	-	-
6	13	PG163	E	1.22	6.32	<0.26	0.950	1.10	<0.038	<0.06	1.79	<0.037	0.033	0.015	<0.064	0.19	<0.09
		PG163 st.dev.	*E*	*0.38*	*2.25*	-	*0.385*	*0.80*	-	-	*1.50*	-	*0.008*	*0.007*	-	*0.03*	-
6	13	PG164	E	1.24	6.64	<0.26	0.928	0.86	<0.038	<0.06	1.09	<0.037	0.031	<0.014	<0.064	0.17	<0.09
		PG164 st.dev.	*E*	*0.05*	*0.17*	-	*0.005*	*0.06*	-	-	*0.26*	-	*0.003*	-	-	*0.00*	-
6	Other Beads	PG169	E	2.14	5.34	<0.26	<0.065	1.12	<0.038	<0.06	1.01	<0.037	0.039	<0.014	0.086	<0.17	<0.09
		PG169 st.dev.	*E*	*0.06*	*0.30*	-	-	*0.07*	-	-	*0.03*	-	*0.002*	-	*0.040*	-	-
6	Other Beads	VG28	F	0.48	2.76	0.155	0.031	0.76	<0.01	0.006	1.06	<0.02	0.089	N/A	<0.09	<0.14	0.11
		VG28 st.dev.	*F*	-	-	-	-	-	-	-	-	-	-	*N/A*	-	-	-
6	Other Beads	VG38	F	1.56	4.99	0.116	0.148	0.63	<0.01	<0.004	0.93	<0.02	0.056	N/A	0.142	<0.14	<0.05
		VG38 st.dev.	*F*	*0.43*	*1.81*	*0.017*	*0.044*	*0.09*	-	-	*0.23*	-	*0.013*	*N/A*	*0.023*	-	-
6	Non-beads	PG59	E	2.37	6.50	<0.26	0.089	0.40	<0.038	<0.06	1.11	<0.037	0.050	<0.014	<0.064	<0.17	0.75
		PG59 st.dev.	*E*	*0.94*	*3.03*	-	*0.015*	*0.05*	-	-	*0.41*	-	*0.007*	-	-	-	*0.48*
6	Non-beads	PG59y	E	2.08	3.39	<0.26	<0.065	2.00	<0.038	<0.06	0.48	<0.037	0.035	<0.014	<0.064	0.61	17.29
		PG59y st.dev.	*E*	*0.11*	*0.48*	-	-	*0.14*	-	-	*0.09*	-	*0.010*	-	-	*0.13*	*2.88*
6	Non-beads	PG60	E	2.42	7.48	<0.26	0.084	0.44	<0.038	<0.06	1.26	<0.037	0.053	<0.014	<0.064	<0.17	0.82
		PG60 st.dev.	*E*	*0.29*	*1.11*	-	*0.012*	*0.02*	-	-	*0.20*	-	*0.006*	-	-	-	*0.32*
6	Non-beads	PG60y	E	1.97	2.55	<0.26	<0.065	1.96	<0.038	<0.06	<0.4	<0.037	0.021	<0.014	<0.064	0.67	19.82
		PG60y st.dev.	*E*	*0.06*	*0.17*	-	-	*0.14*	-	-	-	-	*0.003*	-	-	*0.04*	*1.16*

Chapter	Group	Sample name/st.dev.	XRF unit	K_20	CaO	TiO_2	MnO	Fe_2O_3	CoO	NiO	CuO	ZnO	SrO	ZrO_2	SnO_2	Sb_2O_5	PbO
7	5	PG69-70	E	<1.2	6.55	<0.26	<0.065	0.79	<0.038	<0.06	1.34	<0.037	0.052	<0.014	<0.064	<0.17	<0.09
		PG69-70 st.dev.	*E*	-	*2.37*	-	-	*0.20*	-	-	*0.50*	-	*0.014*	-	-	-	-
7	5	PG71-72	E	<1.2	6.48	<0.26	<0.065	0.92	<0.038	<0.06	<0.4	<0.037	0.053	<0.014	<0.064	<0.17	<0.09
		PG71-72 st.dev.	*E*	*0.06*	*0.77*	-	-	*0.09*	-	-	-	-	*0.008*	-	-	-	-
7	5	PG75-76	E	<1.2	5.21	<0.26	0.878	0.85	<0.038	<0.06	<0.4	<0.037	0.043	<0.014	<0.064	<0.17	<0.09
		PG75-76 st.dev.	*E*	-	*1.16*	-	*0.259*	*0.30*	-	-	-	-	*0.008*	-	-	-	-
7	5	PG154	E	<1.2	7.25	<0.26	<0.065	0.63	<0.038	<0.06	<0.4	<0.037	0.042	<0.014	<0.064	<0.17	<0.09
		PG154 st.dev.	*E*	-	*0.94*	-	-	*0.07*	-	-	-	-	*0.004*	-	-	-	-
7	10	PG1	E	<1.2	9.22	<0.26	<0.065	0.36	<0.038	<0.06	<0.4	<0.037	0.045	<0.014	<0.064	0.36	<0.09
		PG1 st.dev.	*E*	-	*0.52*	-	-	*0.02*	-	-	-	-	*0.004*	-	-	*0.03*	-
7	10	PG2	E	1.31	7.40	<0.26	0.217	0.33	<0.038	<0.06	<0.4	<0.037	0.036	<0.014	<0.064	0.34	<0.09
		PG2 st.dev.	*E*	*0.21*	*2.61*	-	*0.042*	*0.06*	-	-	-	-	*0.005*	-	-	*0.01*	-
7	10	PG7	E	1.44	8.99	<0.26	<0.065	0.69	<0.038	<0.06	<0.4	<0.037	0.058	<0.014	<0.064	0.83	<0.09
		PG7 st.dev.	*E*	*0.04*	*1.69*	-	-	*0.12*	-	-	-	-	*0.007*	-	-	*0.18*	-
7	10	PG8	E	<1.2	8.96	<0.26	<0.065	0.42	<0.038	<0.06	<0.4	<0.037	0.041	<0.014	<0.064	0.67	<0.09
		PG8 st.dev.	*E*	-	*0.53*	-	-	*0.03*	-	-	-	-	*0.004*	-	-	*0.17*	-
7	10	PG9	E	2.23	7.01	<0.26	<0.065	0.56	<0.038	<0.06	<0.4	<0.037	0.060	<0.014	<0.064	<0.17	<0.09
		PG9 st.dev.	*E*	*0.33*	*1.14*	-	-	*0.08*	-	-	-	-	*0.007*	-	-	-	-
7	10	PG10	E	<1.2	6.80	<0.26	<0.065	0.23	<0.038	<0.06	<0.4	<0.037	0.037	<0.014	<0.064	<0.17	<0.09
		PG10 st.dev.	*E*	-	*1.08*	-	-	*0.04*	-	-	-	-	*0.005*	-	-	-	-
7	10	PG11	E	<1.2	7.87	<0.26	<0.065	0.27	<0.038	<0.06	<0.4	<0.037	0.038	<0.014	<0.064	<0.17	<0.09
		PG11 st.dev.	*E*	-	*1.29*	-	-	*0.03*	-	-	-	-	*0.002*	-	-	-	-
7	10	PG12	E	1.57	6.56	<0.26	<0.065	0.39	<0.038	<0.06	<0.4	<0.037	0.038	<0.014	<0.064	<0.17	<0.09
		PG12 st.dev.	*E*	*0.30*	*2.15*	-	-	*0.10*	-	-	-	-	*0.007*	-	-	-	-
7	10	PG13	E	<1.2	6.60	<0.26	<0.065	0.22	<0.038	<0.06	<0.4	<0.037	0.034	<0.014	<0.064	<0.17	<0.09
		PG13 st.dev.	*E*	-	*0.16*	-	-	*0.01*	-	-	-	-	*0.001*	-	-	-	-
7	10	PG14	E	<1.2	8.00	<0.26	<0.065	0.24	<0.038	<0.06	<0.4	<0.037	0.040	<0.014	<0.064	<0.17	<0.09
		PG14 st.dev.	*E*	-	*0.26*	-	-	*0.03*	-	-	-	-	*0.001*	-	-	-	-

Chapter	Group	Sample name/st.dev.	XRF unit	K_20	CaO	TiO_2	MnO	Fe_2O_3	CoO	NiO	CuO	ZnO	SrO	ZrO_2	SnO_2	Sb_2O_5	PbO
7	10	PG15	E	<1.2	5.74	<0.26	<0.065	0.29	<0.038	<0.06	<0.4	<0.037	0.030	<0.014	<0.064	<0.17	<0.09
		PG15 st.dev.	*E*	-	*0.17*	-	-	*0.01*	-	-	-	-	*0.003*	-	-	-	-
7	10	PG31	E	<1.2	7.44	<0.26	<0.065	0.26	<0.038	<0.06	<0.4	<0.037	0.036	<0.014	<0.064	<0.17	<0.09
		PG31 st.dev.	*E*	-	*0.90*	-	-	*0.07*	-	-	-	-	*0.005*	-	-	-	-
7	10	PG33	E	1.43	8.86	<0.26	0.078	0.66	<0.038	<0.06	1.16	<0.037	0.047	<0.014	<0.064	<0.17	<0.09
		PG33 st.dev.	*E*	*0.07*	*0.78*	-	*0.014*	*0.06*	-	-	*0.09*	-	*0.004*	-	-	-	-
7	10	PG63	E	1.64	6.41	<0.26	<0.065	0.39	<0.038	<0.06	1.36	0.040	0.049	<0.014	0.071	<0.17	<0.09
		PG63 st.dev.	*E*	*0.23*	*1.05*	-	-	*0.03*	-	-	*0.15*	*0.009*	*0.005*	-	*0.018*	-	-
7	10	PG67	E	<1.2	7.38	<0.26	<0.065	0.29	<0.038	<0.06	<0.4	<0.037	0.035	<0.014	<0.064	<0.17	<0.09
		PG67 st.dev.	*E*	-	*1.04*	-	-	*0.04*	-	-	-	-	*0.002*	-	-	-	-
7	10	PG68	E	1.67	9.82	<0.26	<0.065	1.11	<0.038	<0.06	<0.4	<0.037	0.054	<0.014	<0.064	<0.17	<0.09
		PG68 st.dev.	*E*	*0.18*	*1.64*	-	-	*0.22*	-	-	-	-	*0.005*	-	-	-	-
7	10	PG95	E	2.47	7.41	<0.26	<0.065	0.77	<0.038	<0.06	<0.4	<0.037	0.040	<0.014	<0.064	0.64	<0.09
		PG95 st.dev.	*E*	*0.22*	*0.17*	-	-	*0.02*	-	-	-	-	*0.001*	-	-	*0.07*	-
7	10	PG96	E	<1.2	6.14	<0.26	<0.065	0.21	<0.038	<0.06	<0.4	<0.037	0.035	<0.014	<0.064	<0.17	<0.09
		PG96 st.dev.	*E*	-	*1.19*	-	-	*0.01*	-	-	-	-	*0.007*	-	-	-	-
7	10	PG104	E	2.98	3.05	0.655	0.663	3.11	<0.038	<0.06	<0.4	<0.037	0.032	0.041	<0.064	<0.17	<0.09
		PG104 st.dev.	*E*	*0.10*	*0.16*	*0.032*	*0.034*	*0.18*	-	-	-	-	*0.001*	*0.006*	-	-	-
7	10	PG116	E	<1.2	5.20	<0.26	0.498	0.35	<0.038	<0.06	1.04	<0.037	0.035	<0.014	<0.064	<0.17	<0.09
		PG116 st.dev.	*E*	-	*0.61*	-	*0.058*	*0.05*	-	-	*0.13*	-	*0.004*	-	-	-	-
7	10	PG117	E	<1.2	5.91	<0.26	<0.065	0.29	<0.038	<0.06	<0.4	<0.037	0.039	<0.014	<0.064	<0.17	<0.09
		PG117 st.dev.	*E*	-	*1.57*	-	-	*0.08*	-	-	-	-	*0.007*	-	-	-	-
7	10	PG118	E	<1.2	4.57	<0.26	<0.065	0.68	<0.038	<0.06	<0.4	<0.037	0.032	0.015	<0.064	<0.17	<0.09
		PG118 st.dev.	*E*	-	*1.18*	-	-	*0.16*	-	-	-	-	*0.002*	*0.002*	-	-	-
7	10	PG119	E	1.60	7.23	<0.26	<0.065	0.58	<0.038	<0.06	<0.4	<0.037	0.051	<0.014	<0.064	0.75	<0.09
		PG119 st.dev.	*E*	*0.13*	*0.63*	-	-	*0.05*	-	-	-	-	*0.003*	-	-	*0.12*	-
7	10	PG120	E	<1.2	8.14	<0.26	<0.065	0.45	<0.038	<0.06	<0.4	<0.037	0.041	<0.014	<0.064	<0.17	<0.09
		PG120 st.dev.	*E*	-	*1.15*	-	-	*0.08*	-	-	-	-	*0.003*	-	-	-	-

Chapter	Group	Sample name/st.dev.	XRF unit	K_20	CaO	TiO_2	MnO	Fe_2O_3	CoO	NiO	CuO	ZnO	SrO	ZrO_2	SnO_2	Sb_2O_5	PbO
7	10	PG137	E	<1.2	8.36	<0.26	<0.065	0.26	<0.038	<0.06	<0.4	<0.037	0.039	<0.014	<0.064	<0.17	<0.09
		PG137 st.dev.	*E*	-	*0.84*	-	-	*0.03*	-	-	-	-	*0.003*	-	-	-	-
7	10	PG140	E	<1.2	7.84	<0.26	<0.065	0.27	<0.038	<0.06	<0.4	<0.037	0.041	<0.014	<0.064	<0.17	<0.09
		PG140 st.dev.	*E*	-	*0.61*	-	-	*0.01*	-	-	-	-	*0.001*	-	-	-	-
7	10	PG142	E	<1.2	7.99	<0.26	<0.065	0.24	<0.038	<0.06	<0.4	<0.037	0.042	<0.014	<0.064	<0.17	<0.09
		PG142 st.dev.	*E*	-	*1.30*	-	-	*0.03*	-	-	-	-	*0.003*	-	-	-	-
7	10	PG143	E	<1.2	8.48	<0.26	<0.065	0.38	<0.038	<0.06	<0.4	<0.037	0.036	<0.014	<0.064	<0.17	<0.09
		PG143 st.dev.	*E*	-	*1.65*	-	-	*0.10*	-	-	-	-	*0.007*	-	-	-	-
7	10	PG145	E	1.81	6.13	<0.26	<0.065	0.67	<0.038	<0.06	<0.4	<0.037	0.040	<0.014	<0.064	0.81	<0.09
		PG145 st.dev.	*E*	*0.33*	*1.54*	-	-	*0.19*	-	-	-	-	*0.004*	-	-	*0.08*	-
7	10	PG146	E	2.38	8.12	<0.26	<0.065	0.48	<0.038	<0.06	<0.4	<0.037	0.048	<0.014	<0.064	0.42	<0.09
		PG146 st.dev.	*E*	*0.54*	*1.89*	-	-	*0.10*	-	-	-	-	*0.011*	-	-	*0.11*	-
7	10	PG147	E	2.09	9.57	<0.26	0.280	0.60	<0.038	<0.06	<0.4	<0.037	0.051	<0.014	<0.064	1.23	<0.09
		PG147 st.dev.	*E*	*0.27*	*2.24*	-	*0.052*	*0.06*	-	-	-	-	*0.007*	-	-	*0.36*	-
7	10	PG148	E	<1.2	0.56	<0.26	<0.065	<0.057	<0.038	0.177	<0.4	<0.037	0.015	<0.014	<0.064	<0.17	<0.09
		PG148 st.dev.	*E*	-	*0.01*	-	-	-	-	*0.064*	-	-	*0.002*	-	-	-	-
7	10	PG153	E	<1.2	8.59	<0.26	<0.065	0.24	<0.038	<0.06	<0.4	<0.037	0.038	<0.014	<0.064	<0.17	<0.09
		PG153 st.dev.	*E*	-	*0.89*	-	-	*0.03*	-	-	-	-	*0.004*	-	-	-	-
7	10	PG165	E	2.28	10.91	<0.26	0.428	0.71	<0.038	<0.06	<0.4	<0.037	0.057	<0.014	<0.064	0.41	<0.09
		PG165 st.dev.	*E*	*0.44*	*1.34*	-	*0.072*	*0.18*	-	-	-	-	*0.012*	-	-	*0.10*	-
7	10	PG171	E	<1.2	3.80	<0.26	0.213	1.05	0.091	0.086	<0.4	0.039	0.025	0.028	<0.064	<0.17	<0.09
		PG171 st.dev.	*E*	-	*0.36*	-	*0.020*	*0.11*	*0.010*	*0.008*	-	*0.005*	*0.001*	*0.002*	-	-	-
7	10	VG14	U	<0.48	7.05	<0.15	<0.039	0.20	<0.024	<0.024	0.10	<0.025	0.029	N/A	N/A	<0.5	<0.018
		VG14 st.dev.	*U*	-	*0.79*	-	-	*0.03*	-	-	*0.17*	-	*0.002*	*N/A*	*N/A*	-	-
7	10	VG48	U	1.56	8.24	<0.15	<0.039	0.55	<0.024	<0.024	<0.02	<0.025	0.053	N/A	N/A	<0.5	<0.018
		VG48 st.dev.	*U*	*0.21*	*1.38*	-	-	*0.10*	-	-	-	-	*0.004*	*N/A*	*N/A*	-	-
7	10	VG49	U	1.74	8.94	<0.15	<0.039	0.69	<0.024	<0.024	<0.02	<0.025	0.060	N/A	N/A	<0.5	<0.018
		VG49 st.dev.	*U*	*0.65*	*3.50*	-	-	*0.32*	-	-	-	-	*0.020*	*N/A*	*N/A*	-	-

Chapter	Group	Sample name/st.dev.	XRF unit	K_20	CaO	TiO_2	MnO	Fe_2O_3	CoO	NiO	CuO	ZnO	SrO	ZrO_2	SnO_2	Sb_2O_5	PbO
7	10	VG52	U	0.25	6.97	0.060	<0.039	0.77	<0.024	<0.024	0.37	<0.025	0.042	N/A	N/A	<0.5	<0.018
		VG52 st.dev.	*U*	*0.43*	*0.70*	*0.105*	-	*0.41*	-	-	*0.07*	-	*0.003*	*N/A*	*N/A*	-	-
7	10	VG53	U	1.87	8.94	<0.15	0.133	0.48	<0.024	<0.024	<0.02	<0.025	0.054	N/A	N/A	<0.5	<0.018
		VG53 st.dev.	*U*	*0.09*	*0.78*	-	*0.025*	*0.09*	-	-	-	-	*0.007*	*N/A*	*N/A*	-	-
7	10	VG57	U	2.13	7.55	<0.15	<0.039	0.74	<0.024	<0.024	0.35	<0.025	0.044	N/A	N/A	0.11	<0.018
		VG57 st.dev.	*U*	*0.17*	*1.17*	-	-	*0.17*	-	-	*0.61*	-	*0.007*	*N/A*	*N/A*	*0.19*	-
7	10	VG61	U	1.33	8.01	<0.15	0.224	0.29	<0.024	<0.024	<0.02	<0.025	0.042	N/A	N/A	<0.5	<0.018
		VG61 st.dev.	*U*	*0.16*	*0.80*	-	*0.024*	*0.02*	-	-	-	-	*0.001*	*N/A*	*N/A*	-	-
7	10	VG62	U	1.88	8.62	<0.15	0.019	0.73	<0.024	<0.024	0.10	<0.025	0.050	N/A	N/A	0.13	<0.018
		VG62 st.dev.	*U*	*0.27*	*1.66*	-	*0.016*	*0.23*	-	-	*0.17*	-	*0.008*	*N/A*	*N/A*	*0.23*	-
7	10	VG63	U	1.99	11.55	<0.15	<0.039	0.71	<0.024	<0.024	0.20	<0.025	0.068	N/A	N/A	<0.5	0.03
		VG63 st.dev.	*U*	*0.09*	*1.07*	-	-	*0.09*	-	-	*0.17*	-	*0.004*	*N/A*	*N/A*	-	*0.00*
7	10	VG82	F	1.08	2.76	0.016	0.029	0.51	<0.01	<0.004	0.92	<0.02	0.026	N/A	<0.09	<0.14	<0.05
		VG82 st.dev.	*F*	*0.13*	*0.82*	*0.028*	*0.001*	*0.12*	-	-	*0.02*	-	*0.001*	*N/A*	-	-	-
7	10	VG83	F	0.68	12.32	0.091	0.023	0.88	<0.01	0.002	0.31	<0.02	0.016	N/A	0.045	0.05	0.06
		VG83 st.dev.	*F*	*0.29*	*13.21*	*0.079*	*0.020*	*0.68*	-	*0.004*	*0.28*	-	*0.015*	*N/A*	*0.039*	*0.08*	*0.06*
7	10	VG84	F	1.19	6.23	0.034	0.035	0.47	<0.01	<0.004	0.02	<0.02	0.047	N/A	<0.09	0.76	<0.05
		VG84 st.dev.	*F*	*0.10*	*0.63*	*0.029*	*0.002*	*0.01*	-	-	*0.00*	-	*0.005*	*N/A*	-	*0.05*	-
7	10	VG87	U	1.82	5.89	<0.15	0.051	0.62	<0.024	<0.024	0.10	<0.025	0.036	N/A	N/A	<0.5	<0.018
		VG87 st.dev.	*U*	*0.48*	*1.38*	-	*0.049*	*0.19*	-	-	*0.17*	-	*0.008*	*N/A*	*N/A*	-	-
7	10	VG89	U	1.45	5.45	<0.15	<0.039	0.35	<0.024	<0.024	<0.02	<0.025	0.036	N/A	N/A	<0.5	<0.018
		VG89 st.dev.	*U*	*0.31*	*0.39*	-	-	*0.13*	-	-	-	-	*0.005*	*N/A*	*N/A*	-	-
7	10	VG90	U	0.64	6.31	<0.15	<0.039	0.13	<0.024	<0.024	<0.02	<0.025	0.028	N/A	N/A	<0.5	<0.018
		VG90 st.dev.	*U*	*0.55*	*0.61*	-	-	*0.04*	-	-	-	-	*0.002*	*N/A*	*N/A*	-	-
7	10	VG102	U	<0.48	6.87	<0.15	<0.039	0.10	<0.024	<0.024	0.31	<0.025	0.030	N/A	N/A	<0.5	<0.018
		VG102 st.dev.	*U*	-	*1.39*	-	-	*0.03*	-	-	*0.01*	-	*0.003*	*N/A*	*N/A*	-	-
7	10	VG103	U	0.87	5.82	<0.15	<0.039	0.26	<0.024	<0.024	0.49	<0.025	0.045	N/A	N/A	<0.5	<0.018
		VG103 st.dev.	*U*	*0.76*	*2.50*	-	-	*0.14*	-	-	*0.10*	-	*0.016*	*N/A*	*N/A*	-	-

Chapter	Group	Sample name/st.dev.	XRF unit	K_20	CaO	TiO_2	MnO	Fe_2O_3	CoO	NiO	CuO	ZnO	SrO	ZrO_2	SnO_2	Sb_2O_5	PbO
7	10	VG104	U	1.34	6.82	<0.15	0.135	0.38	<0.024	<0.024	<0.02	<0.025	0.047	N/A	N/A	<0.5	<0.018
		VG104 st.dev.	*U*	*0.08*	*1.17*	-	*0.024*	*0.11*	-	-	-	-	*0.009*	*N/A*	*N/A*	-	-
7	10	VG105	U	2.91	8.97	<0.15	<0.039	0.74	<0.024	<0.024	<0.02	0.010	0.056	N/A	N/A	<0.5	<0.018
		VG105 st.dev.	*U*	*0.57*	*1.48*	-	-	*0.22*	-	-	-	*0.017*	*0.010*	*N/A*	*N/A*	-	-
7	11	PG39	E	<1.2	9.89	<0.26	0.080	0.57	<0.038	<0.06	1.41	<0.037	0.054	0.018	<0.064	<0.17	<0.09
		PG39 st.dev.	*E*	-	*1.53*	-	*0.008*	*0.04*	-	-	*0.34*	-	*0.007*	*0.003*	-	-	-
7	11	PG88	E	<1.2	8.34	0.389	1.360	1.28	<0.038	<0.06	1.12	<0.037	0.046	0.031	<0.064	<0.17	<0.09
		PG88 st.dev.	*E*	-	*4.28*	*0.153*	*0.687*	*0.61*	-	-	*0.23*	-	*0.012*	*0.009*	-	-	-
7	11	PG89	E	<1.2	9.66	0.327	0.345	0.82	<0.038	<0.06	2.18	<0.037	0.048	0.054	<0.064	<0.17	0.15
		PG89 st.dev.	*E*	-	*4.10*	*0.061*	*0.027*	*0.08*	-	-	*0.79*	-	*0.013*	*0.016*	-	-	*0.04*
7	11	PG136	E	<1.2	3.69	0.310	0.508	0.40	<0.038	<0.06	0.96	<0.037	0.026	0.024	<0.064	<0.17	<0.09
		PG136 st.dev.	*E*	-	*1.20*	*0.082*	*0.228*	*0.14*	-	-	*0.30*	-	*0.004*	*0.009*	-	-	-
7	11	VG15	U	<0.48	2.48	<0.15	<0.039	0.79	0.015	<0.024	0.32	<0.025	0.021	N/A	N/A	<0.5	<0.018
		VG15 st.dev.	*U*	-	*0.65*	-	-	*0.22*	*0.026*	-	*0.01*	-	*0.002*	*N/A*	*N/A*	-	-
7	11	VG86	U	1.42	7.77	<0.15	<0.039	0.49	<0.024	<0.024	<0.02	<0.025	0.044	N/A	N/A	<0.5	<0.018
		VG86 st.dev.	*U*	*0.30*	*2.25*	-	-	*0.21*	-	-	-	-	*0.014*	*N/A*	*N/A*	-	-
7	Other Beads	PG90	E	<1.2	12.19	<0.26	<0.065	0.37	<0.038	<0.06	<0.4	<0.037	0.061	0.024	<0.064	4.04	<0.09
		PG90 st.dev.	*E*	-	*1.13*	-	-	*0.02*	-	-	-	-	*0.004*	*0.000*	-	*0.24*	-
7	Other Beads	PG172	E	1.86	7.43	<0.26	0.366	0.84	<0.038	<0.06	2.08	0.037	0.046	<0.014	<0.064	0.65	0.54
		PG172 st.dev.	*E*	*0.23*	*0.25*	-	*0.095*	*0.06*	-	-	*0.33*	*0.007*	*0.004*	-	-	*0.16*	*0.16*
7	Other Beads	PG172d	E	2.09	5.47	<0.26	0.720	0.94	<0.038	<0.06	0.53	<0.037	0.043	<0.014	<0.064	0.21	0.12
		PG172d st.dev.	*E*	*0.07*	*0.47*	-	*0.024*	*0.06*	-	-	*0.09*	-	*0.002*	-	-	*0.05*	*0.02*
7	Other Beads	VG88	U	1.48	5.29	<0.15	0.010	0.46	<0.024	<0.024	0.74	<0.025	0.032	N/A	N/A	<0.5	0.02
		VG88 st.dev.	*U*	*0.04*	*1.85*	-	*0.015*	*0.04*	-	-	*0.01*	-	*0.003*	*N/A*	*N/A*	-	*0.03*
7	Other Beads	VG88y	U	0.42	4.84	<0.15	0.204	2.85	0.080	<0.024	0.30	<0.025	<0.01	N/A	N/A	2.91	12.84
		VG88y st.dev.	*U*	*0.59*	*0.37*	-	*0.043*	*0.01*	*0.006*	-	*0.01*	-	-	*N/A*	*N/A*	*0.68*	*2.70*
7	Non-beads	PG97	E	<1.2	6.21	<0.26	<0.065	0.69	<0.038	<0.06	2.73	<0.037	0.054	0.024	<0.064	<0.17	<0.09
		PG97 st.dev.	*E*	-	*5.50*	-	-	*0.22*	-	-	*2.29*	-	*0.022*	*0.013*	-	-	-

Chapter	Group	Sample name/st.dev.	XRF unit	K_20	CaO	TiO_2	MnO	Fe_2O_3	CoO	NiO	CuO	ZnO	SrO	ZrO_2	SnO_2	Sb_2O_5	PbO
7	Non-beads	VG114	U	1.50	5.86	<0.15	<0.039	0.38	<0.024	<0.024	0.21	<0.025	0.028	N/A	N/A	<0.5	<0.018
		VG114 st.dev.	*U*	*0.17*	*0.71*	-	-	*0.06*	-	-	*0.18*	-	*0.003*	*N/A*	*N/A*	-	-
7	Non-beads	VG5	U	1.42	7.14	<0.15	<0.039	0.43	<0.024	<0.024	<0.02	<0.025	0.053	N/A	N/A	<0.5	0.05
		VG5 st.dev.	*U*	*0.40*	*1.67*	-	-	*0.12*	-	-	-	-	*0.008*	*N/A*	*N/A*	-	*0.01*
7	Non-beads	VG56	U	3.07	8.54	<0.15	<0.039	0.65	<0.024	<0.024	0.36	<0.025	0.050	N/A	N/A	<0.5	<0.018
		VG56 st.dev.	*U*	*0.12*	*0.44*	-	-	*0.13*	-	-	*0.11*	-	*0.001*	*N/A*	*N/A*	-	-
7	Non-beads	VG6	U	0.43	6.70	<0.15	<0.039	0.32	<0.024	<0.024	<0.02	<0.025	0.047	N/A	N/A	0.25	0.05
		VG6 st.dev.	*U*	*0.75*	*2.36*	-	-	*0.16*	-	-	-	-	*0.016*	*N/A*	*N/A*	*0.22*	*0.02*
8	6	PG16-18	E	<1.2	3.02	<0.26	<0.065	1.56	<0.038	<0.06	<0.4	<0.037	0.017	<0.014	<0.064	0.62	12.15
		PG16-18 st.dev.	*E*	-	*0.55*	-	-	*0.16*	-	-	-	-	*0.001*	-	-	*0.06*	*0.90*
8	6	PG19-21	E	<1.2	2.29	<0.26	<0.065	1.70	<0.038	<0.06	<0.4	<0.037	0.018	<0.014	<0.064	0.68	15.65
		PG19-21 st.dev.	*E*	-	*0.68*	-	-	*0.61*	-	-	-	-	*0.005*	-	-	*0.23*	*6.97*
8	6	PG22-24	E	<1.2	1.94	<0.26	<0.065	1.79	<0.038	<0.06	<0.4	<0.037	0.017	<0.014	<0.064	0.51	11.30
		PG22-24 st.dev.	*E*	-	*0.25*	-	-	*0.28*	-	-	-	-	*0.002*	-	-	*0.01*	*0.83*
8	6	PG25-27	E	<1.2	2.43	<0.26	<0.065	1.89	<0.038	<0.06	<0.4	<0.037	0.020	<0.014	<0.064	0.67	15.30
		PG25-27 st.dev.	*E*	-	*0.22*	-	-	*0.38*	-	-	-	-	*0.005*	-	-	*0.30*	*5.09*
8	6	PG40-42	E	<1.2	1.93	<0.26	<0.065	1.35	<0.038	<0.06	<0.4	<0.037	0.015	<0.014	<0.064	0.46	9.14
		PG40-42 st.dev.	*E*	-	*0.56*	-	-	*0.29*	-	-	-	-	*0.003*	-	-	*0.08*	*2.68*
8	6	PG48-50	E	<1.2	2.54	<0.26	<0.065	1.57	<0.038	<0.06	<0.4	<0.037	0.018	<0.014	<0.064	0.56	15.59
		PG48-50 st.dev.	*E*	-	*0.53*	-	-	*0.26*	-	-	-	-	*0.005*	-	-	*0.06*	*0.93*
8	6	VG66	F	0.79	2.54	0.226	0.030	2.18	<0.01	<0.004	0.13	<0.02	0.024	N/A	<0.09	5.25	29.08
		VG66 st.dev.	*F*	-	-	-	-	-	-	-	-	-	-	*N/A*	-	-	-
8	6	VG67	F	1.08	3.02	0.341	<0.006	2.93	<0.01	<0.004	0.20	<0.02	<0.02	N/A	<0.09	6.75	34.38
		VG67 st.dev.	*F*	-	-	-	-	-	-	-	-	-	-	*N/A*	-	-	-
8	6	VG68	U	<0.48	3.06	<0.15	0.173	1.15	0.063	<0.024	1.49	<0.025	<0.01	N/A	N/A	0.90	16.48
		VG68 st.dev.	*U*	-	-	-	-	-	-	-	-	-	-	*N/A*	*N/A*	-	-
8	6	VG69	U	<0.48	2.31	<0.15	0.214	0.92	0.071	<0.024	0.31	<0.025	<0.01	N/A	N/A	0.64	11.30
		VG69 st.dev.	*U*	-	-	-	-	-	-	-	-	-	-	*N/A*	*N/A*	-	-

Chapter	Group	Sample name/st.dev.	XRF unit	K_20	CaO	TiO_2	MnO	Fe_2O_3	CoO	NiO	CuO	ZnO	SrO	ZrO_2	SnO_2	Sb_2O_5	PbO
8	6	VG70	U	<0.48	2.50	<0.15	0.147	1.48	0.064	<0.024	0.31	<0.025	<0.01	N/A	N/A	0.67	11.14
		VG70 st.dev.	*U*	-	-	-	-	-	-	-	-	-	-	*N/A*	*N/A*	-	-
8	6	VG71	U	<0.48	2.09	<0.15	0.107	0.88	0.059	<0.024	0.30	<0.025	<0.01	N/A	N/A	0.40	8.85
		VG71 st.dev.	*U*	-	-	-	-	-	-	-	-	-	-	*N/A*	*N/A*	-	-
8	6	VG76	U	<0.48	2.01	<0.15	0.088	0.45	0.045	<0.024	0.30	<0.025	<0.01	N/A	N/A	<0.5	4.89
		VG76 st.dev.	*U*	-	-	-	-	-	-	-	-	-	-	*N/A*	*N/A*	-	-
8	6	VG77	U	<0.48	2.49	<0.15	0.123	1.51	0.052	<0.024	0.30	<0.025	<0.01	N/A	N/A	0.55	10.29
		VG77 st.dev.	*U*	-	-	-	-	-	-	-	-	-	-	*N/A*	*N/A*	-	-
8	6	VG78	U	<0.48	2.47	<0.15	0.137	0.82	0.054	<0.024	0.31	<0.025	<0.01	N/A	N/A	0.43	8.08
		VG78 st.dev.	*U*	-	-	-	-	-	-	-	-	-	-	*N/A*	*N/A*	-	-
8	6	VG79	nr.														
		VG79 st.dev.	*nr.*														
8	14	VG37d	U	<0.48	4.01	<0.15	<0.039	8.42	<0.024	<0.024	<0.02	0.026	0.026	N/A	N/A	0.71	0.05
		VG37d st.dev.	*U*	-	-	-	-	-	-	-	-	-	-	*N/A*	*N/A*	-	-
8	14	VG37y	U	<0.48	4.67	<0.15	0.123	0.66	0.056	<0.024	0.32	<0.025	0.021	N/A	N/A	1.25	9.26
		VG37y st.dev.	*U*	-	*0.24*	-	*0.011*	*0.08*	*0.004*	-	*0.00*	-	*0.001*	*N/A*	*N/A*	*0.13*	*0.14*
8	15	VG94	U	1.12	4.11	<0.15	<0.039	0.95	0.180	0.132	0.74	<0.025	0.018	N/A	N/A	<0.5	0.58
		VG94 st.dev.	*U*	-	-	-	-	-	-	-	-	-	-	*N/A*	*N/A*	-	-
8	15	VG94y	U	0.00	3.61	<0.15	0.202	1.82	0.073	<0.024	0.37	0.026	<0.01	N/A	N/A	1.22	12.57
		VG94y st.dev.	*U*	-	-	-	-	-	-	-	-	-	-	*N/A*	*N/A*	-	-
8	15	PG101	E	1.22	4.46	0.288	0.136	8.08	0.075	<0.06	0.63	0.529	0.026	<0.014	<0.064	1.22	18.00
		PG101 st.dev.	*E*	*0.07*	*0.54*	*0.041*	*0.026*	*1.29*	*0.019*	-	*0.10*	*0.087*	*0.006*	-	-	*0.17*	*3.13*
8	15	PG101y	E	<1.2	2.25	<0.26	<0.065	2.09	<0.038	<0.06	0.45	<0.037	0.019	<0.014	<0.064	0.64	14.33
		PG101y st.dev.	*E*	-	*0.36*	-	-	*0.31*	-	-	*0.01*	-	*0.002*	-	-	*0.08*	*1.84*
8	15	PG99	E	<1.2	3.95	<0.26	<0.065	4.86	0.043	<0.06	1.10	<0.037	0.031	<0.014	<0.064	0.69	5.79
		PG99 st.dev.	*E*	-	*0.50*	-	-	*0.60*	*0.012*	-	*0.24*	-	*0.003*	-	-	*0.06*	*0.74*
8	15	PG99y	E	<1.2	4.41	<0.26	0.065	2.30	<0.038	<0.06	0.61	<0.037	0.035	<0.014	<0.064	0.77	7.73
		PG99y st.dev.	*E*	-	*1.55*	-	*0.019*	*0.64*	-	-	*0.06*	-	*0.009*	-	-	*0.27*	*3.39*

Chapter	Group	Sample name/st.dev.	XRF unit	K_20	CaO	TiO_2	MnO	Fe_2O_3	CoO	NiO	CuO	ZnO	SrO	ZrO_2	SnO_2	Sb_2O_5	PbO
8	15	VG101	U	1.26	4.88	<0.15	0.002	1.83	0.444	0.316	0.92	0.019	0.023	N/A	N/A	<0.5	0.83
		VG101 st.dev.	*U*	*0.05*	*0.04*	-	*0.003*	*0.08*	*0.040*	*0.184*	*0.04*	*0.026*	*0.003*	*N/A*	*N/A*	-	*0.02*
8	15	VG101y	U	0.41	2.94	0.084	0.130	1.49	0.040	<0.024	0.32	<0.025	<0.01	N/A	N/A	0.76	10.04
		VG101y st.dev.	*U*	*0.57*	*1.44*	*0.118*	*0.092*	*1.19*	*0.056*	-	*0.03*	-	-	*N/A*	*N/A*	*1.07*	*8.52*
8	17	PG98	E	<1.2	4.49	<0.26	0.106	1.11	<0.038	<0.06	0.63	<0.037	0.024	<0.014	<0.064	0.69	15.47
		PG98 st.dev.	*E*	-	*0.24*	-	*0.023*	*0.14*	-	-	*0.09*	-	*0.003*	-	-	*0.10*	*2.04*
8	17	PG141	E	<1.2	2.54	<0.26	<0.065	0.72	<0.038	<0.06	<0.4	<0.037	0.017	<0.014	<0.064	0.81	12.03
		PG141 st.dev.	*E*	-	*0.60*	-	-	*0.21*	-	-	-	-	*0.001*	-	-	*0.19*	*3.27*
8	17	VG19	U	<0.48	9.82	<0.15	0.167	1.53	0.065	<0.024	1.90	0.009	0.010	N/A	N/A	1.26	10.30
		VG19 st.dev.	*U*	-	*10.41*	-	*0.084*	*0.57*	*0.014*	-	*2.22*	*0.016*	*0.017*	*N/A*	*N/A*	*0.75*	*3.33*
8	17	VG51	U	<0.48	2.29	<0.15	0.127	0.31	0.060	<0.024	<0.02	<0.025	<0.01	N/A	N/A	<0.5	9.34
		VG51 st.dev.	*U*	-	*0.11*	-	*0.016*	*0.03*	*0.008*	-	-	-	-	*N/A*	*N/A*	-	*0.86*
8	18	PG3	E	1.86	2.81	0.307	0.211	2.06	0.320	0.746	0.56	<0.037	0.022	0.014	<0.064	0.38	0.46
		PG3 st.dev.	*E*	*0.17*	*0.22*	*0.063*	*0.017*	*0.29*	*0.028*	*0.092*	*0.02*	-	*0.001*	*0.002*	-	*0.04*	*0.17*
8	18	PG64	E	1.58	2.85	0.378	0.340	9.80	0.097	<0.06	<0.4	<0.037	0.025	0.016	<0.064	<0.17	0.81
		PG64 st.dev.	*E*	*0.08*	*0.09*	*0.005*	*0.034*	*0.89*	*0.014*	-	-	-	*0.000*	*0.005*	-	-	*0.45*
8	18	PG64y	E	<1.2	2.10	<0.26	0.094	2.81	<0.038	<0.06	<0.4	<0.037	0.017	<0.014	<0.064	0.50	12.32
		PG64y st.dev.	*E*	-	*0.06*	-	*0.039*	*0.72*	-	-	-	-	*0.001*	-	-	*0.10*	*2.50*
8	18	VG81g	U	0.24	3.80	0.321	0.040	0.95	<0.024	<0.024	7.09	0.036	0.013	N/A	N/A	0.72	5.78
		VG81g st.dev.	*U*	*0.42*	*0.72*	*0.090*	*0.006*	*0.09*	-	-	*1.18*	*0.004*	*0.002*	*N/A*	*N/A*	*0.21*	*1.31*
8	18	VG81y	U	<0.48	2.15	0.116	0.140	0.86	0.055	<0.024	1.30	0.009	<0.01	N/A	N/A	0.32	7.71
		VG81y st.dev.	*U*	-	*0.44*	*0.201*	*0.070*	*0.45*	*0.014*	-	*2.00*	*0.015*	-	*N/A*	*N/A*	*0.30*	*3.93*
8	Other Beads	VG85	U	0.55	2.86	<0.15	<0.039	0.64	<0.024	<0.024	0.34	<0.025	0.019	N/A	N/A	<0.5	<0.018
		VG85 st.dev.	*U*	*0.48*	*0.58*	-	-	*0.05*	-	-	*0.00*	-	*0.003*	*N/A*	*N/A*	-	-
8	Non-beads	VG3	U	0.25	6.16	<0.15	0.089	0.64	0.062	<0.024	0.20	<0.025	0.032	N/A	N/A	1.45	7.69
		VG3 st.dev.	*U*	*0.44*	*1.27*	-	*0.036*	*0.13*	*0.007*	-	*0.17*	-	*0.006*	*N/A*	*N/A*	*0.30*	*1.11*
8	Non-beads	VG4	U	<0.48	5.08	<0.15	0.096	0.57	0.061	<0.024	0.19	<0.025	0.027	N/A	N/A	1.46	6.81
		VG4 st.dev.	*U*	-	*0.70*	-	*0.032*	*0.09*	*0.008*	-	*0.17*	-	*0.002*	*N/A*	*N/A*	*0.60*	*1.46*

Chapter	Group	Sample name/st.dev.	XRF unit	K_20	CaO	TiO_2	MnO	Fe_2O_3	CoO	NiO	CuO	ZnO	SrO	ZrO_2	SnO_2	Sb_2O_5	PbO
8	Non-beads	VG7	U	0.29	6.47	<0.15	<0.039	0.29	<0.024	<0.024	<0.02	<0.025	0.042	N/A	N/A	2.49	0.12
		VG7 st.dev.	*U*	*0.50*	*1.48*	-	-	*0.09*	-	-	-	-	*0.011*	*N/A*	*N/A*	*0.89*	*0.08*
8	Non-beads	VG9	U	0.54	8.81	<0.15	<0.039	0.36	<0.024	<0.024	<0.02	<0.025	0.061	N/A	N/A	2.46	0.07
		VG9 st.dev.	*U*	*0.47*	*0.66*	-	-	*0.04*	-	-	-	-	*0.003*	*N/A*	*N/A*	*0.33*	*0.02*
9	8	PG81	E	1.26	1.66	<0.26	<0.065	7.73	0.081	<0.06	<0.4	<0.037	0.018	<0.014	<0.064	<0.17	<0.09
		PG81 st.dev.	*E*	*0.12*	*0.15*	-	-	*1.22*	*0.013*	-	-	-	*0.000*	-	-	-	-
9	8	PG83	E	2.05	4.43	0.333	<0.065	9.29	0.102	<0.06	<0.4	<0.037	0.026	0.014	<0.064	<0.17	<0.09
		PG83 st.dev.	*E*	*0.13*	*0.31*	*0.035*	-	*1.00*	*0.017*	-	-	-	*0.002*	*0.002*	-	-	-
9	8	PG105	E	1.47	1.86	0.316	<0.065	13.38	0.136	<0.06	<0.4	<0.037	0.016	0.029	<0.064	<0.17	<0.09
		PG105 st.dev.	*E*	*0.05*	*0.08*	*0.038*	-	*0.79*	*0.026*	-	-	-	*0.001*	*0.002*	-	-	-
9	8	PG106	E	<1.2	3.19	<0.26	<0.065	8.76	0.083	<0.06	<0.4	0.037	0.019	0.014	<0.064	<0.17	<0.09
		PG106 st.dev.	*E*	-	*0.59*	-	-	*1.31*	*0.007*	-	-	*0.008*	*0.002*	*0.003*	-	-	-
9	8	PG125	E	2.26	2.38	0.368	<0.065	6.95	0.070	0.104	<0.4	<0.037	0.020	0.018	<0.064	<0.17	<0.09
		PG125 st.dev.	*E*	*0.12*	*0.12*	*0.026*	-	*0.68*	*0.004*	*0.007*	-	-	*0.000*	*0.002*	-	-	-
9	8	PG126	E	<1.2	2.38	<0.26	<0.065	7.74	0.068	<0.06	<0.4	<0.037	0.020	0.014	<0.064	<0.17	<0.09
		PG126 st.dev.	*E*	-	*0.16*	-	-	*1.05*	*0.009*	-	-	-	*0.001*	*0.002*	-	-	-
9	8	PG128	E	1.37	2.25	<0.26	<0.065	19.72	0.211	<0.06	<0.4	0.080	0.018	<0.014	<0.064	<0.17	<0.09
		PG128 st.dev.	*E*	*0.08*	*0.10*	-	-	*0.95*	*0.008*	-	-	*0.006*	*0.000*	-	-	-	-
9	8	PG129	E	1.56	2.62	<0.26	<0.065	15.68	0.174	<0.06	<0.4	<0.037	0.019	<0.014	<0.064	<0.17	<0.09
		PG129 st.dev.	*E*	*0.12*	*0.38*	-	-	*2.06*	*0.032*	-	-	-	*0.002*	-	-	-	-
9	8	PG130	E	1.33	2.22	<0.26	<0.065	10.03	0.094	<0.06	<0.4	0.047	0.017	0.022	<0.064	<0.17	<0.09
		PG130 st.dev.	*E*	*0.13*	*0.32*	-	-	*1.33*	*0.022*	-	-	*0.007*	*0.001*	*0.006*	-	-	-
9	8	PG131	E	1.27	2.11	0.398	<0.065	13.52	0.137	<0.06	<0.4	<0.037	0.019	<0.014	<0.064	0.22	<0.09
		PG131 st.dev.	*E*	*0.15*	*0.23*	*0.174*	-	*1.71*	*0.022*	-	-	-	*0.000*	-	-	*0.00*	-
9	8	PG132	E	1.27	2.66	<0.26	<0.065	18.08	0.169	<0.06	<0.4	0.077	0.020	<0.014	<0.064	<0.17	<0.09
		PG132 st.dev.	*E*	*0.16*	*0.51*	-	-	*3.39*	*0.031*	-	-	*0.023*	*0.002*	-	-	-	-
9	8	PG133	E	1.47	5.03	<0.26	<0.065	12.19	0.131	<0.06	<0.4	0.056	0.021	0.027	<0.064	<0.17	<0.09
		PG133 st.dev.	*E*	*0.13*	*0.54*	-	-	*1.30*	*0.001*	-	-	*0.007*	*0.002*	*0.014*	-	-	-

Chapter	Group	Sample name/st.dev.	XRF unit	K_20	CaO	TiO_2	MnO	Fe_2O_3	CoO	NiO	CuO	ZnO	SrO	ZrO_2	SnO_2	Sb_2O_5	PbO
9	8	PG157	E	1.30	1.83	<0.26	<0.065	14.16	0.151	<0.06	<0.4	0.044	0.017	0.015	<0.064	<0.17	<0.09
		PG157 st.dev.	*E*	*0.12*	*0.12*	-	-	*2.28*	*0.023*	-	-	*0.009*	*0.001*	*0.005*	-	-	-
9	16	PG4	E	1.49	2.07	<0.26	<0.065	5.57	0.050	<0.06	0.98	<0.037	0.019	<0.014	<0.064	0.25	<0.09
		PG4 st.dev.	*E*	*0.53*	*0.47*	-	-	*3.14*	*0.030*	-	*0.55*	-	*0.004*	-	-	*0.05*	-
9	16	PG4w	E	1.79	3.43	0.316	<0.065	6.32	0.069	<0.06	0.59	0.041	0.020	<0.014	<0.064	0.30	<0.09
		PG4w st.dev.	*E*	-	-	-	-	-	-	-	-	-	-	-	-	-	-
9	16	PG115	E	1.43	3.63	<0.26	<0.065	9.47	0.097	<0.06	<0.4	<0.037	0.027	0.021	<0.064	<0.17	<0.09
		PG115 st.dev.	*E*	*0.16*	*0.50*	-	-	*2.03*	*0.029*	-	-	-	*0.003*	*0.001*	-	-	-
9	16	PG123	E	1.54	3.86	<0.26	<0.065	2.70	0.044	<0.06	<0.4	<0.037	0.029	0.016	<0.064	<0.17	<0.09
		PG123 st.dev.	*E*	*0.08*	*0.37*	-	-	*0.29*	*0.010*	-	-	-	*0.001*	*0.006*	-	-	-
9	16	PG124	E	1.28	3.17	<0.26	<0.065	10.41	0.094	<0.06	<0.4	<0.037	0.026	<0.014	<0.064	<0.17	<0.09
		PG124 st.dev.	*E*	*0.35*	*0.65*	-	-	*2.92*	*0.035*	-	-	-	*0.004*	-	-	-	-
9	16	PG127	E	1.46	5.52	0.292	0.113	16.29	0.161	<0.06	0.79	0.068	0.026	0.014	<0.064	0.30	0.15
		PG127 st.dev.	*E*	*0.07*	*0.18*	*0.014*	*0.055*	*0.37*	*0.007*	-	*0.17*	*0.002*	*0.000*	*0.001*	-	*0.05*	*0.01*
9	16	PG144	E	1.70	2.51	0.345	<0.065	13.20	0.133	0.062	0.51	<0.037	0.019	0.014	<0.064	<0.17	<0.09
		PG144 st.dev.	*E*	*0.28*	*0.46*	*0.083*	-	*2.39*	*0.013*	*0.009*	*0.17*	-	*0.002*	*0.006*	-	-	-
9	16	VG50	U	1.21	2.84	0.200	<0.039	7.63	<0.024	0.012	0.33	<0.025	0.008	N/A	N/A	<0.5	0.09
		VG50 st.dev.	*U*	*0.29*	*0.28*	*0.029*	-	*1.39*	-	*0.021*	*0.01*	-	*0.007*	*N/A*	*N/A*	-	*0.01*
9	Other Beads	PG5	E	1.27	3.66	<0.26	<0.065	2.87	0.041	<0.06	<0.4	<0.037	0.031	0.017	<0.064	0.19	<0.09
		PG5 st.dev.	*E*	*0.38*	*1.41*	-	-	*1.35*	*0.015*	-	-	-	*0.007*	*0.007*	-	*0.03*	-
9	Other Beads	PG5w	E	1.63	5.20	0.305	<0.065	4.06	0.051	<0.06	0.43	<0.037	0.037	0.017	<0.064	0.23	0.75
		PG5w st.dev.	*E*	*0.50*	*1.87*	*0.128*	-	*2.81*	*0.035*	-	*0.10*	-	*0.009*	*0.006*	-	*0.05*	*0.58*
9	Other Beads	PG6	E	1.56	4.49	0.305	<0.065	8.97	0.094	<0.06	<0.4	<0.037	0.031	0.025	<0.064	0.19	<0.09
		PG6 st.dev.	*E*	*0.09*	*0.54*	*0.123*	-	*2.29*	*0.043*	-	-	-	*0.002*	*0.012*	-	*0.04*	-
9	Other Beads	PG6w	E	1.55	5.99	0.332	<0.065	1.75	<0.038	<0.06	0.51	<0.037	0.029	0.015	<0.064	1.73	<0.09
		PG6w st.dev.	*E*	*0.41*	*1.41*	*0.075*	-	*0.44*	-	-	*0.07*	-	*0.001*	*0.007*	-	*0.89*	-
9	Other Beads	PG32	E	<1.2	2.33	<0.26	0.073	7.44	0.066	<0.06	<0.4	<0.037	0.018	<0.014	<0.064	0.33	1.65
		PG32 st.dev.	*E*	-	-	-	-	-	-	-	-	-	-	-	-	-	-

Chapter	Group	Sample name/st.dev.	XRF unit	K_20	CaO	TiO_2	MnO	Fe_2O_3	CoO	NiO	CuO	ZnO	SrO	ZrO_2	SnO_2	Sb_2O_5	PbO
9	Other Beads	PG32w	E	<1.2	4.19	0.332	0.115	5.45	<0.038	<0.06	0.66	<0.037	0.034	0.018	<0.064	0.36	4.67
		PG32w st.dev.	*E*	-	-	-	-	-	-	-	-	-	-	-	-	-	-
9	Other Beads	PG58	E	3.21	5.80	0.449	<0.065	6.50	0.087	<0.06	<0.4	<0.037	0.039	0.020	<0.064	0.20	<0.09
		PG58 st.dev.	*E*	*0.10*	*0.26*	*0.011*	-	*0.19*	*0.014*	-	-	-	*0.003*	*0.001*	-	*0.02*	-
9	Other Beads	PG58w	E	<1.2	4.60	0.296	<0.065	1.37	<0.038	<0.06	<0.4	<0.037	0.069	0.027	<0.064	0.90	0.10
		PG58w st.dev.	*E*	-	*0.42*	*0.072*	-	*0.15*	-	-	-	-	*0.008*	*0.004*	-	*0.16*	*0.01*
9	Other Beads	PG66d	E	1.37	3.74	<0.26	<0.065	10.97	0.106	<0.06	<0.4	0.066	0.023	0.034	<0.064	0.26	<0.09
		PG66d st.dev.	*E*	*0.10*	*0.05*	-	-	*1.68*	*0.026*	-	-	*0.014*	*0.002*	*0.028*	-	*0.02*	-
9	Other Beads	PG66w	E	2.20	9.42	0.451	0.073	12.78	0.141	<0.06	0.56	0.076	0.029	0.015	<0.064	0.31	<0.09
		PG66w st.dev.	*E*	*0.40*	*1.41*	*0.097*	*0.055*	*2.11*	*0.033*	-	*0.09*	*0.016*	*0.004*	*0.003*	-	*0.03*	-
9	Other Beads	PG113	E	<1.2	3.98	<0.26	<0.065	8.24	0.078	<0.06	<0.4	<0.037	0.030	<0.014	<0.064	<0.17	<0.09
		PG113 st.dev.	*E*	-	*0.16*	-	-	*1.30*	*0.010*	-	-	-	*0.002*	-	-	-	-
9	Other Beads	PG114	E	<1.2	2.98	0.323	<0.065	10.48	0.105	<0.06	<0.4	<0.037	0.025	0.032	<0.064	<0.17	<0.09
		PG114 st.dev.	*E*	-	*0.71*	*0.066*	-	*3.21*	*0.025*	-	-	-	*0.004*	*0.026*	-	-	-
9	Other Beads	PG114w	E	<1.2	6.21	0.557	<0.065	6.32	0.081	<0.06	<0.4	<0.037	0.029	0.028	<0.064	0.43	<0.09
		PG114w st.dev.	*E*	-	*0.29*	*0.092*	-	*1.52*	*0.009*	-	-	-	*0.003*	*0.010*	-	*0.17*	-
9	Other Beads	VG18	U	0.65	18.64	0.250	0.043	2.04	0.017	<0.024	1.04	<0.025	0.060	N/A	N/A	0.30	2.23
		VG18 st.dev.	*U*	*0.56*	*7.85*	*0.220*	*0.044*	*1.09*	*0.030*	-	*0.33*	-	*0.024*	*N/A*	*N/A*	*0.26*	*1.22*
9	Non-beads	PG57	E	1.20	5.17	<0.26	0.115	9.60	0.078	<0.06	1.99	<0.037	0.035	<0.014	<0.064	0.41	2.10
		PG57 st.dev.	*E*	*0.34*	*1.40*	-	*0.066*	*3.89*	*0.037*	-	*2.78*	-	*0.006*	-	-	*0.19*	*1.82*
9	Non-beads	PG57y	E	<1.2	2.14	<0.26	<0.065	1.80	<0.038	<0.06	<0.4	<0.037	0.016	<0.014	<0.064	0.80	8.40
		PG57y st.dev.	*E*	-	*0.47*	-	-	*0.88*	-	-	-	-	*0.005*	-	-	*0.12*	*0.96*
9	Non-beads	PG61	E	2.61	3.63	<0.26	0.411	5.56	0.061	<0.06	<0.4	<0.037	0.029	<0.014	0.184	0.26	1.48
		PG61 st.dev.	*E*	*0.35*	*0.33*	-	*0.100*	*0.83*	*0.015*	-	-	-	*0.003*	-	*0.083*	*0.01*	*0.18*
9	Non-beads	PG61y	E	<1.2	3.13	<0.26	<0.065	1.12	<0.038	<0.06	<0.4	<0.037	0.024	<0.014	0.145	0.53	9.30
		PG61y st.dev.	*E*	-	*0.26*	-	-	*0.15*	-	-	-	-	*0.003*	-	*0.055*	*0.05*	*1.50*
9	Non-beads	PG62	E	2.71	4.00	<0.26	0.388	6.51	0.077	<0.06	<0.4	<0.037	0.029	<0.014	0.150	0.26	1.32
		PG62 st.dev.	*E*	*0.32*	*0.45*	-	*0.052*	*1.29*	*0.010*	-	-	-	*0.004*	-	*0.032*	*0.02*	*0.25*

Chapter	Group	Sample name/st.dev.	XRF unit	K_20	CaO	TiO_2	MnO	Fe_2O_3	CoO	NiO	CuO	ZnO	SrO	ZrO_2	SnO_2	Sb_2O_5	PbO
9	Non-beads	PG62y	E	<1.2	3.71	<0.26	0.091	1.92	<0.038	<0.06	<0.4	<0.037	0.026	0.014	0.135	0.69	11.16
		PG62y st.dev.	*E*	-	*0.21*	-	*0.045*	*0.39*	-	-	-	-	*0.002*	*0.006*	*0.018*	*0.04*	*0.49*
9	Non-beads	VG92	U	<0.48	2.98	<0.15	0.193	3.97	0.062	<0.024	0.37	<0.025	<0.01	N/A	N/A	0.51	6.03
		VG92 st.dev.	*U*	-	*0.74*	-	*0.017*	*2.40*	*0.021*	-	*0.06*	-	-	*N/A*	*N/A*	*0.72*	*4.19*
9	Non-beads	VG92y	U	<0.48	3.05	0.110	0.160	1.22	0.023	<0.024	0.18	0.044	0.005	N/A	N/A	0.46	4.03
		VG92y st.dev.	*U*	-	*0.11*	*0.155*	*0.015*	*1.03*	*0.033*	-	*0.25*	*0.062*	*0.008*	*N/A*	*N/A*	*0.17*	*0.85*
9	Non-beads	VG93	U	<0.48	2.72	<0.15	0.145	4.01	0.064	<0.024	0.34	<0.025	<0.01	N/A	N/A	0.56	6.58
		VG93 st.dev.	*U*	-	*0.43*	-	*0.021*	*1.72*	*0.000*	-	*0.03*	-	-	*N/A*	*N/A*	*0.27*	*2.51*
9	Non-beads	VG93y	U	<0.48	3.38	<0.15	0.160	0.72	0.045	<0.024	0.15	<0.025	<0.01	N/A	N/A	0.46	4.46
		VG93y st.dev.	*U*	-	*0.05*	-	*0.002*	*0.03*	*0.002*	-	*0.21*	-	-	*N/A*	*N/A*	*0.17*	*0.83*
9	Non-beads	PG135	E	1.67	3.66	<0.26	<0.065	4.71	0.052	<0.06	<0.4	<0.037	0.027	<0.014	<0.064	<0.17	<0.09
		PG135 st.dev.	*E*	*0.36*	*0.73*	-	-	*1.37*	*0.020*	-	-	-	*0.003*	-	-	-	-
10	9	VG17	U	0.41	46.20	<0.15	0.055	0.03	<0.024	<0.024	1.67	<0.025	0.213	N/A	N/A	<0.5	0.09
		VG17 st.dev.	*U*	*0.58*	*0.71*	-	*0.029*	*0.01*	-	-	*0.71*	-	*0.066*	*N/A*	*N/A*	-	*0.02*
10	9	VG39-41w	F	0.76	1.53	0.016	0.040	0.72	0.042	0.012	0.91	<0.02	0.028	N/A	<0.09	<0.14	<0.05
		VG39-41w st.dev.	*F*	*0.17*	*0.25*	*0.027*	*0.009*	*0.21*	*0.018*	*0.008*	*0.91*	-	*0.004*	*N/A*	-	-	-
10	9	VG42-44b	F	0.33	1.01	0.017	0.035	0.64	0.107	0.029	3.25	0.053	<0.02	N/A	<0.09	0.05	<0.05
		VG42-44b st.dev.	*F*	*0.29*	*0.87*	*0.030*	*0.014*	*0.21*	*0.036*	*0.010*	*0.29*	*0.017*	-	*N/A*	-	*0.09*	-
10	9	VG45-47y	F	0.53	2.09	0.046	0.051	0.52	<0.01	<0.004	0.13	<0.02	0.008	N/A	<0.09	1.71	2.44
		VG45-47y st.dev.	*F*	*0.16*	*1.13*	*0.041*	*0.014*	*0.18*	-	-	*0.00*	-	*0.013*	*N/A*	-	*0.45*	*0.36*
10	Other Beads	VG16	U	<0.48	3.13	<0.15	0.078	2.59	0.121	0.231	1.04	<0.025	0.025	N/A	N/A	0.11	7.31
		VG16 st.dev.	*U*	-	*0.20*	-	*0.003*	*0.41*	*0.052*	*0.306*	*0.12*	-	*0.005*	*N/A*	*N/A*	*0.19*	*0.94*
10	Other Beads	VG27	F	<0.1	2.93	0.056	0.038	0.41	<0.01	<0.004	2.27	<0.02	<0.02	N/A	<0.09	<0.14	<0.05
		VG27 st.dev.	*F*	-	-	-	-	-	-	-	-	-	-	*N/A*	-	-	-

APPENDIX 7. LASER ABLATION INDUCTIVELY COUPLED PLASMA MASS SPECTROMETRY RESULTS.

The LA-ICP-MS results are presented in the two tables below. First table presents the composition of major elements and some elements that were detected in significant concentrations during the XRF analyses as the ones that influence the colour and raw materials impurities. Their values were converted to the respective oxides and standard deviation of the replicate analyses was added to check the dispersion of data. The values in the table 1 are in weight percent. Table 2 contains the block of trace elements data with determined elemental concentrations expressed in ppm and their standard deviations. The number of significant digits in both tables was adjusted to correspond to concentration range of the element (oxide) and their respective standard deviations. The values below the Limits of Quantification were substituted with the "<LOQ". N/A instead of some Zr values means no data on this element were acquired for the corresponding sample. "-" means no standard deviation can be obtained (for the acquisitions with no replicates) or the value in not applicable when the concentration is too low. Polychrome beads were analysed as two (sometimes three) samples – to obtain the base glass composition and the one of the decorations (qualitative). The results of decoration analyses are marked near the name of the sample with a letter: d – dark, g – green, r – red, y – yellow, w – white. Both tables have identical sorting according to the chapter of the main text, where these samples are discussed, typological group of beads and sample name in the ascending order. The PG series precedes the VG series within same group. Samples that did not produce meaningful results are omitted.

Table 1. LA-ICP-MS results for major elements and typical colourants opacifiers and impurities. The values are in weight percent.

Chapter	**Group**	**Sample/ st.dev.**	**Na_2O**	**MgO**	**Al_2O_3**	**SiO_2**	**K_2O**	**CaO**	**TiO_2**	**V_2O_5**	**MnO**	**Fe_2O_3**	**CoO**	**NiO**	**CuO**	**ZnO**	**As_2O_3**	**SnO_2**	**Sb_2O_5**	**PbO**
5	1	PG46	20.14	4.08	5.94	61.42	0.07	5.94	0.046	0.0017	0.299	0.68	0.0605	0.0736	0.0021	0.0577	0.0002	0.0003	0.0006	0.0009
		st.dev.	*4.92*	*0.91*	*1.32*	*14.21*	*0.02*	*1.35*	*0.010*	*0.0003*	*0.068*	*0.16*	*0.0142*	*0.0172*	*0.0018*	*0.0141*	*0.0000*	*0.0002*	*0.0001*	*0.0007*
5	1	PG47	20.51	3.85	6.43	62.64	0.09	<LOQ	0.041	0.0015	0.306	0.70	0.0523	0.0596	0.0015	0.0335	<LOQ	0.0000	<LOQ	0.0005
		st.dev.	*9.92*	*1.77*	*2.99*	*33.36*	*0.04*	-	*0.019*	*0.0008*	*0.142*	*0.30*	*0.0242*	*0.0275*	*0.0008*	*0.0168*	-	*0.0000*	-	*0.0004*
5	1	PG73	30.83	4.23	7.18	53.51	0.15	1.12	0.033	0.0011	0.700	0.75	0.1282	0.0827	0.0023	0.0916	0.0001	0.0009	0.0001	0.0005
		st.dev.	*11.98*	*0.74*	*1.30*	*10.30*	*0.07*	*0.21*	*0.005*	*0.0002*	*0.134*	*0.15*	*0.0228*	*0.0147*	*0.0006*	*0.0186*	*0.0001*	*0.0015*	*0.0000*	*0.0002*
5	1	PG79	23.85	2.77	6.53	60.72	0.08	4.00	0.035	0.0010	0.335	0.66	0.0678	0.0594	0.0044	0.0895	0.0001	0.0000	0.0004	0.0008
		st.dev.	*9.37*	*1.22*	*2.59*	*26.58*	*0.04*	*1.85*	*0.013*	*0.0004*	*0.130*	*0.27*	*0.0259*	*0.0219*	*0.0017*	*0.0337*	*0.0001*	*0.0000*	*0.0001*	*0.0003*
5	1	PG85	18.30	3.82	6.39	63.32	0.10	5.95	0.049	0.0012	0.245	0.61	0.0317	0.0363	0.0091	0.0246	0.0002	0.0000	0.0007	0.0061
		st.dev.	*5.46*	*1.12*	*1.93*	*20.97*	*0.05*	*1.80*	*0.015*	*0.0004*	*0.073*	*0.18*	*0.0093*	*0.0111*	*0.0109*	*0.0066*	*0.0001*	*0.0000*	*0.0002*	*0.0016*
5	1	PG86	26.75	4.53	9.87	49.39	0.06	5.40	0.090	0.0024	0.431	1.96	0.0673	0.0708	0.0094	0.0637	<LOQ	0.0002	0.0015	0.0022
		st.dev.	*10.29*	*1.77*	*4.04*	*35.38*	*0.02*	*2.30*	*0.033*	*0.0009*	*0.168*	*0.76*	*0.0265*	*0.0276*	*0.0078*	*0.0260*	-	*0.0003*	*0.0006*	*0.0009*

Chapter	Group	Sample/ st.dev.	Na_2O	MgO	Al_2O_3	SiO_2	K_2O	CaO	TiO_2	V_2O_5	MnO	Fe_2O_3	CoO	NiO	CuO	ZnO	As_2O_3	SnO_2	Sb_2O_5	PbO
5	1	PG91	18.56	4.13	6.73	64.58	0.19	3.24	0.130	0.0017	0.286	0.84	0.0489	0.0520	0.0062	0.0368	0.0003	0.0003	0.0106	0.0126
		st.dev.	*1.16*	*0.24*	*0.38*	*3.29*	*0.01*	*0.18*	*0.007*	*0.0001*	*0.017*	*0.05*	*0.0026*	*0.0028*	*0.0023*	*0.0025*	*0.0000*	*0.0002*	*0.0042*	*0.0046*
5	1	PG94	18.78	2.73	7.71	64.94	0.22	2.91	0.056	0.0015	0.477	1.11	0.1153	0.0745	0.0032	0.0906	0.0003	0.0002	0.0231	0.0006
		st.dev.	*17.20*	*2.58*	*7.10*	*62.78*	*0.21*	*2.57*	*0.049*	*0.0014*	*0.446*	*1.02*	*0.1063*	*0.0685*	*0.0026*	*0.0857*	*0.0002*	*0.0002*	*0.0441*	*0.0004*
5	1	PG100b	25.97	3.75	5.94	56.35	0.32	4.46	0.092	0.0032	0.535	1.22	0.1047	0.0917	0.0455	0.0983	<LOQ	0.0001	0.0025	0.0011
		st.dev.	*1.98*	*0.32*	*0.58*	*4.96*	*0.21*	*0.42*	*0.005*	*0.0003*	*0.045*	*0.09*	*0.0112*	*0.0109*	*0.0524*	*0.0129*	-	*0.0001*	*0.0012*	*0.0006*
5	1	PG100w	22.13	1.23	1.47	51.48	0.33	13.70	0.168	0.0029	0.063	0.77	0.0145	0.0125	0.1493	0.0263	0.0043	0.0061	8.1197	0.0318
		st.dev.	*20.10*	*1.19*	*1.56*	*114.82*	*0.28*	*12.67*	*0.138*	*0.0022*	*0.112*	*0.71*	*0.0204*	*0.0181*	*0.1132*	*0.0359*	*0.0041*	*0.0103*	*7.7445*	*0.0298*
5	1	PG107	16.25	3.87	6.94	68.17	0.16	2.26	0.051	0.0016	0.251	0.74	0.0465	0.0606	0.0531	0.0373	0.0003	0.0043	0.0024	0.0028
		st.dev.	*4.78*	*1.02*	*1.69*	*20.40*	*0.03*	*0.58*	*0.012*	*0.0003*	*0.068*	*0.19*	*0.0134*	*0.0177*	*0.0290*	*0.0105*	*0.0001*	*0.0029*	*0.0006*	*0.0010*
5	1	PG108	16.65	3.77	6.17	67.51	0.17	3.39	0.062	0.0015	0.292	0.79	0.0377	0.0358	0.0118	0.0283	0.0002	0.0002	0.0134	0.0110
		st.dev.	*3.14*	*0.74*	*1.18*	*13.30*	*0.04*	*0.69*	*0.013*	*0.0003*	*0.054*	*0.15*	*0.0070*	*0.0065*	*0.0022*	*0.0052*	*0.0001*	*0.0002*	*0.0019*	*0.0019*
5	1	PG109w	13.84	0.51	0.78	66.26	0.19	8.18	0.054	0.0014	0.133	0.34	0.0031	0.0035	0.0740	0.0030	0.0093	0.0004	9.4419	0.0445
		st.dev.	*3.34*	*0.28*	*0.60*	*15.88*	*0.05*	*1.69*	*0.011*	*0.0004*	*0.200*	*0.09*	*0.0047*	*0.0051*	*0.0813*	*0.0032*	*0.0022*	*0.0005*	*2.5288*	*0.0098*
5	1	PG109d	15.32	1.31	2.64	72.60	0.25	5.51	0.049	0.0023	0.913	0.45	0.0203	0.0209	0.3340	0.0131	0.0008	0.0026	0.2103	0.0101
		st.dev.	*1.23*	*0.16*	*0.28*	*6.20*	*0.01*	*0.51*	*0.005*	*0.0001*	*0.124*	*0.06*	*0.0020*	*0.0022*	*0.0284*	*0.0014*	*0.0001*	*0.0006*	*0.0149*	*0.0007*
5	1	PG111b	20.75	2.77	4.79	66.05	0.17	2.90	0.048	0.0020	0.496	0.61	0.0251	0.0350	0.1856	0.0210	0.0017	0.0013	0.3768	0.0008
		st.dev.	*2.08*	*0.30*	*0.50*	*6.58*	*0.02*	*0.33*	*0.005*	*0.0002*	*0.050*	*0.07*	*0.0027*	*0.0036*	*0.0197*	*0.0024*	*0.0002*	*0.0000*	*0.0414*	*0.0000*
5	1	PG111w	20.37	0.79	1.17	60.74	0.16	7.77	0.069	0.0012	0.088	0.37	0.0043	0.0067	0.0521	0.0054	0.0117	0.0003	8.1860	0.0024
		st.dev.	*2.85*	*0.33*	*0.66*	*9.03*	*0.03*	*1.96*	*0.012*	*0.0002*	*0.079*	*0.06*	*0.0042*	*0.0063*	*0.0297*	*0.0042*	*0.0034*	*0.0003*	*2.5680*	*0.0006*
5	1	PG112	14.53	0.66	0.88	75.26	0.29	5.63	0.088	0.0019	1.356	0.43	0.0006	0.0008	0.6716	0.0023	0.0023	0.0044	0.0067	0.0131
		st.dev.	*3.13*	*0.13*	*0.22*	*17.44*	*0.06*	*1.14*	*0.021*	*0.0005*	*0.295*	*0.10*	*0.0002*	*0.0003*	*0.1605*	*0.0006*	*0.0006*	*0.0014*	*0.0014*	*0.0035*
5	1	PG139	20.68	2.92	5.74	64.05	0.18	4.38	0.034	0.0010	0.187	0.69	0.0917	0.0773	0.0077	0.1001	0.0004	0.0002	0.0173	0.0011
		st.dev.	*4.27*	*0.20*	*0.41*	*6.18*	*0.07*	*0.32*	*0.003*	*0.0001*	*0.015*	*0.06*	*0.0089*	*0.0080*	*0.0062*	*0.0370*	*0.0001*	*0.0002*	*0.0022*	*0.0002*
5	1	PG150b	22.74	2.41	6.20	62.78	0.12	3.39	0.038	0.0011	0.468	0.87	0.1300	0.0838	0.0029	0.0752	<LOQ	0.0001	0.0013	0.0009
		st.dev.	*8.45*	*0.90*	*2.50*	*24.50*	*0.04*	*1.27*	*0.013*	*0.0004*	*0.173*	*0.32*	*0.0475*	*0.0310*	*0.0011*	*0.0282*	-	*0.0000*	*0.0010*	*0.0003*

Chapter	Group	Sample/ st.dev.	Na_2O	MgO	Al_2O_3	SiO_2	K_2O	CaO	TiO_2	V_2O_5	MnO	Fe_2O_3	CoO	NiO	CuO	ZnO	As_2O_3	SnO_2	Sb_2O_5	PbO
5	1	PG150w	21.15	1.81	0.52	62.27	0.44	6.55	0.038	0.0009	0.028	0.22	0.0055	0.0043	0.0096	0.0059	0.0122	0.0007	6.4406	0.0284
		st.dev.	*5.19*	*0.54*	*0.36*	*15.34*	*0.14*	*1.72*	*0.010*	*0.0002*	*0.031*	*0.07*	*0.0092*	*0.0061*	*0.0017*	*0.0080*	*0.0029*	*0.0002*	*1.5867*	*0.0068*
5	1	PG150b	18.40	2.44	6.01	67.79	0.15	3.03	0.033	0.0010	0.440	0.73	0.1134	0.0726	0.0009	0.0778	0.0002	0.0000	0.0007	0.0011
		st.dev.	*2.14*	*0.37*	*0.89*	*10.82*	*0.02*	*0.44*	*0.005*	*0.0001*	*0.089*	*0.11*	*0.0168*	*0.0111*	*0.0002*	*0.0106*	*0.0000*	*0.0000*	*0.0002*	*0.0007*
5	1	PG150w	17.52	1.82	0.50	65.66	0.68	6.37	0.035	0.0008	0.027	0.21	0.0052	0.0037	0.0033	0.0047	0.0107	0.0009	6.6820	0.0289
		st.dev.	*23.20*	*2.31*	*0.34*	*85.31*	*0.91*	*8.21*	*0.042*	*0.0009*	*0.026*	*0.21*	*0.0087*	*0.0050*	*0.0036*	*0.0048*	*0.0133*	*0.0005*	*7.7927*	*0.0366*
5	1	PG151b	21.28	2.06	2.91	64.63	0.27	6.21	0.049	0.0027	0.943	0.46	0.0157	0.0221	0.3348	0.0095	0.0009	0.0018	0.2164	0.0064
		st.dev.	*6.85*	*0.73*	*1.05*	*21.40*	*0.10*	*2.14*	*0.017*	*0.0009*	*0.321*	*0.17*	*0.0051*	*0.0073*	*0.0926*	*0.0028*	*0.0003*	*0.0006*	*0.0575*	*0.0015*
5	1	PG151w	19.65	0.53	0.53	58.85	0.26	9.65	0.065	0.0016	0.012	0.36	0.0002	0.0005	0.0163	0.0017	0.0104	0.0003	9.8882	0.0379
		st.dev.	*8.34*	*0.23*	*0.24*	*25.40*	*0.09*	*4.20*	*0.028*	*0.0007*	*0.005*	*0.17*	*0.0001*	*0.0004*	*0.0079*	*0.0008*	*0.0043*	*0.0001*	*4.0160*	*0.0156*
5	1	PG156b	20.89	2.59	5.41	64.50	0.14	4.54	0.036	0.0010	0.353	0.62	0.0709	0.0553	0.0015	0.0501	0.0002	0.0001	0.0038	0.0011
		st.dev.	*3.35*	*0.41*	*0.87*	*9.83*	*0.02*	*0.78*	*0.007*	*0.0001*	*0.063*	*0.10*	*0.0107*	*0.0086*	*0.0011*	*0.0074*	*0.0000*	*0.0002*	*0.0039*	*0.0001*
5	1	VG106b	18.90	2.40	5.35	66.65	0.12	4.46	0.036	0.0011	0.456	0.73	0.0809	0.0573	0.0017	0.0661	0.0002	0.0000	0.0031	0.0010
		st.dev.	*1.58*	*0.19*	*0.44*	*5.63*	*0.01*	*0.39*	*0.003*	*0.0001*	*0.044*	*0.07*	*0.0070*	*0.0046*	*0.0018*	*0.0058*	*0.0000*	*0.0000*	*0.0008*	*0.0004*
5	1	VG106w	19.26	1.89	0.33	62.84	0.82	7.15	0.039	0.0009	0.010	0.20	0.0003	0.0008	0.0212	0.0023	0.0110	0.0002	6.9728	0.0184
		st.dev.	*1.70*	*0.21*	*0.05*	*6.22*	*0.08*	*0.78*	*0.005*	*0.0001*	*0.001*	*0.03*	*0.0001*	*0.0002*	*0.0241*	*0.0011*	*0.0009*	*0.0000*	*1.0924*	*0.0027*
5	1	PG110_2	21.90	3.70	6.01	62.02	0.13	3.74	0.130	0.0018	0.301	0.86	0.0558	0.0677	0.0050	0.0302	0.0002	0.0001	0.0006	0.0022
		st.dev.	*8.51*	*1.41*	*2.26*	*24.38*	*0.04*	*1.46*	*0.049*	*0.0007*	*0.113*	*0.34*	*0.0215*	*0.0253*	*0.0011*	*0.0120*	*0.0001*	*0.0000*	*0.0001*	*0.0006*
5	1	PG110_1	19.43	0.66	0.68	71.67	0.28	4.91	0.075	0.0016	1.507	0.36	0.0005	0.0008	0.2351	0.0020	0.0015	0.0029	0.0061	0.0067
		st.dev.	*5.70*	*0.19*	*0.19*	*20.47*	*0.08*	*1.51*	*0.022*	*0.0005*	*0.550*	*0.10*	*0.0002*	*0.0002*	*0.0662*	*0.0006*	*0.0005*	*0.0009*	*0.0032*	*0.0017*
5	2	VG98y	14.14	0.28	0.32	50.87	0.18	3.09	0.097	0.0014	0.021	1.11	0.0007	0.0010	0.0210	0.0043	0.0359	0.0002	5.0410	24.7441
		st.dev.	*5.03*	*0.05*	*0.05*	*14.99*	*0.04*	*0.83*	*0.032*	*0.0004*	*0.022*	*0.31*	*0.0008*	*0.0004*	*0.0028*	*0.0001*	*0.0107*	*0.0002*	*1.5185*	*7.8401*
5	2	VG98b	18.88	1.43	2.89	67.80	0.35	6.07	0.072	0.0026	1.127	0.69	0.0332	0.0253	0.1299	0.0209	0.0010	0.0018	0.1034	0.0165
		st.dev.	*1.50*	*0.13*	*0.25*	*5.04*	*0.03*	*0.49*	*0.006*	*0.0002*	*0.100*	*0.03*	*0.0030*	*0.0023*	*0.0086*	*0.0017*	*0.0001*	*0.0002*	*0.0061*	*0.0084*
5	7	PG28	16.83	0.98	5.29	<LOQ	2.97	<LOQ	0.319	0.0099	0.215	13.00	0.0022	0.0053	0.0491	0.0564	0.1122	0.0117	0.2374	3.5062
		st.dev.	*5.87*	*0.26*	*2.92*	*-*	*1.74*	*-*	*0.093*	*0.0027*	*0.053*	*1.32*	*0.0001*	*0.0020*	*0.0067*	*0.0210*	*0.0261*	*0.0106*	*0.0676*	*1.0236*

Chapter	Group	Sample/ st.dev.	Na_2O	MgO	Al_2O_3	SiO_2	K_2O	CaO	TiO_2	V_2O_5	MnO	Fe_2O_3	CoO	NiO	CuO	ZnO	As_2O_3	SnO_2	Sb_2O_5	PbO
5	7	PG37	13.37	0.68	4.44	59.54	0.88	3.94	0.254	0.0069	0.328	9.93	0.0016	0.0031	0.0559	0.0052	0.0043	0.0190	0.6347	5.8625
		st.dev.	*9.00*	*0.33*	*2.66*	*31.83*	*0.49*	*2.67*	*0.123*	*0.0036*	*0.214*	*6.98*	*0.0010*	*0.0020*	*0.0602*	*0.0045*	*0.0023*	*0.0318*	*0.4351*	*4.3443*
5	7	PG43	16.31	2.17	5.68	70.77	0.10	3.13	0.044	0.0012	0.237	0.74	0.0695	0.0567	0.0040	0.0533	<LOQ	0.0003	0.0014	0.0015
		st.dev.	*1.96*	*0.22*	*0.57*	*8.59*	*0.01*	*0.34*	*0.005*	*0.0002*	*0.023*	*0.07*	*0.0081*	*0.0065*	*0.0004*	*0.0063*	-	*0.0003*	*0.0012*	*0.0003*
5	7	PG51	23.21	1.16	6.83	59.53	1.27	2.58	0.422	0.0090	0.360	3.55	0.3211	0.1448	0.2372	0.0237	0.0216	0.0074	0.0767	0.2002
		st.dev.	*7.67*	*0.17*	*1.26*	*3.17*	*0.42*	*0.40*	*0.060*	*0.0015*	*0.045*	*0.43*	*0.0548*	*0.0330*	*0.0947*	*0.0143*	*0.0105*	*0.0069*	*0.0316*	*0.1089*
5	7	PG158	5.61	0.77	1.84	79.67	7.04	2.79	0.060	0.0020	0.018	1.04	0.1512	0.2810	1.0959	0.0506	0.2633	0.0271	0.2149	0.1049
		st.dev.	*0.69*	*0.12*	*0.26*	*12.00*	*0.93*	*0.37*	*0.009*	*0.0003*	*0.002*	*0.14*	*0.0192*	*0.0349*	*0.1565*	*0.0056*	*0.0297*	*0.0030*	*0.0256*	*0.0145*
5	7	PG159	6.76	1.37	5.47	74.67	5.41	3.45	0.180	0.0069	0.038	1.98	0.1939	0.2713	0.5676	0.0113	0.1720	0.0251	0.0109	0.0024
		st.dev.	*0.16*	*0.05*	*0.15*	*3.64*	*0.31*	*0.08*	*0.005*	*0.0001*	*0.001*	*0.07*	*0.0038*	*0.0047*	*0.0238*	*0.0005*	*0.0047*	*0.0016*	*0.0006*	*0.0003*
5	7	VG22	6.19	0.81	2.10	77.10	10.43	3.32	0.070	0.0024	0.018	0.92	0.1164	0.1841	0.1521	0.0259	0.0549	0.0013	0.0733	0.0580
		st.dev.	*0.54*	*0.11*	*0.30*	*9.96*	*1.29*	*0.45*	*0.008*	*0.0003*	*0.003*	*0.11*	*0.0134*	*0.0206*	*0.0494*	*0.0022*	*0.0051*	*0.0001*	*0.0076*	*0.0057*
5	Non-beads	VG32	22.25	0.50	1.48	64.10	0.31	9.69	0.058	0.0013	0.027	0.51	0.1103	0.0017	0.0274	0.0192	0.0012	0.0102	0.7615	0.0166
		st.dev.	*1.84*	*0.05*	*0.12*	*5.42*	*0.02*	*0.85*	*0.005*	*0.0001*	*0.002*	*0.03*	*0.0057*	*0.0001*	*0.0020*	*0.0017*	*0.0001*	*0.0008*	*0.0777*	*0.0017*
6	3	PG84w	7.29	0.73	2.67	81.94	4.33	2.41	0.089	0.0026	0.023	0.88	0.0042	0.0129	0.1482	0.0067	0.0071	0.0027	0.0032	0.0005
		st.dev.	*1.62*	*0.12*	*0.56*	*31.88*	*1.03*	*0.49*	*0.018*	*0.0005*	*0.006*	*0.16*	*0.0034*	*0.0099*	*0.0642*	*0.0014*	*0.0066*	*0.0023*	*0.0025*	*0.0002*
6	3	PG84b	6.29	1.15	4.12	74.32	4.93	2.91	0.136	0.0043	0.026	1.65	0.0816	0.2404	4.3457	0.0141	0.1940	0.0437	0.0818	0.0066
		st.dev.	*1.11*	*0.25*	*1.33*	*12.86*	*0.82*	*0.52*	*0.027*	*0.0008*	*0.005*	*0.47*	*0.0164*	*0.0478*	*0.8147*	*0.0024*	*0.0349*	*0.0074*	*0.0146*	*0.0012*
6	3	PG87	6.30	0.95	3.08	78.49	4.75	2.20	0.088	0.0028	0.021	0.88	0.0045	0.0098	3.6376	0.0101	0.0056	0.1329	0.0034	0.0058
		st.dev.	*0.68*	*0.11*	*0.34*	*8.02*	*0.50*	*0.25*	*0.011*	*0.0003*	*0.003*	*0.10*	*0.0005*	*0.0012*	*0.4196*	*0.0041*	*0.0007*	*0.0165*	*0.0003*	*0.0009*
6	4	PG121	20.18	3.30	2.46	63.97	1.99	5.60	0.162	0.0031	0.028	1.05	0.0007	0.0069	0.6385	0.0062	0.0025	0.0002	0.0128	0.0142
		st.dev.	*2.54*	*0.46*	*0.29*	*8.07*	*0.23*	*0.71*	*0.020*	*0.0004*	*0.004*	*0.14*	*0.0001*	*0.0008*	*0.0781*	*0.0010*	*0.0004*	*0.0000*	*0.0026*	*0.0053*
6	4	PG122_w_1	19.68	4.07	3.11	55.30	1.75	9.29	0.254	0.0046	0.037	1.44	0.0008	0.0066	0.1904	0.0178	0.0201	0.0001	0.5295	3.4759
		st.dev.	-	-	-	-	-	-	-	-	-	-	-	-	-	-	-	-	-	-
6	4	PG122d	20.57	3.24	2.50	63.60	2.11	6.46	0.212	0.0031	0.026	0.72	0.0004	0.0032	0.0076	0.0036	0.0004	0.0001	0.0015	0.0033
		st.dev.	*1.80*	*0.30*	*0.22*	*6.63*	*0.20*	*0.66*	*0.019*	*0.0002*	*0.003*	*0.06*	*0.0000*	*0.0002*	*0.0038*	*0.0003*	*0.0002*	*0.0001*	*0.0004*	*0.0016*

Chapter	Group	Sample/ st.dev.	Na_2O	MgO	Al_2O_3	SiO_2	K_2O	CaO	TiO_2	V_2O_5	MnO	Fe_2O_3	CoO	NiO	CuO	ZnO	As_2O_3	SnO_2	Sb_2O_5	PbO
6	4	PG122g	21.55	3.93	3.10	57.76	1.51	7.83	0.248	0.0042	0.042	1.48	0.0009	0.0071	1.5554	0.0608	0.0011	0.0002	0.0828	0.0049
		st.dev.	*4.96*	*0.52*	*0.42*	*8.25*	*0.37*	*1.06*	*0.034*	*0.0006*	*0.006*	*0.21*	*0.0001*	*0.0009*	*0.2122*	*0.0065*	*0.0004*	*0.0001*	*0.0114*	*0.0032*
6	Non-beads	PG60y	10.61	0.45	0.88	50.64	0.21	1.72	0.047	0.0020	0.021	1.96	0.0002	0.0017	0.0381	0.0018	1.1672	0.0020	2.0540	30.1040
		st.dev.	*3.26*	*0.16*	*0.28*	*14.88*	*0.08*	*0.56*	*0.015*	*0.0006*	*0.007*	*0.61*	*0.0001*	*0.0005*	*0.0143*	*0.0006*	*0.2222*	*0.0010*	*0.5808*	*7.4114*
6	Non-beads	PG60b	10.38	0.40	0.76	59.10	0.16	1.48	0.040	0.0017	0.018	1.62	0.0002	0.0014	0.0264	0.0013	0.9355	0.0004	1.3752	23.6182
		st.dev.	*2.82*	*0.14*	*0.24*	*11.37*	*0.07*	*0.52*	*0.012*	*0.0005*	*0.006*	*0.48*	*0.0001*	*0.0004*	*0.0116*	*0.0007*	*0.2571*	*0.0006*	*0.3613*	*6.4185*
7	5	PG71	17.26	3.27	0.77	67.24	0.58	9.14	0.072	0.0023	0.124	0.63	0.0003	0.0013	0.0037	0.0030	0.0003	0.0001	0.0008	0.0003
		st.dev.	*4.43*	*0.82*	*0.20*	*18.97*	*0.17*	*2.33*	*0.019*	*0.0006*	*0.030*	*0.17*	*0.0001*	*0.0004*	*0.0011*	*0.0009*	*0.0002*	*0.0000*	*0.0003*	*0.0001*
7	5	PG75	16.51	3.04	0.88	66.42	0.60	9.10	0.068	0.0047	1.908	0.60	0.0006	0.0018	0.0088	0.0040	0.0003	0.0001	0.0006	0.0003
		st.dev.	*0.99*	*0.15*	*0.04*	*3.14*	*0.03*	*0.34*	*0.003*	*0.0002*	*0.105*	*0.03*	*0.0000*	*0.0001*	*0.0010*	*0.0003*	*0.0000*	*0.0000*	*0.0000*	*0.0001*
7	10	PG2	17.16	2.54	0.34	71.58	0.96	6.12	0.030	0.0015	0.247	0.22	0.0002	0.0009	0.0018	0.0035	0.0005	0.0042	0.2049	0.0011
		st.dev.	*2.81*	*0.40*	*0.05*	*11.14*	*0.15*	*0.97*	*0.005*	*0.0002*	*0.042*	*0.04*	*0.0000*	*0.0002*	*0.0006*	*0.0007*	*0.0001*	*0.0033*	*0.0369*	*0.0005*
7	10	PG7	14.37	2.53	0.77	72.65	0.81	6.98	0.054	0.0018	0.023	0.48	0.0003	0.0013	0.0007	0.0032	0.0009	0.0000	0.6873	0.0005
		st.dev.	*0.43*	*0.14*	*0.03*	*2.97*	*0.02*	*0.28*	*0.002*	*0.0001*	*0.001*	*0.02*	*0.0000*	*0.0000*	*0.0002*	*0.0002*	*0.0001*	*0.0000*	*0.0853*	*0.0002*
7	10	PG9	15.97	3.13	0.97	69.47	1.35	7.84	0.045	0.0016	0.043	0.45	0.0037	0.0052	0.0007	0.0058	0.0015	0.0001	0.0008	0.0005
		st.dev.	*5.52*	*1.02*	*0.35*	*22.75*	*0.44*	*2.67*	*0.015*	*0.0005*	*0.015*	*0.15*	*0.0012*	*0.0016*	*0.0001*	*0.0018*	*0.0004*	*0.0000*	*0.0002*	*0.0000*
7	10	PG10	15.28	0.85	0.21	77.16	0.40	5.75	0.022	0.0005	0.006	0.12	0.0001	0.0001	0.0006	0.0009	0.0001	0.0000	0.0005	0.0002
		st.dev.	*3.47*	*0.21*	*0.04*	*14.87*	*0.10*	*1.09*	*0.004*	*0.0001*	*0.001*	*0.03*	*0.0000*	*0.0000*	*0.0001*	*0.0002*	*0.0000*	*0.0000*	*0.0001*	*0.0000*
7	10	PG13	19.30	0.41	0.15	73.77	0.22	5.92	0.016	0.0005	0.004	0.11	0.0001	0.0001	0.0021	0.0006	0.0006	0.0000	0.0005	0.0004
		st.dev.	*0.35*	*0.00*	*0.00*	*1.05*	*0.00*	*0.03*	*0.000*	*0.0000*	*0.000*	*0.00*	*0.0000*	*0.0000*	*0.0010*	*0.0001*	*0.0001*	*0.0000*	*0.0000*	*0.0002*
7	10	PG14	19.86	0.46	0.19	71.93	0.31	6.96	0.025	0.0006	0.005	0.14	0.0001	0.0002	0.0178	0.0011	0.0003	0.0001	0.0006	0.0031
		st.dev.	*4.93*	*0.11*	*0.05*	*17.04*	*0.09*	*1.76*	*0.006*	*0.0002*	*0.002*	*0.05*	*0.0000*	*0.0001*	*0.0148*	*0.0007*	*0.0001*	*0.0001*	*0.0005*	*0.0011*
7	10	PG15	18.39	0.54	0.25	75.02	0.24	5.17	0.055	0.0008	0.008	0.19	0.0001	0.0002	0.0011	0.0012	0.0004	0.0000	0.0007	0.0001
		st.dev.	*1.39*	*0.03*	*0.01*	*5.71*	*0.02*	*0.35*	*0.004*	*0.0001*	*0.001*	*0.02*	*0.0000*	*0.0000*	*0.0003*	*0.0001*	*0.0001*	*0.0000*	*0.0000*	*0.0001*
7	10	PG63	17.67	3.60	0.37	68.45	1.92	6.30	0.033	0.0010	0.023	0.30	0.0004	0.0012	0.4591	0.0209	0.0143	0.0591	0.0088	0.0254
		st.dev.	*1.59*	*0.23*	*0.01*	*4.08*	*0.10*	*0.38*	*0.001*	*0.0000*	*0.001*	*0.01*	*0.0000*	*0.0001*	*0.0259*	*0.0015*	*0.0012*	*0.0014*	*0.0004*	*0.0008*

Chapter	Group	Sample/ st.dev.	Na_2O	MgO	Al_2O_3	SiO_2	K_2O	CaO	TiO_2	V_2O_5	MnO	Fe_2O_3	CoO	NiO	CuO	ZnO	As_2O_3	SnO_2	Sb_2O_5	PbO
7	10	PG68	18.56	2.06	0.52	67.72	0.58	9.61	0.051	0.0012	0.016	0.35	0.0002	0.0007	0.0024	0.0046	0.0002	0.0005	0.0000	0.0017
		st.dev.	*1.08*	*0.11*	*0.04*	*4.70*	*0.02*	*0.49*	*0.004*	*0.0001*	*0.001*	*0.03*	*0.0000*	*0.0004*	*0.0008*	*0.0016*	*0.0000*	*0.0008*	*0.0000*	*0.0014*
7	10	PG96	19.27	0.45	0.18	72.91	0.27	6.68	0.022	0.0006	0.004	0.12	0.0001	0.0001	0.0009	0.0006	0.0000	0.0000	0.0001	0.0012
		st.dev.	*1.63*	*0.04*	*0.01*	*5.80*	*0.02*	*0.55*	*0.002*	*0.0000*	*0.000*	*0.01*	*0.0000*	*0.0000*	*0.0009*	*0.0000*	*0.0000*	*0.0000*	*0.0000*	*0.0000*
7	10	PG104	28.80	1.29	10.47	49.59	1.51	2.84	0.797	0.0117	1.105	3.60	0.0036	0.0025	0.0051	0.0060	0.0107	0.0003	0.0001	0.0014
		st.dev.	*8.80*	*0.43*	*3.25*	*16.75*	*0.46*	*0.89*	*0.292*	*0.0036*	*0.347*	*1.14*	*0.0011*	*0.0007*	*0.0022*	*0.0022*	*0.0034*	*0.0001*	*0.0000*	*0.0004*
7	10	PG116	18.85	0.50	0.30	73.74	0.24	4.76	0.033	0.0016	0.585	0.23	0.0007	0.0010	0.6104	0.0016	0.0019	0.0073	0.0021	0.0140
		st.dev.	*0.25*	*0.03*	*0.02*	*1.51*	*0.01*	*0.08*	*0.000*	*0.0000*	*0.010*	*0.01*	*0.0002*	*0.0002*	*0.0064*	*0.0003*	*0.0001*	*0.0001*	*0.0007*	*0.0014*
7	10	PG118	10.57	0.54	0.37	81.05	0.21	6.76	0.084	0.0012	0.009	0.27	0.0001	0.0003	0.0014	0.0009	0.0005	0.0000	0.0001	0.0005
		st.dev.	*8.15*	*0.10*	*0.07*	*15.67*	*0.06*	*1.20*	*0.016*	*0.0002*	*0.002*	*0.04*	*0.0000*	*0.0001*	*0.0003*	*0.0001*	*0.0001*	*0.0000*	*0.0001*	*0.0001*
7	10	PG119	19.59	3.03	0.65	66.26	0.82	7.77	0.056	0.0020	0.042	0.51	0.0003	0.0012	0.0018	0.0033	0.0015	0.0004	0.4969	0.0008
		st.dev.	*1.28*	*0.18*	*0.03*	*3.61*	*0.06*	*0.55*	*0.004*	*0.0001*	*0.003*	*0.03*	*0.0000*	*0.0001*	*0.0002*	*0.0002*	*0.0001*	*0.0005*	*0.0239*	*0.0004*
7	10	PG137	17.74	0.31	0.12	75.47	0.22	5.92	0.016	0.0005	0.003	0.10	0.0001	0.0001	0.0221	0.0027	0.0006	0.0012	0.0012	0.0021
		st.dev.	*2.77*	*0.06*	*0.02*	*12.85*	*0.03*	*1.08*	*0.003*	*0.0001*	*0.001*	*0.03*	*0.0001*	*0.0001*	*0.0313*	*0.0031*	*0.0003*	*0.0023*	*0.0012*	*0.0032*
7	10	PG142	20.56	0.35	0.15	71.93	0.18	6.59	0.038	0.0006	0.005	0.11	0.0001	0.0001	0.0025	0.0006	0.0005	0.0000	0.0000	0.0001
		st.dev.	*2.67*	*0.05*	*0.02*	*9.54*	*0.02*	*0.86*	*0.005*	*0.0001*	*0.001*	*0.01*	*0.0000*	*0.0000*	*0.0017*	*0.0001*	*0.0000*	*0.0000*	*0.0000*	*0.0001*
7	10	PG143	18.86	0.69	0.32	74.09	0.35	5.25	0.043	0.0009	0.009	0.23	0.0001	0.0002	0.0018	0.0013	0.0005	0.0001	0.0000	0.0016
		st.dev.	*6.90*	*0.25*	*0.11*	*26.87*	*0.12*	*1.91*	*0.015*	*0.0003*	*0.003*	*0.09*	*0.0000*	*0.0001*	*0.0005*	*0.0005*	*0.0002*	*0.0000*	*0.0000*	*0.0006*
7	10	PG147	16.75	4.75	0.47	66.05	2.04	8.15	0.040	0.0013	0.026	0.38	0.0002	0.0011	0.0008	0.0039	0.0012	0.0001	0.2952	0.0005
		st.dev.	*2.57*	*0.74*	*0.07*	*10.64*	*0.30*	*1.24*	*0.006*	*0.0002*	*0.004*	*0.06*	*0.0000*	*0.0002*	*0.0002*	*0.0006*	*0.0002*	*0.0000*	*0.0444*	*0.0001*
7	11	PG39	22.41	0.64	0.78	63.21	0.31	11.64	0.084	0.0018	0.049	0.40	0.0002	0.0009	0.2862	0.0018	0.0061	0.0039	0.0029	0.0061
		st.dev.	*8.25*	*0.25*	*0.38*	*25.36*	*0.13*	*4.53*	*0.034*	*0.0008*	*0.021*	*0.17*	*0.0001*	*0.0003*	*0.0888*	*0.0009*	*0.0017*	*0.0010*	*0.0009*	*0.0019*
7	11	PG89	20.44	0.39	0.41	67.94	0.20	8.02	0.115	0.0019	0.201	0.36	0.0003	0.0020	1.6857	0.0014	0.0180	0.0013	0.0159	0.0830
		st.dev.	*0.79*	*0.02*	*0.02*	*3.54*	*0.01*	*0.39*	*0.004*	*0.0001*	*0.006*	*0.01*	*0.0000*	*0.0001*	*0.0389*	*0.0001*	*0.0010*	*0.0001*	*0.0011*	*0.0076*
7	Other Beads	PG90a	15.19	0.57	0.33	68.34	0.09	11.22	0.061	0.0009	0.010	0.24	0.0001	0.0002	0.0015	0.0013	0.0015	0.0042	3.7618	0.0035
		st.dev.	*5.28*	*0.07*	*0.04*	*6.31*	*0.01*	*1.28*	*0.006*	*0.0001*	*0.001*	*0.02*	*0.0000*	*0.0001*	*0.0013*	*0.0005*	*0.0002*	*0.0030*	*0.3228*	*0.0008*

Chapter	Group	Sample/ st.dev.	Na_2O	MgO	Al_2O_3	SiO_2	K_2O	CaO	TiO_2	V_2O_5	MnO	Fe_2O_3	CoO	NiO	CuO	ZnO	As_2O_3	SnO_2	Sb_2O_5	PbO
7	Other Beads	PG90y	2.08	0.52	0.43	73.95	0.06	7.52	0.067	0.0025	0.010	0.82	0.0002	0.0007	0.0059	0.0026	0.0367	0.0019	2.0642	12.2693
		st.dev.	*1.40*	*0.22*	*0.16*	*31.95*	*0.03*	*3.44*	*0.029*	*0.0002*	*0.005*	*0.34*	*0.0001*	*0.0004*	*0.0018*	*0.0017*	*0.0163*	*0.0014*	*0.8567*	*5.6828*
7	Non-beads	PG97	21.44	0.52	0.55	65.39	0.31	9.09	0.080	0.0014	0.027	0.31	0.0002	0.0014	2.1104	0.0014	0.0248	0.0034	0.0086	0.0073
		st.dev.	*1.87*	*0.09*	*0.11*	*11.82*	*0.05*	*1.54*	*0.013*	*0.0003*	*0.013*	*0.07*	*0.0001*	*0.0002*	*0.3943*	*0.0002*	*0.0075*	*0.0007*	*0.0013*	*0.0024*
7	Non-beads	VG114	17.20	4.52	0.66	65.52	1.76	8.43	0.055	0.0018	0.015	0.43	0.0002	0.0013	0.0007	0.0055	0.0004	0.0000	0.3872	0.0003
		st.dev.	*4.30*	*1.10*	*0.16*	*16.68*	*0.44*	*2.05*	*0.014*	*0.0005*	*0.004*	*0.11*	*0.0001*	*0.0003*	*0.0002*	*0.0014*	*0.0002*	*0.0000*	*0.0931*	*0.0001*
8	6	PG16	9.14	0.64	1.36	44.75	0.14	1.89	0.066	0.0024	0.022	2.16	0.0004	0.0028	0.0351	0.0028	1.4378	0.0003	2.6579	35.5360
		st.dev.	*0.67*	*0.08*	*0.47*	*3.51*	*0.01*	*0.16*	*0.010*	*0.0002*	*0.002*	*0.13*	*0.0000*	*0.0002*	*0.0019*	*0.0002*	*0.1847*	*0.0000*	*0.2949*	*2.8593*
8	6	PG19	6.74	0.24	0.56	45.95	0.07	1.14	0.062	0.0016	0.012	2.00	0.0001	0.0012	0.1245	0.0017	0.0656	0.0007	2.4991	40.4908
		st.dev.	*0.62*	*0.00*	*0.01*	*6.94*	*0.00*	*0.07*	*0.000*	*0.0002*	*0.000*	*0.05*	*0.0000*	*0.0001*	*0.1329*	*0.0007*	*0.0079*	*0.0004*	*0.0269*	*1.1802*
8	6	PG25	11.53	0.30	0.76	49.13	0.12	1.28	0.036	0.0017	0.017	1.78	0.0002	0.0018	0.0236	0.0019	1.5275	0.0001	2.1684	31.2612
		st.dev.	*4.37*	*0.10*	*0.31*	*16.18*	*0.04*	*0.46*	*0.013*	*0.0006*	*0.006*	*0.61*	*0.0001*	*0.0006*	*0.0055*	*0.0002*	*0.2118*	*0.0001*	*0.3739*	*5.9591*
8	6	PG40	6.14	0.29	0.72	<LOQ	0.08	<LOQ	0.089	0.0016	0.075	1.48	0.0003	<LOQ	0.0619	0.0018	0.0132	0.0045	2.1094	43.1864
		st.dev.	*6.14*	*0.25*	*0.64*	-	*0.10*	-	*0.072*	*0.0017*	*0.065*	*1.43*	*0.0003*	-	*0.0664*	*0.0018*	*0.0135*	*0.0033*	*2.0140*	*40.2439*
8	6	PG48	14.41	0.36	0.81	50.03	0.11	1.95	0.098	0.0022	0.090	1.85	0.0003	0.0016	0.0558	0.0021	0.0110	0.0016	1.8934	28.2469
		st.dev.	*2.80*	*0.02*	*0.07*	*2.51*	*0.01*	*0.16*	*0.006*	*0.0001*	*0.034*	*0.13*	*0.0000*	*0.0002*	*0.0091*	*0.0003*	*0.0013*	*0.0009*	*0.0889*	*2.6924*
8	6	VG76	12.10	0.44	1.00	56.78	0.17	2.62	0.109	0.0023	0.020	1.68	0.0003	0.0022	0.0142	0.0020	0.0457	0.0008	2.1116	22.8175
		st.dev.	*5.92*	*0.33*	*0.83*	*25.75*	*0.06*	*1.19*	*0.054*	*0.0011*	*0.010*	*0.76*	*0.0003*	*0.0022*	*0.0085*	*0.0009*	*0.0172*	*0.0002*	*0.9153*	*9.5532*
8	15	PG99y	17.17	0.50	0.86	62.17	0.21	5.31	0.095	0.0018	0.036	2.70	0.0005	0.0016	0.3076	0.0179	0.0994	0.0042	1.2218	9.1907
		st.dev.	*3.29*	*0.09*	*0.45*	*11.00*	*0.03*	*0.98*	*0.024*	*0.0006*	*0.014*	*1.26*	*0.0002*	*0.0006*	*0.0429*	*0.0111*	*0.0150*	*0.0031*	*0.3404*	*1.5752*
8	15	PG99d	17.43	0.57	1.78	53.54	0.49	4.95	0.163	0.0041	0.123	9.32	0.0026	0.0061	0.6966	0.1322	0.0389	0.0048	1.2710	9.3896
		st.dev.	*2.15*	*0.06*	*0.39*	*11.44*	*0.07*	*0.62*	*0.019*	*0.0005*	*0.006*	*0.58*	*0.0005*	*0.0006*	*0.0674*	*0.0368*	*0.0082*	*0.0026*	*0.1510*	*0.7626*
8	15	PG99section	15.64	0.51	2.05	55.00	0.46	4.62	0.157	0.0049	0.106	8.96	0.0024	0.0054	0.7624	0.0800	0.0349	0.0348	1.4294	10.0390
		st.dev.	*2.19*	*0.04*	*0.17*	*4.04*	*0.07*	*0.11*	*0.009*	*0.0001*	*0.013*	*1.23*	*0.0013*	*0.0013*	*0.0210*	*0.0347*	*0.0054*	*0.0238*	*0.1504*	*0.7770*
8	18	PG3	11.56	0.61	3.01	76.83	0.96	2.31	0.172	0.0038	0.144	1.74	0.1260	0.3279	0.2065	0.0145	0.0396	0.0333	0.2697	1.6649
		st.dev.	*4.57*	*0.26*	*1.30*	*10.61*	*0.36*	*0.89*	*0.070*	*0.0015*	*0.053*	*0.66*	*0.0570*	*0.2655*	*0.0862*	*0.0062*	*0.0174*	*0.0146*	*0.1104*	*0.6358*

Chapter	Group	Sample/ st.dev.	Na_2O	MgO	Al_2O_3	SiO_2	K_2O	CaO	TiO_2	V_2O_5	MnO	Fe_2O_3	CoO	NiO	CuO	ZnO	As_2O_3	SnO_2	Sb_2O_5	PbO
8	18	PG64d	18.05	0.98	6.03	61.04	1.01	1.97	0.321	0.0065	0.432	10.06	0.0013	0.0030	0.0292	0.0031	0.0042	0.0009	0.0006	0.0081
		st.dev.	*7.41*	*0.44*	*2.53*	*5.73*	*0.38*	*0.81*	*0.142*	*0.0030*	*0.199*	*4.47*	*0.0006*	*0.0015*	*0.0106*	*0.0012*	*0.0019*	*0.0009*	*0.0003*	*0.0045*
8	18	PG64y	12.80	0.33	0.82	52.12	0.12	1.77	0.046	0.0018	0.019	1.91	0.0002	0.0015	0.0297	0.0013	1.8015	0.0001	2.0257	26.1458
		st.dev.	*2.88*	*0.01*	*0.11*	*2.14*	*0.02*	*0.08*	*0.001*	*0.0001*	*0.001*	*0.05*	*0.0000*	*0.0001*	*0.0033*	*0.0001*	*0.0587*	*0.0000*	*0.0664*	*0.8762*
9	8	PG81	19.67	2.29	1.84	64.37	0.66	1.32	0.199	0.0088	0.009	9.10	0.0011	0.0228	0.0077	0.0019	0.0014	0.0001	0.0001	0.0002
		st.dev.	*4.86*	*0.53*	*0.45*	*17.75*	*0.16*	*0.34*	*0.047*	*0.0022*	*0.002*	*2.20*	*0.0003*	*0.0060*	*0.0017*	*0.0005*	*0.0003*	*0.0000*	*0.0000*	*0.0000*
9	8	PG106	22.02	2.17	2.04	58.59	1.85	2.85	0.115	0.0195	0.013	9.97	0.0004	0.0057	0.0281	0.0056	0.0118	0.0001	0.0043	0.0007
		st.dev.	*2.02*	*0.23*	*0.22*	*5.40*	*0.16*	*0.31*	*0.012*	*0.0018*	*0.001*	*0.93*	*0.0000*	*0.0006*	*0.0014*	*0.0007*	*0.0022*	*0.0000*	*0.0009*	*0.0001*
9	8	PG126	18.16	1.40	1.99	64.97	0.89	2.44	0.155	0.0134	0.012	9.71	0.0011	0.0183	0.0049	0.0017	0.0085	0.0029	0.0006	0.0004
		st.dev.	*1.39*	*0.08*	*0.11*	*4.12*	*0.06*	*0.11*	*0.007*	*0.0006*	*0.001*	*0.53*	*0.0001*	*0.0008*	*0.0006*	*0.0002*	*0.0007*	*0.0023*	*0.0000*	*0.0000*
9	8	PG131_1	18.89	0.54	1.19	60.40	0.77	1.81	0.134	0.0036	0.009	16.20	0.0002	0.0015	0.0100	0.0344	0.0073	0.0003	0.0011	0.0048
		st.dev.	*0.84*	*0.07*	*0.19*	*2.79*	*0.05*	*0.28*	*0.011*	*0.0004*	*0.001*	*0.61*	*0.0000*	*0.0003*	*0.0006*	*0.0009*	*0.0047*	*0.0002*	*0.0008*	*0.0035*
9	8	PG131_2	23.53	1.44	2.22	58.67	1.08	1.57	0.168	0.0115	0.009	11.02	0.0008	0.0115	0.0026	0.0024	0.0221	0.0001	0.0588	0.0008
		st.dev.	*15.81*	*1.07*	*1.58*	*40.84*	*0.76*	*1.05*	*0.111*	*0.0075*	*0.006*	*7.23*	*0.0005*	*0.0076*	*0.0017*	*0.0016*	*0.0137*	*0.0000*	*0.0377*	*0.0005*
9	16	PG4w	13.05	2.33	2.70	69.39	1.48	1.46	0.137	0.0336	0.058	8.46	0.0013	0.0222	0.0962	0.0096	0.0955	0.0001	0.2822	0.0059
		st.dev.	*7.29*	*0.96*	*1.07*	*29.03*	*0.64*	*0.59*	*0.055*	*0.0141*	*0.025*	*3.41*	*0.0005*	*0.0087*	*0.0895*	*0.0033*	*0.0585*	*0.0000*	*0.1325*	*0.0028*
9	16	PG4d	17.84	2.13	2.34	66.22	1.50	1.29	0.128	0.0342	0.053	7.97	0.0013	0.0232	0.0261	0.0067	0.0591	0.0001	0.0457	0.0021
		st.dev.	*7.52*	*0.88*	*0.95*	*26.95*	*0.56*	*0.42*	*0.042*	*0.0115*	*0.019*	*2.85*	*0.0005*	*0.0083*	*0.0083*	*0.0011*	*0.0202*	*0.0000*	*0.0150*	*0.0010*
9	16	PG4_r_1	18.77	1.31	2.41	67.14	1.47	1.61	0.139	0.0203	0.063	6.06	0.0009	0.0114	0.3863	0.0102	0.1082	0.0002	0.3919	0.0068
		st.dev.	-	-	-	-	-	-	-	-	-	-	-	-	-	-	-	-	-	-
9	16	PG115	17.04	2.87	1.65	61.53	0.65	4.10	0.222	0.0091	0.011	11.20	0.0002	0.0014	0.0065	0.0318	0.0057	0.0001	0.0019	0.0006
		st.dev.	*1.38*	*0.24*	*0.14*	*5.80*	*0.06*	*0.37*	*0.018*	*0.0007*	*0.001*	*0.85*	*0.0000*	*0.0001*	*0.0006*	*0.0028*	*0.0005*	*0.0000*	*0.0004*	*0.0003*
9	16	PG123	21.41	3.31	1.73	64.10	0.74	4.34	0.161	0.0033	0.011	3.28	0.0004	0.0064	0.0072	0.0021	0.0727	0.0001	0.0254	0.0004
		st.dev.	*2.54*	*0.44*	*0.24*	*8.30*	*0.07*	*0.56*	*0.021*	*0.0004*	*0.002*	*0.43*	*0.0001*	*0.0007*	*0.0016*	*0.0002*	*0.0074*	*0.0000*	*0.0036*	*0.0001*
9	16	PG124	21.27	2.92	1.57	58.50	0.57	3.02	0.115	0.0071	0.011	11.23	0.0005	0.0026	0.0046	0.0262	0.0049	0.0001	0.0093	0.0088
		st.dev.	*3.24*	*0.40*	*0.23*	*8.05*	*0.09*	*0.43*	*0.019*	*0.0012*	*0.002*	*1.79*	*0.0001*	*0.0004*	*0.0006*	*0.0027*	*0.0004*	*0.0000*	*0.0009*	*0.0007*

Chapter	Group	Sample/ st.dev.	Na_2O	MgO	Al_2O_3	SiO_2	K_2O	CaO	TiO_2	V_2O_5	MnO	Fe_2O_3	CoO	NiO	CuO	ZnO	As_2O_3	SnO_2	Sb_2O_5	PbO
9	16	PG127	16.55	1.33	2.18	55.92	0.69	5.57	0.221	0.0057	0.129	16.62	0.0006	0.0036	0.2102	0.0494	0.1148	0.0001	0.1936	0.0018
		st.dev.	*0.86*	*0.11*	*0.13*	*4.77*	*0.05*	*0.28*	*0.014*	*0.0004*	*0.010*	*1.11*	*0.0000*	*0.0001*	*0.0116*	*0.0033*	*0.0041*	*0.0000*	*0.0110*	*0.0001*
9	16	PG173	17.10	2.84	1.49	64.55	0.62	4.31	0.183	0.0071	0.014	8.17	0.0002	0.0013	0.0054	0.0232	0.0040	0.0003	0.0019	0.0008
		st.dev.	*0.72*	*0.16*	*0.10*	*3.23*	*0.02*	*0.25*	*0.008*	*0.0003*	*0.001*	*0.43*	*0.0000*	*0.0001*	*0.0032*	*0.0015*	*0.0002*	*0.0004*	*0.0002*	*0.0004*
9	16	PG174r	19.01	1.37	1.09	60.48	0.63	3.08	0.149	0.0075	0.009	13.02	0.0005	0.0016	0.7451	0.0491	0.0557	0.0001	0.0528	0.0045
		st.dev.	*6.68*	*0.57*	*0.44*	*21.67*	*0.22*	*1.07*	*0.047*	*0.0026*	*0.003*	*4.54*	*0.0001*	*0.0005*	*0.2398*	*0.0154*	*0.0170*	*0.0000*	*0.0177*	*0.0016*
9	16	PG174d	16.33	1.01	1.10	61.30	0.58	3.09	0.158	0.0068	0.012	16.12	0.0002	0.0013	0.0106	0.0595	0.0338	0.0001	0.0280	0.0009
		st.dev.	*1.00*	*0.05*	*0.03*	*3.97*	*0.02*	*0.06*	*0.019*	*0.0004*	*0.000*	*0.45*	*0.0000*	*0.0001*	*0.0027*	*0.0017*	*0.0086*	*0.0000*	*0.0083*	*0.0005*
9	Other Beads	PG32d	5.60	0.55	1.90	29.11	0.70	3.67	0.112	0.0050	0.227	54.41	0.0167	0.0888	0.1846	0.0035	0.0138	0.0229	0.3476	3.0008
		st.dev.	*3.26*	*0.16*	*0.47*	*16.27*	*0.50*	*1.37*	*0.009*	*0.0017*	*0.039*	*32.35*	*0.0104*	*0.0710*	*0.0635*	*0.0009*	*0.0092*	*0.0134*	*0.2649*	*2.2744*
9	Other Beads	PG32w	0.18	0.22	0.59	75.96	0.02	4.35	0.110	0.0016	0.031	1.22	0.0002	0.0010	0.1139	0.0015	0.0041	0.0032	1.8287	15.3047
		st.dev.	*0.10*	*0.09*	*0.36*	*29.48*	*0.01*	*1.72*	*0.042*	*0.0007*	*0.011*	*0.55*	*0.0001*	*0.0009*	*0.0686*	*0.0004*	*0.0016*	*0.0021*	*0.8935*	*3.8132*
9	Other Beads	PG58d	20.09	4.42	7.25	54.11	1.72	4.97	0.270	0.0162	0.052	6.06	0.0008	0.0090	0.0090	0.0049	0.0200	0.0029	0.0443	0.0023
		st.dev.	*2.83*	*0.69*	*0.86*	*7.59*	*0.24*	*0.76*	*0.036*	*0.0020*	*0.006*	*0.77*	*0.0001*	*0.0007*	*0.0008*	*0.0016*	*0.0061*	*0.0032*	*0.0185*	*0.0009*
9	Other Beads	PG58y	0.33	0.44	4.76	85.44	0.04	2.81	0.160	0.0025	0.005	1.06	0.0000	0.0002	0.0051	0.0014	0.3738	0.0010	4.1528	0.0181
		st.dev.	*0.07*	*0.06*	*0.41*	*12.72*	*0.00*	*0.41*	*0.019*	*0.0003*	*0.001*	*0.12*	*0.0000*	*0.0000*	*0.0006*	*0.0003*	*0.0645*	*0.0005*	*0.2399*	*0.0014*
9	Other Beads	PG113	18.78	4.17	1.14	59.67	0.62	5.90	0.113	0.0037	0.009	8.48	0.0002	0.0011	0.0031	0.0224	0.0028	0.0002	0.0007	0.0007
		st.dev.	*5.62*	*1.19*	*0.32*	*17.88*	*0.18*	*1.63*	*0.031*	*0.0009*	*0.003*	*2.21*	*0.0000*	*0.0003*	*0.0004*	*0.0053*	*0.0010*	*0.0002*	*0.0004*	*0.0004*
9	Other Beads	PG114d	16.42	2.87	1.06	55.68	0.59	3.69	0.358	0.0050	0.007	18.64	0.0002	0.0015	0.0025	0.0258	0.0086	0.0002	0.0043	0.0019
		st.dev.	*0.84*	*0.19*	*0.07*	*1.18*	*0.06*	*0.46*	*0.058*	*0.0012*	*0.001*	*10.38*	*0.0001*	*0.0013*	*0.0001*	*0.0035*	*0.0012*	*0.0002*	*0.0015*	*0.0017*
9	Other Beads	PG114w	16.23	3.01	1.13	61.09	0.61	3.98	0.330	0.0045	0.008	12.81	0.0002	0.0009	0.0033	0.0251	0.0096	0.0002	0.0835	0.0050
		st.dev.	*1.32*	*0.51*	*0.17*	*5.35*	*0.04*	*0.80*	*0.033*	*0.0007*	*0.001*	*1.23*	*0.0000*	*0.0001*	*0.0000*	*0.0010*	*0.0006*	*0.0000*	*0.0314*	*0.0006*
9	Non-beads	PG57y	10.59	0.23	0.65	54.01	0.11	0.79	0.035	0.0016	0.014	1.72	0.0002	0.0014	0.0072	0.0011	0.1000	0.0012	4.0070	27.6971
		st.dev.	*2.08*	*0.06*	*0.17*	*16.84*	*0.01*	*0.19*	*0.009*	*0.0003*	*0.004*	*0.38*	*0.0001*	*0.0003*	*0.0018*	*0.0002*	*0.0115*	*0.0011*	*0.8918*	*6.4861*
9	Non-beads	PG57b	16.02	1.67	5.12	55.58	0.84	6.43	0.181	0.0068	0.159	12.09	0.0009	0.0074	0.0137	0.0059	0.0058	0.0019	0.2079	1.3284
		st.dev.	*5.62*	*0.53*	*1.91*	*19.36*	*0.35*	*1.87*	*0.058*	*0.0022*	*0.053*	*4.05*	*0.0003*	*0.0022*	*0.0039*	*0.0015*	*0.0021*	*0.0024*	*0.0599*	*0.3758*

Chapter	Group	Sample/ st.dev.	Na_2O	MgO	Al_2O_3	SiO_2	K_2O	CaO	TiO_2	V_2O_5	MnO	Fe_2O_3	CoO	NiO	CuO	ZnO	As_2O_3	SnO_2	Sb_2O_5	PbO
9	Non-beads	PG62y	0.04	0.23	0.37	75.72	0.01	2.76	0.077	0.0012	0.007	0.94	0.0001	0.0004	0.0101	0.0009	0.0202	0.0002	2.0563	17.6957
		st.dev.	*0.01*	*0.06*	*0.06*	*17.99*	*0.00*	*0.72*	*0.019*	*0.0002*	*0.002*	*0.22*	*0.0000*	*0.0001*	*0.0009*	*0.0001*	*0.0044*	*0.0001*	*0.5872*	*3.7386*
9	Non-beads	PG62b	12.49	0.85	1.97	74.93	1.18	2.69	0.108	0.0031	0.309	4.14	0.0009	0.0026	0.0535	0.0041	0.0166	0.1098	0.1006	0.9749
		st.dev.	*10.23*	*0.67*	*1.61*	*5.89*	*0.94*	*2.14*	*0.087*	*0.0024*	*0.243*	*3.30*	*0.0007*	*0.0020*	*0.0378*	*0.0031*	*0.0130*	*0.0888*	*0.0812*	*0.7663*
10	9	VG39	0.14	0.06	0.22	93.51	0.08	0.50	0.046	0.0029	0.024	0.98	0.0004	0.0004	0.0093	0.0018	0.0018	0.0000	1.3385	3.0870
		st.dev.	*0.05*	*0.01*	*0.10*	*19.87*	*0.04*	*0.28*	*0.016*	*0.0008*	*0.010*	*0.36*	*0.0001*	*0.0002*	*0.0018*	*0.0003*	*0.0004*	*0.0000*	*0.4393*	*0.6991*

Table 2. LA-ICP-MS results for the trace elements. Values are in ppm.

Chapter	Group	Sample/ st.dev.	Rb	Sr	Zr	Cs	Ba	La	Ce	Nd	Sm	Eu	Gd	Tb	Dy	Er	Yb	Lu	Hf	Tl	Th	U
5	1	PG46	1.32	164.56	N/A	0.08	34.98	2.57	9.50	9.80	2.96	0.80	3.28	0.42	2.34	1.22	0.95	0.14	0.43	0.009	1.38	0.95
		st.dev.	*0.25*	*36.21*	*N/A*	*0.04*	*8.42*	*0.64*	*2.18*	*2.23*	*0.59*	*0.17*	*0.67*	*0.10*	*0.49*	*0.31*	*0.19*	*0.03*	*0.12*	*0.007*	*0.39*	*0.25*
5	1	PG47	1.65	177.06	N/A	0.04	38.39	2.66	9.66	10.00	2.75	0.72	3.59	0.47	2.75	1.19	1.46	0.16	0.50	0.012	1.42	1.04
		st.dev.	*0.79*	*81.43*	*N/A*	*0.01*	*17.06*	*1.24*	*4.19*	*4.15*	*1.45*	*0.33*	*1.82*	*0.21*	*1.91*	*0.38*	*0.49*	*0.10*	*0.26*	*0.023*	*0.63*	*0.48*
5	1	PG73	3.00	31.67	N/A	0.10	20.66	2.19	9.38	11.06	3.25	0.91	4.14	0.55	3.17	1.68	1.39	0.20	0.21	0.007	0.86	0.77
		st.dev.	*1.77*	*5.47*	*N/A*	*0.06*	*2.88*	*0.42*	*1.67*	*2.10*	*0.52*	*0.18*	*0.83*	*0.11*	*0.63*	*0.31*	*0.28*	*0.04*	*0.04*	*0.004*	*0.14*	*0.16*
5	1	PG79	1.42	121.02	N/A	0.04	29.89	2.30	8.47	7.10	1.95	0.52	2.30	0.27	1.52	0.68	0.73	0.08	0.31	<LOQ	0.97	0.49
		st.dev.	*0.73*	*48.62*	*N/A*	*0.01*	*11.46*	*0.94*	*3.37*	*2.86*	*0.72*	*0.19*	*0.92*	*0.08*	*0.58*	*0.33*	*0.32*	*0.02*	*0.18*	-	*0.34*	*0.20*
5	1	PG85	2.36	172.86	N/A	0.10	38.17	2.84	10.68	11.92	4.14	1.24	4.88	0.61	3.38	1.55	1.19	0.16	0.43	0.021	1.31	0.95
		st.dev.	*1.76*	*55.64*	*N/A*	*0.13*	*12.07*	*0.89*	*3.30*	*3.67*	*1.25*	*0.35*	*1.29*	*0.21*	*1.07*	*0.45*	*0.40*	*0.05*	*0.12*	*0.041*	*0.38*	*0.30*
5	1	PG86	1.30	146.81	N/A	0.08	41.07	5.83	15.06	10.84	3.38	0.79	3.38	0.52	3.43	1.83	1.49	0.19	0.67	0.017	1.21	7.69
		st.dev.	*0.48*	*58.62*	*N/A*	*0.01*	*16.53*	*2.75*	*6.25*	*4.45*	*1.14*	*0.25*	*1.34*	*0.14*	*1.28*	*0.91*	*0.43*	*0.12*	*0.40*	*0.038*	*0.27*	*3.05*
5	1	PG91	2.10	123.66	90.60	0.06	30.96	4.48	11.30	9.69	2.70	0.77	3.37	0.45	2.70	1.39	1.12	0.15	1.88	0.001	1.55	1.05
		st.dev.	*0.26*	*7.34*	*4.15*	*0.02*	*1.66*	*0.16*	*0.73*	*0.69*	*0.24*	*0.06*	*0.27*	*0.03*	*0.24*	*0.12*	*0.06*	*0.02*	*0.15*	*0.003*	*0.04*	*0.06*
5	1	PG94	4.52	121.73	25.85	0.13	42.65	3.12	9.37	7.18	1.81	0.48	2.00	0.29	1.44	0.87	0.71	0.10	0.51	0.001	0.95	0.76
		st.dev.	*4.14*	*108.76*	*23.19*	*0.13*	*38.50*	*2.83*	*8.59*	*6.72*	*1.70*	*0.43*	*1.98*	*0.27*	*1.29*	*0.81*	*0.73*	*0.09*	*0.45*	*0.002*	*0.87*	*0.68*

Chapter	Group	Sample/ st.dev.	Rb	Sr	Zr	Cs	Ba	La	Ce	Nd	Sm	Eu	Gd	Tb	Dy	Er	Yb	Lu	Hf	Tl	Th	U
5	1	PG100b	3.32	229.45	N/A	0.12	56.44	3.12	6.32	5.21	1.31	0.36	1.83	0.20	1.21	0.89	0.74	0.08	0.95	0.022	0.69	3.75
		st.dev.	*1.16*	*26.02*	*N/A*	*0.03*	*9.82*	*0.33*	*0.43*	*0.45*	*0.10*	*0.01*	*0.81*	*0.05*	*0.17*	*0.46*	*0.00*	*0.01*	*0.19*	*0.035*	*0.00*	*0.74*
5	1	PG100w	14.55	373.38	N/A	0.77	95.65	7.18	12.10	7.03	1.27	0.28	1.31	0.17	0.91	0.74	0.59	0.10	3.43	0.121	1.30	1.92
		st.dev.	*11.51*	*316.50*	*N/A*	*0.49*	*85.40*	*5.62*	*10.63*	*5.44*	*1.15*	*0.33*	*1.06*	*0.17*	*0.75*	*0.75*	*0.60*	*0.08*	*3.12*	*0.087*	*1.17*	*1.90*
5	1	PG107	4.40	74.47	N/A	0.28	40.71	3.21	10.38	11.00	3.21	0.91	3.60	0.47	2.80	1.62	1.30	0.19	0.67	0.008	1.51	1.20
		st.dev.	*0.84*	*17.89*	*N/A*	*0.17*	*9.26*	*0.47*	*1.99*	*2.68*	*0.84*	*0.22*	*1.01*	*0.12*	*0.53*	*0.48*	*0.27*	*0.04*	*0.09*	*0.009*	*0.19*	*0.31*
5	1	PG108	4.99	93.49	N/A	0.15	34.29	3.26	9.72	9.92	2.94	0.80	2.93	0.34	2.00	0.95	0.85	0.12	0.74	0.005	1.08	0.86
		st.dev.	*1.50*	*16.91*	*N/A*	*0.02*	*6.82*	*0.61*	*2.05*	*1.99*	*0.57*	*0.15*	*0.48*	*0.06*	*0.46*	*0.18*	*0.13*	*0.03*	*0.14*	*0.005*	*0.22*	*0.18*
5	1	PG109w	4.22	269.98	N/A	0.13	57.79	4.20	6.86	4.36	1.05	0.25	0.91	0.13	0.85	0.48	0.40	0.06	1.03	0.006	0.78	1.74
		st.dev.	*1.14*	*53.75*	*N/A*	*0.02*	*37.89*	*0.89*	*1.59*	*1.59*	*0.50*	*0.15*	*0.53*	*0.07*	*0.37*	*0.29*	*0.15*	*0.02*	*0.26*	*0.003*	*0.18*	*0.40*
5	1	PG109d	6.63	183.20	N/A	0.15	162.70	2.85	7.01	7.52	2.06	0.58	2.49	0.34	1.84	0.91	0.88	0.11	0.80	0.004	0.87	0.84
		st.dev.	*0.54*	*14.85*	*N/A*	*0.02*	*14.18*	*0.23*	*0.82*	*0.93*	*0.23*	*0.06*	*0.42*	*0.04*	*0.27*	*0.11*	*0.08*	*0.01*	*0.08*	*0.002*	*0.07*	*0.05*
5	1	PG111b	3.42	85.50	N/A	0.08	59.62	3.57	9.14	7.95	2.47	0.73	3.23	0.42	2.06	0.90	0.71	0.09	0.59	0.009	1.19	1.09
		st.dev.	*0.52*	*8.59*	*N/A*	*0.00*	*6.52*	*0.29*	*1.07*	*0.59*	*0.10*	*0.09*	*0.39*	*0.08*	*0.26*	*0.10*	*0.05*	*0.02*	*0.08*	*0.010*	*0.16*	*0.17*
5	1	PG111w	3.16	207.05	N/A	0.09	36.91	3.45	5.98	3.91	1.00	0.22	0.98	0.13	0.79	0.37	0.37	0.04	0.96	0.007	0.64	0.56
		st.dev.	*0.49*	*52.52*	*N/A*	*0.01*	*6.84*	*0.59*	*0.96*	*0.98*	*0.29*	*0.09*	*0.39*	*0.05*	*0.28*	*0.05*	*0.14*	*0.00*	*0.21*	*0.005*	*0.10*	*0.13*
5	1	PG112	8.71	241.40	N/A	0.29	341.54	7.39	10.08	6.68	1.19	0.25	1.18	0.14	1.04	0.47	0.63	0.08	1.18	0.062	1.20	0.99
		st.dev.	*1.81*	*50.70*	*N/A*	*0.06*	*74.84*	*1.90*	*2.59*	*1.59*	*0.66*	*0.10*	*0.13*	*0.04*	*0.38*	*0.05*	*0.21*	*0.06*	*0.14*	*0.031*	*0.38*	*0.36*
5	1	PG139	2.97	260.56	12.11	0.10	51.04	4.38	11.07	8.44	2.43	0.61	2.69	0.31	1.71	0.76	0.65	0.08	0.25	0.022	1.30	0.92
		st.dev.	*1.24*	*20.93*	*1.25*	*0.02*	*3.59*	*0.29*	*1.00*	*0.76*	*0.35*	*0.05*	*0.25*	*0.05*	*0.25*	*0.08*	*0.04*	*0.01*	*0.03*	*0.018*	*0.08*	*0.12*
5	1	PG150b	2.47	138.10	N/A	0.09	33.11	2.31	8.48	10.30	3.71	1.10	5.41	0.68	3.41	1.65	1.11	0.14	0.31	0.006	0.69	0.44
		st.dev.	*0.77*	*51.77*	*N/A*	*0.04*	*11.98*	*0.86*	*3.30*	*3.71*	*1.44*	*0.36*	*1.68*	*0.29*	*1.09*	*0.64*	*0.47*	*0.07*	*0.16*	*0.006*	*0.25*	*0.19*
5	1	PG150w	3.62	271.63	N/A	0.10	65.93	1.13	2.43	1.42	0.34	0.09	0.39	0.06	0.37	0.19	0.16	0.03	0.43	0.009	0.40	0.22
		st.dev.	*0.69*	*71.78*	*N/A*	*0.04*	*17.28*	*0.29*	*0.87*	*0.75*	*0.17*	*0.08*	*0.38*	*0.05*	*0.20*	*0.11*	*0.05*	*0.01*	*0.09*	*0.004*	*0.27*	*0.07*
5	1	PG150b	2.19	140.53	17.29	0.10	36.39	2.45	8.55	10.29	3.93	1.16	5.29	0.67	3.56	1.58	1.03	0.14	0.40	0.006	0.73	0.47
		st.dev.	*0.39*	*21.10*	*2.52*	*0.05*	*5.27*	*0.43*	*1.43*	*1.69*	*0.81*	*0.23*	*0.79*	*0.11*	*0.61*	*0.27*	*0.19*	*0.03*	*0.07*	*0.011*	*0.13*	*0.06*

Chapter	Group	Sample/ st.dev.	Rb	Sr	Zr	Cs	Ba	La	Ce	Nd	Sm	Eu	Gd	Tb	Dy	Er	Yb	Lu	Hf	Tl	Th	U
5	1	PG150w	4.07	295.19	20.52	0.11	72.09	1.38	2.75	1.53	0.39	0.10	0.44	0.06	0.41	0.20	0.21	0.02	0.47	0.008	0.34	0.25
		st.dev.	*4.98*	*377.38*	*25.31*	*0.13*	*91.63*	*1.48*	*2.75*	*1.31*	*0.25*	*0.07*	*0.29*	*0.04*	*0.29*	*0.13*	*0.18*	*0.02*	*0.56*	*0.015*	*0.33*	*0.27*
5	1	PG151b	5.17	157.24	N/A	0.12	130.05	1.76	4.83	4.53	1.46	0.42	1.81	0.26	1.45	0.72	0.61	0.10	0.58	0.006	0.56	0.55
		st.dev.	*2.09*	*55.22*	*N/A*	*0.02*	*47.05*	*0.76*	*1.77*	*1.39*	*0.16*	*0.19*	*0.54*	*0.08*	*0.64*	*0.28*	*0.24*	*0.05*	*0.08*	*0.012*	*0.18*	*0.12*
5	1	PG151w	5.26	241.33	N/A	0.12	29.92	3.53	5.79	3.29	0.58	0.12	0.79	0.10	0.62	0.31	0.33	0.04	0.92	0.005	0.54	1.29
		st.dev.	*1.85*	*107.81*	*N/A*	*0.08*	*13.56*	*1.53*	*2.68*	*1.22*	*0.23*	*0.04*	*0.27*	*0.06*	*0.42*	*0.19*	*0.17*	*0.02*	*0.57*	*0.005*	*0.23*	*0.53*
5	1	PG156b	1.77	179.23	16.60	0.07	43.93	2.23	7.98	9.67	3.51	1.17	4.98	0.65	3.51	1.68	1.23	0.16	0.38	0.003	0.74	0.52
		st.dev.	*0.20*	*28.94*	*2.69*	*0.03*	*6.43*	*0.31*	*1.18*	*1.63*	*0.55*	*0.23*	*0.75*	*0.09*	*0.51*	*0.29*	*0.22*	*0.02*	*0.07*	*0.004*	*0.10*	*0.09*
5	1	VG106b	1.49	171.60	16.64	0.06	36.53	2.12	7.58	9.10	3.35	1.04	4.75	0.58	3.40	1.38	1.04	0.13	0.34	0.006	0.76	0.49
		st.dev.	*0.22*	*13.32*	*1.38*	*0.01*	*2.77*	*0.13*	*0.84*	*0.83*	*0.14*	*0.09*	*0.56*	*0.07*	*0.21*	*0.05*	*0.10*	*0.01*	*0.07*	*0.005*	*0.07*	*0.10*
5	1	VG106w	6.73	317.31	21.58	0.18	73.50	1.35	2.58	1.34	0.26	0.07	0.26	0.03	0.21	0.16	0.15	0.02	0.48	0.017	0.36	0.23
		st.dev.	*1.71*	*32.49*	*2.80*	*0.03*	*6.20*	*0.11*	*0.22*	*0.11*	*0.05*	*0.01*	*0.09*	*0.01*	*0.05*	*0.03*	*0.03*	*0.01*	*0.05*	*0.021*	*0.11*	*0.01*
5	1	PG110_2	1.77	104.09	76.45	0.04	31.02	4.82	11.39	9.04	2.41	0.73	2.85	0.39	2.28	1.16	1.00	0.14	1.67	0.003	1.59	0.94
		st.dev.	*0.39*	*40.45*	*29.84*	*0.00*	*11.51*	*1.88*	*4.52*	*3.14*	*0.97*	*0.30*	*1.15*	*0.16*	*1.05*	*0.42*	*0.30*	*0.06*	*0.59*	*0.005*	*0.61*	*0.30*
5	1	PG110_1	4.14	180.39	38.63	0.09	255.03	5.45	6.48	4.76	0.93	0.21	0.98	0.13	0.69	0.41	0.39	0.06	0.97	0.038	0.71	0.74
		st.dev.	*1.11*	*51.79*	*11.36*	*0.02*	*74.63*	*1.50*	*1.74*	*1.42*	*0.32*	*0.09*	*0.32*	*0.05*	*0.19*	*0.14*	*0.10*	*0.03*	*0.33*	*0.006*	*0.21*	*0.23*
5	2	VG98y	2.47	80.91	136.67	0.08	22.70	2.62	5.02	2.54	0.51	0.12	0.62	0.07	0.46	0.33	0.34	0.05	2.80	0.100	0.61	0.62
		st.dev.	*0.60*	*23.16*	*46.32*	*0.00*	*4.28*	*0.80*	*1.49*	*0.63*	*0.06*	*0.02*	*0.14*	*0.01*	*0.11*	*0.10*	*0.10*	*0.01*	*0.98*	*0.054*	*0.19*	*0.11*
5	2	VG98b	6.42	172.87	44.05	0.15	127.05	3.53	9.23	10.48	3.22	0.84	3.44	0.43	2.38	1.20	0.90	0.12	0.90	0.004	0.86	0.75
		st.dev.	*0.58*	*13.37*	*3.18*	*0.02*	*8.91*	*0.35*	*0.61*	*0.91*	*0.56*	*0.12*	*0.40*	*0.02*	*0.14*	*0.02*	*0.10*	*0.02*	*0.21*	*0.003*	*0.08*	*0.07*
5	7	PG28	520.68	637.04	N/A	8.81	365.07	32.60	57.46	21.85	3.46	0.63	2.55	0.30	2.09	1.62	1.30	0.22	6.30	0.536	12.65	9.68
		st.dev.	*228.28*	*350.73*	*N/A*	*3.01*	*103.83*	*7.33*	*11.09*	*6.13*	*0.61*	*0.40*	*0.51*	*0.12*	*0.69*	*0.20*	*0.53*	*0.12*	*1.91*	*0.737*	*2.23*	*2.38*
5	7	PG34	95.10	314.07	N/A	8.14	409.11	21.80	47.05	18.20	3.35	0.76	2.50	0.37	1.97	1.16	1.23	0.18	3.58	0.334	9.82	4.15
		st.dev.	*86.19*	*143.91*	*N/A*	*10.98*	*182.07*	*10.45*	*26.04*	*8.42*	*1.31*	*0.43*	*1.11*	*0.21*	*1.11*	*0.58*	*0.64*	*0.07*	*1.87*	*0.455*	*5.31*	*1.86*
5	7	PG43	2.58	223.67	N/A	0.11	52.90	3.49	11.61	9.38	2.55	0.75	3.40	0.46	3.11	1.46	1.35	0.17	0.50	<LOQ	1.11	0.71
		st.dev.	*0.51*	*24.50*	*N/A*	*0.04*	*5.93*	*0.27*	*1.35*	*0.87*	*0.57*	*0.10*	*0.43*	*0.04*	*0.41*	*0.22*	*0.18*	*0.04*	*0.06*	-	*0.15*	*0.07*

Chapter	Group	Sample/ st.dev.	Rb	Sr	Zr	Cs	Ba	La	Ce	Nd	Sm	Eu	Gd	Tb	Dy	Er	Yb	Lu	Hf	Tl	Th	U
5	7	PG51	53.63	153.65	N/A	1.70	385.81	13.54	28.11	12.78	2.88	0.50	2.61	0.41	2.52	1.85	1.81	0.21	3.33	0.343	4.28	2.29
		st.dev.	*16.20*	*18.96*	*N/A*	*0.86*	*59.93*	*2.09*	*4.48*	*2.69*	*0.36*	*0.09*	*0.22*	*0.10*	*0.34*	*0.34*	*0.53*	*0.02*	*0.66*	*0.233*	*1.04*	*0.20*
5	7	PG158	163.96	160.13	N/A	0.58	68.38	3.52	7.39	3.17	0.75	0.16	0.62	0.09	0.58	0.34	0.34	0.04	0.54	0.025	1.18	0.28
		st.dev.	*23.09*	*23.28*	*N/A*	*0.10*	*10.82*	*0.46*	*1.27*	*0.59*	*0.11*	*0.01*	*0.02*	*0.02*	*0.07*	*0.05*	*0.09*	*0.01*	*0.08*	*0.006*	*0.16*	*0.06*
5	7	PG159	118.68	195.66	N/A	1.13	156.01	8.70	18.39	8.90	1.93	0.43	1.80	0.26	1.69	0.92	0.98	0.13	1.34	0.035	2.95	0.79
		st.dev.	*5.95*	*3.93*	*N/A*	*0.08*	*3.99*	*0.14*	*0.59*	*0.26*	*0.09*	*0.04*	*0.08*	*0.02*	*0.05*	*0.08*	*0.06*	*0.01*	*0.11*	*0.004*	*0.14*	*0.05*
5	7	VG22	131.74	173.23	20.73	0.60	75.69	3.87	8.07	3.59	0.74	0.17	0.81	0.11	0.69	0.43	0.41	0.06	0.60	0.021	1.46	0.32
		st.dev.	*20.68*	*22.35*	*2.89*	*0.05*	*10.81*	*0.51*	*0.48*	*0.40*	*0.10*	*0.03*	*0.10*	*0.01*	*0.12*	*0.08*	*0.11*	*0.01*	*0.13*	*0.006*	*0.18*	*0.02*
5	Non-beads	VG32	4.98	351.73	56.75	0.06	107.71	5.74	7.87	5.53	1.21	0.27	1.04	0.15	0.87	0.54	0.49	0.07	1.23	0.005	0.60	0.65
		st.dev.	*0.33*	*30.55*	*4.81*	*0.01*	*9.25*	*0.42*	*0.67*	*0.44*	*0.13*	*0.03*	*0.05*	*0.01*	*0.14*	*0.14*	*0.03*	*0.01*	*0.13*	*0.006*	*0.08*	*0.06*
6	3	PG84w	93.55	158.75	N/A	0.53	87.20	4.99	10.07	4.66	0.96	0.20	1.03	0.15	0.94	0.52	0.53	0.09	0.82	0.015	1.68	0.42
		st.dev.	*22.52*	*34.66*	*N/A*	*0.14*	*20.85*	*0.93*	*2.08*	*0.79*	*0.21*	*0.03*	*0.19*	*0.02*	*0.08*	*0.16*	*0.12*	*0.02*	*0.27*	*0.005*	*0.34*	*0.10*
6	3	PG84b	119.72	168.20	N/A	0.98	101.47	6.34	12.95	6.00	1.28	0.29	1.25	0.18	1.10	0.68	0.69	0.09	0.95	0.011	2.56	0.56
		st.dev.	*22.88*	*30.78*	*N/A*	*0.20*	*19.53*	*1.14*	*2.60*	*1.17*	*0.26*	*0.10*	*0.19*	*0.03*	*0.23*	*0.18*	*0.19*	*0.02*	*0.19*	*0.002*	*0.59*	*0.13*
6	3	PG87	90.12	128.74	N/A	0.82	91.77	5.09	10.82	4.59	1.04	0.20	0.99	0.14	0.89	0.50	0.52	0.08	0.85	0.048	1.98	0.56
		st.dev.	*9.62*	*13.28*	*N/A*	*0.14*	*12.60*	*0.27*	*1.50*	*0.56*	*0.10*	*0.02*	*0.08*	*0.02*	*0.13*	*0.06*	*0.03*	*0.01*	*0.09*	*0.014*	*0.24*	*0.06*
6	4	PG121	15.06	174.53	44.76	0.23	46.55	8.89	19.26	8.96	1.95	0.39	1.83	0.25	1.52	0.86	0.83	0.12	1.30	0.005	2.95	0.51
		st.dev.	*1.49*	*23.85*	*5.97*	*0.02*	*5.97*	*1.16*	*2.39*	*1.21*	*0.28*	*0.04*	*0.19*	*0.05*	*0.25*	*0.10*	*0.14*	*0.01*	*0.16*	*0.004*	*0.37*	*0.07*
6	4	PG122_w_1	18.22	213.98	N/A	0.44	76.73	11.07	23.37	11.12	3.28	0.58	2.66	0.38	2.43	1.20	0.95	0.16	2.23	0.052	3.41	0.99
		st.dev.	-	-	*N/A*	-	-	-	-	-	-	-	-	-	-	-	-	-	-	-	-	-
6	4	PG122d	20.65	158.74	N/A	0.27	55.23	9.96	19.89	9.57	2.41	0.53	2.36	0.31	1.89	1.06	1.04	0.14	1.61	0.005	2.75	1.18
		st.dev.	*1.66*	*14.47*	*N/A*	*0.02*	*4.75*	*0.99*	*1.93*	*0.78*	*0.46*	*0.04*	*0.25*	*0.01*	*0.21*	*0.11*	*0.03*	*0.02*	*0.28*	*0.004*	*0.14*	*0.19*
6	4	PG122g	14.85	215.95	N/A	0.26	73.40	10.25	21.33	9.55	1.96	0.42	1.85	0.26	1.62	0.86	0.81	0.12	1.37	0.006	3.30	0.61
		st.dev.	*3.44*	*29.21*	*N/A*	*0.08*	*11.19*	*1.42*	*3.01*	*1.55*	*0.26*	*0.08*	*0.30*	*0.03*	*0.23*	*0.13*	*0.14*	*0.02*	*0.24*	*0.004*	*0.48*	*0.12*
6	Non-beads	PG60y	6.57	63.89	N/A	0.15	29.57	2.05	3.99	1.99	0.43	0.11	0.46	0.07	0.46	0.26	0.24	0.03	0.39	0.071	0.61	2.56
		st.dev.	*1.99*	*21.44*	*N/A*	*0.05*	*9.54*	*0.66*	*1.27*	*0.66*	*0.14*	*0.04*	*0.18*	*0.02*	*0.14*	*0.08*	*0.08*	*0.01*	*0.11*	*0.019*	*0.23*	*0.79*

Chapter	Group	Sample/ st.dev.	Rb	Sr	Zr	Cs	Ba	La	Ce	Nd	Sm	Eu	Gd	Tb	Dy	Er	Yb	Lu	Hf	Tl	Th	U
6	Non-beads	PG60b	5.35	49.18	N/A	0.13	22.92	1.65	3.18	1.57	0.41	0.10	0.40	0.05	0.37	0.20	0.19	0.03	0.28	0.045	0.47	2.01
		st.dev.	*2.21*	*19.07*	*N/A*	*0.04*	*7.05*	*0.43*	*0.77*	*0.48*	*0.09*	*0.02*	*0.10*	*0.01*	*0.14*	*0.06*	*0.07*	*0.01*	*0.12*	*0.013*	*0.18*	*0.62*
7	5	PG71	3.66	467.02	N/A	0.07	233.98	2.71	11.43	2.71	0.59	0.13	0.52	0.07	0.46	0.25	0.21	0.03	0.40	0.002	0.40	0.49
		st.dev.	*0.90*	*120.76*	*N/A*	*0.02*	*51.32*	*0.75*	*2.98*	*0.81*	*0.14*	*0.03*	*0.11*	*0.02*	*0.12*	*0.06*	*0.03*	*0.01*	*0.10*	*0.004*	*0.13*	*0.11*
7	5	PG75	3.72	455.93	N/A	0.06	515.79	2.67	9.83	2.68	0.60	0.18	0.62	0.09	0.46	0.31	0.32	0.04	0.42	0.004	0.37	0.59
		st.dev.	*0.26*	*20.29*	*N/A*	*0.01*	*22.99*	*0.05*	*0.36*	*0.12*	*0.03*	*0.03*	*0.04*	*0.01*	*0.02*	*0.03*	*0.04*	*0.00*	*0.06*	*0.002*	*0.02*	*0.04*
7	10	PG2	5.21	257.19	<LOQ	0.17	45.69	1.34	3.08	1.20	0.26	0.06	0.23	0.03	0.23	0.12	0.10	0.02	0.28	0.015	0.33	1.75
		st.dev.	*0.85*	*40.01*	-	*0.03*	*7.86*	*0.20*	*0.56*	*0.18*	*0.09*	*0.03*	*0.05*	*0.01*	*0.04*	*0.02*	*0.02*	*0.01*	*0.03*	*0.015*	*0.08*	*0.28*
7	10	PG7	5.67	442.36	<LOQ	0.15	67.63	3.31	26.47	3.09	0.61	0.12	0.55	0.08	0.47	0.26	0.25	0.03	0.50	0.001	0.58	0.73
		st.dev.	*0.08*	*16.16*	-	*0.03*	*2.74*	*0.14*	*1.19*	*0.08*	*0.05*	*0.01*	*0.04*	*0.01*	*0.06*	*0.01*	*0.03*	*0.01*	*0.04*	*0.002*	*0.03*	*0.06*
7	10	PG9	3.26	531.00	<LOQ	0.08	101.87	3.91	15.51	4.15	0.85	0.21	0.81	0.09	0.64	0.34	0.32	0.05	0.43	0.000	0.56	0.91
		st.dev.	*1.14*	*169.75*	-	*0.03*	*32.89*	*1.23*	*4.96*	*1.36*	*0.30*	*0.06*	*0.28*	*0.03*	*0.18*	*0.11*	*0.14*	*0.02*	*0.14*	*0.002*	*0.17*	*0.29*
7	10	PG10	3.18	229.79	<LOQ	0.07	59.90	1.01	1.86	0.89	0.17	0.04	0.18	0.02	0.20	0.11	0.12	0.02	0.34	0.003	0.25	0.24
		st.dev.	*0.55*	*41.14*	*0.00*	*0.02*	*11.62*	*0.19*	*0.37*	*0.16*	*0.05*	*0.01*	*0.05*	*0.01*	*0.04*	*0.04*	*0.03*	*0.00*	*0.07*	*0.002*	*0.06*	*0.06*
7	10	PG13	1.78	213.33	6.43	0.05	43.65	0.79	1.39	0.74	0.20	0.05	0.23	0.02	0.16	0.13	0.11	0.01	0.13	0.003	0.17	0.39
		st.dev.	*0.04*	*2.34*	*0.10*	*0.01*	*0.81*	*0.01*	*0.04*	*0.05*	*0.08*	*0.01*	*0.05*	*0.01*	*0.03*	*0.03*	*0.01*	*0.00*	*0.02*	*0.005*	*0.04*	*0.04*
7	10	PG14	2.71	256.30	16.71	0.08	54.64	1.07	1.82	0.95	0.28	0.03	0.15	0.03	0.18	0.10	0.14	0.02	0.42	0.003	0.18	0.33
		st.dev.	*1.20*	*65.48*	*3.82*	*0.04*	*14.50*	*0.29*	*0.52*	*0.32*	*0.10*	*0.01*	*0.08*	*0.01*	*0.09*	*0.06*	*0.04*	*0.01*	*0.12*	*0.011*	*0.01*	*0.11*
7	10	PG15	3.13	167.52	60.93	0.09	26.20	3.36	5.24	3.09	0.64	0.13	0.62	0.09	0.45	0.29	0.30	0.05	1.45	<LOQ	0.51	0.46
		st.dev.	*0.24*	*13.27*	*4.03*	*0.01*	*1.91*	*0.24*	*0.36*	*0.10*	*0.14*	*0.01*	*0.10*	*0.02*	*0.06*	*0.06*	*0.10*	*0.00*	*0.23*	-	*0.07*	*0.07*
7	10	PG63	10.74	449.67	<LOQ	0.32	42.92	1.72	3.68	1.36	0.27	0.07	0.28	0.04	0.23	0.13	0.12	0.02	0.15	0.040	0.35	0.14
		st.dev.	*0.33*	*26.13*	-	*0.03*	*0.68*	*0.25*	*0.78*	*0.08*	*0.05*	*0.01*	*0.02*	*0.01*	*0.05*	*0.01*	*0.04*	*0.00*	*0.03*	*0.022*	*0.10*	*0.03*
7	10	PG68	4.40	379.45	N/A	0.12	76.32	2.16	4.17	2.05	0.45	0.11	0.45	0.06	0.44	0.28	0.26	0.04	0.56	0.010	0.44	0.40
		st.dev.	*0.80*	*26.36*	*N/A*	*0.08*	*6.10*	*0.17*	*0.23*	*0.18*	*0.04*	*0.02*	*0.02*	*0.01*	*0.05*	*0.04*	*0.03*	*0.00*	*0.06*	*0.010*	*0.07*	*0.04*
7	10	PG96	2.05	227.12	11.94	0.06	43.95	0.79	1.39	0.70	0.24	0.03	0.13	0.02	0.16	0.13	0.08	0.02	0.27	0.001	0.17	0.20
		st.dev.	*0.10*	*15.27*	*0.66*	*0.01*	*3.61*	*0.06*	*0.12*	*0.01*	*0.05*	*0.00*	*0.04*	*0.01*	*0.02*	*0.06*	*0.03*	*0.00*	*0.06*	*0.002*	*0.01*	*0.04*

Chapter	Group	Sample/ st.dev.	Rb	Sr	Zr	Cs	Ba	La	Ce	Nd	Sm	Eu	Gd	Tb	Dy	Er	Yb	Lu	Hf	Tl	Th	U
7	10	PG104	55.28	198.05	N/A	1.67	673.44	23.76	50.60	22.74	4.91	1.05	4.96	0.71	4.88	3.36	3.45	0.51	7.31	0.066	7.34	3.21
		st.dev.	*17.96*	*64.19*	*N/A*	*0.49*	*213.19*	*7.58*	*15.99*	*7.07*	*1.51*	*0.33*	*1.60*	*0.23*	*1.65*	*1.08*	*1.02*	*0.15*	*2.27*	*0.016*	*2.25*	*1.03*
7	10	PG116	2.37	208.87	31.11	0.08	110.76	1.51	2.69	1.46	0.31	0.06	0.38	0.05	0.25	0.17	0.20	0.03	0.70	0.014	0.31	0.48
		st.dev.	*0.21*	*2.50*	*0.46*	*0.00*	*0.52*	*0.06*	*0.04*	*0.06*	*0.03*	*0.01*	*0.07*	*0.01*	*0.02*	*0.03*	*0.01*	*0.01*	*0.07*	*0.011*	*0.03*	*0.02*
7	10	PG118	2.09	211.74	105.41	0.07	31.59	4.19	6.51	3.70	0.80	0.15	0.73	0.10	0.62	0.42	0.43	0.06	2.27	0.005	0.74	0.68
		st.dev.	*0.41*	*39.23*	*20.02*	*0.02*	*6.21*	*0.73*	*1.21*	*0.77*	*0.14*	*0.01*	*0.22*	*0.04*	*0.12*	*0.09*	*0.09*	*0.01*	*0.38*	*0.003*	*0.15*	*0.11*
7	10	PG119	4.98	342.00	N/A	0.09	60.64	3.10	16.76	3.06	0.62	0.14	0.61	0.07	0.34	0.22	0.25	0.03	0.34	<LOQ	0.38	0.74
		st.dev.	*0.21*	*16.77*	*N/A*	*0.02*	*3.37*	*0.14*	*1.09*	*0.25*	*0.05*	*0.03*	*0.07*	*0.01*	*0.05*	*0.02*	*0.03*	*0.01*	*0.03*	-	*0.05*	*0.07*
7	10	PG137	2.67	210.01	7.62	0.10	51.05	0.71	1.56	0.74	0.13	0.05	0.22	0.02	0.14	0.10	0.11	0.01	0.16	0.028	0.11	0.23
		st.dev.	*1.09*	*35.33*	*1.31*	*0.08*	*8.83*	*0.17*	*0.86*	*0.18*	*0.04*	*0.04*	*0.07*	*0.01*	*0.02*	*0.02*	*0.03*	*0.01*	*0.07*	*0.031*	*0.04*	*0.12*
7	10	PG142	1.83	228.44	51.25	0.07	34.28	1.66	2.84	1.48	0.31	0.07	0.33	0.05	0.27	0.16	0.19	0.03	1.15	0.000	0.29	0.78
		st.dev.	*0.25*	*32.58*	*6.75*	*0.02*	*4.83*	*0.26*	*0.55*	*0.15*	*0.08*	*0.01*	*0.04*	*0.01*	*0.05*	*0.04*	*0.02*	*0.01*	*0.21*	*0.004*	*0.03*	*0.17*
7	10	PG143	3.58	230.67	34.29	0.10	38.85	2.00	3.61	1.80	0.40	0.07	0.37	0.07	0.36	0.20	0.20	0.04	0.71	<LOQ	0.41	2.19
		st.dev.	*1.28*	*84.65*	*12.21*	*0.05*	*14.10*	*0.76*	*1.35*	*0.75*	*0.28*	*0.05*	*0.14*	*0.04*	*0.14*	*0.08*	*0.14*	*0.02*	*0.30*	-	*0.20*	*0.89*
7	10	PG147	7.51	401.50	<LOQ	0.10	61.93	2.52	8.69	2.40	0.50	0.10	0.44	0.06	0.34	0.21	0.18	0.03	0.37	0.001	0.43	1.14
		st.dev.	*1.18*	*62.19*	-	*0.02*	*9.35*	*0.38*	*1.38*	*0.43*	*0.04*	*0.01*	*0.02*	*0.01*	*0.06*	*0.03*	*0.04*	*0.01*	*0.08*	*0.001*	*0.06*	*0.18*
7	11	PG39	8.43	407.89	105.71	0.22	71.06	4.97	8.07	4.70	0.89	0.24	0.99	0.14	0.90	0.52	0.54	0.08	2.13	0.015	0.84	2.83
		st.dev.	*3.70*	*159.43*	*40.21*	*0.08*	*26.41*	*2.06*	*3.31*	*2.00*	*0.35*	*0.07*	*0.35*	*0.05*	*0.32*	*0.22*	*0.24*	*0.04*	*0.83*	*0.010*	*0.38*	*1.18*
7	11	PG89	4.40	297.77	280.12	0.38	51.27	4.68	6.97	4.34	1.04	0.18	0.84	0.13	0.77	0.49	0.58	0.09	6.36	0.038	0.82	1.34
		st.dev.	*0.25*	*13.11*	*11.61*	*0.11*	*1.69*	*0.13*	*0.37*	*0.17*	*0.12*	*0.04*	*0.07*	*0.00*	*0.09*	*0.06*	*0.07*	*0.02*	*0.09*	*0.007*	*0.03*	*0.11*
7	Other Beads	PG90a	2.14	433.19	<LOQ	0.06	38.37	5.02	7.16	4.65	0.98	0.19	0.91	0.12	0.82	0.56	0.45	0.08	3.15	0.024	0.66	1.24
		st.dev.	*0.99*	*50.86*	-	*0.01*	*3.97*	*0.47*	*0.52*	*0.59*	*0.10*	*0.01*	*0.13*	*0.01*	*0.15*	*0.09*	*0.05*	*0.01*	*0.35*	*0.015*	*0.08*	*0.07*
7	Other Beads	PG90y	3.21	297.62	<LOQ	0.11	40.91	6.22	8.59	5.55	1.04	0.25	1.05	0.15	0.91	0.60	0.58	0.08	2.81	0.095	0.93	3.80
		st.dev.	*1.13*	*134.16*	-	*0.01*	*17.38*	*2.56*	*3.44*	*2.39*	*0.42*	*0.09*	*0.47*	*0.07*	*0.43*	*0.24*	*0.23*	*0.04*	*1.20*	*0.041*	*0.41*	*0.20*
7	Non-beads	PG97	25.26	391.88	106.95	0.51	54.48	4.76	7.67	4.49	0.94	0.20	0.91	0.10	0.77	0.47	0.49	0.07	2.32	0.057	0.81	2.77
		st.dev.	*4.33*	*65.74*	*18.47*	*0.15*	*10.14*	*0.75*	*1.36*	*0.85*	*0.18*	*0.06*	*0.16*	*0.01*	*0.11*	*0.08*	*0.12*	*0.02*	*0.43*	*0.027*	*0.18*	*0.43*

Chapter	Group	Sample/ st.dev.	Rb	Sr	Zr	Cs	Ba	La	Ce	Nd	Sm	Eu	Gd	Tb	Dy	Er	Yb	Lu	Hf	Tl	Th	U
7	Non-beads	VG114	6.94	302.20	14.57	0.18	45.32	2.41	5.35	2.27	0.51	0.12	0.45	0.06	0.38	0.25	0.22	0.03	0.32	0.000	0.45	1.60
		st.dev.	*1.76*	*74.13*	*3.63*	*0.06*	*11.51*	*0.63*	*1.34*	*0.68*	*0.21*	*0.04*	*0.11*	*0.03*	*0.12*	*0.09*	*0.07*	*0.00*	*0.10*	*0.001*	*0.11*	*0.45*
8	6	PG16	2.62	74.94	19.08	0.14	29.99	2.45	5.01	2.30	0.54	0.13	0.57	0.09	0.58	0.31	0.29	0.04	0.49	0.071	0.78	2.41
		st.dev.	*0.21*	*6.92*	*1.63*	*0.02*	*2.63*	*0.14*	*0.31*	*0.09*	*0.04*	*0.02*	*0.04*	*0.01*	*0.05*	*0.04*	*0.05*	*0.01*	*0.09*	*0.016*	*0.13*	*0.17*
8	6	PG19	3.58	65.54	N/A	0.12	69.89	6.15	10.19	5.12	0.94	0.18	0.95	0.15	0.98	0.57	0.57	0.07	0.84	0.157	1.56	3.02
		st.dev.	*1.16*	*4.69*	*N/A*	*0.03*	*51.46*	*0.05*	*0.23*	*0.16*	*0.03*	*0.03*	*0.06*	*0.01*	*0.04*	*0.02*	*0.03*	*0.01*	*0.14*	*0.012*	*0.04*	*0.08*
8	6	PG25	3.39	39.58	10.20	0.13	22.65	1.62	3.14	1.54	0.40	0.09	0.36	0.06	0.37	0.21	0.21	0.02	0.26	0.058	0.51	3.50
		st.dev.	*1.17*	*14.19*	*3.47*	*0.05*	*7.47*	*0.55*	*1.13*	*0.53*	*0.15*	*0.03*	*0.14*	*0.03*	*0.16*	*0.07*	*0.06*	*0.01*	*0.12*	*0.009*	*0.18*	*1.23*
8	6	PG40	9.18	68.95	N/A	0.18	32.61	6.01	10.06	5.05	0.86	0.19	0.72	0.17	1.16	0.59	0.49	0.06	1.23	0.154	1.91	3.14
		st.dev.	*3.60*	*56.68*	*N/A*	*0.13*	*25.16*	*4.86*	*9.06*	*4.38*	*1.15*	*0.18*	*0.73*	*0.17*	*0.95*	*0.46*	*0.43*	*0.06*	*1.25*	*0.179*	*1.69*	*2.19*
8	6	PG48	6.94	59.65	N/A	0.18	24.90	4.65	8.38	4.01	0.85	0.18	0.78	0.12	0.79	0.44	0.44	0.06	1.23	0.090	1.22	2.17
		st.dev.	*1.95*	*5.49*	*N/A*	*0.10*	*2.79*	*0.28*	*0.86*	*0.36*	*0.05*	*0.03*	*0.05*	*0.02*	*0.14*	*0.04*	*0.02*	*0.00*	*0.32*	*0.009*	*0.10*	*0.33*
8	6	VG76	3.86	62.98	74.42	0.10	22.37	4.39	7.60	3.76	0.78	0.18	0.77	0.11	0.71	0.40	0.42	0.06	1.68	0.103	1.09	3.23
		st.dev.	*1.29*	*24.73*	*30.15*	*0.02*	*9.12*	*2.15*	*3.79*	*1.83*	*0.41*	*0.09*	*0.39*	*0.06*	*0.38*	*0.21*	*0.24*	*0.02*	*0.67*	*0.036*	*0.54*	*1.33*
8	15	PG99y	10.04	222.22	N/A	0.45	102.61	7.84	10.40	5.80	0.92	0.26	0.90	0.11	0.63	0.42	0.41	0.07	1.62	0.049	1.05	4.97
		st.dev.	*2.30*	*53.68*	*N/A*	*0.21*	*57.34*	*5.07*	*4.25*	*2.92*	*0.41*	*0.13*	*0.33*	*0.03*	*0.14*	*0.14*	*0.10*	*0.02*	*0.34*	*0.028*	*0.38*	*0.93*
8	15	PG99d	27.47	197.84	N/A	1.57	237.90	9.58	16.80	7.50	1.46	0.32	1.32	0.15	0.93	0.55	0.54	0.08	1.92	0.046	2.74	4.17
		st.dev.	*4.17*	*25.65*	*N/A*	*0.17*	*40.26*	*1.21*	*1.56*	*0.71*	*0.18*	*0.05*	*0.09*	*0.00*	*0.24*	*0.09*	*0.08*	*0.02*	*0.16*	*0.005*	*0.28*	*0.43*
8	15	PG99section	31.99	297.20	N/A	2.05	437.66	30.15	30.38	15.91	2.43	0.53	1.81	0.22	1.19	0.59	0.59	0.08	1.98	0.146	3.13	4.67
		st.dev.	*5.97*	*71.27*	*N/A*	*0.64*	*129.13*	*21.90*	*12.12*	*7.54*	*0.76*	*0.19*	*0.62*	*0.06*	*0.25*	*0.10*	*0.14*	*0.01*	*0.15*	*0.056*	*0.40*	*0.30*
8	18	PG3	26.84	80.33	N/A	0.63	167.45	6.46	13.18	6.11	1.30	0.29	1.26	0.19	1.23	0.78	0.82	0.11	1.48	0.004	2.07	1.50
		st.dev.	*10.09*	*30.49*	*N/A*	*0.25*	*66.91*	*2.55*	*5.29*	*2.51*	*0.56*	*0.10*	*0.47*	*0.08*	*0.59*	*0.36*	*0.30*	*0.04*	*0.72*	*0.004*	*0.90*	*0.65*
8	18	PG64d	32.27	112.63	N/A	1.00	252.48	12.25	25.69	11.34	2.58	0.50	2.38	0.35	2.33	1.39	1.49	0.21	2.01	0.027	4.08	2.55
		st.dev.	*12.03*	*48.61*	*N/A*	*0.38*	*110.00*	*5.36*	*11.42*	*4.97*	*1.15*	*0.22*	*1.03*	*0.15*	*1.02*	*0.63*	*0.69*	*0.10*	*0.83*	*0.012*	*1.79*	*1.18*
8	18	PG64y	3.13	45.24	N/A	0.15	22.40	1.76	3.23	1.67	0.37	0.09	0.43	0.05	0.36	0.21	0.20	0.03	0.42	0.073	0.51	2.41
		st.dev.	*1.07*	*1.58*	*N/A*	*0.05*	*0.55*	*0.06*	*0.23*	*0.05*	*0.04*	*0.01*	*0.04*	*0.00*	*0.02*	*0.03*	*0.02*	*0.00*	*0.05*	*0.019*	*0.06*	*0.15*

Chapter	Group	Sample/ st.dev.	Rb	Sr	Zr	Cs	Ba	La	Ce	Nd	Sm	Eu	Gd	Tb	Dy	Er	Yb	Lu	Hf	Tl	Th	U
9	8	PG81	11.86	52.37	N/A	0.26	104.25	7.18	14.86	6.34	1.16	0.18	0.89	0.10	0.67	0.51	0.49	0.07	1.20	0.013	2.28	0.94
		st.dev.	*2.96*	*11.63*	*N/A*	*0.07*	*26.00*	*1.69*	*3.73*	*1.65*	*0.37*	*0.05*	*0.18*	*0.02*	*0.21*	*0.15*	*0.15*	*0.01*	*0.31*	*0.009*	*0.49*	*0.26*
9	8	PG106	25.32	145.88	66.13	0.63	35.42	11.06	18.17	9.58	2.04	0.33	1.81	0.29	1.72	1.18	1.07	0.16	1.71	0.011	3.70	1.82
		st.dev.	*1.83*	*13.52*	*6.77*	*0.02*	*3.57*	*0.98*	*1.57*	*0.93*	*0.20*	*0.02*	*0.16*	*0.03*	*0.18*	*0.13*	*0.06*	*0.04*	*0.23*	*0.004*	*0.32*	*0.10*
9	8	PG126	20.00	86.45	N/A	0.53	150.79	9.57	19.58	8.29	1.50	0.25	1.23	0.18	1.18	0.72	0.74	0.10	2.07	0.011	3.48	1.44
		st.dev.	*0.82*	*5.40*	*N/A*	*0.02*	*5.04*	*0.37*	*0.97*	*0.31*	*0.13*	*0.02*	*0.11*	*0.01*	*0.06*	*0.05*	*0.02*	*0.01*	*0.20*	*0.009*	*0.02*	*0.10*
9	8	PG131_1	14.90	52.65	N/A	0.37	37.11	11.15	22.09	9.23	1.86	0.28	1.72	0.21	1.35	0.79	0.79	0.10	2.12	0.041	4.74	2.92
		st.dev.	*1.53*	*7.11*	*N/A*	*0.07*	*5.43*	*0.65*	*1.26*	*0.51*	*0.20*	*0.03*	*0.08*	*0.03*	*0.13*	*0.08*	*0.16*	*0.01*	*0.21*	*0.007*	*0.20*	*0.19*
9	8	PG131_2	14.27	41.77	53.53	0.35	51.22	6.33	13.74	5.73	1.07	0.17	1.00	0.16	0.89	0.58	0.52	0.07	1.30	0.020	2.07	0.92
		st.dev.	*9.23*	*28.05*	*36.34*	*0.25*	*34.85*	*4.23*	*9.17*	*3.96*	*0.64*	*0.12*	*0.61*	*0.10*	*0.67*	*0.42*	*0.35*	*0.05*	*1.00*	*0.017*	*1.31*	*0.61*
9	16	PG4w	30.73	48.95	<LOQ	1.65	72.03	10.66	14.54	9.44	1.81	0.45	1.40	0.17	1.05	0.64	0.69	0.09	1.11	0.553	2.10	1.18
		st.dev.	*16.17*	*19.52*	-	*1.63*	*29.48*	*6.14*	*5.38*	*4.27*	*0.83*	*0.23*	*0.61*	*0.08*	*0.47*	*0.26*	*0.26*	*0.04*	*0.58*	*0.073*	*0.82*	*0.44*
9	16	PG4d	17.11	45.79	<LOQ	0.39	65.73	6.66	14.71	6.75	1.57	0.41	1.11	0.13	0.80	0.57	0.56	0.10	1.03	0.119	1.99	1.02
		st.dev.	*5.02*	*16.06*	-	*0.14*	*22.91*	*2.92*	*7.79*	*3.20*	*0.71*	*0.19*	*0.34*	*0.04*	*0.43*	*0.17*	*0.19*	*0.03*	*0.44*	*0.118*	*0.74*	*0.30*
9	16	PG4_r_1	19.65	81.80	<LOQ	0.51	128.49	9.71	18.89	8.01	1.70	0.34	1.18	0.15	0.94	0.63	0.59	0.10	1.05	0.009	2.32	1.02
		st.dev.	-	-	-	-	-	-	-	-	-	-	-	-	-	-	-	-	-	-	-	-
9	16	PG115	16.16	170.81	N/A	0.42	37.23	14.64	29.96	12.74	2.48	0.30	2.08	0.29	1.70	0.99	0.97	0.15	2.14	0.035	7.14	2.06
		st.dev.	*1.27*	*16.50*	*N/A*	*0.05*	*3.35*	*1.41*	*2.59*	*1.17*	*0.22*	*0.01*	*0.18*	*0.03*	*0.10*	*0.07*	*0.05*	*0.01*	*0.11*	*0.008*	*0.60*	*0.20*
9	16	PG123	16.75	170.83	N/A	0.41	33.96	8.80	17.90	7.76	1.38	0.21	1.26	0.18	1.14	0.67	0.66	0.10	1.43	0.007	3.42	1.14
		st.dev.	*1.66*	*21.92*	*N/A*	*0.05*	*5.22*	*1.24*	*2.45*	*1.01*	*0.16*	*0.03*	*0.16*	*0.02*	*0.18*	*0.10*	*0.14*	*0.01*	*0.24*	*0.002*	*0.50*	*0.18*
9	16	PG124	16.65	121.36	N/A	0.43	37.40	8.33	17.40	7.83	1.67	0.26	1.55	0.21	1.39	0.80	0.81	0.11	1.08	0.055	2.69	1.79
		st.dev.	*2.53*	*17.01*	*N/A*	*0.06*	*6.37*	*1.36*	*3.16*	*1.27*	*0.23*	*0.08*	*0.23*	*0.04*	*0.23*	*0.09*	*0.20*	*0.01*	*0.15*	*0.009*	*0.47*	*0.29*
9	16	PG127	15.91	123.34	N/A	0.47	81.13	9.80	20.67	8.95	1.78	0.35	1.80	0.25	1.69	0.89	0.81	0.11	1.99	0.082	3.34	2.38
		st.dev.	*0.39*	*6.33*	*N/A*	*0.02*	*4.42*	*0.76*	*1.42*	*0.44*	*0.07*	*0.01*	*0.17*	*0.02*	*0.03*	*0.02*	*0.07*	*0.01*	*0.22*	*0.000*	*0.30*	*0.21*
9	16	PG173	15.38	177.96	N/A	0.43	42.55	11.90	24.55	10.44	2.12	0.27	1.87	0.27	1.66	0.97	0.93	0.13	1.85	0.031	5.73	2.00
		st.dev.	*0.56*	*10.80*	*N/A*	*0.05*	*3.00*	*0.68*	*1.76*	*0.72*	*0.08*	*0.03*	*0.13*	*0.02*	*0.10*	*0.02*	*0.05*	*0.01*	*0.14*	*0.011*	*0.39*	*0.13*

Chapter	Group	Sample/ st.dev.	Rb	Sr	Zr	Cs	Ba	La	Ce	Nd	Sm	Eu	Gd	Tb	Dy	Er	Yb	Lu	Hf	Tl	Th	U
9	16	PG174r	12.37	88.51	N/A	0.29	27.53	8.51	18.14	7.64	1.41	0.22	1.07	0.18	0.93	0.69	0.60	0.08	1.07	0.056	2.95	1.75
		st.dev.	*4.84*	*31.39*	*N/A*	*0.12*	*9.62*	*2.96*	*6.35*	*2.77*	*0.68*	*0.08*	*0.35*	*0.05*	*0.32*	*0.33*	*0.25*	*0.03*	*0.34*	*0.023*	*1.05*	*0.60*
9	16	PG174d	11.86	53.54	N/A	0.25	28.00	7.69	15.93	7.06	1.28	0.20	1.11	0.14	0.93	0.54	0.57	0.09	1.26	0.066	2.65	1.88
		st.dev.	*0.44*	*1.76*	*N/A*	*0.01*	*1.42*	*0.50*	*0.83*	*0.38*	*0.06*	*0.02*	*0.04*	*0.01*	*0.08*	*0.04*	*0.03*	*0.00*	*0.23*	*0.017*	*0.24*	*0.12*
9	Other Beads	PG32d	57.70	131.32	N/A	1.86	151.12	9.14	20.10	7.58	1.42	0.31	1.21	0.15	0.90	0.58	0.64	0.08	2.32	0.059	3.77	1.28
		st.dev.	*28.92*	*59.12*	*N/A*	*0.68*	*100.88*	*1.35*	*1.33*	*0.76*	*0.14*	*0.07*	*0.19*	*0.03*	*0.06*	*0.08*	*0.08*	*0.01*	*0.46*	*0.006*	*0.69*	*0.60*
9	Other Beads	PG32w	14.17	156.95	N/A	1.03	45.04	10.03	17.84	7.66	1.88	0.33	1.43	0.20	1.09	0.63	0.69	0.10	4.41	0.146	2.30	2.82
		st.dev.	*11.01*	*57.62*	*N/A*	*0.86*	*15.77*	*4.73*	*9.07*	*3.58*	*0.99*	*0.15*	*0.71*	*0.11*	*0.50*	*0.32*	*0.28*	*0.05*	*1.77*	*0.097*	*1.23*	*1.03*
9	Other Beads	PG58d	53.93	201.18	N/A	2.01	218.33	30.96	69.61	28.34	4.31	0.88	3.38	0.44	2.73	1.64	1.59	0.21	2.16	0.081	5.57	3.27
		st.dev.	*4.60*	*22.25*	*N/A*	*0.22*	*21.78*	*3.53*	*8.64*	*3.49*	*0.64*	*0.10*	*0.35*	*0.04*	*0.22*	*0.21*	*0.22*	*0.02*	*0.16*	*0.053*	*0.36*	*0.30*
9	Other Beads	PG58y	41.93	592.12	N/A	1.68	2502.03	75.81	29.99	60.67	11.92	2.17	10.21	1.25	7.46	4.14	3.61	0.45	3.12	0.573	5.40	2.07
		st.dev.	*3.00*	*169.96*	*N/A*	*0.16*	*1207.85*	*9.48*	*3.63*	*5.48*	*1.17*	*0.22*	*1.65*	*0.16*	*0.76*	*0.62*	*0.54*	*0.04*	*0.31*	*0.063*	*0.53*	*0.38*
9	Other Beads	PG113	13.86	248.97	N/A	0.36	35.59	7.27	14.84	6.38	1.31	0.21	1.21	0.18	0.99	0.56	0.52	0.08	1.02	0.028	2.44	1.77
		st.dev.	*3.09*	*64.94*	*N/A*	*0.10*	*7.28*	*1.93*	*3.95*	*1.97*	*0.40*	*0.07*	*0.35*	*0.05*	*0.30*	*0.19*	*0.18*	*0.02*	*0.19*	*0.019*	*0.77*	*0.57*
9	Other Beads	PG114d	11.76	155.01	N/A	0.33	32.75	10.92	23.76	9.51	1.78	0.25	1.65	0.24	1.49	0.86	0.79	0.11	1.38	0.047	5.75	2.60
		st.dev.	*0.41*	*5.27*	*N/A*	*0.05*	*4.65*	*0.22*	*2.34*	*0.25*	*0.10*	*0.09*	*0.55*	*0.14*	*0.93*	*0.43*	*0.27*	*0.04*	*0.07*	*0.002*	*0.29*	*0.09*
9	Other Beads	PG114w	12.94	166.37	N/A	0.46	38.86	11.07	24.78	9.42	1.80	0.24	1.40	0.18	1.11	0.67	0.61	0.10	1.42	0.084	5.57	2.58
		st.dev.	*0.90*	*21.56*	*N/A*	*0.04*	*5.92*	*0.93*	*2.07*	*1.05*	*0.19*	*0.04*	*0.06*	*0.02*	*0.05*	*0.08*	*0.04*	*0.01*	*0.07*	*0.003*	*0.54*	*0.33*
9	Non-beads	PG57y	2.61	27.57	13.38	0.12	18.82	2.06	4.09	1.83	0.42	0.10	0.40	0.06	0.34	0.20	0.21	0.03	0.31	0.063	0.61	4.87
		st.dev.	*0.34*	*6.83*	*3.56*	*0.02*	*4.43*	*0.47*	*1.12*	*0.50*	*0.11*	*0.03*	*0.10*	*0.02*	*0.09*	*0.06*	*0.05*	*0.01*	*0.10*	*0.012*	*0.17*	*1.50*
9	Non-beads	PG57b	20.93	218.82	47.76	0.53	266.49	9.18	16.49	7.49	1.53	0.43	1.36	0.20	1.05	0.68	0.77	0.11	1.28	0.057	3.00	5.71
		st.dev.	*7.68*	*73.41*	*16.31*	*0.18*	*89.25*	*3.31*	*5.64*	*2.68*	*0.57*	*0.14*	*0.45*	*0.06*	*0.27*	*0.33*	*0.21*	*0.05*	*0.38*	*0.026*	*0.99*	*2.01*
9	Non-beads	PG62y	10.03	76.72	N/A	0.19	22.35	3.11	5.04	2.71	0.60	0.12	0.55	0.07	0.47	0.29	0.27	0.05	1.39	0.230	0.66	4.31
		st.dev.	*2.56*	*21.07*	*N/A*	*0.06*	*5.74*	*0.70*	*1.18*	*0.67*	*0.16*	*0.03*	*0.16*	*0.02*	*0.13*	*0.07*	*0.07*	*0.02*	*0.35*	*0.045*	*0.07*	*1.14*
9	Non-beads	PG62b	23.43	124.16	N/A	1.02	539.20	5.02	9.76	4.23	0.86	0.18	0.81	0.11	0.79	0.50	0.57	0.08	1.25	0.040	1.56	1.19
		st.dev.	*17.77*	*97.37*	*N/A*	*0.80*	*422.01*	*3.94*	*7.55*	*3.27*	*0.68*	*0.13*	*0.61*	*0.08*	*0.63*	*0.37*	*0.43*	*0.06*	*1.03*	*0.024*	*1.24*	*0.96*

Chapter	Group	Sample/ st.dev.	Rb	Sr	Zr	Cs	Ba	La	Ce	Nd	Sm	Eu	Gd	Tb	Dy	Er	Yb	Lu	Hf	Tl	Th	U
10	9	VG39	13.93	60.46	9.88	0.68	41.81	1.65	3.06	1.44	0.32	0.06	0.32	0.04	0.28	0.17	0.15	0.02	0.22	1.794	0.33	0.67
		st.dev.	*5.97*	*30.14*	*3.27*	*0.26*	*12.95*	*0.71*	*1.28*	*0.69*	*0.14*	*0.02*	*0.12*	*0.02*	*0.08*	*0.06*	*0.09*	*0.01*	*0.09*	*0.249*	*0.25*	*0.42*